Reprint of

ESSA TECHNICAL REPORT NESC 51, rev.

(including Supplement, Nov. 1971, and Supplement #2, March 1973)

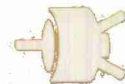# Application of Meteorological Satellite Data in Analysis and Forecasting

Anderson, Ralph K., et al.

March 1974

de Environmental Science Services Administration
NESC-51, rev.

BEST
SCAN
AVAILABLE

noaa / NATIONAL OCEANIC AND ATMOSPHERIC ADMINISTRATION / de NATIONAL ENVIRONMENTAL SATELLITE SERVICE

NESC-51, rev.

208-8-7?

## National Environmental Satellite Service Series

The National Environmental Satellite Service (NESS) is responsible for the establishment and operation of the National Operational Meteorological Satellite System and of the environmental satellite systems of NOAA. The three principal offices of NESS are Operations, Systems Engineering, and Research. The NOAA Technical Report NESS series is used by these offices to facilitate early distribution of research results, data handling procedures, systems analyses, and other information of interest to NOAA organizations.

Publication of a report in NOAA Technical Report NESS series will not preclude later publication in an expanded or modified form in scientific journals. NESS series of NOAA Technical Reports is a continuation of, and retains the consecutive numbering sequence of, the former series, ESSA Technical Report National Environmental Satellite Center (NESC), and of the earlier series, Weather Bureau Meteorological Satellite Laboratory (MSL) Report. Reports 1 through 37 are listed in publication NESC 56 of this series.

Reports 1 through 50 in the series are available from the National Technical Information Service (NTIS), U.S. Department of Commerce, Sills Bldg., 5285 Port Royal Road, Springfield, Va. 22151. Price $3.00 paper copy; $1.45 microfiche. Order by accession number, when given, in parentheses. Beginning with 51, printed copies of the reports are available through the Superintendent of Documents, U.S. Government Printing Office, Washington, D.C. 20402. Price as indicated. Microfiche available from NTIS (use accession number when available). Price $1.45.

### ESSA Technical Reports

NESC 38 Angular Distribution of Solar Radiation Reflected From Clouds as Determined From TIROS IV Radiometer Measurements. I. Ruff, R. Koffler, S. Fritz, J. S. Winston, and P. K. Rao, March 1967. (PB-174-729)

NESC 39 Motions in the Upper Troposphere as Revealed by Satellite Observed Cirrus Formations. H. McClure Johnson, October 1966. (PB-173-996)

NESC 40 Cloud Measurements Using Aircraft Time-Lapse Photography. Linwood F. Whitney, Jr., and E. Paul McClain, April 1967. (PB-174-728)

NESC 41 The SINAP Problem: Present Status and Future Prospects; Proceedings of a Conference Held at the National Environmental Satellite Center, Suitland, Maryland, January 18-20, 1967. E. Paul McClain, October 1967. (PB-176-570)

NESC 42 Operational Processing of Low Resolution Infrared (LRIR) Data From ESSA Satellites. Louis Rubin, February 1968. (PB-178-123)

NESC 43 Atlas of World Maps of Long-Wave Radiation and Albedo--for Seasons and Months Based on Measurements From TIROS IV and TIROS VII. J. S. Winston and V. Ray Taylor, September 1967. (PB-176-569)

NESC 44 Processing and Display Experiments Using Digitized ATS-1 Spin Scan Camera Data. M. B. Whitney, R. C. Doolittle, and B. Goddard, April 1968. (PB-178-424)

NESC 45 The Nature of Intermediate-Scale Cloud Spirals. Linwood F. Whitney, Jr., and Leroy D. Herman, May 1968. (AD-673-681)

NESC 46 Monthly and Seasonal Mean Global Charts of Brightness From ESSA 3 and ESSA 5 Digitized Pictures, February 1967-February 1968. V. Ray Taylor and Jay S. Winston, November 1968. (PB-180-717)

NESC 47 A Polynomial Representation of Carbon Dioxide and Water Vapor Transmission. William L. Smith, February 1969. (PB-183-296)

NESC 48 Statistical Estimation of the Atmosphere's Geopotential Height Distribution From Satellite Radiation Measurements. William L. Smith, February 1969. (PB-183-297)

NESC 49 Synoptic/Dynamic Diagnosis of a Developing Low-Level Cyclone and Its Satellite-Viewed Cloud Patterns. Harold J. Brodrick and E. Paul McClain, May 1969. (PB-184-612)

NESC 50 Estimating Maximum Wind Speed of Tropical Storms From High Resolution Infrared Data. L. F. Hubert, A. Timchalk, and S. Fritz, May 1969. (PB-184-611)

Reprint of
# ESSA TECHNICAL REPORT NESC 51
(including Supplement, Nov. 1971, and Supplement #2, March 1973)

# Application of Meteorological Satellite Data in Analysis and Forecasting

Anderson, Ralph K., et al.

WASHINGTON, D.C.
March 1974

# APPLICATION OF METEOROLOGICAL SATELLITE DATA
## IN ANALYSIS AND FORECASTING

## PREFACE

Environmental satellites, first equipped with cameras, and now with scanning radiometers, have rapidly become an important data-gathering mechanism. Cloud-cover data with excellent resolution are received regularly at ground APT stations throughout the world. These views are used advantageously to fill the observational voids of normally data-sparse areas and to supplement normal information in areas where data are more plentiful.

Many researchers are engaged in constant study to determine the correlations between the satellite's "view from the top" and the conventional observations and measurements of weather elements. Many correlations are already established and others are being established; these will enable us to obtain the maximum value from this observational technique.

Until the initial publication of this report in 1969, guidance in the interpretation of satellite cloud photographs was available mainly from the World Meteorological Organization Technical Note 75 (1966) and the "Guide for Interpretation of Satellite Photography and Nephanalyses" (1967) by Project FAMOS (U.S. Navy).

This report represents the combined efforts of personnel of the Applica. ans Group, National Environmental Satellite Center (NESC), now the National Environmental Satellite Service (NESS); the Naval Air Systems Command Project FAMOS; and the Satellite Section, USAF Environmental Technical Applications Center (ETAC). The report is a simultaneous publication: AIR WEATHER SERVICE TECHNICAL REPORT 212 and ESSA TECHNICAL REPORT NESC 51. A Supplement adding Chapter 6 was issued in November 1971; Supplement #2, adding material for Chapters 2, 3, and 5, was published in March 1973. Both supplements have been incorporated in this printing but are not identified as such.

The following personnel were directly involved with the preparation of this technical report and its supplements:

Original Report, September 1969

### USAF ETAC (AWS)

Golden R. Farr, Maj USAF, Primary Author
Jerome P. Ashman, Capt USAF, Primary Author
Arthur H. Smith, Primary Author
Leo F. Ritter, TSgt USAF, Illustrator
Darryl G. Grage, TSgt USAF, Illustrator
Lawrence Berry, Editor

Reprint March 1974

NESC (ESSA)

Ralph K. Anderson, Primary Author
Vincent J. Oliver, Primary Author
Edward W. Ferguson, Primary Author
Frances C. Parmenter, Contributor
LaRue R. Amacher, Illustrator

FAMOS (Navy)

Walter N. Cottrell, LCdr, Contributor
Fred E. Bittner, Primary Author

## Supplement, Nov. 1971

NESS (NOAA)

Ralph K. Anderson, Primary Author
Edward W. Ferguson, Contributor
Frances C. Parmenter, Contributor
LaRue F. Amacher, Illustrator

USAF ETAC (AWS)

Arthur H. Smith, Primary Author
Jerome P. Ashman, Maj USAF, Contributor
Jerome O. Siebers, Maj USAF, Contributor
Rance W. Skidmore, Capt USAF, Contributor

## Supplement #2, Mar. 1973

NESS (NOAA)

James F. W. Purdom, Primary Author
Vincent J. Oliver, Contributor
Ralph K. Anderson, Contributor
Edward W. Ferguson, Contributor
LaRue F. Amacher, Illustrator

USAF ETAC (AWS)

Rance W. Skidmore, Capt, USAF,
  Primary Author
Jerome O. Siebers, Maj USAF, Contributor
Arthur H. Smith, Contributor (now NESS)
Elden C. Taylor, Capt.USAF, Contributor
Wayne Neff, Sgt USAF, Illustrator

---

TABLE OF CONTENTS

Chapter 1

INTRODUCTION

---

Since the advent of the operational ESSA weather satellites in 1966, rou-
tine use of satellite cloud photographs has increased steadily.  Meteorolo-
gists worldwide now depend on these data to supplement conventional observa-
tions and rely completely on satellite cloud observations where other data are
not available.  The problem of "sparse data" areas has been greatly alleviated
since weather satellites now provide analysts with a timely view of the cloud
conditions over all parts of the earth.  Even so, the advantages of the satel-
lite data are not limited to isolated areas but also provide additional intel-
ligence over areas where conventional observations are dense.

If the maximum value of these data is to be realized, correct interpreta-
tion of the cloud photographs is essential.  This technical report furnishes
guidance in the interpretation of satellite cloud photographs and presents the
latest relationships as determined by research and study in this field.  The
material is arranged and presented in such a way that the user has a quick and
easy reference for the application of satellite data to weather analysis and
forecasting.  Each picture or schematic which illustrates a relationship is
located near the textual entry which describes it.  The satellite pictures are
identified by letters and numbers, i.e., E-7 indicates ESSA 7.  Most analyses
used in this report are based on the operational analyses prepared by the
National Meteorological Center at Suitland, Maryland.  However, any time dif-
ferences between the pictures and the analyses have been considered in the
interpretation of cloud patterns.  In some cases, slight adjustments have been
made to the original analyses.

Future research with improved satellite data will undoubtedly result in
the determination of new concepts and a better understanding of the relation-
ships between satellite data and the dynamics of the atmosphere.  For this
reason, this report is published in loose-leaf form to allow it to accommodate
new information as it becomes available.

A Satellite Cloud Atlas and Glossary is included to assist in identifica-
tion of cloud types and to define terms currently employed by the Applications
Group, National Environmental Satellite Center, the Naval Air Systems Command
Project FAMOS and the Satellite Section, USAF Environmental Technical Applica-
tions Center.

Chapter 2

SATELLITE CLOUD ATLAS AND GLOSSARY

---

Introduction

This pictorial glossary includes some of the more common terms used in satellite meteorology; defines or describes each item and shows photographic examples.  The meaning and definition of some of these terms vary among satellite meteorologists.  The Satellite Section, USAF ETAC; Applications Group, NESC; and Project FAMOS, U.S. Navy have coordinated in defining and describing all the terms in an attempt to standardize definitions.

The glossary is not all-inclusive.  It does, however, include cloud types, a few terms for which standardization is desired, and other items which can be adequately described without being assigned a full section of this report.

Cloud codes from the International Cloud Atlas are appended to each definition of cloud type to aid in associating satellite pictures with ground observations.

Familiarity with the glossary definitions and descriptions will assist in better understanding of the chapters following.

## Terms

ALTOSTRATUS — When seen in conjunction with synoptic scale patterns, alto-
stratus appears in satellite photographs as a very white (bright) cloud with a
uniform surface, generally organized into extensive sheets or bands.  An alto-
stratus layer without underlying cloud can vary from white to gray, depending
on its vertical thickness.  Variations in the top appear as a result of shad-
ows and breaks, often caused by internal convection.  The brightest parts of
these cloud areas are often associated with precipitation.  Altostratus clouds
usually appear in large connected sheets and are associated mainly with synop-
tic-scale systems such as cyclones and fronts.  Altostratus is frequently in-
distinguishable from cirrostratus.  The convective cloud elements of altocu-
mulus are usually below the resolution of the camera system; thus, altocumulus
is usually not distinguishable from altostratus.  Cloud Atlas codes M2, M5,
M7, apply.
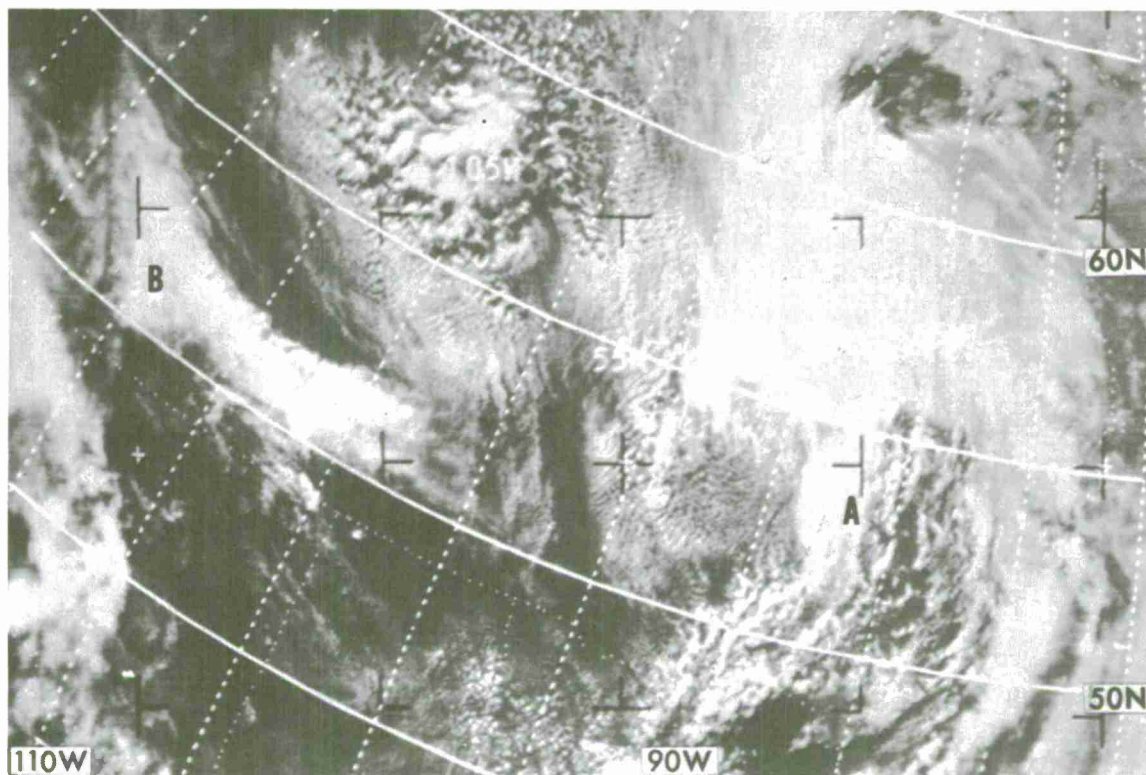


E-5 790-4 2034Z 21 Jun 67

Figure 2-1.  Altostratus is reported by surface observation
at points A and B.  These clouds, associated with a low pressure
area and a frontal system, are very white and have a uniform sur-
face.  The altostratus at A is organized in a sheet and at B, in-
to a band; both have well-defined boundaries.  These very white
cloud areas are associated with precipitation at both A and B.

Figure 2-2. Multilayered alto-
stratus and cirrostratus clouds cover
most of the area between A and B.
Identification of middle clouds in
this area may not be possible. Alto-
stratus is reported at A and B, but
at A the usual distinguishing char-
acteristics of altostratus are not
apparent.
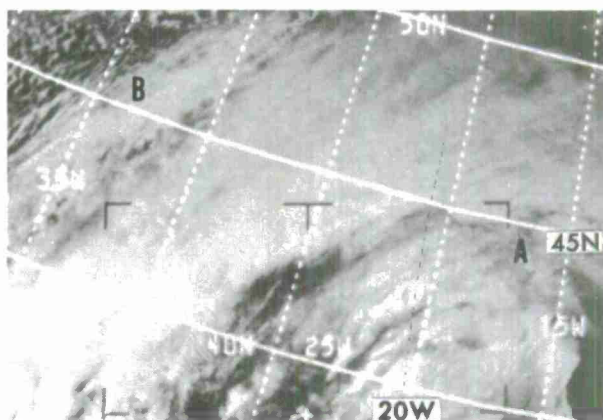


E-3 1785-3 1453Z 21 Feb 67

Figure 2-3. Cloud types change
from multilayered altostratus and
cirrostratus at C, to cirrostratus
at B. At A, altostratus is reported
and can be identified, even with a
thin cirrostratus cover. Altocumulus,
reported at D, cannot be distinguished
from altostratus.
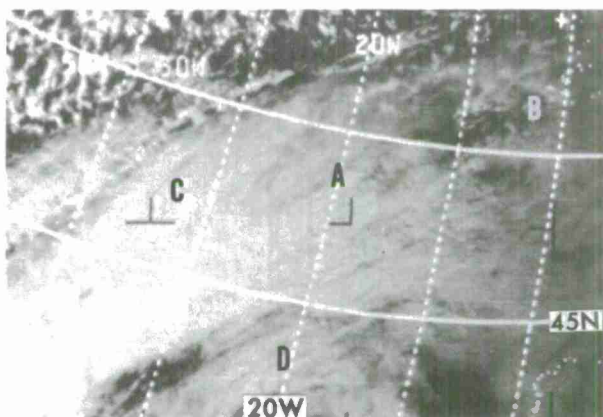


E-3 1785-2 1458Z 21 Feb 67

Figure 2-4. Convection within
the frontal band and cyclone has re-
sulted in shadows and striations in
the top of the altostratus and alto-
cumulus layer north of 53N-10W.
South of 53N the middle clouds are
covered by a smooth deck of cirrus.
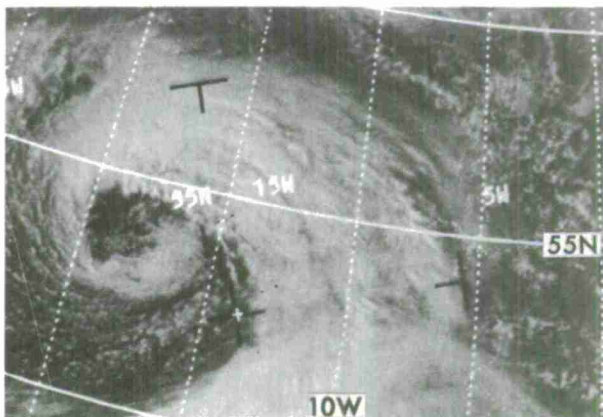


E-5 1738-4 1523Z 4 Sep 67

ANOMALOUS LINE — A highly persistent cloud line found in oceanic anticy-
clones.  It appears as a bright line in a very thin stratus or fog area, or in
a nearly clear region.  The lines vary in length up to several hundred miles
and are normally under 20 miles wide.  Anomalous lines are aligned in ways
which are initially unrelated to any patterns of synoptic circulation and of-
ten cross each other.  They are assumed to be condensation trails produced by
ships or low flying aircraft.

Figure 2-5.  Anomalous lines
shown have formed in stratiform
clouds under a high pressure area.
Low level winds tend to bend anoma-
lous lines with time.  Note the sharp
change in direction of the anomalous
line at A, while at B there is a
gradual change in the orientation of
the line.
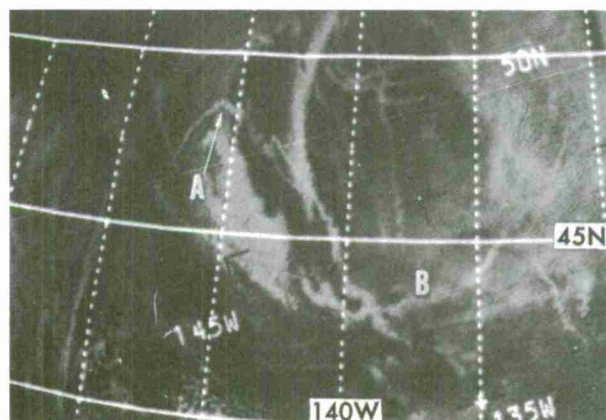


E-3 1927-3 2214Z 4 Mar 67

Figure 2-6.  An example of anoma-
lous lines which have formed in the
mostly clear area of a high pressure
cell.



E-3 1914-2 2128Z 3 Mar 67

Figure 2-7. These anomalous
lines, in a "tic-tac-toe" pattern,
are unrelated to any synoptic flow.
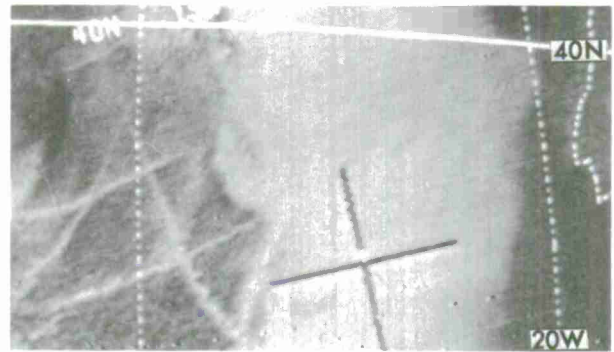
E-1 2285-8 1413Z 12 Jul 66

ANVIL CIRRUS — A smooth-textured cloud which forms from cumulonimbus and
extends downwind in the form of an anvil or plume. The plume is aligned par-
allel to the wind shear in the layer in which the cumulonimbus and the anvil
are embedded. It has a distinct sharp edge on the upwind side and a fuzzy
edge downwind. Anvil cirrus is brighter over the parent cloud, decreasing in
brightness away from the source. The plumes often extend downwind several de-
grees and may thin to a filmy veil with fibrous texture. Cloud Atlas codes
L9, H2, H3, apply.
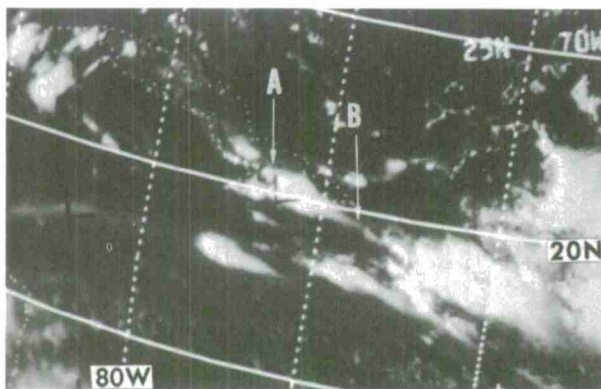


E-5 853-6 1942Z 26 Jun 67



E-5 841-6 2059Z 25 Jun 67

Figure 2-8. Anvil cirrus plumes
extend from cumulonimbus over the
Caribbean. At A, note the sharp
edges and bright cirrus. Further
downstream the plume decreases in
brightness and thickness, becoming
fuzzy at B.

Figure 2-9. Anvil cirrus is seen
over Florida and Gulf of Mexico. The
sharp edge at A decreases in bright-
ness and thins at B. Notice the
cells embedded near A and the dif-
ference in texture and brightness
between A and B.

CIRCULATION CENTER — See VORTICITY CENTER.

CIRROSTRATUS — This cloud is normally a smooth uniform-appearing cloud, sometimes fibrous in texture, which may appear as long bands extending hundreds of miles, or as an extensive sheet. Cirrostratus is usually light gray when thin and becomes brighter with increasing thickness. Shadows from thick cirrostratus are frequently seen on lower clouds and terrain. A thin cloud layer through which lower clouds or landmarks can be detected is usually cirrostratus. Thin cirrus is difficult for the camera system to detect, and unless it is connected with cirrostratus or anvil cirrus, it is not seen. Cloud Atlas codes H5, H6, H7, H8, apply.
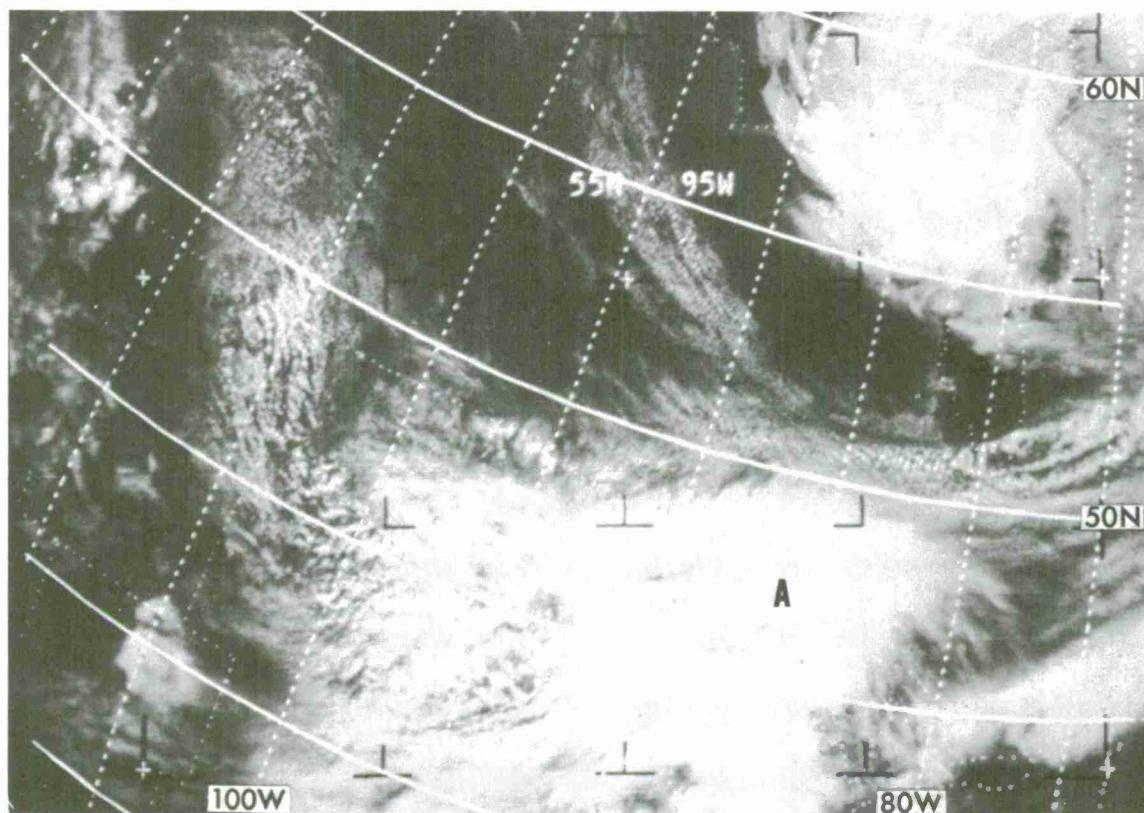


E-5 828-4 2031Z 24 Jun 67

Figure 2-10. A thick sheet of bright, smooth cirrostratus over a frontal wave, at A, decreases in density becoming fibrous and grayer around the edges to the east.
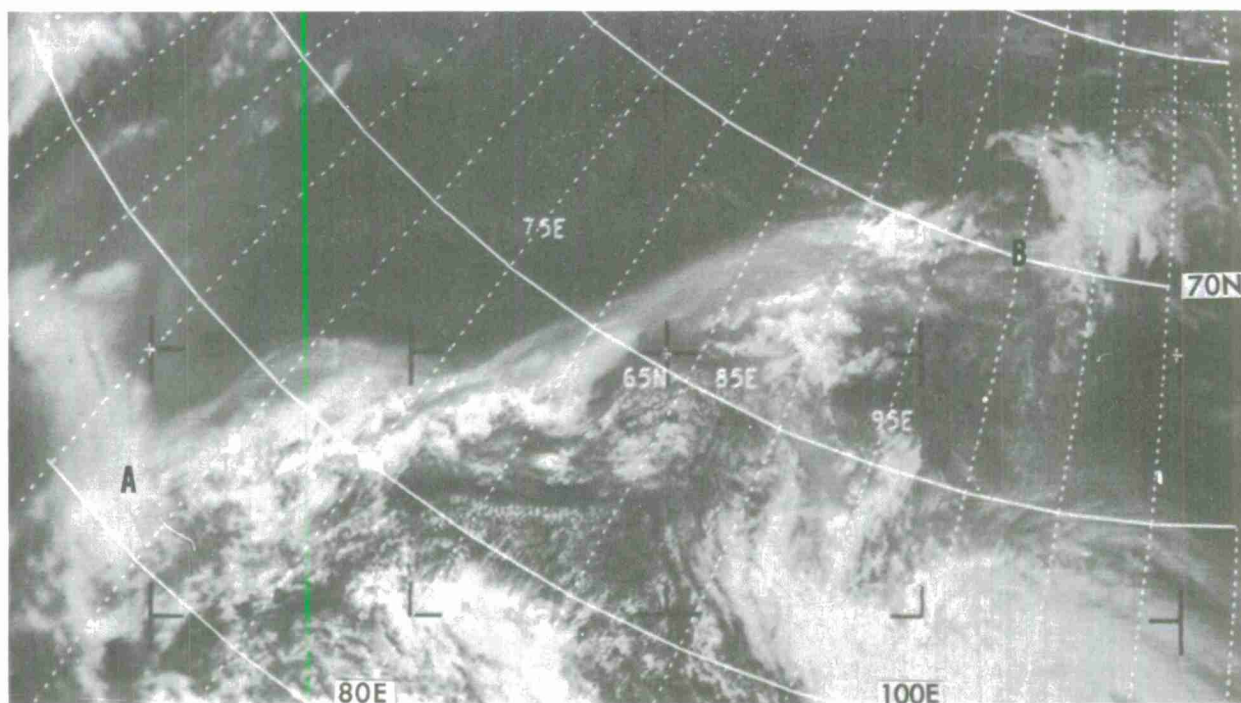
E-5 1227-3 0801Z 26 Jun 67

Figure 2-11.  Denser low and middle clouds can be seen through a
band of thin cirrostratus extending from A to B.
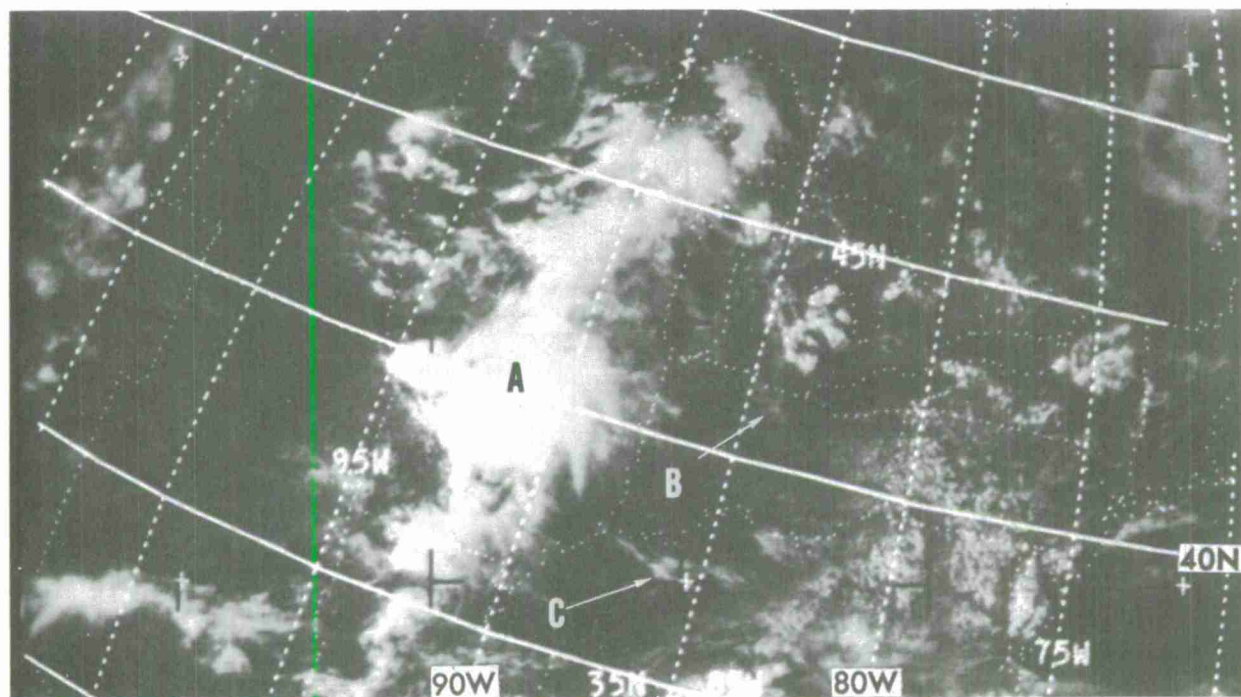


E-5 866-5 2022Z 27 Jun 67
     Figure 2-12.  A dense cirrostratus shield at A thins to semi-
transparent gray clouds at B, over some fair weather cumulus.
Dense cirrus is observed at C.

CIRRUS SPISSATUS — A dense globular cirrus cloud formation which is convective in appearance and gives an impression of cumulonimbus when viewed from satellite altitude.  It is frequently seen in long bands associated with strong winds.  A distinguishing feature of cirrus spissatus is that the shadows cast by cirrus spissatus are usually of uniform width (from the edge of the cloud away from the sun to the edge of the shadow), while a field of cumulonimbus and cumulus clouds cast shadows of different sizes depending on their vertical development.  Cirrus spissatus produces recognizable shadows most often over the desert regions of the subtropics.  Cloud Atlas codes H2, H3, apply.
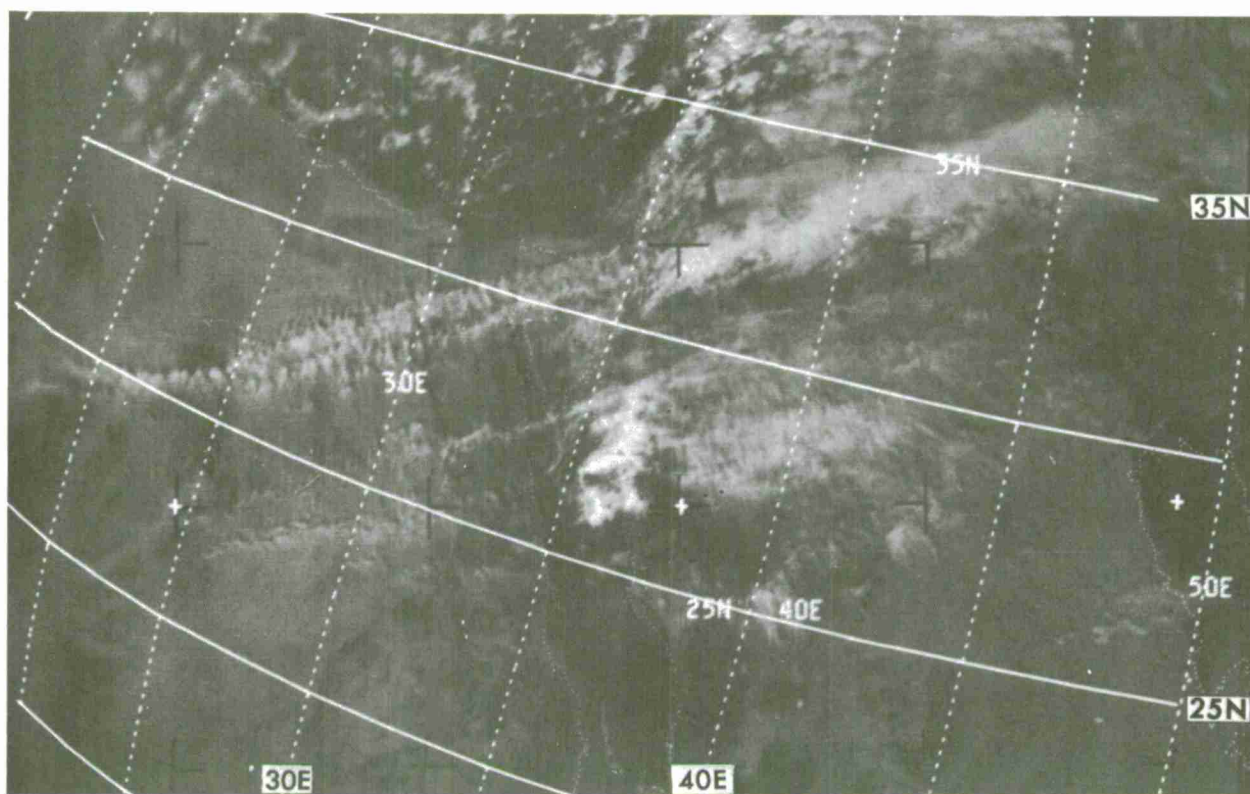


E-3 5538-3 1001Z 17 Dec 67

Figure 2-13.  Cirrus spissatus appears as bands of convective-like clouds associated with strong winds over Egypt and the Red Sea.  Shadows of equal size can be seen along the northern edge of the cloud band.
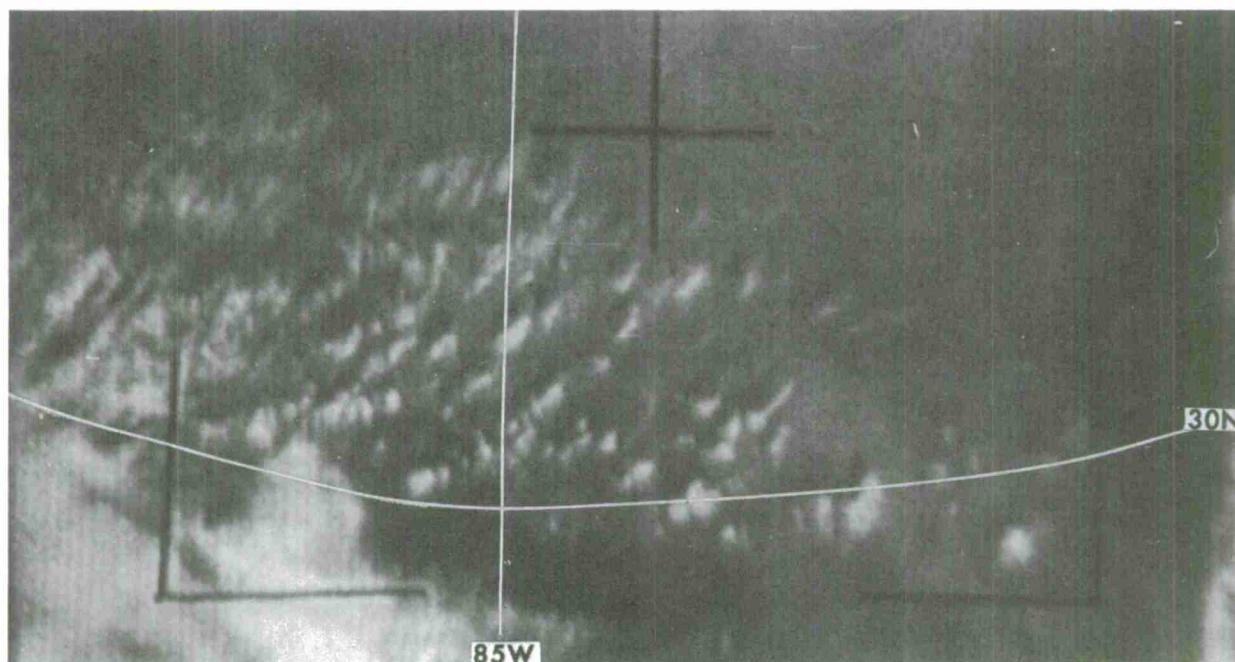
T-7 3108D 1541Z 15 Jan 64

Figure 2-14. Cirrus spissatus in the form of dense globs creates the impression of cumulonimbus. Shadows of uniform width to the northwest of each cloud aids in differentiation of cirrus spissatus from cumulonimbus.

Figure 2-15. A band of cirrus spissatus, extending from A to B over northwest India, is characterized by a convective appearance and shadows of uniform width.
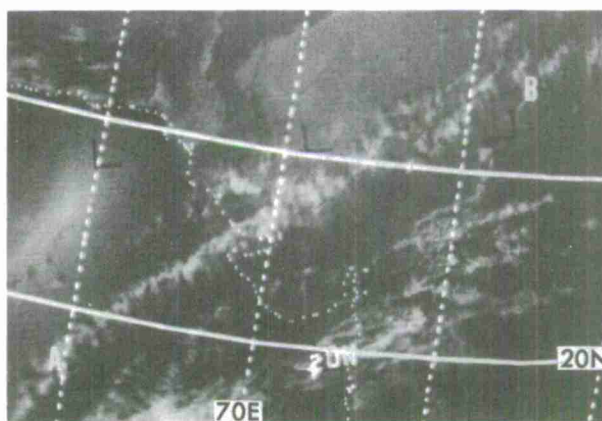


E-3 840-3 0908Z 8 Dec 67

CLOUD BAND — A nearly continuous cloud formation with a distinct long axis where the ratio of length to width is at least 4 to 1 and the width is greater than 1 degree latitude.

Figure 2-16. Bands at A and B are greater than 1 degree in width and conform to the length-width ratio of at least 4 to 1.
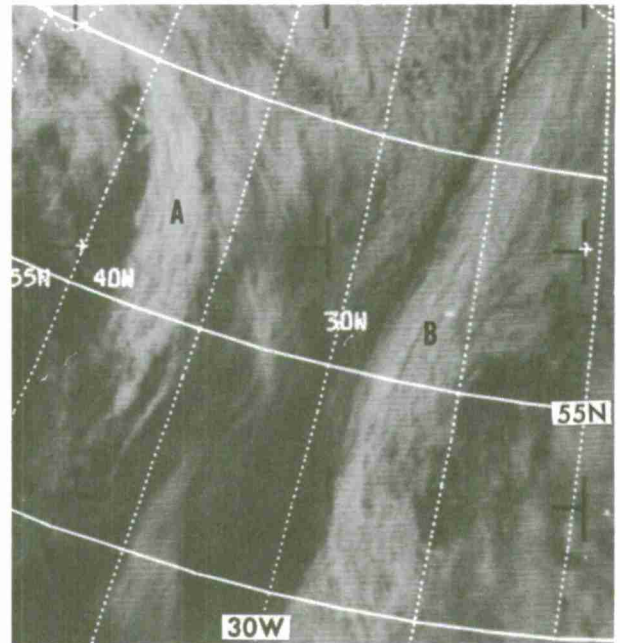


E-5 5948-3 1803Z 1 Aug 68

Figure 2-17. A band of clouds associated with a frontal system is seen over the Atlantic. The clouds, extending southeastward at A, do not constitute a separate band since the length, as seen protruding from the front, is less than 4 to 1.
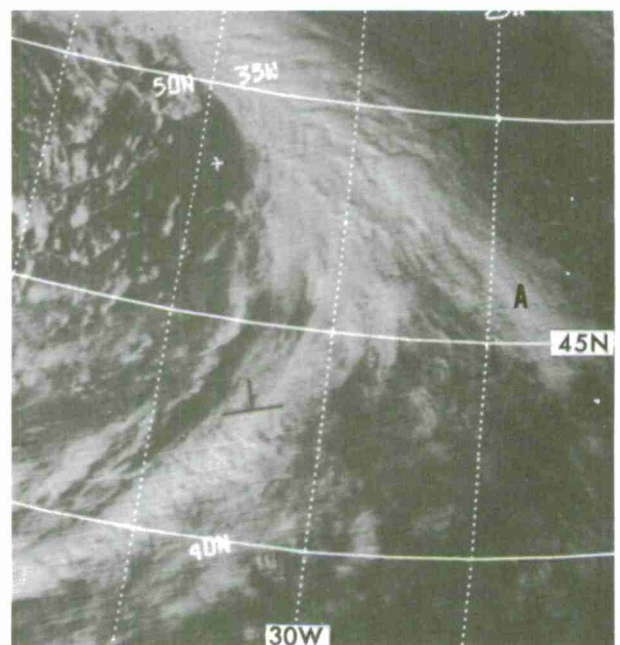


E-7 653-3 1619Z 7 Oct 68

CLOUD ELEMENT — The smallest distinguishable cloud unit that can be re-
solved in a satellite picture.  Clouds larger than the resolution of the cam-
era system can be made up of more than one element.
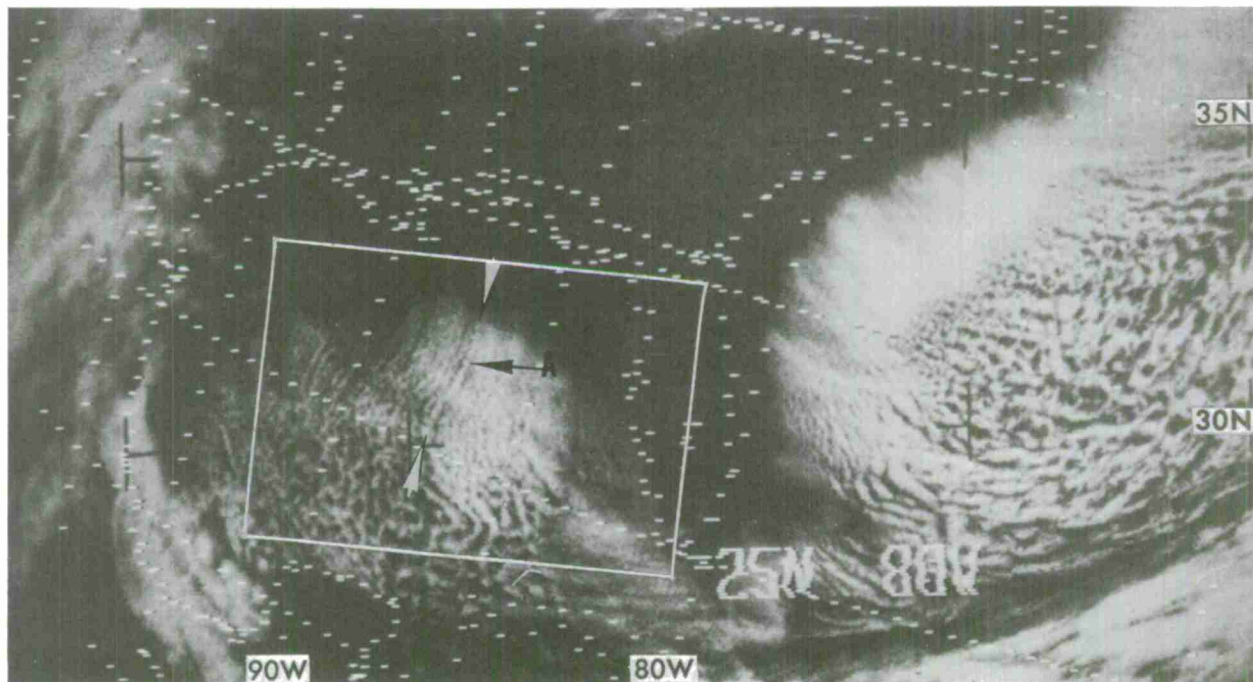


E-3 6484-3 1830Z 1 Mar 68

Figure 2-18.  Careful examination of the cloud lines forming over the
Gulf of Mexico will reveal individual cloud elements.  These elements are
small bright cells, separate from each other, making up the cloud line
between the two arrowheads.  At A is a cloud element within a cumulus
mass.

Figure 2-19.  This enlargement
of a portion of Figure 2-18 shows
the individual cloud elements in
greater detail at points A, B, and
C.
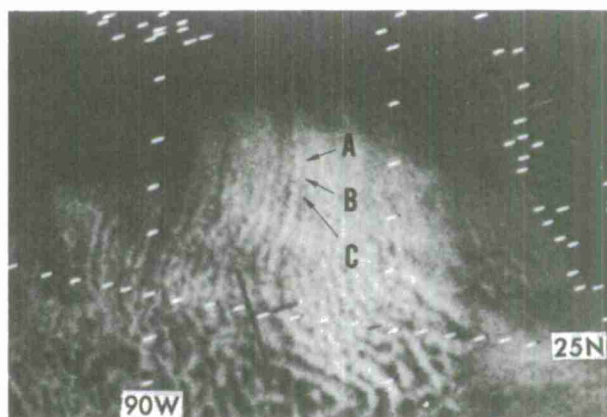


Enlargement of E-3 6484-3

CLOUD LINE — A line composed of a series of clouds nearly all of which are connected and which is less than 1 degree latitude in width.
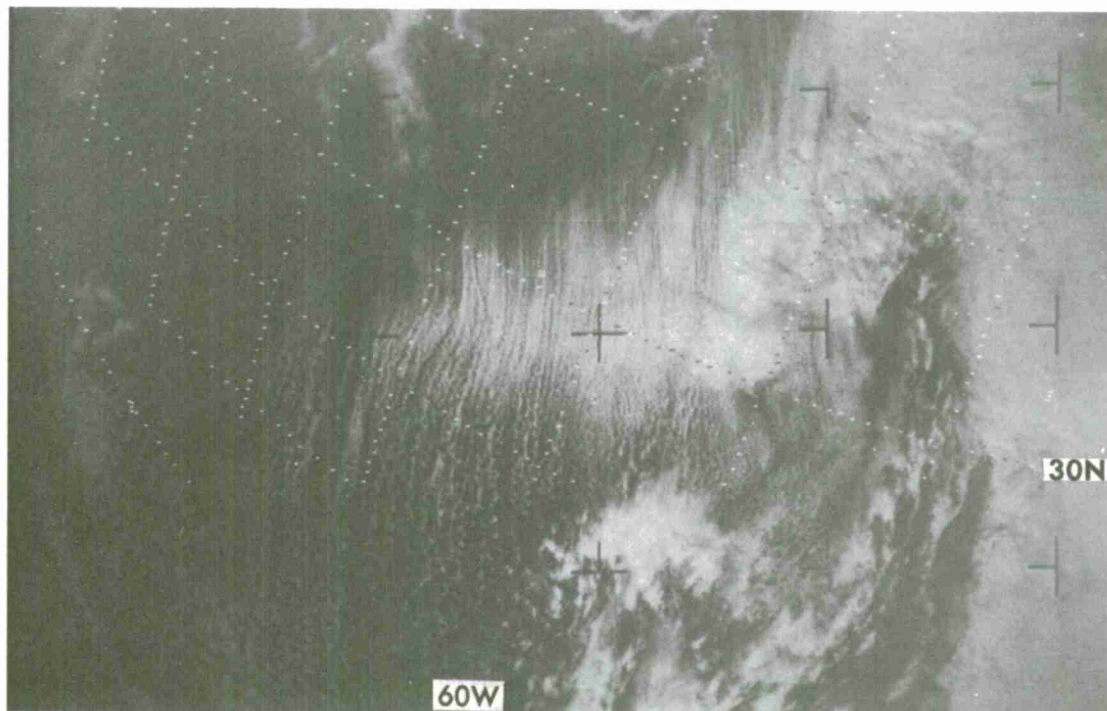


E-3 6571-3 1600Z 8 Mar 68

Figure 2-20. A large number of nearly parallel cloud lines are seen in the Atlantic Ocean off the southeastern coast of the United States. South of 30N some of the lines widen to almost 1 degree latitude.
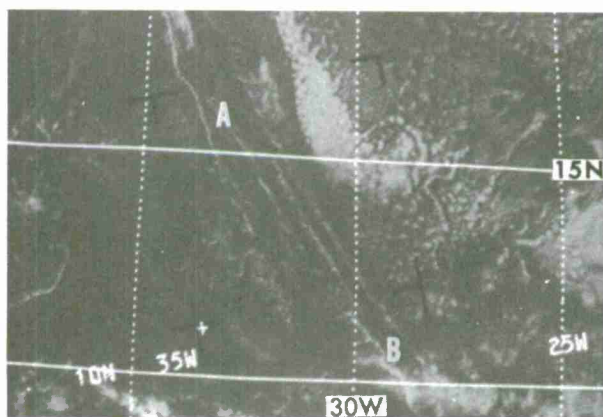
Figure 2-21. A series of cloud lines, one element wide, extends from A to B.



E-5 1790-7 1737Z 8 Sep 67

CLOUD STREET — A series of aligned cloud elements which are not connected. Usually streets form in a pattern of rows parallel to each other. They occur in a scale below the resolution of the 1968 APT camera system.
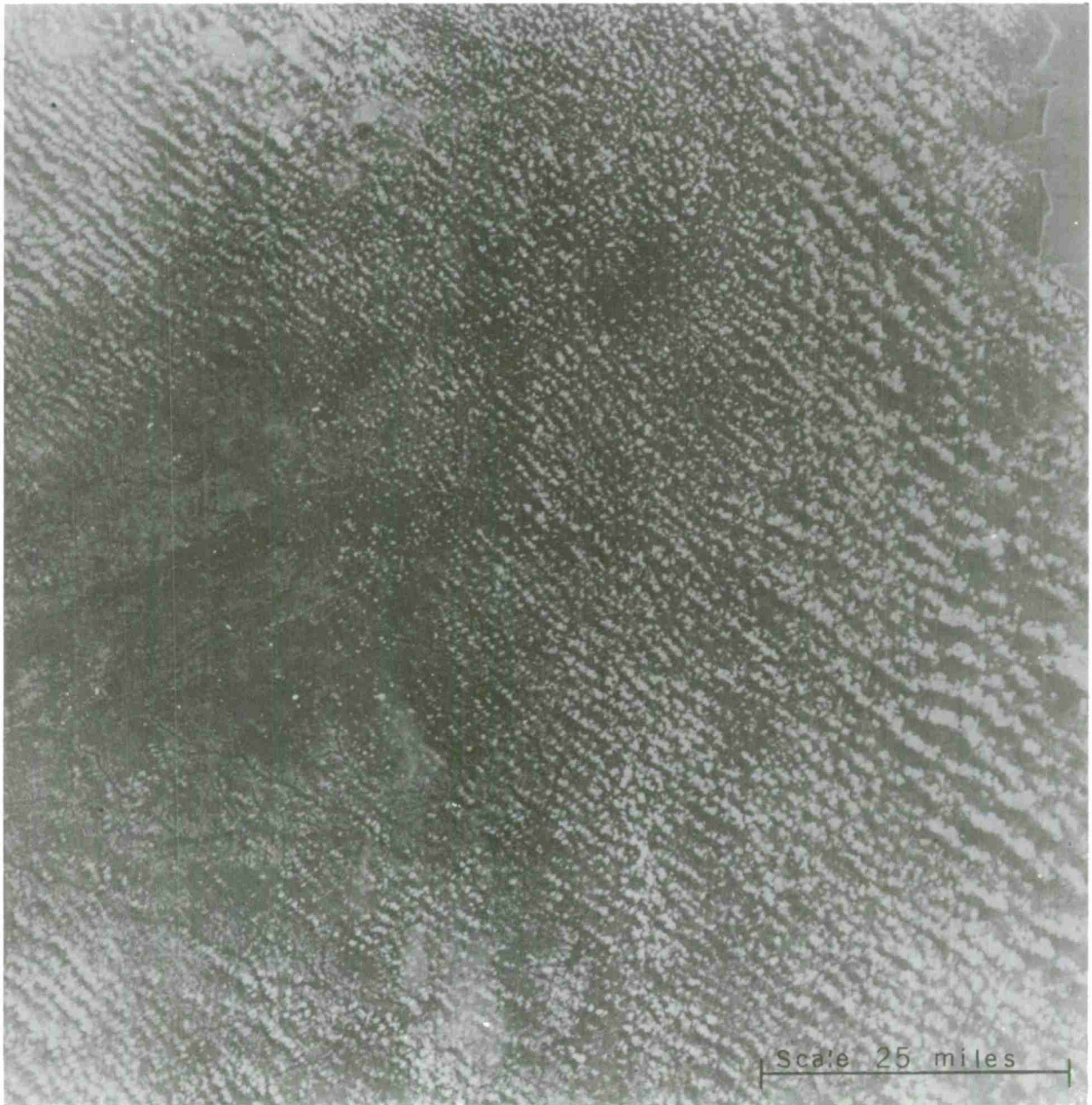


G-4 Orbit 45 Frame 39 7 Jun 65

Figure 2-22. Cloud streets over South Carolina and Georgia are seen from Gemini IV. The cumulus cloud elements form into nearly parallel rows.


COMMA CLOUD — See VORTICITY CENTER.

CUMULONIMBUS — A very white cloud with uniform top which often has a distinct sharp edge on one side and a cirrus plume emanating from the other side. Cumulonimbus may appear in satellite pictures as an isolated, nearly circular cell or as a large cirrus shield produced by a cluster of cumulonimbi. Shadows are usually present and are especially helpful in identifying cumulonimbus protruding through a stratiform cloud layer. Cumulonimbus without anvils appear as bright dots. Cloud Atlas codes L3, L9, apply.
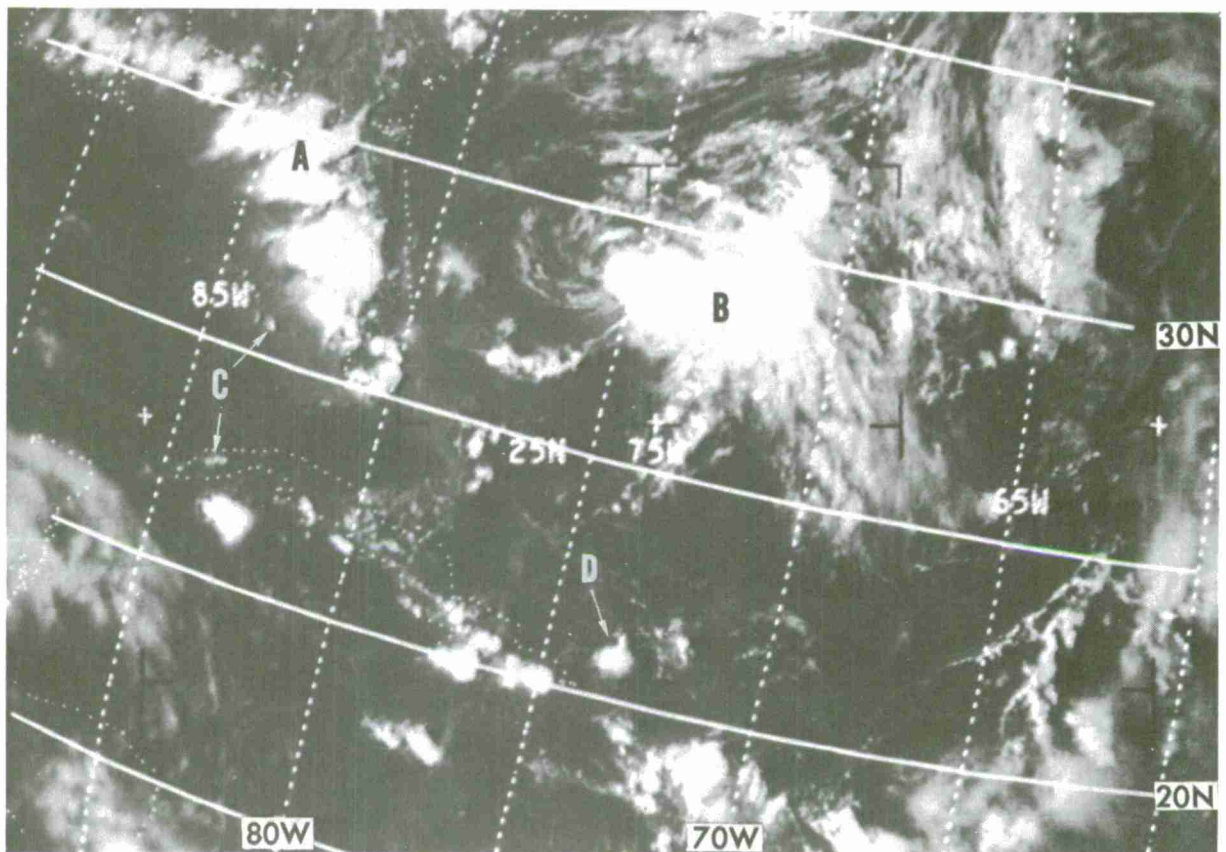


E-5 777-6 1948Z 20 Jun 67

Figure 2-23. Cumulonimbus clouds at A have a very white uniform top with plumes extending southwestward from the sharp edge to the east. A cluster of cumulonimbus clouds has produced a large cirrus shield at B, while the bright dots at points C are cumulonimbus without anvils. An isolated, nearly circular cumulonimbus cluster is at point D.

Figure 2-24. Shadows, in the
area around A, aid in identifying
several groups of cumulonimbus
clouds protruding through a lower
stratiform cloud layer.
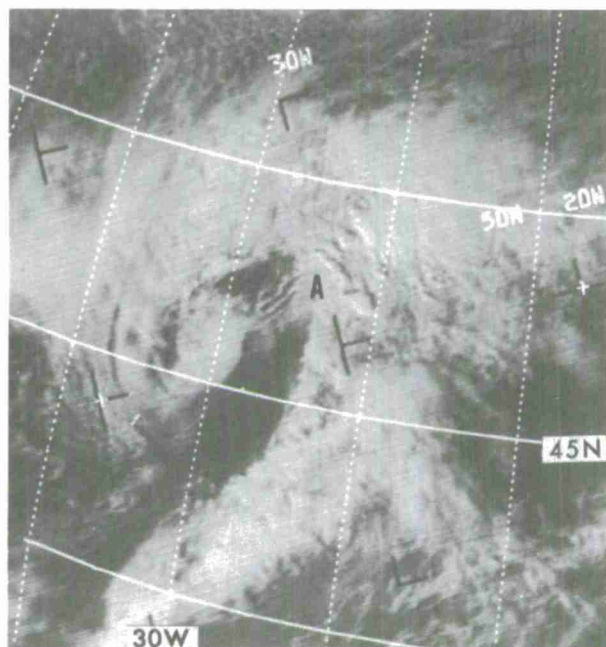


E-7 690-3 1514Z 10 Oct 68

Figure 2-25. Cumulonimbus clouds
associated with the ITC over Africa
cover the lower portion of the fig-
ure. Two nearly circular clusters of
cumulonimbus clouds can be seen at A.
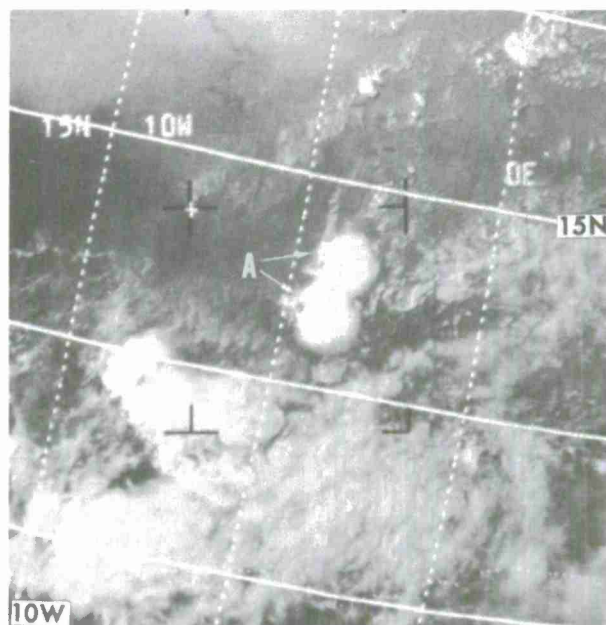


E-5 610-7 1534Z 7 Jun 67

CUMULUS, CUMULUS CONGESTUS — A field of these clouds has a lumpy, uneven texture and is frequently organized into lines, bands, or cellular patterns. The uneven texture is due to varying height, thickness, irregular shape, and shadow.  The smallest individual cumulus clouds, such as fair weather cumulus, are normally smaller than the resolution capability of the satellite camera system.  As the number and size of these small clouds increases over a given area, the contrast between the clouds and land or water increases.  Because of the distribution of small cumulus, terrain features, such as rivers, lakes, and hills, can be easily identified.  Cloud Atlas codes L1, L2 apply.
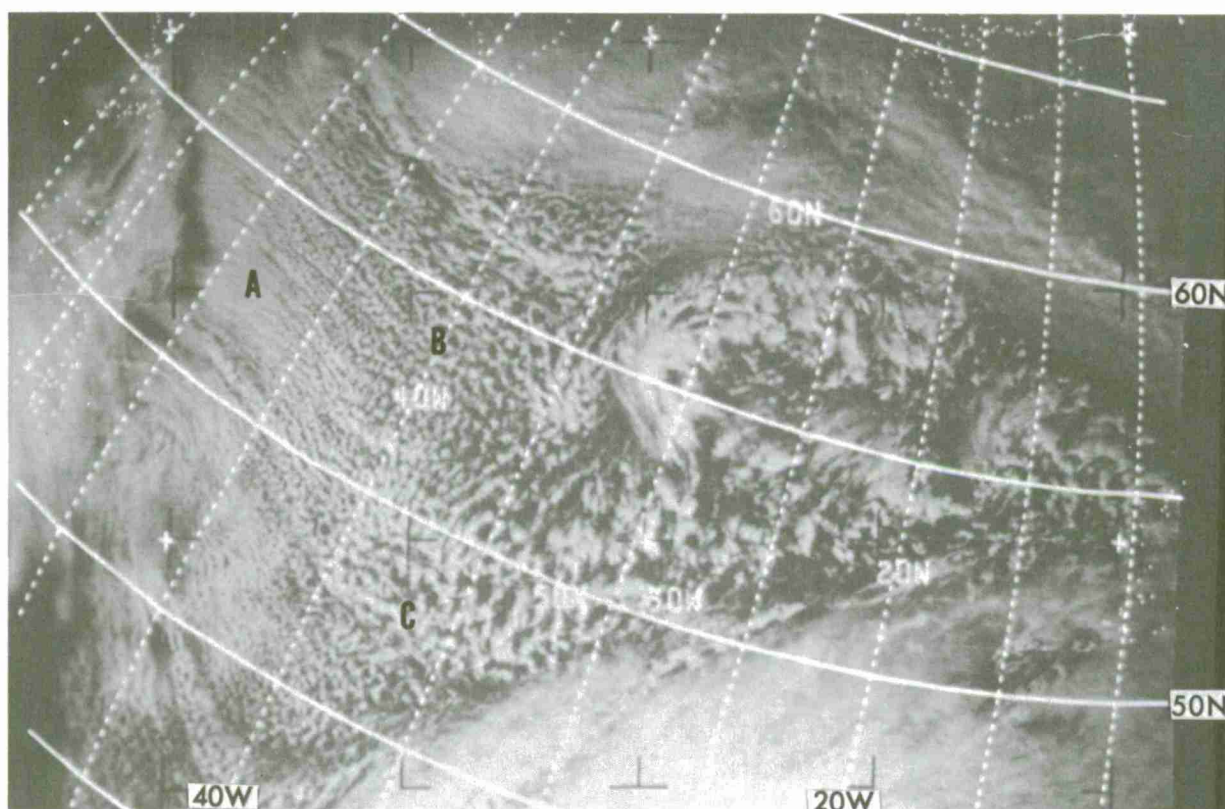


E-3 1785-2 1485-2 1458Z 21 Feb 67

Figure 2-26.  Cold air streaming off the continent gives rise to a large field of cumulus and cumulus congestus.  Cumulus, which are in lines at A, form into open cellular patterns at B, with cumulonimbus seen at C.  The texture of these cumulus are typically uneven due to variations in height and shape.
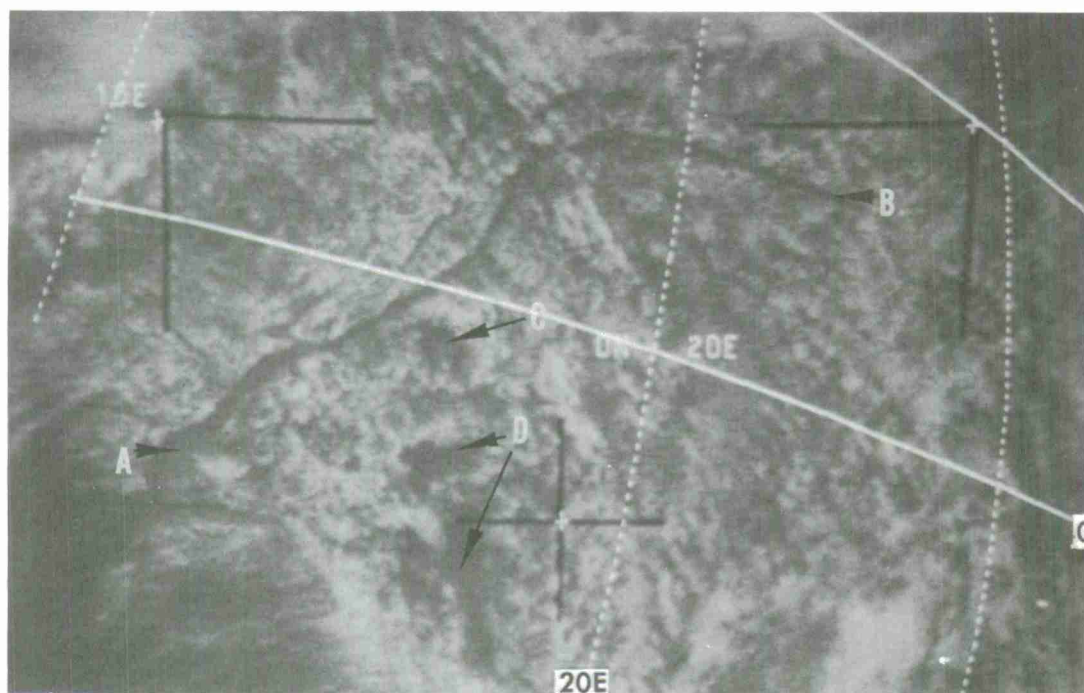
E-1 3145-12 1213Z 10 Sep 66

Figure 2-27.  Cumulus are seen over Africa.  The Congo River from A to B, Lake Tumba at C, and Lake Leopold II at D, are free of cumulus and are distinctly outlined.
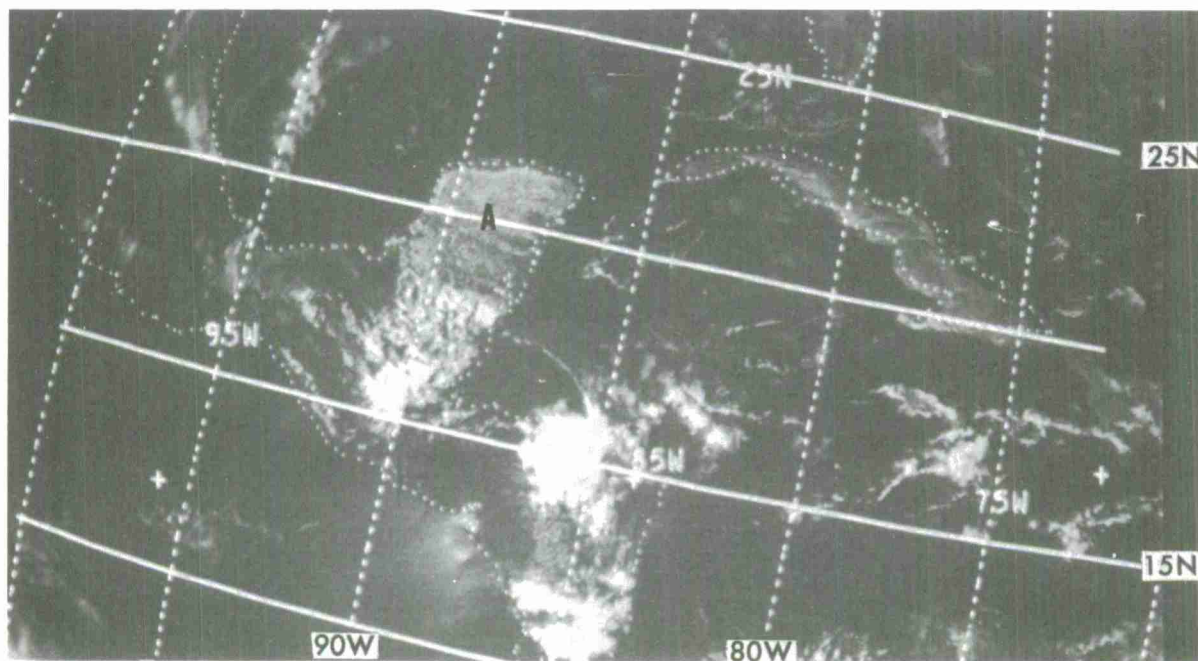


E-3 2026-5 1916Z 12 Mar 67

Figure 2-28.  Small cumulus at A cover the Yucatan Peninsula while the adjacent water body is virtually cloud-free.

DUST STORMS-SAND STORMS — An obscuration resulting from wind-driven parti-
cles of sand or dust which dims or obliterates surface features.  Dust storms
and sand storms are characterized by a dull, hazy, filmy appearance similar to
thin cirrostratus.  The sand and dust can extend over adjacent water bodies
obscuring the coastline.  The edges of sand and dust storm areas usually taper
off uniformly.
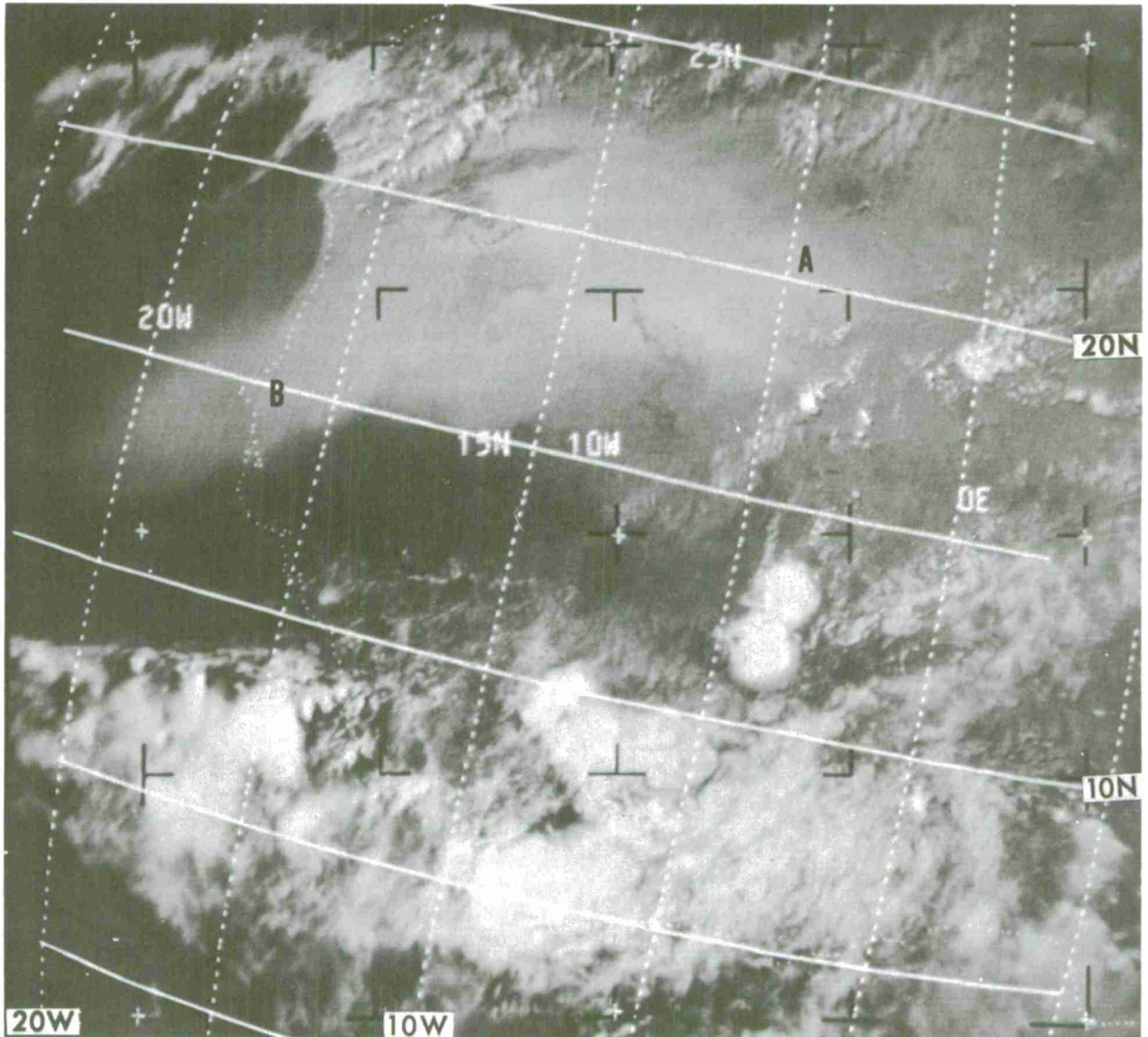


E-5 610-7 1534Z 7 Jun 67

Figure 2-29.  Widespread sand and dust obliterates much of the
terrain of northwestern Africa from A to B with a hazy, filmy ap-
pearance similar to thin cirrostratus.  This sand and dust extends
westward over the Atlantic partially obscuring the coastline at B.

EDDY — A spiral pattern in low clouds that forms beneath a strong subsidence inversion in the wake of steep-sided land barriers. The term eddy has also been applied to swirls of stratus and fog that are produced by shear in oceanic high pressure areas.
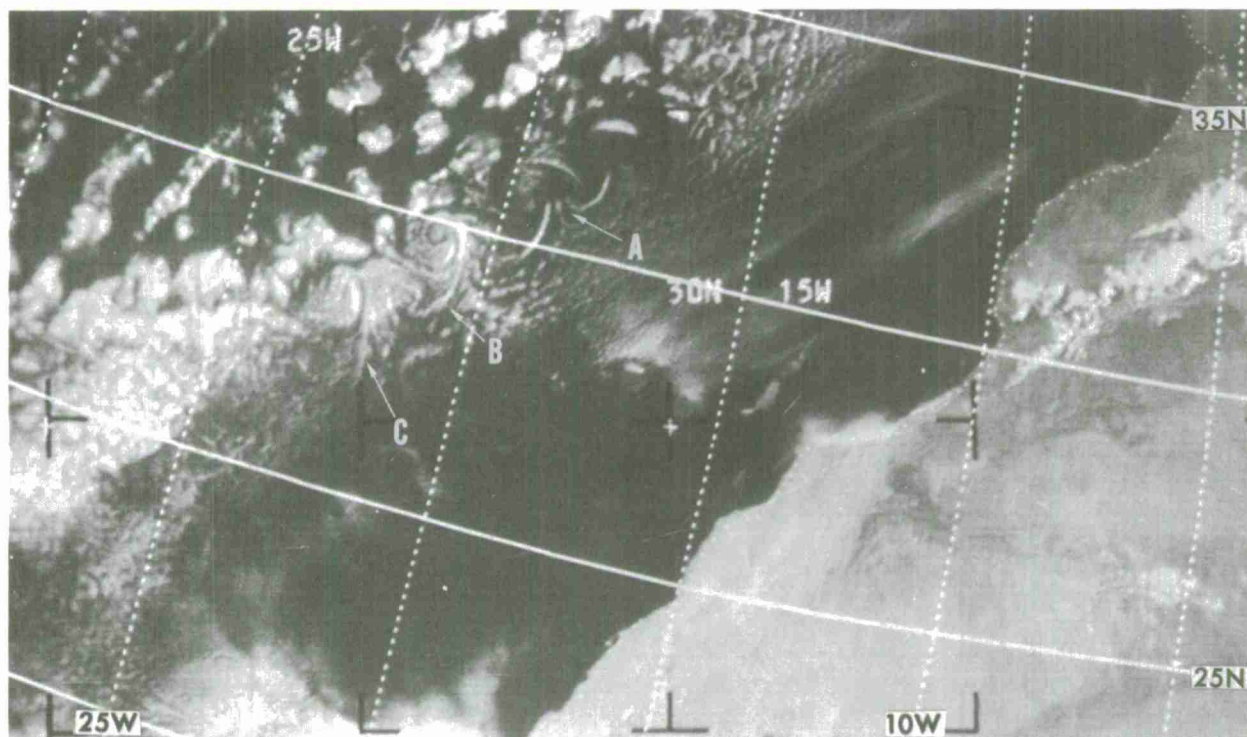


E-5 1206-6 1602Z 24 Jul 67

Figure 2-30. Eddies formed on the downwind side of the Madeira Islands at A, B, and C are under a strong subsidence inversion.

FOG and STRATUS — A flat, uniform-textured cloud, white or gray depending on density and sun angle. Boundaries are sharply defined and the shape of a fog or low stratus area often outlines topography, such as coastlines, mountains, valleys, etc. Cloud Atlas codes L6, L7 apply.
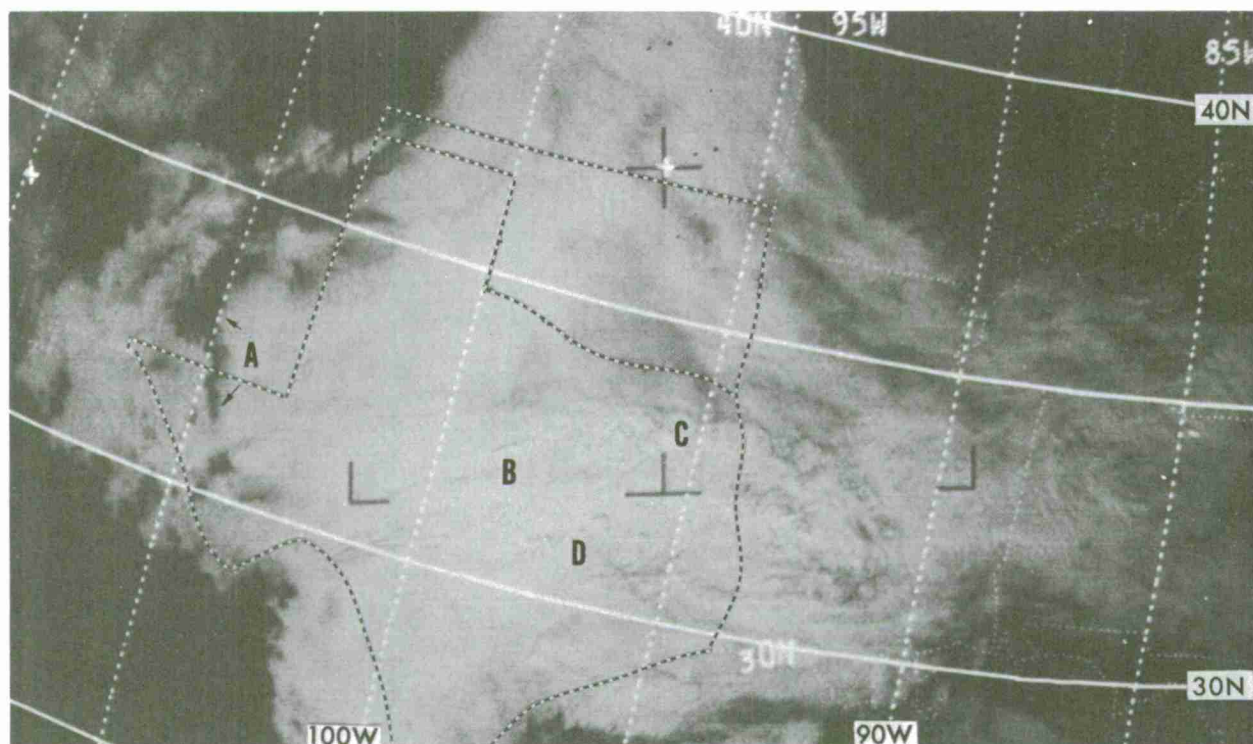


E-3 5304-3 1857Z 28 Nov 67

Figure 2-31. Many stations west of 95W report fog and stratus in the large cloud shield covering the southern plains and Gulf states. The main fog area is from eastern New Mexico to the Texas Panhandle. The western edge of the fog and stratus is sharply defined and, over New Mexico, outlines the topography of the Sacramento and Guadalupe Mountains, point A. The lumpy texture of the higher clouds and shadows cast by them at B, C, and D aid in identifying the lower clouds.

Figure 2-32.  Fog and stratus at
A, off the California coast, is char-
acterized by a flat uniform upper
surface and sharp well-defined edges.
Its eastern boundary generally con-
forms to the coastline.  A cellular
pattern of stratocumulus is seen at
C and D.  As the cell-size decreases
towards B, the stratocumulus becomes
similar in appearance and is indis-
tinguishable from the fog and stratus.
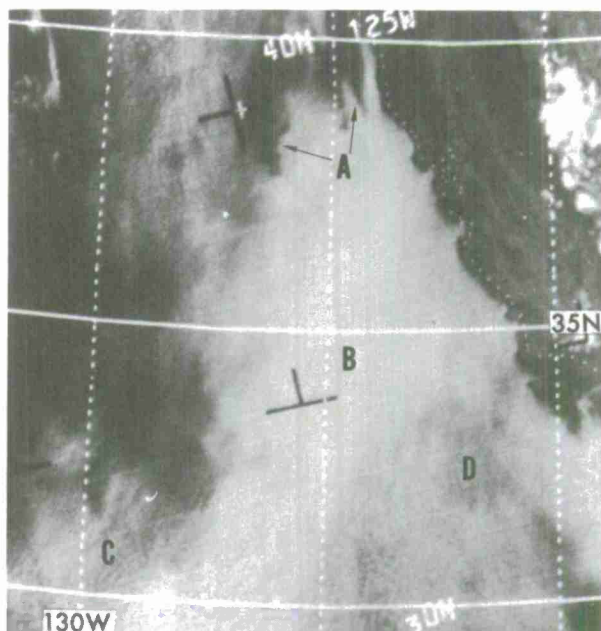


E-5 1476-5 2317Z 14 Aug 67

Figure 2-33.  Fog and stratus at
A outlines the San Joaquin Valley.
Thick radiation fog generally has a
uniform-textured upper surface.
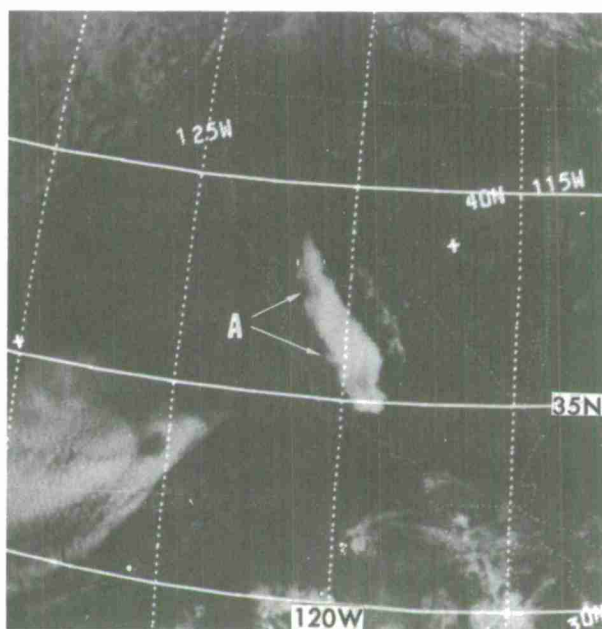


E-3 5267-3 2015Z 25 Nov 67
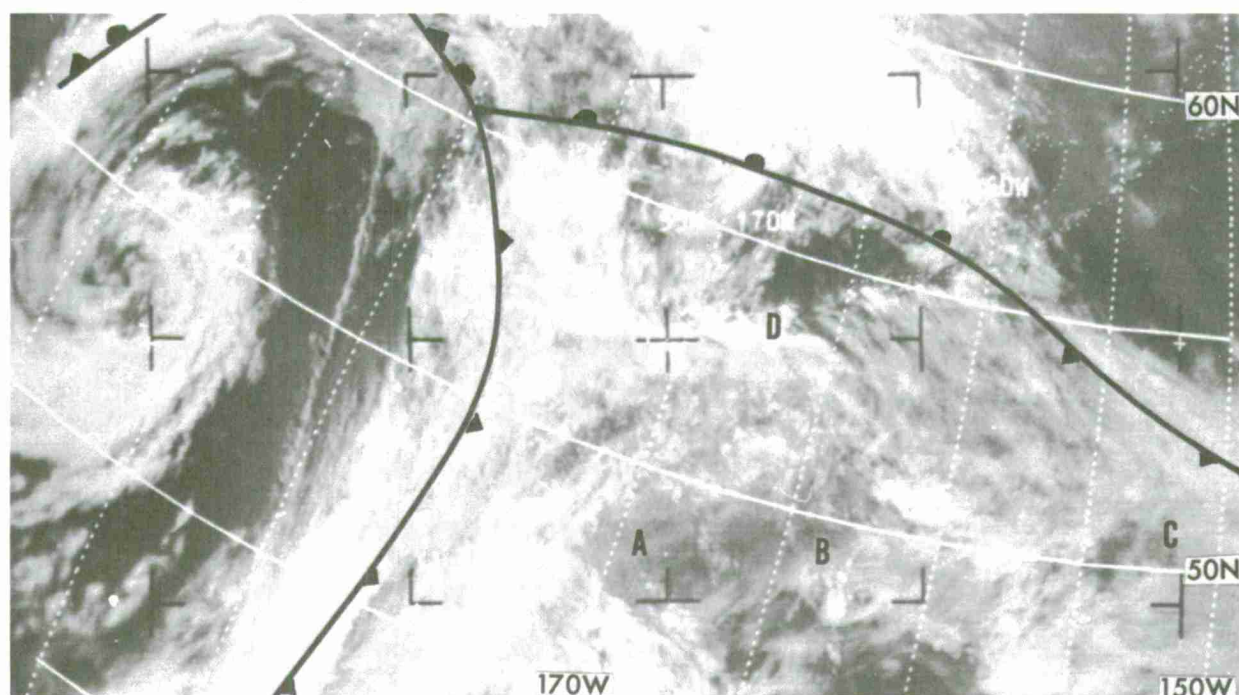
E-5 1173-4 0141Z 22 Jul 67

Figure 2-34.  Fog and stratus at A, B, and C, covering a portion of
the Pacific Ocean, is associated with warm air advection around a sub-
tropical high.  Variations in density or other cloud layers cause dif-
fering shades of gray throughout the fog and stratus area.  The moun-
tainous Aleutian Islands, D, cause the break in the fog in their lee.


ICE and SNOW — The bright appearance of ice and snow varies from very white
to gray depending on terrain, vegetation, age of snow and solar illumination.
Snow areas are smooth, except for dendritic patterns which outline mountains
and valleys, while clouds generally have a more textured appearance.

Figure 2-35.  Ice and snow-
covered lakes at A and B are very
smooth while the rugged snow-covered
terrain of the Canadian Rockies,
from C to D, displays a dendritic
pattern.
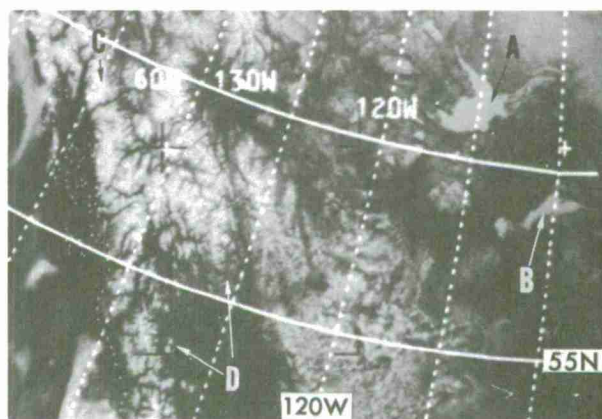


E-3 2680-3 2109Z 3 May 67

Figure 2-36. Shadows cast by
clouds at A, B, and C distinguish
them from the smooth ice and snow
covering most of Greenland.
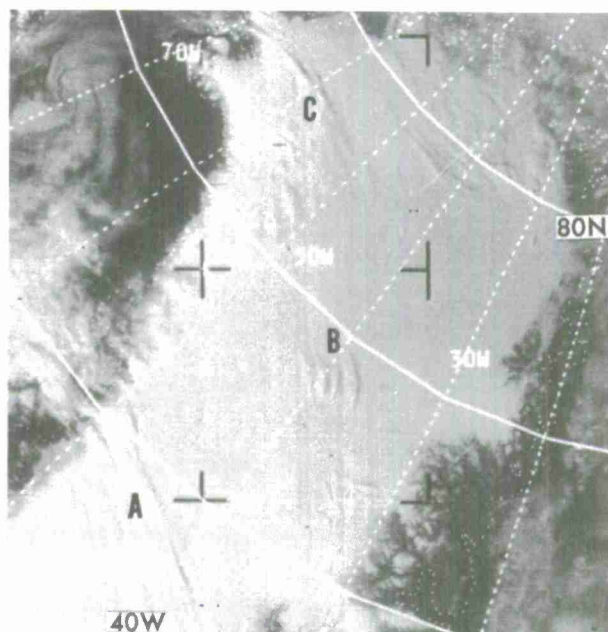


E-5 1510-2 1551Z 17 Aug 67

Figure 2-37. Snow, north of the
tree line extending from A to B, is
very white, while south of this line,
trees, vegetation, and frozen lakes,
cause the snow to appear mottled.
Evergreen tree-covered mountains at
C, D, and E are dark, while Lake
Winnipeg at F and Nipigon Lake at G
are bright. The surface of Hudson
Bay is white and smooth except for
sections of open water along the
coastline, which are black.
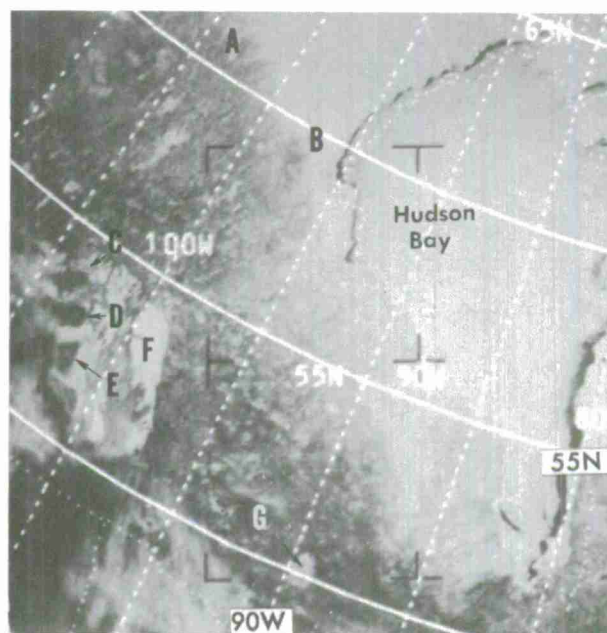


E-3 2553-3 1828Z 23 Apr 67

SHADOW — Cloud shadows appear as dark lines or blobs in, or adjacent to, bright cloud patterns. Shadows are seen most frequently on underlying clouds, snow, or ice; less often on land surfaces; and rarely over dark water surfaces. Shadows assist in estimating relative cloud height. A shadow, unless the sun angle is very low, indicates middle or high clouds, or cumulonimbi. Shadows cast with a low sun angle show detail of the vertical structure of clouds. The observed width of a shadow depends on the sun angle, the difference in cloud height, and the position of the satellite relative to the sun.
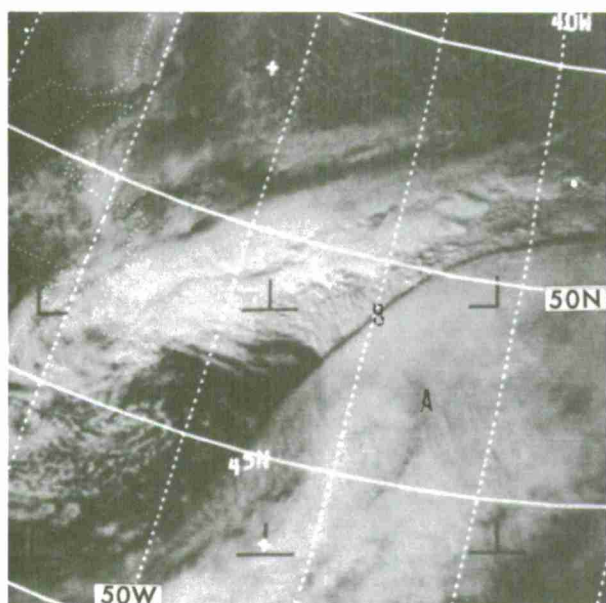


E-3 4850-2 1532Z 23 Oct 67

Figure 2-38. A large shield of cirrus at A is casting an exceptionally well-defined shadow at B on the middle clouds. Numerous shadows, resulting from a low sun angle, show considerable detail in the vertical structure of the middle clouds north of the cirrus shield.
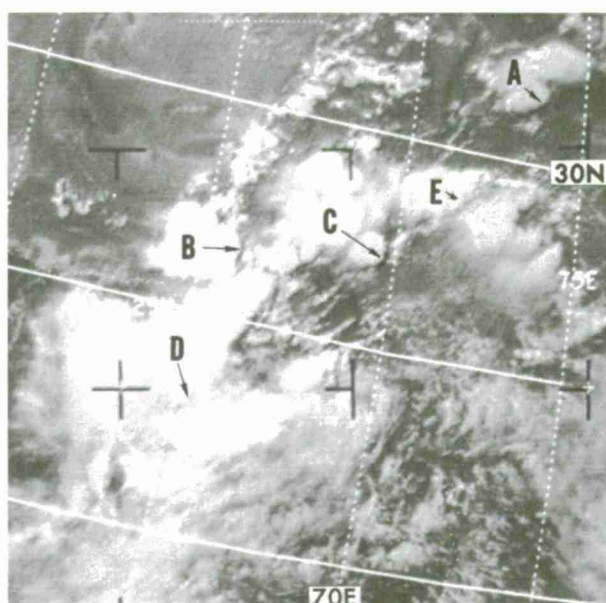


E-5 1292-6 1058Z 31 Jul 67

Figure 2-39. Clusters of cumulonimbus clouds are casting numerous shadows on both the land and underlying clouds. Some of these shadows on the land can be seen at A, B, and C while shadows on lower clouds are at D and E.

STRATOCUMULUS — Lumpy, globular clouds, generally grouped into an exten-
sive sheet or aligned in bands.  They are commonly seen in closed cellular
patterns with large numbers of relatively bright globular centers often con-
nected to each other with darker, less dense clouds.  As these cells decrease
in size, they become similar in appearance to stratus.  Cloud Atlas codes L4,
L5, and L8, apply.
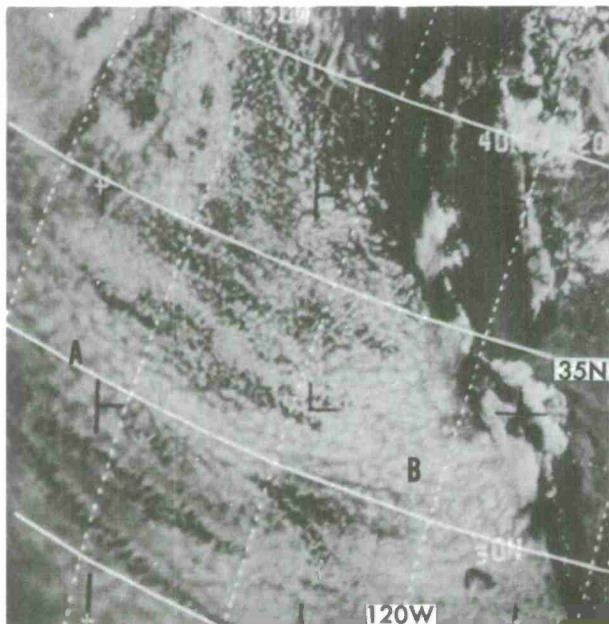
E-5 639-5 2236Z 9 Jun 67                    E-3 2026-8 1903Z 12 Mar 67

Figure 2-40.  An extensive sheet
of stratocumulus over the western Pa-
cific is primarily composed of closed
cells.  The bright globular centers
of the closed cells can be seen in a
band extending from A to B.

Figure 2-41.  Stratocumulus sheet
at A, off the west coast of South
America, is composed of small cells.
As these cells continue to decrease
in size, they take on a stratiform
appearance and it becomes difficult
to distinguish stratocumulus from
stratus near B.

STRIATIONS — Narrow, straight or curved streaks in clouds which appear in an overcast area.  A low sun angle causes highlights and shadows which produce the striated pattern.  Striations frequently give indications of the orientation of the thickness lines.

Figure 2-42.  Striations associated with an occluded front are readily seen from A to B.  The striations in this photograph are aligned parallel to the thickness lines from 1000 to 500 mb ahead of the front.
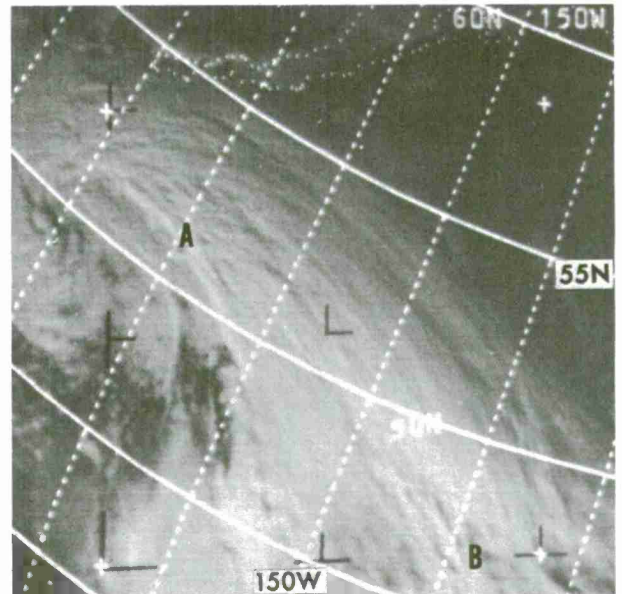


E-3 1048-1 2244Z 24 Dec 66

Figure 2-43.  Striations can be seen curving across an occluded frontal system between A and B.
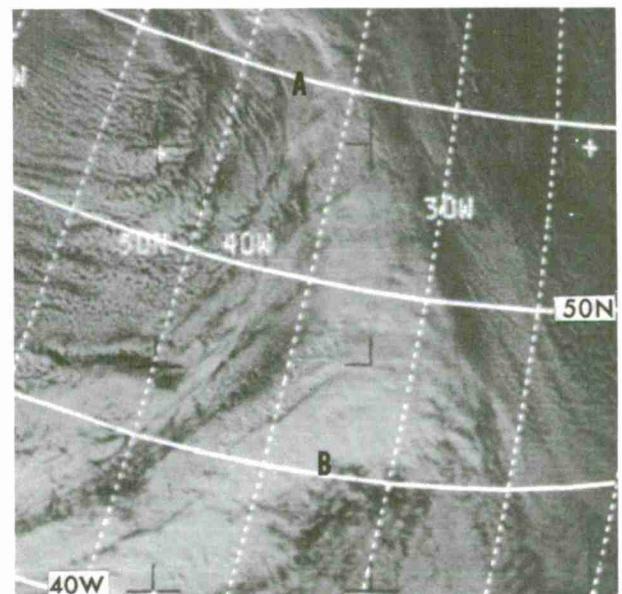


E-3 1371-2 1915Z 19 Jan 67

SUN GLINT — The image of the sun on water surfaces appearing as a bright area or spot. Variations in the size and brightness of a sun glint are dependent on the roughness of the water body on which it appears.
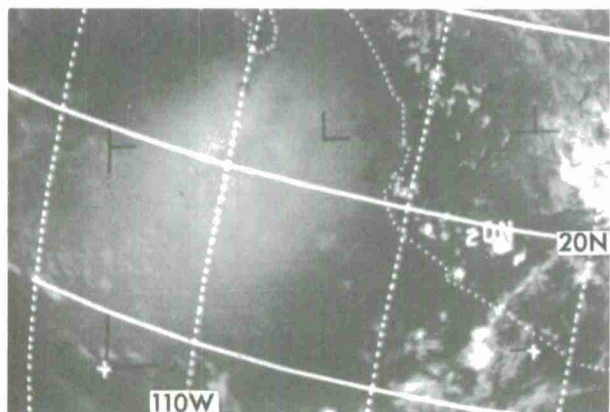


E-3 620-3 2045Z 20 Nov 66

Figure 2-44. A large diffused sun glint off the west coast of Mexico is centered near 20N and 110W.
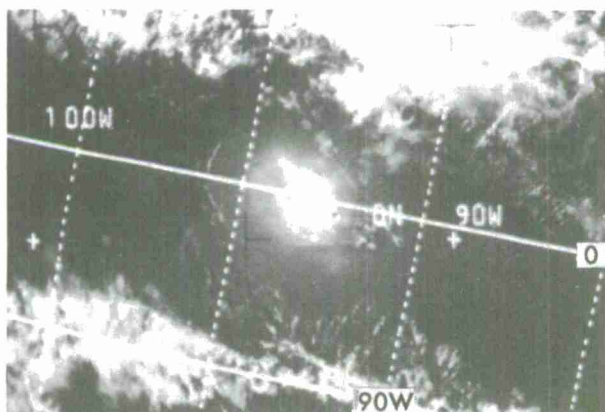


E-3 2064-6 1947Z 15 Mar 67

Figure 2-45. A small intense sun glint off the west coast of South America is centered at the equator and 93W.

Figure 2-46. Sun glint on the water surrounding Florida outlines the coastline in great detail. Tampa Bay is seen at A and Cape Kennedy at B. The very bright spots at C are from sun glint on the many lakes of central Florida, while sun glint on Lake Okeechobee is seen at D.
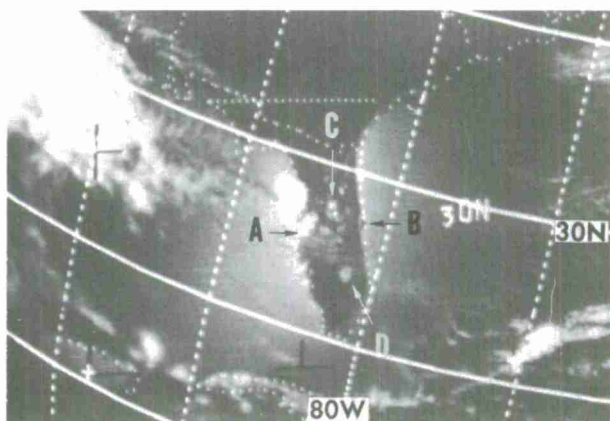


E-3 1586-3 1838Z 5 Feb 67

VORTEX — The cloud pattern which appears in satellite pictures as one or more bands spiraling toward a common center and which is associated with a vortex in the atmosphere. The term applies to both tropical and extratropical cloud systems. In the case of well-developed extratropical spiral patterns, one of the cloud bands is often associated with a front. Certain vortical cloud patterns, which identify areas of possible cyclonic development, have been given specific names. See VORTICITY CENTER.
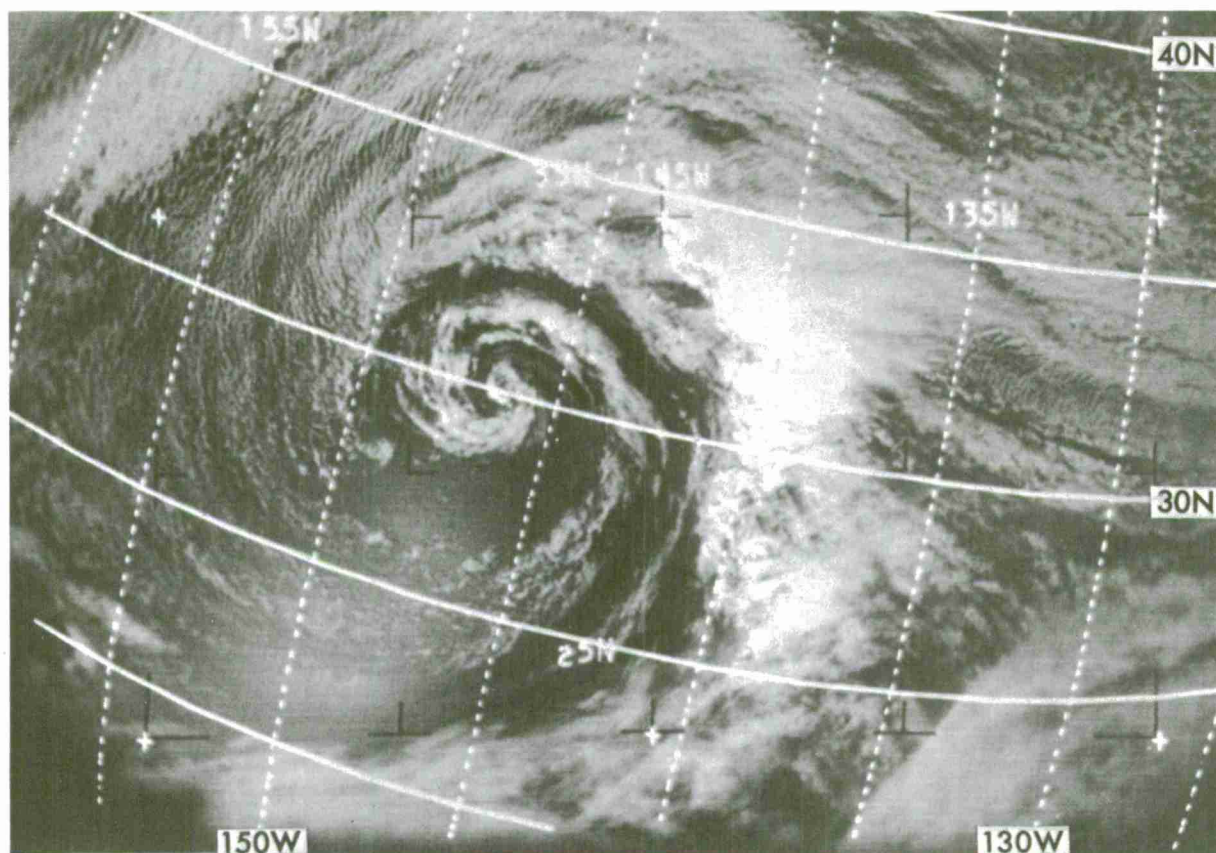


E-3 1199-3 2308Z 5 Jan 67

Figure 2-47. An extratropical vortex consisting of a number of bands, one of which is associated with a front, spirals toward a common center.
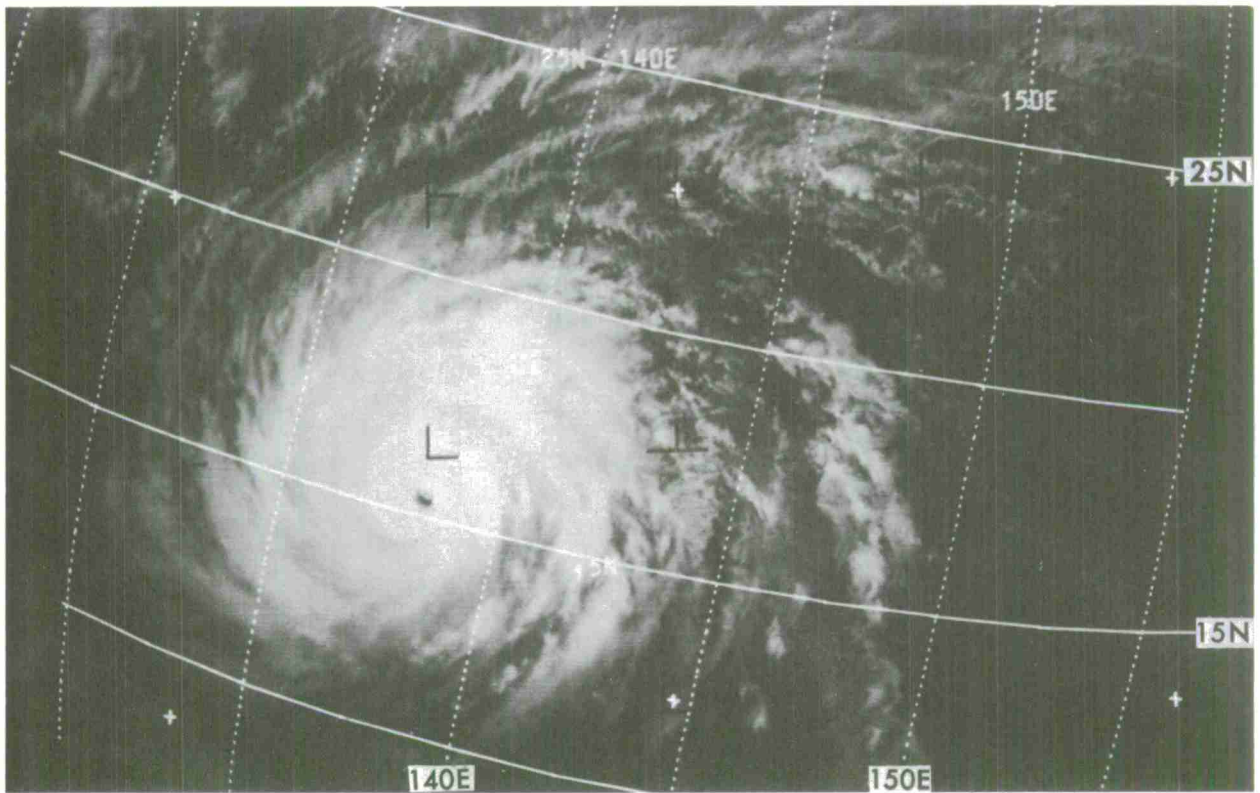
E-3 5120-4 0317Z 14 Nov 67

Figure 2-48. Typhoon GILDA over the Pacific shows a number of bands converging towards a common center.
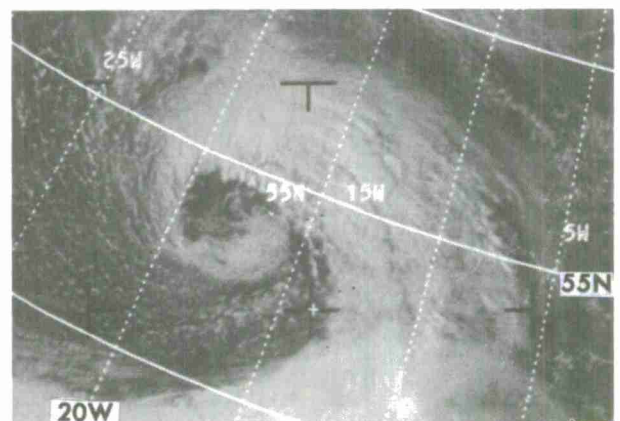


Figure 2-49. A vortex formed by a frontal band spirals into a center within a field of cumulus.

E-5 1738-4 1523Z 4 Sep 67

VORTICITY CENTER — Many cloud patterns in fields of cumulus clouds are as-
sociated with a maximum of cyclonic vorticity in the atmosphere.  These gener-
ally consist of curved cloud lines organized about a center.  When observed in
open-cellular cumulus, where cold air advection is occurring behind the polar
front, lines of cumulus generally curve spiral-like toward a common center.
In the cumulus fields beneath a deep quasi-stationary polar low, or beneath a
cut-off low in the subtropics, the lines of cumulus tend to be concentric, but
still suggest a common center.  Secondary centers of vorticity rotating around
the main center are commonly seen as areas of enhanced cumulus.

A moving vorticity center to the rear of a polar front produces a cloud
mass or grouping of cloud elements ahead of the center that assume the charac-
teristic shape of a comma.  In the polar westerlies, these comma-shaped forma-
tions are often observed in the areas of strongest mid-tropospheric positive
vorticity advection (PVA maximum).  A PVA maximum in a cumulus field will
initially lack the comma shape and appear as a small area of brighter, more
active, but as yet, unorganized convection.  As the cloud system develops,
middle and higher clouds are produced and the formation takes on its comma
shape.  A clear zone is often seen ahead of a well-developed comma cloud.

Vorticity centers also occur in the tropics and produce distinctive cloud
patterns that will be discussed in Chapter 4.

Figure 2-50.  Cumulus lines, in
open-cellular cumulus curving towards
a common center, are associated with a
maximum of cyclonic vorticity.
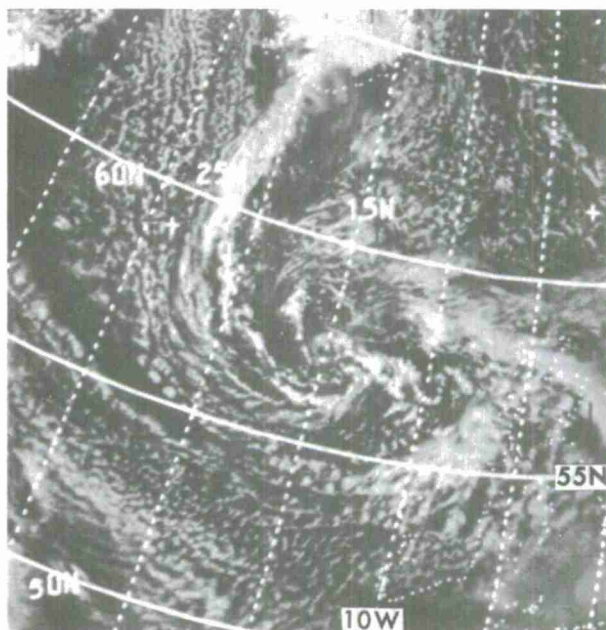


E-3 2513-3 1403Z 20 Apr 67

Figure 2-51.  A well-developed
comma-shaped cloud is the result of a
moving vorticity center to the rear
of a polar front.  The comma cloud is
composed of middle and high clouds
over the lower-level cumulus and is
preceded by a clear slot.
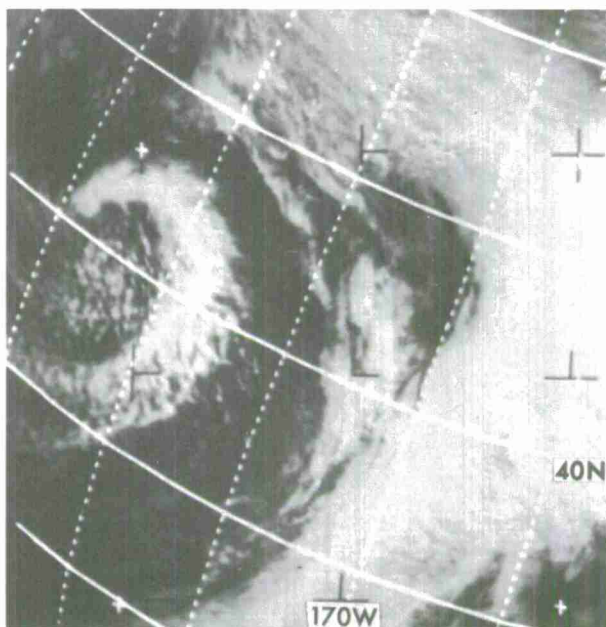


E-3 1815-2 0016Z 24 Feb 67

Figure 2-52. Brighter, more ac-
tive cumulus at A identifies a region
of positive vorticity advection in a
field of open-cellular cumulus. The
clearing in advance of the enhanced
cumulus is typical of sinking motion
ahead of positive vorticity advec-
tion areas.
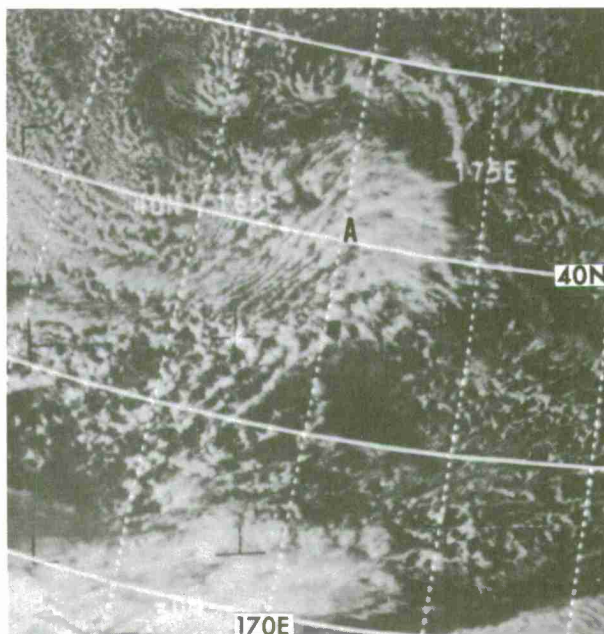


E-3 1590-3 0216Z 6 Feb 67

Figure 2-53. A vorticity center
is indicated in the clouds near A.
Enhanced cloudiness at points B is
the result of positive vorticity ad-
vection on the forward side of the
vorticity center.
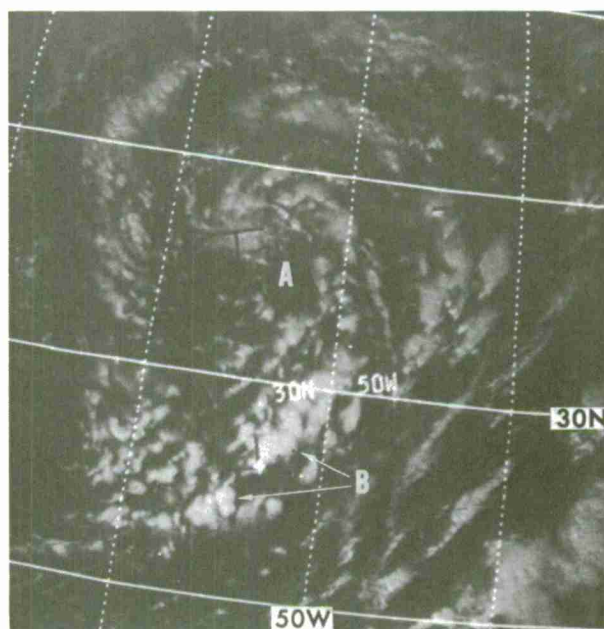


E-3 5403-3 1604Z 6 Dec 67

WAVE CLOUDS - Wave clouds caused by terrain barriers appear as a pattern of vermiculated bands that range from a few miles up to 20 miles in width. The bands are separated by clear spaces of the same size. The appearance of wave clouds may vary depending on the shape of the barrier. These patterns usually consist of stratocumulus and altocumulus.

These criteria must be met for formation of mountain wave clouds: (1) Wind direction is more or less perpendicular to the mountains through a deep layer of the atmosphere, (2) winds at the top of the mountain are at least 25 knots, (3) winds increase steadily with height to about 300-mb., (4) the atmosphere is stable for vertical displacement of air parcels and, (5) sufficient moisture for cloud formation is present.
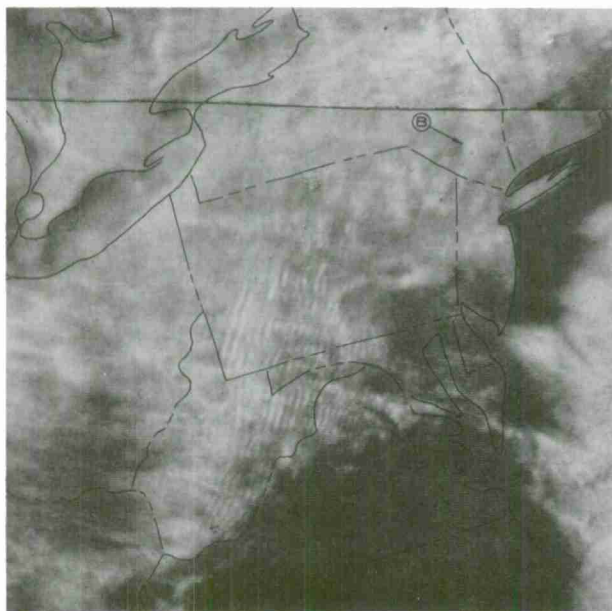


E-8 752-    1455 GMT February 13, 1967

Figure 2-54. Wave clouds associated with the Appalachian Mountains extend southward from central Pennsylvania into North Carolina. This pattern lies under the jet stream. A second area with waves of shorter length (B) lies just east of the Catskill Mountains. The cloud type forming the waves is predominately stratocumulus.



IR ITOS-1 0800 GMT December 20, 1970

Figure 2-55. Wave clouds (A) produced by the Appalachian Mountains are over eastern Pennsylvania. These wave clouds are at a relatively low level and show a small thermal contrast with the surrounding earth's surface. The cloud-free portion of Lake Huron appears dark in the upper left-hand corner of the picture; the warmer waters of the Atlantic appear dark on the eastern side of the picture.

Chapter 3

SYNOPTIC CLOUD PATTERNS

---

SECTION A

VORTICITY AND VORTICES

Introduction

Cyclonic disturbances in the atmosphere produce cloud patterns which are
easily recognized in satellite pictures.  By properly identifying these pat-
terns, analysts can locate significant centers of low pressure and centers of
vorticity as well as diagnose the stage of storm development.

The sequence of cloud patterns associated with the life cycle of a vortex
depends on the way in which a storm develops.  Several different modes of
storm development are observed at mid and high latitudes.  Some disturbances
develop entirely within the cold air and form a separate cloud system behind a
major frontal band; others form along the frontal band itself.  The latter
type exemplifies classical frontal wave development which culminates in an
occluded storm.  Some cut-off lows may be associated with a major frontal
cloud band in their initial stages, while others form ahead and equatorward of
the major frontal band.

The cloud pattern observed at a given stage of storm development depends
on the dynamical processes which are contributing most at that particular time
to cloud production and organization.  The widespread cloud patterns produced
by cyclonic disturbances represent the combined effect of active condensation
from upward vertical motion and horizontal advection of cloud.  Storm dynamics
restrict the production of cloud to those areas within a storm where extensive
upward vertical motion or active convection is taking place.  For disturbances
in their early stages, the limits of the vertical motion distribution are the
most important factor controlling cloud distribution.  The comma-shaped cloud
formation which precedes an upper tropospheric vorticity maximum is an example.
Here, the clouds are closely related to the upward motion produced by positive
vorticity advection (PVA).  The pattern of vertical motion also plays an im-
portant role in determining cloud distribution for deepening frontal storms.
Here, vertical motions caused by thermal advection strongly influence the
cloud pattern.  As disturbances mature, cloud advection becomes increasingly

important in shaping the pattern.  It plays an important role in producing the
well-developed spiral band that accompanies a deep slow-moving or stationary
vortex.  The effects of vertical motion and horizontal advection combine to
produce a similarity of patterns [19] [20].

## Vorticity

The cloud patterns associated with upper tropospheric vorticity are gener-
ally restricted to areas where convective cloud is present.  Thus, they are
most commonly observed over the oceans in the fields of open cellular cumulus
behind cold fronts.  There are two significant patterns: enhanced cumulus and
the comma-shaped cloud.  Both are caused by increased convection due to gener-
al lifting in the areas of maximum positive vorticity advection.  Cloud pat-
terns associated with upper tropospheric vorticity are called vorticity cen-
ters [1].

Enhanced Cumulus.  This is an area, 3 to 5 degrees across, of brighter
cumulus clusters lying within a larger field of cellular cumulus.  A vorticity
maximum and associated 500-mb trough are located along the upwind edge of the
area.  Often the cumulus organization suggests a spiral pattern.  (This form
of the pattern is also called a maximum vorticity center formation.)  Middle
or high cloudiness is either absent or forms a small part of the cloud cover
within an area of enhanced cumulus.  Figure 3-A-1 shows an example.

Comma-Shaped Cloud Patterns.  The comma-shaped cloud formation (also
called PVA MAX formation) is more easily recognized than the enhanced cumulus
pattern.  It is a bright, layer-type cloud mass formed from tops of cumulonim-
bus.  A zone of clear skies is often present on the downwind side.  The typi-
cal relationship of a comma-shaped cloud to the vorticity maximum and trough
line at 500 mb is shown in Figure 3-A-2.  There is usually a surface low pres-
sure center associated with a fully-developed comma-shaped cloud.

## Vortex Development in the Cold Air

Vortices which develop within the cold air behind a major cloud band first
appear as an area of enhanced cumulus.  Not all such areas necessarily con-
tinue to develop.  The comma-shape cloud indicates a developing stage.  As
these storms reach maturity, they develop a regular spiral vortex pattern
with a long, narrow cloud band similar in appearance to a frontal band.  The
north-south dimensions of these storms rarely exceed 15 degrees of latitude.
During its life cycle, the entire cloud system remains poleward and separate
from the major cloud band of the polar front.

Figure 3-A-1. An area of en-
hanced cumulus (PVA MAX) appears
near 45N, 145W. Note the 500-mb
trough from the center of the low
to A. The enhanced area has a more
congested look and a brighter ap-
pearance.
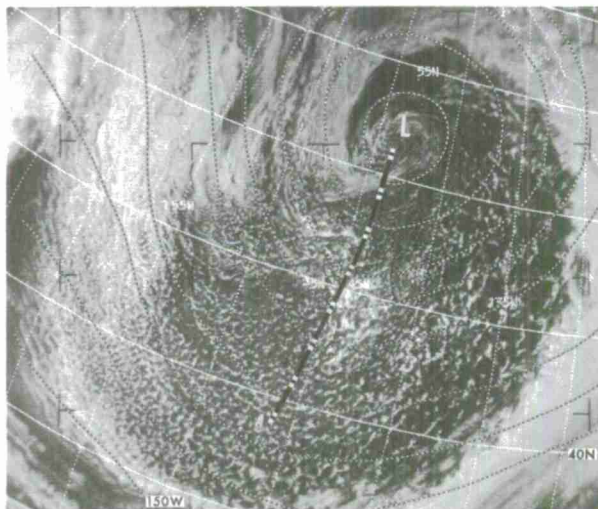


E-9 457-4,5 2319Z 3 Apr 69
500-mb Analysis 0000Z 4 Apr 69

Figure 3-A-2. The relationship
of the comma-shaped cloud to the
500-mb flow is shown in this pic-
ture. The black dot indicates the
position of the 500-mb vorticity
center. Note the clear area in ad-
vance of the comma-shaped cloud. A
portion of the major frontal cloud
band appears in the upper right-
hand corner. The comma-shaped
cloud is in the cold air region be-
hind this front. Trough at 500 mb
is shown extending from A to B.
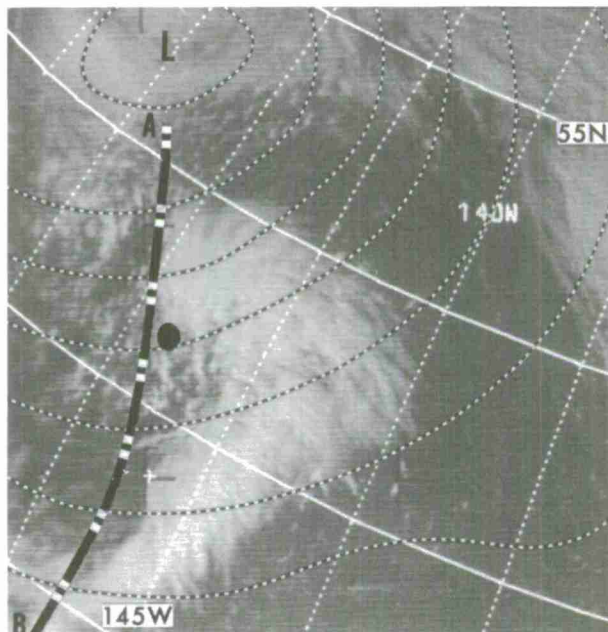


E-7 1007-2 2248Z 4 Nov 68
500-mb Analysis 0000Z 5 Nov 68

## Vortex Development Along a Frontal Band

   Wave Stage.  The frontal wave is the first of four stages in vortex de-
velopment which occurs along a baroclinic frontal zone.  The wave appears with
the approach of an upper level vorticity maximum on the cold side of the front.
The presence of vorticity advection is indicated by the enhanced cumulus or a
comma-shaped cloud.  If such a pattern moves to within 5 to 9 degrees of a
frontal system, wave development may be expected.  As a vorticity-associated
cloud pattern approaches the frontal band, the front broadens and forms a con-
vex bulge towards the cold air.  Surface wave development may be directly
associated with this bulge.  The surface position of the wave is under the
bulge near the position where the curvature of the rear edge of the frontal
band changes from concave to convex.  The clouds over the low along the front
show no evidence of a vortex pattern during the wave stage.
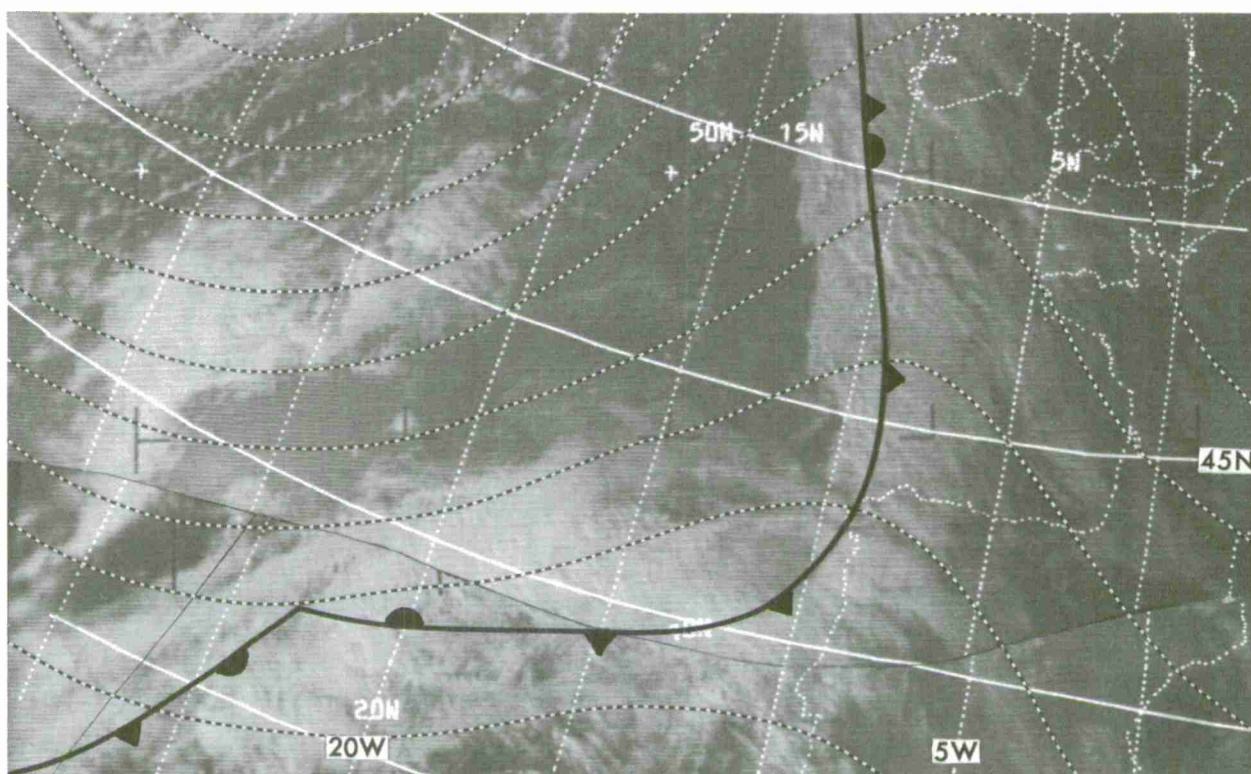


E-7 1003-2,3 1506Z 4 Nov 68   500-mb and Surface Analyses 1200Z 4 Nov 68

   Figure 3-A-3.  The indications of wave formation appear along front
near 37N, 25W.  Vorticity, as evidenced by the cloud formation at about
43N, 30W is approaching the frontal band causing it to widen and bulge
backward into the cold air.  Notice the clear area between the front and
the comma-shaped cloud.

As the wave develops, but before occlusion, the curvature of the bulge be-
comes more pronounced; the back edge of the high clouds near the surface wave
becomes more concave; and an area of lower, less solid cloud cover appears
along the back edge of the wave.  This change in the clouds is a prelude to
the initial appearance of a dry slot between the vortex and the frontal band.
The rapid deepening of the circulation along the front begins at about this
time.
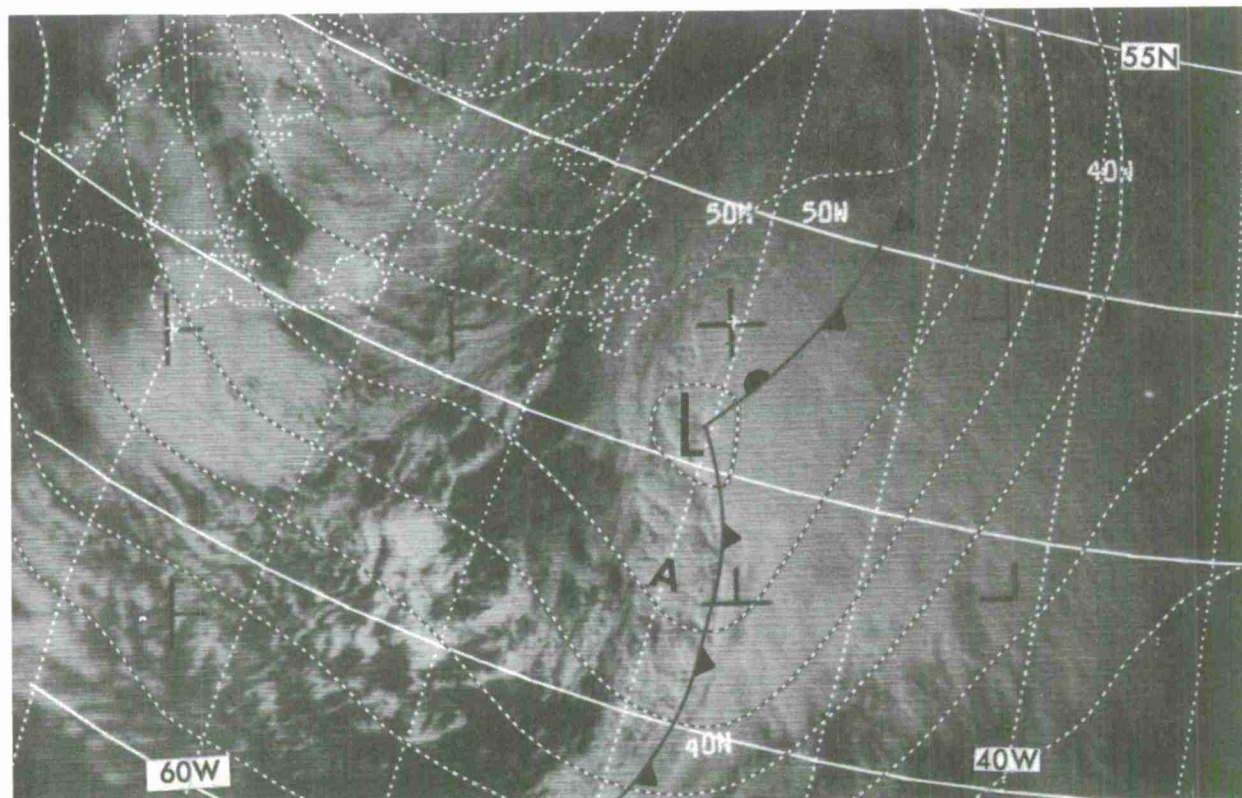


E-7 904-3 1723Z 27 Oct 68   Surface Analysis 1800Z 27 Oct 68

Figure 3-A-4.  Several cloud changes appear in the wave as it de-
velops.  High clouds which formerly covered the frontal cloudiness ap-
pear inward from the back edge and leave the lower cloudiness visible
at A.

   Occluding Stage.  In the occluding stage, the clouds begin to take on a
definite spiral pattern.  A definite dry slot begins to form behind the front.
The occluding frontal band curves into the vortex center along with the non-
frontal cumuliform cloud-lines in the cold air to form the vortex.
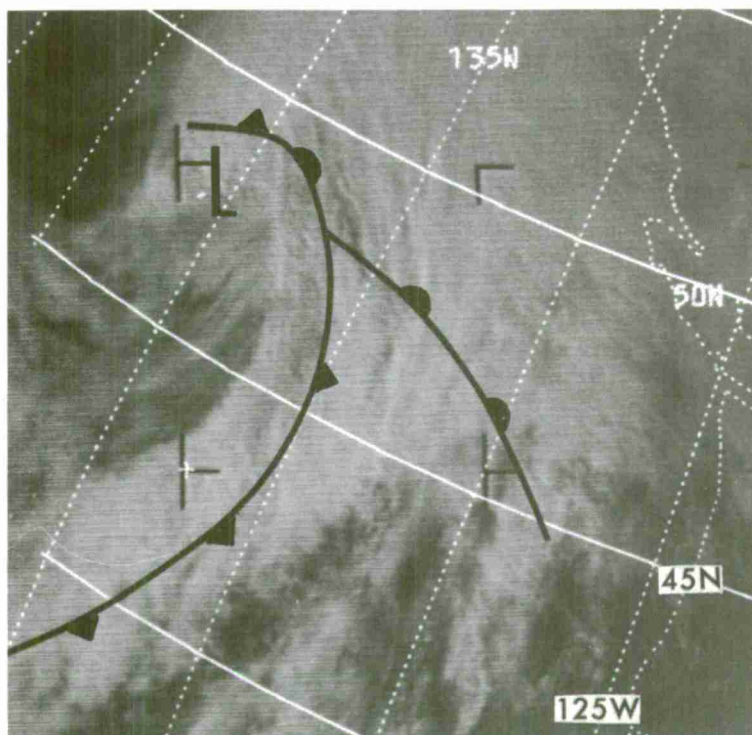


E-7 894-3 2213Z 26 Oct 68
Surface Analysis 0000Z 27 Oct 68


        Figure 3-A-5.  A frontal system is
     shown in an early stage of occlusion.
     The spiral pattern of the vortex is not
     as obvious as in many cases.  The appear-
     ance of the cloud pattern suggests the
     beginning stage of formation of the dry
     slot.

Mature Stage.  At this stage, the cyclonic development of the cloud pat-
tern has reached its peak of organization with the "dry slot" having intruded
all the way to the center of the vortex.  The movement of the dry air towards
the center of the vortex suggests a cut-off of the moisture available to the
cyclone and implies that the system is reaching its next stage of development.
At the mature stage, the vortex center and the surface and mid-tropospheric
pressure centers are in the closest coincidence due to minimum tilt of the
pressure centers with height.
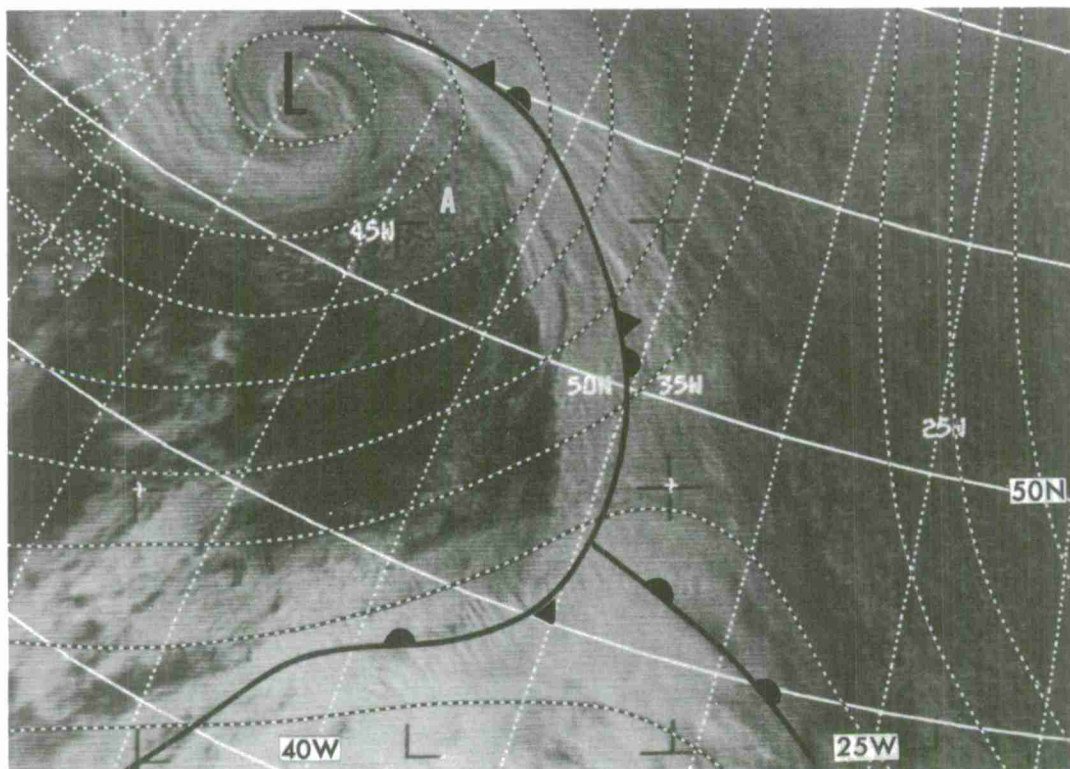


E-7 966-2 1613Z 1 Nov 68  500-mb and Surface Analyses 1800Z 1 Nov 68

Figure 3-A-6.  A vortex with an occluded front in the mature
stage shows the obvious spiral pattern of the vortex and the dry slot
at A.  Note the nearness of the cold-core 500-mb low to the vortex
position.

Dissipating Stage.  In the dissipating stage, the vortex bands become
fragmented with cloud-free areas appearing between the bands.  The clouds
forming the bands are middle and/or low-level cumuliform and stratiform.  This
cloud pattern is usually associated with a cold-core low pressure center and a
well-developed, but dissipating, surface low.  The frontal band is separated
from the vortex center and the area surrounding the vortex center is usually
cloud-free except for convective clouds due to heating from below.
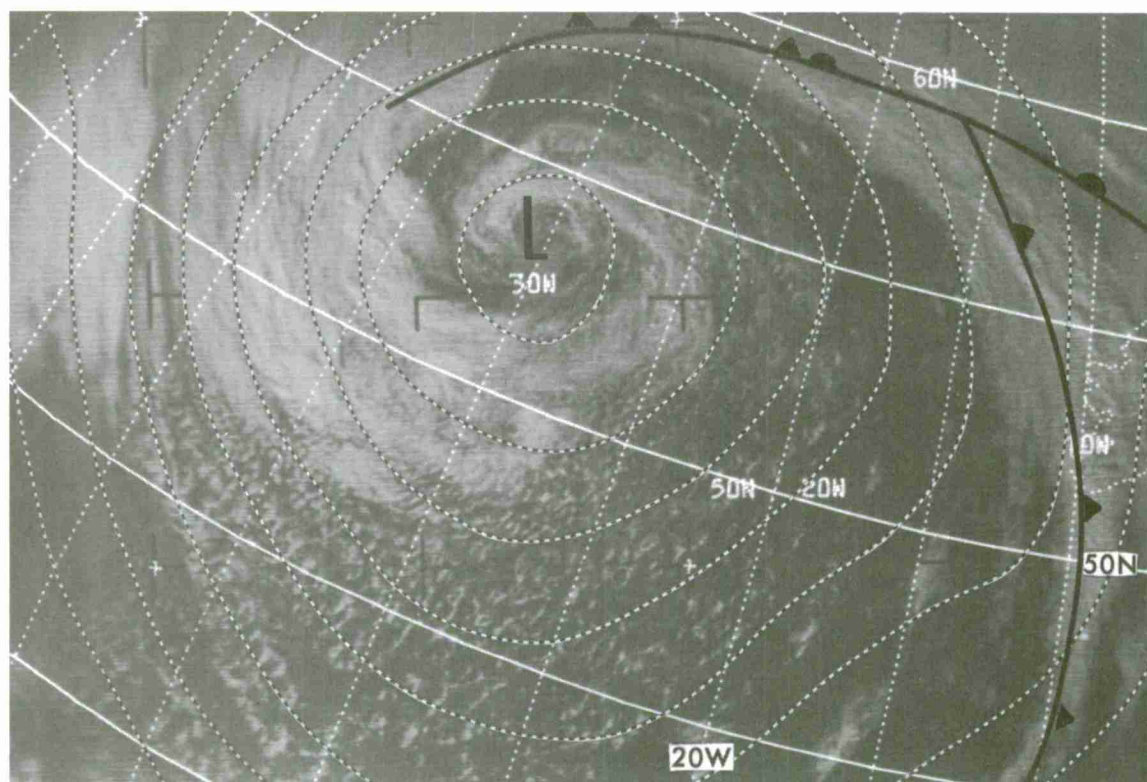


E-7 615-3 1529Z 4 Oct 68   500-mb and Surface Analyses 1200Z 4 Oct 68

Figure 3-A-7.  A vortex is seen in the dissipating stage.  The low is
fully closed.

Dissipating low pressure centers produce poorly-organized spiral patterns. They are composed predominantly of cumuliform, spiral cloud bands which are fragmented. Some cirriform clouds are likely to be present. These cloud patterns are no longer associated with frontal systems.
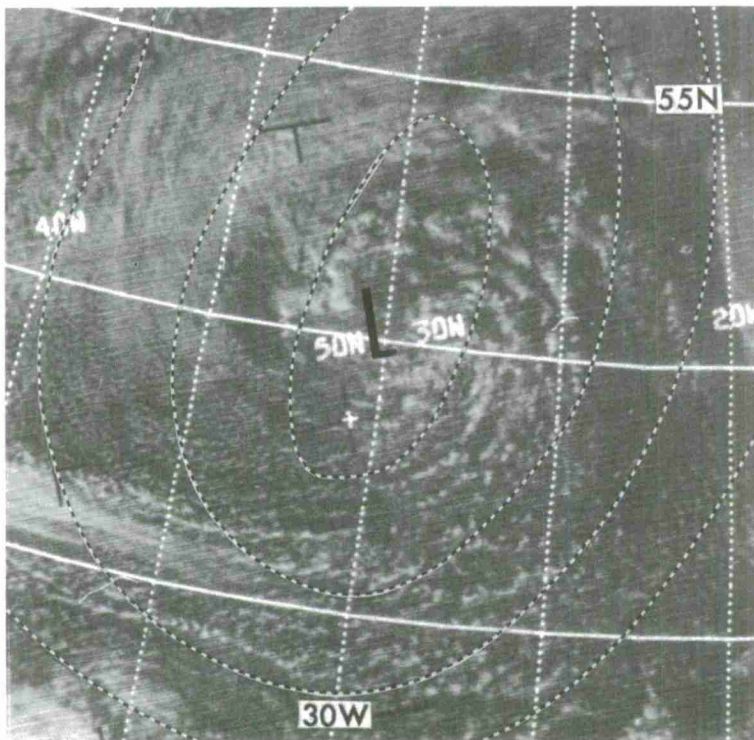


E-7 1016-2 1603Z 5 Nov 68
500-mb Analysis 1200Z 5 Nov 68

Figure 3-A-8. An example of a low in
the final stages of decay can be seen.
The weak spiral pattern in the cumulus
cloud field shows a circulation center
near 50N, 30W. The unstable air is deep-
est near the center of the low where
there is more convection and the cumulus
has an enhanced appearance.

## Cut-Off Lows

Well-developed cut-off lows produce spiral vortex patterns that appear much the same as those produced by the occlusion process. Low latitude cut-offs that develop at the base of existing upper level troughs produce a sequence of cloud patterns during the cutting-off process similar to those observed with frontal vortex development [21]. Instead of moving poleward as in the case of true wave development, the cloud system with the cut-off either remains stationary or tracks toward the equator. It thus becomes separated from the major cloud band and lies to the south of it. Cut-offs can also form aloft as the result of unstable anticyclonic flow over a ridge. In this case, they may not be associated with a cloud band in their early stages but initially form to the south of the polar front. The cloud systems that develop with these storms may have no history of having been connected with a front, however, they often contain cloud bands that appear similar to fronts. (The cloud patterns associated with cut-off lows in the subtropics are discussed in Chapter 4, Section F.)
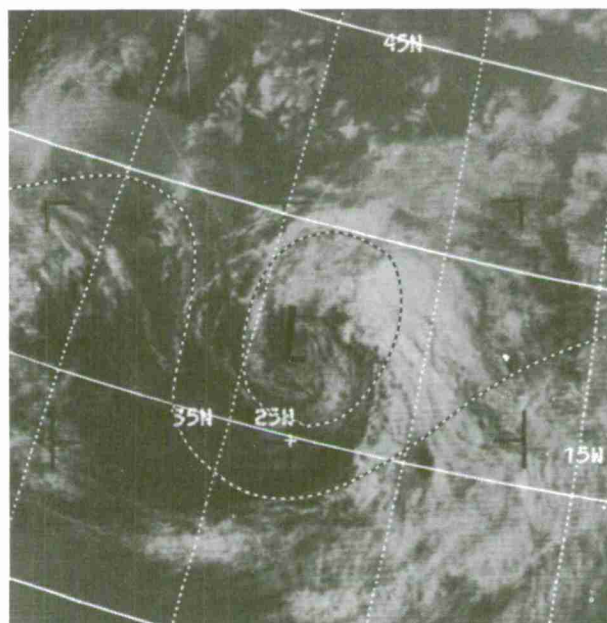


Figure 3-A-9. A cut-off cold low is shown. This system is strongest in the upper troposphere and has a weak surface circulation. The dominant clouds near the vortex center are cumulus and strato-cumulus.

E-7 753-4 1555Z 15 Oct 68
500-mb Analysis 1800Z 15 Oct 68

Chapter 3

---

SECTION B

FRONTS

## Introduction

Fronts are identified on satellite pictures by their distinctive cloud
bands. As a rule the well defined cloud bands that occur with active cold
fronts and occluded fronts occur in zones of strong baroclinicity. Active
warm fronts also occur in strong baroclinic zones but the bands, if they ex-
ist, are covered by high cirrus shields. The frontal cloud bands generally
extend several thousand miles and may exceed 300 miles in width. The bands
generally consist of multilayered clouds with a cirriform cloud cover. In ad-
dition to long cloud bands, fronts can sometimes be located from the difference
in cloud patterns on each side of a frontal system.

Active cold fronts have upper air winds parallel, or nearly parallel, to
the frontal zone. This results in a broad band of multilayered low, middle
and high clouds. Inactive cloud fronts have upper air winds perpendicular to
the frontal zone which result in considerable subsidence caused by downglide
over the frontal zone. This reduces the amount of clouds associated with the
front [1] [2] [3].

## Cold Fronts

Active cold fronts are seen as continuous, well-developed cloud bands. The frontal cloud bands are associated with strong baroclinic zones that have considerable thermal advection and strong vertical shear. The upper level winds are parallel, or nearly parallel, to an active cold front and this along with the strong baroclinic factors lead to the well developed cloud bands. The bands are made up of lower stratiform and cumuliform layers with cirriform clouds over the top.

Figure 3-B-1. A well developed cold front approaching northern Europe. The band shows stratiform, cumuliform and cirriform layers.
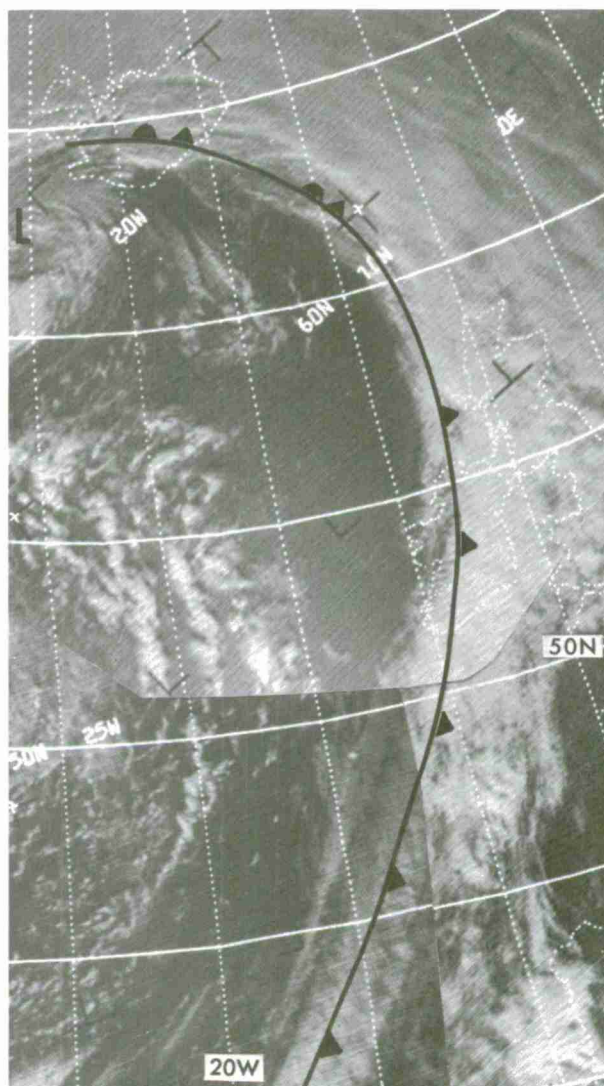
E-7 802-2,3; 803-3 1354Z, 1549Z 19 Oct 68
Surface Fronts 1200Z 19 Oct 68

Inactive cold fronts are often seen as narrow, fragmented, discontinuous
cold bands.  Inactive cold fronts over water occasionally have the same ap-
pearance as active cold fronts over land.  The inactive cold fronts are asso-
ciated with weak baroclinic zones that suggest weak cold air advection and
slight vertical shear.  The upper level winds tend to be perpendicular, or
nearly perpendicular, to the fronts.  The light winds and weak vertical shear
associated with the baroclinic zone are the contributing factors in the frag-
mented appearance of the cloud band.  The band of clouds is comprised mainly
of low level cumuliform and stratiform clouds but some cirriform clouds may be
present.  Inactive cold fronts over land may have few or no clouds.
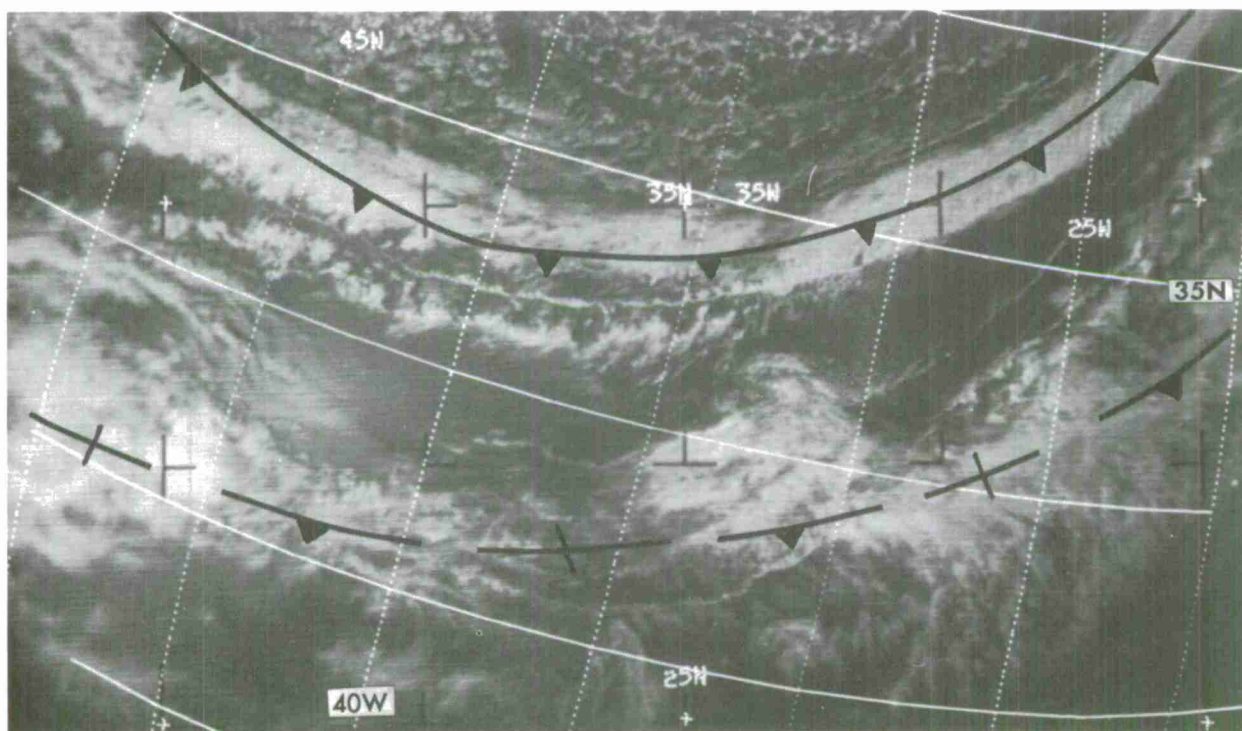


E-7 791-4 1644Z 18 Oct 68   Surface Fronts 1800Z 18 Oct 68

Figure 3-B-2.  The fragmented band of clouds from about 25N, 50W to
about 34N, 20W shows the location of an inactive cold front.  This front
is undergoing frontolysis.  A more active front characterized by the solid
band of clouds to the north can be compared with the inactive front.

When considering a quasi-stationary front, there are active and inactive systems to consider. The active quasi-stationary front tends to have the upper flow parallel, or nearly parallel, to the frontal zone. Active quasi-stationary fronts appear as wide cloud bands. Waves frequently develop on such frontal bands.

Inactive quasi-stationary fronts are usually found in lower latitudes with a generally east-west orientation. It is the presence of a subtropical high which leads to the dissipation of the clouds in the frontal zone. Inactive quasi-stationary fronts are seen as fragmented cloud bands, often devoid of low and middle clouds due to the subsidence associated with the subtropical high.

When a frontal cloud band is weak and difficult to orient, it is sometimes helpful to examine the cloud character in the region of the suspected front. In the cold air behind a front, especially over water, there will be cumuliform clouds, often open and closed cellular in aspect; while ahead of the front, there will be a mixture of cumuliform and stratiform clouds.

With a mature vortex the occluded front may be located near the trailing edge of the cloud band. The stationary front is normally located near the leading edge of the cloud band and the cold frontal portion somewhere in between.
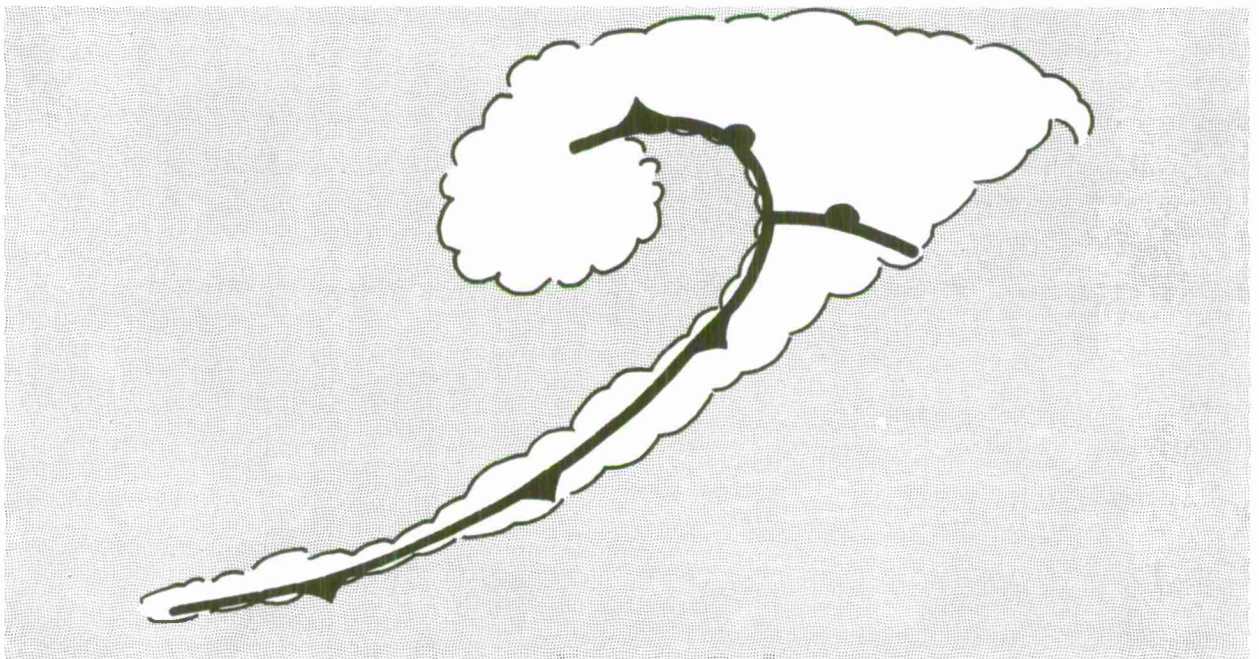


Figure 3-B-3. An idealized schematic showing frontal positions with relation to the cloud band. The occluded front is placed near the trailing edge of the cloud band and the slow-moving portion of the cold front is located near the leading edge.
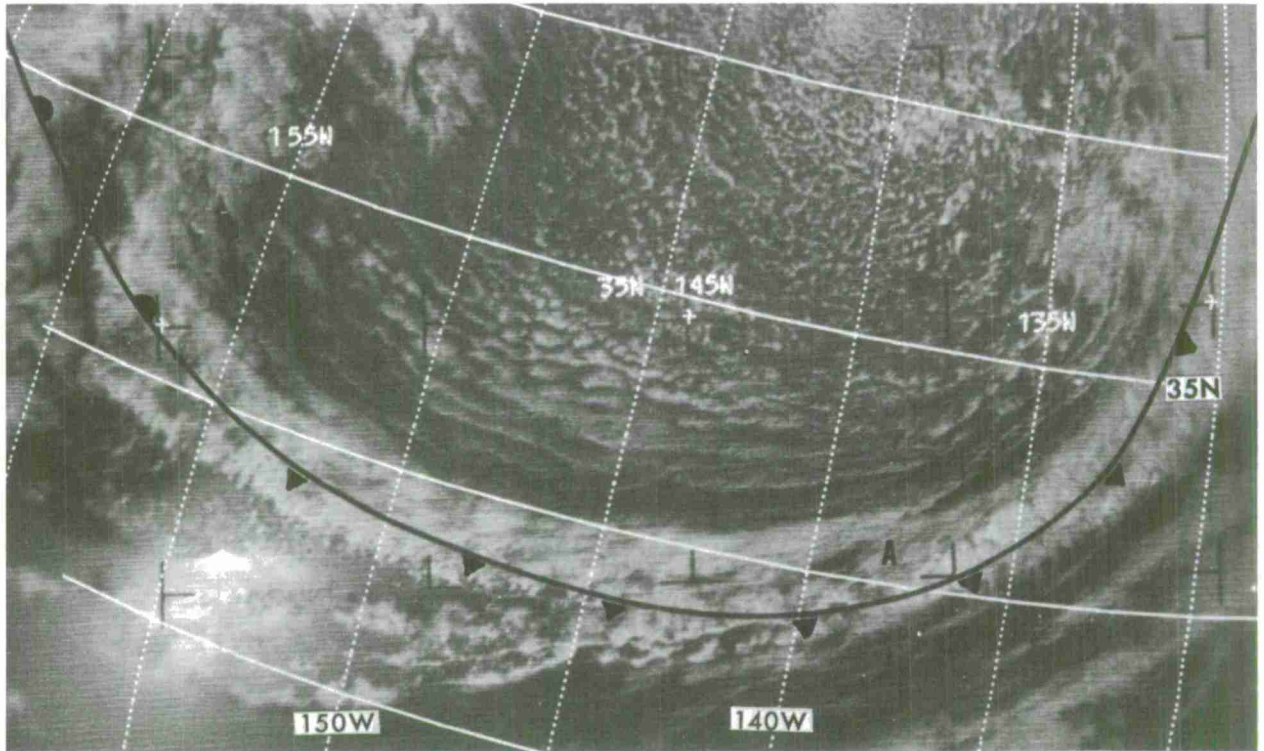
E-7 920-4 2359Z 28 Oct 68   Surface Front 0000Z 29 Oct 68

Figure 3-B-4.  A slow-moving, nearly stationary cold front is shown
between high pressure areas.  The frontal cloud band is in the first
stage of dissipation from point A westward.  There are cumuliform cellu-
lar clouds behind the front and some cumuliform and stratiform clouds
ahead of the front.  In the area where this front is moving slowly, the
frontal position  is placed near the leading edge of the cloud band.

## Warm Fronts

Active warm fronts are, at best, difficult to locate on satellite cloud
pictures, and inactive warm fronts cannot be located at all. An active warm
front will be associated with strong baroclinicity and may be associated with
a well organized cloud band, but the frontal zone will be difficult to locate.
An active warm front may be placed somewhere under the bulge of clouds that is
associated with the peak of the warm sector of a frontal system. The clouds
in the bulging portion of a mature frontal system with an active warm front
are combinations of stratiform and cumuliform beneath a cirriform canopy. In-
active warm fronts usually have very little baroclinicity associated with them
and very few clouds.
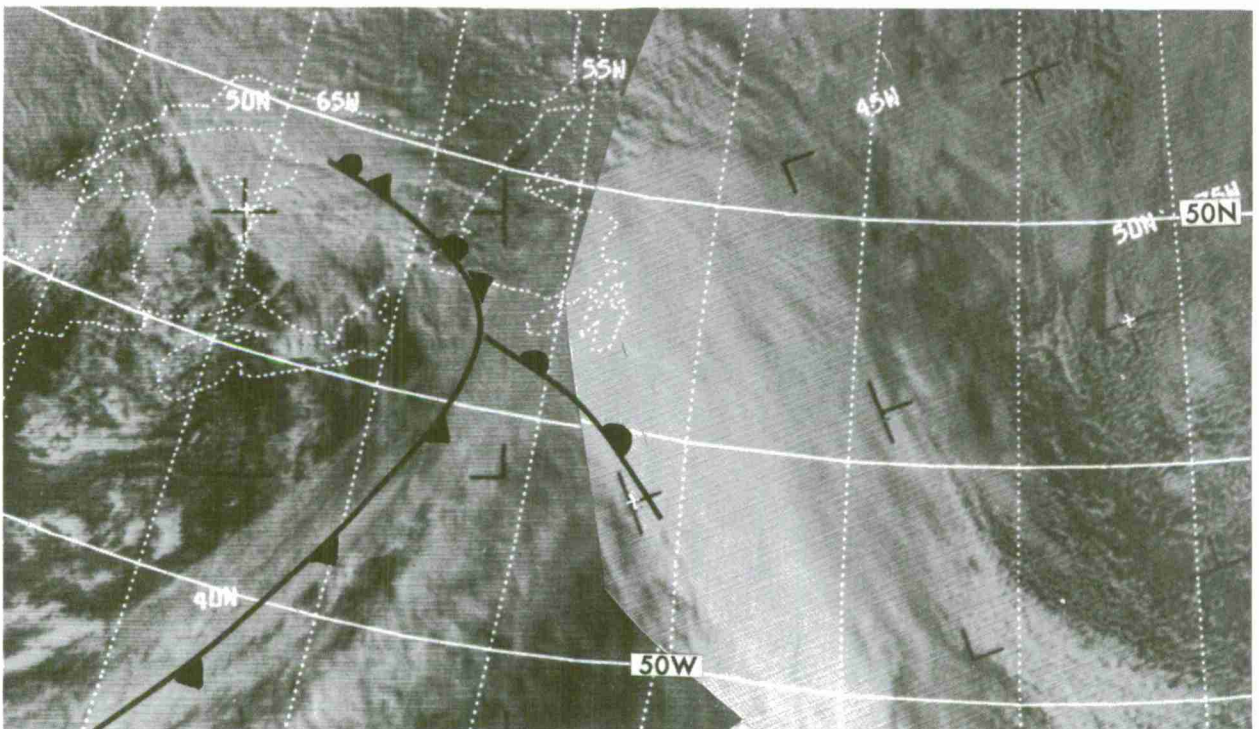


E-7 891-3; 892-3 1628Z, 1823Z 26 Oct 68  Surface Fronts 1800Z 26 Oct 68

Figure 3-B-5. The surface analysis places the warm front under the
cirrus shield ahead of the cold front and occlusion. Beoause of the exten-
sive cirrus cover over the band of clouds associated with the warm front,
this band cannot be seen. As a result, the warm front cannot be accurately
located from the cloud picture alone.

## Occluded Fronts

The occluded front is located in the band of clouds poleward of the bulge of cirrus over the front.  The occluded front is associated with that part of the cloud band that curves in a spiral away from the peak of the warm sector toward the associated vortex.  The peak of the warm sector is located equatorward of the cirrus shield under the bulge in the frontal band.  Present analysis techniques do not carry the front completely around the vortex but end it in the north or northwest quadrant.

Sometimes there is a change in cloud character from smooth-appearing cirriform over the bulge of a frontal system to lumpy-appearing cumuliform poleward of the bulge.  This change in cloud character helps to position the point of occlusion and the peak of the warm sector.

Figure 3-B-6.  The jet stream cuts across the frontal band near A and a change in cloud character is noticed near this point.
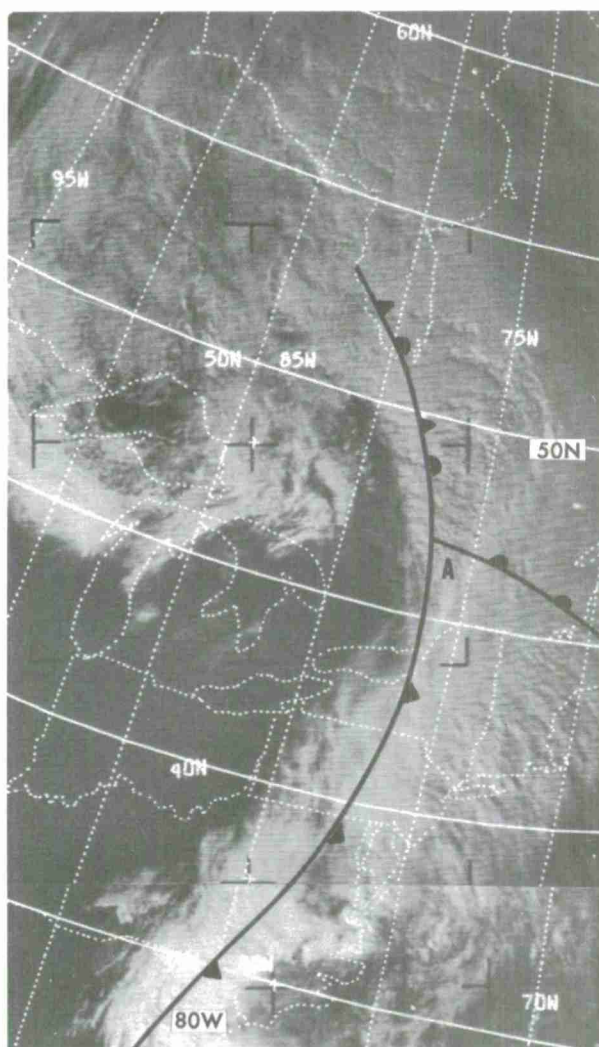


E-7 805-3,4 1932Z 19 Oct 68
Fronts 1800Z 19 Oct 68

Occluded Frontogenesis

A phenomenon shown on satellite photographs that is not usually described
in conventional frontal theory is occluded frontogenesis or the "instant"
occlusion. This is a situation where an occluded-like front forms by fronto-
genesis rather than by the occluding process. When a comma cloud, reflecting
a maximum of positive vorticity advection approaches a frontal band, wave for-
mation may begin. As the comma cloud formation continues to intensify, cy-
clonic flow becomes accentuated resulting in a more northerly flow in the cold
air behind the vorticity center and a more southerly flow in the warm air
ahead of the vorticity center. As the comma cloud formation merges with the
frontal wave, the cold and warm air masses appear separated. From the stand-
point of continuity in analysis this results in a frontal system that appears
to "jump" from the wave stage to the mature occlusion without going through
the entire occlusion process. The resulting cloud pattern produced by the
merging of the vorticity comma and the frontal wave gives the appearance of a
system that has occluded and is analyzed as a fully occluded system. Continu-
ity from the satellite pictures will show that the system is actually the re-
sult of frontogenesis. This occurrence is seen in synoptic situations as the
merging of a trough with a wave on an east-west front.

Figure 3-B-7 and Figure 3-B-8 (facing). Figure 3-B-7 shows a vorticity
comma centered at 46N, 147W and the leading edge of a front at about 37N,
132W. Figure 3-B-8 shows the two systems about 24 hours later. Note that the
clouds associated with the vorticity center have merged with the frontal
clouds and the surface analysis shows an occluded front from 37N northward.
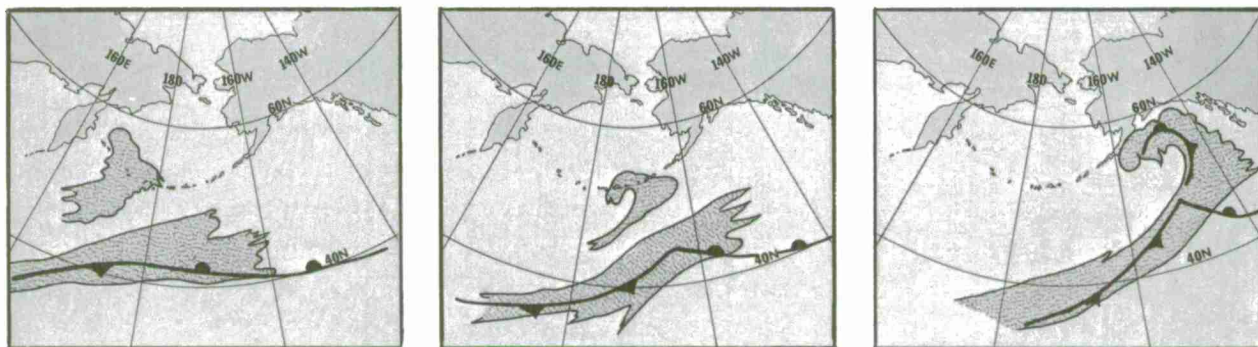


Figure 3-B-9 a, b, c. An idealized schematic showing occluded fronto-
genesis.
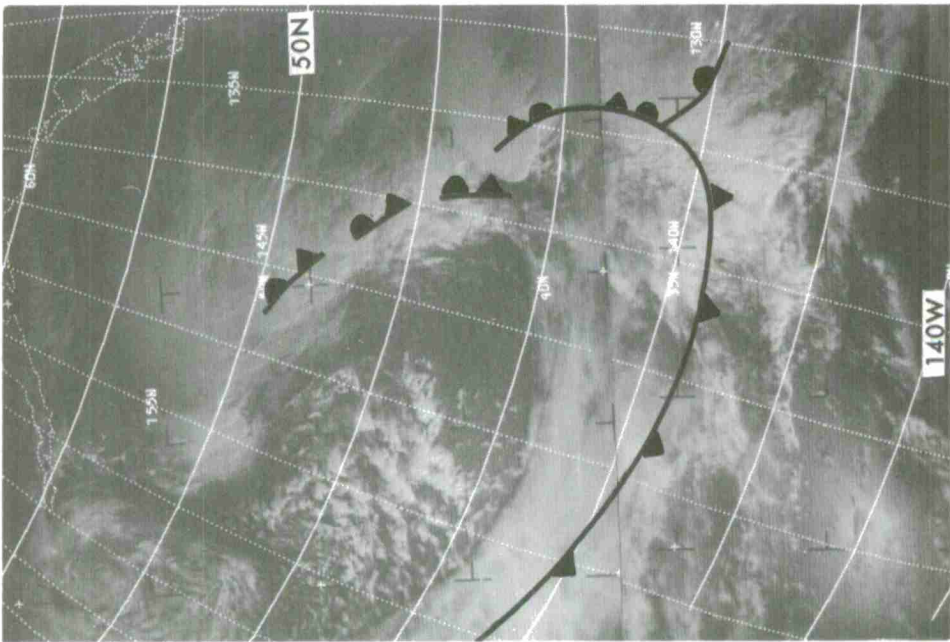
E-7 1020-2,3  2335Z 5 Nov 68
Fronts 0000Z 6 Nov 68

Figure 3-B-8.
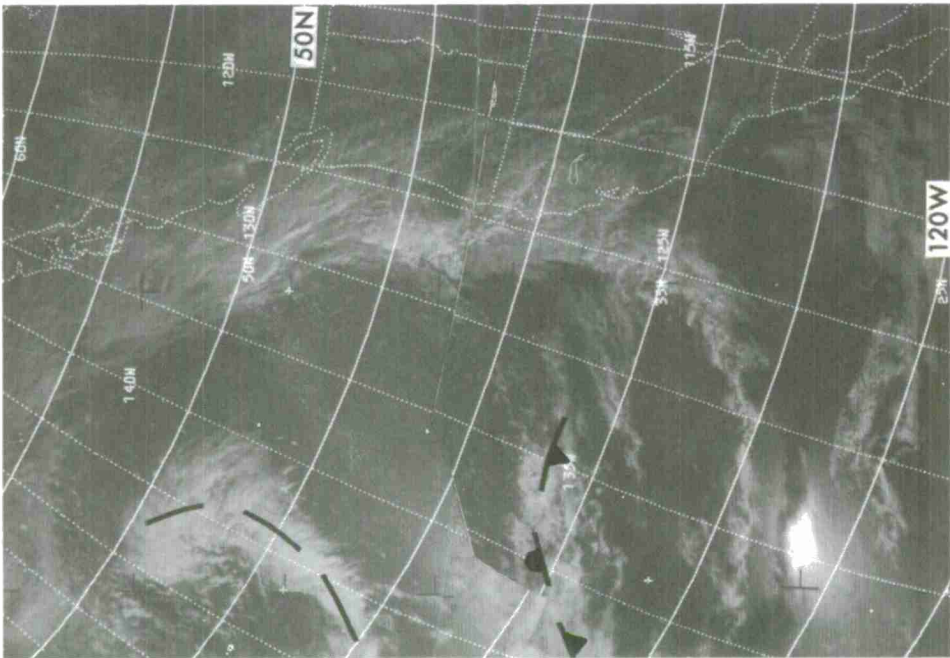


E-7 1007-2,3  2245Z 4 Nov 68
Fronts 0000Z 5 Nov 68

Figure 3-B-7.

Another cloud pattern that is often analyzed as occluded frontogenesis or an "instant" occlusion occurs in the Pacific near Japan. The southern end of a north-south oriented cloud band, associated with a cold trough and usually analyzed as a cold front, will often merge with a stable wave on a front that is oriented east-northeast to west-southwest. The merger of the north-south cloud band into the wave produces a cloud pattern similar to the occluded frontal band.
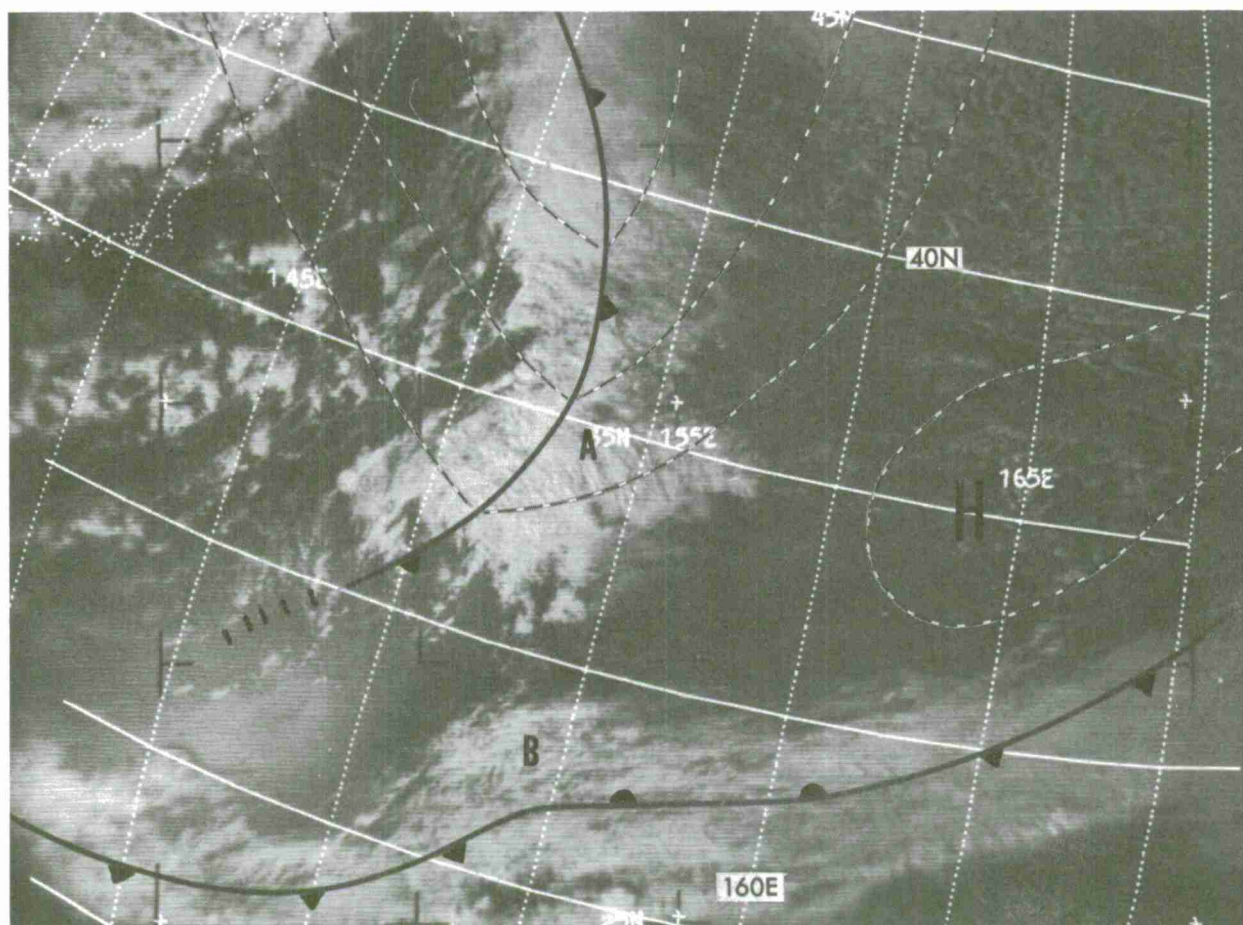


E-7 1160-3 0358Z 17 Nov 68   Analysis 0600Z 17 Nov 68

Figure 3-B-10. A north-south cloud band, at A, is approaching a stable wave, at B, on an east-west frontal band. Satellite pictures on 18 November showed the two cloud bands merged into what appeared to be an occluded front. At 0000Z on 18 November an occlusion was analyzed which extended almost 900 miles out of a wave on the front.

## Fronts Over Land and Water

Frontal cloud bands usually change character as they move inland after having had an over-water trajectory. Similarly, frontal cloud bands moving offshore change in appearance after a sufficiently long trajectory over water. A well-developed continuous frontal cloud band over water can change to a discontinuous, fragmented collection of clouds as the associated front moves over land. This change in cloud character is the result of a decrease in the amount of moisture available over land. As a rule, frontal cloud bands tend to have more continuous clouds over water than over land although there are cases of continuous frontal cloud bands over land.



Figure 3-B-11. A frontal cloud band is shown that is partly over land and partly over water. Note that the portion of the front that is over water is well developed while the part that is inland, north of A, is less organized.
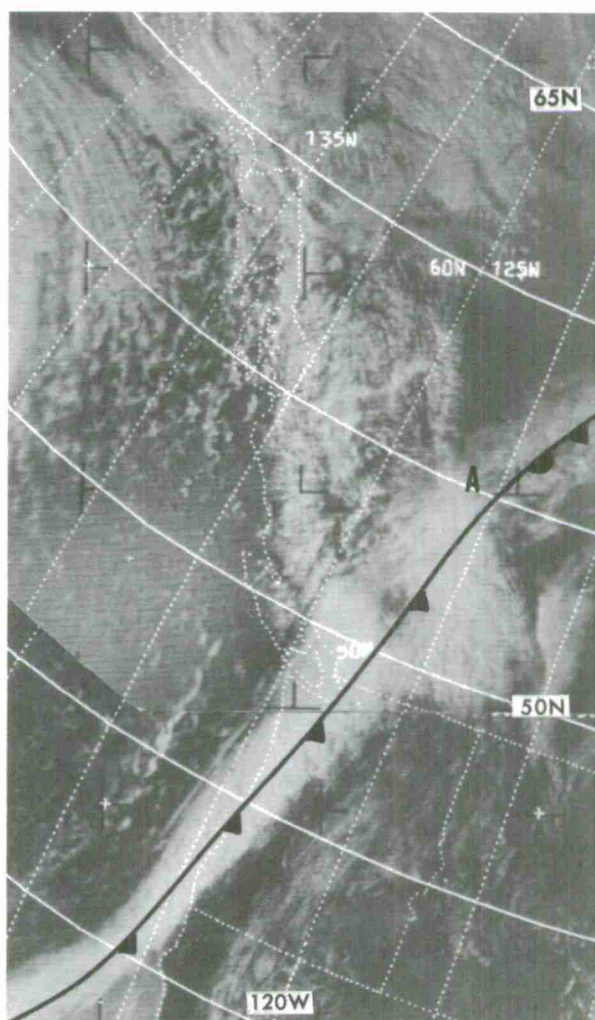
E-7 781-2,3 2137Z 17 Oct 68
Front 0000Z 18 Oct 68

### Non-Frontal Cloud Bands

Some of the long cloud bands seen on satellite photographs are not associated with fronts, yet may give the appearance of a frontal band. In many cases these cloud bands are associated with regions of surface confluence. Other cloud bands may be the result of northward advection of moist tropical air. North-south oriented bands often appear in the convergent flow on the back side of a high pressure cell as a low approaches the area.

Figure 3-B-12. The band of clouds south of the front is associated with confluence along a trough and with winds related to a sub-tropical jet. The band appears similar to frontal cloudiness. In cases like this, it is necessary to investigate the formation of the cloud band on earlier passes and to check previous synoptic analyses at several levels to determine if frontal discontinuities exist.
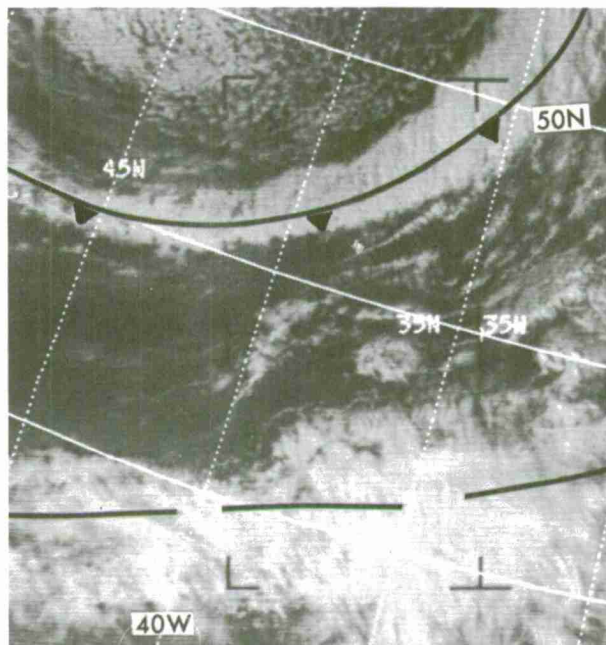
E-7 816-4 1639Z 20 Oct 68
Front 1800Z 20 Oct 68

Figure 3-B-13 and Figure 3-B-14 (facing). A cloud band with a north-south orientation formed in a confluence zone with northward advection of warm moist air. On 28 September the clouds have a broken appearance without a solid cover. By 29 September cirrus covers most of the band.
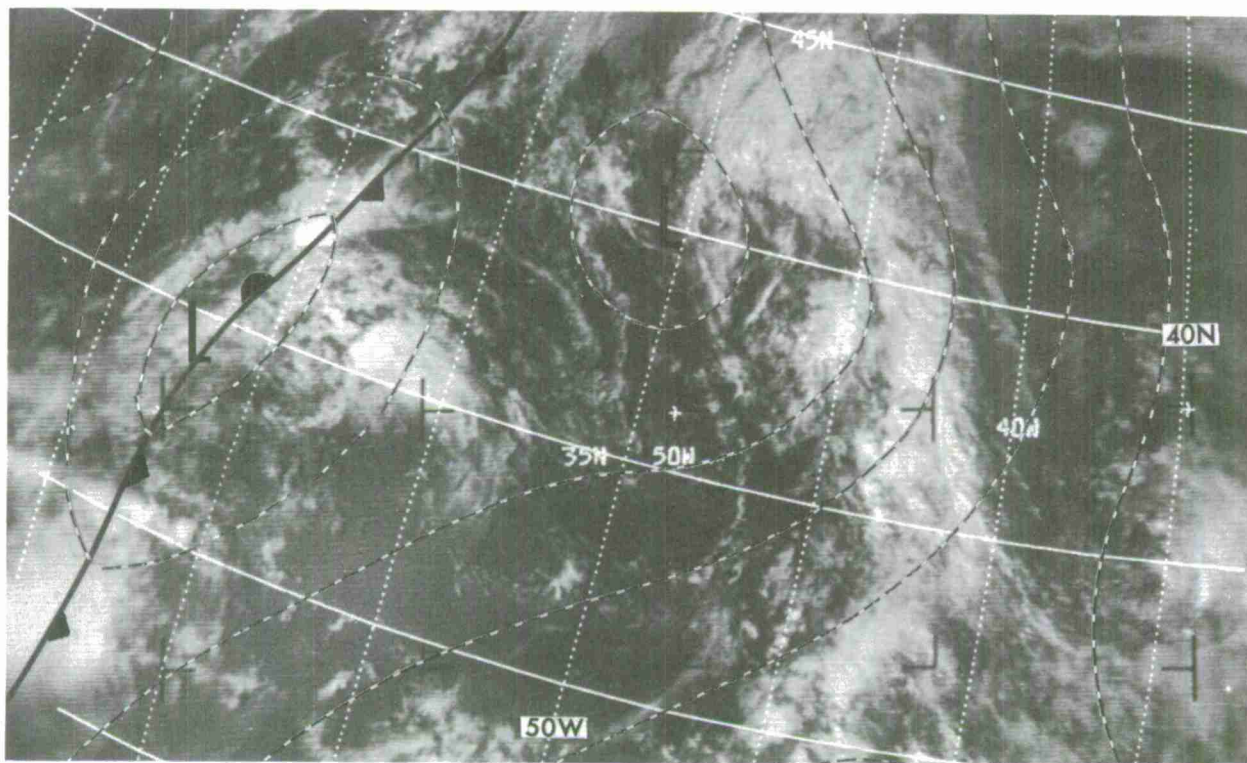
E-7 541-4 1735Z 28 Sep 68   Analysis 1800Z 28 Sep 68

Figure 3-B-13.
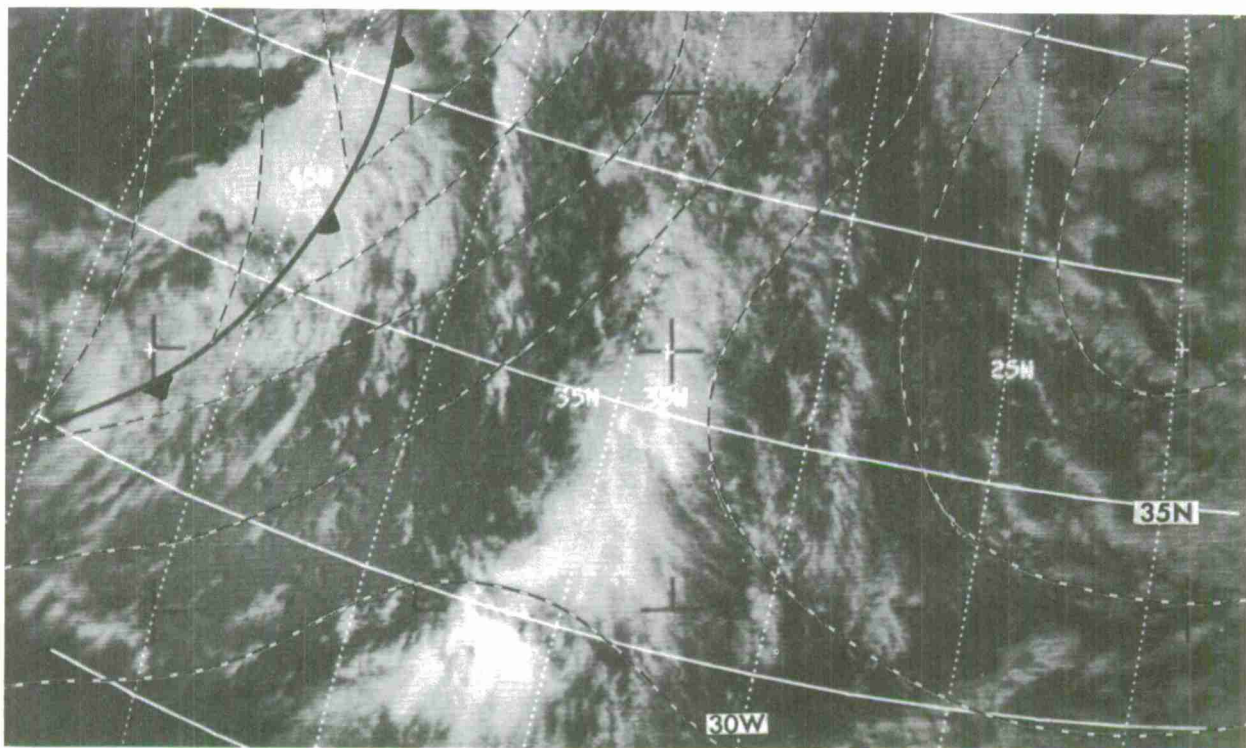


E-7 553-4 1635Z 29 Sep 68   Analysis 1800Z 29 Sep 68

Figure 3-B-14.

Squall Lines

Squall lines are often seen in the cloud patterns ahead of a cold front. In some cases a thin line of cumulus and cumulonimbus appears ahead of, and parallel to, a frontal band. In other instances groups and clusters of clouds form bands that may have a scalloped appearance.

Figure 3-B-15. A narrow pre-frontal squall line, at A, with tops reported above 40,000 feet moves ahead of a cold front. The anvil cirrus of the cumulonimbus has dissipated in the sinking air behind the upper trough which just passed to the east of the squall line.
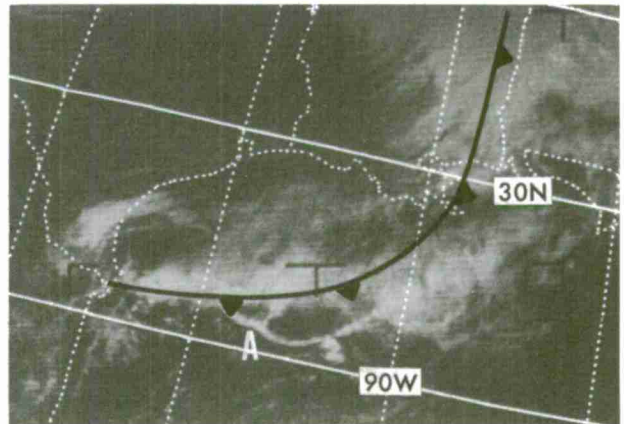


E-7 1031-4 2039Z 6 Nov 68
Front 1800Z 6 Nov 68

Figure 3-B-16. Two large areas of cirrus-covered thunderstorms coincide with squall lines. The cold front is positioned by a thin line of cumuliform clouds.
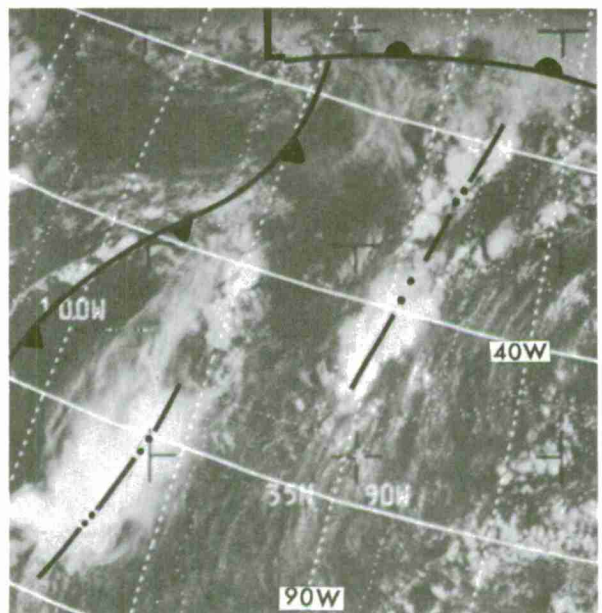


E-5 676-5 2038Z 12 Jun 67
Fronts 1800Z 12 Jun 67

## Back-Door Cold Front

One of the many ways in which the Middle Atlantic States get temporary relief from hot, humid weather conditions is by the passage of a back-door cold front. Fronts of this type move towards the south or southeast along the Atlantic seaboard of the United States (57) and displace a westerly or south-westerly flow of warm, humid maritime tropical (mT) air with a cool north-east flow of modified continental polar (cP) air.

The 500-mb flow associated with a back-door cold front has a northerly com-ponent over eastern Canada. This northerly component occurs when a 500-mb ridge intensifies as it moves from central to eastern Canada. Concurrently a 500-mb low deepens and moves south over eastern Canada. As the 500-mb flow increases in amplitude, the surface high in eastern Canada strengthens and moves off the coast of North America. North of the front, the easterly flow at the surface is blocked by the Appalachians and is deflected to the south, undercutting the prevailing mT air. After frontal passage there is a significant lowering of the temperature and often of the dew point. Many times low clouds and fog are advected onshore in the low level easterly flow which occurs within one to two hundred miles north of the front. Further north, towards the center of the high, mostly clear skies prevail. This cloudiness aids in locating the front and outlining the shallow layer of cool modified cP air as it moves southward behind the front and spreads westward over the Coastal and Piedmont sections of the Middle Atlantic States. The Appalachian Mountains limit the westward push of the cool air. After the passage of a back-door cold front, cool conditions prevail over the normally warm, humid lowlands while in the mountains to the west of the front, high temperatures continue.

A back-door cold front moving southward along the Atlantic Coast is seen on the ESSA-9 photographs (Figures 3-B-17 and 3-B-18) at approximately 1800 GMT on May 14 and 15, 1970. The 24-hour movement of the frontal system can be traced with the satellite cloud patterns. Along the coastal area, the front moves southward from Delaware to South Carolina, while from the mountains west, the front moves northward from western Maryland to Canada. On both days most of the cloudiness is north of the front. The southern and western edges of the clouds outline the southern and western limits of the cool air. On the 15th, the clouds behind the front cover the Coastal and Piedmont sections of the Middle Atlantic States where an onshore flow takes place in the shallow layer of cool air.
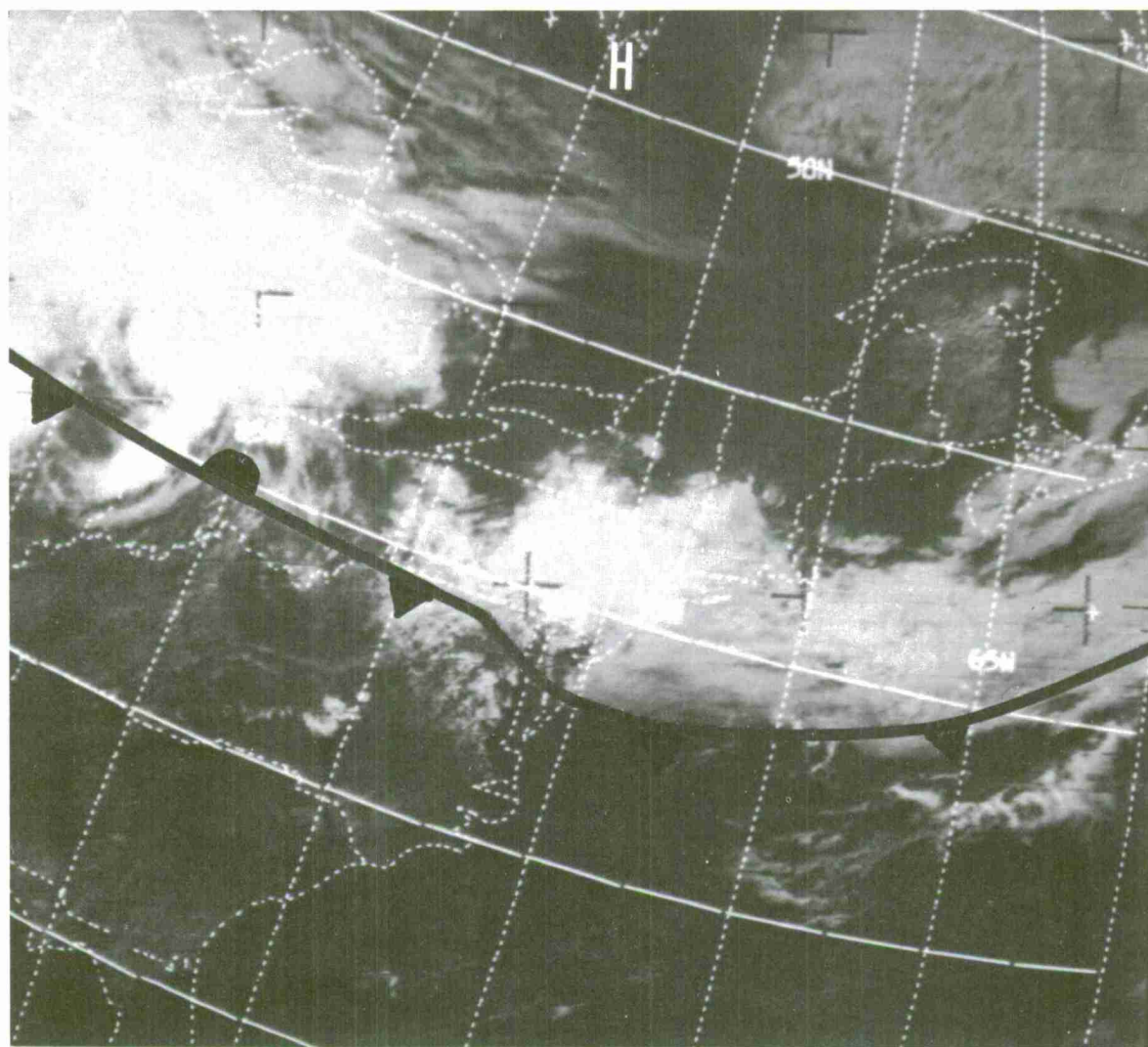


E-9 5526-4   1857 GMT May 14, 1970;Surface Front 1800 GMT  May 14, 1970.

Figure 3-B-17.  Clouds associated with onshore easterly winds behind a back-door cold front.  Maximum temperatures (Fahrenheit) are in the 90's south of the front and between 70 and 80 in the cloudy zone north of the front.  The center of the surface high is indicated by H.

3-B-16
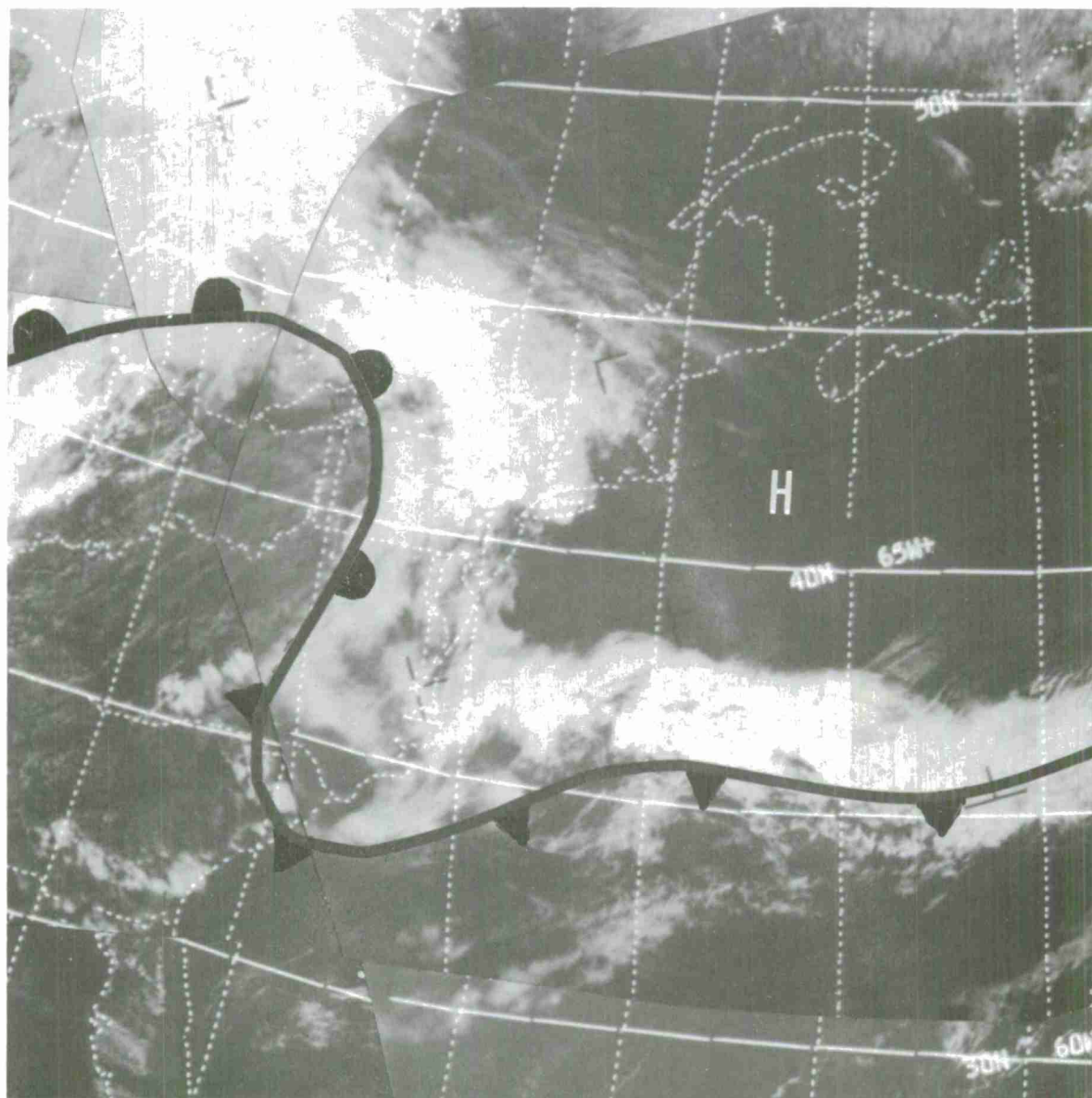
E-9 Mosaic of Pass 5538 (1800 GMT) and Pass 5539 (1955 GMT) May 15, 1970;
Surface Front for 1800 GMT  May 15, 1970.

Figure 3-B-18.  Fog and stratus over the Piedmont and coastal sections of the
Middle Atlantic States outline the southwestward extent of the shallow layer
of modified cP air.  The surface front continues to lie along the leading
edge of the cloud band.  Maritime tropical air to the south and west is
characterized by some cumulonimbus and much fair weather cumulus.  Maximum
temperatures are near 70°F in the cloudy cold air north of the front and in
the 90's south of the front.  The Washington sounding showed marked cooling
below 850 mb.  The center of the surface high is indicated by H.
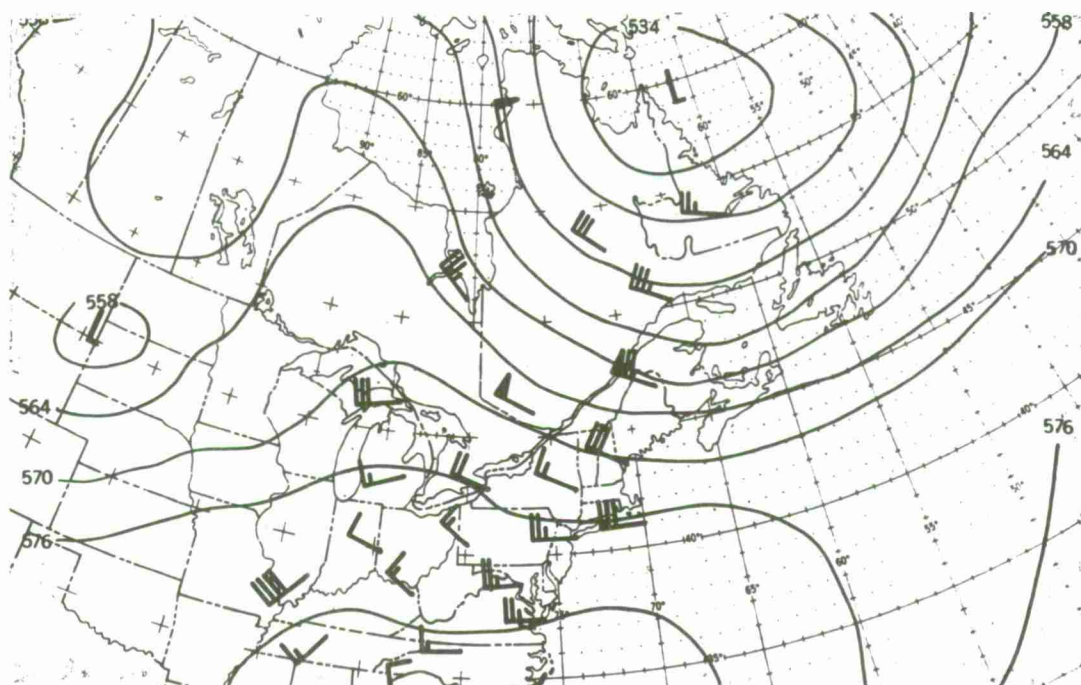
500-mb Analysis  1200 GMT  May 14, 1970.

Figure 3-B-19.  The 500-mb analysis six hours prior to figure 3-B-17.  At this time there is a sharpening ridge over central Canada with closed lows over South Dakota and northern Labrador.
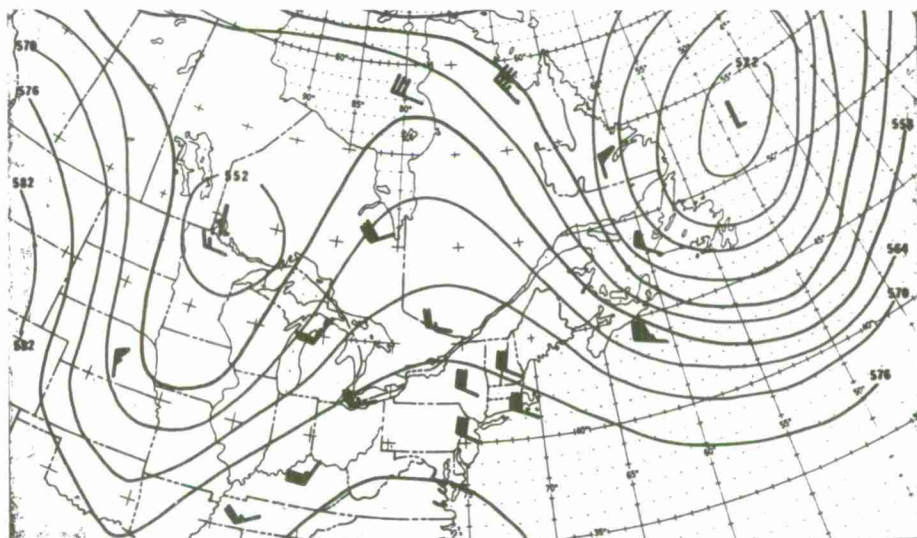


500-mb Analysis  0000 GMT  May 16, 1970.

Figure 3-B-20.  The 500-mb analysis six hours after figure 6-B-18.  The axis of the ridge is over eastern Canada and the Labrador low has moved southeastward.

Chapter 3

SECTION C

CELLULAR CLOUDS

Introduction

    The most common cloud formations found in satellite pictures are open and
closed cellular patterns.  Recognition and interpretation of these cellular
cloud patterns will enable the meteorologist to identify regions of cold air
advection and areas of cyclonic, anticyclonic and divergent flow in the cold
air behind polar fronts over oceanic areas.  Cellular cloud patterns aid in
the identification of cloud types, location of jet streams, and regions of
positive vorticity advection.  They also provide indications of surface wind
direction and speed and atmospheric stability.  Additional information on jet
streams, vorticity, and surface winds is included in other sections of this
chapter.

## Cellular Cloud Patterns

These cloud patterns form as a result of mesoscale convective mixing within the large scale flow. As the cold air to the rear of a cold front is advected over warmer water, there is a heating of the air mass from below. Open cells form where there is a large air-sea temperature difference and closed cells form where a weaker air-sea temperature contrast exists. The open cells are composed of cloudless, or less cloudy, centers surrounded by cloud walls with a predominant ring- or U-shape. The closed cells are characterized by approximately polygonal, cloud covered areas bounded by clear or less cloudy walls. These cellular patterns are a result of a mixing process of the moist air in the lower levels where a slow turnover process is initiated. The vertical motion of this process is capped by either a subsidence inversion away from the area of strongest cyclonic activity or by dry air entrainment near the more active cyclonic areas. The final result is an atmospheric balance of upward and downward vertical motion in the lower levels giving a mesoscale cellular pattern. The cell type, open or closed, is dependent on the intensity of heating from below. Cellular patterns associated with subtropical high cells form under more stable conditions and lack strong cold air advection [1] [2] [4] [15] [25].
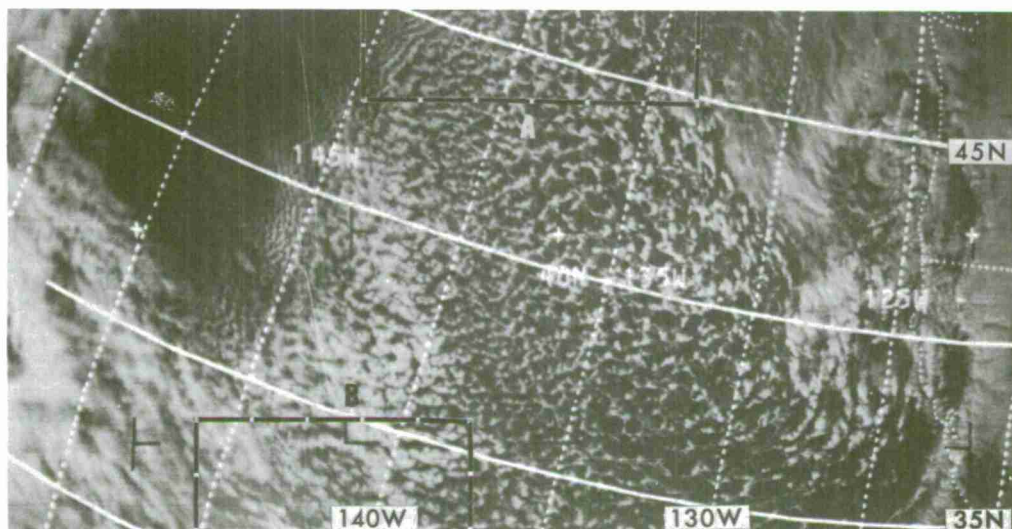


E-3 621-2 2244Z 20 Nov 66

Figure 3-C-1. A large area of the eastern Pacific is covered by cellular patterns which formed as cold air moved over the warmer ocean surface. Open cells are located at A, closed cells at B. Blocked-in areas of this photograph are shown enlarged as Figures 3-C-2 and 3-C-3.

Enlargement of E-3 621-2 20 Nov 66



Enlargement of E-3 621-2 20 Nov 66

Figure 3-C-2. A typical open cellular pattern is formed behind a polar front. A single cell of the open cellular pattern, showing the open center and the cloud walls, is shown in the boxed-in area. These walls may be ring- or U-shaped.

Figure 3-C-3. A typical closed cellular pattern is formed behind a polar front. A single cell of the closed cellular pattern is shown in the boxed-in area. It shows the polygonal cloud cell surrounded by clear air or less cloudy areas.
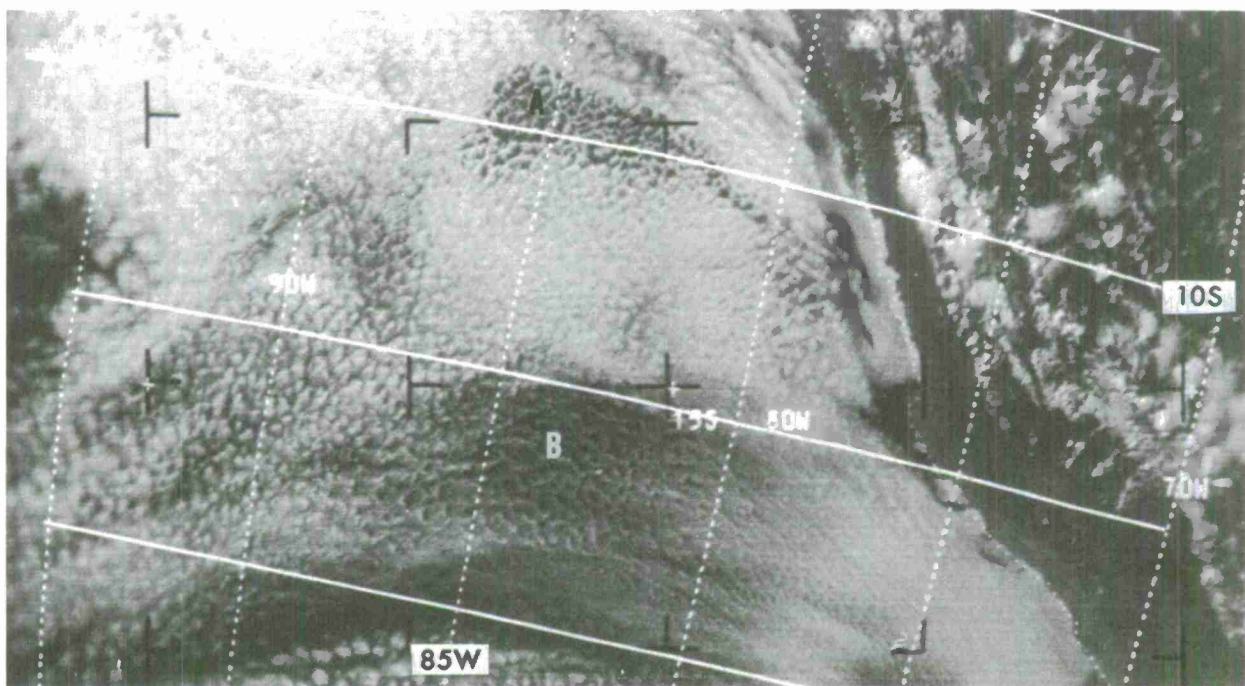


E-5 1475-9 2106Z 14 Aug 67

Figure 3-C-4. Closed cells of various diameters in the subtropical high west of South America surround open cells at A and B.

The vertical shear, speed or directional, in a three-dimensional cellular
pattern composed of either open or closed cells, must be small or nonexistent.
When strong shear exists, the cells break down and form into lines or bands
that are oriented along the shear vector.  The pattern thereby gives indica-
tions of the vertical wind structure.  If the shear is exclusively due to a
change in wind speed with height, the orientation of the shear, wind direction,
and bands or lines will be coincident.

Figure 3-C-5.  Lines of cumuli-
form clouds at A and B indicate strong
shear through the cloud layer parallel
to the low level wind direction.  At
C and D an open cellular cumuliform
pattern prevails while at E and F, an
increase in vertical shear through the
cloud layer breaks the open cellular
pattern down into lines and bands.
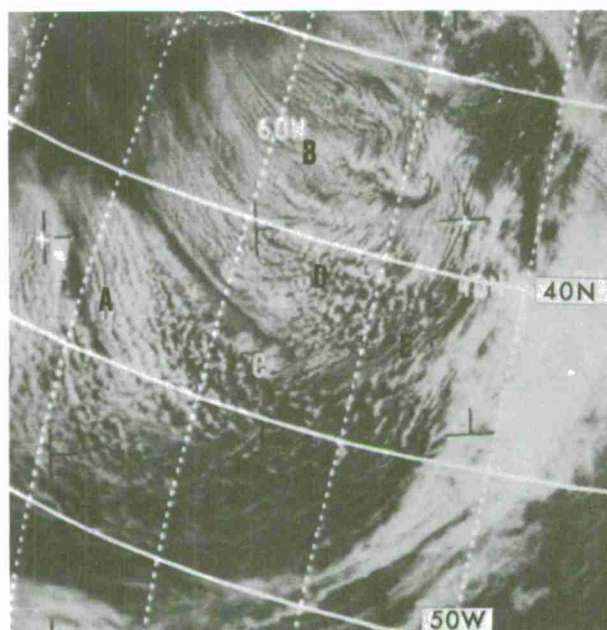
E-3 1899-3 1644Z 2 Mar 67

In the subtropical cellular patterns an unusual radial or crystal-like
cloud formation is occasionally seen in the open or closed cells.  This is
called an actiniform cloud pattern and it may be a transitional phase between
open and closed cells.  They are most commonly seen off the west coast of
South America.
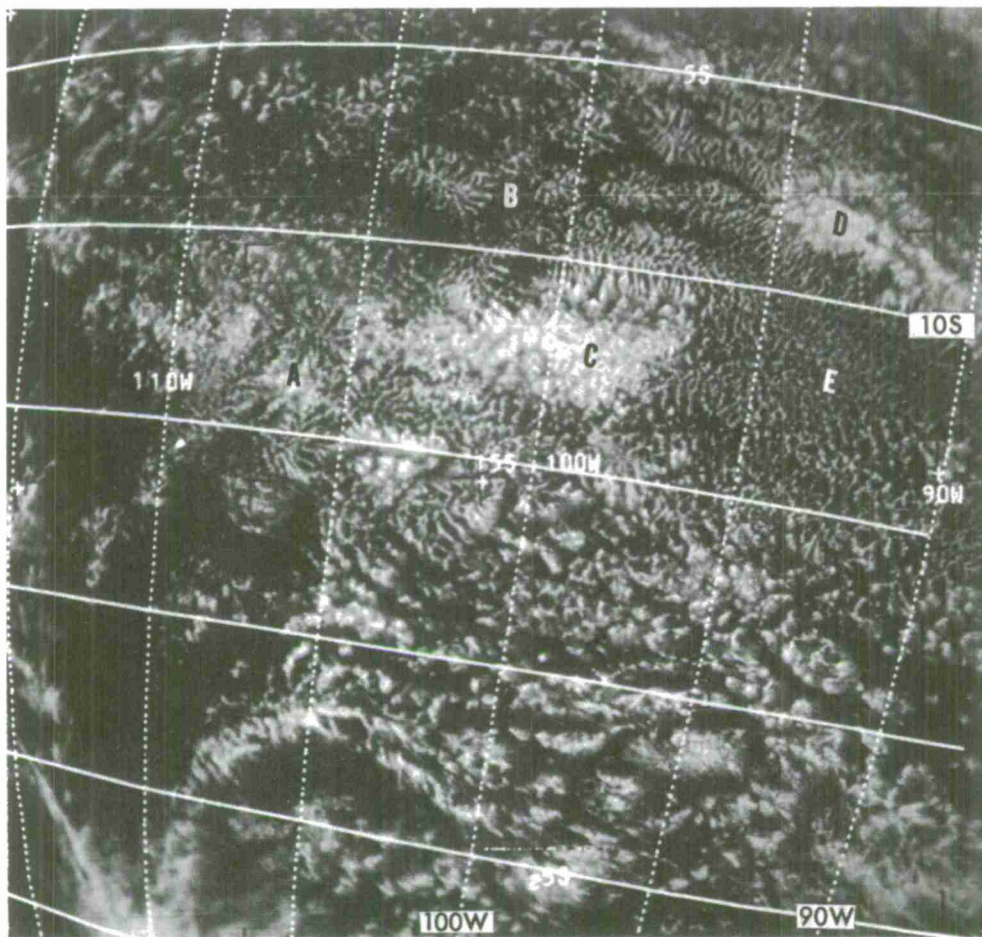
E-3 4413-8 2099Z 18 Sep 67

Figure 3-C-6.  The semipermanent subtropical high pressure
cell off the west coast of South America is characterized by
many types of cellular cloud patterns.  The radial or crystal-
like formation of the actiniform cloud pattern can be seen at
A and B.  Closed cells are present at C and D, and open cells
at E.

### Open Cellular Cloud Patterns

Open cellular patterns are most commonly found to the rear of cold fronts in cold unstable air. These patterns are made up of many individual cumuliform cells. The cells are composed of cloudless, or less cloudy, centers surrounded by cloud walls with a predominant ring- or U-shape. In the polar air mass the open cellular patterns that form in the deep cold air are predominantly cumulus congestus and cumulonimbus. The open cells that are found in the subtropical high are mainly stratocumulus, cumulus and cumulus congestus clusters. In order for open cells to form in a polar high, there must be moderate to intense heating (a large air-sea temperature difference) of the air mass from below. When the cold continental air moves over water, the moist layer is shallow and capped by a subsidence inversion near the coast. Further downstream the vertical height of the moist layer increases, as does the height of the clouds, and the capping is caused by dry air entrainment.

Behind the polar front open cells are observed where the low level flow is cyclonic.

Vorticity centers associated with positive vorticity advection are frequently observed in regions of open cellular clouds. The positive vorticity advection can be identified where there is a small area of enhanced convective activity or, in certain cases, a formation in the shape of a comma.

The presence of open cells indicates warming of the air mass from below and conditional instability in the lower levels. This instability is capped by either a subsidence inversion or dry air entrainment.
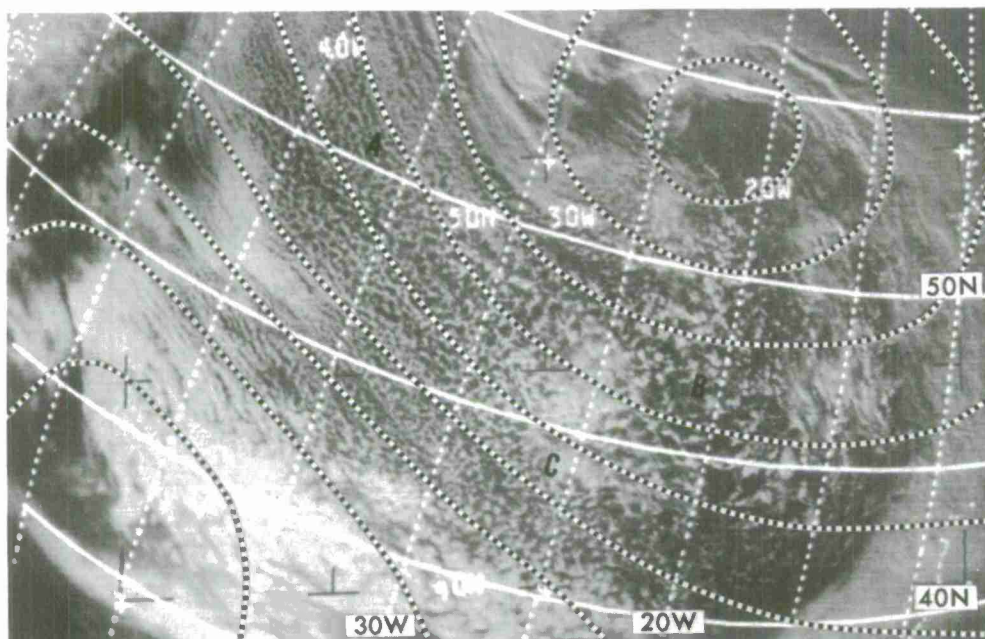
E-3 1358-2 1503Z 18 Jan 67   Analysis 1800Z 18 Jan 67

Figure 3-C-7.  Open cells behind a polar front over the North At-
lantic indicate cold air advection and cyclonic curvature of the low
level wind flow.  Vertical thickness of the cumulus at A is small but
increases eastward towards B.  The bright enhanced area at C is an
indicator of positive vorticity advection.

Figure 3-C-8.  A large area of
the subtropical high west of Peru is
covered with open cells.  The open
cells which form in subtropical highs
are not associated with low level cy-
clonic flow or strong cold air advec-
tion.
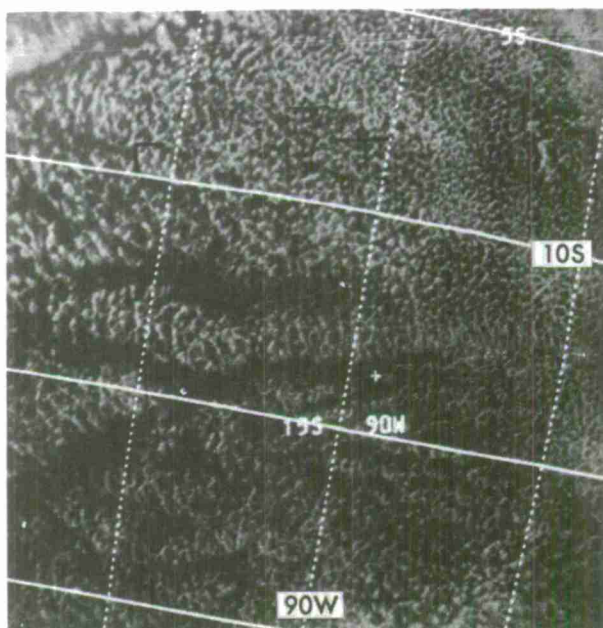


E-5 1171-9 2133Z 21 Jul 67

### Closed Cellular Cloud Patterns

Closed cellular patterns which occur behind the cold front are commonly found in the southeastern quadrant of polar highs. These patterns are characterized by approximately polygonal cloud-covered areas bounded by clear or less cloudy walls. Atmospheric conditions necessary for the formation of closed cellular patterns are weak convective mixing in the lower levels and a cap to this mixing. The convective mixing is the result of surface heating of the air or radiative cooling of the cloud tops. This convection is not as intense as that associated with open cells. The cap to the instability associated with these closed cellular cloud patterns is in the form of a subsidence inversion in both polar and subtropical situations. Closed cellular patterns are made up of stratocumulus elements in both the polar and subtropical air masses and may also be accompanied by trade wind cumulus in the subtropical high. Closed cells, when associated with subtropical highs, are located in the eastern sections of the high pressure areas.

Behind the polar front closed cells are observed where the lower level flow is anticyclonic.

Surface winds in closed cellular cloud patterns of a polar high are usually 20 knots or less.

Closed cells are associated with limited low level instability below the subsidence inversion and extensive vertical convective activity is not likely.
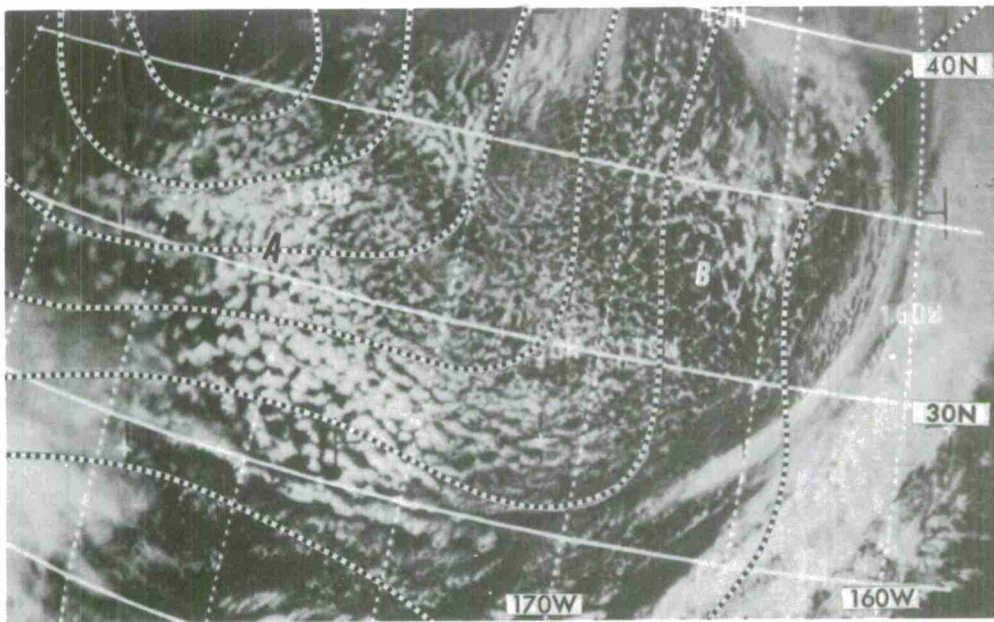
E-5 1941-4 0055Z 6 Mar 67   Analysis 0000Z 6 Mar 67

Figure 3-C-9.  Closed cells in the southeastern portion of a
polar high over the Pacific are at A.  The closed cells prevail
where the low level flow is anticyclonic while, at B, open cells
prevail in a cyclonic flow.

Figure 3-C-10.  Closed cells are
seen in the eastern portion of a sub-
tropical high in the South Pacific.
West of A the closed cells are com-
posed of stratocumulus with some
clear walls and east of A the walls
are composed of thinner clouds.
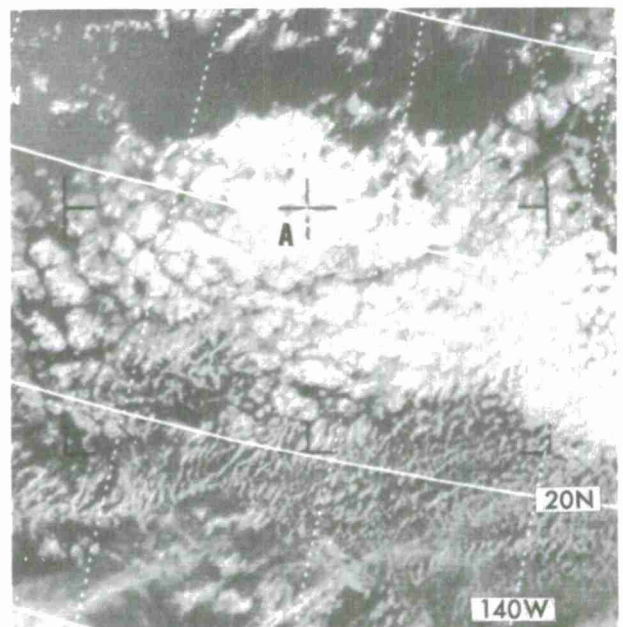


E-5 1236-6 0049Z 27 Jul 67

Transitional Features

Areas of divergence can be located when a well-developed open and closed cellular pattern exists, especially in the polar air mass. The open cells are associated with cyclonic flow and the closed cells are found with anticyclonic flow. From this, it follows, that the area between the open and closed cells would be an area of low level directional divergence or an asymptote of divergence for streamline analysis.

Jet streams can sometimes be located with the aid of cellular cloud patterns. When a jet stream is known to cross over a cellular pattern from a poleward direction, it will be found above the dividing line between the open and closed cells.
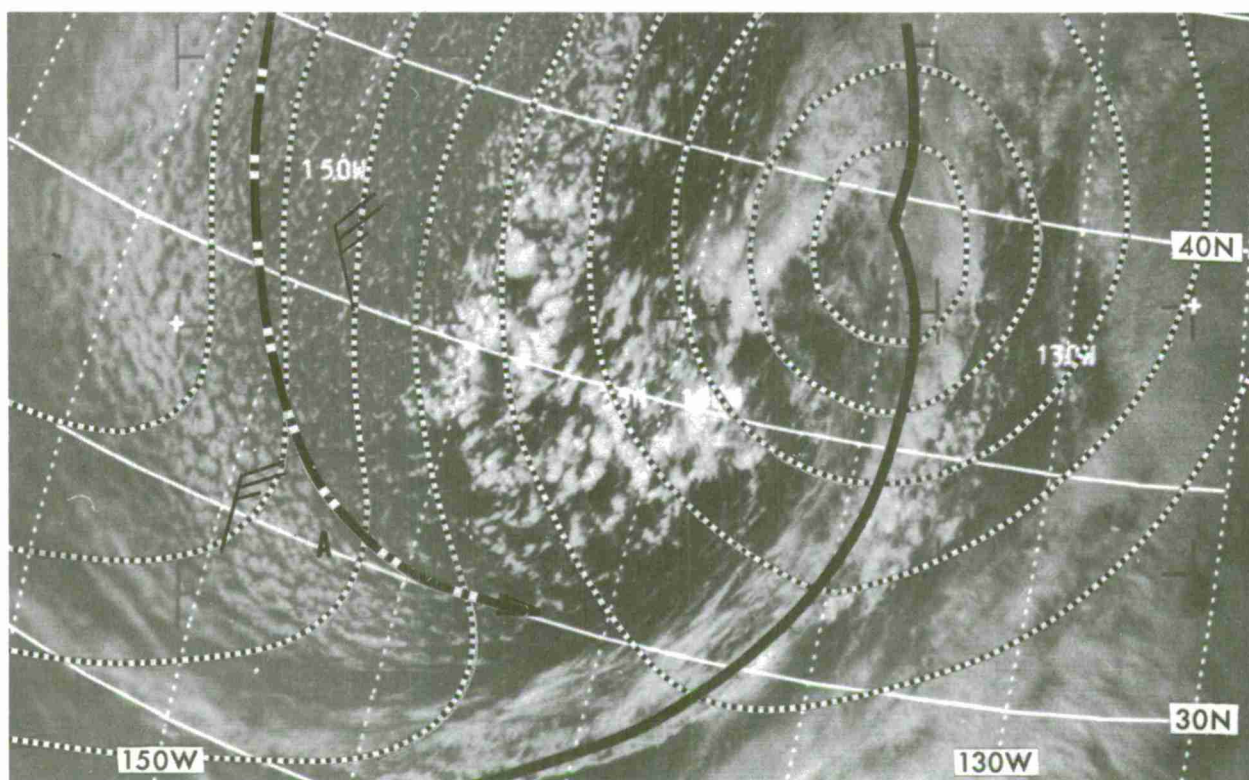
E-3 5092-3 2152Z 11 Nov 67   Analysis 0000Z 12 Nov 67

Figure 3-C-11. Surface isobars on the picture near A emphasize the change from cyclonic to anticyclonic curvature occurring where the closed cells end and the open cells begin. The plotted ship winds in the same region also show divergence in the low level wind pattern. A jet stream crosses over the cold air mass approximately over the transitional zone between the open and closed cells.

3-C-10

Cellular Clouds Over Land

Cellular cloud patterns are usually observed over water areas but, in certain instances, may be seen over land. As previously noted, a prerequisite for the formation of a cellular cloud pattern is a sufficiently warm surface temperature with respect to the air above the surface. Ideally, this condition occurs when cold air moves over a warmer water surface. However, formation of cellular cloud patterns can happen over land when the surface terrain is comprised of many lakes, viz., parts of Canada and Minnesota, or after very heavy rains that leave considerable amounts of standing water.
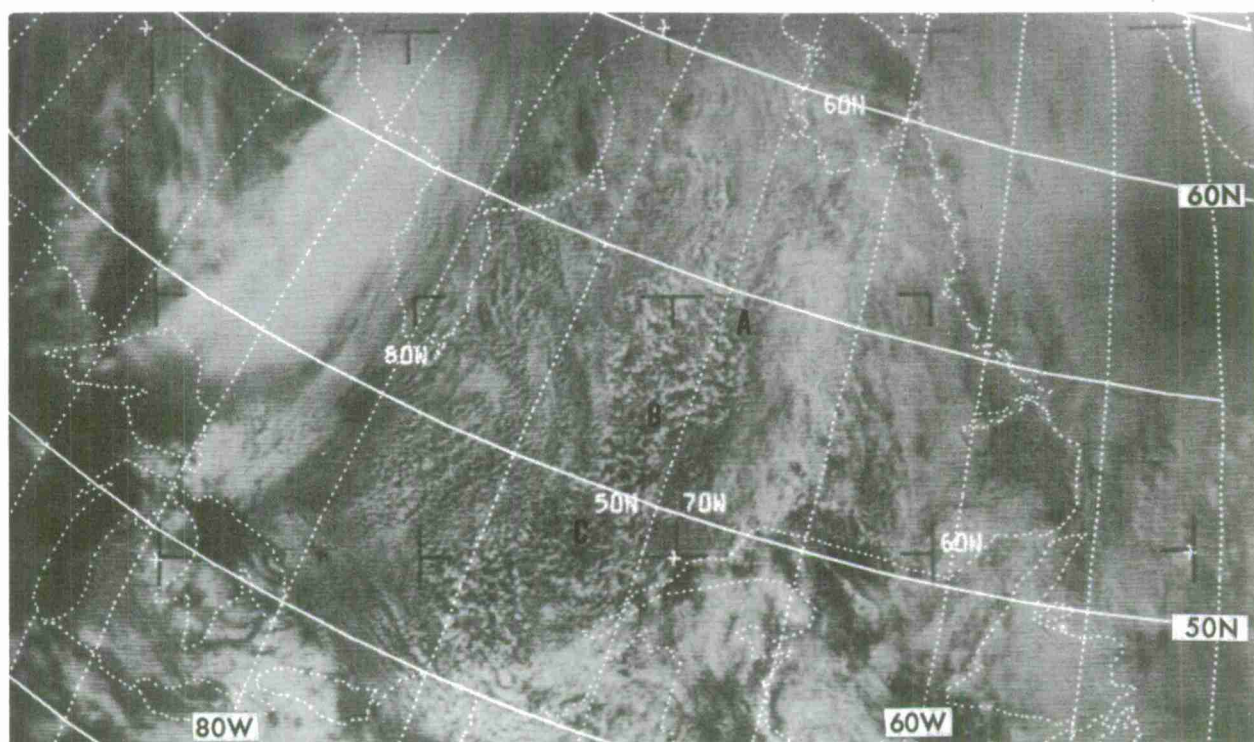


E-7 554-3 1835Z 29 Sep 68

Figure 3-C-12.  An open cellular cloud pattern is recognizable at A, B, and C over northeastern Canada. Colder air over the warmer water of the numerous lakes of this part of Canada has led to the formation of this cellular cloud pattern.

Chapter 3

SECTION D

JET STREAMS

<u>Introduction</u>

The location of the jet stream or maximum wind zone can be accurately po-
sitioned by examining the cloud patterns shown in satellite pictures.  Verti-
cal and horizontal motions in the upper troposphere in the vicinity of jet
streams have a very marked effect on the distribution of cirrus clouds in
their vicinity.  Because of this, it is possible to determine the location of
such wind maxima from cloud pictures taken by weather satellites.  Cirrus
clouds predominate on the equatorial side of the jet stream and in the anti-
cyclonically-turning portion of the jet.  The poleward boundary of the cirrus
is often very abrupt; it lies under or slightly equatorward from the jet axis,
and frequently casts a shadow on the lower clouds which is clearly visible in
satellite pictures.

Over the oceans, where the jet stream curves cyclonically, the differences
in stability on each side of the core are reflected in the appearance of the
clouds.  On the left side, looking downstream, cold temperatures and unstable
air occur resulting in great vertical development of the convective clouds in
the open cellular patterns.  On the right-hand side of the core, subsidence
and warmer air occur and subdued stratiform cloudiness appears in closed cel-
lular patterns.

The main jet-stream cloud features are long shadow lines, large cirrus
shields with sharp boundaries, long cirrus bands, cirrus streaks, and trans-
verse bands within cirrus cloud formations.  Once a jet stream has been iden-
tified on a cloud photograph, it is possible to deduce other meteorological
information, such as wind direction, wind shear, direction of horizontal tem-
perature gradient, and areas where clear air turbulence is possible.

## Cirrus Shields and Shadow Lines

The cloud pattern most frequently associated with the polar jet is the large, slightly anticyclonically-curved cirrus shield with a sharp poleward edge. These clouds usually are seen in the frontal zone east of an upper level trough and extend downwind to the upper level ridge where the upward motion usually ceases and downward motion begins. Where the curvature of the jet stream changes from anticyclonic to cyclonic, most of the cirrus dissipates. The small amount of cirrus that is advected over the ridgeline into the generally sinking zone to the rear of the downstream trough continues to thin out or evaporate so that it is infrequently visible on satellite pictures [1] [2] [3].
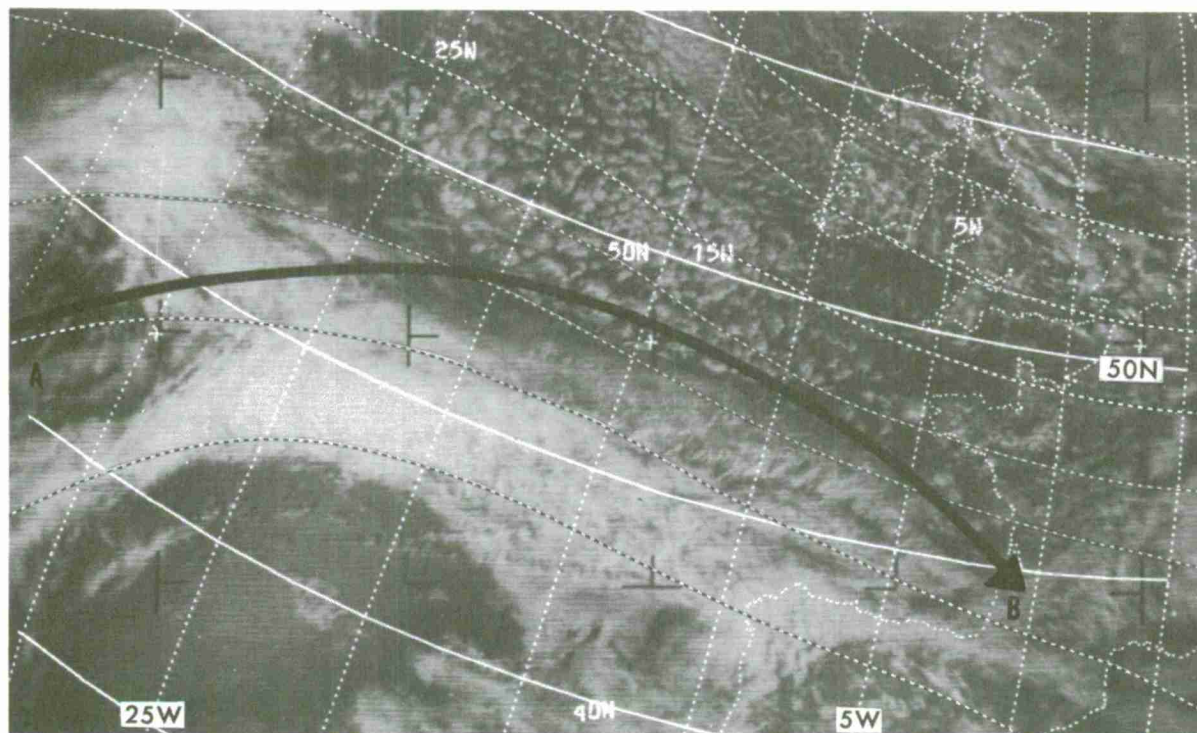


E-7 477-3 1500Z 23 Sep 68   200-mb Analysis 1200Z 23 Sep 68

Figure 3-D-1. A cirrus shield from A to B has an anticyclonically-curved edge and indicates the approximate location of a jet stream.

Jet-stream cirrus clouds are usually much higher than other widespread cloud patterns, thus the shadow they cast on lower clouds or surface features extends relatively far from the edge of the cloud. This shadow appears as a long, narrow, dark line with a slight anticyclonic turning. The polar jet will be located parallel to and within one degree of latitude poleward of the shadow.

The edge of a cirrus shield may also be located by examining the difference in texture and brightness of the clouds near the jet. Poleward from jet streams the clouds present a "lumpy" appearance, while on the equatorward side the clouds look much more even due to the smoothness of the cirrus which obscures details below it.
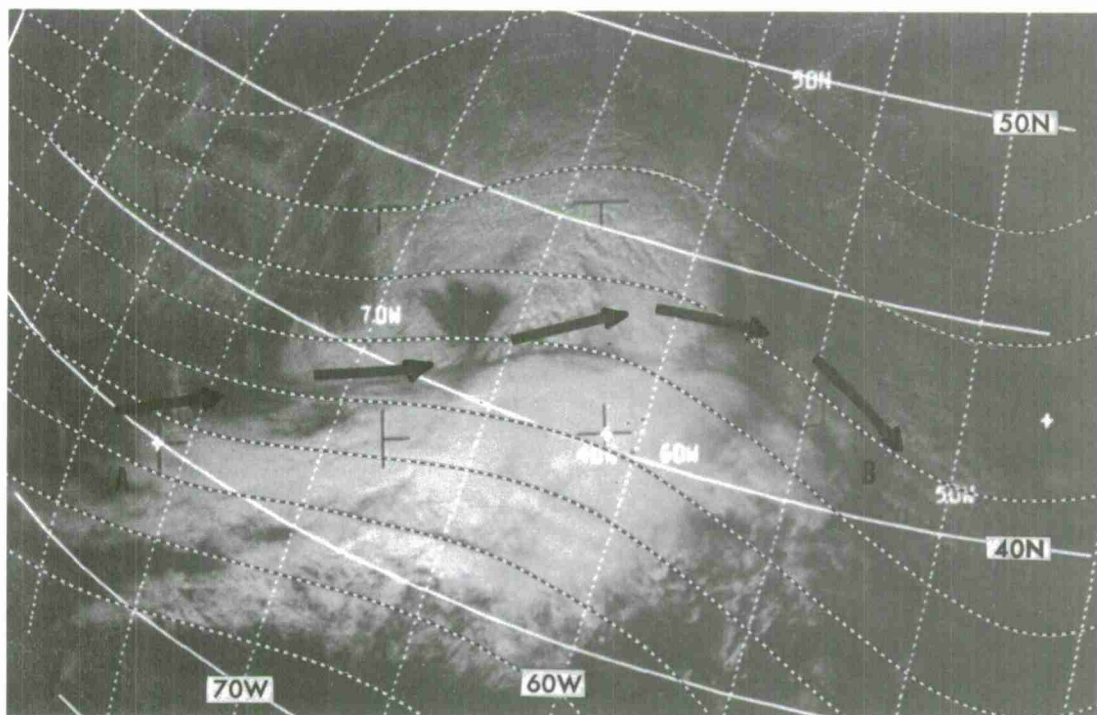


E-3 5805-2 1616Z 7 Jan 68   200-mb Analysis 1200Z 7 Jan 68

Figure 3-D-2. The anticyclonically-curved cirrus sheet from A to B ends near the jet axis and shows the higher cirrus casting shadows on the lower cloud deck. The cirrus shield is easily identified by its smooth appearance and is in contrast to the "lumpy" texture of the lower clouds north of the jet.

It is common to observe a widening of the frontal cloud band where a jet stream crosses an occluded front. Where the cirrus shield crosses a frontal band, the cirrus partly obscures from view the top of the frontal altostratus. Poleward from the jet, the top of the unobscured altostratus will appear very "lumpy" due to the convective cells extending up from the altostratus. To the south of the jet axis, highlights and shadows of the convective clouds will be obscured by the cirrus shield, thereby causing the sharp change in texture seen in the pictures.

When a surface wave develops on a front, the rear edge of the frontal cloud band becomes anticyclonically curved and bulges back toward the cold air. Jet-associated cirrus is often seen over this formation.
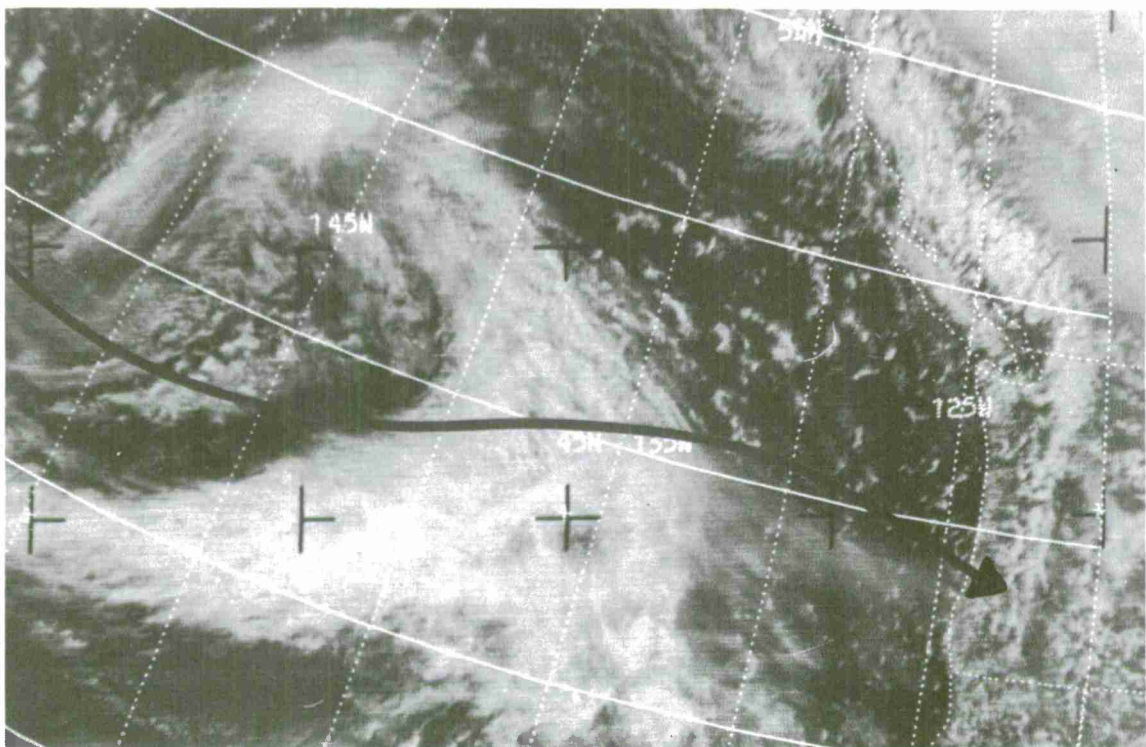


E-9 719-4 2246Z 24 Apr 69   200-mb Analysis 0000Z 25 Apr 69

Figure 3-D-3. The northern edge of an extensive, anticyclonically-curved cirrus sheet from A to B to C defines the position of the jet stream. The smooth texture of the cirrus south of the jet stream is evident when compared to the "lumpy" texture of the middle clouds of the frontal band north of the jet. Notice the increase in width of the cloud band where the jet crosses the front.

Jet-stream cirrus is usually observed in the upper-level ridge area. The poleward edge of the cirrus shield ends in a line parallel to the jet axis. Lines in the jet cirrus tend to have a slightly greater amplitude than the contour pattern at any one level. They often cross the contours toward lower height values between the trough and downstream ridge and toward higher values between the ridge and downstream trough.

A comparison of jet-stream cloud patterns and reported winds shows the poleward edge of the cirrus shield and the shadow it casts are usually nearly parallel to the wind [5] [23]. Small contour-crossing angles, on the order of 30 degrees, are often observed in the vicinity of troughs and ridges. Wherever the winds along the jet are accelerating, some cross-contour flow should be expected.
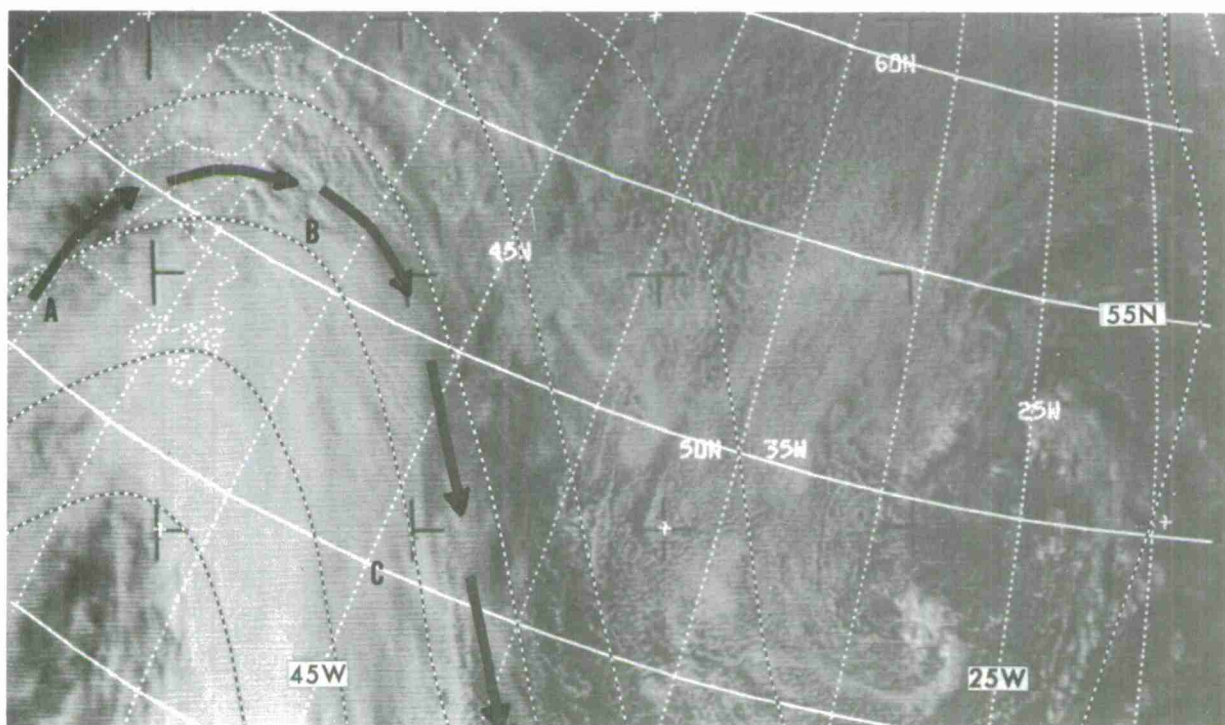


E-7 891-3 1628Z 26 Oct 68   200-mb Analysis 1200Z 26 Oct 68

Figure 3-D-4. The cirrus shield and its shadow from A to B to C illustrate both the anticyclonically-curved edge and the change in cloud texture to the south. Notice some cross-contour flow toward lower height values near the ridge.

## Cirrus Streaks

Long narrow streaks of cirrus are frequently seen with jet streams that do
not have extensive cloud shields.  The lack of underlying clouds make these
streaks easy to see.  The streaks are observed to be nearly parallel to the
winds and equatorward of the jet.  Lack of continuity of these streaks makes
accurate location of the jet more difficult.  The orientation of these streaks
may be used as a good indicator of the direction of the upper level flow.
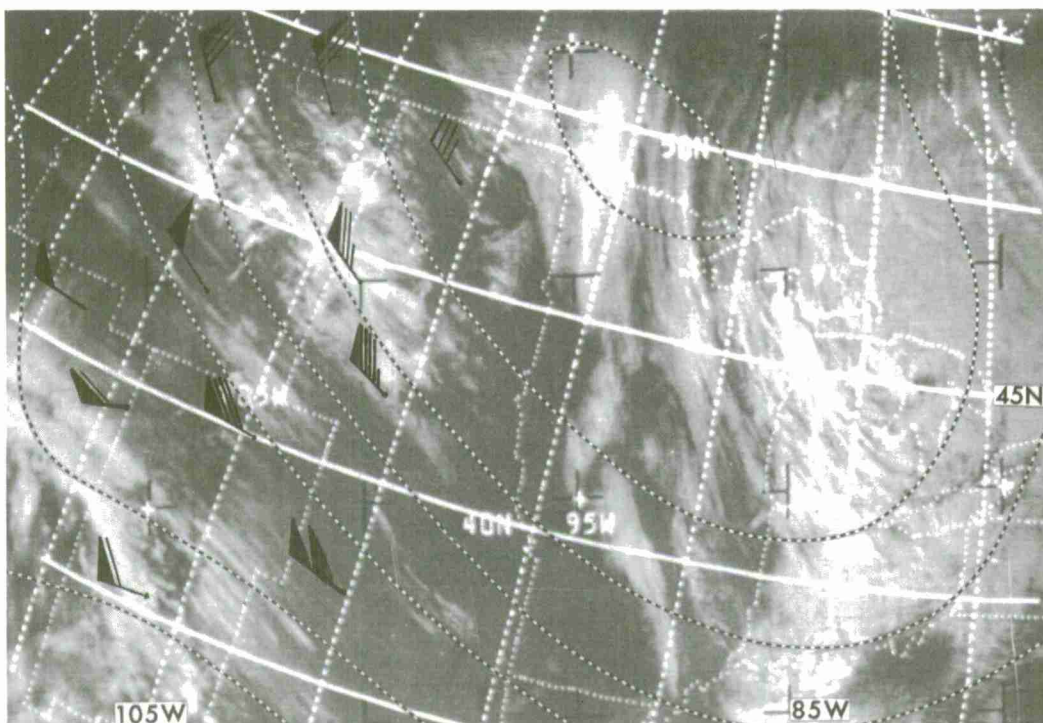


E-3 406-3 1955Z 3 Nov 66   200-mb Analysis 0000Z 4 Nov 66

Figure 3-D-5.  The long straight cirrus streaks west of 100W ac-
company a strong northwesterly flow over the mountains at the cirrus
level.  These streaks are easy to detect where they are not over some
underlying clouds or snow of similar brightness.  The cloud lines
just west of the Great Lakes are associated with the cyclonic flow
at lower levels.

Transverse Lines (Cloud Trails)

        Transverse lines are often observed in jet-stream cirrus.  These cloud
patterns appear as small-scale lines at an angle almost perpendicular to the
main jet, or maximum wind flow.  These lines look somewhat like waves but are
much more irregular than mountain waves and are observed over oceans as well
as over land.  Studies of these wavelike lines, made with the help of motion
pictures from the Applications Technology Satellites (ATS 1 and ATS 3), sug-
gest that most of these lines are the result of horizontal, and possibly ver-
tical, shear.  These lines are now being called CLOUD TRAILS.  Due to the ef-
fects of shear, it is common for the ends of the lines farthest from the jet
stream to curve upwind.  The lines are oriented between 50 and 90 degrees to
the wind direction.  Cloud trails are usually associated with wind speeds of
80 knots or higher.

        Some evidence has been collected showing that this type of cirrus may be
more turbulent than the smoother-looking cirrus shields.  Detailed examination
of these trails shows strong anticyclonic shear through most of the cloud line
with the strongest winds along the poleward edge of the clouds.  Severe and
extreme turbulence has been reported more frequently in cases associated with
transverse lines than in cases where this feature was not observed [5].
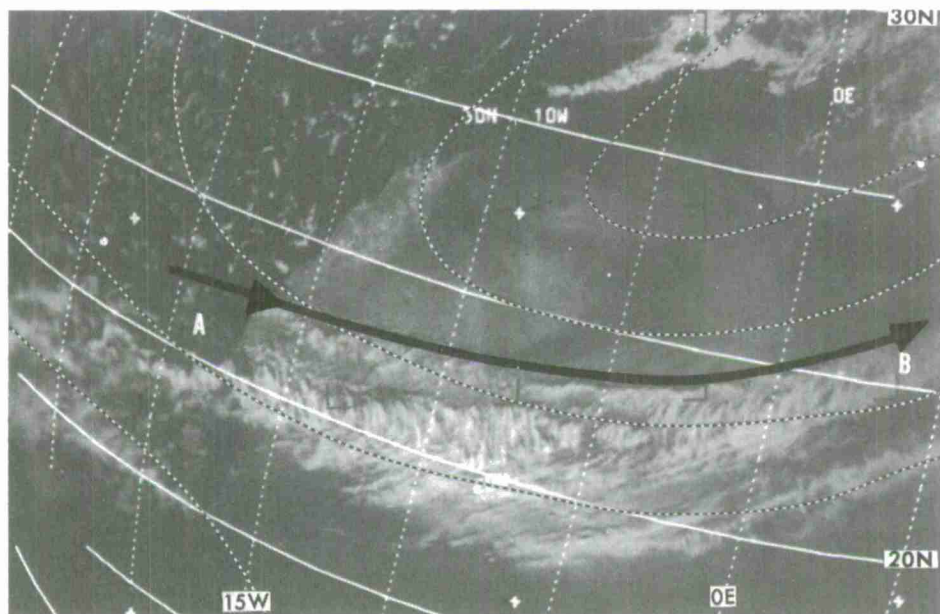


E-3 5728-3 1304Z 1 Jan 68   200-mb Analysis 1200Z 1 Jan 68

        Figure 3-D-6.  Transverse lines in jet-stream cirrus are seen over
Africa where lower clouds are absent.  The southern edge of the lines
trails off to the west due to slower wind speeds farther away from the
jet core.

## Cellular Cloud Patterns

When a jet stream crosses over an area of open and closed cellular clouds from a poleward direction, the jet axis is located at the boundary between the open and closed cellular patterns.
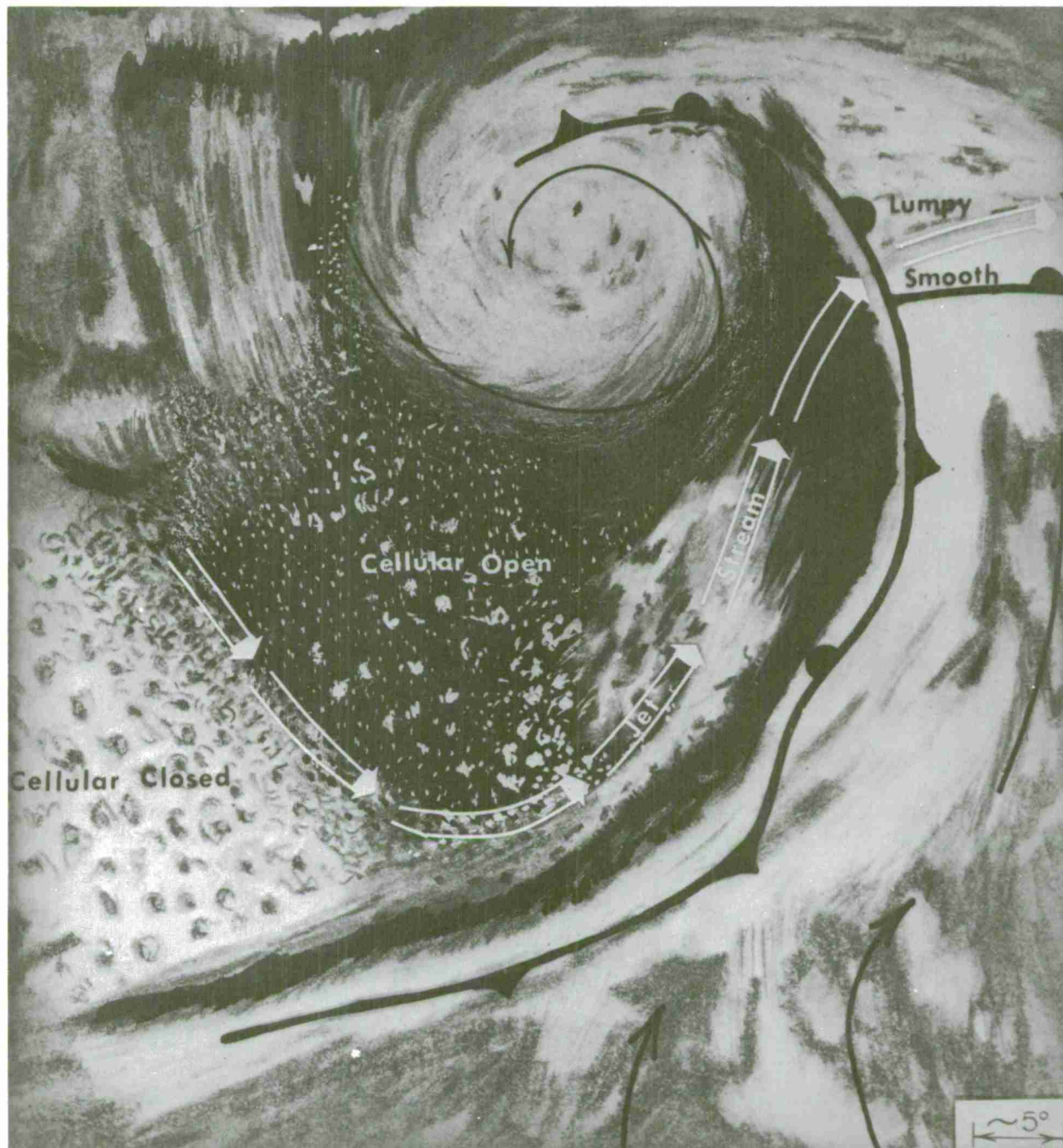


Figure 3-D-7.  An idealized illustration showing a jet stream over the dividing line between open and closed cellular clouds.  The jet stream east of the upper air trough is shown crossing over an occluded front.
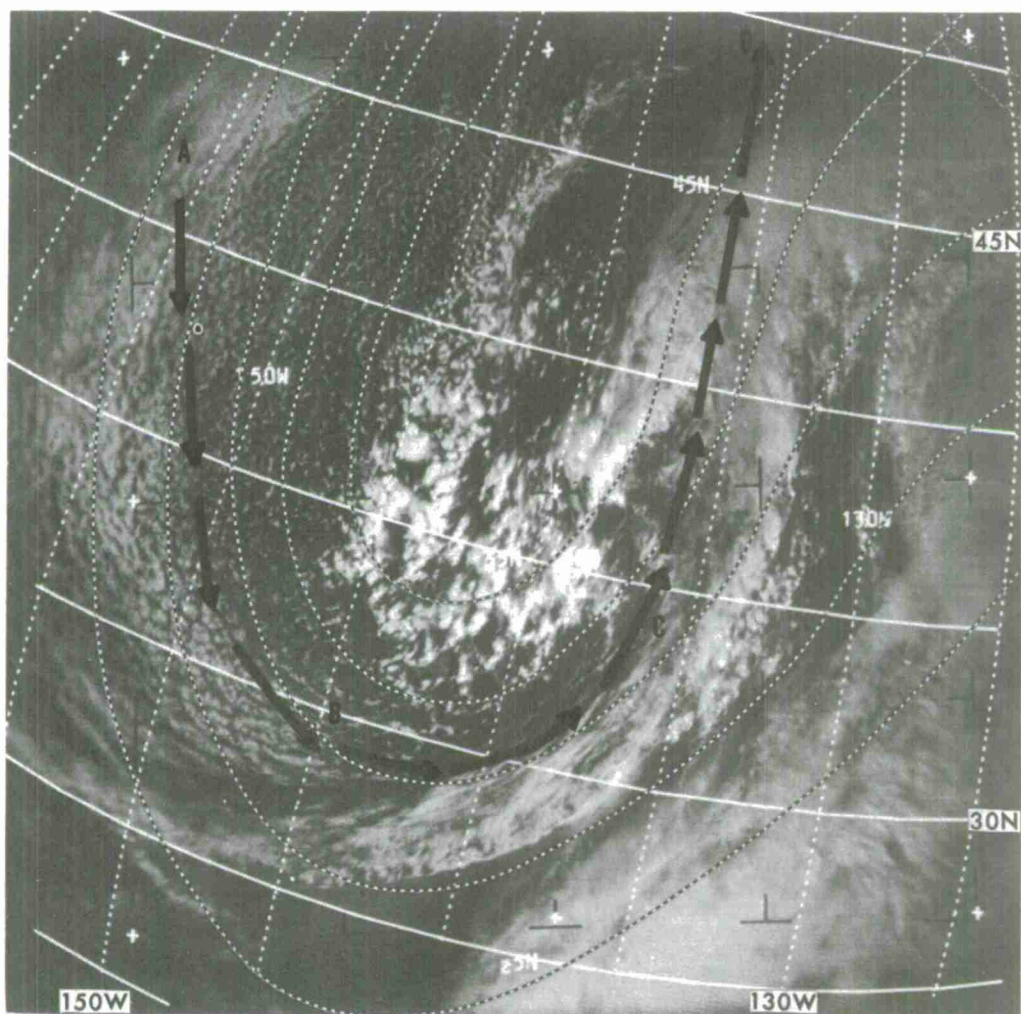
E-3 5092-3 2152Z 11 Nov 67   200-mb Analysis 0000Z 12 Nov 67

Figure 3-D-8.  A jet stream from A to D is located along
the transition zone from A to B between open and closed cumu-
lus cells.  The cirrus from C to D positions the jet stream
east of the trough line.

Non-Jet Stream Cloud Patterns

There are two cloud patterns that are seen in satellite photographs that
are not directly associated with jet streams but give the impression of being
jet-related.  In the first case, a frontal band may have a sharp, distinct,
trailing edge that gives the impression of being the poleward edge of a polar
jet.  A misinterpretation of this type may be avoided by remembering that the
polar jet-stream cirrus is usually straight or anticyclonically-curved while
frontal bands normally show cyclonic curvature.  In the second case, a cirrus
cloud edge, similar to the cirrus sheet seen with jet streams, is observed in
an area where the winds are very light.  In this instance, the clouds are as-
sociated with the poleward section of a cut-off low and the winds along the
cirrus edge are light.
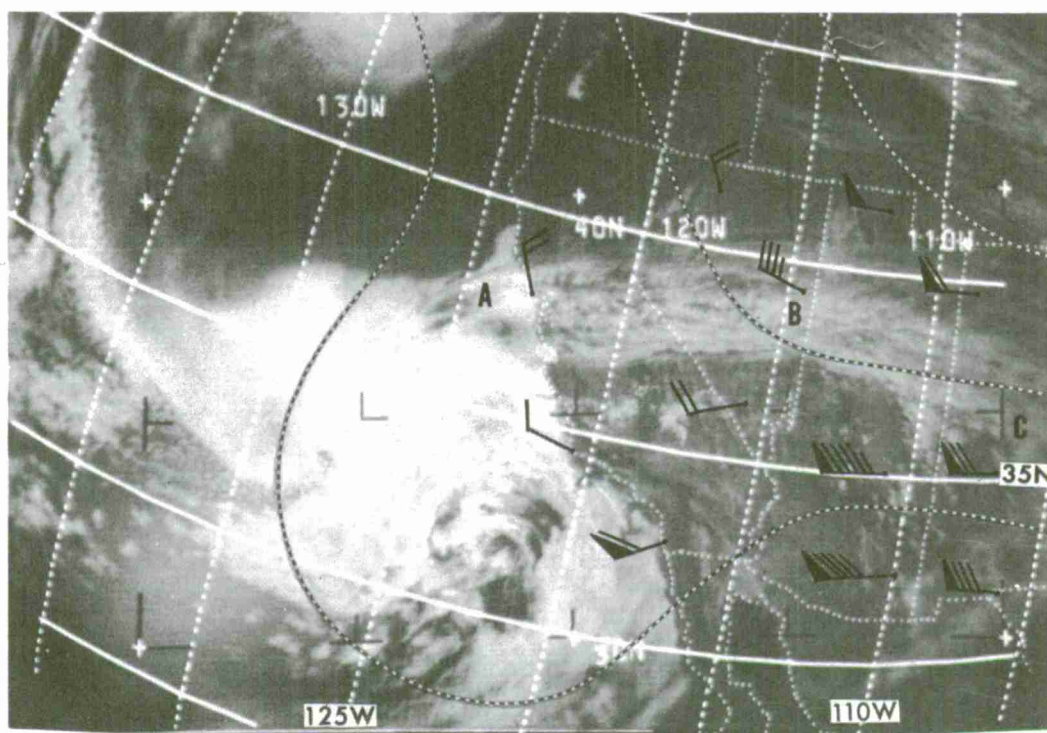


E-3 407-3 2150Z 3 Nov 66   200-mb Analysis 0000Z 4 Nov 66

Figure 3-D-9.  Cirriform streaks from A to B extend from a cut-
off low and give the impression of jet-stream cirrus.  The upper
level winds in this case are light.  The winds do increase from B
to C and, east of C are associated with a jet stream.

## Cirrus Bands in Cyclonically-Curved Flow

Cirrus is not often seen along the cyclonically-curved portion of the jet stream (58). Usually jet-stream cirrus dissipates in the sinking air between a ridge and the next trough downstream. If cirrus is present, sun angle, camera resolution, and the amount of cirrus determine whether or not the cirrus is detectable visible data.
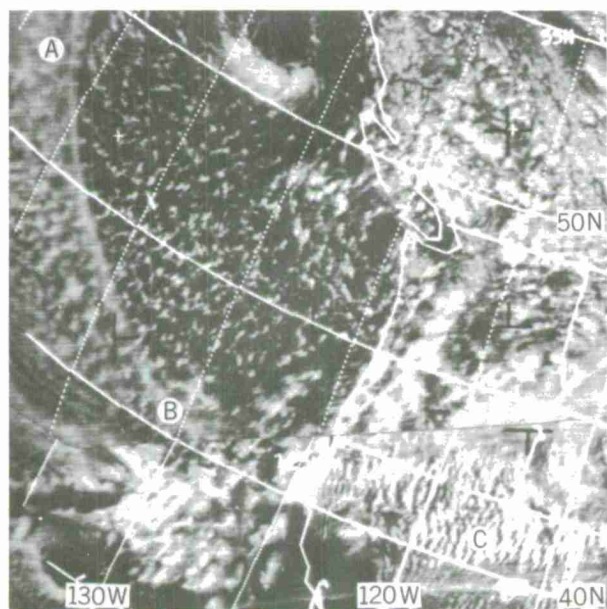


E-9 5290-3, 4 2130 GMT 25 April 1970

Figure 3-D-10. An extensive sheet of thin cirrus, associated with the cyclonically-curved portion of the polar jet stream, extends from A to B. The large area of mountain wave clouds at C is further evidence of this belt of strong winds. The difference in cellular cloud type across the jet axis west of B is less than usual. The normal pattern of open cells poleward of the jet and closed cells equatorward appears between B and the coast.
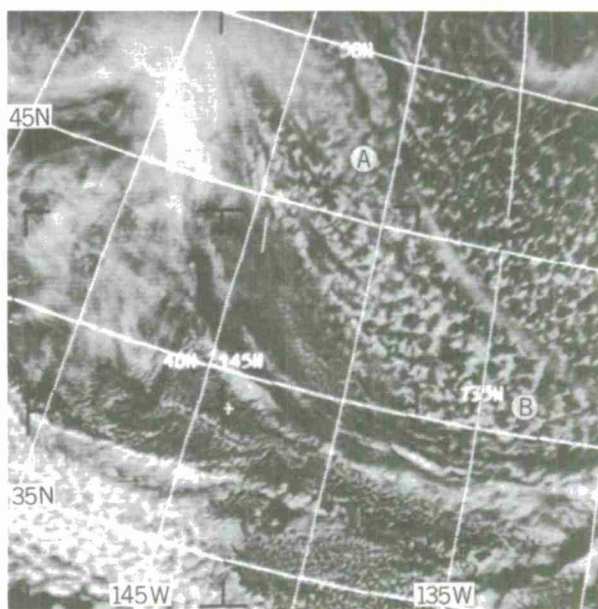
E-9 5291-4 2330 GMT 25 April 1970

Figure 3-D-11. Cirrus associated with the jet stream extends from A to B. This photograph is approximately two hours later than Figure 3-D-10 and illustrates the rapid dissipation of the cirrus during the 2-hour period.
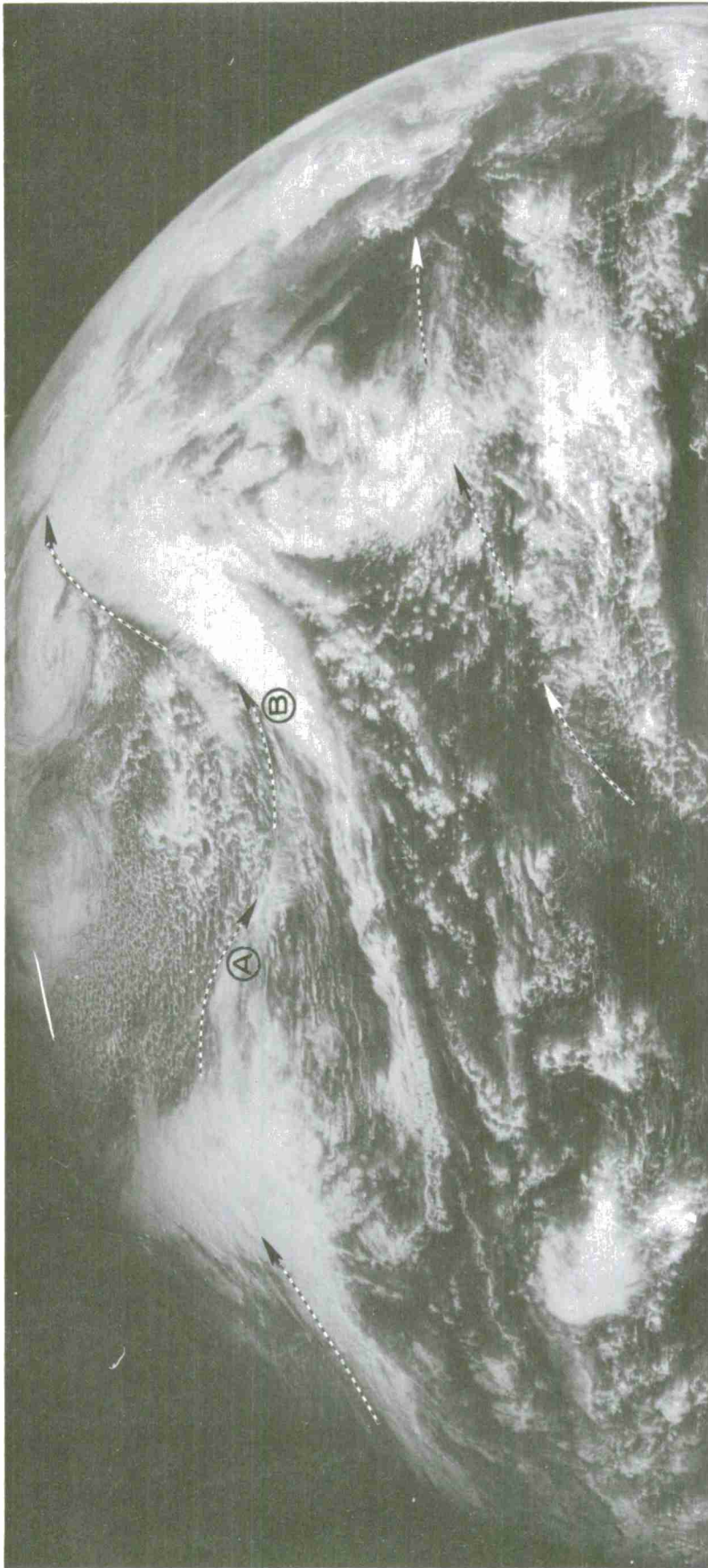
ATS-1 2043 GMT January 22, 1970. 200-mb Jet Superimposed.

Figure 3-D-12. Cyclonically curved cirrus associated with the polar jet stream is seen between A and B. It is unusual to observe as much cirrus through the trough as is visible here. An ill-defined subtropical jet stream to the south is weak so the cirrus associated with it has no sharply defined northern edge.

Chapter 3

SECTION E

UPPER LEVEL TROUGHS

Introduction

The location of upper level troughs is one of the techniques of satellite
meteorology readily applied to conventional synoptic analysis.  The change in
sign of the vertical motion and the change in the wind direction at the trough-
line are reflected in a number of differing cloud patterns which aid in locat-
ing the upper trough.  Cloud patterns used to position troughs include en-
hanced cumulus, comma-shaped clouds, breaks in frontal bands, and cirrus
trails.  Frequently, more than one point can be located on the same trough
which will allow the analyst to extrapolate between the points and deduce the
orientation and location of the entire troughline [1] [2] [22].

## Locating Troughs from Frontal Bands

The upper level trough can frequently be located where a frontal band and the trough intersect. At this point of intersection the clouds along the front will lessen or disappear where the mid-tropospheric vertical motion changes from upward to downward at the troughline. The trough crosses at the point where the cloud band either ends abruptly, forks with changes in character, or changes character from solid to breaks and holes.
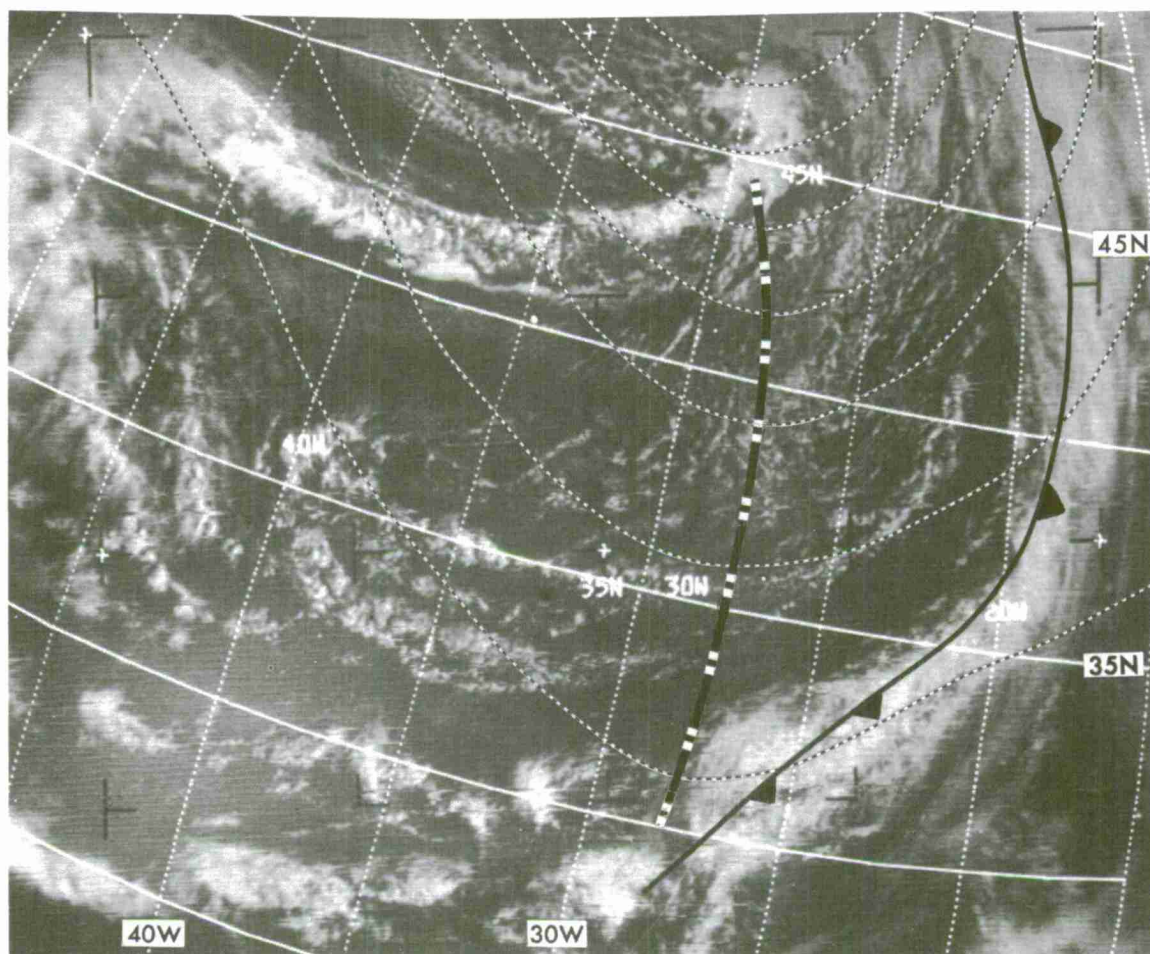


E-7 603-4 1625Z 3 Oct 68
500-mb Analysis 1200Z 3 Oct 68
Front 1800Z 3 Oct 68

Figure 3-E-1. A solid band of clouds, representing a cold front, becomes fragmented west of 27W. The 500-mb trough is located at this point.
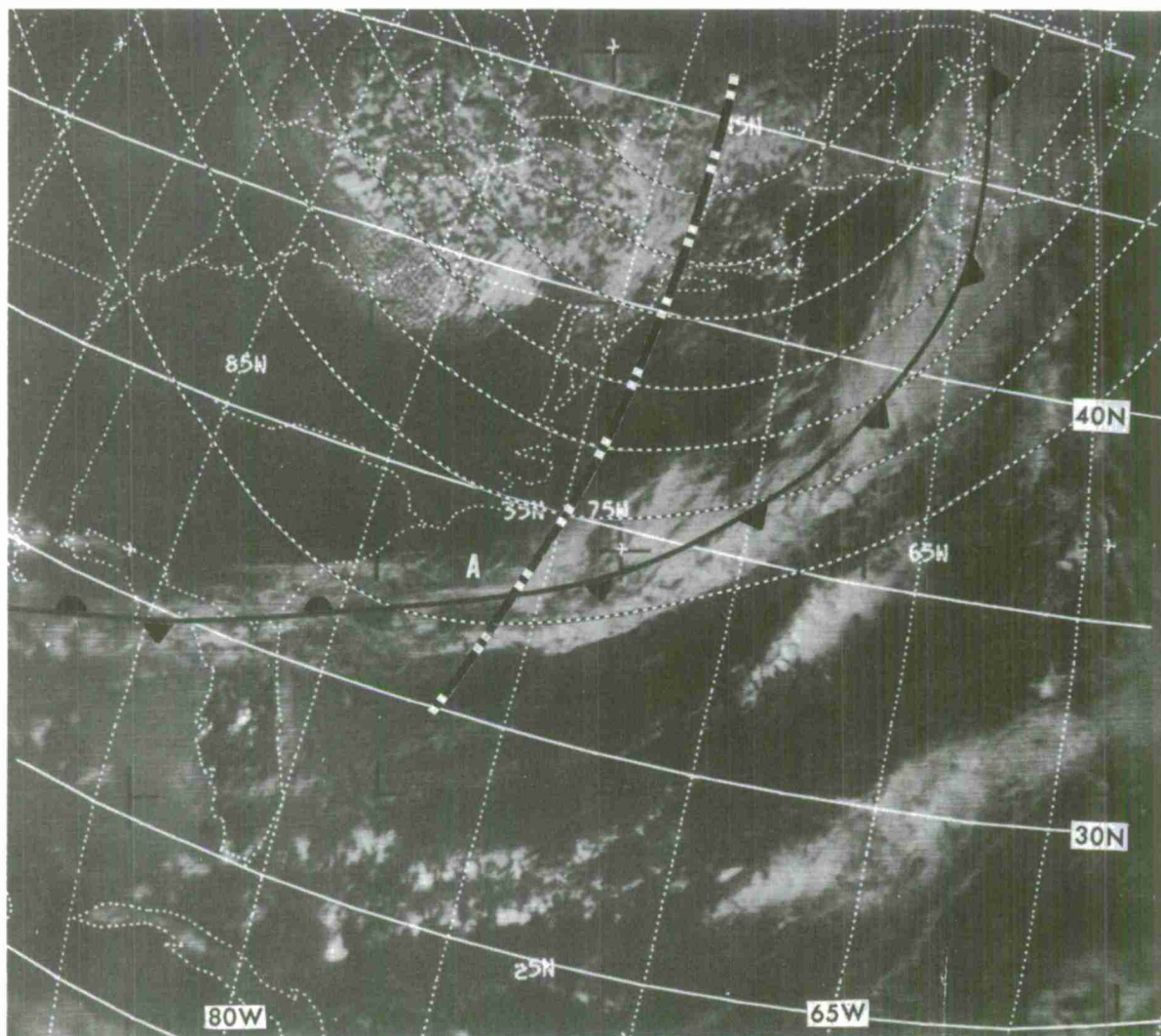
E-7 617-4 1914Z 4 Oct 68
500-mb Analysis 0000Z 5 Oct 68
Front 1800Z 4 Oct 68

Figure 3-E-2.  The middle and high clouds in the frontal band off
the east coast of North America show the first signs of dissipating at
point A.  At picture time the trough was located just west of A where
the change in cloud character begins.

## Locating Troughs from Vorticity Maxima

As discussed in Section A (VORTICITY AND VORTICES) of this chapter, areas of positive vorticity advection are reflected in the appearance of the cellular clouds to the rear of cold fronts. The upward motion produces areas of enhanced cumulus which form comma-shaped cloud masses. A secondary trough in the broad cyclonic flow can be located along the rear or trailing edge of the enhanced cumulus or comma-shaped cloud.
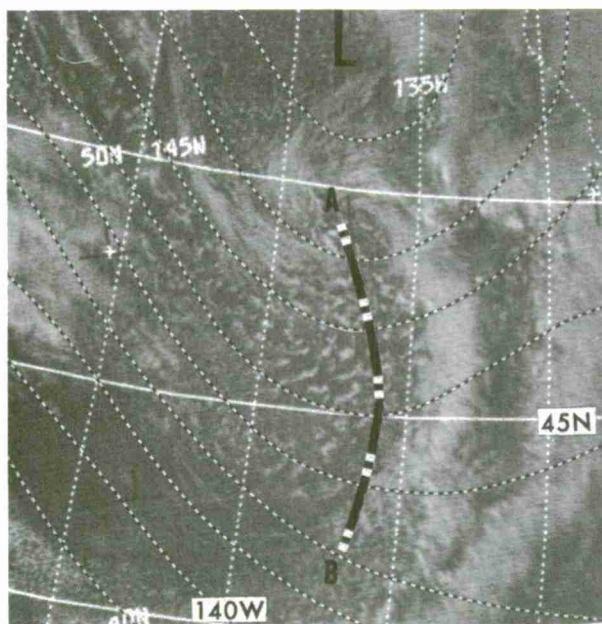


E-7 732-3 2343Z 13 Oct 68
500-mb Analysis 0000Z 14 Oct 68

Figure 3-E-3. A comma-shaped cloud associated with a short wave trough is just off the west coast of the US. Points A and B along the rear edge of the comma cloud give two points on the short wave 500-mb trough.
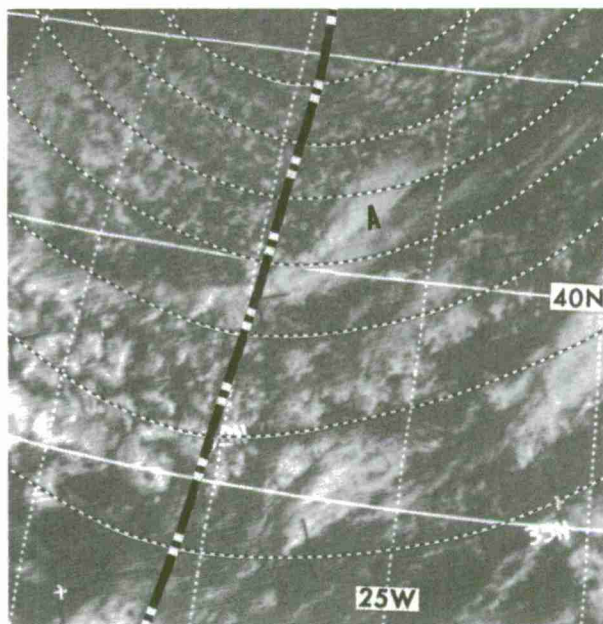


E-7 803-4 1544Z 19 Oct 68
500-mb Analysis 1200Z 19 Oct 68

Figure 3-E-4. The upwind edge of the mass of cumulus activity at A closely approximates the short wave 500-mb trough moving around a huge low in the Atlantic.

## Locating Troughs from Cirrus Clouds

The positioning of upper troughs, primarily at 200 mb, can be accomplished by determining the wind direction from cirrus plumes (see Chapter 4). The wind directions obtained by this method will be used in much the same way conventional winds are used in analyzing and locating the trough.
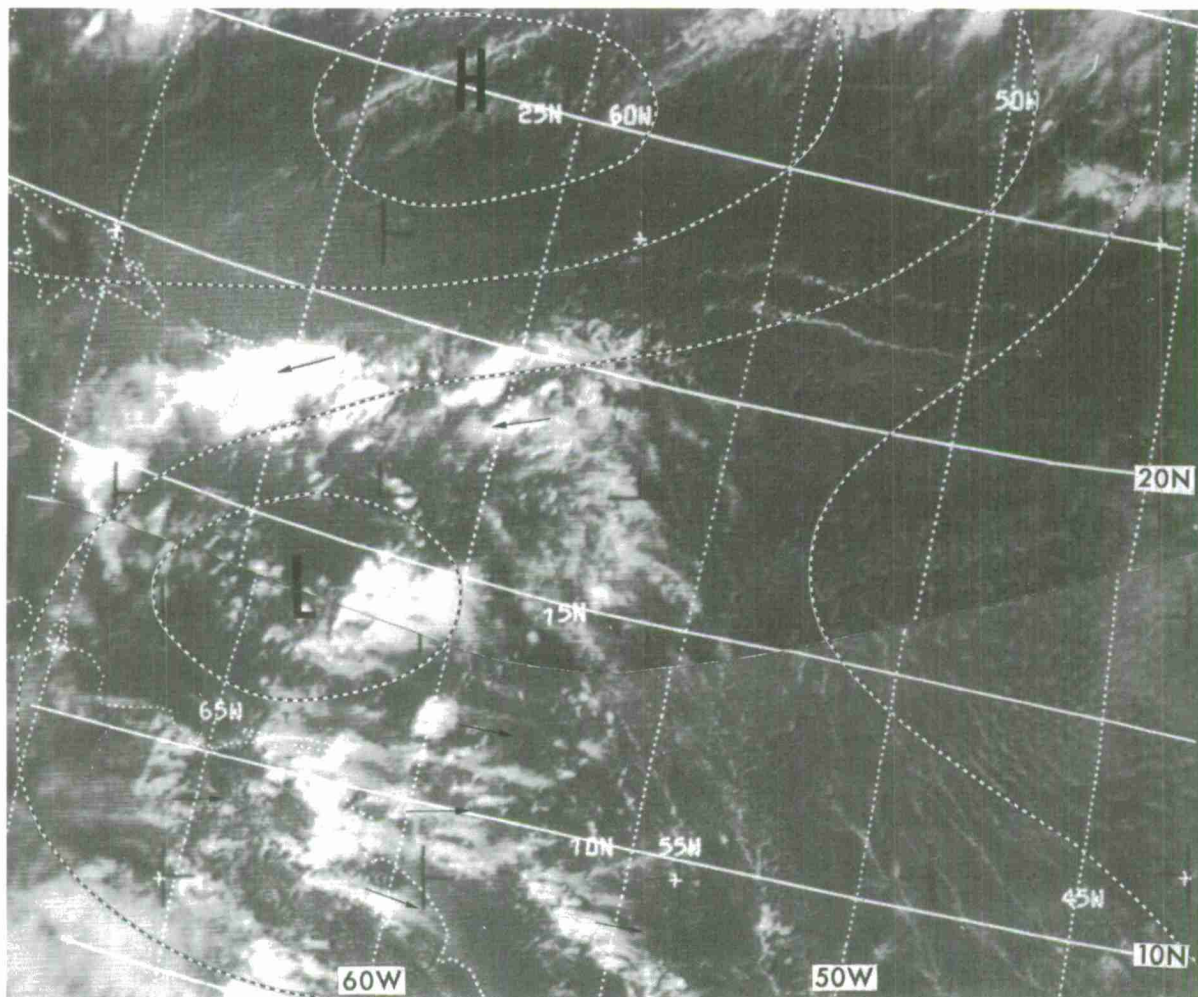


E-7 554-5,6 1821Z 29 Sep 68   200-mb Analysis 0000Z 30 Sep 68

Figure 3-E-5. Wind directions derived from cirrus plumes, represented by arrows on the satellite photographs above, show an easterly flow north of 15N and a westerly flow south of 15N. The troughline can be accurately positioned using these wind directions in conjunction with available conventional data.

## Locating Troughs from Major Cloud Masses

There are many instances where large masses of middle or high clouds occur in the broad field of upward vertical motion between an upper trough and down-stream ridge. Clear skies or low clouds are found to the rear of the trough where the air is sinking. The troughline can be located at or a few degrees behind the rearward edge of the middle or upper clouds.
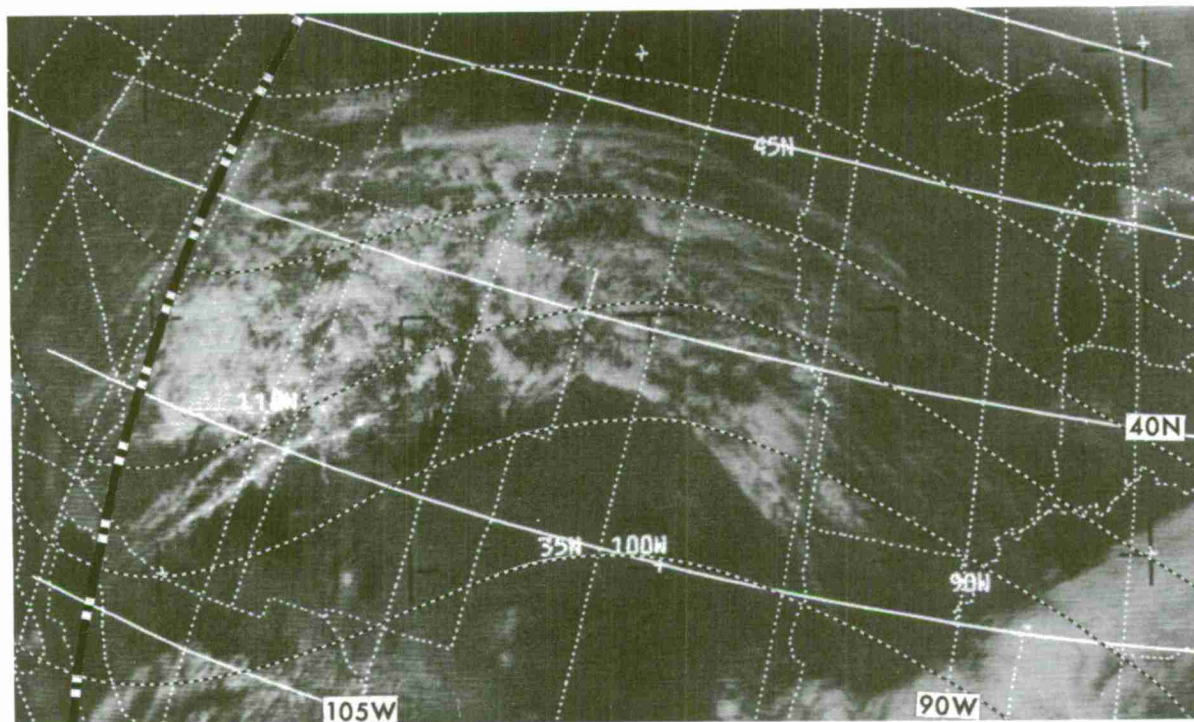


E-7 693-4 2054Z 10 Oct 68   500-mb Analysis 0000Z 11 Oct 68

Figure 3-E-6. A trough, oriented in a north-south direction along 115W, can be positioned along the rearward boundary of a mass of middle and high clouds in an area of upward motion over the western United States.
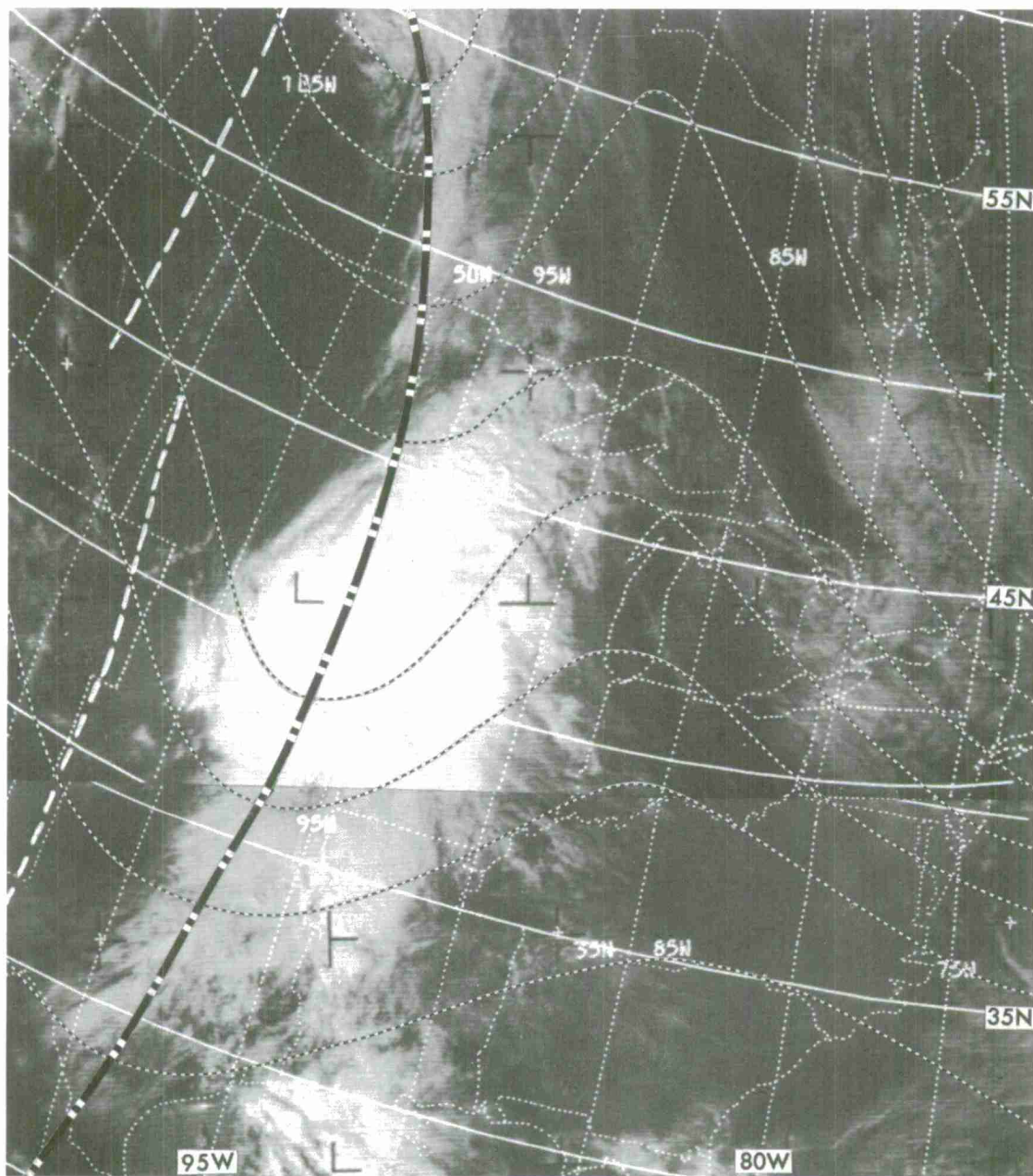
E-7 630-4 2009Z 5 Oct 68   500-mb Analysis 0000Z 6 Oct 68

Figure 3-E-7.  The western edge of a large mass of multilayered clouds
over the central United States conforms well to a rapidly moving upper
level trough.  Further north, the cloud mass is not as intense but still
can be used to locate the troughline.  The dashed line to the west of the
cloud mass was the position of the trough at 1200Z 5 Oct 68.
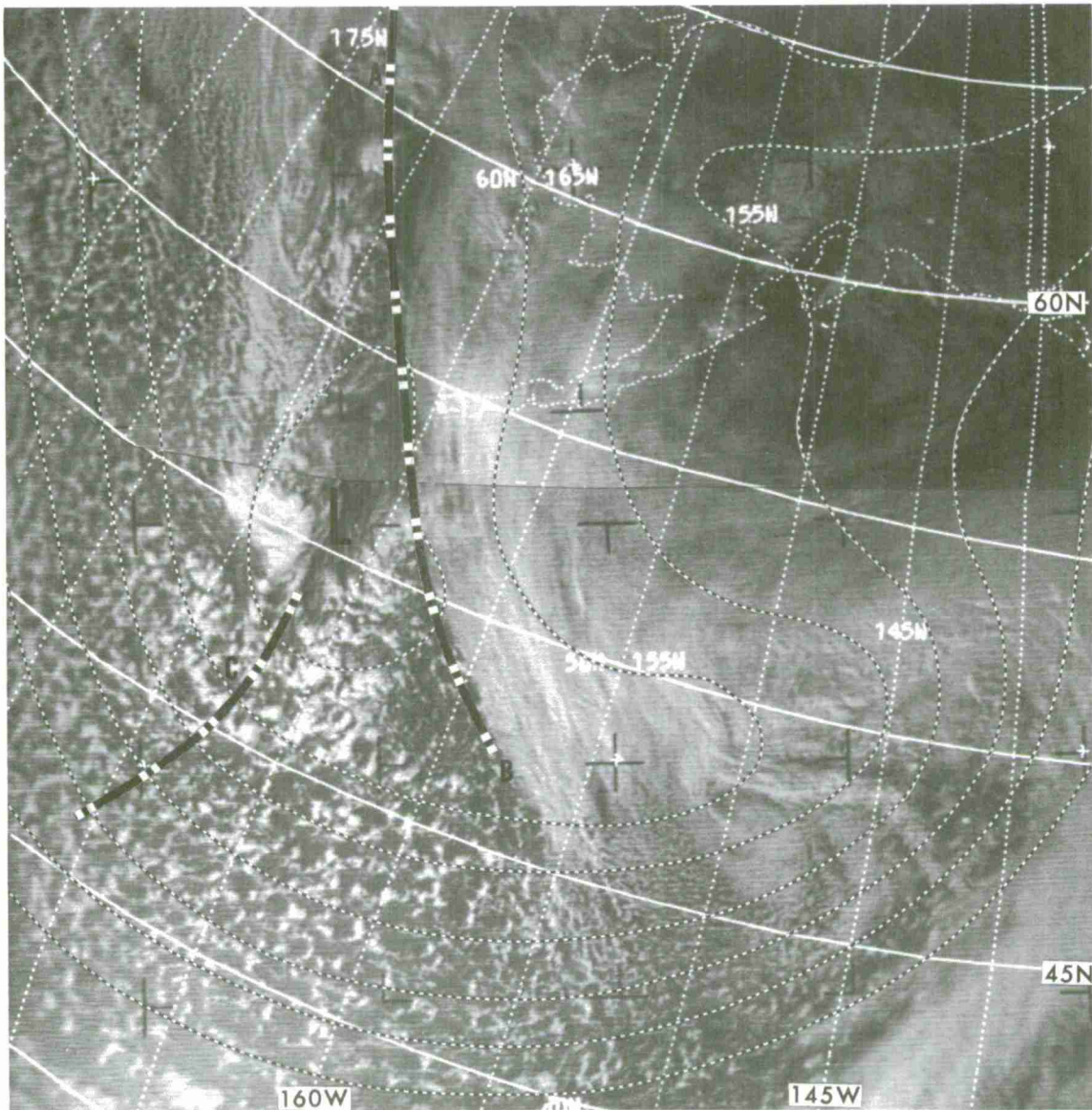
E-7 845-3 0018Z 23 Oct 68   500-mb Analysis 0000Z 23 Oct 68

Figure 3-E-8.   The mass of high and middle clouds east of A-B suggests
a southerly flow in advance of a trough located just west of the clouds.
West of A-B, open cellular cumulus identifies a deep northwesterly flow of
unstable air.   An area of enhanced cumulus at C is indicative of a short
wave trough in the broad cyclonic flow.

Troughs in the mid-Pacific are often difficult to position due to the
sparsity of data.  Easterly winds that occur on the northern side of these
troughs often go unnoticed in the broad expanse of west winds.  Small closed
circulations at high levels are often associated with the trough and may be
reflected in the clouds as vortices or areas of cumulonimbus activity.  As the
trough extends into the tropical areas, a wide band of clouds often develops
in the westerly flow ahead of the trough.  The vortices and the wide band of
clouds extending out of the tropics toward the northeast are indicators of an
upper level trough.



E-7 694-4; 695-4; 696-5 2250Z, 0040Z, 0236Z 10-11 Oct 68
500-mb Analysis 0000Z 11 Oct 68

Figure 3-E-9.  A mid-Pacific trough is shown south of the main belt of
westerlies located over small tropical and subtropical disturbances.  The
trough will be located at or slightly north of the clouds extending out of
the tropics toward the northeast.
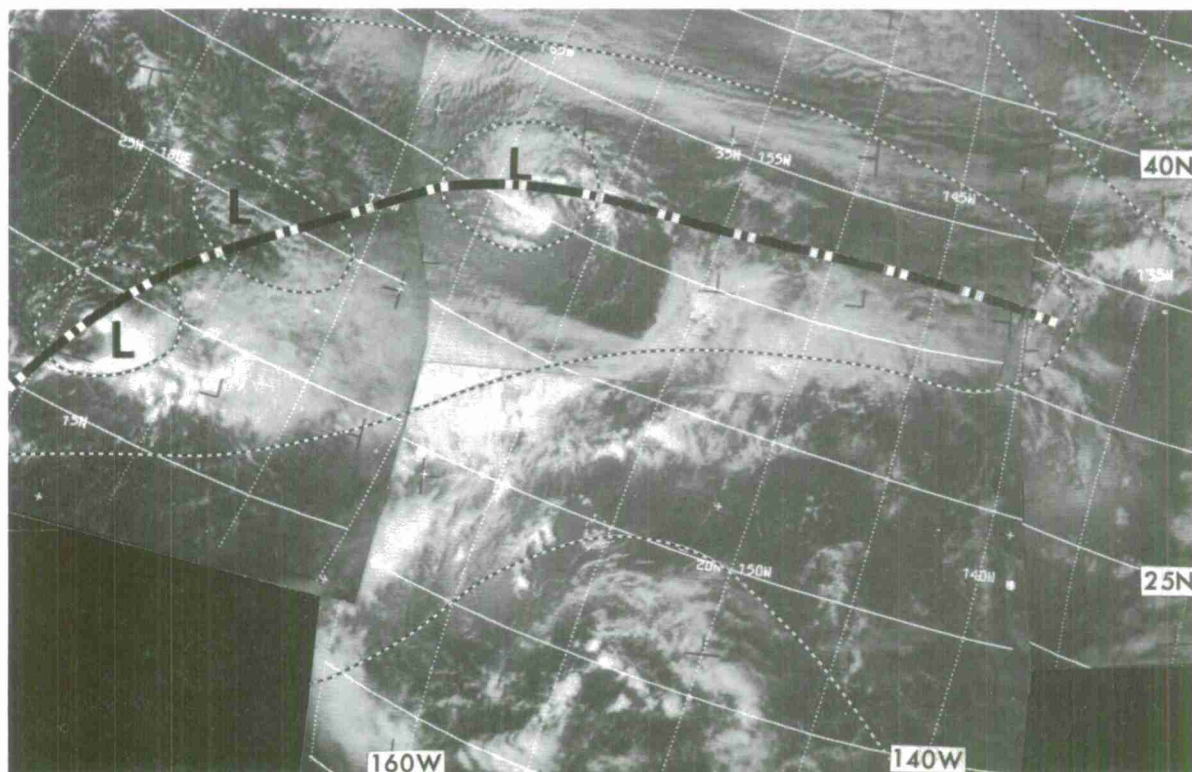
Chapter 3

SECTION F

UPPER LEVEL RIDGES

## Introduction

The cloud distribution seen in satellite photographs makes possible a very
accurate positioning of upper level ridgelines.  The distribution of middle
and high clouds is the main tool used to locate and orient upper ridges.  Up-
per ridges can be categorized into three main groups consisting of sharp,
medium and broad ridges, plus a number of special cases.  A measure of the
amplitude or sharpness of the ridge can often be determined from the width of
the cloud pattern and from the characteristics of its leading edge.  The ef-
fect of moisture variations over continents may cause these cloud patterns to
appear different over land than over water.  After an upper level ridgeline is
located, the upper level wind direction can be determined [1] [2] [3].

## Sharp Ridges

The cloud band associated with a sharp ridge will be relatively narrow due to the close spacing of the trough and ridge which results in a narrow area of upward vertical motion. The middle and high clouds along the leading edge of the cloud band will end abruptly due to a rapid change from upward motion to downward motion at the ridgeline.

Sharp ridgelines are normally found at the leading edge of the cloud band, and under certain circumstances are ahead of the leading edge by several degrees. Clouds will rarely be found downwind of a sharp ridgeline due to the downward vertical motion beyond the ridgeline.
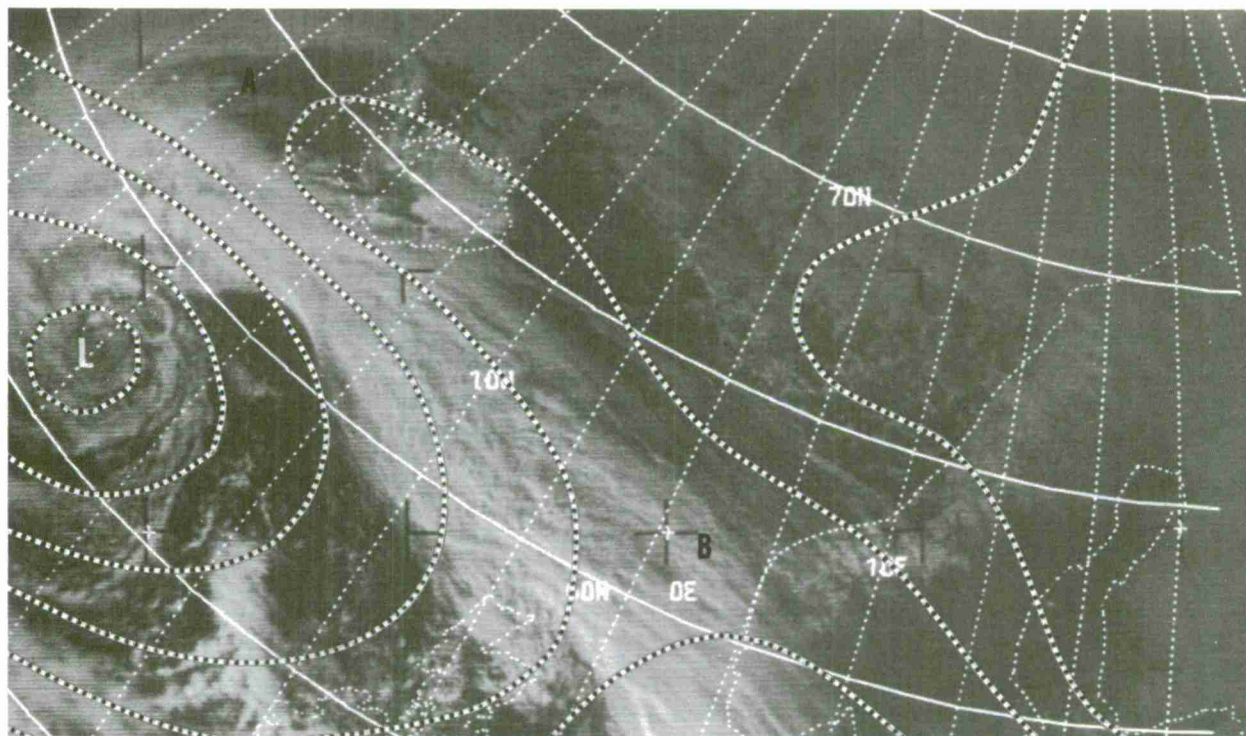


E-7 689-2 1323Z 10 Oct 68   500-mb Analysis 1200Z 10 Oct 68

Figure 3-F-1. A relatively narrow cloud band over the north Atlantic, from A to B, is representative of a sharp ridgeline. In this example, the ridgeline is positioned where the clouds terminate along the leading edge of the cloud band. South of B the clouds appear to be higher and spill over the ridgeline as the amplitude of the ridge decreases.
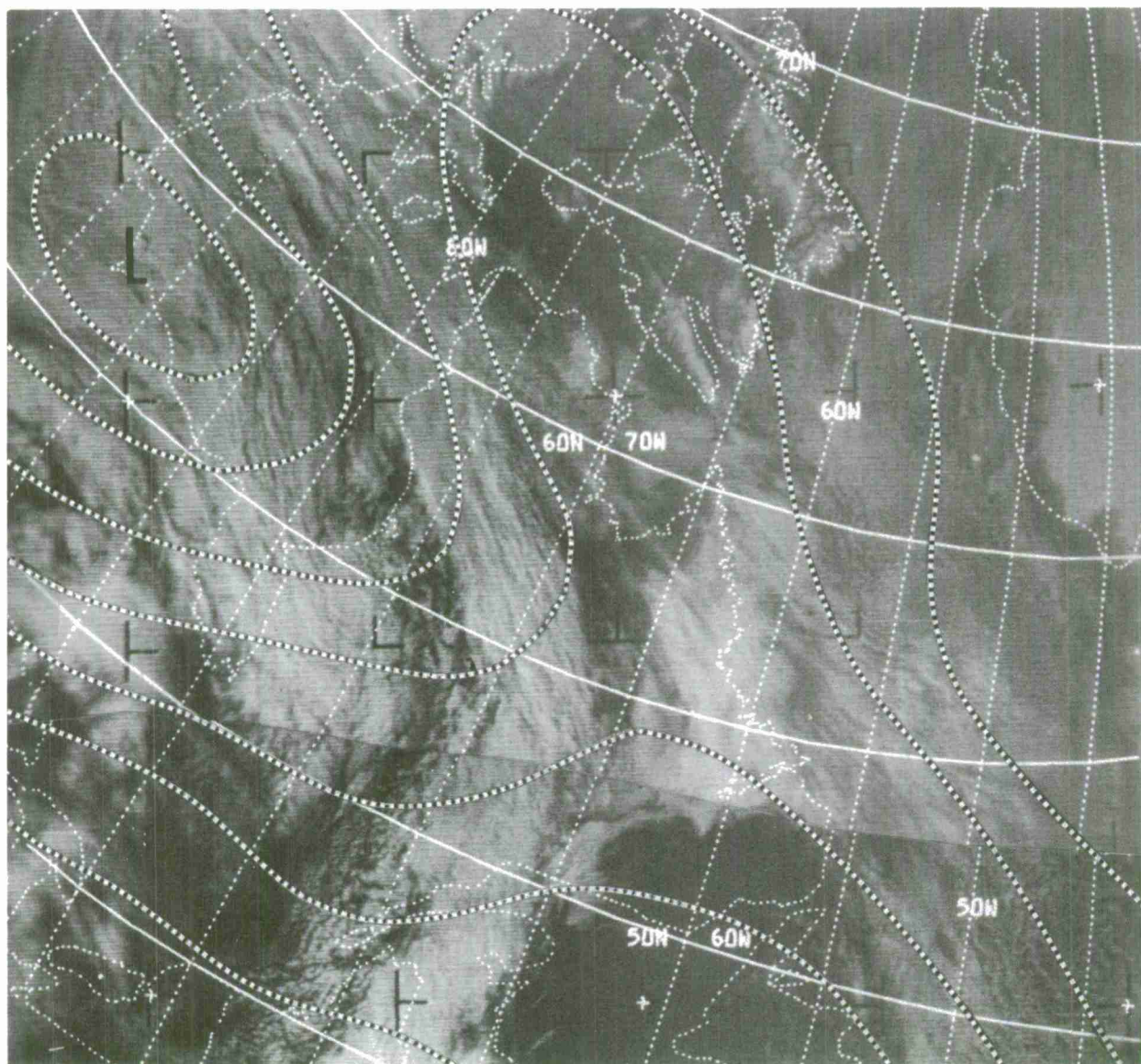
E-7 704-3 1804Z 11 Oct 68   500-mb Analysis 1800Z 11 Oct 68

Figure 3-F-2.  The leading edge of a narrow cloud band over eastern
Canada ends a few degrees west of the main 500-mb ridge.  A minor ridge is
seen near 50N, 65W.  A cloud band, ahead of a low which is slowing down or
stationary, will often have its leading edge a few degrees behind the main
ridgeline.  In the above situation, if more moisture were available ahead
of the trough, the leading edge of the cloud band could extend out to the
main ridgeline.

Medium Ridges

The band of clouds associated with medium ridges will normally be broader
than those associated with sharp ridges and the leading edge of the cloud pat-
tern will not end nearly as abruptly as with the sharp ridge.

The location of these ridgelines will range from the leading edge of the
cloud pattern to a few degrees back into the cloud pattern. The change in di-
rection of the vertical motion at the ridgeline will be gradual thus allowing,
in some cases, clouds to extend beyond the ridgeline. The clouds will usually
be cirrus and the ridgeline will closely approximate the leading edge of the
middle clouds frequently seen under the cirrus. If cirrus is not present to
be advected over the ridgeline, the ridgeline will be located at or slightly
behind the leading edge of the middle clouds of the overall cloud pattern.

Figure 3-F-3. A ridge-
line of medium amplitude be-
tween A and B is located sev-
eral degrees back into the
cloud pattern. Between A
and C the amplitude of the
ridgeline increases and the
cloud band ends at the ridge-
line. The leading edge of
this cloud band from A to B
is rather ragged but as the
amplitude of the ridge in-
creases from A to C, the
leading edge of the cloud
band becomes less ragged.
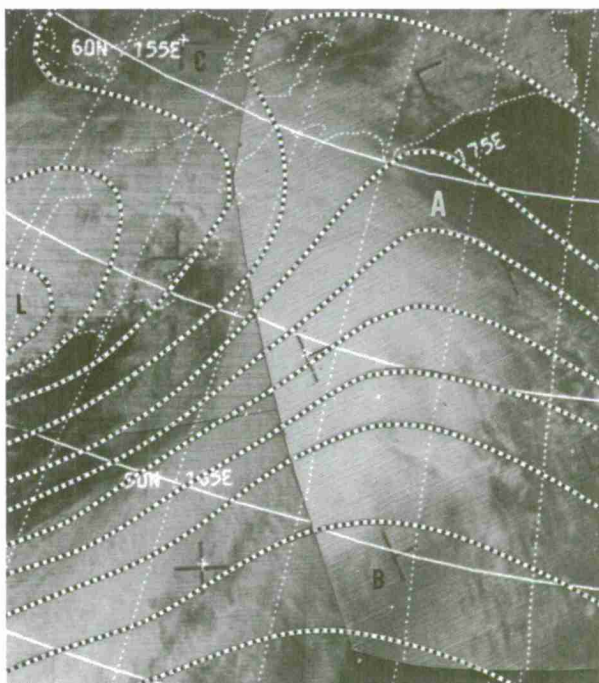
E-7 645-2 0105Z 7 Oct 68
500-mb Analysis 0000Z 7 Oct 68

Figure 3-F-4. Middle clouds end
at the ridgeline from A to B and ex-
tend a few degrees downstream of the
ridgeline from B to C.
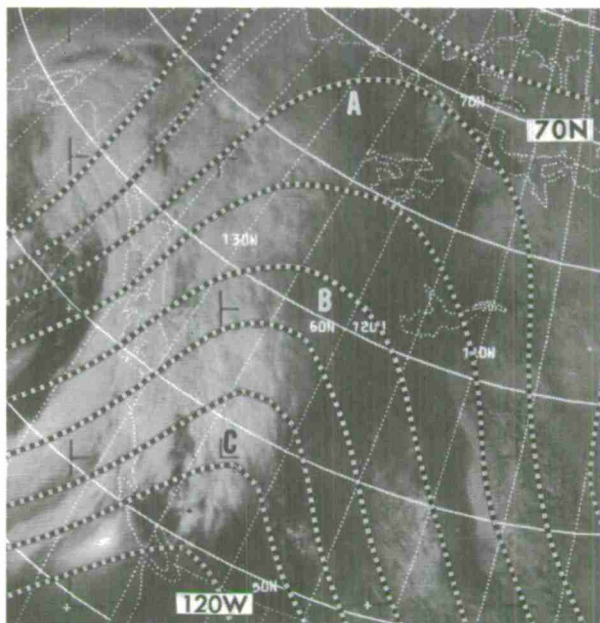


E-7 593-2 2123Z 2 Oct 68
500-mb Analysis 0000Z 3 Oct 68

Figure 3-F-5. A band of middle
clouds north of A extends a few de-
grees east of the ridgeline. South
of A, cirrus is over the middle
clouds and is advected a considerable
distance downstream of the ridgeline.
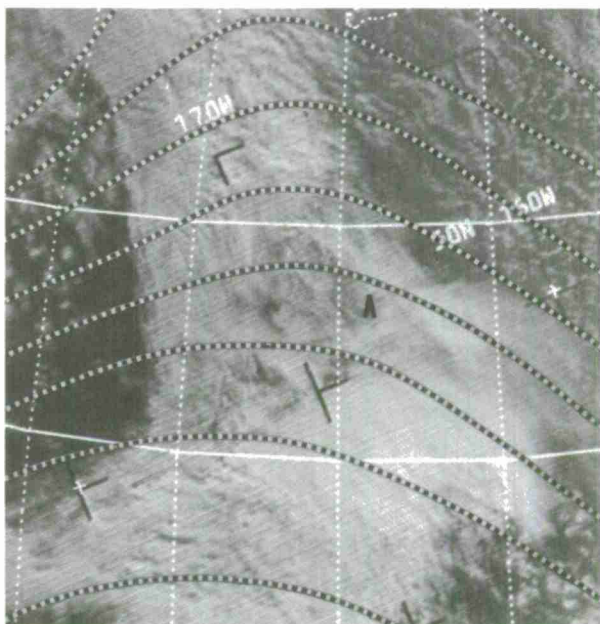


E-7 770-3 0033Z 17 Oct 68
500-mb Analysis 0000Z 17 Oct 68

## Broad Ridges

The clouds seen with flat, low amplitude ridges are the broadest of the three categories due to the large region of upward vertical motion between the widely-spaced trough and ridge.  The clouds along the forward edge of the mass will dissipate slowly as the magnitude of the downward motion gradually increases.

These ridgelines will be found well back into the cloud pattern as the change from upward motion to downward motion at the ridgeline is very gradual, allowing widespread advection of clouds over the ridgeline.  Anticyclonically-curved striations are frequently seen in these broad cloud patterns.  The upper ridgeline will be very close to the apparent ridgeline as seen in the curved striations of the cloud mass.
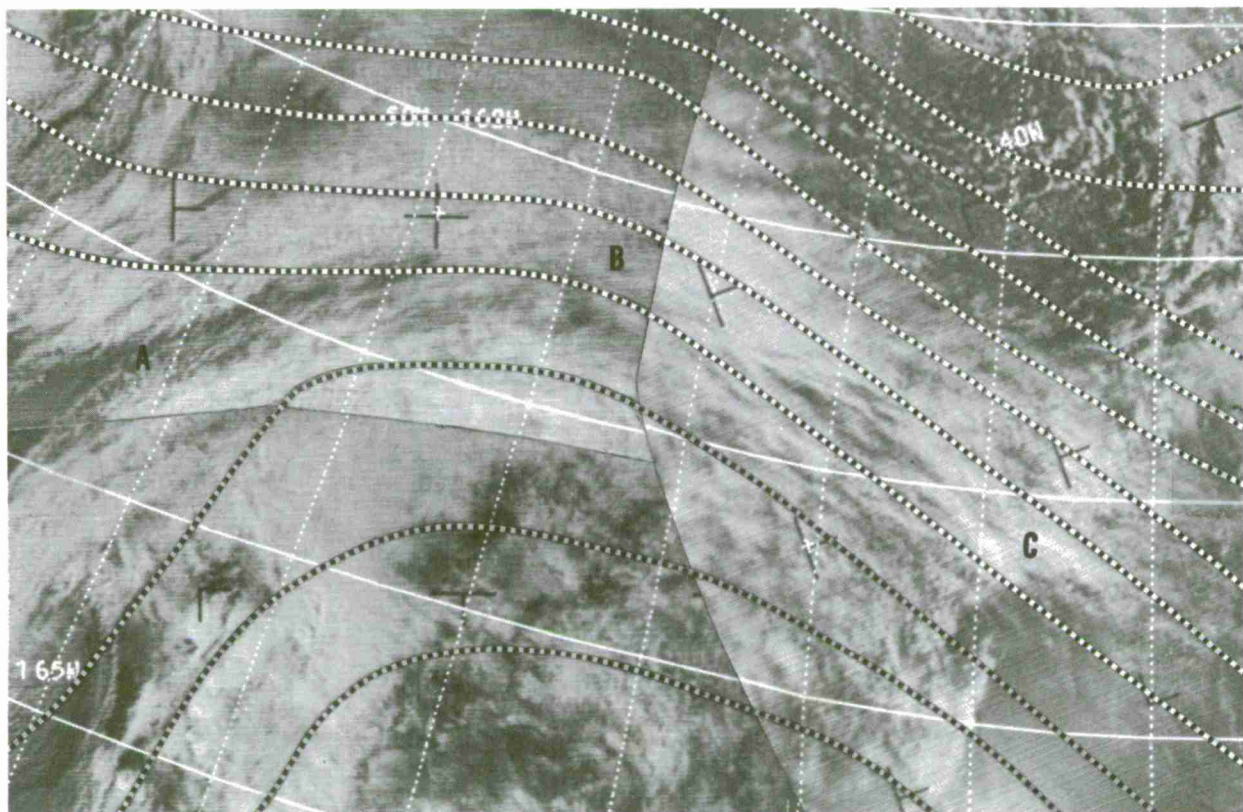


E-7 745-3 0038Z 15 Oct 68   500-mb Analysis 0000Z 15 Oct 68

Figure 3-F-6.  A broad area of clouds with a ragged leading edge over the Pacific characterizes a low amplitude ridge.  Breaks and striations curve anticyclonically across the entire cloud mass from A to C.  The location of the upper ridgeline will closely approximate the apparent ridgeline of the striations in the vicinity of B.

3-F-6
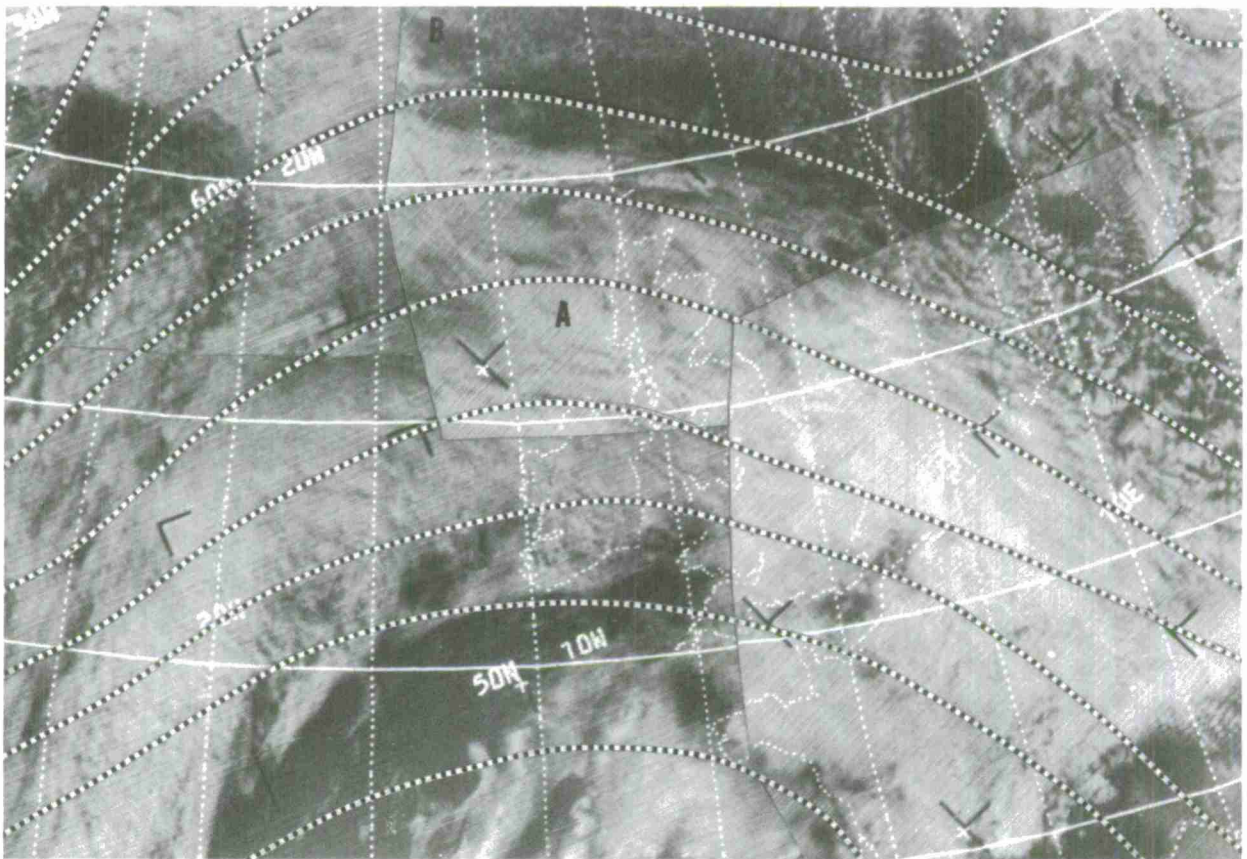
E-7 577-3 1439Z 1 Oct 68   500-mb Analysis 1200Z 1 Oct 68

Figure 3-F-7.  An extensive cloud band over the eastern Atlantic re-
veals the existence of a broad upper ridge.  The exact location of the up-
per ridgeline is difficult to ascertain since striations through the cloud
band are ill-defined.  Assuming that there is little difference between
the flow and the orientation of the striations, the few striations at A
which are oriented slightly towards the southeast indicate the ridgeline
is to the west.  At B, the ridge increases in amplitude and a point on
the ridgeline can be located along the leading edge of the cloud band.
Using the point selected at B in conjunction with the apparent ridgeline
that can be inferred from the anticyclonic curvature of the entire cloud
mass, the ridgeline can be located with an acceptable degree of accuracy.

## Minor Ridges

Omega Blocks. A large ridge forming the omega block pattern often has minor ridges within the large scale flow. These minor ridges will normally be oriented in a more east-west fashion than the north-south configuration of the main omega block. The first minor ridge will be located along the leading edge of the observed cloud band. This cloud band will be quite similar in appearance to those associated with sharp ridges.
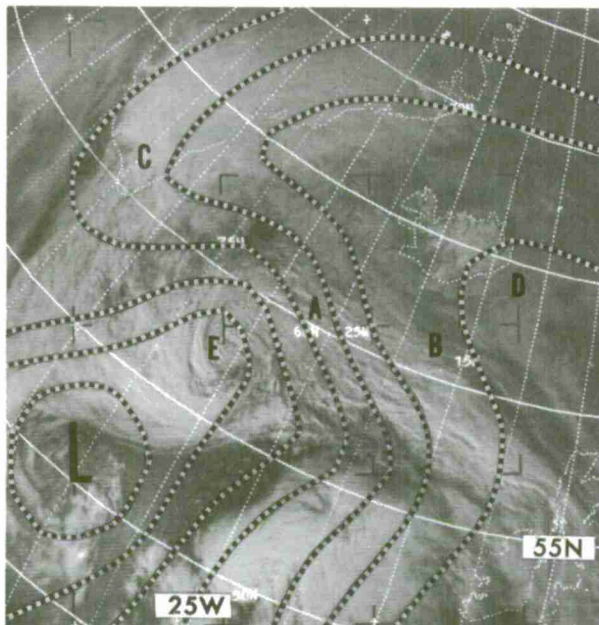


E-7 790-2 1458Z 18 Oct 68
500-mb Analysis 1200Z 18 Oct 68



E-7 777-2 1403Z 17 Oct 68
500-mb Analysis 1200Z 17 Oct 68

Figure 3-F-8. A number of minor ridges can be found within a well-developed omega block. One of these is from A to B. The major ridge is from C to D. The minor ridgeline from A to B closely approximates the northern edge of the cloud band spiralling into the vortex at E.

Figure 3-F-9. The minor ridge within the omega block can be positioned near the northern edge of the cloud band from A to B. The main axis of the omega block is from C to D.

   Large Scale Flow.  Frequently minor ridges will be imbedded in the large
scale westerly flow.  These ridges are often detected by a weakening of the
major cloud bands in the vicinity of the upper ridge.
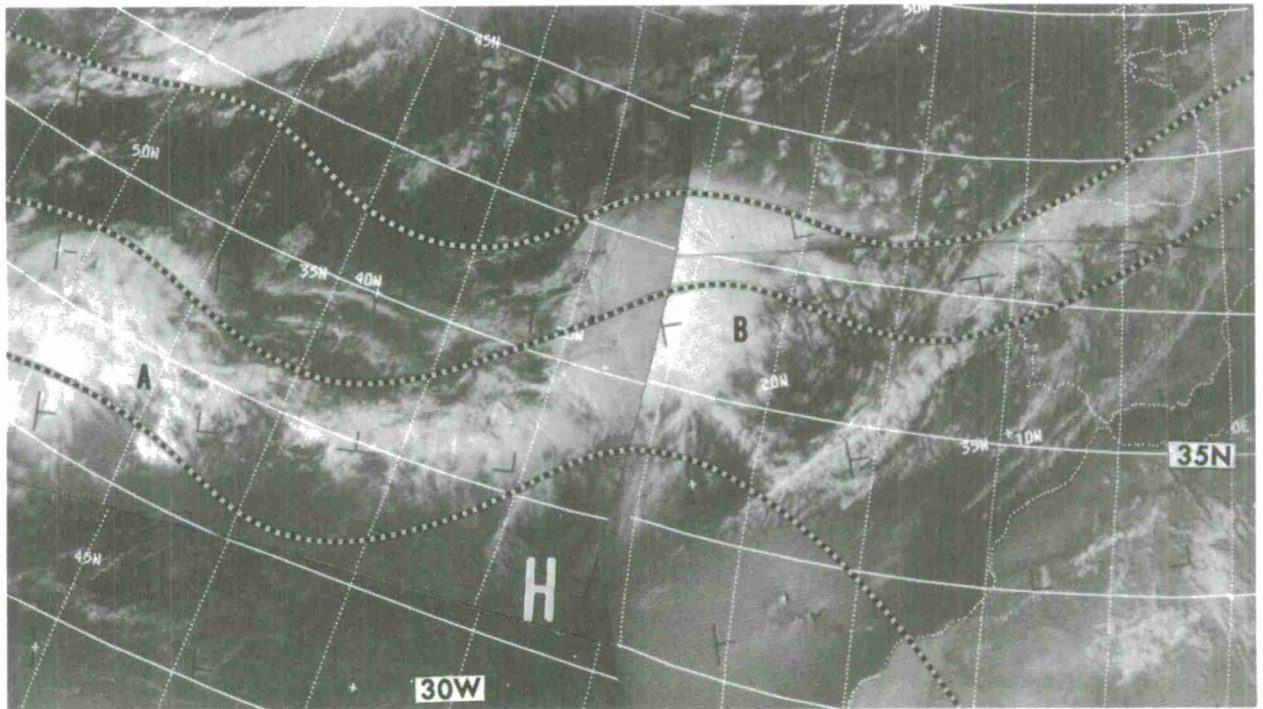


E-7 740-4; 741-5 1459Z, 1650Z 14 Oct 68   500-mb Analysis 1200Z 14 Oct 68

   Figure 3-F-10.  The broad scale west to southwest flow at upper levels
across the Atlantic is interrupted by a series of minor ridges and troughs.
The heavy cloud masses protrude poleward, at A and B, giving a trough and
ridge effect.  The profile of the northern edge of the cloud band is an
approximation of the minor trough and ridge positions.
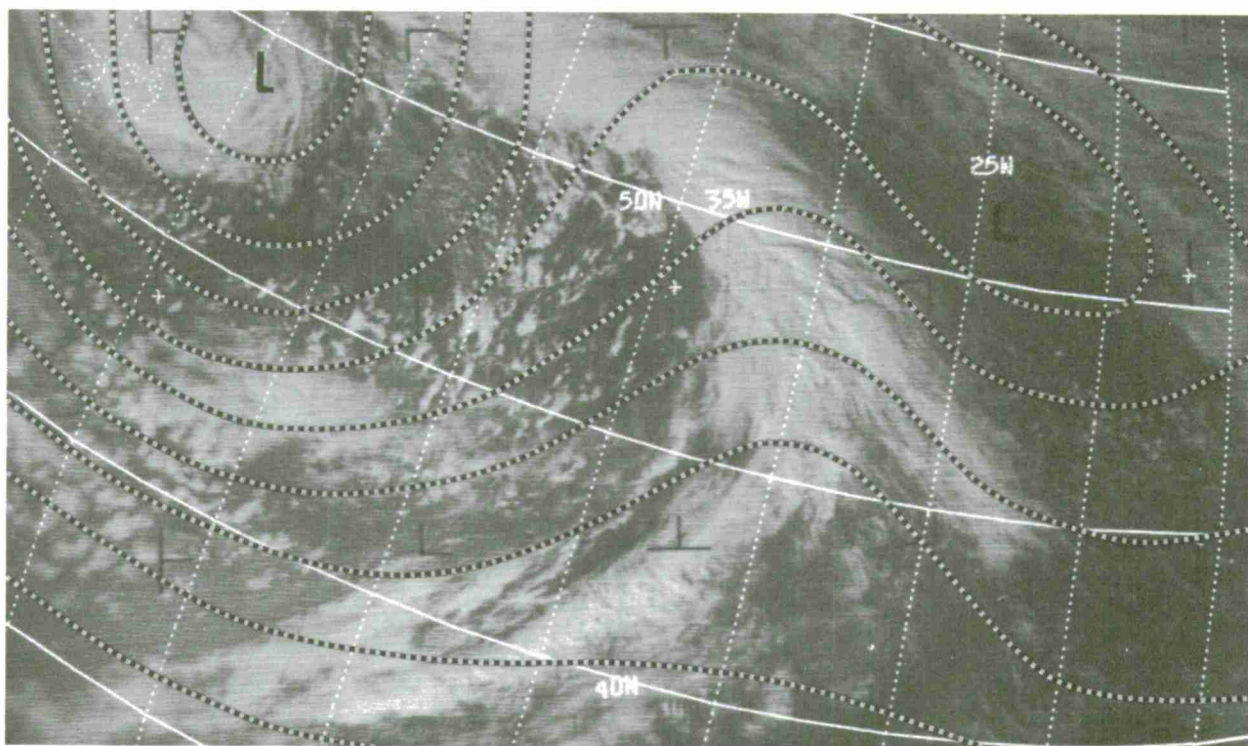
E-7 653-3 1619Z 7 Oct 68   500-mb Analysis 1800Z 7 Oct 68

Figure 3-F-11.  A broad belt of westerlies traversing the Atlantic at middle latitudes is interrupted by a narrow ridge.

Chapter 3

SECTION G

THERMAL PATTERNS

### Introduction

Cloud patterns in satellite photographs correlate with the 1000-500 mb thickness patterns. This is because the cloud patterns are basically the result of integrated motions through the atmosphere. Thus, cloud pictures may be used to considerable advantage when constructing 1000-500 mb thickness analyses [1] [46].

Lines or bands of convective clouds are useful in identifying thermal shear in the atmosphere. These lines and bands are aligned parallel to the vector representing the shear in wind through the cloud layer. The lines or bands are a visual representation of the thermal shear vector, or the thickness pattern, through the cloud layer.

The following are the most commonly used rules regarding thickness:

(1) Thickness lines lie nearly parallel to and are closely packed behind strong surface cold fronts. Thickness lines are also parallel to and are packed ahead of warm fronts but the packing is farther removed from the warm front than it is from the cold front. The degree of packing of the thickness lines is a measure of the thermal gradient associated with the front.

(2) Thickness lines should curve anticyclonically where they intersect surface fronts with the frontal zone being a "thickness ridge."

(3) Thickness contours over the peak of a developing frontal wave should curve anticyclonically with the tightest gradient, the thermal jet, being located just poleward of the peak.

(4) In general, there should not be more than two (60-meter interval) thickness lines through the warm sector of an occluding cyclone, since the warm sector is usually homogeneous.

(5) The thickness pattern should reflect the development or dissipation of synoptic-scale systems. In filling situations, the thermal field should be either in phase with or slightly ahead of height contours.

(6) In deepening baroclinic zones, the thermal troughs and ridges should lag the 500-mb troughs and ridges by about five to seven degrees.

(7)   In quasi-barotropic areas the thermal pattern should be in phase with the 500-mb contours.

(8)   Thermal troughs lie east of surface high pressure centers, reflecting cold, equatorward flow.

(9)   Cold lows are quasi-barotropic and have little tilt with height. The thickness pattern in these cases should indicate the coldest air nearly coincident with the position of the surface and 500-mb low center.

(10)   Thickness is a relatively conservative feature.  It seldom changes more than 60 to 120 meters in 24 hours, except where strong development is occurring.

The following photographs show how the general rules described above are applied to satellite-observed cloud patterns.  Vertically-developed convective clouds, such as cumulus congestus and cumulonimbus, form into cloud lines or bands which are often aligned parallel to the 1000-500 mb thickness contours. The thickness contours can also be drawn parallel to the striations which are often observed in cloud bands or large cloud masses.

In areas where upper air data are sparse, the forecaster may prepare a 1000-mb analysis from the surface analysis, and graphically add a satellite-adjusted thickness pattern to obtain a 500-mb pattern.  In this way, vertical consistency is almost always assured, and the analyst will find the resultant 500-mb analysis fits the rules described in other sections for upper level troughs and ridges.

## Surface Waves

The widening of a frontal cloud band which accompanies surface wave forma-
tion often produces a large cloud mass with striations. The striations within
the cloud mass curve anticyclonically and are parallel to the thickness lines.
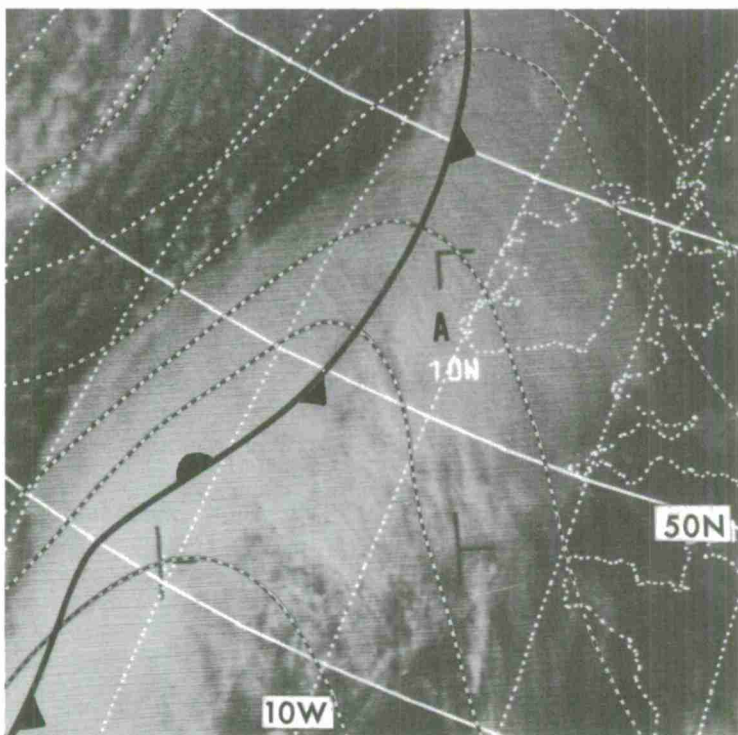


E-7 1065-2 1359Z 9 Nov 68
1000-500 mb Thickness 1200Z 9 Nov 68

Figure 3-G-1. This example shows the broad portion of a frontal band
typical of a surface wave. NW-SE oriented striations appear near A. The
thickness lines show the thermal ridge over the frontal cloud band with the
thermal jet located near 45N, 20W. The orientation of the thickness contours
is in agreement with the striations near A. This is an example of rules (3)
and (6).
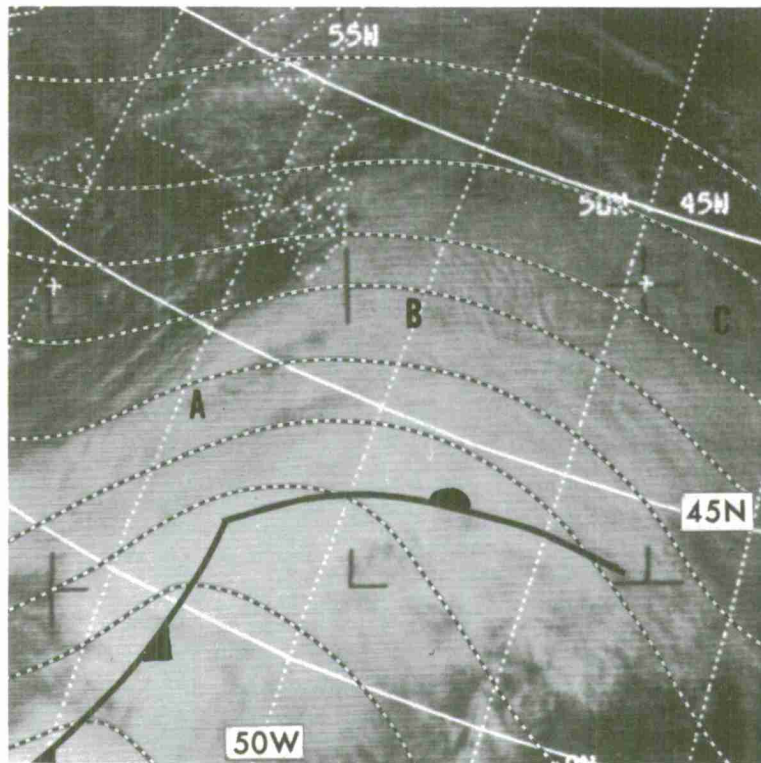
E-7 1029-2 1658Z 6 Nov 68
1000-500 mb Thickness 1800Z 6 Nov 68

Figure 3-G-2.  A large cloud mass associated with a developing surface wave is shown above.  The poleward edge of the cirrus shield which positions the jet stream is along the line ABC.  The thickness ridge south of the jet is nearly coincident with the striations observed in the cloud mass, with the tightest packing of the isolines just poleward of the surface wave.  The clouds south of the jet extend through a deep layer of the atmosphere.  The striations in this cloud mass relate to the 1000-500 mb thickness pattern. North of the jet, where the clouds are lower and not as thick, the striations represent thermal shear for a lower layer.  The surface wave is just develop- ing and the warm front is not well-defined in the thickness field, thus more thickness lines appear in the warm sector than previously indicated in rule (4).

Thickness Ridges and Mature Cyclones

    The clouds seen on satellite photographs associated with mature cyclones and occluded frontal systems often have striations that are helpful in determining the related thermal pattern. This thermal pattern may be used to subjectively prepare a thickness chart which may be graphically added to a 1000-mb analysis to obtain a realistic 500-mb pattern in data sparse areas.
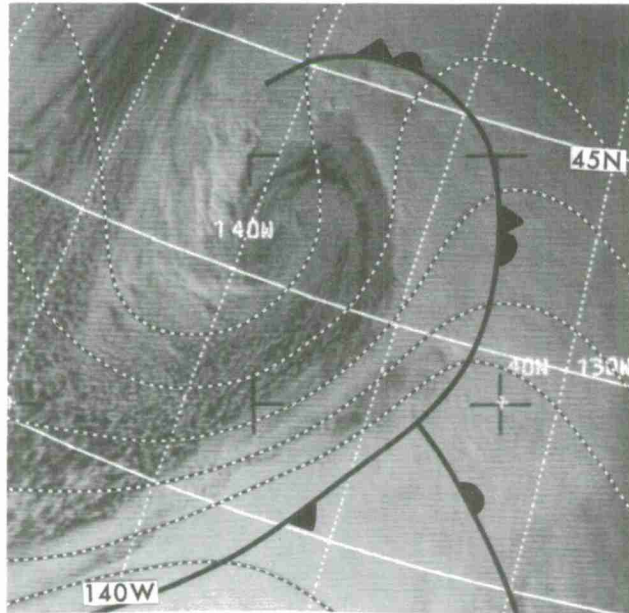


E-7 1483-2 2303Z 12 Dec 68
1000-500 mb Thickness 0000Z 13 Dec 68

    Figure 3-G-3. A nearly-mature cyclone is shown with its associated cloud vortex pattern centered near 41N, 139W. The analysis shows only one thickness line through the warm sector. The curvature of the cloud lines in the open cellular field are used as an aid in placing the thermal trough. The thickness pattern shows the ridging over the occluded portion of the frontal cloud band, with the maximum thermal gradient behind the front. The center of the cold air is west of the 500-mb center and, the cyclone center is analyzed as being cold. This is reflected in the picture by the dry tongue that has penetrated almost to the center of the system. This is an example of rules (2), (4), and (5).

## Dissipating Vortex and Thermal Trough

When a vortex reaches the dissipating stage, the vortex cloud pattern is
made up of less clouds than in the developing and mature stages and the cirrus
clouds are often absent. It is possible to identify thermal patterns associ-
ated with dissipating vortices from the alignment of low and middle clouds.
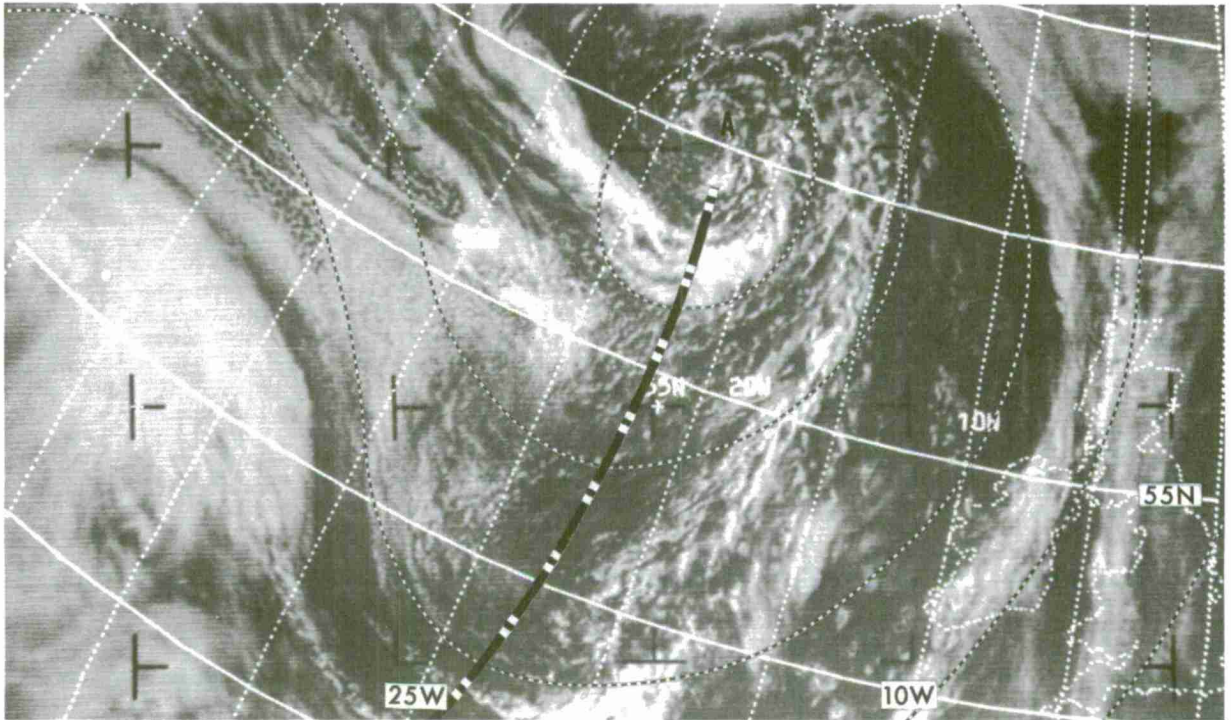


E-5 5174-3 1639Z 1 Jun 68   1000-500 mb Thickness 1800Z 1 Jun 68

Figure 3-G-4. The vortex at A has progressed from the mature stage to the
dissipating stage as evidenced by a lack of middle and upper-level cloudiness;
only cumuliform cloud lines remain to identify the spiral. Near the vortex,
the thickness contours are nearly parallel to the cumuliform cloud lines, with
the center of the cold air nearly coincident with the center of the cloud
spiral. The maximum curvature in the cumuliform cloud lines equatorward of
the spiral is nearly coincident with both the thickness trough and the 500-mb
trough. This shows that there is little change in direction of the geostroph-
ic wind with height.

## Thickness Troughs

The curvature of cumuliform cloud lines in open cellular cloud patterns may be used to locate thermal trough lines. Striations or lines in closed cellular or stratocumulus cloud patterns are not as helpful since these patterns relate to the thermal field of a shallow layer near the surface. As a general rule, to the rear of a developing system, a 500-mb trough line may be placed five to seven degrees downstream from the thermal trough. To the rear of a mature and/or dissipating system, the distance between the thermal trough and the 500-mb trough is usually less than five to seven degrees.
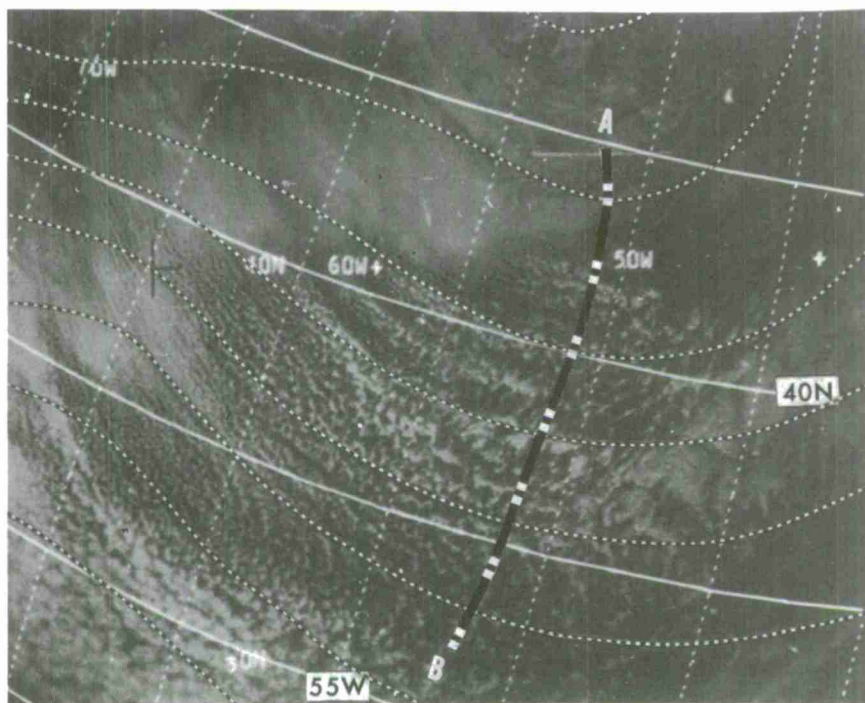


E-3 5830-2 1603Z 9 Jan 68   1000-500 mb Thickness 1800Z 9 Jan 68

Figure 3-G-5. Cumuliform lines that are produced by cold dry continental air flowing offshore over a warmer water surface are shown southwest of a major cyclone. The cells structure changes from fine lines to an open cellular pattern after the air has had an adequate trajectory over water. The curvature of the cloud lines in the open cellular cloud pattern locates the position of the thickness trough from A to B.

## Positive Vorticity Advection (PVA) Maxima and Vorticity Centers

The PVA MAX or comma-shaped cloud patterns which occur in the cold air to the rear of, or around the periphery of, cloud vortices are usually associated with small amplitude ridges in the 1000-500 mb thickness analyses. Thickness lines are generally normal to the cloud band of the comma, with one or two contours curving anticyclonically near the head of the comma-shaped cloud pattern [22]. The associated thickness trough is nearly in phase with the 500-mb trough.
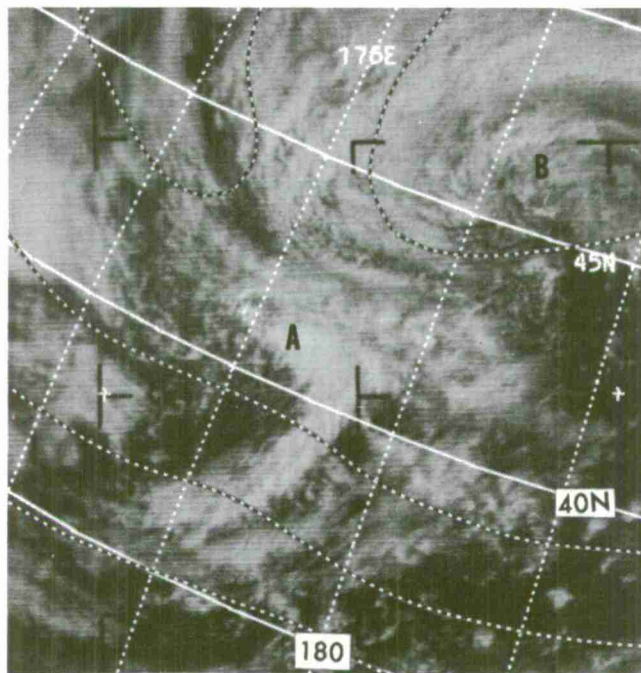


E-5 5205-4 0317Z 4 Jun 68
1000-500 mb Thickness 0000Z 4 Jun 68

Figure 3-G-6. A comma-shaped cloud pattern near A is rotating around the main vortex near B. The maximum 1000-500 mb thickness gradient is equatorward of the head of the comma, with the thermal and flow trough lines nearly in phase. These thickness contours are nearly normal to the N-S oriented cloud band associated with the PVA maximum.

Vorticity center cloud patterns also frequently appear in the cold air to the rear of, or around the periphery of, cloud vorticies and are associated with cyclonic curvature or a trough in the thickness field.  The degree to which the vorticity center is reflected in the thickness pattern is dependent upon the strength and organization of the vorticity center.
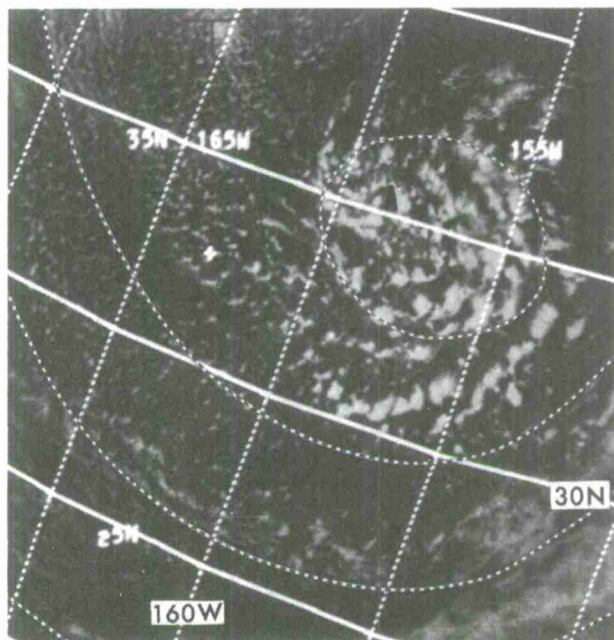


E-3 6424-3 2301Z 25 Feb 68
1000-500 mb Thickness 0000Z 26 Feb 68

Figure 3-G-7.  A positive vorticity center is implied by the curved lines of enhanced cumuliform clouds around A.  The vorticity center is located in the cold air between two lows outside of the area shown, one to the northwest and one to the east.

Cut-Off Cyclones

Cold-core systems often have a surface low pressure center nearly coincident with the center of circulation aloft. The 1000-500 mb thickness pattern usually reflects this by exhibiting a closed contour nearly concentric with the 500-mb contours.
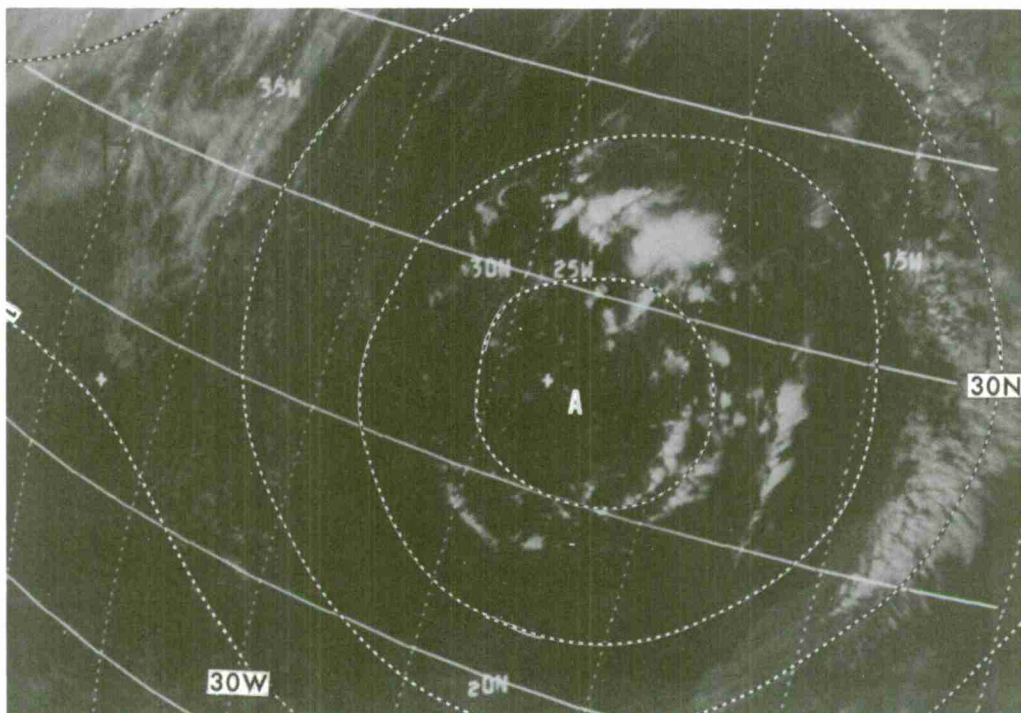


E-3 5942-3 1359Z 18 Jan 68   1000-500 mb Thickness 1200Z 18 Jan 68

Figure 3-G-8. This picture presents one of a variety of cloud patterns associated with a cut-off cyclone. The curvature of the cloud lines around the system centered at A suggests a center of circulation aloft. Both the picture and the thermal pattern show that the cyclone has little tilt with height.

Chapter 3

SECTION H

SURFACE RIDGES

Introduction

Surface ridgelines and high pressure cells, in both the northern and
southern hemisphere, are characterized by certain cloud patterns or sun glints.
Rules describing these relationships were tested and have proven useful during
the past two years.  The use of these ridgeline rules in data-sparse regions
will assist in a better analysis of surface features, such as, centers of
highs, surface troughs, changes from cyclonic to anticyclonic flow, determin-
ing gradients, etc.  The surface ridgeline indicators cannot always be found
in every high cell.  The indicators should be applied only to the type of high
cell for which they were formulated, and in the region of the high cell for
which they apply.  For example, rapidly-moving cold highs have different cloud
patterns than nearly stationary warm highs [6] [22] [23].

## Northern Hemisphere Ridgelines

TYPE A

On the forward edge of the frontal band, cloud fingers are often tied in a
nearly-continuous fashion to the frontal clouds [1].  These fingers generally
extend in a more southerly direction than the frontal bands.  Points on the
surface ridgeline, on the western or southwestern side of a subtropical high,
are located on the extreme end of the nearly-continuous cloud fingers extend-
ing from the frontal band.  This procedure is subjective and, until experience
is gained, care must be taken in selecting the cloud finger and the resultant
ridgeline position.





E-3 5366-3 1721Z 3 Dec 67
Analysis 1800Z 3 Dec 67

Figure 3-H-1 is a schematic of
Type A illustrating the surface
ridgeline extending west from the
center of the subtropical high and
located at the end of the cloud
fingers extending from the frontal
band.

Figure 3-H-2, Type A.  A continu-
ous cloud finger extends from the
frontal band A to B.  A point on the
surface ridgeline is located at B.
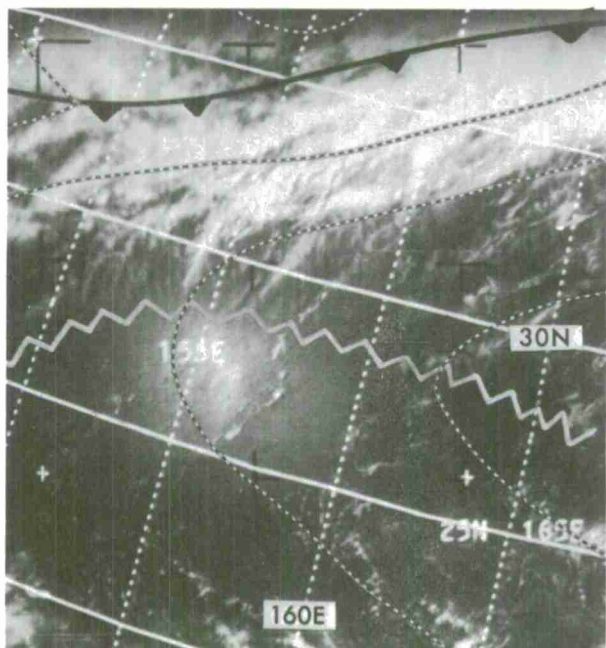
E-5 794-6 0400Z 22 Jun 67
Analysis 0600Z 22 Jun 67



E-3 1083-4 1725Z 27 Dec 66
Analysis 1800Z 27 Dec 66

Figure 3-H-3, Type A.  Several
continuous cloud fingers extend from
this front.  The ridgeline is located
at the extreme end of the fingers.

Figure 3-H-4, Type A.  A point on
the surface ridgeline, in the south-
western side of the subtropical high,
is positioned at the extreme end of a
cloud finger.

Figure 3-H-5.  Errors of several
degrees in determining the proper
position would be made if points on
the surface ridgeline were selected
at A and B instead of the extreme
ends of the cloud fingers at C and D.
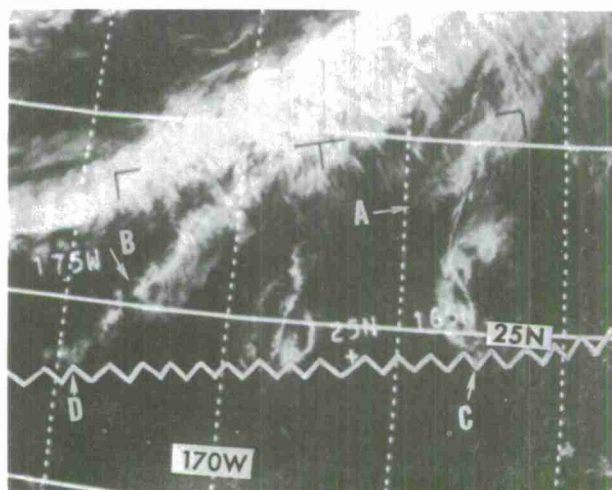


E-3 1539-4 0045Z 2 Feb 67

TYPE B

On the western side of subtropical high cells a change in the character of
the clouds from cumuliform to stratiform occurs where the low level winds
change direction from southeasterly or easterly to southwesterly or southerly.
Points on the surface ridgeline are positioned where the greatest change oc-
curs in the cloud character.  The change in character from cumulus globs to
clouds more stratified in nature is caused by the difference in heating and
stability; the air is unstable with heating from below in the southeasterly or
easterly flow, and more stable with cooling or less heating from below in the
southwesterly or southerly flow.  The change in cloud character selected must
be associated with a surface ridge rather than some other phenomenon.





E-3 1861-3 1605Z 27 Feb 67
Analysis 1200Z 27 Feb 67

Figure 3-H-6, Type B.  This sche-
matic illustrates the surface ridge-
line located where clouds change char-
acter from cumuliform to a more
stratified nature in the western side
of a subtropical high.

Figure 3-H-7, Type B.  Clouds
change character where the wind direc-
tion changes from an easterly flow to
a southerly flow.  The change in
cloud character can be seen at points
A and B.
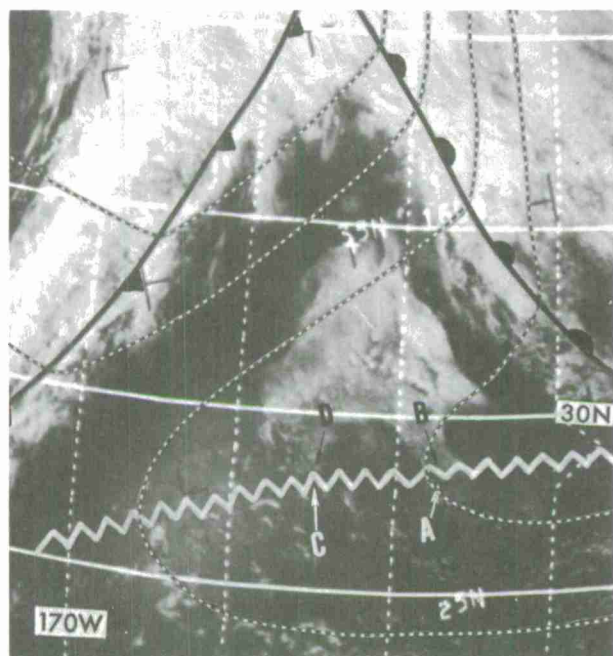
E-3 1815-3 0011Z 24 Feb 67
Analysis 0000Z 24 Feb 67



E-3 2380-3 2349Z 9 Apr 67
Analysis 0000Z 10 Apr 67

Figure 3-H-8, Type B.  The clouds
change character from cumuliform to
stratiform from points A to B and
from C to D.  The change in cloud
form is more pronounced here than in
many cases.  This ridge is located in
the western portion of a subtropical
high.

Figure 3-H-9, Type B.  Points on
a surface ridgeline are selected
where clouds change character from
cumuliform to stratiform from point
A to B and from point C to D.

Figure 3-H-10.  This photograph,
while showing changes in cloud char-
acter, does not show the cumuliform to
stratiform change required for Type B
classification and is not coincident
with a surface ridge.  In this case,
surface flow changes from cyclonic to
anticyclonic with cloud cells changing
from open to closed along a line from
A to B.
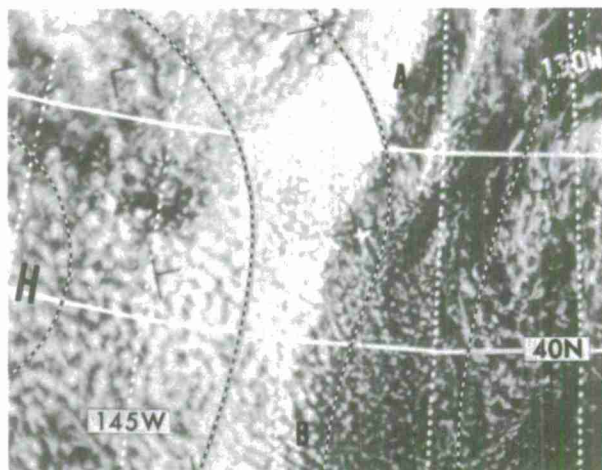


E-3 2555-4 2213Z 23 Apr 67
Analysis 0000Z 24 Apr 67

TYPE C

When two cyclones come in close proximity, a sharp polar ridge at the sur-
face is found between them.  On the northern side of the polar high there will
be a wind shift from southwesterly or westerly to northwesterly or northerly.
The surface ridge is positioned along a line where the low level cumuliform
clouds first develop in the low level cold air having a northerly component
over warmer water.  This line is usually coincident with the forward edge of
the overcast from the western storm in the belt of strong westerlies.  It is
important that the initial formation of the cold air cumuli is determined.
Such clouds often form under higher clouds and are barely discernible.





E-3 1715-2 0112Z 16 Feb 67
Analysis 0000Z 16 Feb 67

Figure 3-H-11, Type C.  This is a
schematic which illustrates a surface
ridgeline located where the cumulus
clouds first develop and where the
solid overcast ends in the northern
portion of a polar high wedged be-
tween two cyclones.

Figure 3-H-12, Type C.  A surface
ridgeline, on the northern side of a
polar high, can be positioned between
.A and B, where the high level over-
cast ends and cumulus clouds initial-
ly develop.
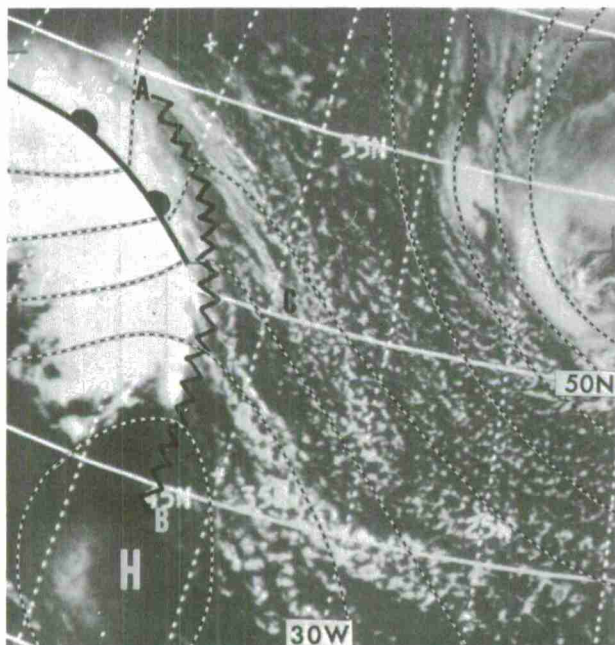
E-3 2903-4 1511Z 21 May 67
Analysis 1800Z 21 May 67



E-3 987-2 0206Z 20 Dec 66
Analysis 0000Z 20 Dec 66

Figure 3-H-13, Type C.  Points on the surface ridgeline associated with a polar high wedged between two lows can be found along line AB.  Care must be taken to determine points where the cumulus first develops.  The selection of a point at C, rather than along AB, would result in a large error.

Figure 3-H-14, Type C.  The surface ridge is positioned along a line from A to B.  This line is where the cumulus clouds first develop in the cold surface air which is moving southward over the warmer water.

Figure 3-H-15, Type C.  Errors of several degrees in ridgeline placement will occur if the initial formation of the cumulus activity is not detected, i.e., by placing the ridgeline at A instead of B.  Note that B is the correct location of the ridgeline since cumulus clouds under a higher thin cloud layer can be identified at the B points.
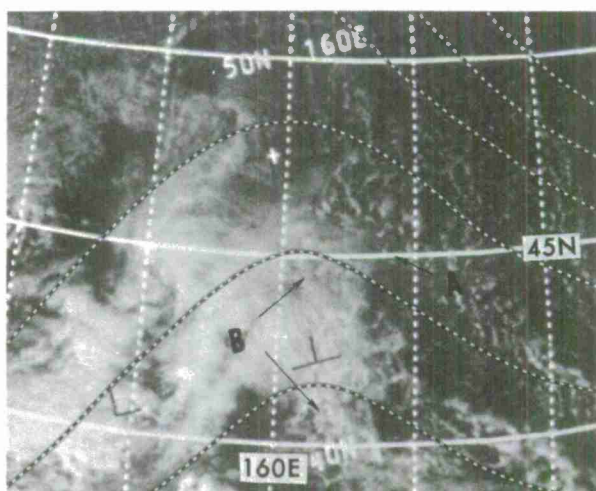


E-3 1138-2 0239Z 1 Jan 67
Analysis 0000Z 1 Jan 67

TYPE C (Variation)

A variation of the Type C polar-ridgeline rule may be found in some cases
on the northern side of a modified polar high.  In these cases, the cumuliform
clouds will not develop when the wind shifts to west or northwest, because the
contrast in the air-sea temperature is not as great as with a shift to the
north.  In these cases, points on the surface ridgeline can be approximated
where high level stratiform clouds end and a clear zone begins.

Frequently in the warmer months, even with a wind shift to a northerly di-
rection, the cumulus will not form due to a small air-sea temperature differ-
ence.  A clear slot in advance of the frontal band will indicate the location
of the surface ridgeline.
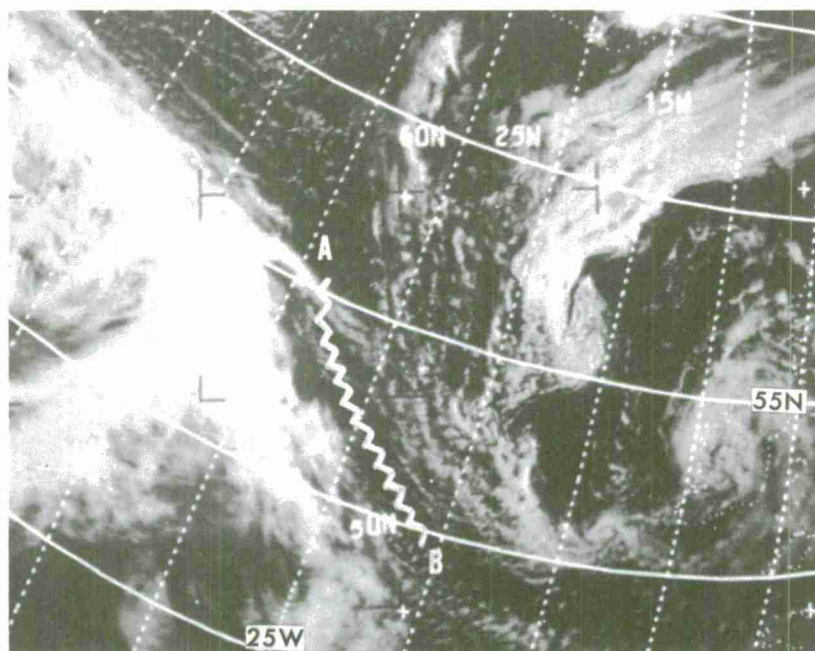


E-3 2915-3 1411Z 22 May 67

Figure 3-H-16.  An illustration of where a clear
slot, from A to B, is coincident with the surface
ridgeline.

Southern Hemisphere Ridgelines

The three rules for determining surface ridgelines in the northern hemis-
phere generally apply in the southern hemisphere. Lack of synoptic data in
the southern hemisphere precludes a definite correlation between the rules and
specific cloud patterns associated with surface ridgelines [7].

In the southern hemisphere, the cloud fingers associated with Type A can
be continuous or discontinuous. However, care must be taken when following
discontinuous cloud fingers to the north and northwest to ascertain that the
same cloud type exists on both sides of the break in the cloud-finger forma-
tion.

When the cloud finger (Type A) has breaks and is discontinuous, the type
of cloud will often change character at the point of discontinuity. This
change in cloud character can be treated as a Type B and the surface ridge
placed where the cloud type of the cloud finger changes.

Initial formation of cumulus clouds on the poleward side of a high pres-
sure center (Type C) is applied similarly in the southern hemisphere as it is
in the northern hemisphere.

E-3 4938-7,8 1515Z 30 Oct 67
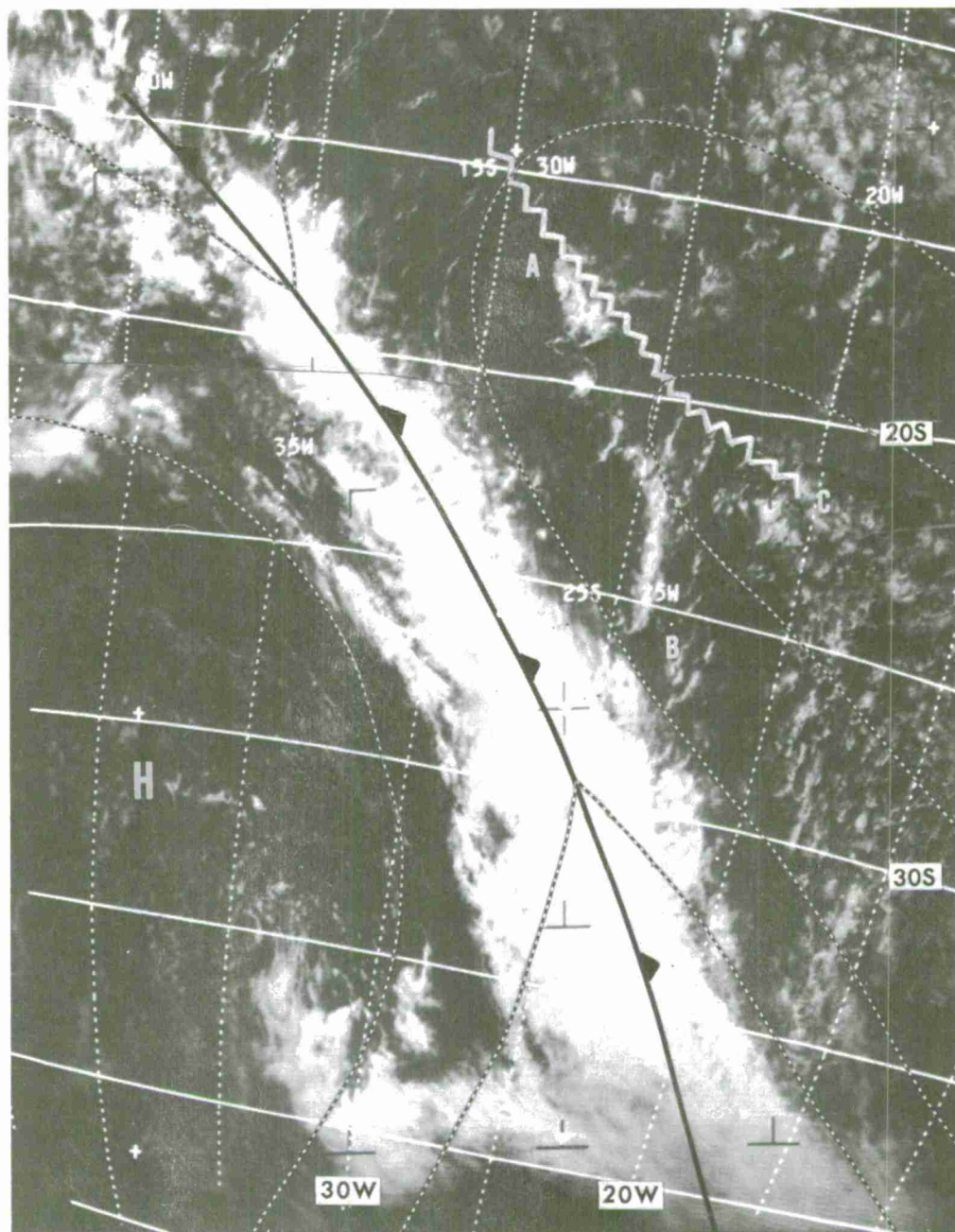
Figure 3-H-17.  The northern end of the nearly-continuous cloud fin-
ger from A to B locates a point on a surface ridgeline in the southern
hemisphere.  The ridgeline is from A to C.
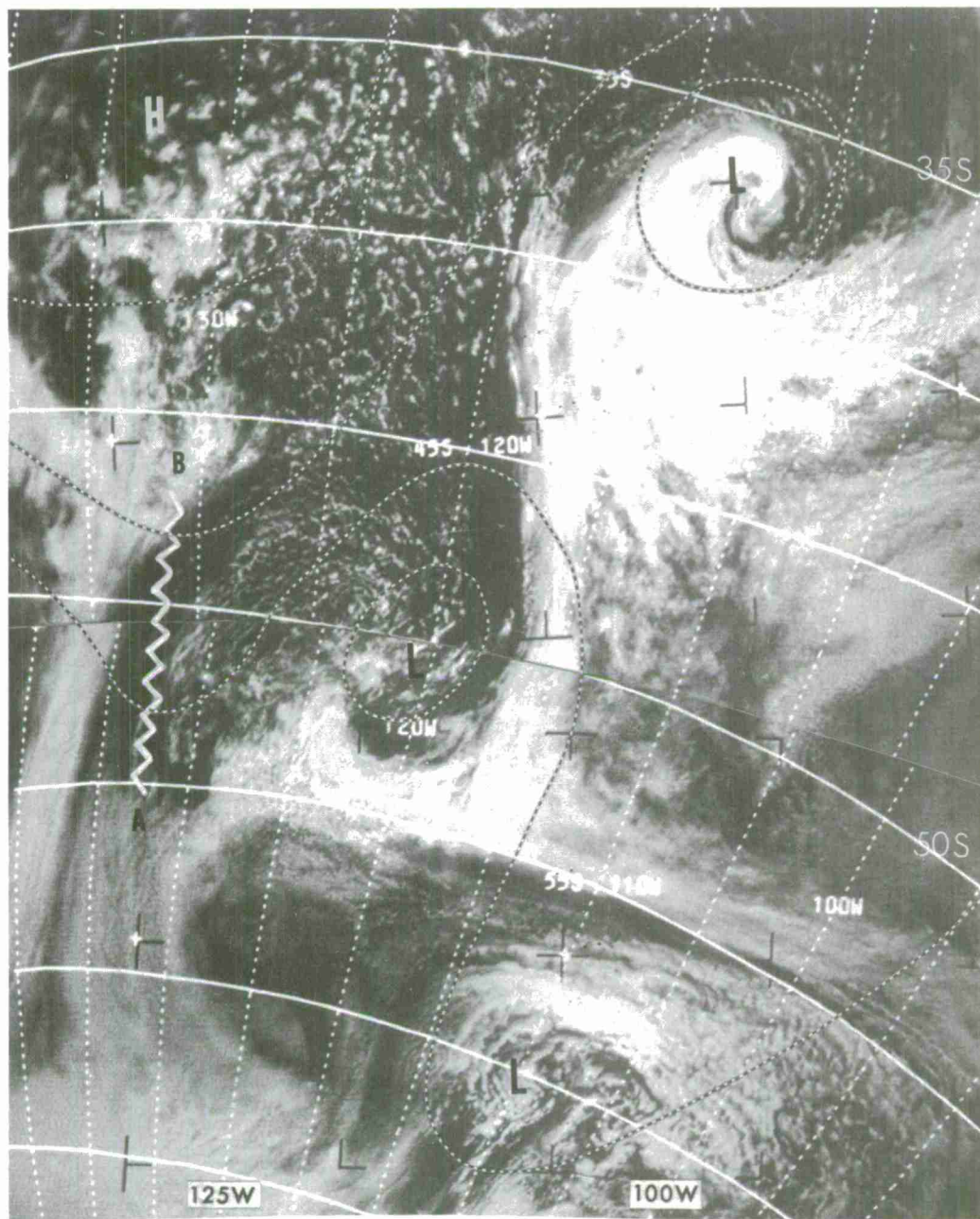
E-3 5067-9,10 2135Z 9 Nov 67  Analysis 1200Z 9 Nov 67

Figure 3-H-18.  A surface ridgeline, from A to B, can be located
by the initial formation of cumulus in the clear slot in advance of a
cold front.

In the southern hemisphere, a clear zone ahead of a cold front is frequent-
ly coincident with the surface ridgeline.  The surface ridgeline should be
analyzed near the center of the clear zone.  Preliminary studies indicate a
surface ridgeline can also be found in the northern hemisphere in a clear area
in the stratocumulus ahead of a cold front.
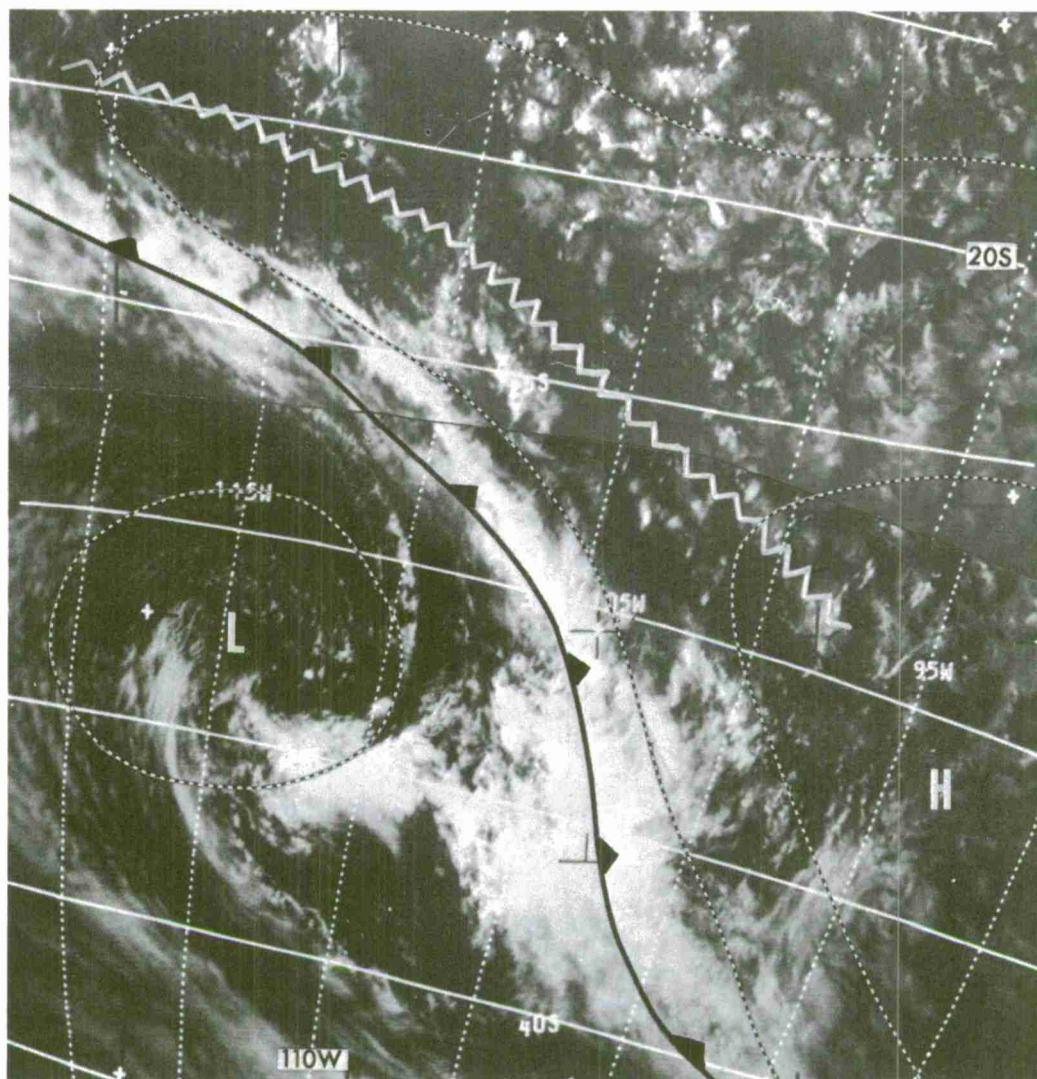


E-3 4991-7,8 2031Z 3 Nov 67   Analysis 0000Z 4 Nov 67

Figure 3-H-19.  A clear area in advance of a cold front,
west of South America, closely approximates the location of
the surface ridgeline.  Cloud fingers along 110W also indi-
cate points on the ridgeline.
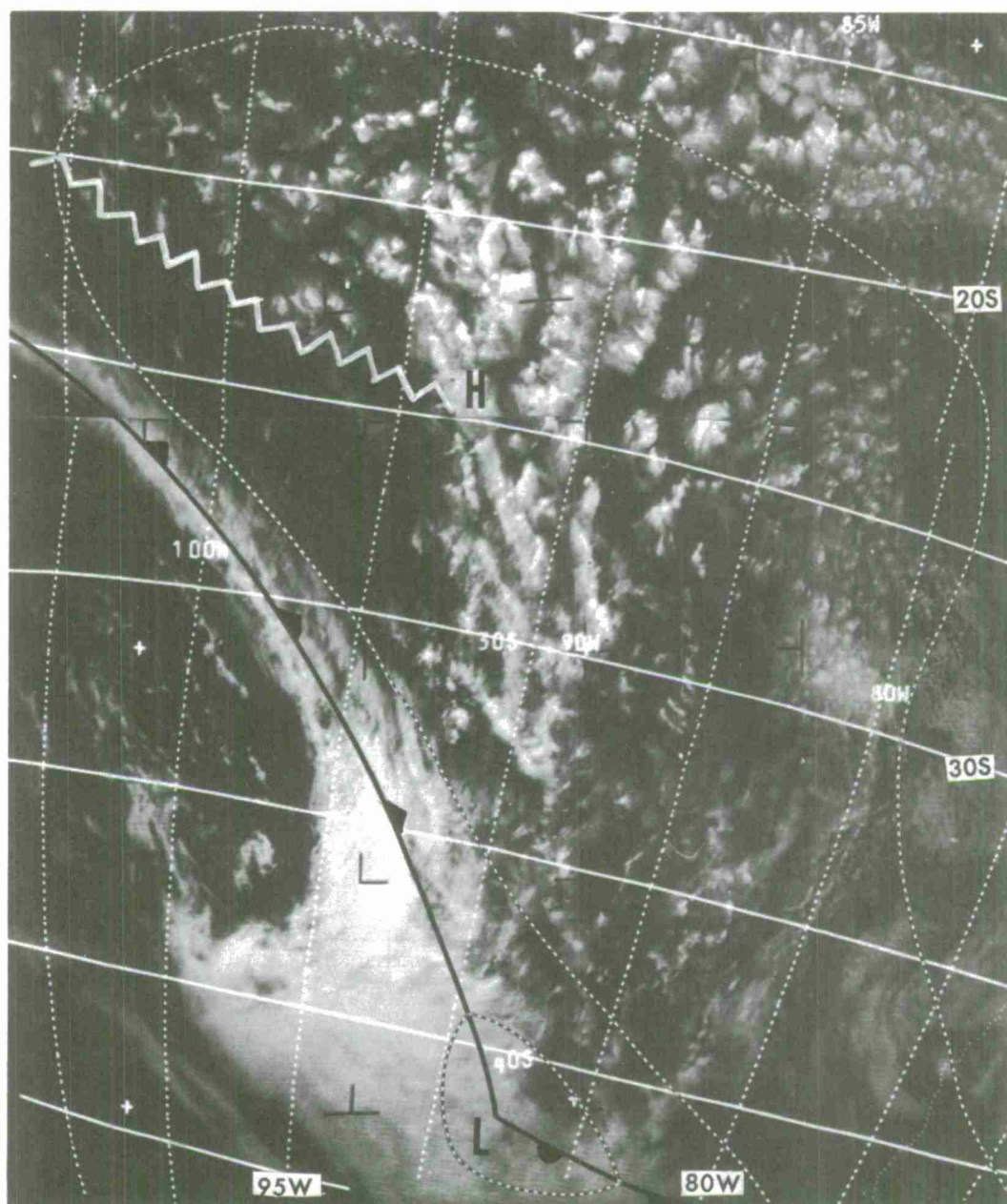
E-3 5003-7,8 1927Z 4 Nov 67   Analysis 0000Z 5 Nov 67

Figure 3-H-20.  A view of the same area as Figure 3-H-19 on the
next day shows the clear area still persisting.  In the analysis it
appears that the ridgeline position is in the more northerly part
of the clear zone.
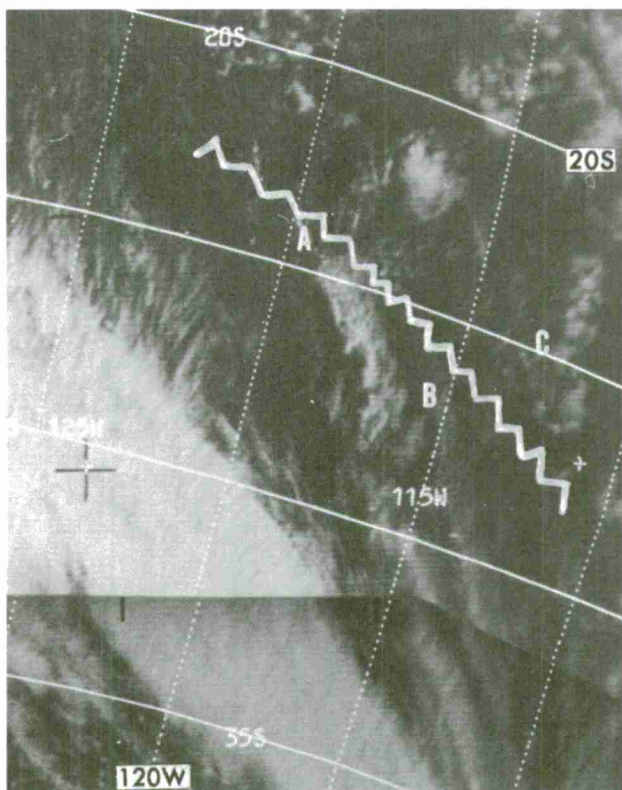
E-7 1208-8,9 2336Z 20 Nov 68

Figure 3-H-21. Cloud fingers extend
from a front approaching the west coast
of South America. The surface ridgeline
can be located at the end of the fingers
A and B. The ridge can also be positioned
between B and C where the clouds change
from cumuliform at C to stratiform in the
finger.

## Sun Glint

When the sun and satellite are in the correct relationship to each other, a sun glint will exist in the resulting photograph. Recent studies show these sun glints useful for determining surface ridgeline location and orientation in both the northern and southern hemispheres. A sharp well-defined sun glint is often located along a surface ridgeline. There may be very dark bands or patches on either side of this type of sun glint. The surface ridgeline will be oriented in the direction of the elongated axis of the sun glint through the two dark regions. This type of sun glint occurs most often in the center of an elongated high pressure cell. When a ridgeline is located in an area of sun glint, the very light winds associated with the ridgeline and the high pressure center will cause a smooth ocean with a highly-reflective surface resulting in a bright sun glint [8].

These sun glints will appear only in a relatively small or specific area of the picture. Ridgelines will not be discernible using the sun-glint method unless the ridgeline and the sun glint are in the same area of the photograph.



Figure 3-H-22. A sharp well-defined sun glint is located just to the west of the analyzed high center. Dark bands to the east and west of the sun glint are aligned along the axis of the ridge.
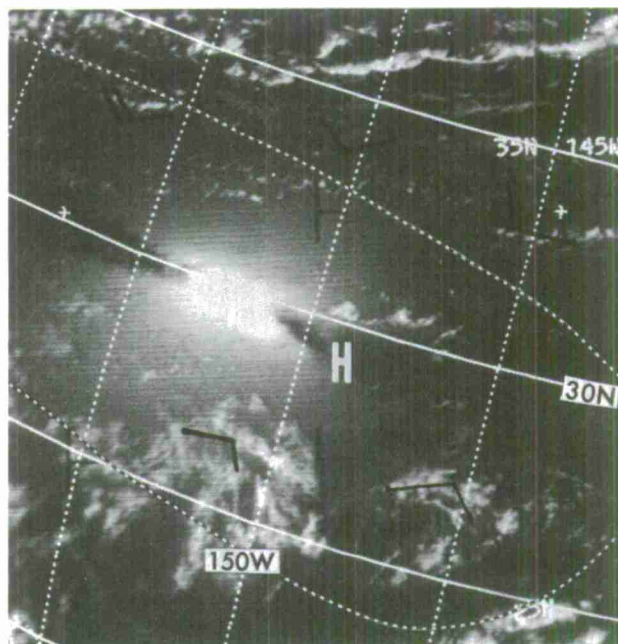
E-7 344-4 0000Z 13 Sep 68
Analysis 0000Z 13 Sep 68

Figure 3-H-23.  A bright sun
glint is located in the center of a
high pressure area in the eastern
Pacific.  The dark bands are oriented
along the east-west axis of the
ridge.
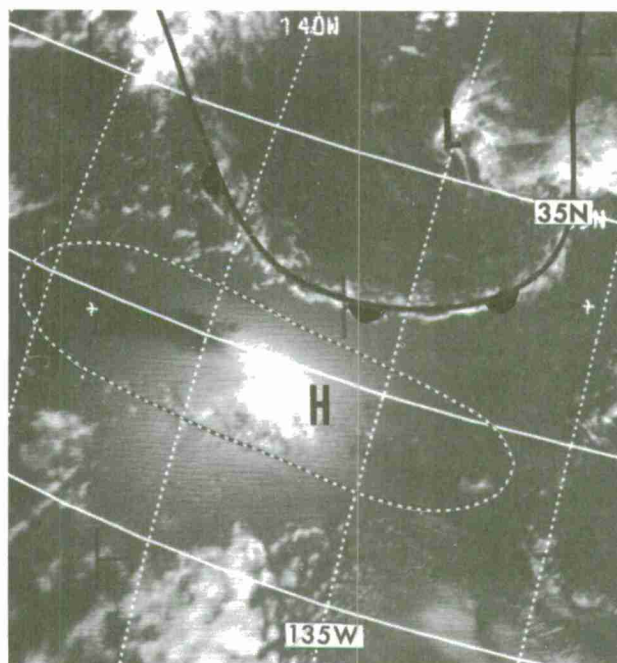


E-7 331-4 2305Z 11 Sep 68
Analysis 0000Z 12 Sep 68

Figure 3-H-24.  The bright sun
glint at A locates a surface ridge-
line in the western Atlantic.  The
general southwest-northeast orienta-
tion of the ridgeline is shown by the
very dark area at B which extends
from the sun glint.  The cloud trails
at C should not be confused with
cloud fingers which normally would
denote a surface ridgeline.
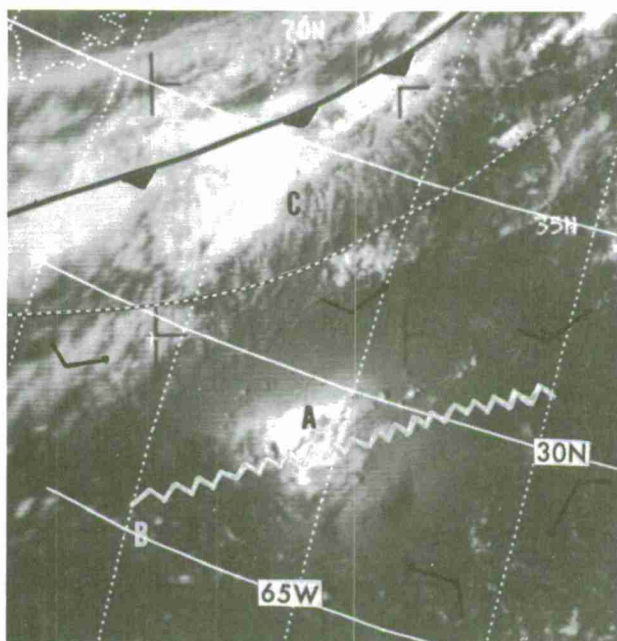


E-7 341-4 1815Z 12 Sep 68
Analysis 1800Z 12 Sep 68
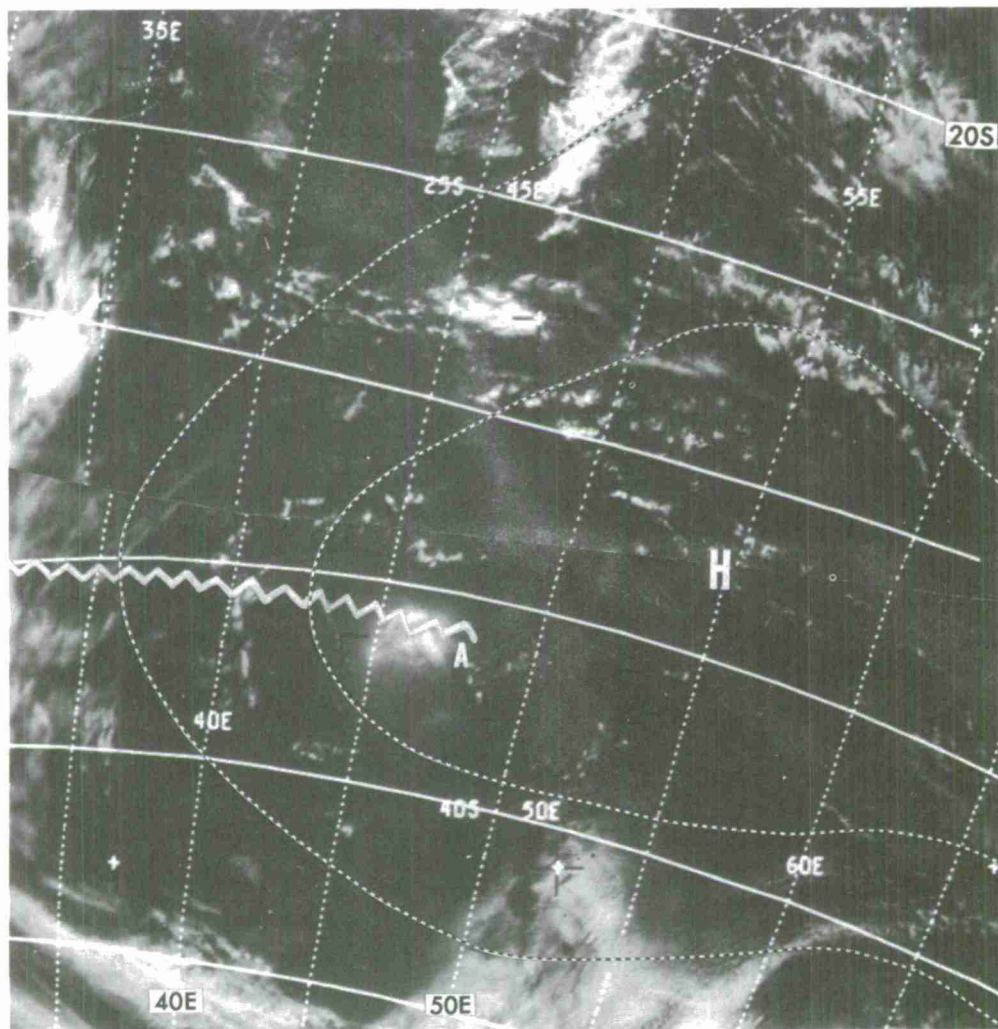
E-3 4948-8,9 1017Z 31 Oct 67   Analysis 0000Z 31 Oct 67

Figure 3-H-25.  A surface ridgeline in the southern hemisphere
passes through a sharp well-defined sun glint, at A, that does not
have dark bands or patches.

Chapter 3

SECTION I

SURFACE WIND DIRECTION AND SPEED

Introduction

Indications of surface wind direction and speed are found in many of the
cloud patterns associated with the low-level flow.  Variations in the large
fields of cumulus clouds in the cold air to the rear of the polar fronts pro-
vide information of direction, curvature of the flow, and speed [9] [10] [11]
[12] [13].  These variations take the form of open and closed cellular patterns,
long narrow lines of cumulus, and streaky patterns within the cumulus field.
The size and intensity of sun glint on the ocean surface give a clue to the
surface wind speed.  The distribution of clouds due to the sea breeze, moun-
tain ranges, and the effects of islands on large regions of stratus and fog
may yield information on surface wind direction.  Variations in the size of
areas of open water or thin fresh ice around large ice fields can give indica-
tions of persistent surface wind direction.  Anomalous cloud lines in areas of
fog and stratus will, at times, provide some indication of surface wind speed
[22].

## Cumulus Patterns to the Rear of Polar Fronts

Wind Direction.  The patterns that appear in large fields of cumulus clouds
associated with extratropical cyclones frequently give an indication of low-
level wind direction.  The cumulus clouds form where there is advection of
cold air over a relatively warm surface.  The cumulus clouds will initially
form as narrow lines which closely approximate the surface wind direction.  As
they increase in vertical extent, the narrow lines often form into open cells.
The open cells can be arranged in lines parallel to the vertical wind shear
through the cloud layer.  Near frontal zones the shear is usually large and
the low-level wind directions cross the lines at large angles.

In cold lows the isotherms parallel the wind direction, and the vertical
wind shear is therefore parallel to the wind direction at all levels.  The
cumulus cloud lines will also be parallel to the wind direction at all levels.
In the developing wave or in a rapidly moving cyclone, the isotherms do not
parallel the upper wind direction, and the cumulus cloud lines may cross the
low-level wind direction at large angles.  A condition of little vertical
change in wind direction may also exist further to the rear of cyclones where
the isotherms parallel the contours.  The lines in this situation will be
parallel to the low-level wind direction.

Figure 3-I-1.  Narrow
lines of cumulus at A and B
are parallel to the surface
wind direction.  The lines
widen and gradually form
into open cellular patterns
as the clouds build in
height.  At C and D, the
lines are nearly parallel
to the vertical wind shear
through the cloud layer and
almost perpendicular to the
surface wind direction.
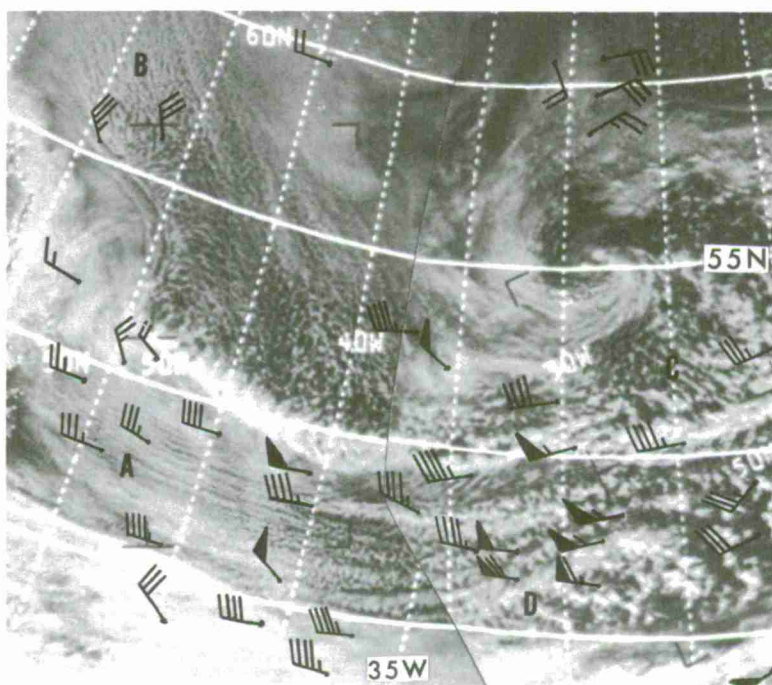


E-3 1747-2 1748-2 1615Z 18 Feb 67
Winds 1200Z and 1800Z 18 Feb 67

Open and closed cellular cloud patterns can be used as indicators of sur-
face wind direction.  Open cellular cloud patterns are found in areas of cy-
clonic flow and closed cellular cloud patterns occur most often in anticyclonic
flow.  A surface streamline pattern can be drawn cyclonically-curved over an
open cellular pattern and anticyclonically-curved over a closed cellular pat-
tern.
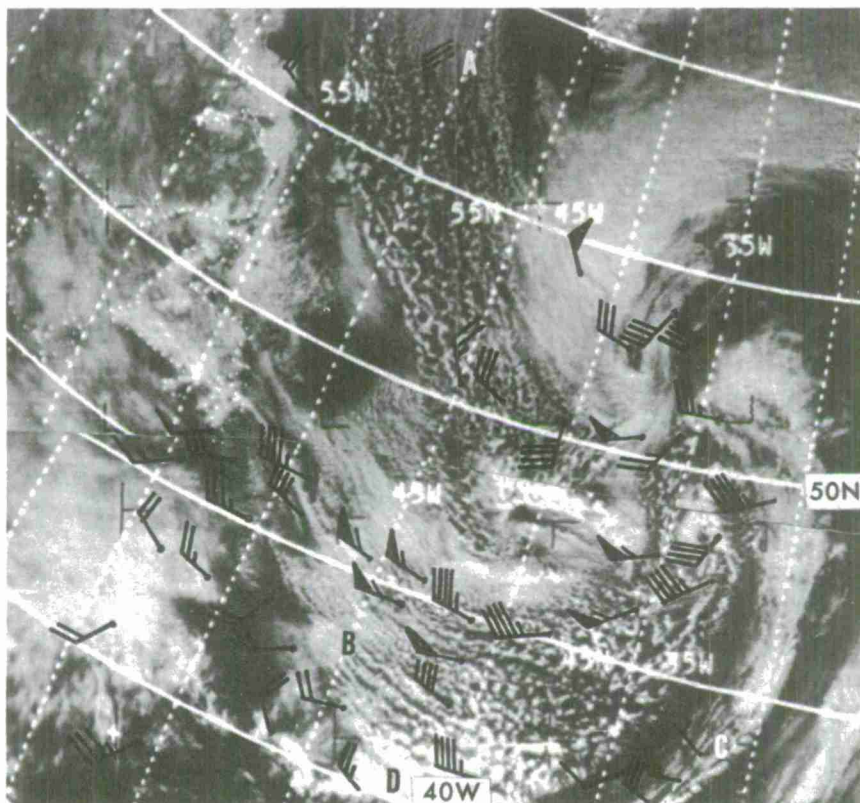


E-3 1911-2,3 1540Z 3 Mar 67
Winds 1200Z and 1800Z 3 Mar 67

Figure 3-I-2.  Narrow lines of cumulus par-
allel to the low level wind initially form around
points A and B.  As the clouds build in height,
the lines widen and gradually form an open cel-
lular pattern.  Banding occurs in the clouds at
point C parallel to the shear with the front.
Near D the cellular pattern changes to closed
cells and the flow begins turning in an anticy-
clonic direction.

Wind Speed. Wind speeds in the cold air behind polar fronts can be esti-
mated to a limited degree from satellite photographs.  In a closed cellular
pattern the winds are associated with anticyclonic flow and are relatively
lighter than those found with open cellular patterns.  Winds found in closed
cellular cloud patterns are generally less than 20 knots.  The winds in open
cellular cloud patterns are generally 20 knots or higher.  When cellular
clouds are seen in lines close to a vortex, the winds are sometimes 50 knots
or higher.  Investigations indicate that specific categories of wind speed
based on cellular cloud patterns may be found in some local areas [13].
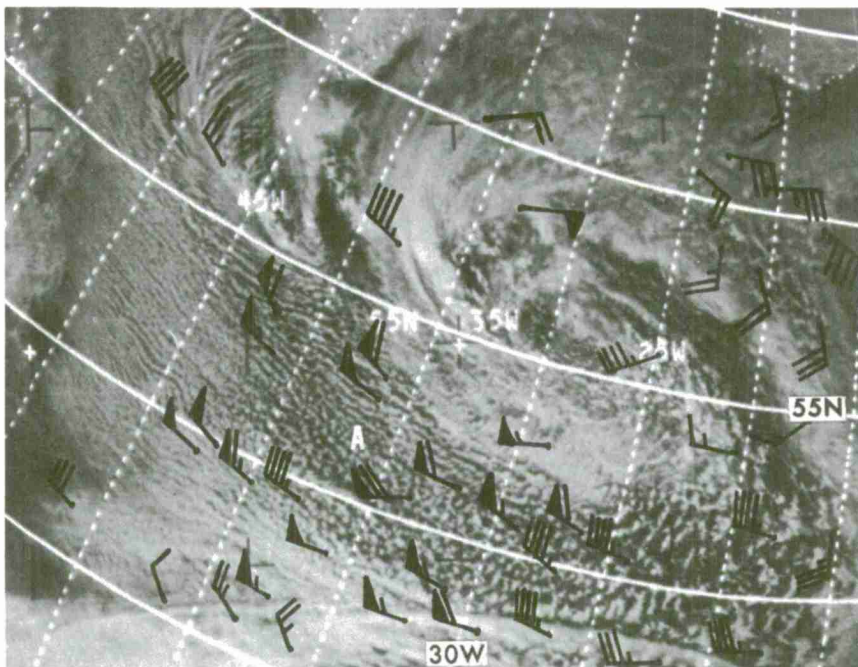


E-3 1986-2 1500Z 9 Feb 67
Winds 1200Z and 1800Z 9 Feb 67

Figure 3-I-3.  Winds of 50 knots or greater are
located at A, south of the vortex.  Notice the tendency
of the open cells to form into lines.

Wind Speed from Narrow Cloud Lines Near Continents

When cold air streams off the continents, cumulus clouds form over the warmer ocean surface.  Observation has shown that, if these cumulus clouds initially form as narrow lines, the surface wind speed will be on the order of 20 knots or greater.
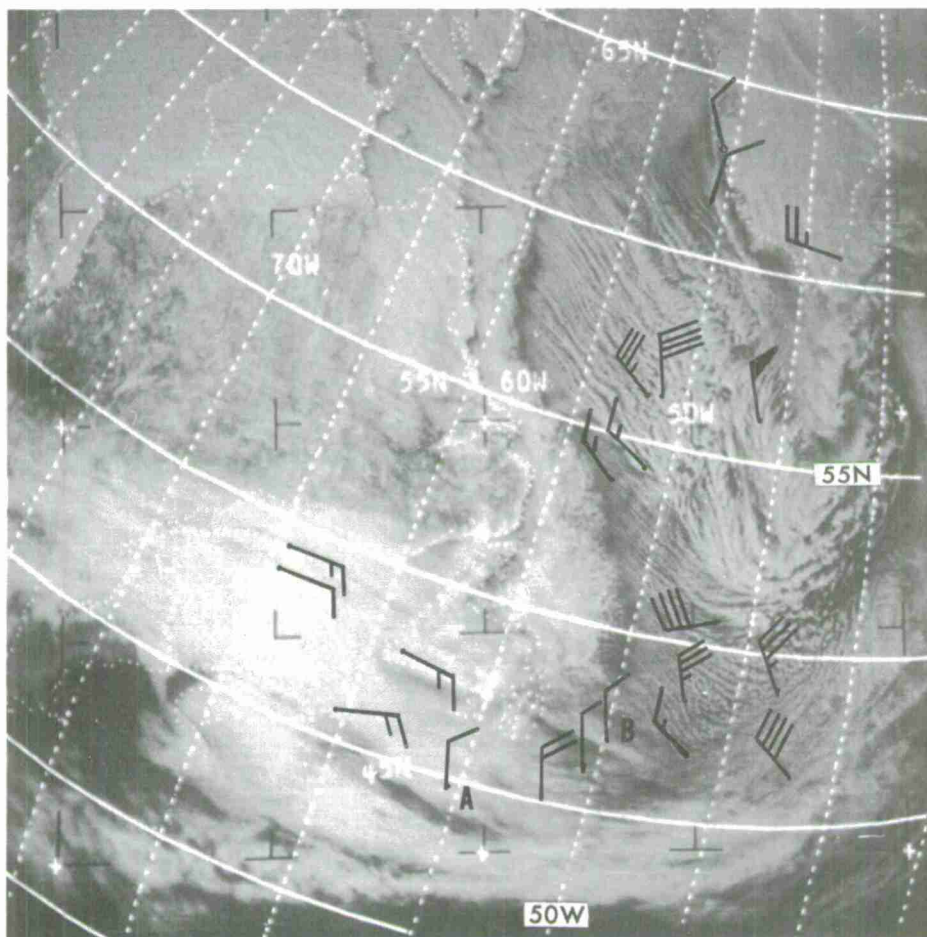


E-3 2012-2 1645Z 11 Mar 67
Winds 1200Z and 1800Z 11 Mar 67

Figure 3-I-4.  Narrow cloud lines initially forming off the coast of Newfoundland north of 47N are associated with surface winds greater than 20 knots.  From A to B the winds blowing off the continent are generally less than 20 knots and narrow cloud lines are not observed.  This is the region where the flow turns anticyclonically and the pressure gradient is weaker.

Wind Direction from Sea Breeze

    The sea breeze is indicated by the distribution of clouds along the coast-
lines of large water bodies.  This pattern consists of a narrow cloud-free
area along the immediate coast corresponding to a diurnal onshore low-level
flow.  Further inland, convective cloudiness will form in an area of upward
vertical motion.  Offshore, in the region of downward vertical motion, there
will usually be an area of relatively clear skies.

    Figure 3-I-5.  The cloud pattern
resulting from a sea breeze can be
readily seen along the coasts of Viet-
nam, China, and Hainan Island.  Surface
reports showed light onshore winds.
From A to B and along the east coast of
Hainan Island, the low-level flow is
easterly while from B to C, the low-
level flow is southerly.  Cumulus and
cumulonimbi form a sea breeze front a
few miles inland along the Vietnam
coast, marking the westward penetra-
tion of the sea breeze.  The clear
area surrounding Hainan Island south-
ward to the equator outlines an area
of downward vertical motion due to the
sea breeze.
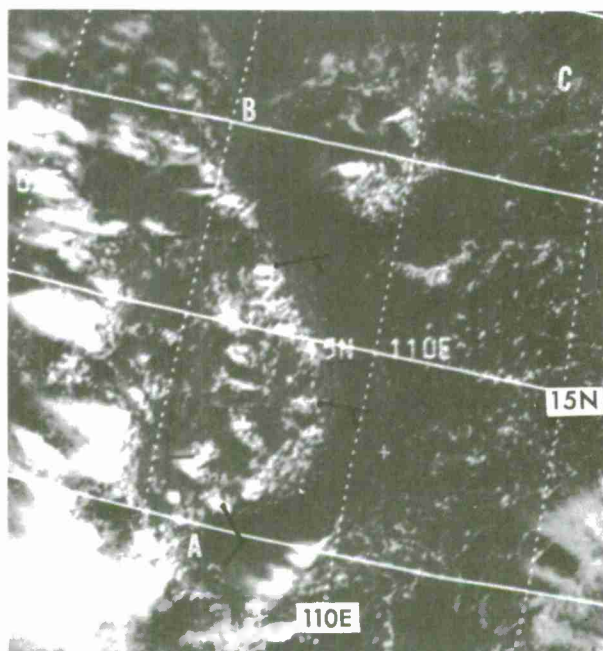


E-5 1151-7 0750Z 20 Jul 67
Winds 1200Z 20 Jul 67

Figure 3-I-6.  Mostly clear skies
encircle Lake Michigan, at A, and
Lake Superior, at C, outlining the
limits of the lake breeze.  The lake
breeze is less pronounced in the pre-
vailing southerly flow over Lake On-
tario, at B.
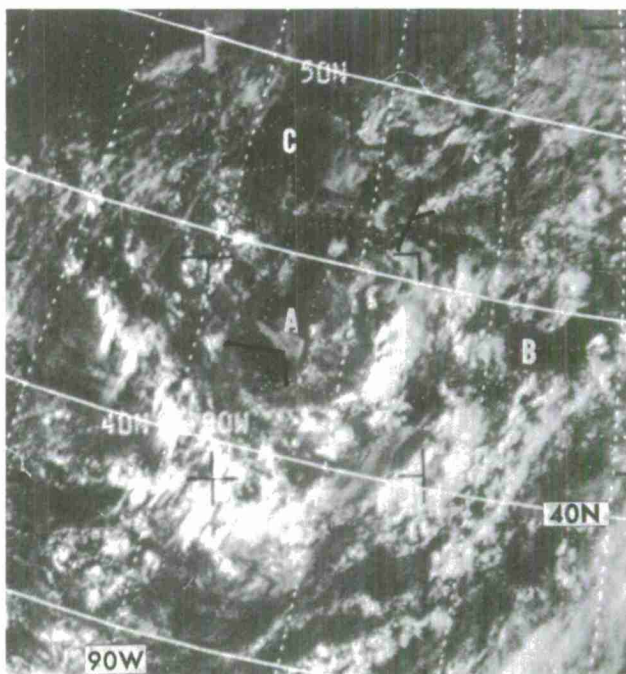
E-5 1145-5 2036Z 19 Jul 67
Winds 1800Z 19 Jul 67



Figure 3-I-7.  Cumulus clouds are
widespread over the jungle lowlands
of eastern Brazil except along the
immediate coastal region.  This clear
land area between A and B is a result
of the sea breeze and indicates a
low-level easterly wind nearly per-
pendicular to the coastline.
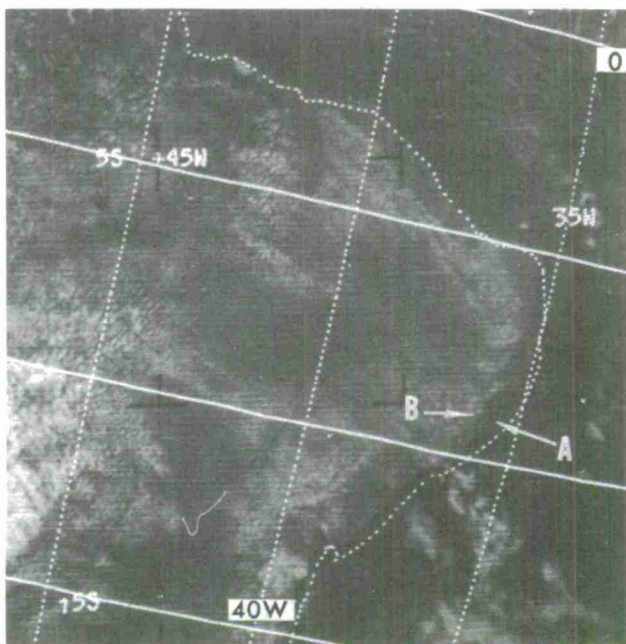
E-7 654-7 1757Z 7 Oct 68

## Wind Speed from Sun Glint

There are certain angles between the sun and the satellite cameras that can result in the observation of a sun glint from a water body. When the water body is very smooth, it acts like a mirror as it reflects the incident light. When the reflected light enters directly into the camera, a very bright image is seen but, if the reflection lies outside the camera view, the water surface will appear darker than the surrounding regions. For this situation to occur, it is necessary for the water surface to be extremely calm and smooth. A rougher water surface will result in more reflecting surfaces and will yield a more diffuse sun glint [24].

In general, small bright sun glints will be associated with lighter surface winds than large diffuse sun glints [8] [14]. The very dark zone which may be adjacent to the bright sun glints marks the axis of weakest winds and may coincide with a surface ridgeline. Winds of 10 knots or less are most often associated with very bright sun glints and winds of 10 knots or greater are probable with more diffuse sun glints.
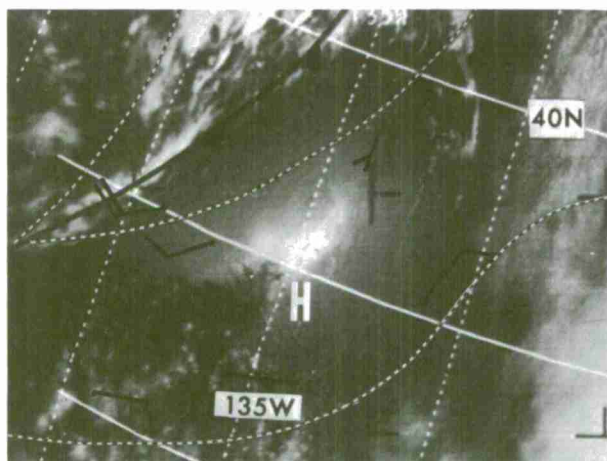


E-5 1476-5 2317Z 14 Aug 67
Analysis 0000Z 15 Aug 67

E-3 620-3 2045Z 20 Nov 66
Analysis 1800Z 20 Nov 66

Figure 3-I-8. A bright sun glint with a very dark zone to the southwest identifies an area of light winds. The axis of the bright and dark zone coincides with the calm zone along the surface ridgeline.

Figure 3-I-9. A sun glint of moderate intensity south of Baja California coincides with an area of relatively light surface winds averaging 5 to 10 knots.

## Wind Direction from Island Effects

The interruption of large areas of fog, stratus, or stratocumulus by is-
lands often gives a clue to the low-level wind direction.  The low-level
clouds are usually advected along with the low-level winds and will accumulate
on the upwind side of the island and be absent for a distance on the downwind
side of the island.  Further downstream the clouds will re-form.
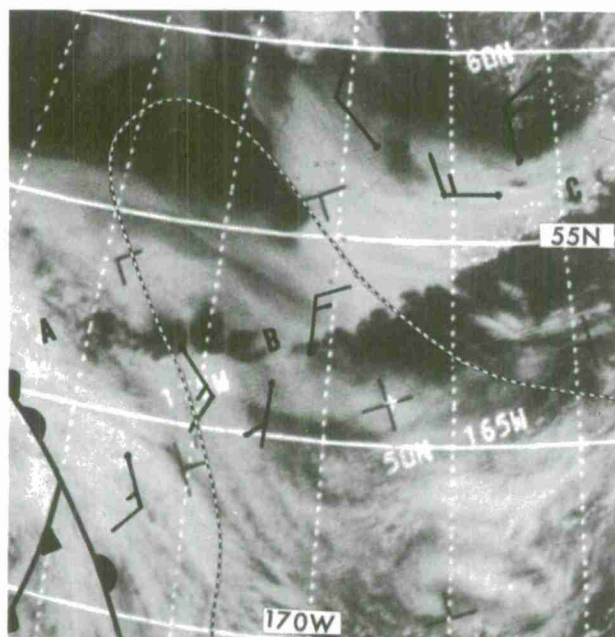


E-5 894-4 0128Z 30 Jun 67
Analysis 0000Z 30 Jun 67



E-7 656-4 2200Z 7 Oct 68
Analysis 0000Z 8 Oct 68

Figure 3-I-10.  The Aleutian
Chain, from A to C, is surrounded by
a large field of fog and stratus.
From A to B the winds are primarily
southerly with a resultant clear area
to the north of the islands.  Surface
winds are north to northwest from B
to C causing the fog and stratus to be
blocked along the north shore of the
chain with a corresponding clear zone
to the south.

Figure 3-I-11.  A large field of
stratocumulus formed by the advection
of cold air, capped by a strong in-
version, over warmer water is inter-
rupted at A, by Guadalupe Island.
The breaks in the clouds and some
eddies on the southern or downwind
side of the island indicates a north-
westerly surface wind direction.

Wind Information from Anomalous Cloud Lines

The presence of anomalous cloud lines in satellite pictures is usually in-
dicative of relatively light low-level winds.  Anomalous cloud lines tend to
persist for periods of several days.  Distortions in these lines from day to
day indicate either differences in low-level wind direction or in low-level
wind speed.  Different wind directions can move the cloud lines in different
directions and different wind speeds can move one portion of an anomalous line
faster than another portion of the same line.
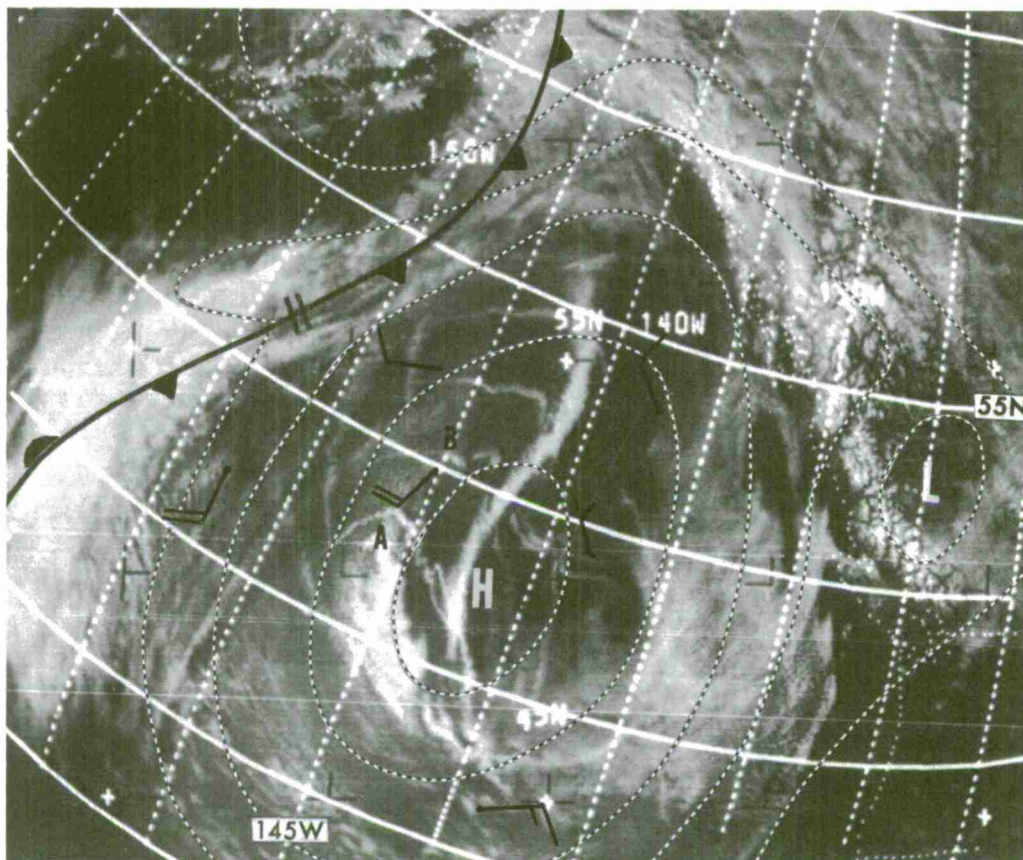


E-3 1927-2 2218Z 4 Mar 67   Analysis 0000Z 5 Mar 67

Figure 3-I-12.  Anomalous lines in the vicinity of a high
pressure cell, in the Eastern Pacific, are associated with rela-
tively light low-level winds.  At A and B the anomalous lines
are bowed to the north indicating a possible southerly low-level
wind.

Wind Direction from Ice Movement

Regions of ice will often be pushed away from the lee shore by low-level winds that persist over long periods of time. A narrow black line indicating the location of open water or newly-formed ice will result as the old ice pack is pushed away from the shoreline.
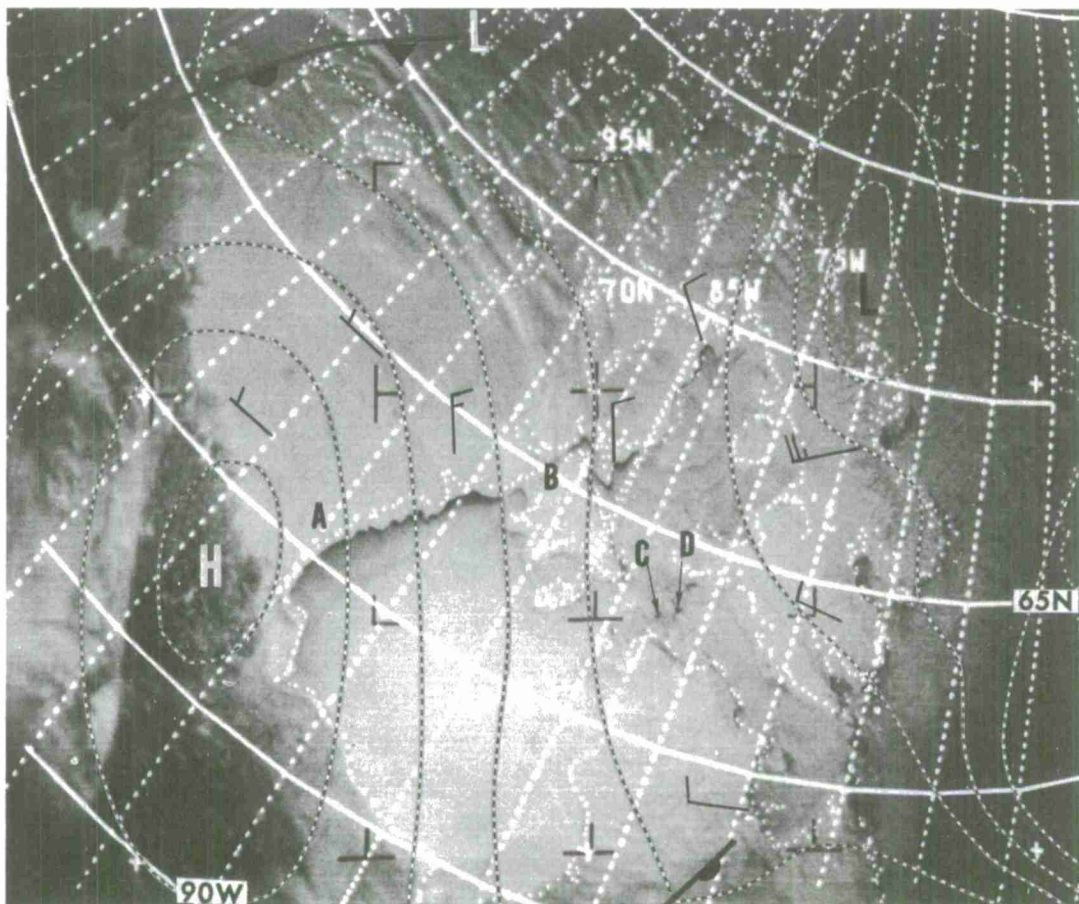


E-3 2113-1 1748Z 19 Mar 67   Analysis 1800Z 19 Mar 67

Figure 3-I-13. Open water or newly-formed ice along the shoreline of Hudson Bay, from A to B, is the result of a persistent north to northwesterly surface wind. These winds have also caused the ice to pile up along the windward shore of the bay. Small regions of open or new ice can also be seen downwind of Nottingham and Salisbury Islands, C and D, respectively. Patches of open water or new ice are widespread along the east coast of Baffin Island in the general offshore flow.

## Wind Direction from Orographic Effects

There are many areas in the world where terrain-induced cloudiness will give an indication of the low-level wind direction. In many cases, this process will consist of an upslope flow producing clouds that are finally blocked by higher mountains.
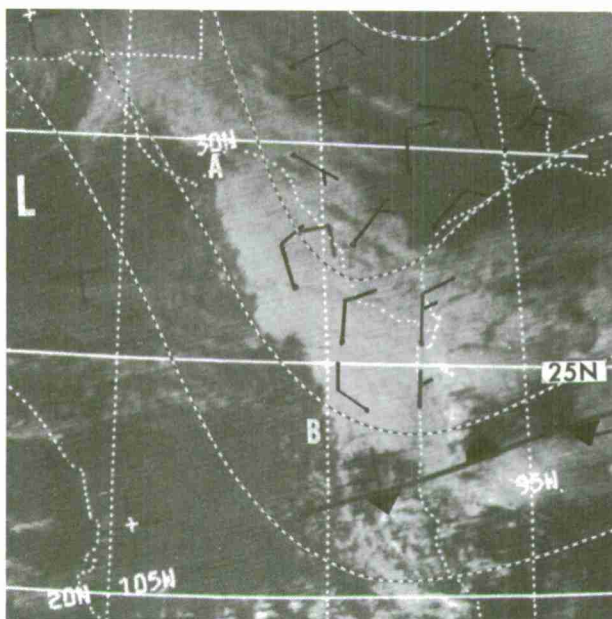


E-7 1044-4 2134Z 7 Nov 68
Analysis 2100Z 7 Nov 68
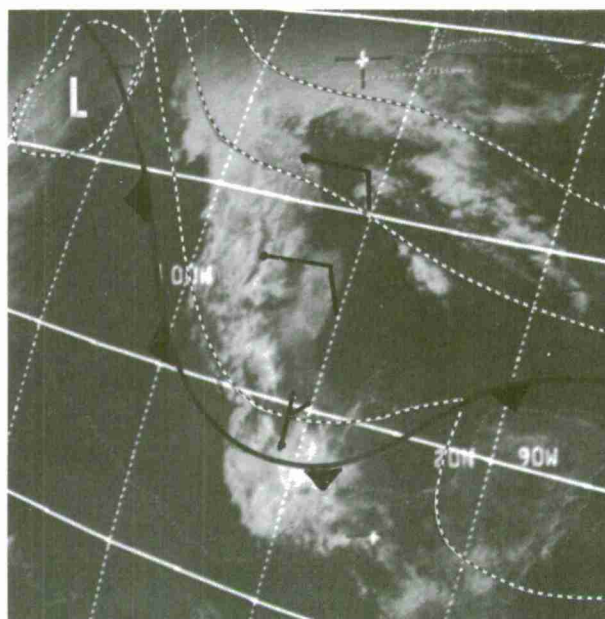


E-3 6271-4 1834Z 13 Feb 68
Analysis 1800Z 13 Feb 68

Figure 3-I-14. The deck of low clouds along the east coast of Mexico is the result of an upslope north to northeasterly low-level flow. The clouds pile up and end along the eastern slopes of the Sierra Madre Oriental Mountains from A to B.

Figure 3-I-15. Low clouds consisting mostly of stratocumulus are the result of an onshore low-level wind. The western boundary of these clouds conforms to the mountains of central Mexico.

Chapter 3


SECTION J


MEAN WIND SPEED IN THE TROPOSPHERE


An estimate of the mean wind speed through the troposphere (U) can be obtain-
ed from wave clouds by using the equation $U = 6L + 10$ where L = the wave-
length, in nautical miles, which is obtained by measuring the total distance
covered by a representative sample of mountain wave clouds divided by the
number of wave clouds in the sample (59). The equation shows that wind speed
increases as wavelength increases.
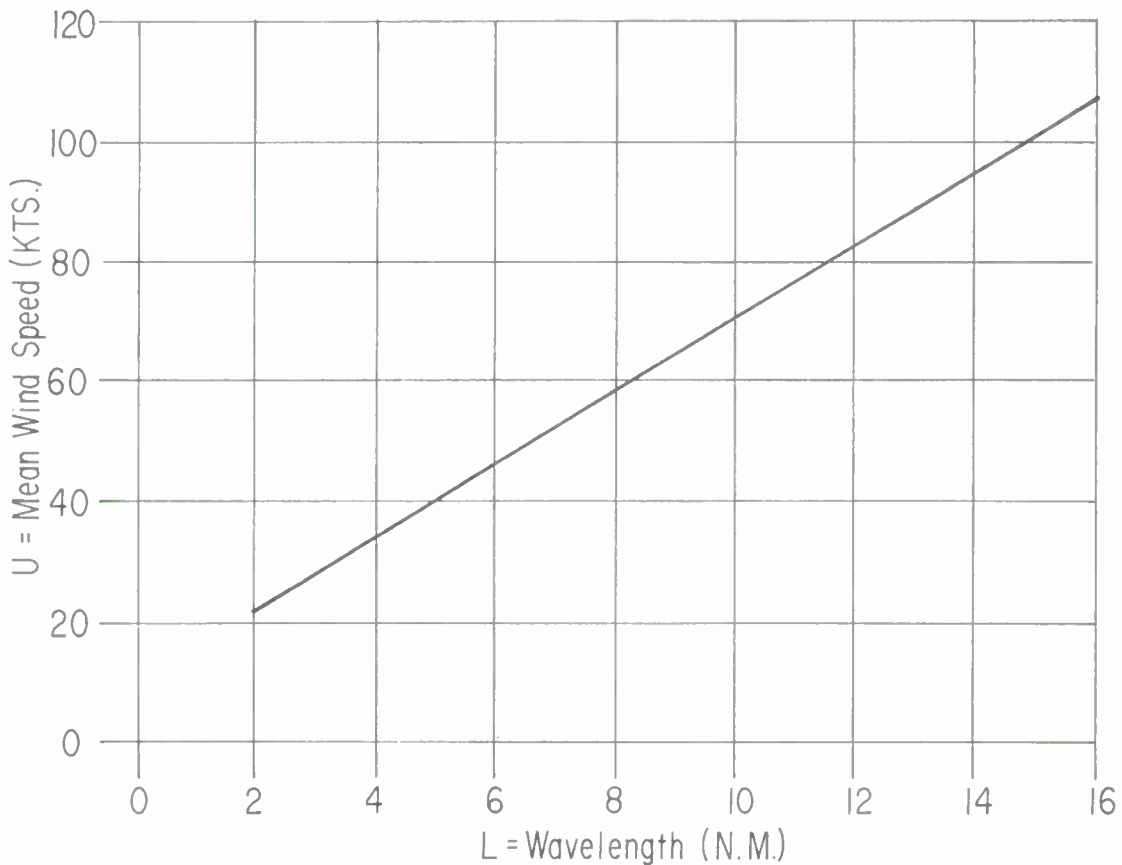


Figure 3-J-1. This graph shows the variation of mean wind speed with wave-
length in the troposphere. For example, a measured wavelength (L) of 10
nautical miles indicates a mean wind speed (U) of 70 knots.

Figure 3-J-2. Mountain wave clouds from Oregon to Utah are imbedded in a northwesterly flow that averages 89 knots from 5 to 40 thousand feet. Twelve individual wave clouds between A and B gives a wavelength (L) of 13.3 nautical miles and a calculated mean tropospheric wind speed of 90 knots.
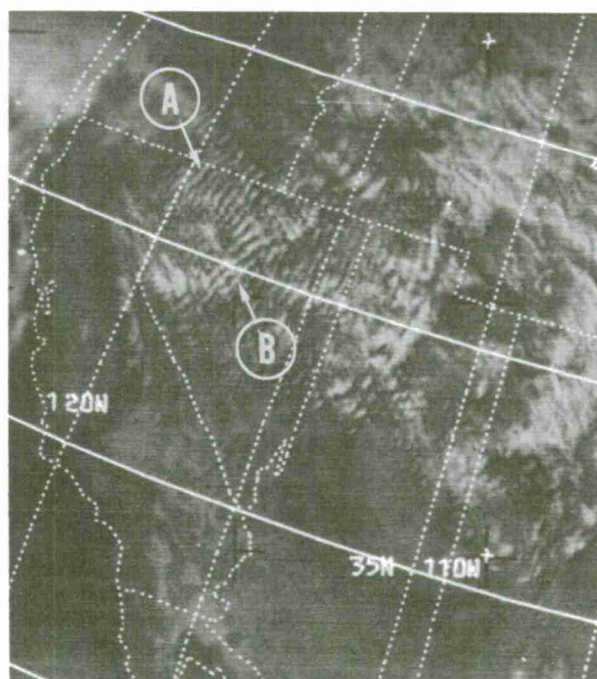


ESSA-7 1069-3   2135 GMT November 9, 1968

Figure 3-J-3. A wavelength (L) of 9.6 nautical miles for the 10 waves between A and B results in a calculated mean tropospheric wind speed of 68 knots. The observed mean tropspheric wind speed is 61 knots from 5 to 40 thousand feet. These mountain waves over and downstream of the Allegheny Mountains are in a northwesterly flow with a maximum speed of 86 knots at 36,000 feet.
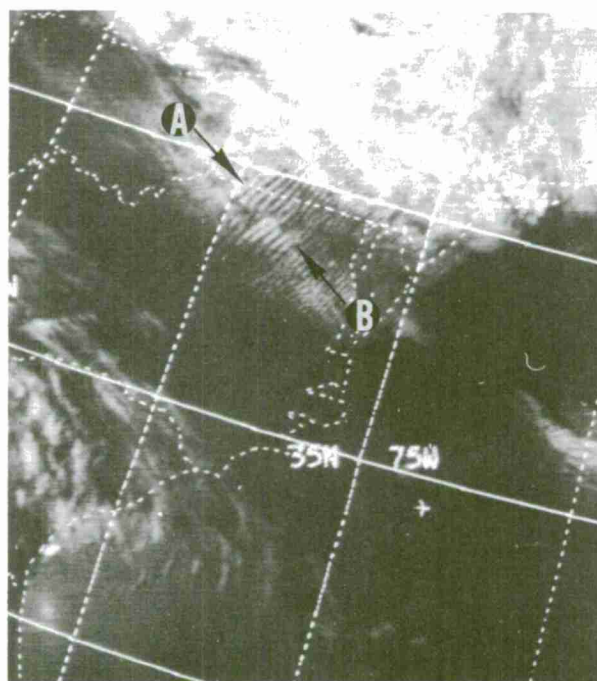


NOAA-1 1695-2   1930 GMT   April 25, 1971

Chapter 4

APPLICATION OF SATELLITE DATA TO SYNOPTIC ANALYSIS IN THE TROPICS

SECTION A

INTRODUCTION

In the tropics, direct analysis of the wind field plays an important role
in daily synoptic analysis.  Clouds over the tropics, viewed from satellite
altitude, reveal many features of the flow.  First, the distribution of wide-
spread cloud systems has  definite relationships to major trough and ridge po-
sitions and make possible qualitative estimates of the general flow.  Secondly,
wind estimates for both upper and lower tropospheric levels can be obtained
from an analysis of cumulus and cirrus cloud formations.  These estimates are
based either on the interpretation of a single picture or on actual measure-
ments of cloud motion from a series of pictures.

Wind speeds associated with tropical storms can be accurately assessed (±
20 knots) by the application of empirical rules concerning the appearance of
the associated cloud systems.  Thus, by interpreting satellite data in terms
of wind flow and storm intensity, it is possible to make daily synoptic analy-
ses over large areas of the tropics where other data are sparse or nonexistent.
Before discussing in detail methods of interpretation, we will first summarize
and define some features of tropical flow.

The majority of tropical storm development in each hemisphere is restrict-
ed, for the most part, to the summer and early fall.  During this season,
there are certain features of the large-scale flow which control cloud distri-
bution and define areas where tropical disturbances are most likely to form or
to intensify.  Near the equator, the equatorial trough is a breeding ground
for storms; in the trades, the upper tropospheric (300-200 mb), mid-oceanic
troughs [34] are responsible for disturbances with potential for development.
The position of the subtropical high pressure belt also controls the area
where storms can form.  In the day-to-day interpretation of satellite data,
these characteristics of the broad-scale flow must be kept in mind.  To assist
in this, Figure 4-A-1 has been prepared.  It shows the mean summer positions
of the upper level mid-Pacific and mid-Atlantic troughs and ridges for the
Northern Hemisphere [34]; the mean summer position of the surface subtropical
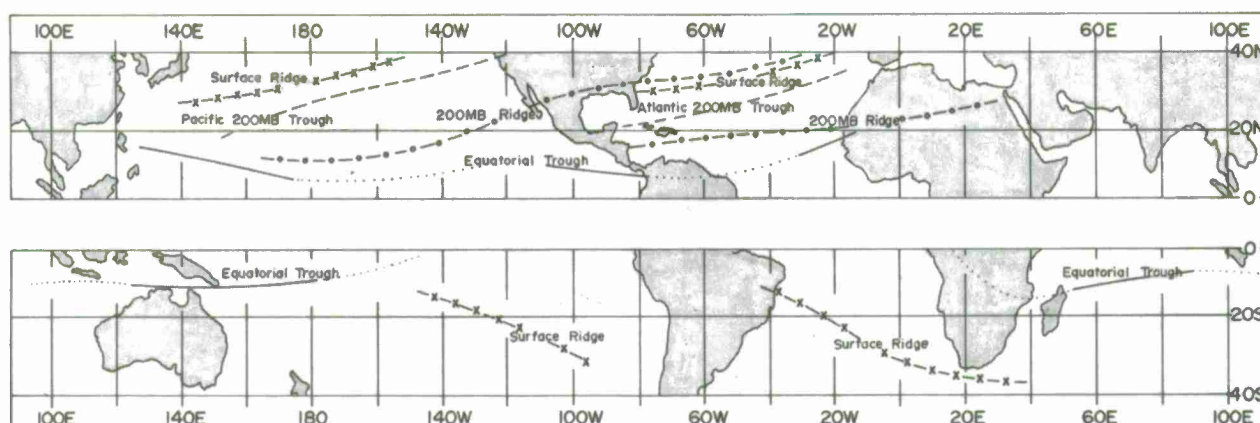
Figure 4-A-1.  Climatological positions of controlling circulation features of the tropical atmosphere for the Northern Hemisphere and Southern Hemisphere summer seasons.  A solid line indicates the active portion of the equatorial trough with respect to tropical storms; the dotted line the inactive portion.

highs in both hemispheres [36]; and the mean summer position of the equatorial trough in both hemispheres [33].  The solid line depicts the doldrum portion of the trough where the air is calm along the trough.  The dotted portion is the trade wind equatorial trough where surface easterlies replace calm conditions.  No mean positions for Southern Hemisphere mid-oceanic troughs are shown since these are not yet established.
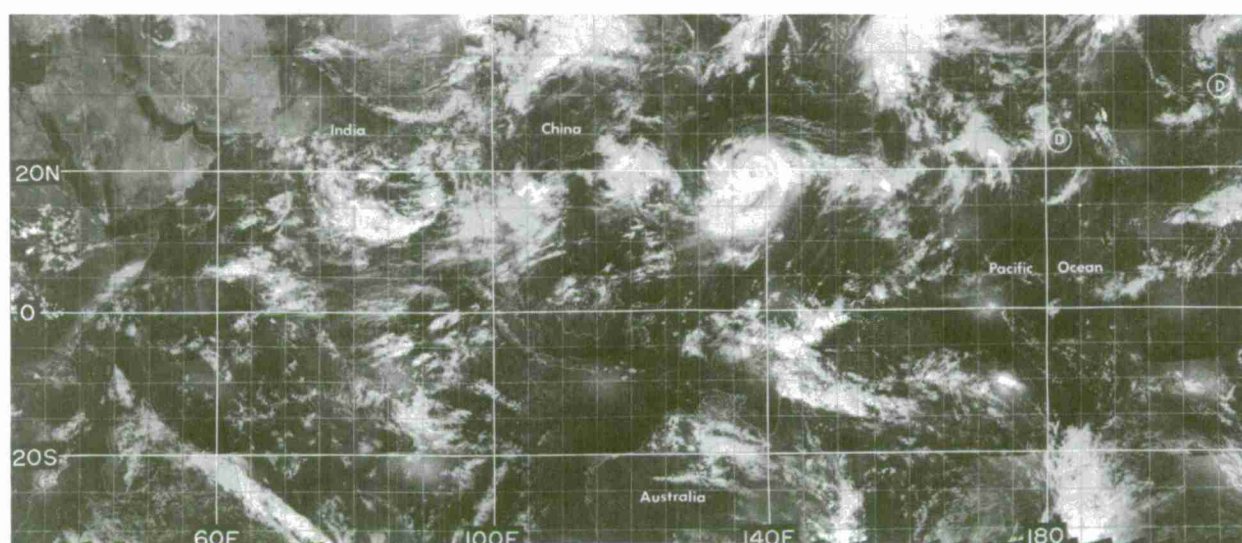


Figure 4-A-2.  Global view of the tropics for 1500 local time, 5-6 Septem-

A view of the clouds over the tropics in September appears in Figure 4-A-2.
This composite picture of mapped digital data covers a 24-hour period begin-
ning at 1300Z, 5 September 1968 on the right, and ending at 1200Z, 6 September
1968 on the left.  This picture contains an example of most of the cloud for-
mations that will be discussed in this chapter.

On this day, the extensive cloud band associated with the zone of Inter-
tropical Confluence (ITC)[1] appears between 5 and 10 degrees north and extends
over the eastern Pacific as well as the eastern Atlantic and western Africa.
This band generally lies immediately north of the equatorial trough.  The ITC
cloud band may appear as a narrow (2-3 degree latitude), continuous formation
thousands of miles long or as a series of discontinuous synoptic-scale cloud
systems.  On this particular day, it is both relatively active and continuous
over the eastern Pacific and Africa.

Several waves in the easterlies appear over Africa and the eastern Atlan-
tic in the form of increased convective cloudiness along, and just to the
north of, the ITC band.  These are identified by letter "W's" in the picture.
Disturbances are also visible at higher latitudes in the trade wind belt in

---

[1] Intertropical Confluence (ITC) is defined by the Regional Tropical Analysis
Center at Miami as follows: "A nearly continuous fluence line (usually con-
fluent) representing the principal asymptote of the Equatorial Trough." [26]
This terminology is used in place of the older concept of an Inter-Tropical
Convergence Zone (ITCZ).
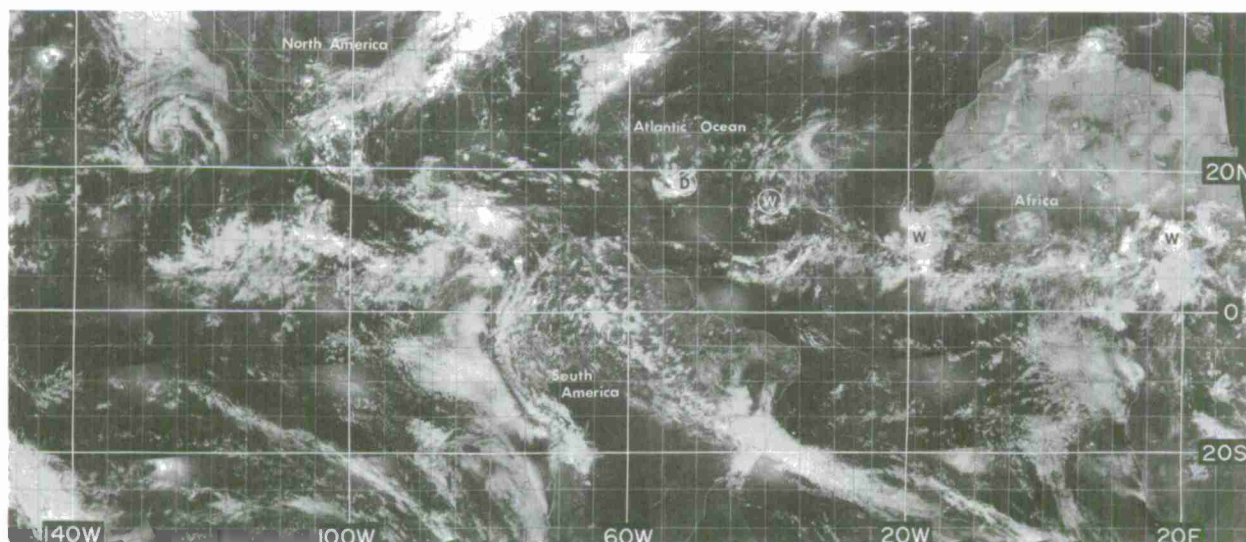


ber 1968, ESSA 7.

both the North Pacific and North Atlantic.  These cloud formations lie along
the mid-oceanic troughs and are indicated by letter "D's" in the picture.

Three mature tropical storms are visible in the North Pacific: the one
west of Mexico (27N, 127W) has lost its cirrus canopy and is dissipating; the
storm at 20N, 137E, has just reached maturity and is a full-fledged typhoon;
the tropical storm at 20N, 120E, is weaker and shows less organization.  Vari-
ations in cloud-system size and degree of organization, such as appear here,
allow storms to be classified as to their intensity.

The organized appearance of cirrus plumes over the western tropical Pacif-
ic and Indian Oceans is apparent in Figure 4-A-2, even at the reduced scale of
the picture.  The plume structure is aligned along, and defines, the high-
level easterly flow over that area.  On any one day, 100 or more wind esti-
mates from cirrus plumes are possible over the tropics [37].

In the Southern Hemisphere, cloud bands representing fronts and frontal
shear lines are seen deep in the tropics over Brazil, in the eastern Pacific,
and in the Indian Ocean.  The only tropical disturbance in the Southern Hemi-
sphere is near the equator just north of New Guinea.

Routine daily satellite coverage, such as that mapped in Figure 4-A-2, re-
veals definite interactions that occur between the mid-latitude westerlies and
the tropical cloud system along the ITC.  These produce surges of clouds and
moisture poleward into temperate latitudes with accompanying significant
changes in the weather.

Daily cloud pictures increase our ability to define both the broad-scale
flow as well as the perturbations within it.  This leads to a much better un-
derstanding of the types of flow patterns which produce the synoptic-scale
cloud formations which we observe daily in the pictures.  At this time, our
understanding of the dynamics and the energetics of the tropics is too incom-
plete to model the tropical atmosphere to the degree that has been possible at
higher latitudes.  But, with our increasing knowledge of the relationships of
clouds to upper and lower tropospheric flow, descriptive models are being de-
veloped which help with day-to-day analysis problems.  This chapter discusses
some of these models and shows how they can be combined with wind-estimating
procedures to produce a meaningful analysis over tropical, sparse-data areas.

Chapter 4

_____

SECTION B


SEASONAL CHANGES IN TROPICAL CLOUD DISTRIBUTION


Seasonal shifts of the basic atmospheric currents produce significant
changes in tropical cloud distribution.  These changes are clearly revealed by
mean cloud charts prepared from mapped digital satellite data.  This section
presents a series of pictures (Figures 4-B-1 to 4-B-4) showing three-month
cloud brightness averages for the year 1967.  These were prepared by photo-
graphically averaging individual daily ESSA montages (such as Figure 4-A-2)
for the required period of time [38].  Because the ESSA satellites are in an
afternoon sun-synchronous orbit, the picture averages represent conditions for
1500 local sun time over the entire world.

The 1967 mean cloud charts reveal the following:

a.  The degree of seasonal meridional displacement of the cloud band asso-
ciated with the ITC;

b.  Changes in the amount of stratocumulus cloud present in the eastern
portion of oceanic subtropical highs as these highs intensify and weaken with
the seasons;

c.  Changes in convective cloud amount which occur over tropical land
areas with the coming of the summer season;

d.  The influence of topography and surface temperature on mean cloud con-
ditions.

It is important to keep in mind variations in the reflectivity of the
earth's surface when interpreting these pictures in terms of average cloud
cover.  For example, the bright appearance of North Africa is not due to cloud
but to the highly reflective Sahara Desert area.  Other desert areas appear
similarly bright and they, too, are mainly cloud-free for the periods averaged.
Dark areas in North Africa are black rock formations.  They form a recogniz-
able pattern that appears in the picture averages of all four seasons.  Bright-
ness variations in Figure 4-A-2 furnish information on the difference in re-
flectivity between desert and vegetated regions when related to known geo-
graphical features.  Such information can be used to identify regions which
are commonly cloud-free but likely to appear bright in the averages.  Other

Fig. 4B1
Jan. - Mar.
Average 1967

Fig. 4B2
Apr. - Jun.
Average 1967
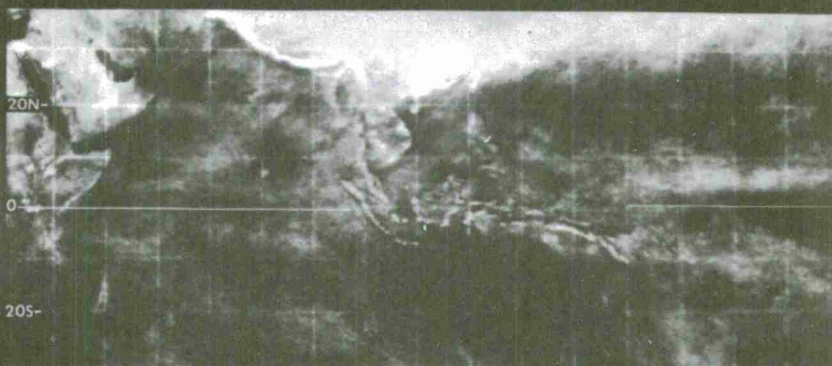
Fig. 4B3
Jul. - Sep.
Average 1967
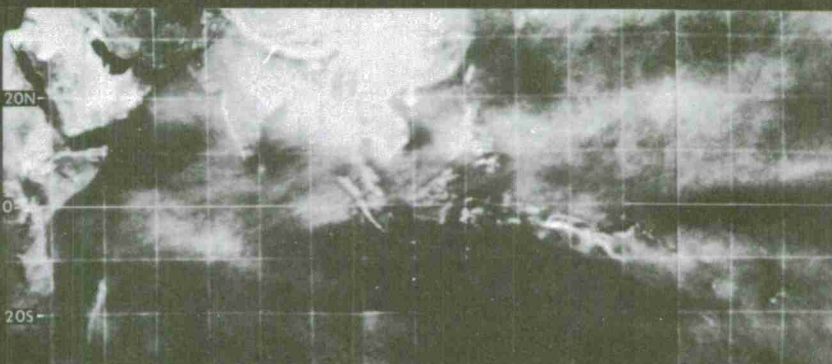
Fig. 4B4
Oct. - Dec.
Average 1967
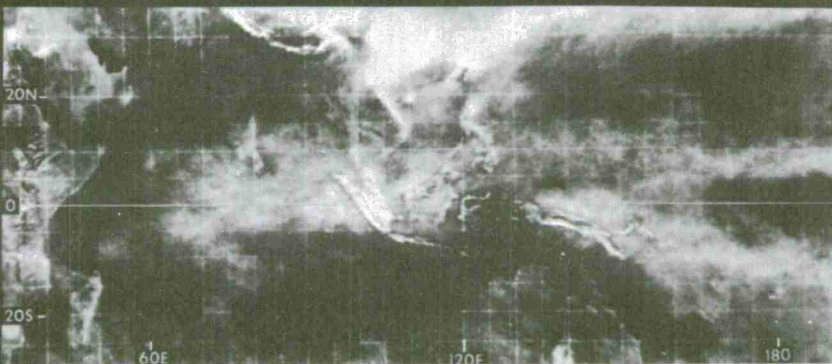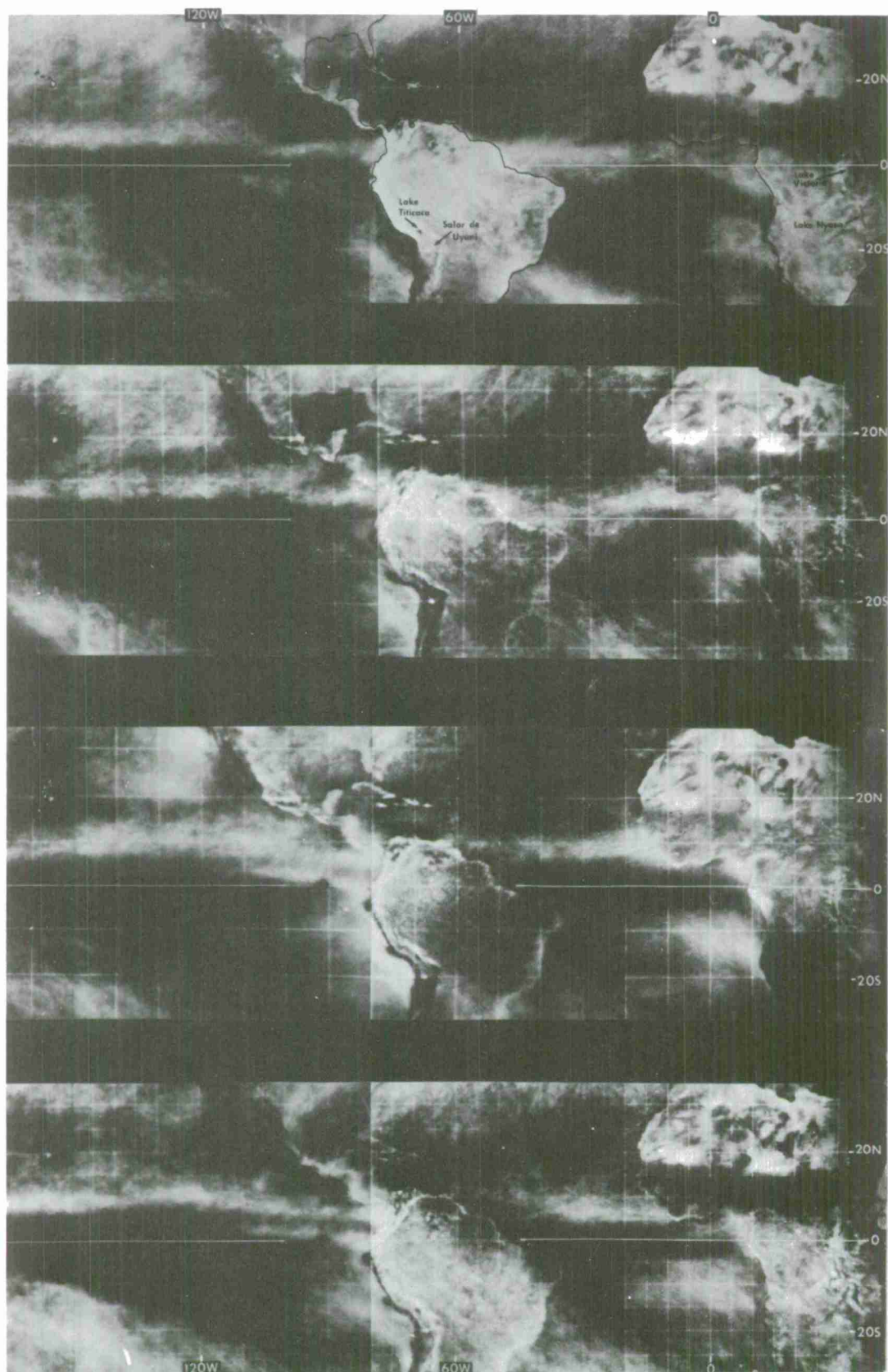
smaller, highly reflective areas also appear in the averages and these should
not be confused with cloud.  An example is the salt flat, Salar de Uyuni,
Bolivia, which appears as a white spot at 20S, 68W (Figure 4-B-1).  This fea-
ture is detectable in the averages for each of the four seasons.

The mean cloud pictures reveal that the ITC cloud band has somewhat dif-
ferent characteristics in different parts of the world.  In the Atlantic, it
is centered 3N in the winter season and moves to about 8N by late summer.  In
the Pacific, the seasonal fluctuation of the cloud band is not readily ap-
parent in that part of the band east of 150W.  West of this point in 1967, the
movements were not well defined.  Seasonal pressure changes over North America
may be responsible for the seasonal shift of the ITC cloud band in the eastern
part of the Pacific ocean.  The large area of relatively cloud-free skies
which appears southwest of Central America and Mexico in the picture for the
winter season suggests that dry wintertime continental outflow pushes the ITC
cloud band to the south in this area.  There is some evidence of a second
cloud band associated with the ITC in the eastern Pacific.  Besides the main
band north of the Equator, a weak band appears at 5S in the January through
March average.  The strength of this second band varies from year to year; in
some instances it fails to develop at all.  The ITC cloud band in the Indian
Ocean during the Southern Hemisphere summer is much broader than those of
either the Atlantic or eastern Pacific Oceans.

Seasonal changes in cloudiness over the continents are marked.  Over
Africa, the greatest changes occur over southwestern Africa which is nearly
cloud-free during the Southern Hemisphere winter but quite cloudy in the sum-
mer.  A similar effect has been noticed in Australia and India.

The inhibiting effects of cool water on cumulus formation are readily seen
in these averages.  The abrupt southern edge of the ITC cloud band in the
eastern Pacific parallels the northern edge of the cold Humbolt current.  No
deep convection occurs over the cold water in any season.  Over Africa, Lake
Nyasa (12S, 35E) and Lake Victoria (2S, 33E) (Figure 4-B-1), both appear dark,
which is attributed to less cumulus forming over the lakes than over the sur-
rounding land and foliage.

The averages show that mountains play a strong role in the distribution of
mean cloudiness.  The Andes mountains through tropical South America are most-
ly cloud-covered throughout the entire year.  Here, the "chimney effect" of
the mountains produces local convergence and convection over the mountain
ridges.  The orographic effect of mountain ranges on clouds can be seen by
noting conditions along the entire west coast of India in the July to Septem-
ber averages.  The Western Ghats block the southwest monsoonal flow and pro-
duce a seasonal increase in clouds along the windward side of the range.  An

example of marked downwind clearing occurs west of the Philippines during winter.  The northeast monsoonal flow is blocked by the mountains of northern Luzon resulting in a reduction of average cloudiness to the west.

The effects of local sea breeze circulations in concentrating clouds along the coastlines are also apparent in the averages.  This is particularly evident along the coastline of Brazil (Figure 4-B-3), and the northeast coastline of Australia (Figure 4-B-1).  Besides concentrating clouds immediately onshore, the sea breeze circulation often produces a minimum of clouds offshore.  Evidence of this can also be seen along many of the coastlines in the seasonal illustrations.

The concentration of clouds over islands is quite clearly shown.  The islands in the Caribbean have more clouds, relative to surrounding oceans during all seasons, as do the islands in the North and South Pacific.  Note the island of Hawaii (19N, 155W), New Caledonia (22S, 165E), Fiji (17S, 178E), and the islands of Indonesia.

The seasonal averages clearly depict the seasonal shifts in the large-scale cloud formations.  They also show where topography and surface conditions combine to produce cloud distributions which change with seasonal wind shifts.  Only a very few examples are discussed.  It should be kept in mind that these averages represent only one year.

Chapter 4

SECTION C

SUBTROPICAL JET STREAMS

Subtropical jet streams can often be located in satellite data by the
clouds associated with them.  Cloud shields that are associated with a sub-
tropical wind maximum have certain visual characteristics.  In general,

a.  Ratio of the length of the cloud formation to its width is quite large.

b.  Cloud shields are usually connected with the ITC cloud band or emanate
from the area immediately to the north of this feature.

c.  Cloud shields often possess numerous small-scale bands oriented per-
pendicular to the direction of the main cloud band.  (Transverse bands or
cloud trails.)

As in the case of polar jet streams, the poleward edge of the cirrus shield
parallels the isotach maximum.  This edge is straight except over pressure
ridges where it curves following the anticyclonic flow.  Cirrus along the sub-
tropical jet stream is most commonly observed when the wind maximum originates
over the tropical oceans where there is a source of moisture.
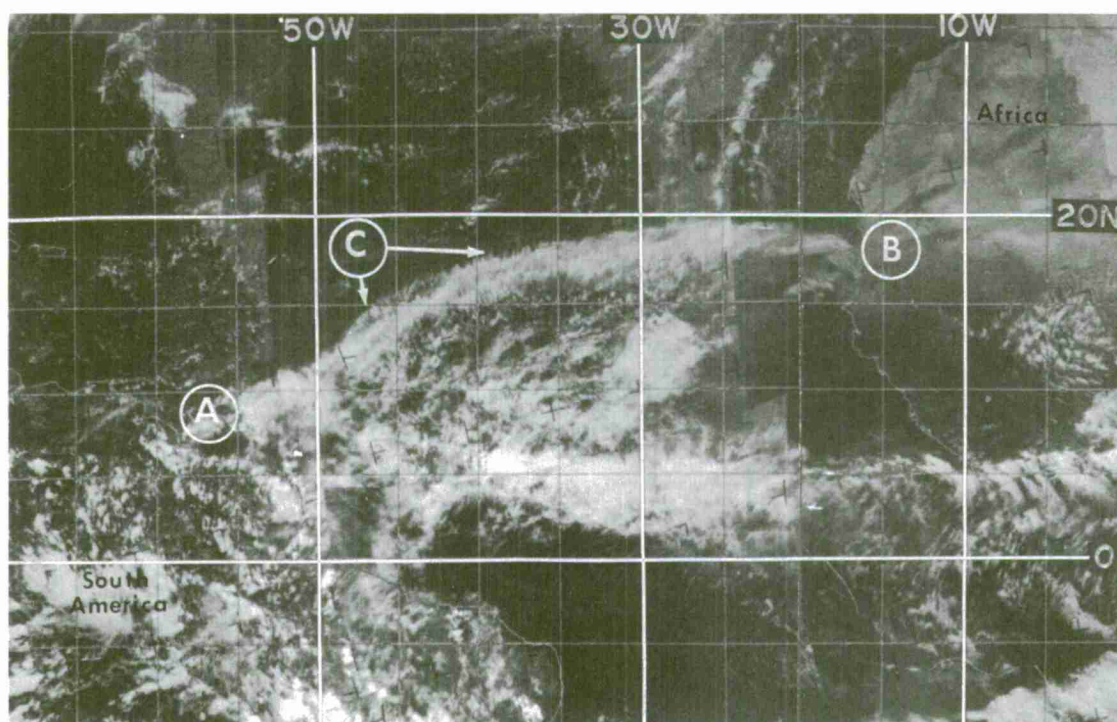
Figure 4-C-1.  Subtropical Jet Stream Cloud Formation, Atlantic
Ocean, 19 November 1968, ESSA 7.  The cloud shield from A to B is asso-
ciated with an upper wind maximum that stretches from the northeast
coast of South America to the west coast of Africa.  The poleward edge
of the shield curves slightly as the winds turn anticyclonically.  The
many small-scale lines (C) oriented perpendicular to the main shield
are typical of this formation.
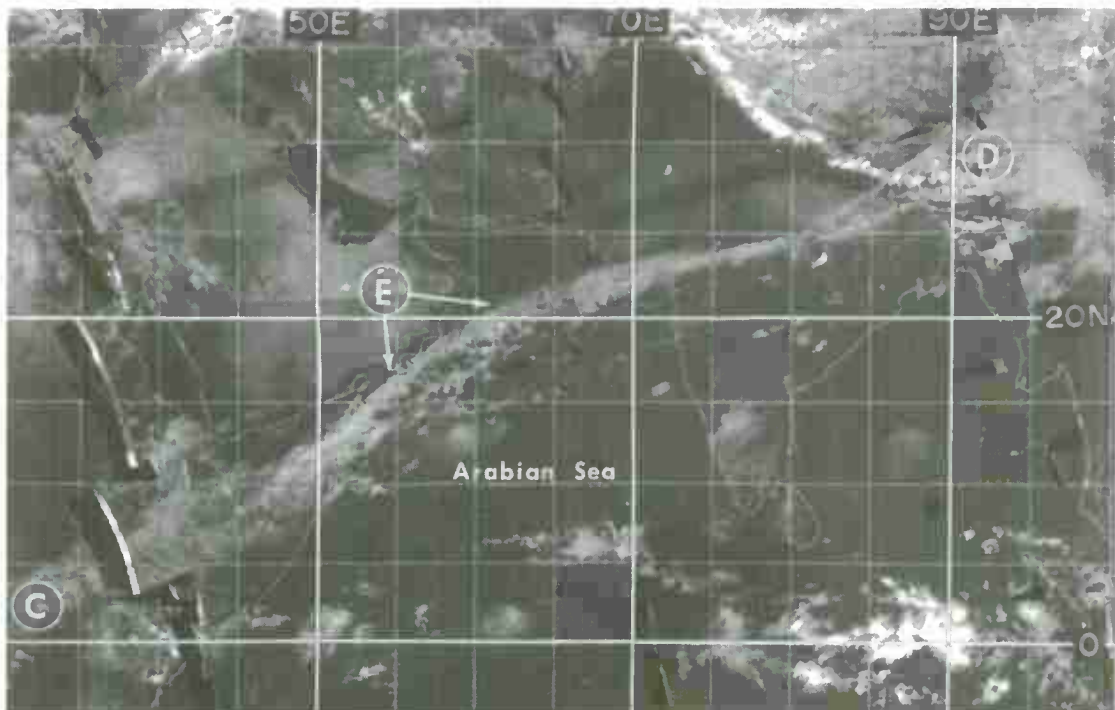
Figure 4-C-2. Subtropical Jet Stream Cloud Formation, Middle East,
15 April 1968, ESSA 3. This band of cirriform cloud is similar in ap-
pearance to the cloud shield in Figure 4-C-1 and is associated with a
high level wind maximum across the Arabian Sea. The clouds originate
in the ITC over eastern Africa (C) and are continuous from there to
Tibet (D). The characteristic transverse banding is evident at E.
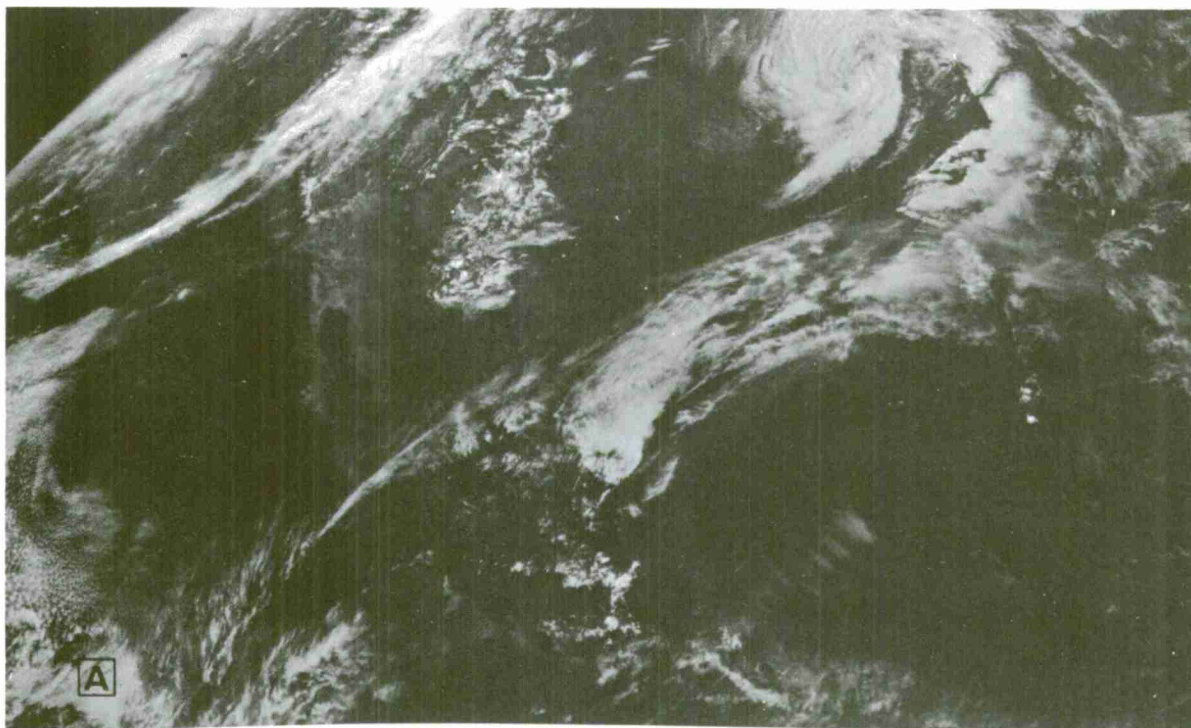
Figure 4-C-3. Subtropical Jet Stream Cloud Formation, North America, 23 April 1968, ATS-III. The long band of high level clouds which extends northeastward from A is located just to the south of a subtropical jet stream. The clouds represent a northward transport of energy from a disturbed area in the equatorial eastern Pacific Ocean. The winds obtained by measuring the movement of the cirrus clouds in this formation are shown in Figure 4-D-4.

Chapter 4

SECTION D

ESTIMATING WINDS FROM SATELLITE DATA

## Introduction

Experience has shown that two types of cloud patterns in ESSA AVCS pic-
tures provide information which can be used in defining upper level flow:

a.  Plumes from the tops of cumulonimbus clouds;

b.  Cirrus cloud shields associated with subtropical jet streams.

## Estimating Upper Winds from Cumulonimbus Plumes

Vertical wind shear through an atmospheric layer containing clouds is one
of the prime factors governing the shape of cloud formations.  Most of the
cloud lines and bands seen in satellite pictures are oriented parallel to the
thermal wind through the layer from cloud base to cloud top.  Under some cir-
cumstances, the direction of shear is the same, or nearly the same, as the
direction of motion of the air containing the cloud.  This is the case if:

a.  The wind changes speed with height but not direction;

b.  The wind changes direction with height but the winds at the top of a
cumulonimbus are much stronger than those near its base.

When these conditions occur, it is possible to estimate wind direction
directly from the orientation of cumulonimbus plumes.  These conditions are
common in tropical regions where the speed of the wind at the level of cumu-
lonimbus anvils is several times greater than the mean speed of the wind
through the lower portion of the cumulonimbus cloud.  In these cases, wind
estimates based on the orientation and dimensions of cirrus blow-off are quite
accurate and closely approximate the winds near the cloud tops.  Examples of
cirrus plumes appear in Figure 4-D-1.
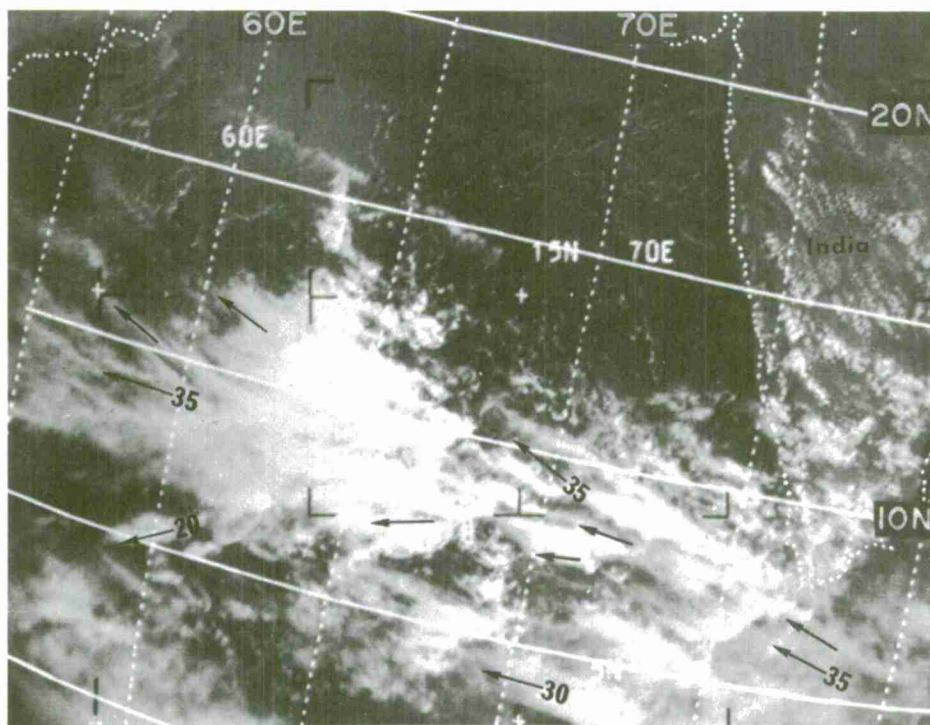
Figure 4-D-1. Long cirrus plumes, such as those seen
here over the Arabian Sea, indicate wind speeds of greater
than 20 knots. The orientation of the plumes suggests a
200-mb flow denoted by the arrows. Numbers near the arrows
are the wind speed estimates at cirrus level based on the
cloud appearance.


There are two conditions which can cause considerable error in wind direc-
tion estimates derived from cumulonimbus plumes:

a.  Light winds at cirrus level;

b.  A large difference between the direction of the shear through the con-
vective layer and the direction of the wind at the top of the layer.

When the speed is light (less than 20 knots), the wind direction is vari-
able causing the correlation between plume orientation and wind direction to
be less reliable.  If there is a large difference between the direction of the
shear through the convective layer and the direction of the wind at the top of
the layer, the plumes will be parallel to the shear but not to the wind at the
layer top.  This condition is common in frontal areas where temperature advec-
tion is strong, but occurs less frequently in the tropics.

Estimating Upper Level Flow from Cirrus Cloud Shields

It is common to observe huge masses of cirriform clouds extending poleward
from the tropics.  These clouds occur in advance of 200-mb troughs and repre-
sent a poleward transport of momentum and high level moisture from the tropi-
cal region.  A wind maximum is usually located on the poleward edge of these
cloud formations.  As with strong jet streams, the direction of the upper level
wind parallels the cloud edge.  Because the air is moving away from the equator
and accelerating, it is crossing the contour pattern toward lower pressure.
For this reason, the general orientation of the cloud shield and the stria-
tions within it can differ as much as 15 degrees from that of the upper tropo-
spheric contours.  When this is taken into account, cirrus formations of this
type provide good estimates of wind direction but less precise information as
to wind speed.  A typical cirrus cloud shield appears in Figure 4-D-2.
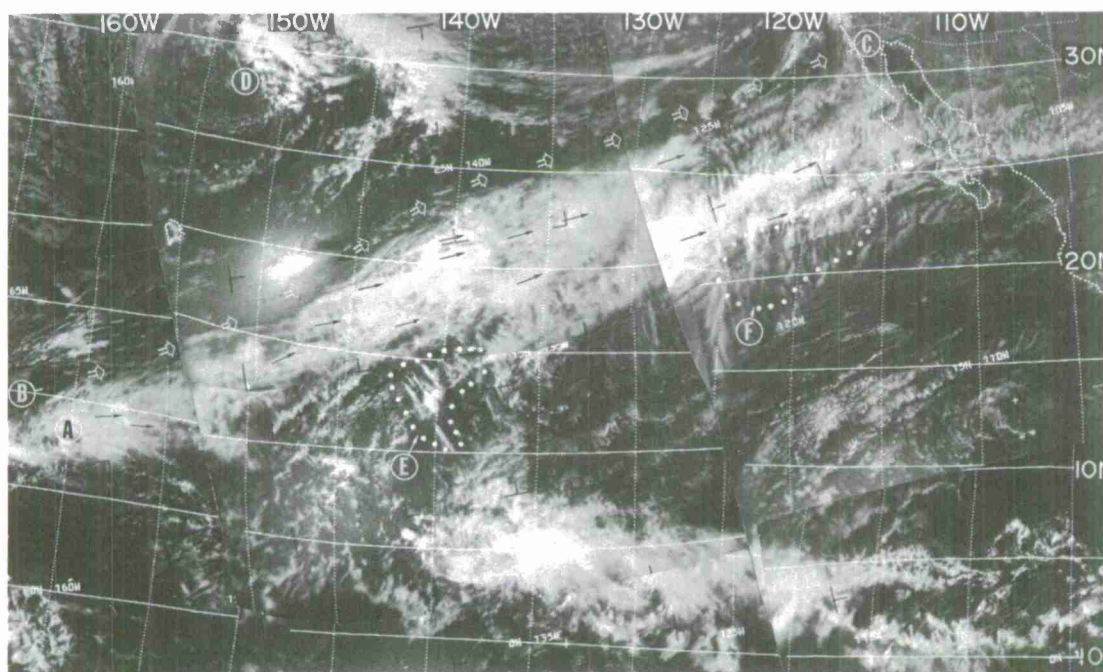


Figure 4-D-2.  Cirrus Cloud Shield Used to Estimate High Level Winds.  The
double-shafted, white arrows (B to C) represent the 200-mb wind maximum sug-
gested by the cirrus cloud edge.  The black, single-shafted arrows represent
200-mb flow based on individual cirrus elements that lie within the larger
scale formation.  The vortical cloud pattern (D) is associated with a cut-off
low.  Southeast of D, a cirriform cloud shield extends northeast from A in ad-
vance of an upper level trough associated with the vortex.  There are numerous
small-scale lines of clouds (E and F) which are oriented approximately perpen-
dicular to the wind direction.  These lines are believed to be caused by hori-
zontal shear and should not be confused with cumulonimbus plumes which are
oriented parallel to the vertical shear.

Rules and Guidelines for Estimating High Level Wind Speed

The techniques for assigning values to the wind speed are more complex and subjective and are based on the appearance of the clouds, climatology and continuity of flow. The estimates are best correlated with 200-mb winds. The following rules for making wind estimates are based on experience and research [37]. As used in the rules, wind strength is defined as follows: light wind, less than 20 knots; moderate wind, 20 to 50 knots; strong wind, greater than 50 knots.

a. Study climatological wind roses, mean wind direction, and wind speed charts to help make estimates of wind speeds within reasonable limits for a given area.

b. In dealing with wind maxima, such as those associated with jet streams, it is often desirable to make corrections for the change of speed with height. The use of a climatological atlas to determine a normalized wind profile gives the best results.

c. Westerly flow originating in equatorial areas generally becomes progressively stronger with increasing latitude.

d. Check continuity and nearby wind reports from recent upper air charts to guard against making unreasonable wind estimates.

e. If a cirriform cloud formation suggests the proximity of a jet axis, the winds are considered strong along the axis of the cloud formation.

f. The presence of transverse bands in cirrus indicates strong winds.

g. In a very general sense, the longer the plumes from cumulonimbus, the stronger the winds.

h. Over the tropics, the presence of diverging filaments of cirriform cloud from areas of solid convective cloudiness are generally indicative of weak high level outflow and light winds.

i. Streaky cirrus extending in one direction for hundreds of miles is associated with large-scale currents of moderate speed. This cloud formation is made up of rather long plumes oriented in the same or nearly the same direction.

j. Areas exhibiting a change in orientation of cloud trails within short distances indicate the presence of weak winds.

k. Empirical rules for various local areas are helpful. For example, some Indian meteorologists have found the strength of high level easterlies over the Bay of Bengal are directly related to greater convective activity.

l. If in doubt about a wind speed or direction, do not make an estimate.

## Estimating Low Level Winds from Cumulus Cloud Lines

Research has shown that many cumulus cloud lines observed between 10N and
10S over the Atlantic and eastern Pacific Oceans are oriented approximately
parallel to the surface wind direction [39].  Because the orientation of cloud
lines relates to the shear, these lines may depart considerably from the sur-
face wind direction.  Therefore, a great deal of caution must be exercised
when using them to define low-level wind flow.  There are no hard, fast rules
which permit positive identification of the particular cloud lines which are
approximately parallel to the surface wind.  It has been observed that cloud
lines which are very long, very narrow, and either wavy, zig-zag, or have
knots (wide places along a line) are the type most often parallel to the sur-
face wind [39].
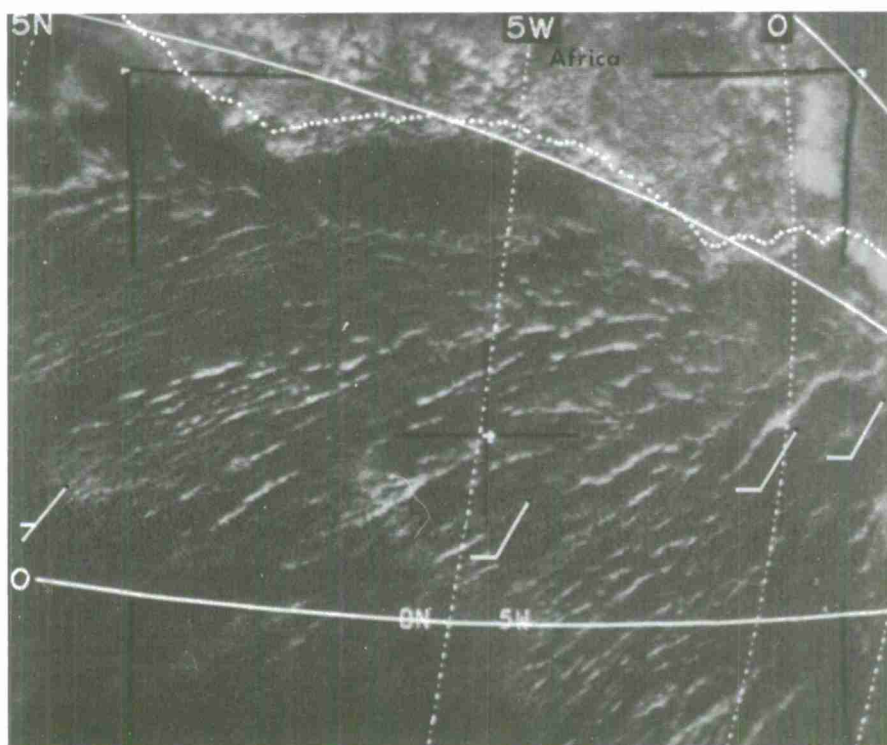


E-1 1441Z 19 Mar 66

Figure 4-D-3.  Cloud lines off the coast of Africa
are shown which are approximately parallel to the flow.
Surface wind reports are entered on the picture (white
arrows).

## Wind Estimates from Geostationary Satellite Data

More recently, the Applications Technology Satellites (ATS) have permitted continuous monitoring of weather patterns over much of the sunlit earth.  Time-lapse movies, prepared from pictures taken at 20-minute intervals, allow investigators to study time changes in size, shape, and location of clouds.  Research to date [40] [41], suggests that the observed motion of clouds relates closely to the wind direction and speed at cloud level.  The objective technique for determining wind direction and speed from ATS data is simple and straightforward.  A time-lapse movie made from cloud pictures is projected; the motions of individual cloud elements over the time interval between pictures are represented by velocity vectors.  After a correction for perspective is applied, this vector approximates mean horizontal motion of the cloud elements, neglecting apparent motion due to cloud growth or dissipation.

Comparison between ATS wind estimates over a limited area with rawinsonde data shows that over the tropics and subtropics wind estimates from high level clouds correlate well with the wind at about 30,000 feet (300 mb) [42].  Wind estimates from low clouds agree closely with the observed wind at 5000 feet and 6000 feet [42].  Although the motion of the cloud elements can be measured quite accurately, there is uncertainty as to the height of the cloud element being tracked.  Correct wind estimates are, therefore, strongly dependent on accurate cloud height estimates.  Though we must be aware of the limitations in using ATS wind estimates, it is significant to note that studies have thus far shown that about 70 percent of the ATS wind estimates based on high clouds are within 10 degrees in direction and 15 knots in speed of the observed 30,000-foot wind.  At low levels, 70 percent of the satellite-derived winds are within 25 degrees and 6 knots of the observed 6000-foot winds [42].

An impressive number of wind data points can be derived from cloud motion over a relatively small area.  This permits nonrepresentative motions to be identified and eliminated.

An operational program for extracting wind information from ATS data is now being developed.  This will provide several hundred additional wind observations daily for input to numerical analyses prepared by the National Meteorological Center.
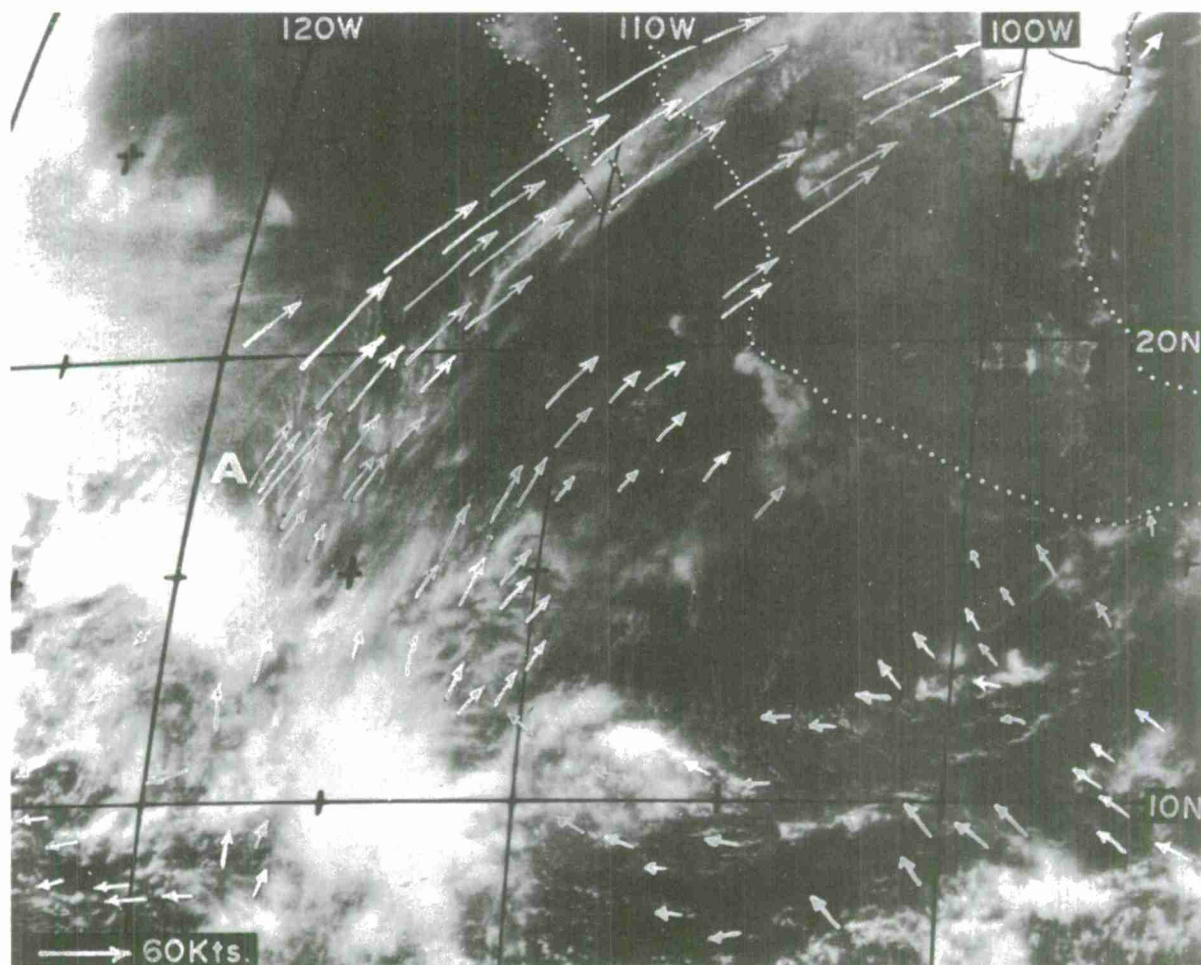
Figure 4-D-4.  Selected wind vectors (all levels) derived from ATS-I data.  The wind vectors were derived from data acquired between 1742 and 2000Z, 23 April 1968.  Additional wind-data points were calculated for the area shown here, but lack of space on the photograph precluded entry of all the vectors.  The narrow band of high level clouds which extends northeast from A is associated with a subtropical jet stream.  Strong horizontal shear near the jet core is reflected in the vectors.

Chapter 4

SECTION E

TROPICAL STORMS*

## Introduction

The cloud systems produced by tropical storms in their early stages of de-
velopment take on a variety of forms.  The shape and appearance of these cloud
systems depends both on the type of atmospheric perturbation initiating their
convection and the vertical wind shear of the storm's environment.  Since the
latter is closely related to aspects of the quasi-stationary planetary circu-
lation, such as the subtropical high pressure ridge or the high level mid-
oceanic troughs, storms that develop in different regions of the world appear
somewhat different as they evolve.  As a tropical storm matures, it modifies
its immediate environment to the extent that storms in the later stages of
their development look much the same worldwide.

On any one day, numerous synoptic-scale cloud systems appear in the trop-
ics and the subtropics.  Only a limited number of these tropical disturbances
develop into mature tropical cyclones.  A classification system has been de-
veloped for these tropical cloud formations.  It first seeks to identify those
areas of convection which, based on their appearance, seem most likely to de-
velop and, secondly, attempts to classify storms as to their intensity.

## Current Classification System
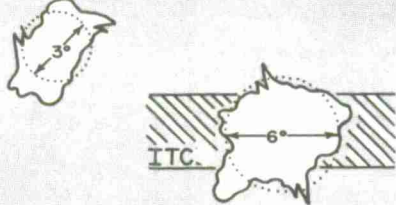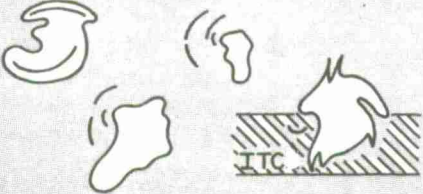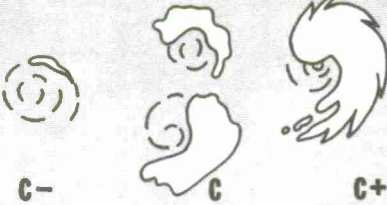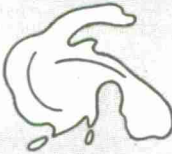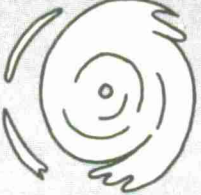
The system currently in use at the National Environmental Satellite Center
combines two early classification schemes.  One was developed to identify pre-
typhoon stage storms in the Pacific [43] and the other was developed to deter-
mine the maximum wind speed of a storm from cloud parameters observed in the
satellite data [44].  The current combined system is a more general version of
the original ones, with modifications that incorporate four years of experi-
ence.  It classifies tropical cloud systems into four groups:  Stages A, B, C,
and X.  Table 1 summarizes the criteria used to define each stage and shows

---

* The use of the term storm (with small 's') in the context of this Section
  does not necessarily imply Tropical Storm intensity.

TABLE 1

# TROPICAL AND SUBTROPICAL DISTURBANCE CLASSIFICATION FROM SATELLITE DATA

| | | |
|---|---|---|
| **A**<br><br>NO CURVED CLOUD LINES OR BANDS | | Stage A is a dense amorphous cloud mass composed of cumuliform, cirriform, and layered middle cloud in any combination. Some cirrus outflow is usually present.<br><br>The cloud mass must have an average diameter of 3° latitude or more.<br>　Exceptions: (1) If the cloud mass is contiguous to or within the ITC in the Atlantic, Pacific, or south Indian Ocean, it must have an average diameter of 6° latitude or more and be partially isolated by breaks from the general cloudiness.<br>　　　　　　(2) In the Arabian Sea and the Bay of Bengal, the cloud mass must be 8° latitude or more in diameter. |
| **B**<br><br>POORLY ORGANIZED CURVED CLOUD LINES AND BANDS<br><br>ILL-DEFINED CENTER | | Stage B is a dense cloud mass with adjacent curved cumulus cloud lines and/or curved bands of middle cloud which are either detached from, or form part of, the major overcast area. The curved cloud lines and bands are often poorly organized.<br><br>The pattern produced by the curved lines and bands is poorly defined--it does not appear to have one definite center.<br><br>Along the ITC , the cloud mass and associated curved cumulus cloud lines and/or bands must be separated from the ITC cloudiness on at least one side and cirrus outflow must be evident. |
| **C**<br><br>WELL ORGANIZED CURVED CLOUD LINES AND BANDS<br><br>WELL DEFINED CENTER OUTSIDE DENSE CLOUD MASS | C−　　C　　C+ | Stage C has well organized, curved cumulus cloud lines and/or broad curved bands of middle and high cloud.<br><br>The pattern produced by the various curved lines and bands has a well defined single center.<br><br>The center of the pattern generally lies outside but adjacent to an associated dense cloud mass, but it can be on the edge or as much as one-half degree latitude within the cloud mass.<br><br>A C− has no associated dense cloud mass.<br><br>A C+ appears very well organized with a large amount of curved cirrus outflow. |
| **X CAT. 1**<br><br>POORLY ORGANIZED SPIRAL BANDS<br><br>ILL-DEFINED CENTER OF ORGANIZATION WITHIN CENTRAL CLOUD MASS | | Category 1 has a bright generally circular central overcast which is cirriform in appearance. Curved cirrus outflow is often restricted to one quadrant.<br><br>Poorly organized, slightly curved cumuliform cloud bands appear near the periphery of the central overcast and cross into it at a large angle. This banding remains close to the overcast edge; away from the overcast, organized curved bands are usually absent.<br><br>An eye is not visible. The center of the spiral pattern can be located approximately by extrapolating inward along the curved peripheral bands. This estimated center must be more than one-half degree latitude within the central cloud mass. |
| **X CAT. 2**<br><br>WELL ORGANIZED BANDS<br><br>SPIRAL BANDS DEFINE CENTER WITHIN CENTRAL CLOUD MASS | | Category 2 has a bright, often asymmetrical central overcast. Cirrus outflow is curved and more extensive.<br><br>At least one long, major, well organized band spirals at a large angle into the central cloud mass. A linear curved break accompanies this band. Within the central cloud mass, the break is covered by thin cirrus but is readily detectable. Minor peripheral bands outside the overcast are poorly organized.<br><br>An eye is not visible. The central tip of the major spiral band defines the center. This center must be more than one-half degree latitude within the central cloud mass. |
| **X CAT. 3**<br><br>MODERATE DEGREE OF CONCENTRICITY TO CLOUD BANDS<br><br>IRREGULARLY SHAPED EYE WITHIN CENTRAL CLOUD MASS | | Category 3 has a bright central overcast that is compact and tends to be circular. There is considerable curved cirrus outflow visible at the edge of the central overcast.<br><br>Curved striations within the central cloud mass define spiral cloud bands which are moderately concentric about a visible eye. Well organized peripheral bands, some with well developed cirrus, are present.<br><br>A ragged and irregularly shaped eye is normally visible. This defines the storm center. |
| **X CAT. 4**<br><br>HIGH DEGREE OF CONCENTRICITY TO CLOUD BANDS<br><br>ROUND EYE NEAR CENTER OF CENTRAL CLOUD MASS | | Category 4 has a very circular bright central overcast. The edge is often sharp and smooth over one or two quadrants, otherwise, it is striated cirrus.<br><br>Highly concentric striations appear within the central overcast. Banding outside the central overcast is very well organized and circular. The entire cloud system is very symmetrical in appearance.<br><br>A well defined eye appears as a small dark circular area surrounded by a bright ring. This defines the storm center. |

cloud models typical of each group.  The basic parameters used in the classifi-
cation are the size and geographical position of the overcast area, the degree
of circularity of the spiral band structure, and the location of the center of
the spiral band structure either inside or outside the major cloud mass of the
storm.

With disturbances classified A, B, or C, the center of the pattern pro-
duced by the curved cloud bands either does not exist (as in Stage A), or, if
it does exist, lies outside or very near the edge of the overcast cloud area
(Stages B and C).  In Stage X storms, the center of the spiral band structure
lies well within the overcast cloud area.  In general, A and B represent form-
ative stages within the classification system and C applies to storms which
are either growing or decaying.  Although Stage X is primarily thought of as
the mature stage, it should be pointed out that this category derives from a
classification system of disturbances according to degree of organization
ranging from weak to very strong.  Thus, the weakest Stage X disturbances or
Category 1 systems bracket subtropical and tropical storm intensities from
about 25 to 45 knots.  On the strong end of the scale (Stage X, Category 4),
maximum wind intensities run from about 75 to 150 knots.  The characteristics
of each stage are discussed below.
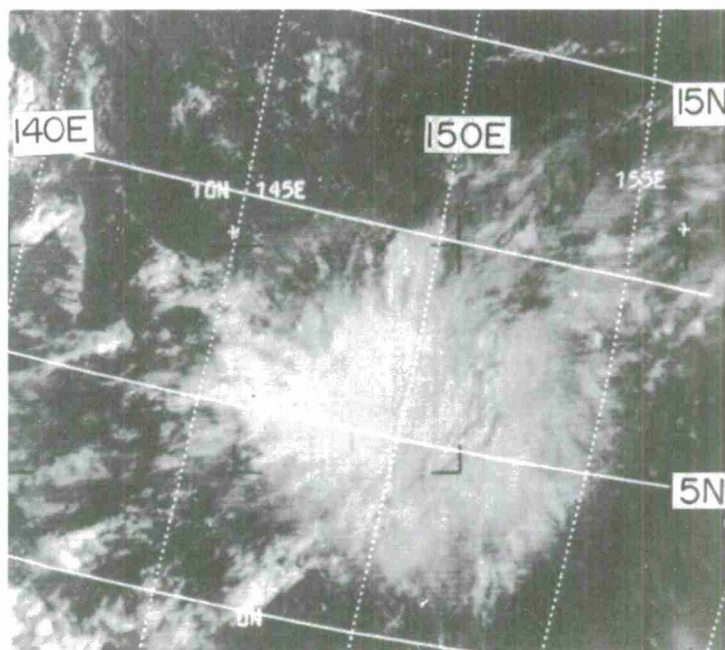
Figure 4-E-1.  Stage A,
Western Pacific.



E-5 497-6 0506Z 25 Sep 68

Stage A.  This stage represents the least intense tropical disturbance.
Stage A is a dense, amorphous cloud mass which occurs over a region where
stronger than normal convection is taking place.  The pattern usually appears

poleward and separate from the ITC and must have a cloud system with a minimum
average diameter of three degrees of latitude.  For those cases when it lies
within, or contiguous to the ITC in the Atlantic, Pacific, and South Indian
Oceans, the cloud-system diameter must be larger than six degrees latitude.
In the Arabian Sea and the Bay of Bengal, the equatorial cloud band appears
much broader and the minimum diameter for a Stage A is eight degrees of lati-
tude.  For a disturbance lying within the equatorial cloud band to be classi-
fied as a Stage A, it must be separated by a break on either one side or the
other from the general cloudiness along the zone.

Clouds associated with a Stage A disturbance are of all types and show no
curved lines or bands, so it is impossible to locate a center using these fea-
tures.  Centers for Stage A's are estimated by picking the geometrical center
of the cloud system.  A Stage A disturbance is often, but not necessarily as-
sociated with, a wave or perturbation in the low level easterlies.  When this
is the case, the clouds most often lie to the east of the low level perturba-
tion axis.  In no case is there a vortex present in the low level wind flow,
nor are there closed surface isobars.  Wind speeds are generally light but may
approach 25-30 knots in the cloudy area where active convection is occurring.
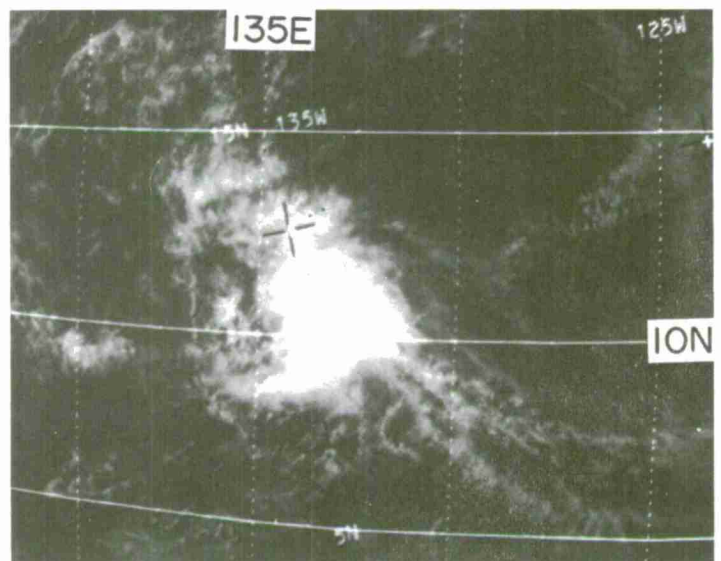


Figure 4-E-2.  Stage B,
Mid-Pacific.

E-3 5833-4 2137Z 9 Jan 68

Stage B.  At this stage, some curved cloud lines or bands are observed,
but there is no definite center to the pattern.  These curved, cumulus cloud
lines are adjacent to, and often immediately west of, a dense cloud mass.
Curved bands and breaks sometimes appear in the dense cloud mass.  While the
curved cloud lines of a Stage B pattern suggest rotation in the wind field, a
closed rotation will be detected in the measured winds only when the speed of
rotation exceeds the speed of translation of the center of the disturbance.

Thus, the curved cloud bands of Stage B do not necessarily imply that a closed
circulation exists in the measured wind field at the surface or at any other
level.  Wind speed near the rotation center of this cloud pattern generally
will not exceed 20 knots, although winds of 30 to 40 knots may be observed in
the area of maximum convective cloudiness.  This area is usually northeast of
the rotation center in the Northern Hemisphere and southeast of the center in
the Southern Hemisphere.
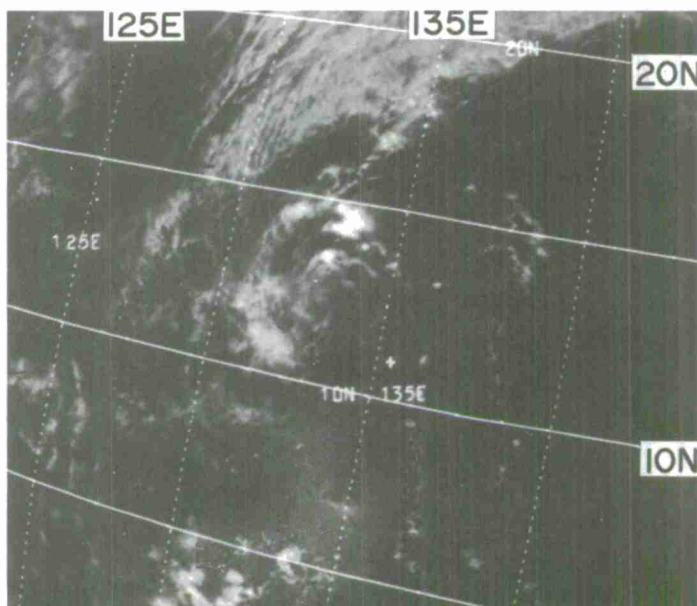
Figure 4-E-3.  Stage C Minus,
Western Pacific.



E-3 5585-4 2103Z 21 Dec 67

Stage C.  This stage is divided into three subcategories:  C minus, C, and
C plus.  Characteristic of all categories are the well-defined, curved cloud
lines and bands which define a definite pattern center.

Stage C is a combination of a large cloud mass and curved cloud lines.  In
this stage, the dense cloud mass assumes an arc which forms one side of the
pattern, and cumulus cloud lines, which spiral towards a center, complete the
other side of the pattern.  Wind speeds near the center of curvature average
between 20 to 40 knots.  It is not uncommon to find wind speeds of 50 plus
knots in the area of overcast convective cloud.

The C minus Stage lacks the large area of convective cloudiness character-
istic of Stages A and B.  Instead, it is defined by thin cumuliform cloud
lines which spiral cyclonically into a center.  Maximum wind speeds near the
center of curvature of a C minus Stage range from 20 to 40 knots.
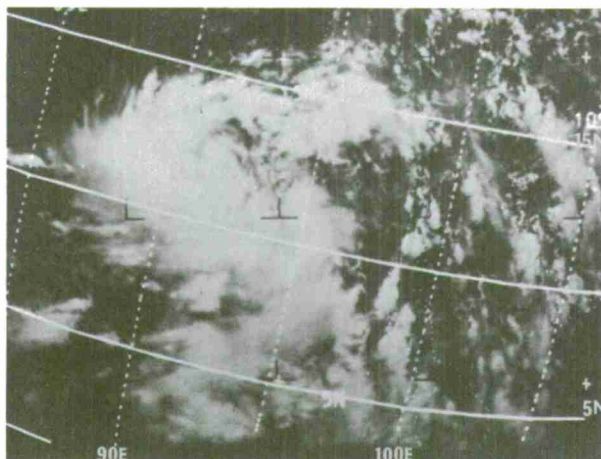
E-3 4906-4 0223Z 28 Oct 67                    E-7 574-6 0842Z 1 Oct 68

    Figure 4-E-4.  Stage C,              Figure 4-E-5.  Stage C Plus,
Western Pacific.                     Bay of Bengal.


    Stage C plus has spiral bands both in the main cloud mass and in the thin
cumulus lines.  The center of curvature of the cloud lines lies near, or is
somewhat obscured by, the edge of the main cloud mass.  C plus cloud systems
are usually indicative of disturbances of Tropical Storm intensity.  At this
stage of development, outflow characteristics become pronounced.  The overcast
cloud shield surmounting the storm center may range from one to three degrees
in diameter becoming larger as intensity increases.  However, the center of
the circulation, as defined by the curved cloud bands, remains near the edge
of the overcast; it is never imbedded more than about one-half degree inside
of the cloud pattern.  Thick spiral bands up to two degrees or more in width
spiral around the center.

    In Stage C plus, typical wind speeds range from 30-65 knots.  However,
speeds up to 75 knots occasionally have been observed in cyclones with the
attributes of this stage.

    Stage X.  The major characteristic of storms in this class is that the
center of curvature lies within the major cloud mass.  The degree of organiza-
tion in the curved and spiral clouds have a wide range.  Four divisions or
categories are used to describe the cloud organization.  These categories are
discussed below and appear in Table 4-E-1.

E-5 972-7, 0456Z 6 Jul 67

Figure 4-E-6.  Stage X,
Category 1, West Pacific.

Category 1.  The Category 1 disturbance has a bright, generally circular
overcast which is cirriform in appearance.  Poorly-organized, cumuliform cloud
bands, which cross into the overcast area at a large angle, appear near the
edge of the central overcast.  No "eye" is visible, so the center of the spiral
pattern, which must be more than one-half a degree in latitude, must be lo-
cated by extrapolating inward from these curved peripheral bands.  Curved
cirrus outflow is often restricted to only one quadrant.



E-3 1440-7 0323Z 25 Jan 67

Figure 4-E-7.  Stage X,
Category 2, South Pacific.
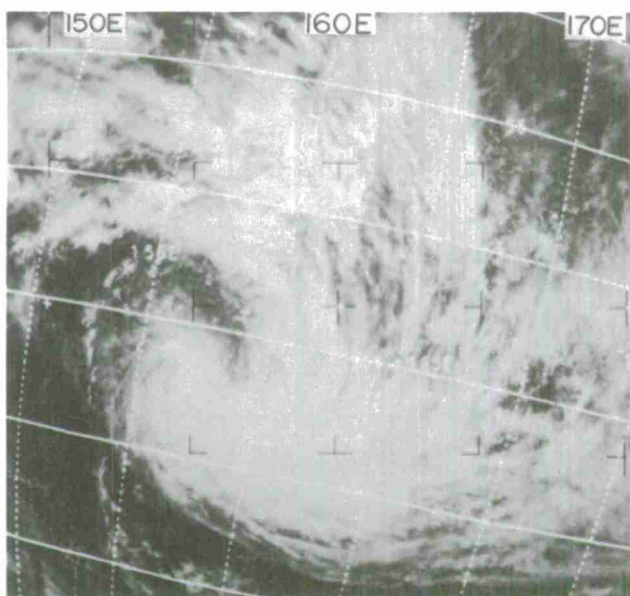
Category 2.  A distinguishing characteristic of the Category 2 disturbance
is at least one long, well-organized band (or tail) usually 120 nm or more in
width which spirals at a large angle in toward the central cloud mass.  An-
other characteristic of Category 2 is a curved break or dry tongue which

accompanies this spiraling band into the center. Within the often bright,
asymmetrical overcast, the break is covered with cirrus, but it is still read-
ily detectable. Cirrus outflow is curved and more extensive than with Cate-
gory 1. Minor peripheral bands which are outside the overcast are poorly or-
ganized. No "eye" is discernable at this stage. The center is defined by the
central tip of the major spiral band.
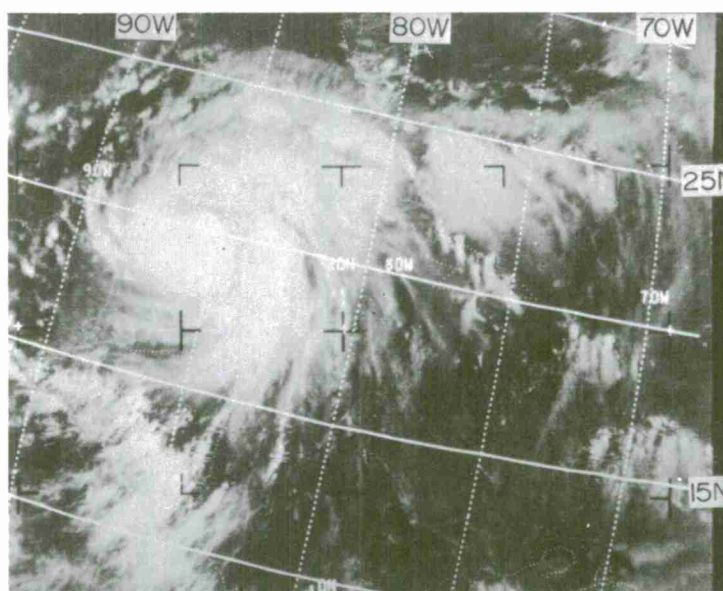


Figure 4-E-8. Stage X,
Category 3, Atlantic.

E-5 1893-4 2039Z 16 Sep 67

Category 3. A Category 3 storm has a bright central overcast that is com-
pact and tends to be circular. This is the earliest stage at which an eye
appears. The eye is usually ragged or irregularly shaped, but it marks the
center of the storm. (Note: the appearance of an eye automatically places a
storm in Category 3 or 4, but a visible eye is not a necessary condition for
either Category 3 or 4, because the eye may be obscured by clouds, especially
if the storm is viewed at an oblique angle.) Curved striations within the
central cloud mass define spiral cloud bands which are moderately concentric
about the eye. Well-organized peripheral bands, some with well-developed
cirrus, and considerable curved cirrus outflow at the edge of the central
overcast are usually visible.

Figure 4-E-9.  Stage X,
Category 4, Atlantic.
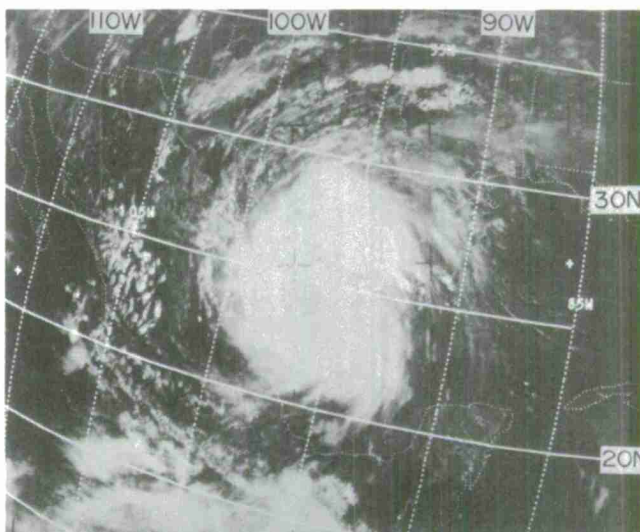
E-3 4425-5 1840Z 19 Sep 67

Category 4.  Characteristic of a Category 4 storm is a well-defined eye
which marks the center of the storm.  This dark circular area is surrounded by
a very bright circular overcast which contains highly concentric striations.
The edge of the overcast is often sharp and smooth over one or two quadrants;
otherwise it is striated with cirrus.  Banding outside the central overcast is
very well organized and circular, thus giving the entire cloud system a sym-
metrical appearance.  The four categories of Stage X can be used as a measure
of storm organization that can be used in conjunction with the diameter of the
storm's overcast area to estimate the maximum wind speed of a storm.  Research
shows that these two parameters, category and diameter, when used together,
yield the wind speed estimates accurate to ± 20 knots.  Of the four categories,
the relationship between diameter and wind speed is least reliable for Cate-
gory 1.  For this reason and because Stage X, Category 1 formations are dif-
ficult to distinguish from Stage B, Stage X, Category 1 is seldom used.

Estimating the Winds in Stage X Storms

After the organization or category has been established, the diameter of
the overcast must be determined to obtain the maximum wind speed of the storm.
Certain guidelines have been established for measuring the diameter of the
storm.  This diameter is used for entry in the nomogram, Figure 4-E-10.  The
amount of clouds produced by the storm is used to determine the diameter size.
Figure 4-E-11 illustrates the amount of cloudiness to be considered or in-
scribed in the diameter circle for Categories 1 through 4 according to the
rules listed below.  If the cloud brightness decreases with increasing diame-
ter, it is important to exclude thin gray cirrus which probably occurs where
there are no low clouds beneath a thin upper layer.  Care should be taken,

Figure 4-E-10. Nomogram used to de-
termine wind speeds in Stage X storms
[46]. The range of wind speeds usually
associated with Stage A, B, and C storms
is indicated in the lower right-hand
corner.
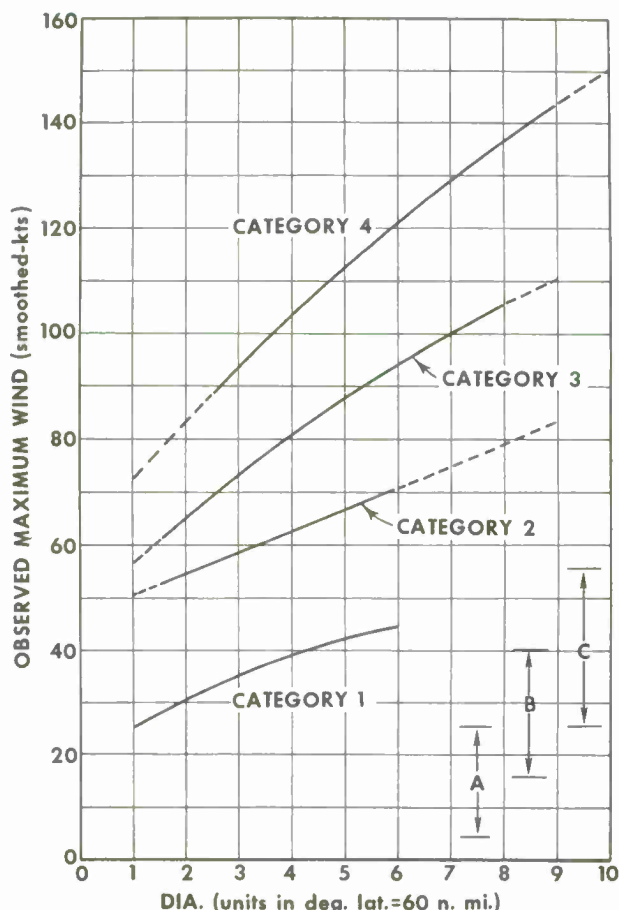


Figure 4-E-11. Schematic Ex-
ample of the four categories of
Stage X. Black circles indicate
area of overcast to be used to
measure diameter of storm.
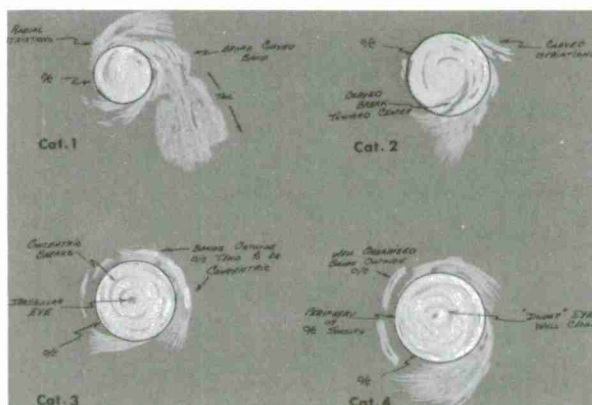


however, to include all of the thick cirrus even if it has no underlying cloud
deck.

Rule 1: The storm diameter is determined by measuring in degrees of latitude
the largest circle which can be inscribed within the highly reflec-
tive cloud area which is continuously overcast or which contains only
minor breaks. Minor breaks are defined as follows:

a. Breaks which are less than 60 nm wide and covered with a thin
high-level overcast, i.e., no apparent cloud-free areas.

   b.  Breaks must be nearly concentric about the pattern center or
the eye.  Category 2 is an exception to this rule.  In this category,
a narrow, curved break spirals in at a large angle toward the pattern
center.  This break is _included_ within the overcast if the break is
less than 60 nm wide and is covered with thin cloud.

Rule 2:  The overcast area which is included outside the concentric breaks
         must contain clearly identifiable curved bands or striations.

Rule 3:  Enter the nomogram (Figure 4-E-10) with diameter of overcast circle
         (degrees latitude) and category to determine the maximum wind speed.

   A storm will not be classified as Stage X if the area within the inscribed
circle is less than 7/8 covered with bright cloud.  If the area covered with
breaks approaches 1/8 of the total area within the inscribed circle, they must
be narrow, concentric, and covered with thin cloud so they appear gray in
color.  If these conditions are not satisfied, the disturbance should be clas-
sified as either A, B, C minus, C, or C plus.

## Classifying Storms from Infrared Data

   Caution must be exercised in applying the classification which has been
developed for television data to the analog infrared data available by APT.
An insufficient number of storms were viewed by Nimbus I and II IR radiometers
to draw valid conclusions as to the applicability of the current system.
Study of the limited number of  HRIR-viewed storms indicates that measurements
of a storm's central overcast diameter from IR analog pictures may be consist-
ently smaller than those made from television pictures of the same storm.
This data sample also suggests that the circular-banded structure within the
area covered by the cirrus canopy is less clearly defined in analog IR pic-
tures while the eye is more clearly visible.  Although more research is needed
before the classification scheme developed for video data can be applied di-
rectly to analog IR pictures, the IR pictures can be used quite successfully
to locate storms and to diagnose development.

Chapter 4

---

SECTION F

WEAK TROPICAL DISTURBANCES

Introduction

On any given day, the tropics and subtropics contain many weak disturb-
ances which have an important effect on local weather.  In satellite pictures,
these disturbances appear as areas where groups of cumulonimbus clouds are
generating altostratus and cirrus which constitutes a rather large cloud sys-
tem.  Weak disturbances, those that correspond to Stage A in the classifica-
tion system, are sometimes quite transient.  They can develop within a 24-hour
period and then dissipate just as rapidly.  Most disturbances which do develop
into Tropical Storms produce cloud systems that can be tracked for several
days prior to the time that they actually reach Tropical Storm intensity.  For
a weak tropical disturbance to be considered significant with regard to po-
tential development, its cloud system must be at least 100 miles in diameter
and it must persist for more than 24 hours [26].  Such cloud formations are
usually associated with a detectable perturbation in the wind field, but, on
occasion, the changes in wind are so small and subtle that the perturbation in
the wind field is, with the present observation equipment and network, unde-
tectable [27].

Perturbations most commonly responsible for synoptic-scale cloud systems
are:

a.  The so-called easterly waves which are observed in the lower and mid-
dle tropospheric easterly flow immediately poleward of the equatorial trough;

b.  Vortices (cold-core lows) in the upper tropospheric flow; and

c.  Weak, low level vortices along the equatorial trough.

Easterly-wave type perturbations which produce significant cloud forma-
tions are frequently observed in the tropical Atlantic [28] [29].  In that
region, perturbations, strong enough to have associated cloud systems, show
the most development between 5000 and 20,000 feet [29].  Weak easterly waves
appear as westward-moving troughs in the low level easterlies with the major
area of cloudiness to the east of the trough axis.  Strong easterly waves
often develop a closed circulation in the surface wind flow which produces the

vortical cloud pattern characteristic of Stage C disturbances.  Other types of westward-moving perturbations are also observed.  Some of these produce significant amounts of cloud and weather but are only slightly noticeable or completely undetectable in the wind field.

A study of those 1967 tropical Atlantic disturbances east of 60W which reached Tropical Depression intensity showed that only one half developed vortical patterns [31] and, of these Stage C disturbances, only 50 percent continued development to reach Tropical Storm intensity.  Figure 4-F-1 shows the relationship of the surface vortex to the overcast shield and cloud bands accompanying a strong easterly wave disturbance in the Atlantic [31].

Figure 4-F-1.  Schematic of a Tropical Vortex Cloud Pattern [31].
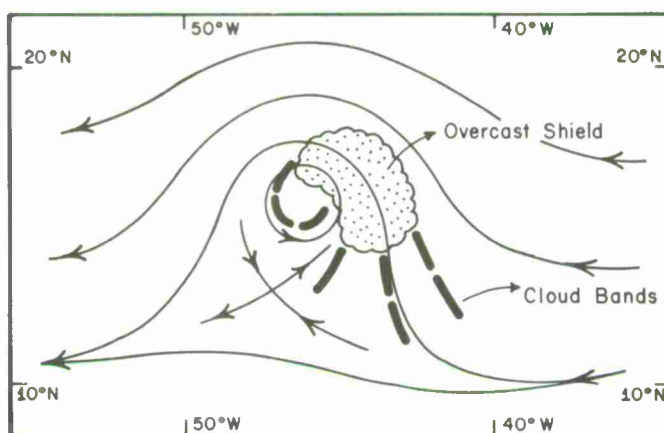


Upper cold-core lows are most obvious near the 200-mb surface.  Depending on their strength, they are reflected in the surface flow as a weak trough or as a weak vortex.  The movement of the upper level vortex governs the movement of the associated cloud system.  Therefore, a cloud system in the region of surface easterlies which is either stationary or moves in opposition to the low level flow indicates an upper circulation and is not associated with an easterly wave.  It is worth noting that not all upper level circulations over the tropics and subtropics produce convection and associated cloud systems [30].

The disturbances which occur along the equatorial trough produce cloud systems which are contained within, or are contiguous to, the ITC cloud band. At times, this cloud band is narrow (2-3 degrees latitude) and continuous for thousands of miles.  At other times, it is discontinuous and is characterized by a number of large cloud areas 5-10 degrees latitude across [32].  On occasion, vortical cloud patterns are observed within the ITC cloud band.  Generally, disturbances along the ITC move from east to west and can move poleward and develop into tropical storms.  These disturbances are most frequent in the

TYPICAL SURFACE WIND FLOW
RELATIVE TO EQUATORIAL TROUGH (Eq.T.)



Figure 4-F-2. Portrayal of Typical Doldrum and Trade-Wind Equatorial Troughs (Eq. T.) in both the Northern and Southern Hemispheres. Dashed line on poleward side of doldrum Eq. T. represents typical location of initial disturbance genesis [33].
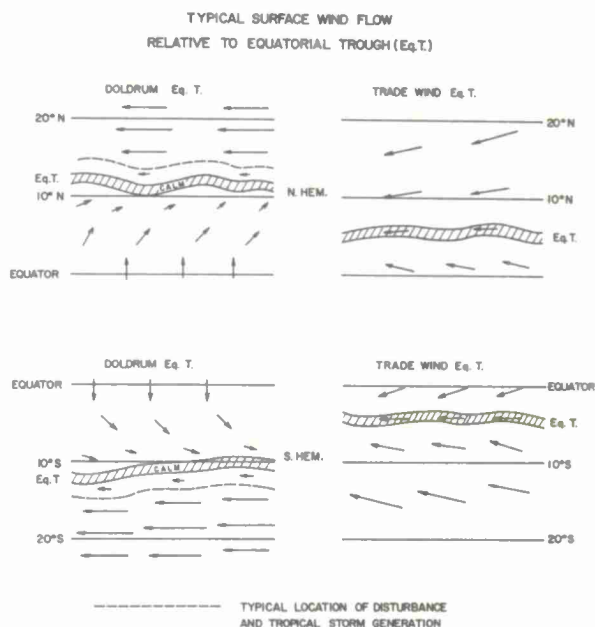
Figure 4-F-3. Typical Satellite-Observed Cloud Cluster Patterns Relative to a Doldrum Equatorial Trough. Tropical storms develop from persistent cloud cluster patterns on the poleward side of a Doldrum Equatorial Trough [33].
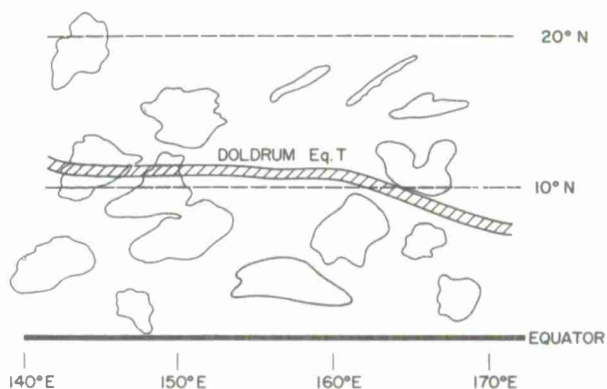


doldrum portions of the equatorial trough [33]. In that area low-level cyclonic wind shear is present over large areas. This, together with friction, produces the forced convergence necessary for development of the individual cloud systems which form the ITC cloud band [33]. The largest of these cloud formations meets the classification criteria of Stage A or B. Figure 4-F-2 shows the typical wind regimes for active (doldrum) and inactive (trade wind) portions of the equatorial grough. Figure 4-F-3 shows the cloud pattern typical of an active doldrum trough in the western Pacific. The mean summer season positions of the trough appear in Figure 4-A-1.

A recent study using ATS data [32] shows that surges of flow from one hemisphere to the other are another factor controlling ITC clouds. As air moves across the equator, anticyclogenesis takes place. This results in a reduction or clearing of cloud along one portion of the ITC cloud band and an intensification of the cloud band in advance of the "burst" of cross-equatorial flow.

The cloud systems produced by weak-to-moderate disturbances exhibit strong regional characteristics. These are produced by (a) latitudinal variation in the position of the mid-oceanic troughs and ridges, (b) differences in the height of the trade-wind inversion, (c) the type of convergent flow into the Equatorial Trough, and (d) continental influences. The degree of cloud development, as well as the appearance of cloud formations that are associated with all weak disturbances, is affected by these factors. Only about 10 percent of the weak disturbances observed in the tropics intensify into mature cyclones [26]. There are several indications in satellite pictures which show whether a disturbance will intensify:

a. The area of strong convection becomes larger or convection increases in strength. This is reflected by an increase in the area of cirrus from one day to the next;

b. A vortical pattern develops in the clouds. This can be related to one of the tropical storm stage classifications.

c. There are indications of weak shear in the region of strong convection. Short cirrus streamers in a diverging pattern around the periphery of the convective area indicate weak shear. Recent research [33] suggests that disturbances which occur where the 850 mb - 200 mb wind shear approaches zero are most likely to intensify; provided other environmental conditions are favorable.

The dynamics of tropical disturbances in their weak and developing stages are still imperfectly understood. Satellite pictures provide insight into the variety and behavior of tropical cloud systems but complete models that explain the life-cycle of tropical storms are presently lacking. Some tentative findings for specific areas are presented in the remainder of this section.

Easterly Waves in the Tropical Atlantic — The "Inverted V" Formation

Weak easterly waves which cross the Atlantic between Africa and the Antilles produce a readily recognizable cloud pattern [29].  As a disturbance moves off the African coast, the clouds become organized in narrow bands which bulge poleward along the axis of the wave.  These resemble a series of inverted letter "V's", as represented in Figure 4-F-4.  The picture for 25 June 1967 in Figure 4-F-5 shows a well-developed example.  The banded "Inverted V" pattern is associated with weak easterly waves that have no surface vortex.  The perturbation in the wind field for these waves, while they are near the African coast, is strongest between 5000 and 15,000 feet.  The wave has a small amplitude in the surface wind field; the cloud bands are aligned to the low-level wind shear and can have more amplitude than the surface flow.  The ITC cloud band may or may not widen and bulge northward at the wave axis as shown in the schematic.  Often, only parts of the pattern appear, as can be seen in Figure 4-F-5.  This series shows the progression of a wave across the Atlantic on seven successive days.

Figure 4-F-4.  A schematic showing the relationship between the lower tropospheric flow and the "Inverted V" cloud pattern [29].
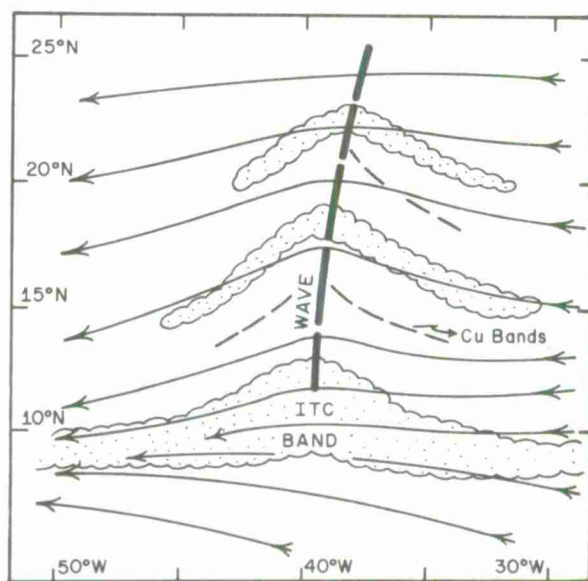


The following discussion gives an insight into the historical progression of this type of disturbance.  Tropical disturbances can be initially identified as they move across Africa by their associated convection.  As a disturbance moves off the African coast, the cloud amount increases due to the increase in available moisture.  Cloud amount decreases with further westward motion, but the "Inverted V" banded pattern becomes more pronounced west of 25W.  The disturbances continue to weaken as they approach the Antilles.  Some dissipate completely before reaching the eastern Caribbean.  Those that persist
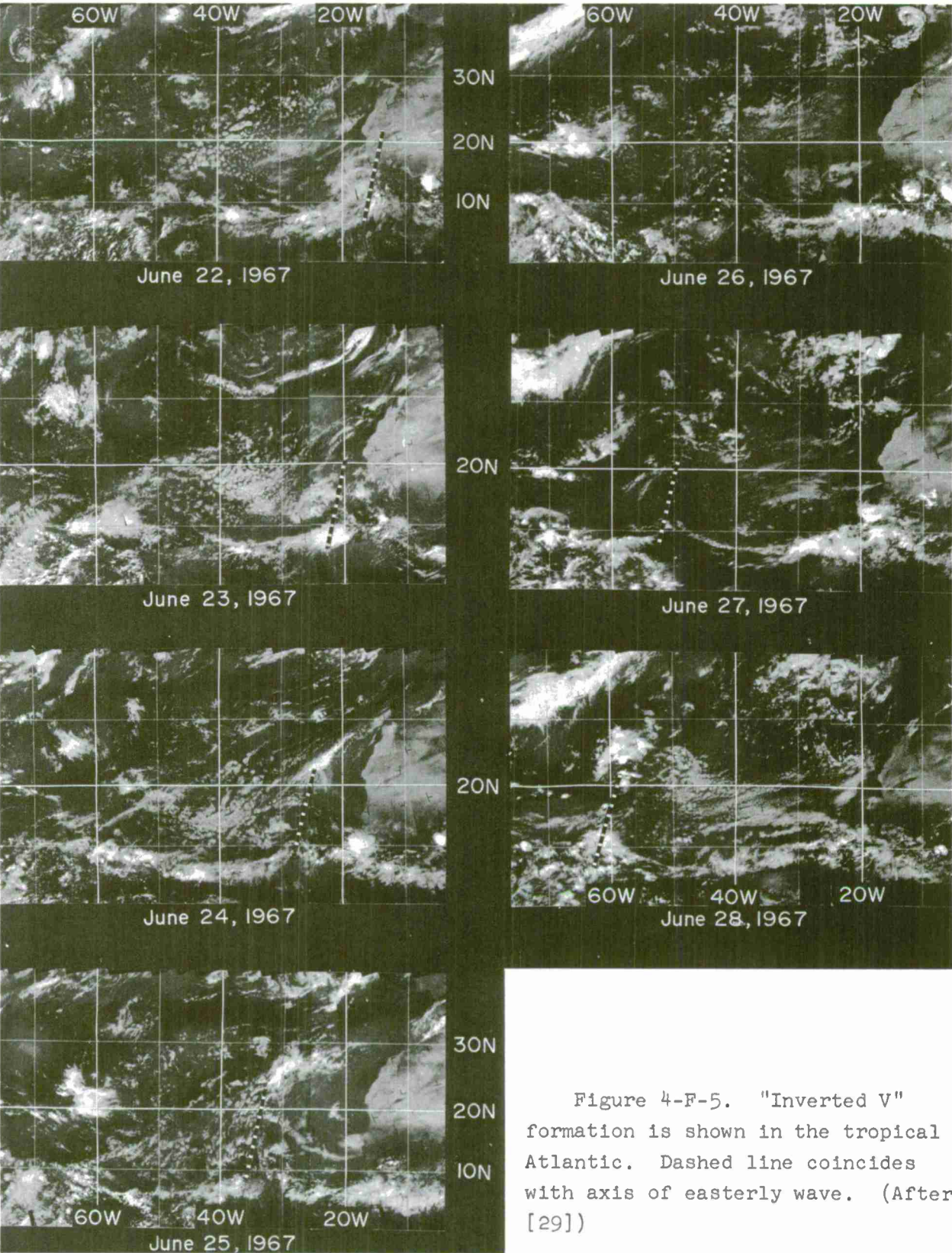
Figure 4-F-5. "Inverted V" formation is shown in the tropical Atlantic. Dashed line coincides with axis of easterly wave. (After [29])

frequently interact with the upper level, mid-oceanic trough.  As they ap-
proach the trough, there is a rapid increase in convection near the wave axis
of the low level, westward-moving disturbance.  This occurs as the wave moves
under the region of southwest flow aloft which is east of the upper level
(200 mb) trough line.  Such an increase in cloud may be present for only one
day.  As the low level wave moves west, the cloud system remains to the east
of the upper level trough and slowly dissipates.  Not all easterly waves are
strong enough to produce this temporary increase in cloud.  Figure 4-F-6,
based on 1967 data [29], shows the mean position of the 200-mb trough during
one month and the region to the east where an increase in cloud occurred as
trade-wind disturbances approached from the east.  In Figure 4-F-5, the in-
crease in the cloud at 25N, 55W that occurs between 27 June and 28 June is an
example of this effect.
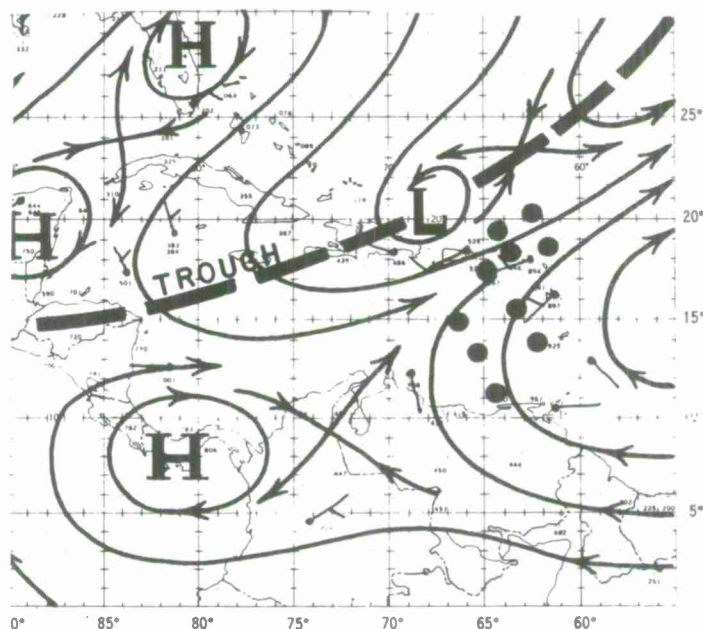


Figure 4-F-6.  The mean 200-mb stream-
line map for July 1967.  The cloudiness as-
sociated with easterly waves is frequently
enhanced in the eastern Caribbean Sea.  The
geometric center of the enhanced cloudy
area relative to the upper trough is shown
by the closed dots [29].

Disturbances Associated with the Mid-Pacific and Mid-Atlantic Troughs

The upper tropospheric troughs (mid-oceanic troughs) which occur in the summer over both the North Pacific and the North Atlantic exert a major control over the weather in these areas. Mid-oceanic troughs are generally more evident at 200 mb. In the mean, their axis lies 5 to 10 degrees south of the subtropical high, surface ridgeline (see Figure 4-A-1). At times, mid-oceanic troughs exist only as shear lines with no detectable vortices. At other times, they consist of a series of well-developed vortices.

The cloud distribution around the mid-oceanic troughs is as follows: There is a minimum of cloud centered along the trough axis, except in the vicinity of an upper level vortex. If the vortex extends to low levels, organized convection occurs beneath the upper low. Otherwise, major convective cloud systems are located in the westerly flow south or southeast of the trough line and are often removed by several degrees of latitude. A first approximation of the trough position can be obtained from satellite pictures by (a) identifying the line of convective disturbances which are associated with the upper tropospheric southwesterly flow and, (b) by identifying the axis of minimum cloud which surrounds the trough line. The trough can be more precisely located by evidence of upper level vortices in the form of curved cumulus lines and by estimates of upper level wind direction based on cirrus plumes.

Upper level vortices along the mid-oceanic troughs produce convective cloud systems which vary in cloud amount and degree of organization. These differences depend on the size of the upper circulation, its depth of penetration, and conditions in the lower troposphere. The latter are controlled by sea surface temperatures, the height and strength of the trade-wind inversion, and other factors which affect the moisture content and stability of the lower atmosphere. Thus, the cloud systems produced by upper level vortices in the eastern side of oceans are different in appearance than those which appear further west.

Not all upper level vortices produce clouds. A study based on Atlantic data showed that in about two-thirds of the cases less than 35 percent of the area around the circulation center is covered with broken or overcast clouds [30]. A Pacific study showed the speed of the cloud formations associated with vortices to average ten knots toward the west [34]. Upper level vortices do occur separately from the mid-oceanic troughs. In these cases, they are either quasi-stationary, cut-off lows or lows at the base of large amplitude troughs in the westerlies that extend into the tropics.

200 mb.

500 mb.

700 mb.

Surface

a.

b.

c.
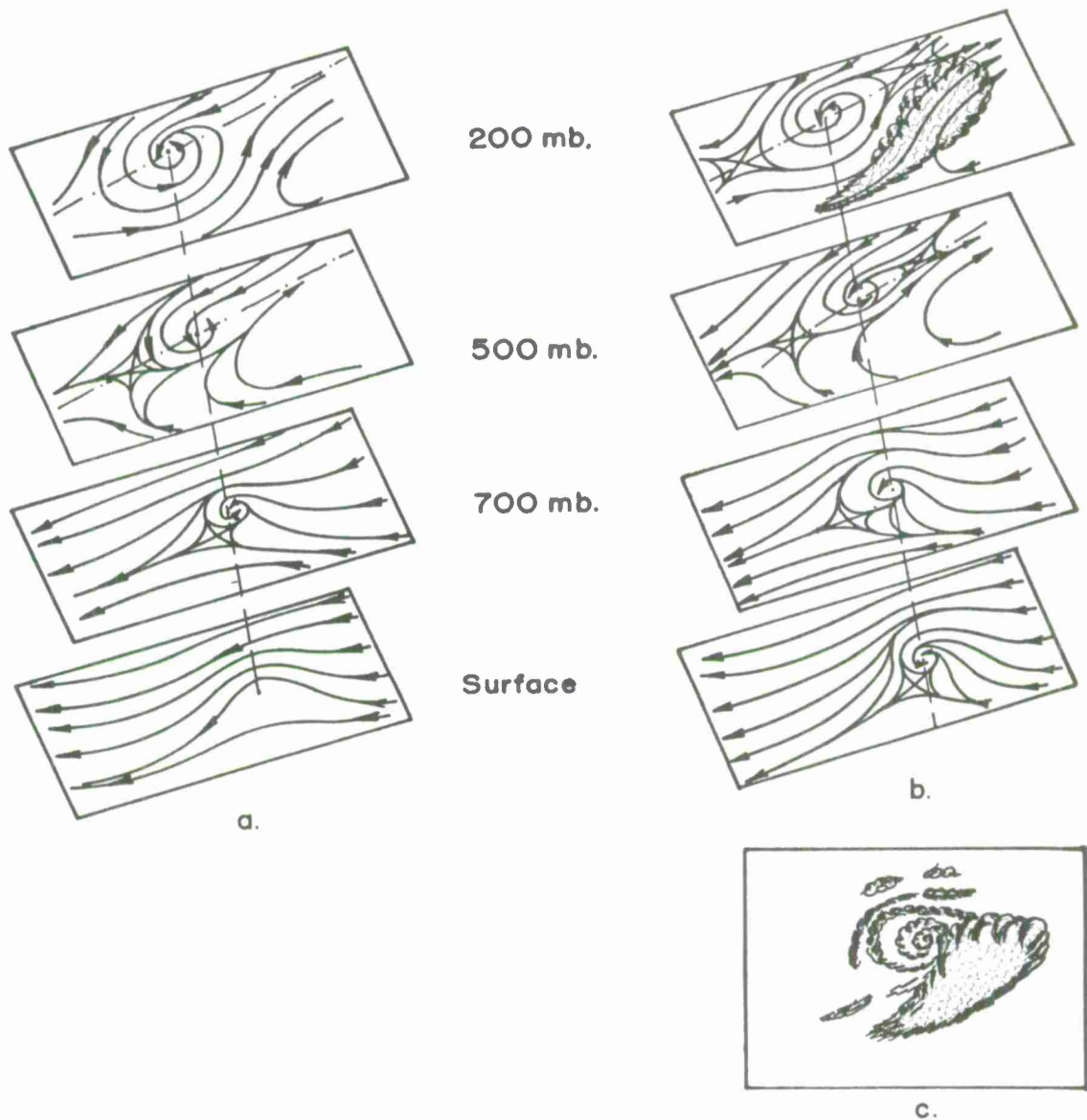
Figure 4-F-7. Three-dimensional structure of the mid-Pacific
trough vortices and a commonly-observed cloud system [35].

The penetration intensity in Figure 4-F-7 is moderate to strong. In (a)
the vortex has penetrated through the 700-mb surface but only shows at the
surface level as an induced trough, whereas in (b), the penetration is to the
surface and a vortex is present in the trade-wind easterlies. Pulsations in
the penetration depth of the system can produce weak vortices that alternately
appear and disappear at the surface level. This can lead to surface analysis
difficulties. The cloud system with the disturbance is more conservative with
time and provides a reliable means of tracking the perturbation from day to
day.

A model, Figure 4-F-7, has been developed using satellite data which describes the general features of cold-low cloud systems in the Pacific [35]. The essential features of the model are as follows:

a.   The slope of the vortex is usually toward the northwest with increasing height.

b.   The surface circulation observed is dependent upon the areal extent, intensity, and penetration depth of the upper vortex.

c.   The surface circulation, whatever its character, is an integral part of the upper level vortex, and neither forms independently, nor moves under or away from the vortex.  Even if the upper system is moving eastward (which is not uncommon during the transition seasons in the Hawaiian region), the surface trough or vortex will move upstream against the surface easterlies.

d.   The observed cloud system depends on the penetration intensity, geographic location, and slope of the system.  The schematic cloud system (Figure 4-F-7c) is the type observed with a moderate to strong cold low in the central Pacific when the circulation has a northwest tilt with increasing altitude.  The model is equally applicable to both circulations in Figure 4-F-7 because the vortex extends down as far as 700 mb in both cases.  The low level convergence is in the east sector of the surface perturbation and, because of the slope, it is under the divergent region of the upper circulation.  The direction of the curved cloud lines forming the vortex pattern is often best associated with the direction of the wind at 700 mb.  The vortex cloud pattern is often less well organized than shown in the schematic; occasionally it is partially obscured by the higher cirrus.

Initially weak, cold-core disturbances can, under proper environmental conditions, become warm-core storms and develop into mature tropical storms. In the eastern Pacific, disturbances remain cold-core and weak.  Even so, they are still the primary source of heavy rains at trade-wind latitudes.  In the western Pacific, disturbances become much better developed and often intensify into typhoons.

An example of the relationship of the clouds to the mid-Pacific trough is shown in Figure 4-F-8.  This illustration shows a computer-derived montage of the clouds alone and one of the clouds with the surface pressure analysis (black) and the 250-mb streamline analysis (white) superimposed.  The black arrows represent surface wind direction.  The analyses combine the cloud data with other available wind reports.  The cloud data is for 0000Z, 7 September 1968.  A view of the same area for the previous day appears in Figure 4-A-2.
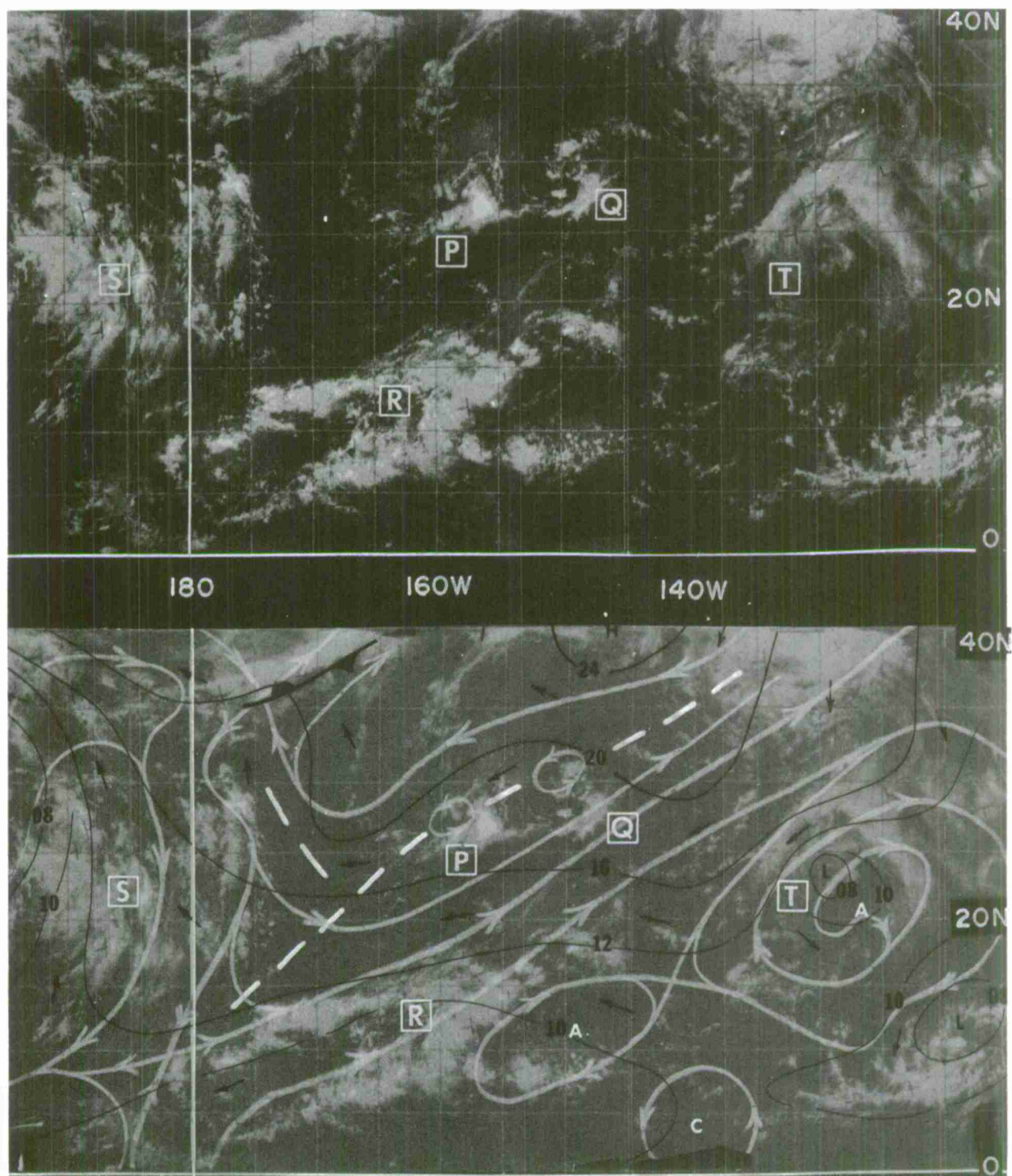
Figure 4-F-8.  Mid-Pacific Trough, 0016Z, 7 September 1968.

Note the isolated cloud systems at P and Q.  These formations are associated with two vortices along the mid-Pacific trough.  The axis of the trough

lies immediately northwest of the two formations. Southwest of them, the trough is centered in the clear area. The large area of cloud centered at R that extends northeast from 10N, 175W lies in the region of southwest flow aloft. Contrast this with the cloud centered at S where the upper level flow is predominantly northerly. In both cases, the alignment of the larger cloud bands is parallel to the shear of the upper tropospheric flow. The shear direction here is similar in direction to that of the upper flow itself. This banded structure, the clear zone, and the vortex cloud systems establish the upper level trough position and help to determine the flow pattern over a large area. The upper westerlies are shown in the analysis to extend over the major cloud systems of P and Q, as suggested in the model just discussed. The appearance of the weakening tropical storm at T can also be used to estimate the upper flow direction. The storm here is typical of those in the eastern Pacific that have moved northward through the near-equatorial 250-mb ridgeline into the region of upper tropospheric westerlies [34]. The storm has lost its cirrus canopy and the clouds that appear in the picture are confined to the lower troposphere. Therefore, the appearance of this storm (T) and the position of cloud systems P and Q establish the limits (width) of the 250-mb southwesterly current along 25N.

Figure 4-F-9 is an enlargement of the cloud systems associated with the vortices P and Q in Figure 4-F-8. Curved cumulus bands are only present around Q, but, even so, are poorly developed. The cloud formation at Q is a weakly-developed example of the cloud model presented in Figure 4-F-7. Cloud system (P) shows even less organization. For this reason, no surface vortex would be expected.

Figure 4-F-9. Disturbances associated with upper level vortices along the mid-Pacific trough, E-7, 0016Z, 7 September 1968.
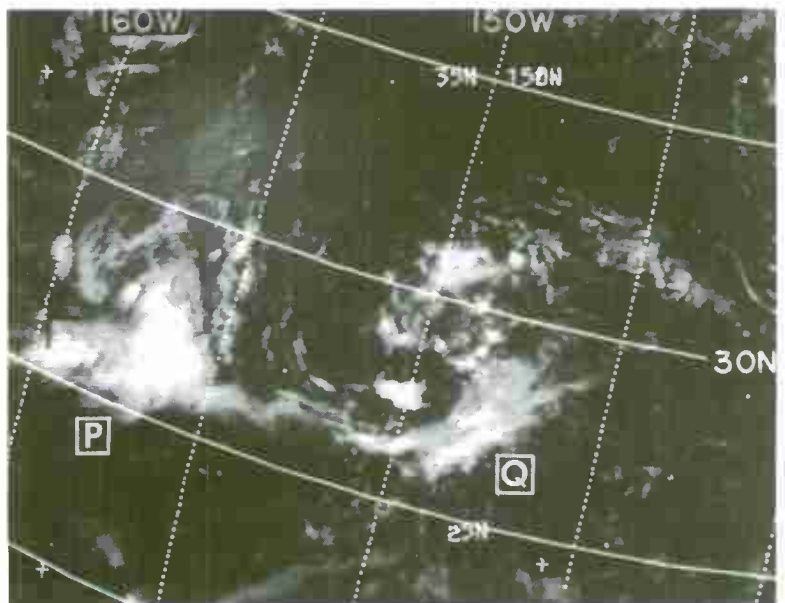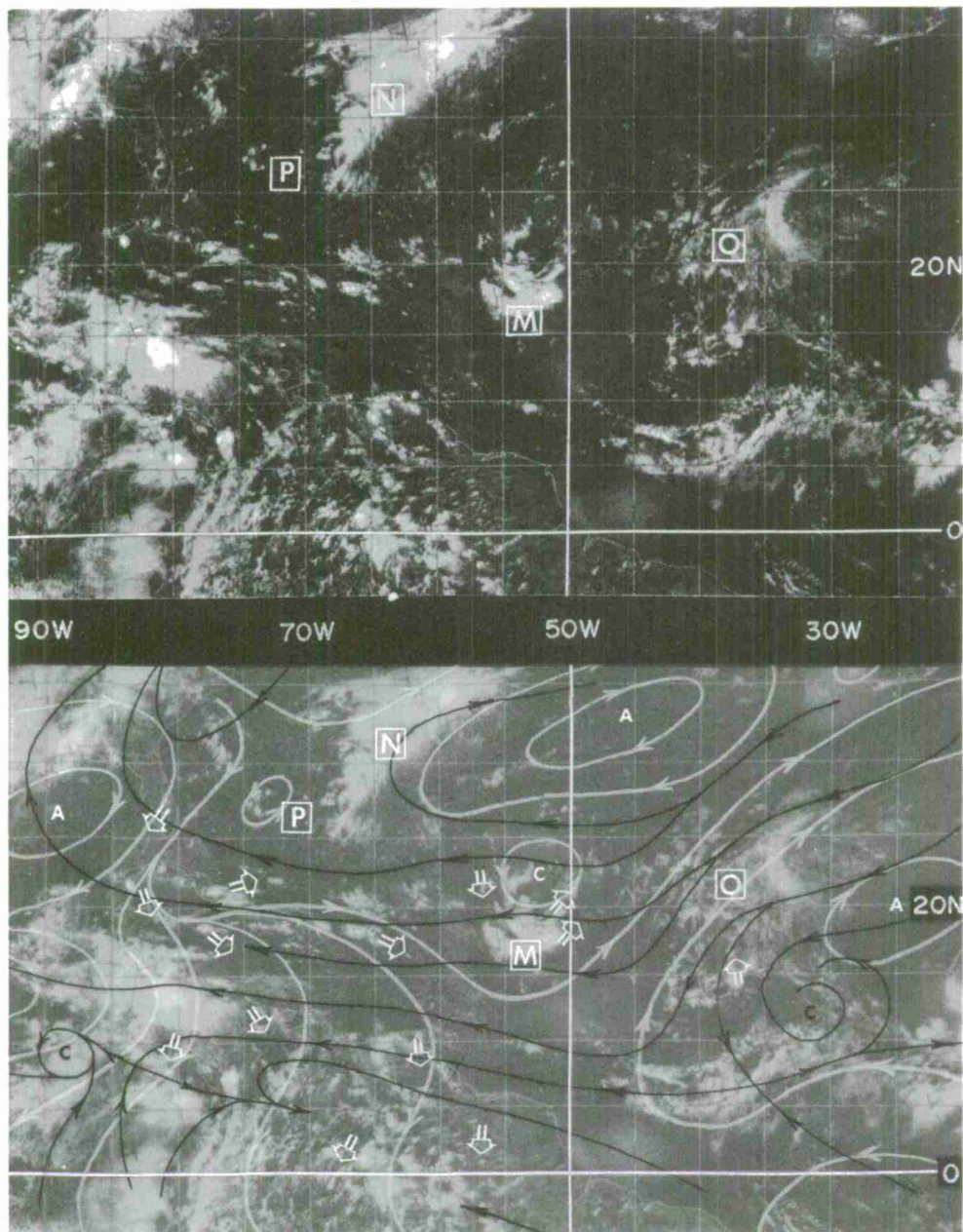
Figure 4-F-10.  Mid-Atlantic Trough, Cloud Patterns with
Surface and 200-mb Streamline Analysis, 1200Z, 5 September 1968.

An example of the relationship of the clouds to the mid-Atlantic trough is
shown in Figure 4-F-10.  The computer-mapped cloud data cover  a 6-hour time
interval centered near 1800Z, 5 September 1968.  The analyses superimposed are
the 200-mb streamline analysis based on the 1200Z wind data (white) and the
surface streamline analysis (black) for the same period.  In this case, both
the positions of the major cloudy areas and the upper-air wind direction esti-
mates from cirrus plumes must be combined to deduce the upper wind flow.

The cloud formation at M is the only evidence of an upper level vortex. The alignment of the cloud elements making up this formation (Figure 4-F-11), suggest that the vortex lies due north of the major cloud area. The cloud at N is in the southwesterly flow in advance of a moving trough in the westerlies. The relatively clear area between M and N (Figure 4-F-10) lies predominantly under upper-level easterly flow. Southwesterly flow aloft extends across the cloud area O which lies to the east of M. These three features roughly establish the direction of the upper level flow in the central Atlantic.
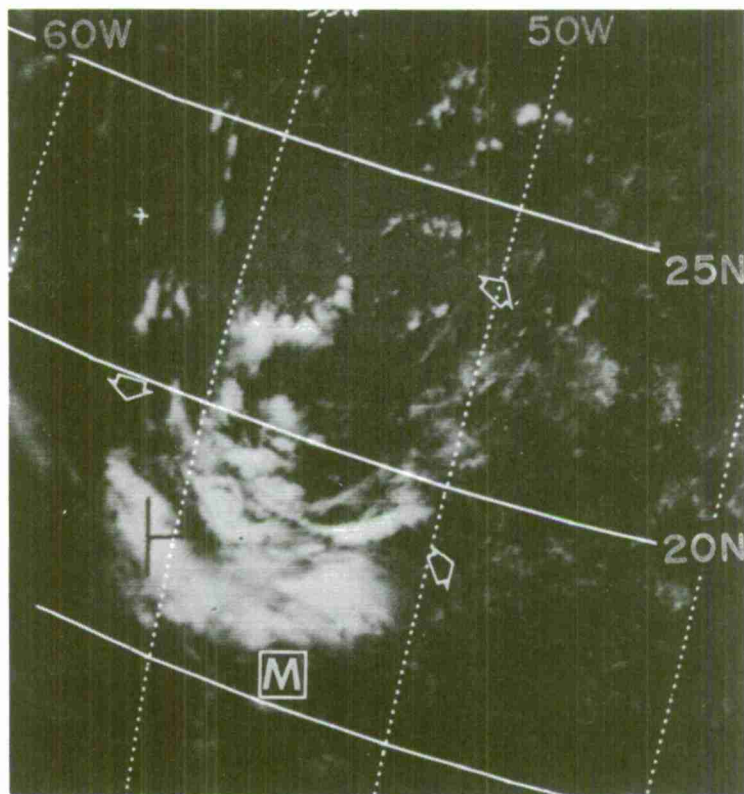


Figure 4-F-11. Enlargement of Cloud Formation from Figure 4-F-10 Associated with an Upper Low. ESSA-7, 1732Z, 5 September 1968.

In the western Atlantic, it is necessary to examine the cirrus plumes to determine upper-level wind flow. Figure 4-F-12 is a more detailed view of the clouds over the Caribbean. Wind direction arrows determined from the clouds, indicated by white arrows, are entered on the picture. Note that the anvil plume direction defines the trough across Cuba quite well. The cumuliform clouds at P exhibit little shear and, therefore, are near the trough axis. Such small cumuliform cloud elements, when surrounded by a large clear area, lie near the center of an upper vortex and help to locate it.
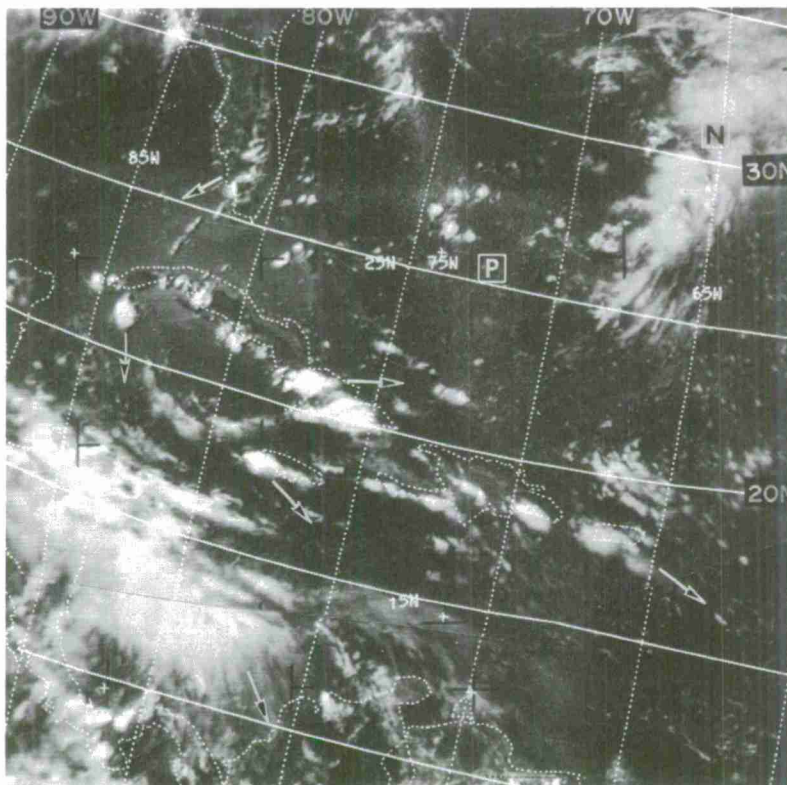


Figure 4-F-12.  Clouds in the Western Atlantic, 1923Z, 5 September 1968.

## Equatorial Anticyclones and "Burst Band" Disturbances

The results of research based on motion fields, as determined from ATS
data, are just becoming available.  A recent study uses this data to show how
flow from the Southern Hemisphere influences the behavior of the ITC cloud
band [32].  In Figure 4-F-13, we see the clouds over the tropical eastern Pa-
cific as viewed by ESSA-3.  Wind vectors obtained from ATS cloud-motion meas-
urements are superimposed.  The vectors represent flow near the surface.
Figure 4-F-14 shows the low level streamlines drawn from this data plus avail-
able ship reports.  The winds reveal that the break in the ITC cloud band at A
is associated with an anticyclone.  The vectors also show three cyclonic cir-
culation centers (B), (C), and (D) along the ITC band in the western portion
of the picture.  These lie along the area of ITC cloudiness which is character-
ized by converging streamlines with cyclonic curvature.



VELOCITY OF LOW CLOUDS
1948-2152 Z, SEPT 17, 1967
← 10 kt   ← 20 kt   ← 30 kt
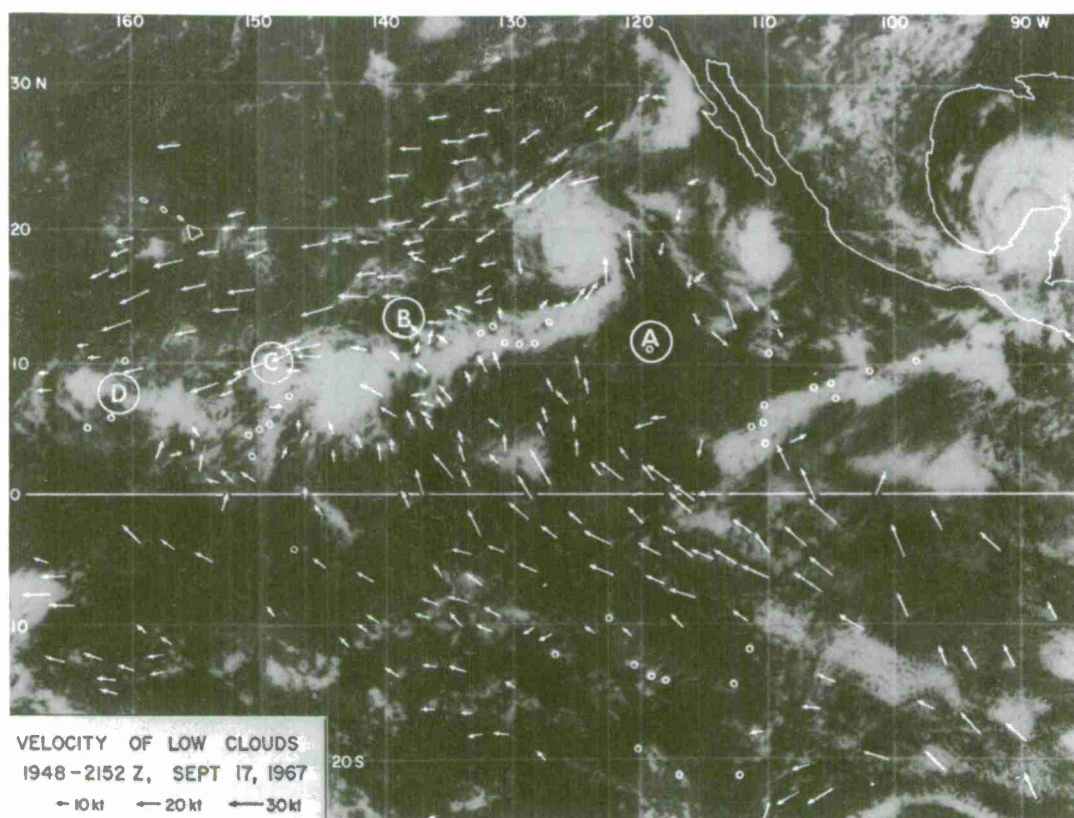
Figure 4-F-13.  ESSA-3 Digital Composite with ATS-I Wind
Vectors Superimposed [32]; Wind Analysis, 2152Z, 17 September
1967.
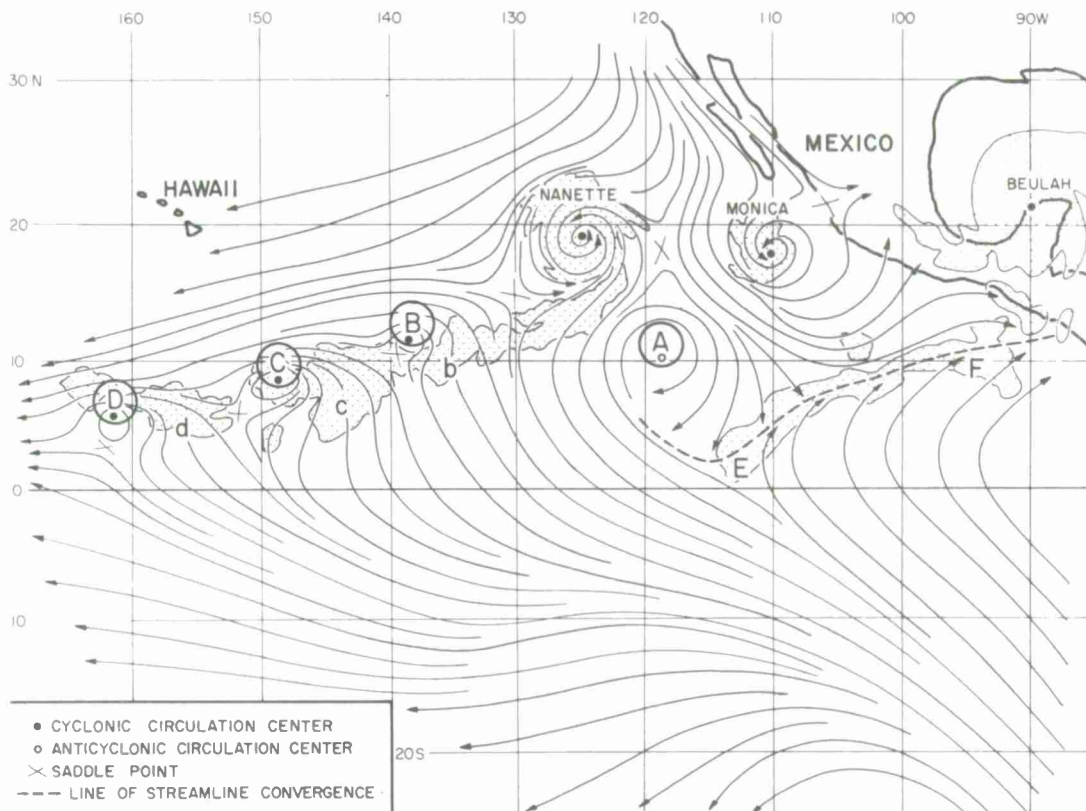
Figure 4-F-14.   Low-Level Wind Flow Based on ATS-I Wind
Data, 17 September 1967.

The anticyclone at A forms as a surge of air moves northward into the
Northern Hemisphere.  As this anticyclone migrates westward, a cloud band de-
velops in advance.  This band, an active weather producer, is called the
"burst band."  A model of the life-cycle of a migratory equatorial anticyclone
and its associated "burst band" is shown in Figure 4-F-15 [32].  There are six
stages to the cycle which require about two weeks to complete.

   1.  Pushing Stage.  A large-scale flow from the Southern Hemisphere pushes
north deforming the band of intertropical cloudiness.  During the pushing
stage, the band can move as far as 1000 km to the north.  At this time, vor-
tices tend to form along the ITC cloud band where wind shear and cyclonic
relative vorticity are greatest.


   2.  Recurving Stage.  Within one to three days after the air initially
moves into the Northern Hemisphere, the increase in anticyclonic relative vor-
ticity causes it to recurve.  Tropical depressions formed in the pushing stage
tend to move out of the region of the tropical cloud band at this stage.


   3.  Cut-off Stage.  A closed anticyclonic circulation forms.  The ITC
cloud band is now broken with relatively clear skies around the center of the
anticyclone.


   4.  Mixing Stage.  Air from both hemispheres mixes around the anticyclonic
circulation.


   5.  Burst Stage.  As the anticyclone moves west, the portion of the ITC
cloud band on the leading edge of the anticyclone intensifies to form a "burst
band."  This formation can produce heavy rains.  The disturbance is primarily
detectable in the wind field; it is not readily detectable from pressure
changes.  A "burst band" lasts for one or two days, then disintegrates quickly
into small fragments or isolated cloud clusters.


   6.  Interacting Stage.  After the disintegration of the "burst band," the
southeasterly flow to the south of the equatorial anticyclone often remains
fairly strong.  This can impede the southeastward movement of a cold front
causing a wave to form.
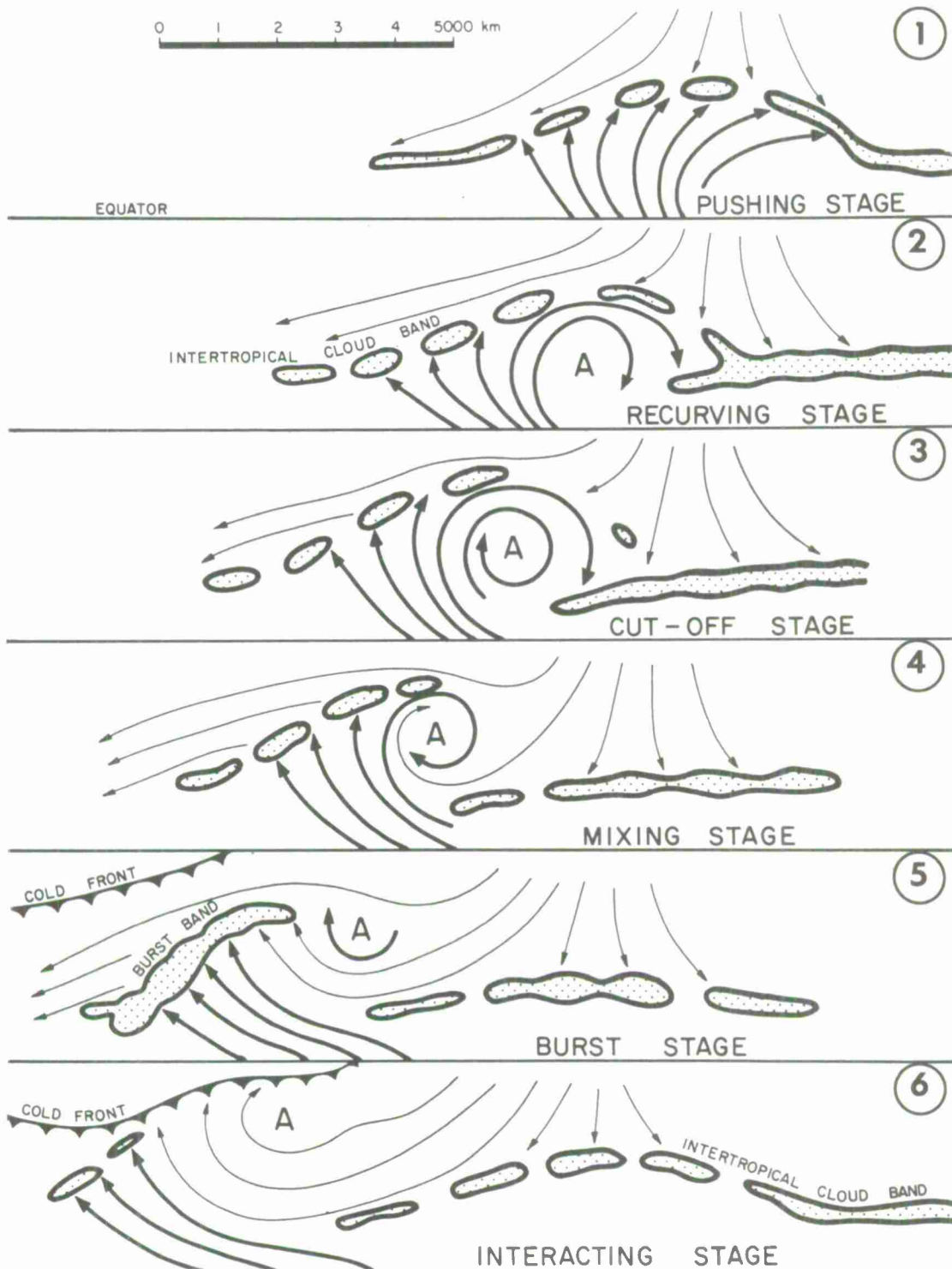
Figure 4-F-15. Model showing the life-cycle of an equatorial anticyclone produced by cross equatorial flow [32].

Figure 4-F-16 shows an analysis [32] of the eastern Pacific over a 14-day period. The low level flow lines for this series are based on wind estimates derived from ATS-I data and available surface reports. It shows the complete development cycle of one anticyclone.

Figure 4-F-16. Low Level Flow in the Eastern Pacific during September 1967. Tropical storms are indicated by letters, anticyclones by the letter A [32].
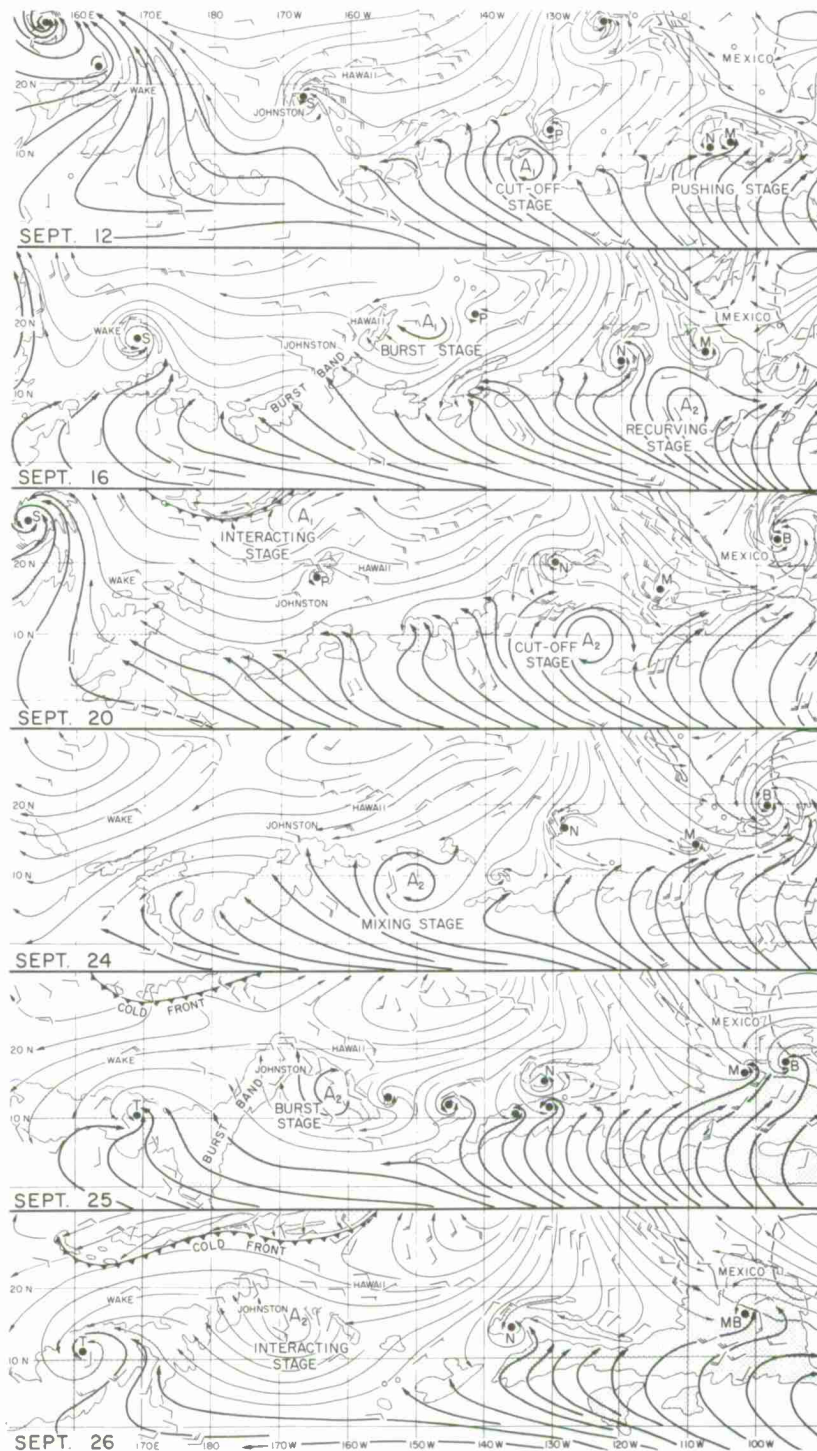
Chapter 4

SECTION G

FRONTAL SHEAR LINES

Bands of clouds observed at low latitudes over oceanic areas are often as-
sociated with shear in the low level wind field.  Satellite pictures, taken on
consecutive days, show that many of these narrow bands are the remnants of
polar cold fronts.  When a polar front moves into the tropics, the cold air
behind it is modified by passage over a warm surface and by subsidence aloft.
Eventually, the density discontinuity disappears leaving a narrow line of cy-
clonic shear in the wind field (Figure 4-G-1).  The low level wind is stronger
on the poleward side of the shear line than on the equatorward side.  A shear
line may persist for several days and often continues to move slowly equator-
ward [45].  Satellite pictures show that a narrow band of cumulus clouds in-
terspersed with cumulonimbus lies in this zone of cyclonic shear.  Accurate
location of this cloud feature permits a more accurate analysis of the wind
field and allows the forecaster to locate these areas of probable shower ac-
tivity and locally gusty winds.
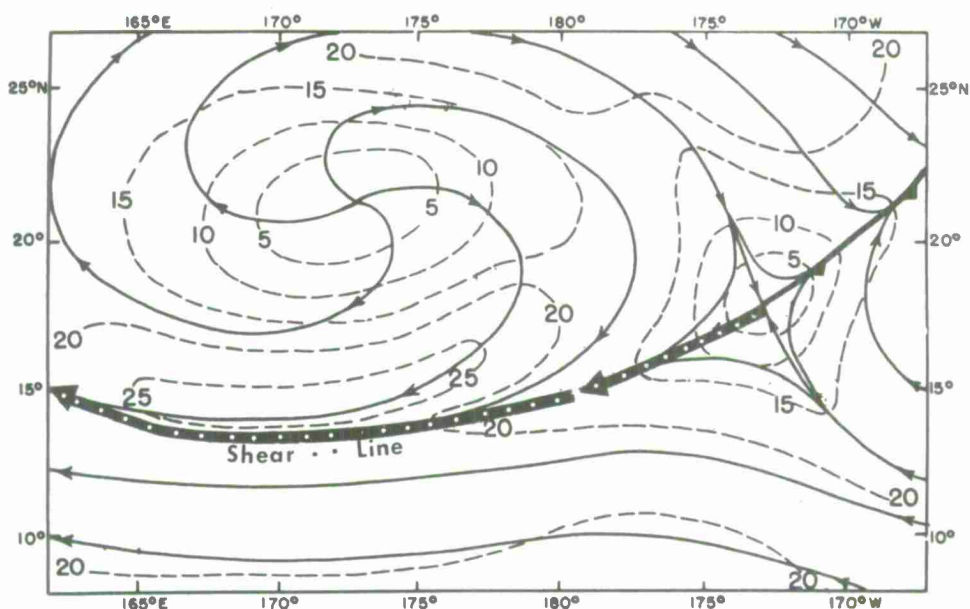


Figure 4-G-1.  A shear line in the wind field [21].

Figure 4-G-2 is a 7-day sequence of digitized satellite data which shows the penetration of two frontal shear lines into the tropics. The cloud band (A to B) accompanying the first system changes considerably in appearance from day to day but can be followed through the entire period. The fronts that are superimposed on the picture are based on the National Meteorological Center's operational analyses. A portion of the front was dropped from the analysis midway through the period and was deleted entirely by the 26th. Surface reports in the vicinity of the shear line on 26 and 27 December showed the band to be composed mainly of cumuliform clouds with some rain shower activity. The picture at the lower right of Figure 4-G-2 is an enlargement of a portion of the shear-line clouds observed on 27 December. The brightest elements are clouds with the greatest vertical development.

The frontal cloud band between C and D on 24 December identifies another outbreak of cold air. This cloud system is maintained through the remainder of the period and, by the 27th, the southern portion of the band coincides with a shear line in the wind field.
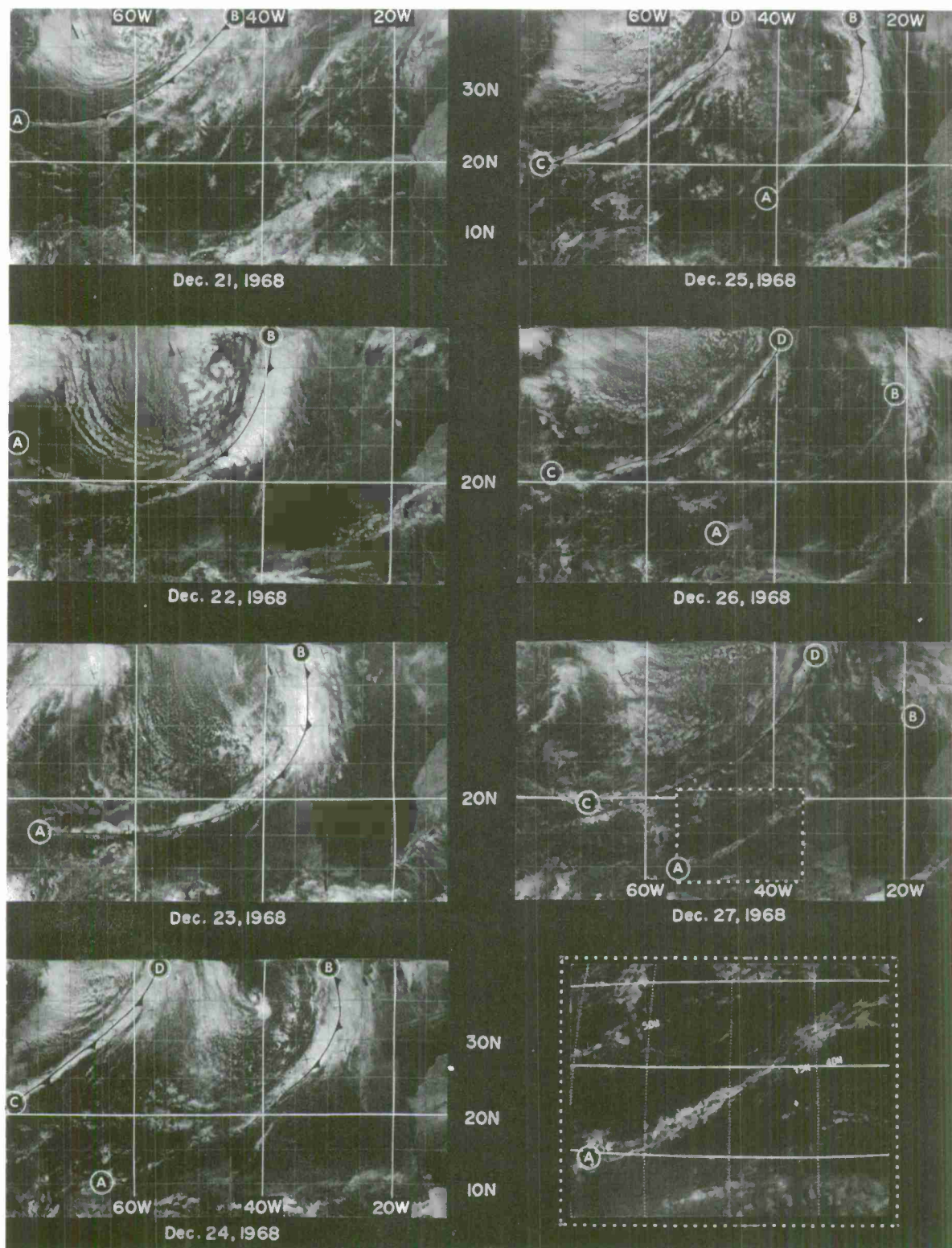
Figure 4-G-2. Sequence of ESSA-7 digital data showing the clouds associated with polar frontal systems. Picture at lower right is an enlargement of the clouds associated with a shear line observed on 27 December 1968.

Chapter 4

SECTION H

INTERACTION BETWEEN HIGH AND LOW LATITUDES IN THE NORTHERN HEMISPHERE

Periodically, portions of the main upper level westerly current of mid-latitudes shift from a zonal to a meridional flow regime. When this occurs, large amplitude troughs develop. These often extend to within 10 to 20 degrees latitude of the equator. Satellite pictures show that amplification of the upper level troughs in mid-latitudes is accompanied by an extensive northward intrusion of clouds and moisture from the tropics. Many times, such cloud formations appear to begin within or near the ITC cloud band. These cloud surges are important weather producers both in the subtropics and further north. Because the clouds move poleward from data-sparse regions, they are primarily detectable by means of satellites.

The evolution and characteristics of these large-scale surges are as follows:

a. The ITC cloud band broadens and begins to extend toward the northeast. This northeast surge of cloud lies in the developing southwesterly current immediately ahead of a deepening trough.

b. With time, this extension lengthens into a broad cloud band within the southwesterly flow. The eastern or leading end of the band moves northeastward at about 25 knots, while the southwestern end remains merged with the east-west ITC cloud band.

c. Discrete cloud systems are often embedded in the northeast-southwest cloud band. These are associated with upper-level vorticity maxima forced northeastward out of the subtropics as the upper level trough "digs" southward to the west of their initial position. There is usually little evidence of these disturbances noted in the surface isobars.

d. Clouds originating in the tropics are usually ahead of the cloud band along the front associated with the amplifying trough and remain a separate and distinct formation.

An example of the northward surge of tropical cloud produced by an amplifying trough is shown in Figures 4-H-1 through 4-H-4.  Mapped digital data for four consecutive days are shown alone and also with the surface and 200-mb analysis superimposed.  The surface fronts and isobars are in black; the 200-mb contours and streamlines are in white.

On the first day of this series, 10 November, the belt of strongest westerlies lies north of 35N.  South of this latitude the 200-mb flow is weak and meanders around two upper level vortices, one near 28N, 170E, and the other near 25N, 145W.

By 11 November, strong pressure rises occur north of 30N at 170W.  This is reflected both at the surface and at the 200-mb surface.  East of 180 degrees, the winds have a much more northerly component than on the previous day.  The frontal cloud band ahead of the digging upper level trough now extends to 32N at 160W.  Southeast of the building ridge, a major increase in cloud has occurred between 15N and 30N at 140W.  Here, the clouds have started to extend northward in response to the deepening trough.

By the third day, 12 November, a large amplitude trough has developed along 145W.  The tropical cloud surge has now reached the California-Oregon coastline.  It covers a broad area ahead of the front, but is still separated from the frontal cloud band by a narrow clear zone.

The break in the northeast-southwest cloud band between 10N and 20N at 135W is associated with a short-wave trough which is accelerating out of the subtropics in advance of the digging trough to the west.

On the last day, 13 November, the tropical cloud surge is well into the western states.  It still remains separate from the frontal clouds.  The northeast-southwest band still extends to the ITC region at 8N, but the break in the band at 20N has become wider, suggesting that the connection is weakening.
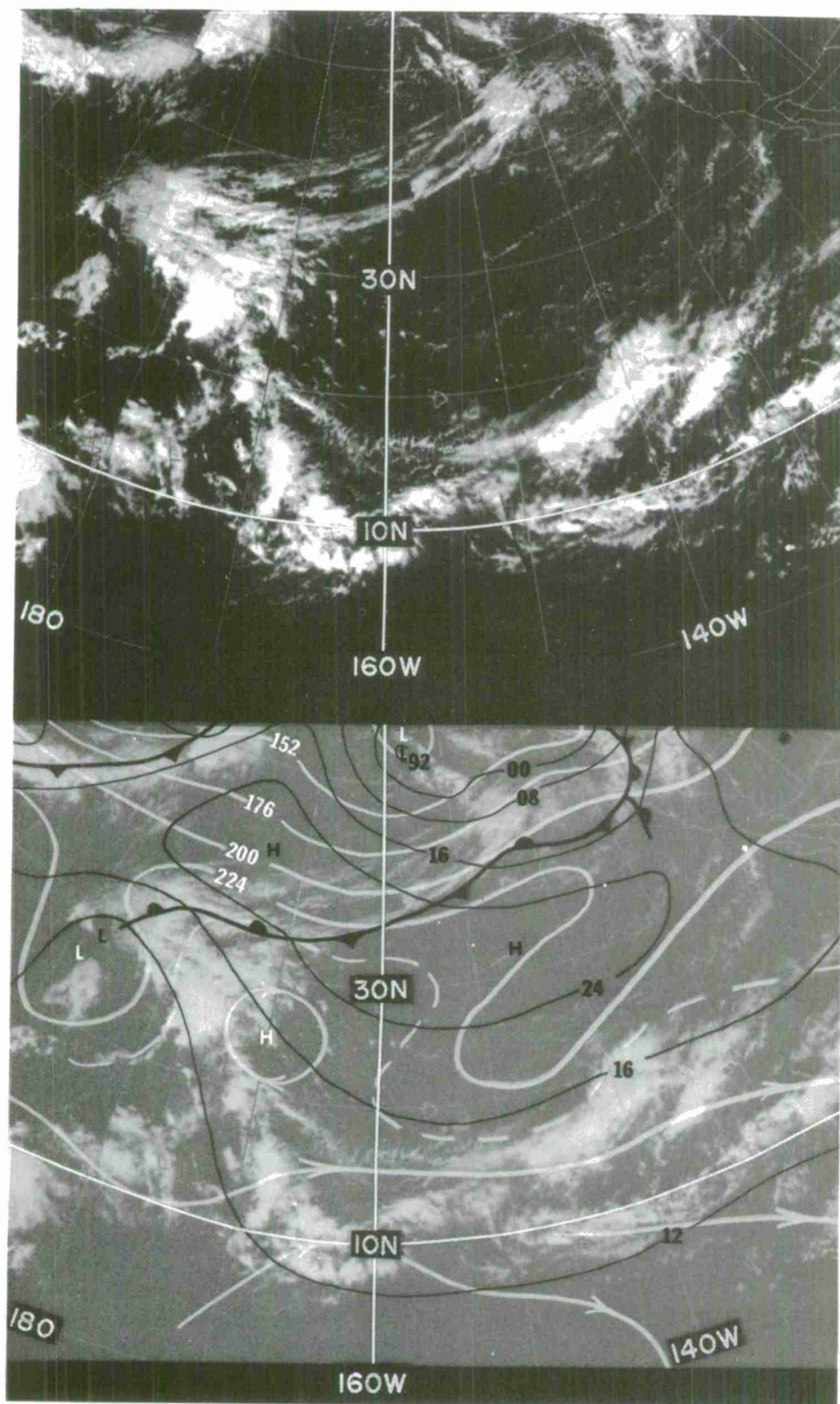
Figure 4-H-1.  E-3 Surface Analysis 0000Z, 10 Nov 67.
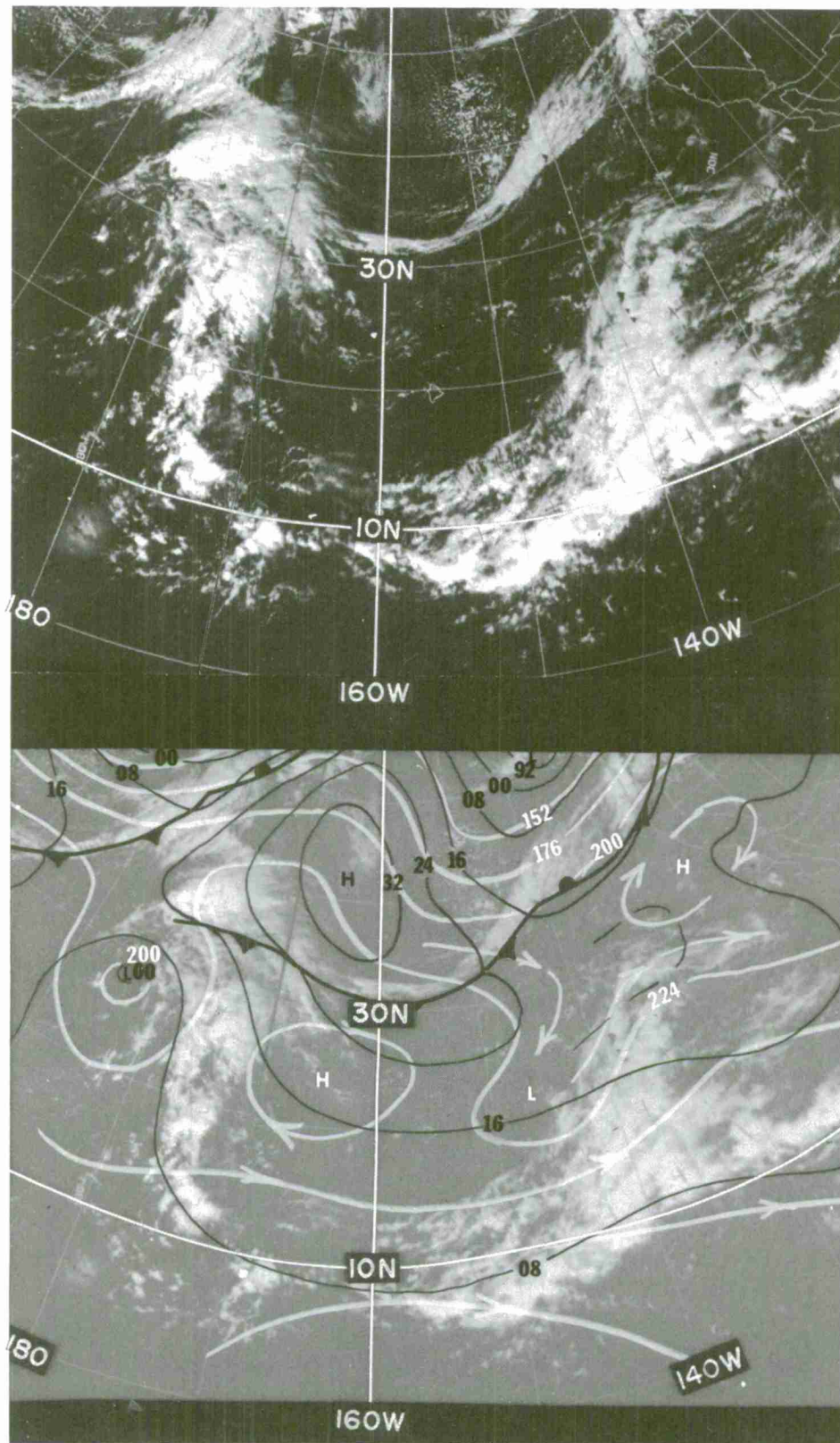
Figure 4-H-2.   E-3 Surface Analysis 0000Z, 11 Nov 67.
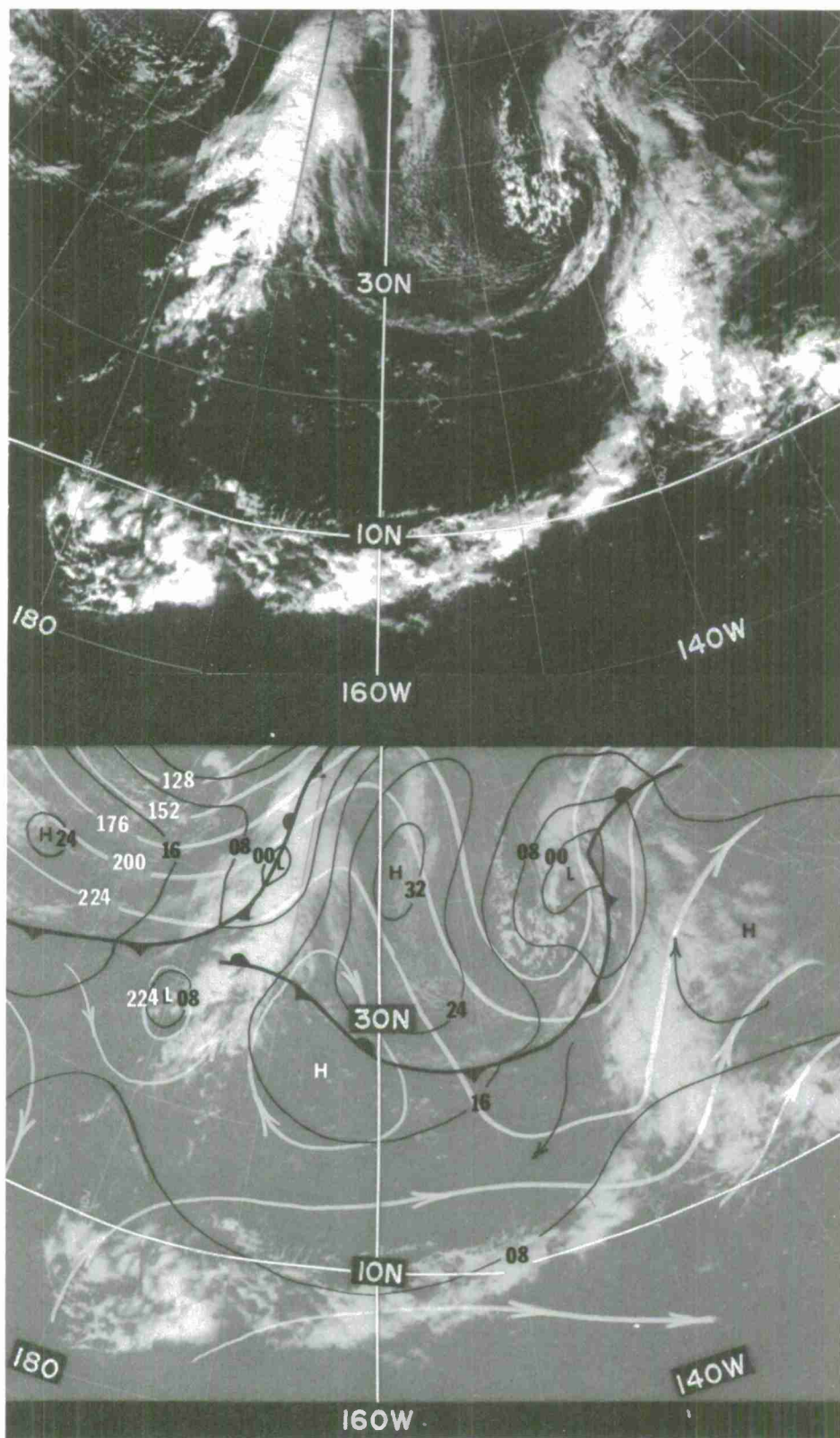
Figure 4-H-3.   E-3 Surface Analysis 0000Z, 12 Nov 67.
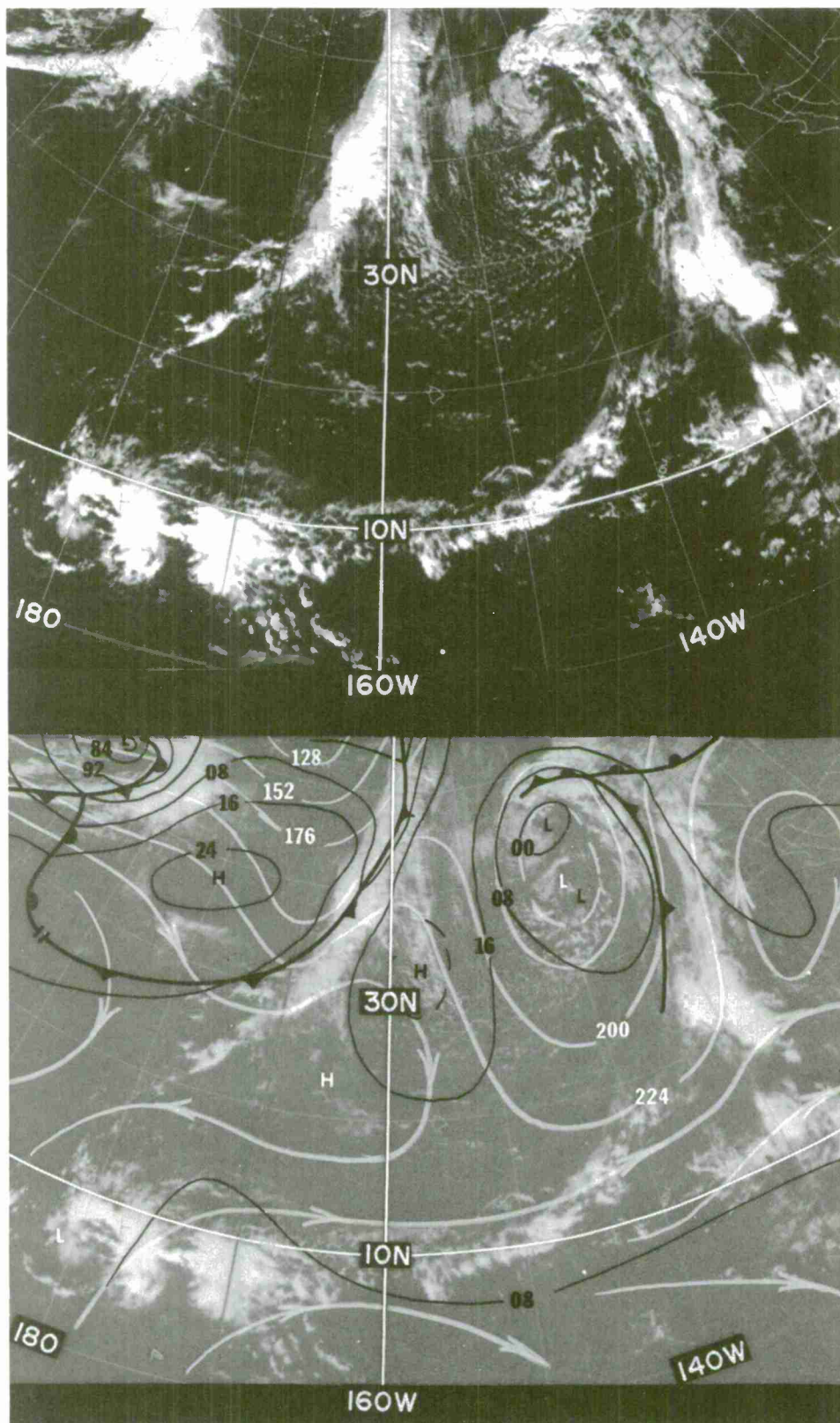
Figure 4-H-4.   E-3 Surface Analysis 0000Z, 13 Nov 67.

Chapter 4

SECTION I

DIURNAL CLOUD CHANGES IN THE TROPICS

Convective processes are the main source of clouds in the equatorial re-
gions of the world.  Thus, the amount of clouds over tropical land areas at
any given time is dependent on diurnal effects.  Typical convective clouds
range from small, isolated, fair-weather cumulus to the large cumulonimbus
clusters found in the Intertropical Convergence Zone.  Cirrus and middle
clouds found in the tropics are usually produced by cumulonimbus activity.

Convective-type clouds over land areas in the tropics are the result of
diurnal heating.  This dependence on diurnal heating causes a greater daily
fluctuation in cloud amount than is generally noted at higher latitudes.
Therefore, it is necessary to consider the time of day a picture is taken when
using satellite photographs for assessing the strength of tropical disturb-
ances, especially those in the developing stages.  Diurnal cloud fluctuation
becomes extremely relevant when only one satellite view per day is available
for study.  Changes in cloud amounts noted in ATS pictures, taken at one-half
hour intervals, further emphasize the importance of considering time of day
when making short-period forecasts based on a single picture.  The cloud
amount accompanying a weak disturbance varies considerably over a 24-hour per-
iod even though the strength of the disturbance remains fairly constant.

Other factors which influence the amount and distribution of convective
cloud over land surfaces include differential heating, frictional effects,
topography, available moisture, convergence, and atmospheric stability.  Their
effects are clearly revealed in picture series available from geostationary
satellites.

Figure 4-I-1, an ATS-III photograph taken at 1547Z, provides a general
view of the synoptic cloud patterns surrounding the area which is shown in de-
tail in succeeding illustrations.  The axis of ITC cloudiness (dashed line)
stretches from the Pacific Ocean, across northern South America, and into the
Atlantic.  The area outlined in Figure 4-I-1 appears enlarged in Figures 4-I-2
to 4-I-6.
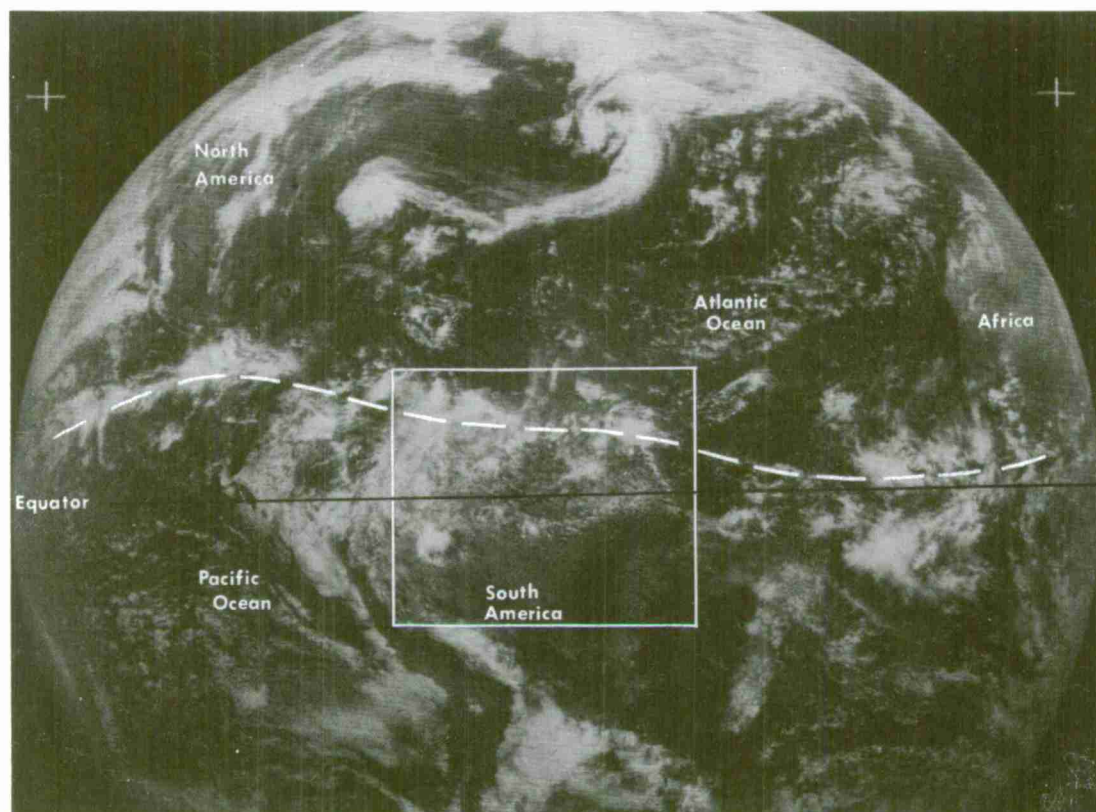


Figure 4-I-1.  ATS-III View of South America, 1547Z,
6 Jan 68. (The axis of the ITC cloud band is dashed.)

The following series of photographs (Figures 4-I-2 through 4-I-6) show the
diurnal changes in cloud amount over a tropical continent.  These were taken
over a 9-hour period by the geostationary ATS-III satellite.  They show
changes in the synoptic-scale systems which make up the ITC band in northern
South America and the effect of surface variations on convective cloud devel-
opment.  The identifying letters used on the photographs appear in the same
geographical location in each picture.

In the early morning (0731 local time, 1131Z) ATS view in Figure 4-I-2,
most of the convective cloudiness associated with the ITC (A-B) lies to the
north of the Amazon River (C-D).  These large cumulonimbus clusters have well-
pronounced cirrus plumes extending northward from the source.  The tops of
cumulonimbi at E and F are highlighted by the sun and produce locally bright
areas in the general overcast.  The low and high cloud area at K is composed
of radiation fog under the debris from earlier thunderstorm activity.  In the
following pictures, it is interesting to note the increase in clouds between
G and H as the sea breeze intensifies during the day.
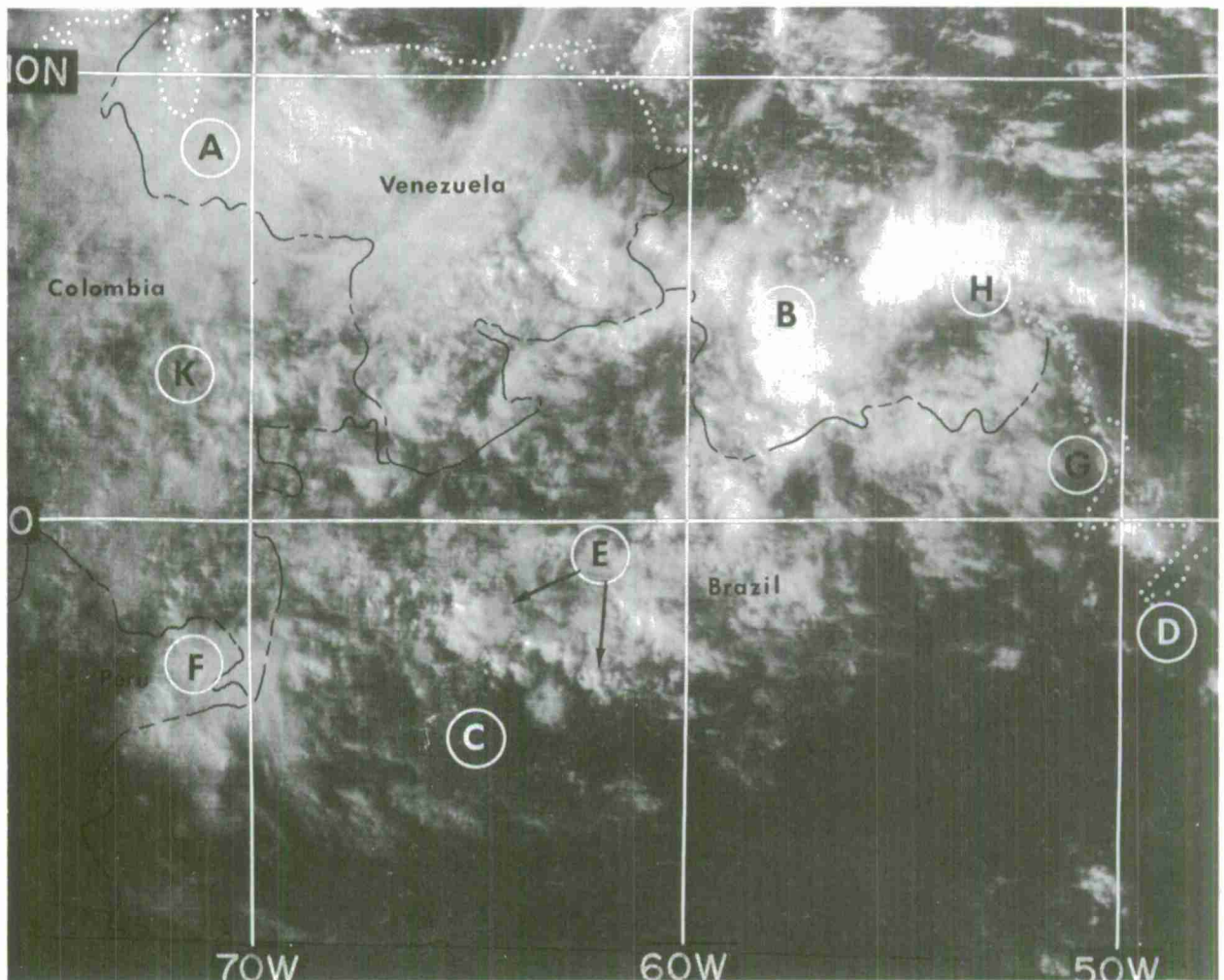


Figure 4-I-2.  ATS-III, 1131Z, 6 Jun 68.  Northeast
South America.

A slight increase in clouds as solar heating increases can be noted in
Figure 4-I-3.  The most striking change appears over the hilly terrain of
northeast Brazil where a large field of fair weather cumulus has formed by
0938 local time.  In Figure 4-I-3, the convective cloud area from A to F is
viewed under more direct sunlight.  This results in a much larger area of
bright clouds which give the impression of more cloudiness, but close inspec-
tion reveals that little change in amount has taken place.
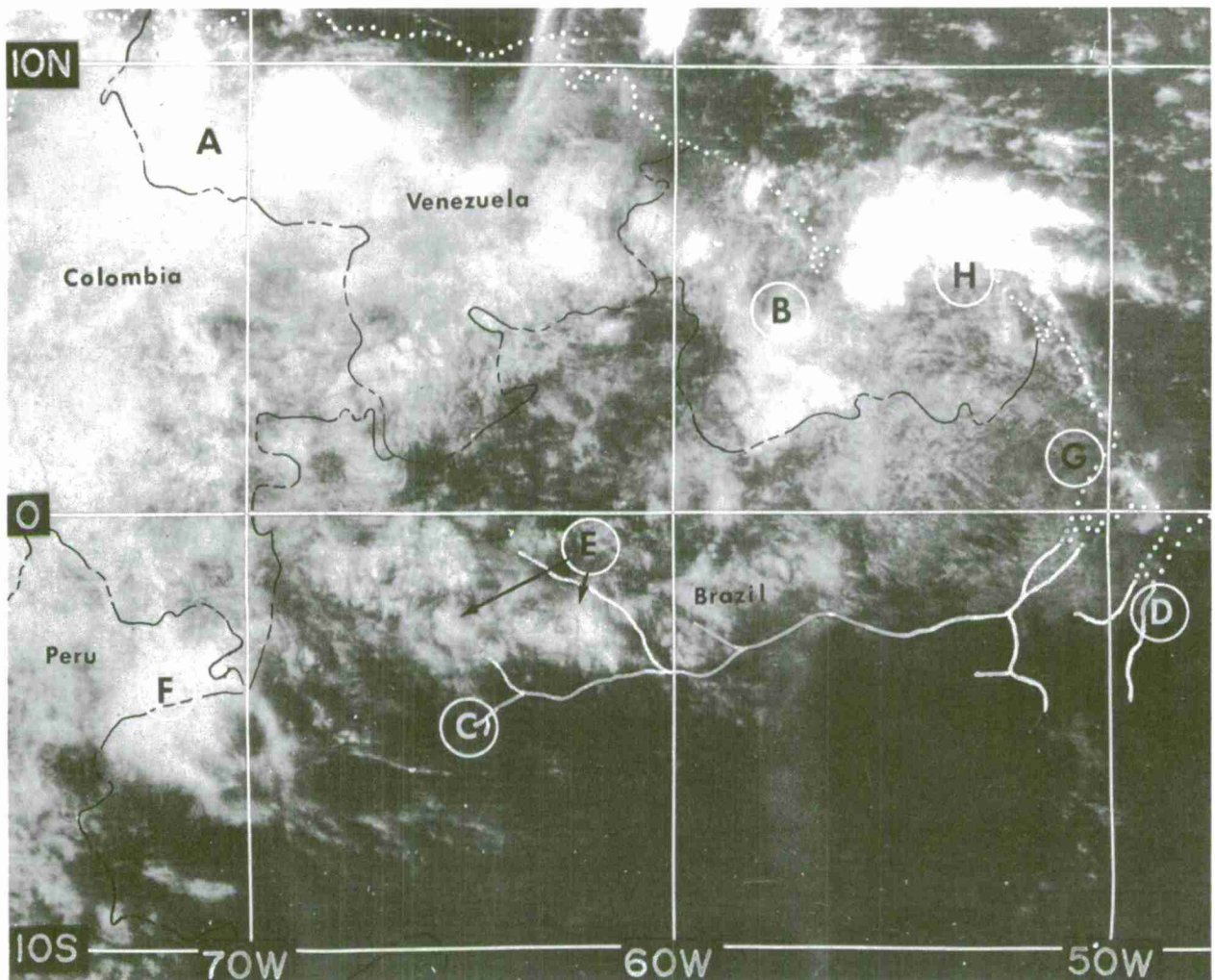


Figure 4-I-3.  ATS III, 1338Z, 6 Jun 68.  Amazon River
indicated by white line.

In Figure 4-I-4, fair weather cumulus appear south of the Amazon River
(C-D).  Since these individual cloud elements are too small to be resolved by
the satellite camera, the area appears quite gray.  These convective clouds
rarely form over relatively cool bodies of water.  The dark vein-like pattern
east of C is indicative of the cloud-free areas over the Amazon and its tribu-
taries.  Two of its larger tributaries, the Tapajos River and the Ningu River
appear at I and J, respectively.  At this time, a decrease in convective
clouds can be noted along the northern coast while the thunderstorm mass at F
remains unchanged.  A slight increase in cloud amount along the coast from G
to H suggests that the sea breeze is beginning to develop.
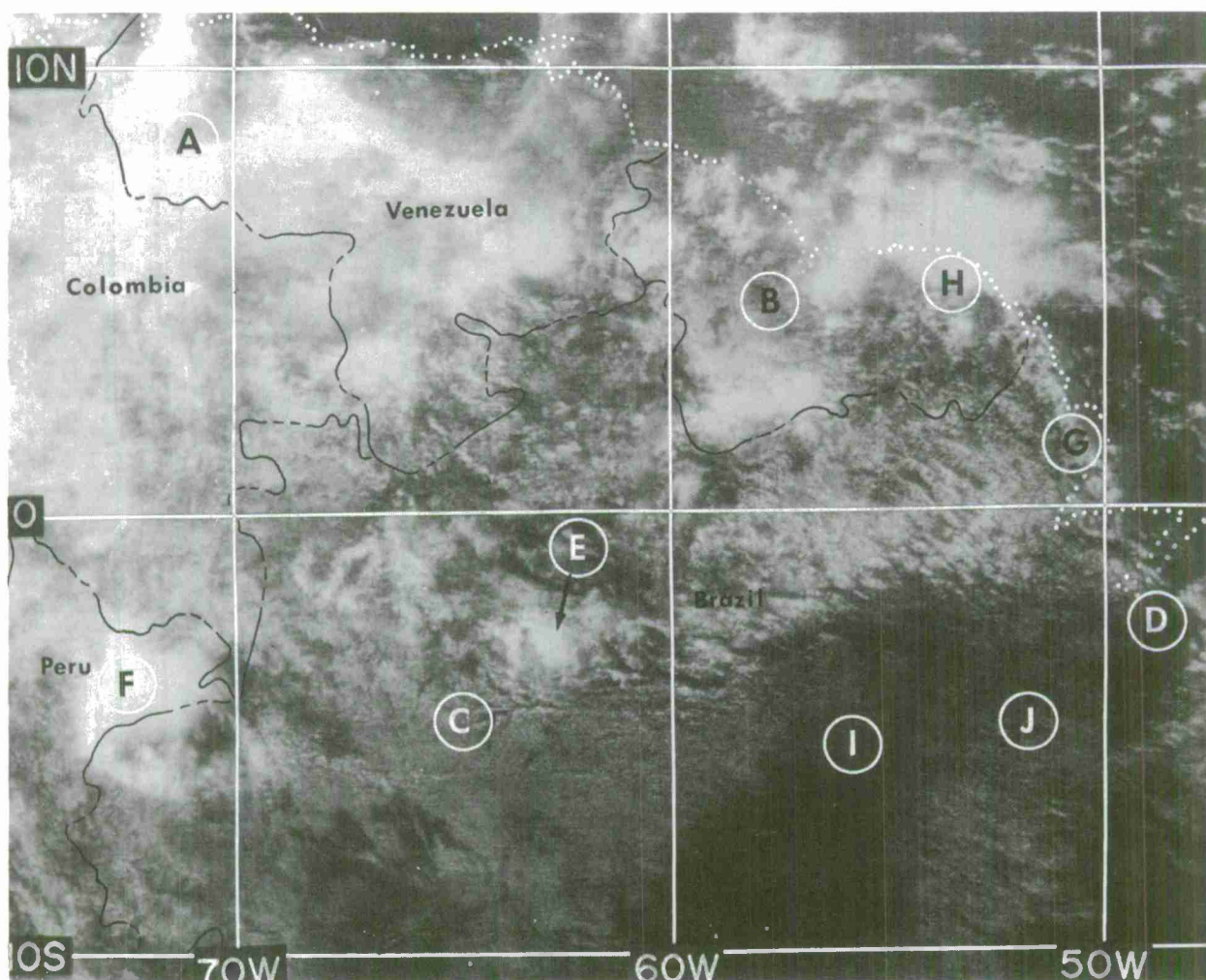


Figure 4-I-4.  ATS III, 1526Z, 6 Jun 68.  Northeast
South America.

By 1332 local time (Figure 4-I-5), an increase in convective activity can
be noted throughout the area. Cirrus plumes emanating from the increased con-
vective activity in southern Venezuela suggest northerly flow, while a south-
westerly flow is evident near B. This defines the center of an upper level
cyclone over eastern Venezuela. The rows of cumulus clouds over the hilly
area south of I and J are oriented parallel to the southeasterly flow at the
surface. Cirrus outflow from the storm at F seems to have increased and the
convective clouds in the sea breeze convergence zone at G and H cover a larger
area. The offshore divergence resulting from the sea breeze circulation pro-
duces a cloud-free zone immediately to the east of G. Clouds begin to form
again further east beyond this divergence area.
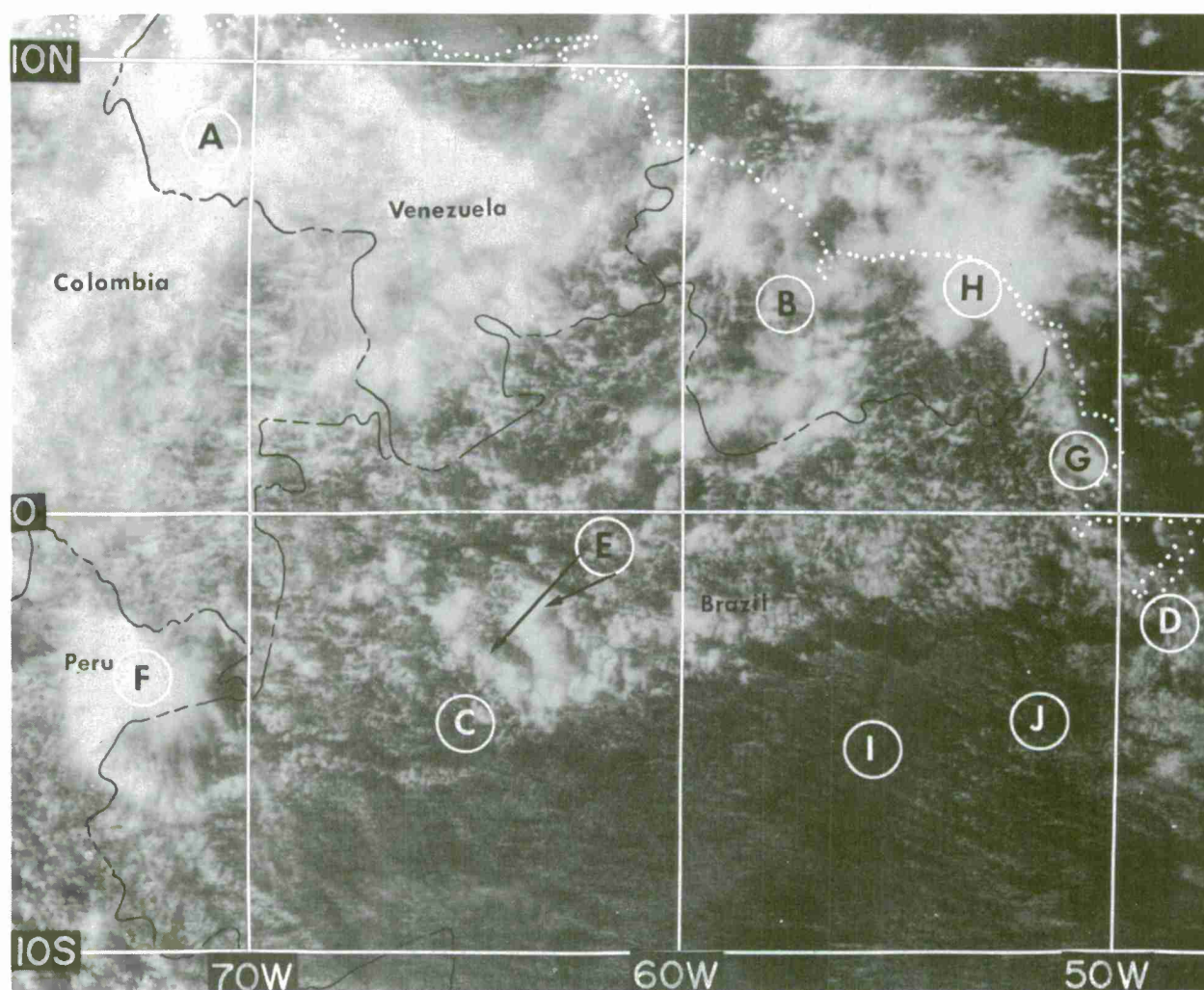


Figure 4-I-5. ATS III, 1732Z, 6 Jun 68. Northeast
South America.

As the source of heat needed to sustain convection decreases, the smaller clouds with the least vertical development quickly disappear.  In Figure 4-I-6, taken at 1540 local time, only a few cloud elements can be seen south of the Amazon.  Further north, the larger, more active cumulonimbi continue to increase in number and size.  The cirrus plumes visible here are the type which aid in upper level analyses.  The clouds in the sea breeze convergence zone between G and H have doubled in size and now are topped with cirrus.
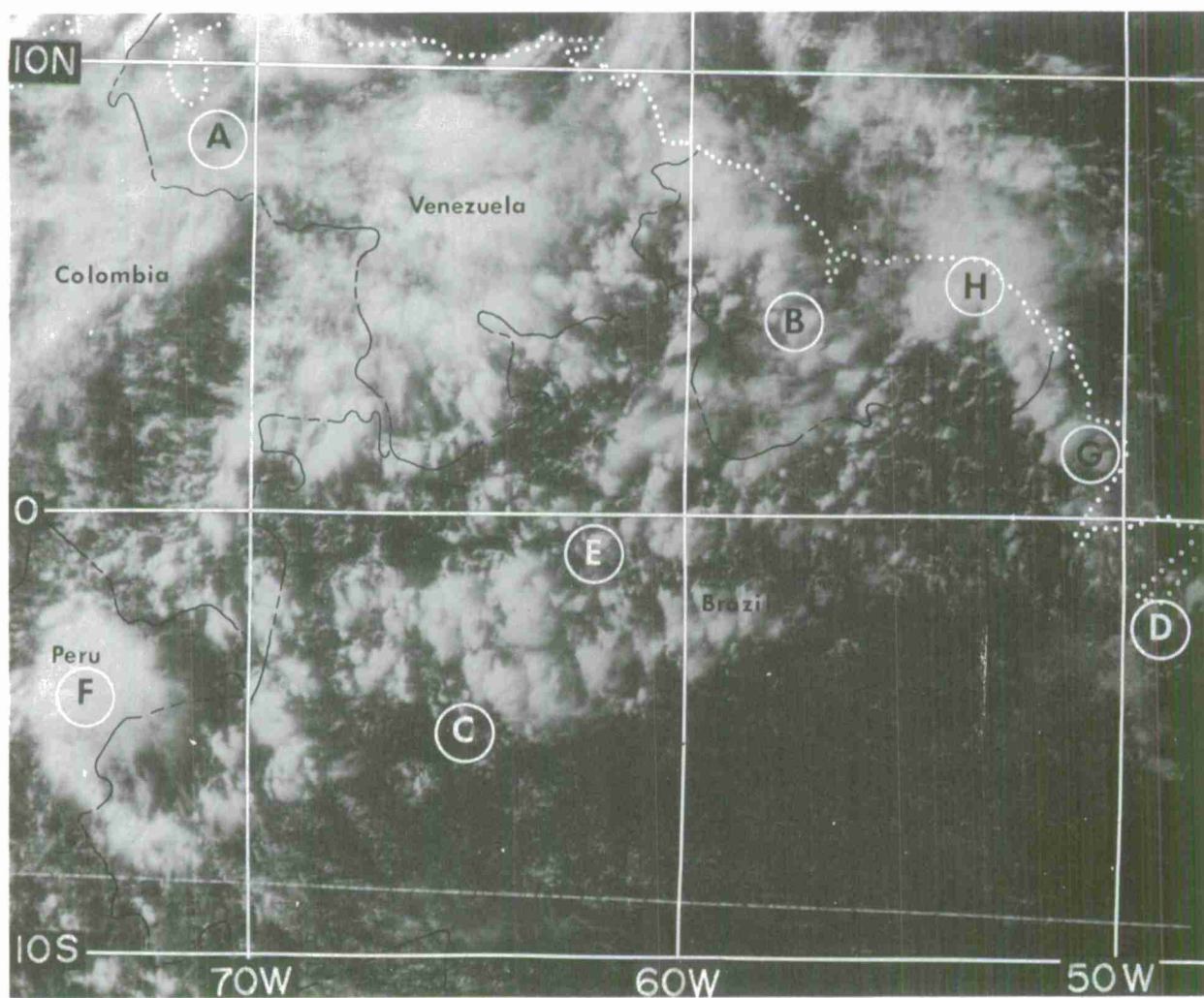


Figure 4-I-6.  ATS III, 1940Z, 6 Jun 68.  Northeast South America.

In Figure 4-I-7, the low sun angle highlights the remaining convective storms along the western edge of the picture.
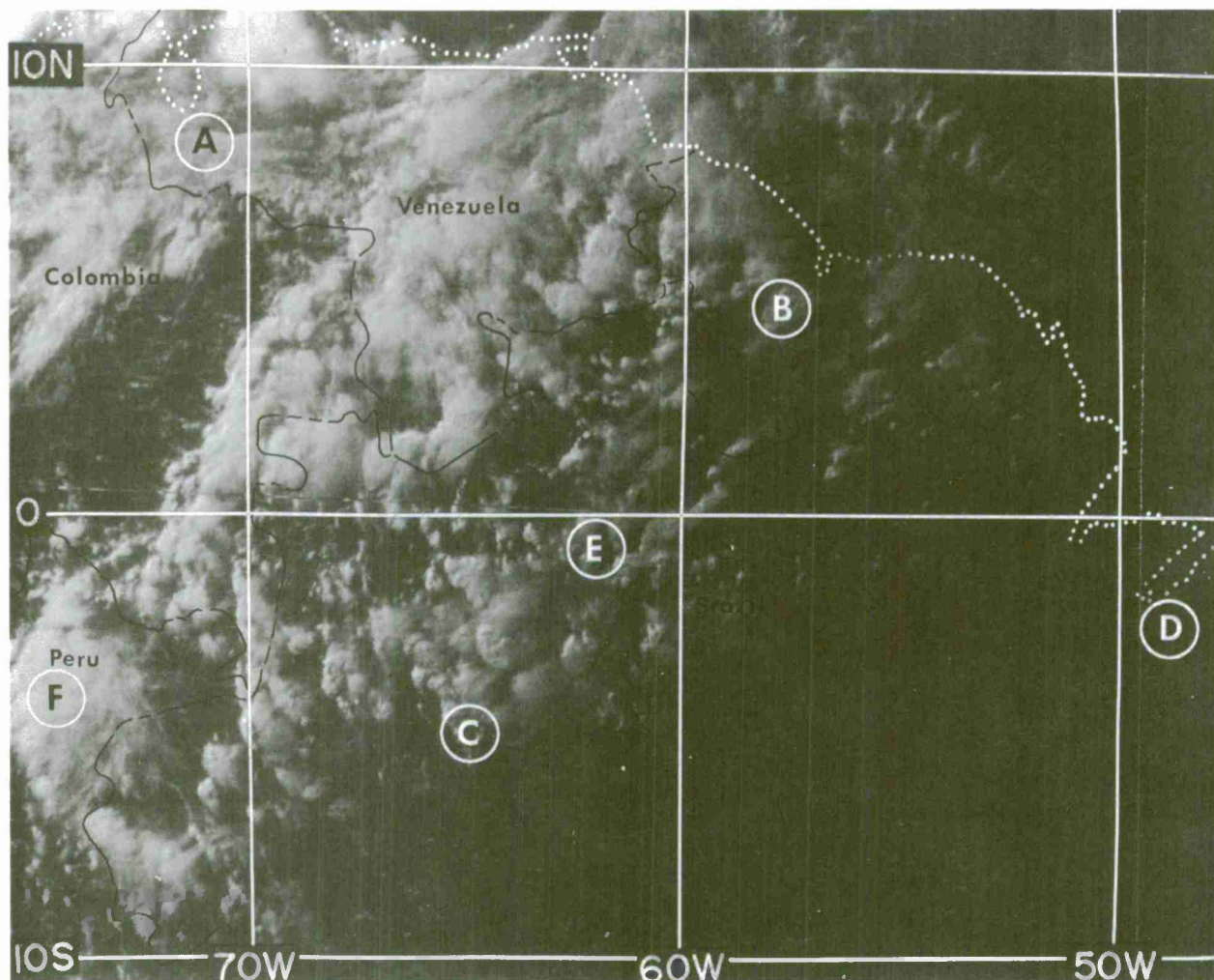


Figure 4-I-7.   ATS III, 2127Z, 6 Jun 68.   Northeast South America.

Chapter 5

LOCAL PHENOMENA

---

SECTION A

SNOW COVER AND SNOW DEPTH

## Introduction

Snow cover, as seen from satellite photographs, can be identified with differing degrees of ease according to the type of terrain and vegetation over which it occurs. Snow is quite easily distinguished over a mountainous area by a characteristic dendritic pattern. A snow cover is less easy to identify over plains or grasslands regions and it is difficult to recognize in a wooded area.

An operational technique to determine snow cover and snow depth from satellite pictures has been developed for use in the upper Mississippi-Missouri River Basins [16] [17]. This technique can probably be used with minor modifications in other regions with similar terrain and vegetation. Usable snow depth estimates in categories of less than 1 inch, 1 to 4 inches, and greater than 4 inches can be made from the brightness patterns of relatively new snow. When conventional reports are available and are used in conjunction with the satellite data, a more detailed analysis can be prepared.

## Snow Identification

To map areas of snow-covered terrain from satellite pictures, it is necessary to distinguish snow from clouds. This can best be accomplished by comparing satellite views of the same area on successive days or, when available, pictures which were taken several hours apart. Except for terrain-induced clouds or valley fog, clouds seldom retain the same shape or location for more than a few hours; nonchanging patterns are indicative of snow cover.

Snow cover can further be distinguished from clouds by comparing the visual characteristics of the two phenomena. Snow-covered plains usually have a smooth texture while clouds are often rough or "lumpy" in appearance. Snow fields over level terrain have sharper, more definite edges than cloud areas, with the exception of fog and stratus. Rivers, lakes, and mountains can often be identified in a snow field while a cloud shield over snow usually obscures such terrain features. Snow cover in forested areas produces little variation in brightness as snow depth increases. A snow-covered forest area with a few inches of snow will have a gray or mottled appearance and can usually be distinguished from one without snow with its dark appearance. The dendritic pattern seen in mountain regions is due to the lack of snow in the lower elevations in stream and river valleys.

Figure 5-A-1. A band of snow
along 50N merges into a large cloudy
area at C. The smooth texture and
sharp edges of the snow contrast with
the "lumpy" appearance of the clouds.
Dark lines at A and B are the Don and
Volga Rivers, respectively. An area
of snow is seen at D with forests
showing up as darker spots.
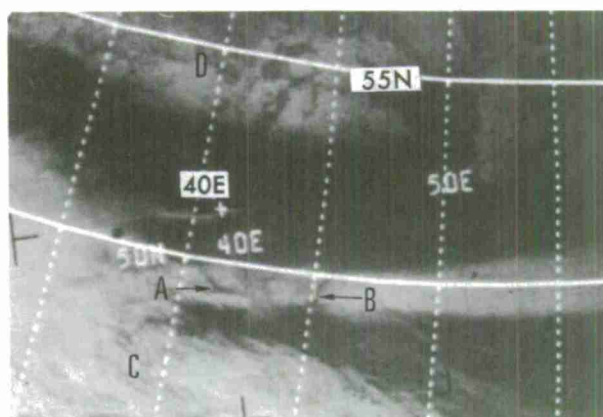


E-3 376-2 1039Z 1 Nov 66

Figure 5-A-2. The band of snow-
covered ground shown in Figure 5-A-1
is easily identified the following
day by its shape. The sharp southern
boundary of the snow field can still
be clearly recognized. On this day
clouds partially cover portions of
the snow band and make it difficult
to positively identify terrain-
produced patterns within the band.
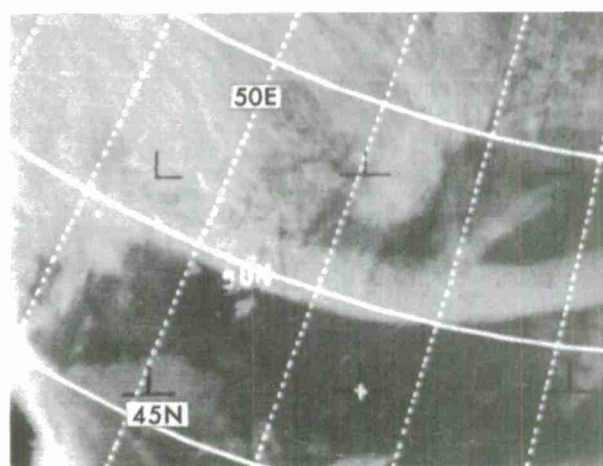


E-3 388-2 0937Z 2 Nov 66

In mountainous regions snow-cover boundaries can often be mapped quite
easily, but the snow depth cannot, as of now, be determined from satellite
pictures [18].  Correct placement of individual river valleys permits accurate
identification of the dendritic pattern observed in mountainous regions.
Snow-line elevation may be discerned over ridges with gradual slopes if de-
tailed topographic maps are used.  The elevation at which the snow ends on
each ridge which has a gradual slope can be plotted as a point on a topograph-
ic map.  These points usually fall close to a given contour line.
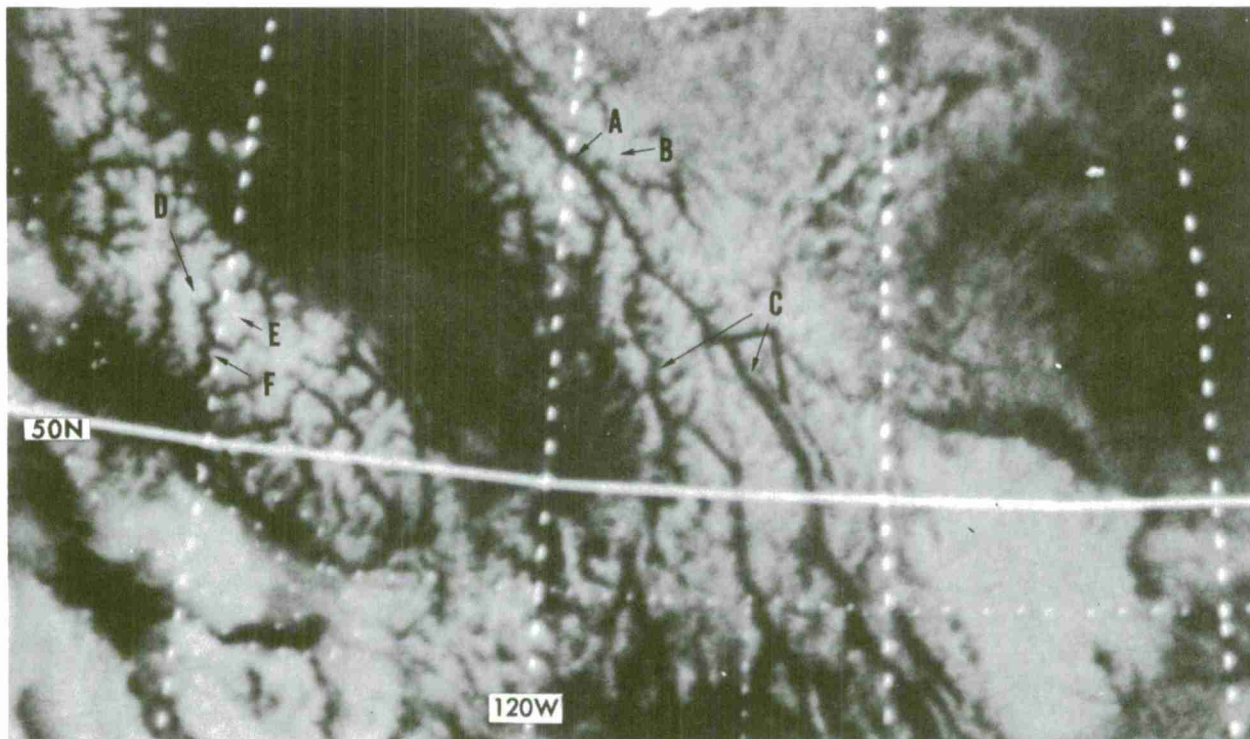


E-3 2680-4 2105Z 3 May 67

Figure 5-A-3.  Two mountain ranges of southwest Canada have a dendritic
snow pattern that permits easy identification of river valleys and individ-
ual mountains.  A, Fraser River; B, Mt. Robson, 12,072 feet; C, east and
west branches of the Columbia River; D, Mt. Waddington, 13,260 feet; E,
Mt. Queen Bess, 10,700 feet; and F, Bute Inlet.  The snow line is very
apparent.  A topographic map could be used to determine which of the ridges
in this picture have a gradual slope.  The point where the snow line ends
could then be related to a particular elevation.

Figure 5-A-4. An APT picture shows snow cover in wooded regions of Newfoundland and Quebec at A. There is a stratus deck west of the snow cover, at B, and higher clouds casting shadows are also seen. The stratus deck can be distinguished from the snow cover by noting that the clouds extend beyond the land to cover part of the Gulf of St. Lawrence, C, and the St. Lawrence River, D to E.
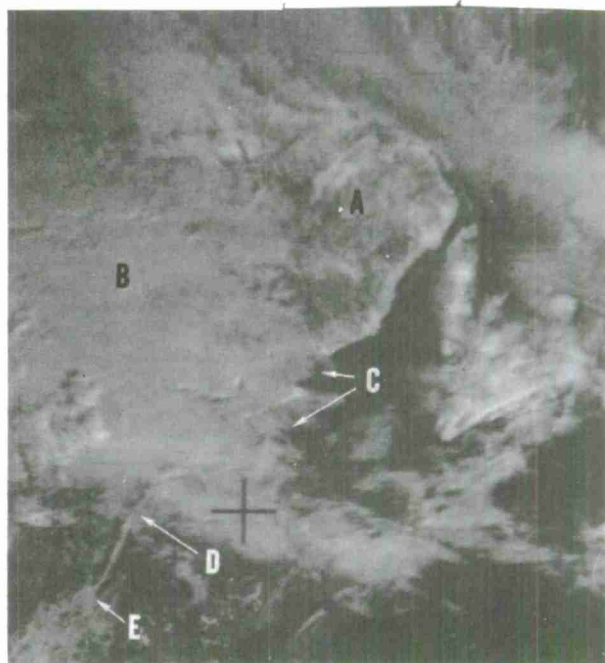
E-8 488-1 1409Z 23 Jan 69



Figure 5-A-5. Snow covers most of the terrain from the Great Lakes northward. The Adirondacks, A, have several inches of snow, but the trees cause the area to appear dark. Variations in gray shades of the snow-covered areas north of the Great Lakes are due to various types of vegetation and ice covered lakes. Scattered cirrus clouds at B cause variations in the brightness of the snow. Note that the geographical boundary lines are displaced considerably relative to the grid and cloud patterns, due to an error by the computer.
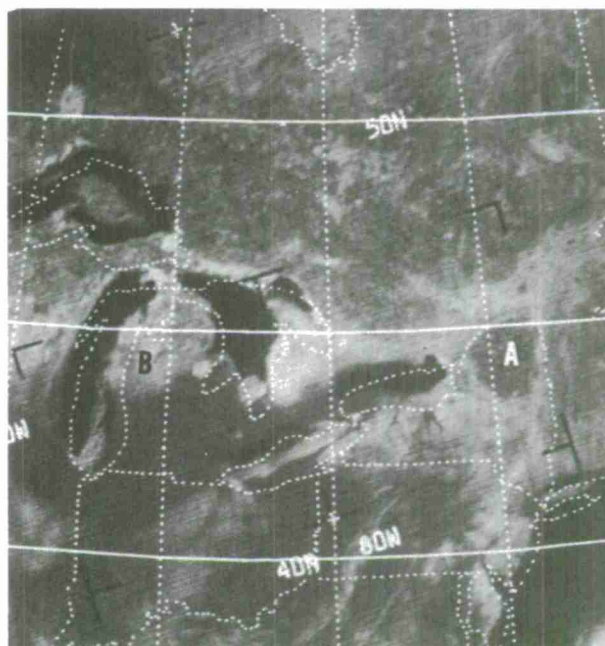
E-7 2508-3 1935Z 4 Mar 69

## Interpretation of Snow Depth

Three shades of gray appear to be the maximum that can normally be dis-
cerned in snow-covered plains-like areas, although more shades may be evident
in particular pictures.  By comparing the three shades of gray with the darker
regions surrounding the snow cover, the following relationships between bright-
ness and snow depth were derived for the non-forested areas in the upper
Mississippi-Missouri Basins:

1.  No snow:  Darkest or black.

2.  Less than 1 inch:  A mottled area of alternating black and gray indi-
cates a trace or an area of noncontinuous snow cover and represents a snow ac-
cumulation of less than 1 inch.

3.  1 to 4 inches:  The area located between the darkest and/or mottled
areas and the brightest shade represents a continuous snow cover with a depth
of 1 to 4 inches.  The boundary between continuous snow cover and the darker
areas represents the one-inch snow line.

4.  Greater than 4 inches:  The outlined edges of the brightest, or white,
areas represent  the four-inch snow line.  This area is usually white, not
just a lighter gray.  The snow cover inside this area corresponds to a depth
of greater than 4 inches.

Figure 5-A-6.  Isolines for the 1-
and 4-inch snow depth were analyzed
using the snow depth mapping proce-
dures described above.  Compare this
analysis with the reported accumula-
tions in Figure 5-A-7.  The isolines
can easily be transferred to a map.
Conventional data may also be used
for a more detailed analysis.
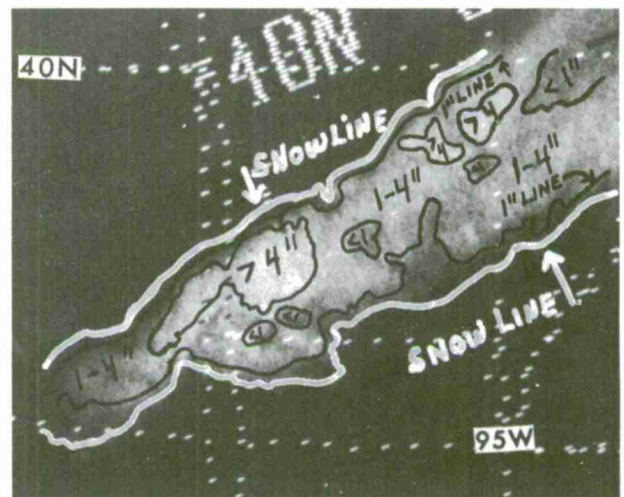


E-3 6635-3 1810Z 13 Mar 68

Figure 5-A-7. Snow was
deposited in this area by a
storm during a 24-hour peri-
od. Snow accumulations from
synoptic reporting stations
are plotted to verify the a-
nalysis shown on the previous
figure. The gray shades re-
late well to the reported
snow depths.
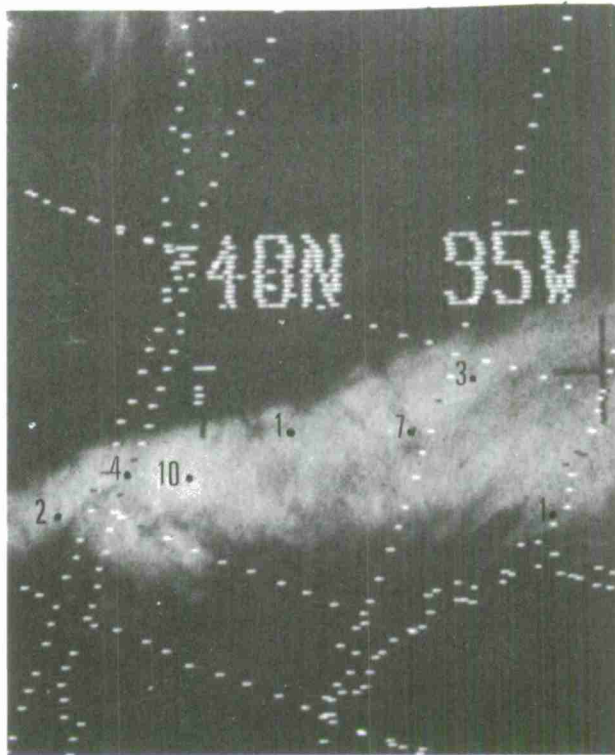
E-3 6635-3 1810Z 13 Mar 68
Data 1200Z 13 Mar 68

Caution should be used when estimating snow depths from gray scale shades
since the relationship between brightness and snow depth in non-forested areas
can be affected by several factors. Some of these factors are:

1. Age of snow: Reflectivity decreases with the age of snow cover.

2. Rainfall: Rain that has fallen on a snow-covered area can reduce its
reflectivity. Rain generally causes melting of the snow which results in a
significant decrease in reflectivity of the snow.

3. Terrain and/or vegetation: The roughness of terrain can influence the
reflectivity of snow cover, particularly for small accumulations. The bright-
ness of snow cover is greatly reduced by high grass, grain stubble, or rough
terrain.

4. Fog, haze, or thin clouds over snow cover: Under these conditions,
even a light covering of snow could appear bright. Snow depth estimates
should not be made in regions where clouds are present.

5. The most important factor affecting the brightness of snow is the
local sun angle. The reflectiveness decreases rapidly when the sun angle is
below 45 degrees.

A Procedure for Snow-Depth Mapping in Non-Forested Areas

The following procedures for snow-depth mapping is suggested:

1.  For snow-depth mapping, APT pictures can be used in their original size.  AVCS pictures should be enlarged to 8 to 12 inches on a side for interpretation of snow cover.

2.  An analysis of snow depth should be made on an acetate overlay before the picture is gridded.  Outline on the acetate the different shades of gray using the established relationships between brightness and snow depth.  Label the 1- and 4-inch isolines.

3.  Accurate gridding is necessary in transferring the snow-cover outline to a base map.  A one-degree grid may have to be drawn over the snow area after the analysis has been made.

4.  Transfer the snow-cover outline to a base map, using the grid as a guide.  Where conventional reports are available, plot them on the base map also.  Additional detail may be gained in the analysis by using conventional reports and estimates of snowfall amount.

Since the relationships reported in this section were derived from a study which dealt with a specific geographical area with certain types of terrain and vegetation, it is suggested that this procedure be used only as a guide.

Chapter 5

Section B

Fog and Stratus

## Introduction

A flat texture, frequently sharp edges, and patterns conforming to topograph-
ical features are the distinguishing characteristics of fog and stratus.
These characteristics make fog and stratus easy to identify when it is not
covered by higher clouds or is not over a snow field. When patches of higher
clouds are present over stratus and fog they cast shadows that give the stra-
tus layer a non-uniform appearance. The shadows are usually large and dis-
tinct because of the large separation between the low stratus tops and the
upper clouds. It is impossible to distinguish fog from stratus in satellite
photographs.

Fog, and to a large extent stratus, is formed by two physical processes: the
air temperature is lowered to the dew-point temperature, or the dew-point
temperature is increased to that of the air temperature. Air mass fogs form
when the temperature falls; frontal fogs form in the presence of precipitation
which raises the dew-point temperature (60).

Radiation fog, a type of air mass fog, is common to many continental areas.
It usually occurs as a thin layer and dissipates after sunrise. Being thin,
it appears gray in satellite pictures. In certain areas, radiation fog can
become relatively thick and persist throughout the day. Thick fog and stratus
such as this has a relatively bright appearance.

## Radiation Fog

Certain areas of the world have high frequencies of fog and stratus. Fog and stratus in these areas often have characteristic shapes caused by local topography; such shapes can be used as an aid in fog and stratus identification.
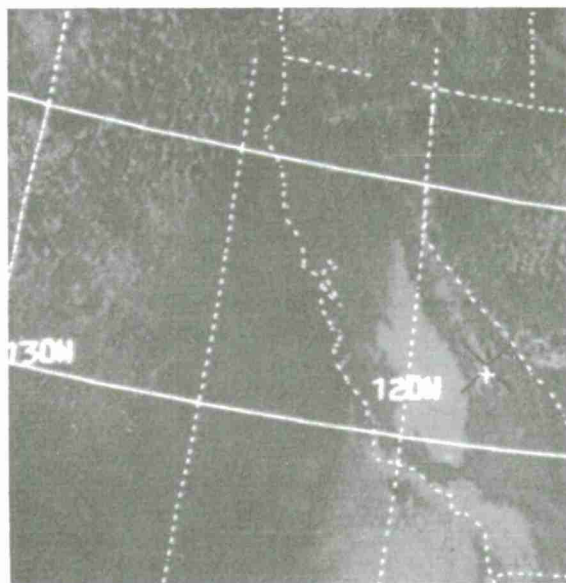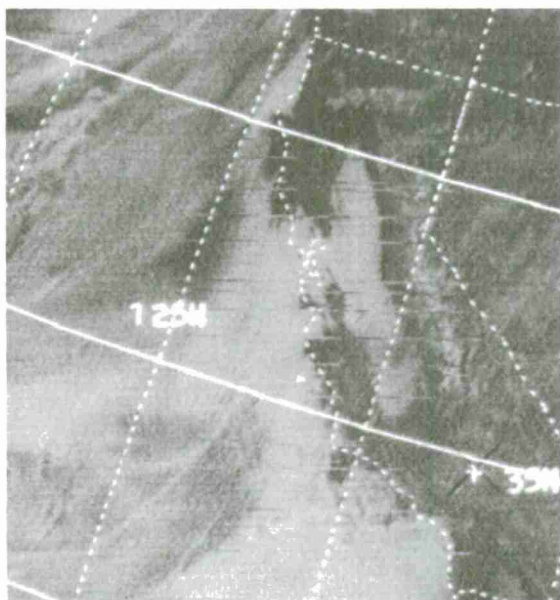


ITOS-1 4684-2 2250 GMT Feb. 1, 1971    ITOS-1 4697-2 2345 GMT  Feb. 2, 1971

Figure 5-B-1. This is an example of radiation fog in the Sacramento-San Joaquin Valley. The strength of the inversion and thickness of the fog layer prevented its dissipation during daytime. This fog formed during the night of January 26 and persisted through February 2. On February 1 the fog covered the entire valley westward through San Francisco Bay. On February 2 a weak cold front moved southward over the region breaking the inversion and clearing the fog in the northern part of the valley. The stratus and stratocumulus also dissipated along the coast north of the cold front.

Figure 5-B-2. This photograph shows
an extensive area of radiation fog (A)
over Europe north of the Alps. The
southern boundary of the fog is along
the foothills of the Alps and the
northern boundary is along the higher
terrain of southern Germany and west-
ern Czechoslovakia. The jagged edge
of the southern boundary is the result
of fog extending into the many valleys
on the northern slope of the Alps.
Other areas of radiation fog are visi-
ble at B and C.
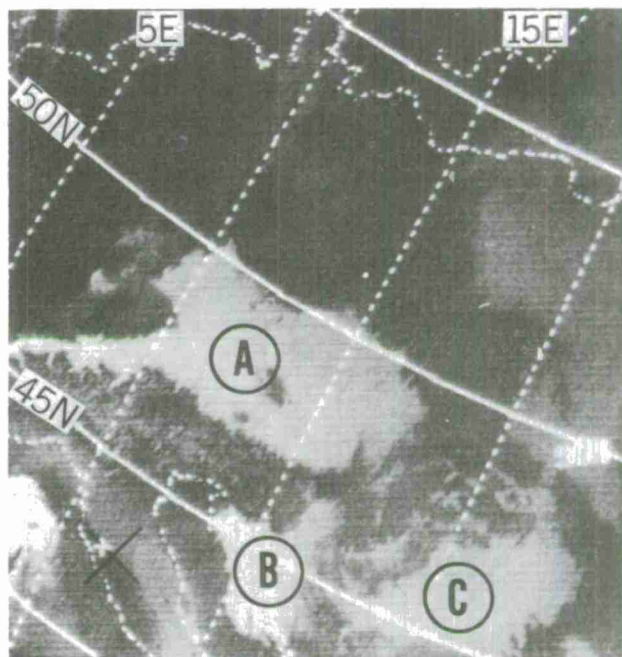


ITOS-1 3828-1 1245 GMT  Nov. 25, 1970

Figure 5-B-3. This is an example of
fog in the Po Valley of northern Italy
(A). It is most common during late
fall and winter. The eastern end of
the valley opens into the Adriatic
Sea. The low level winds were east
or southeast and moist air from the
Adriatic was being advected into the
valley. Radiational cooling occurred
and fog formed. The fog conforms to
the shape of the valley. The fog-
filled smaller valleys of the Alps
and Apennine Mountains gives most of
the perimeter a jagged edge.
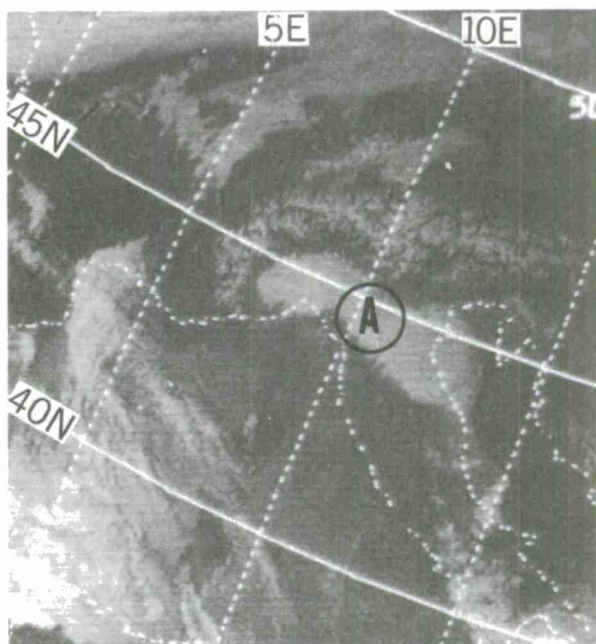


ITOS-1 3966-1 1330 GMT  Dec. 6, 1970

Other Fog Types
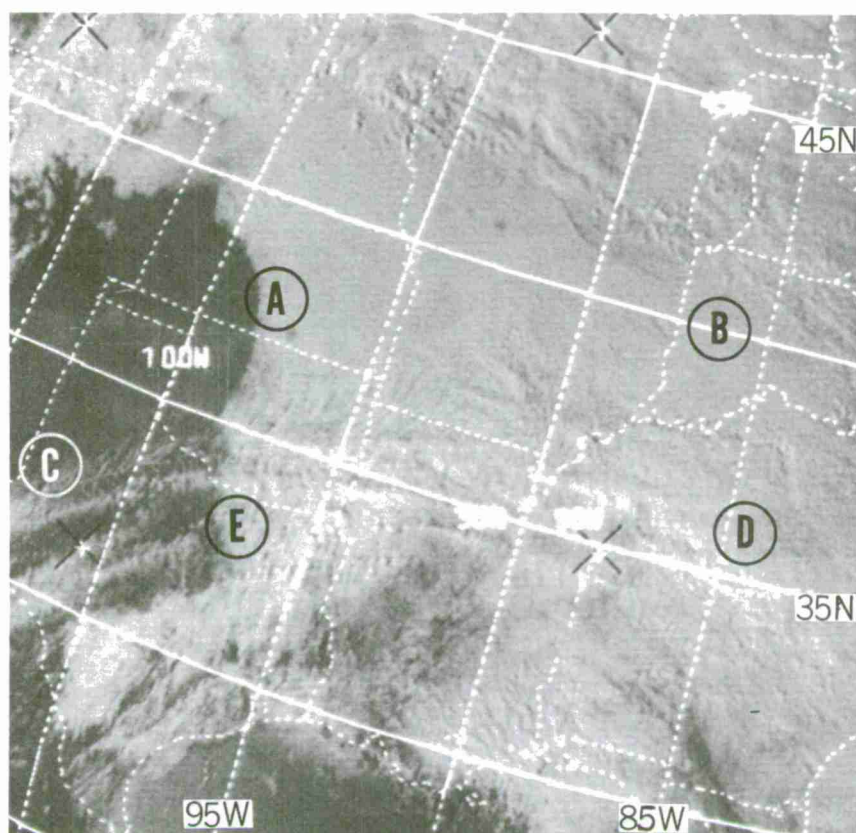


ITOS-1  4708-2  2050 GMT  February 3, 1971

Figure 5-B-4.  A combination of advection, radiation, and upslope cooling pro-
duced this extensive fog and stratus layer over the central United States.
Ship observations in the northwest Gulf of Mexico indicate Fahrenheit water
temperatures in the low 70's and air temperatures in the mid-70's.  The dew-
point depression was five to eight degrees.  When this warm, moist air was
advected northward, cooled, and lifted, fog and stratus formed.  From A to B
the clouds have the characteristic flat texture of fog and stratus seen in
satellite photographs.  The sharp edge (A) is another typical characteristic.
Further south, the fog and stratus lies under cirrus associated with the sub-
tropical jet stream (C to D).  The shadows from the cirrus give this area an
uneven appearance.  The sharp western edge of the fog and stratus (E) can be
seen through the jet stream clouds.

Figure 5-B-5. Fog and stratus covers the Sea of Okhotsk and the Pacific Ocean south and southeast of the Kamchatka Peninsula. The fog and stratus over the open water (A to B) has a characteristic sharp edge. It also terminates abruptly along the coastline on the western side of Kamchatka. The clouds extending inland across the coastline (C) are cirrus from a cluster of thunderstorms at D. The smooth, gray, somewhat mottled appearance of the formation is typical of summertime oceanic fogs. This fog and stratus formed as warmer air from Asia drifted over the water and was cooled from below.
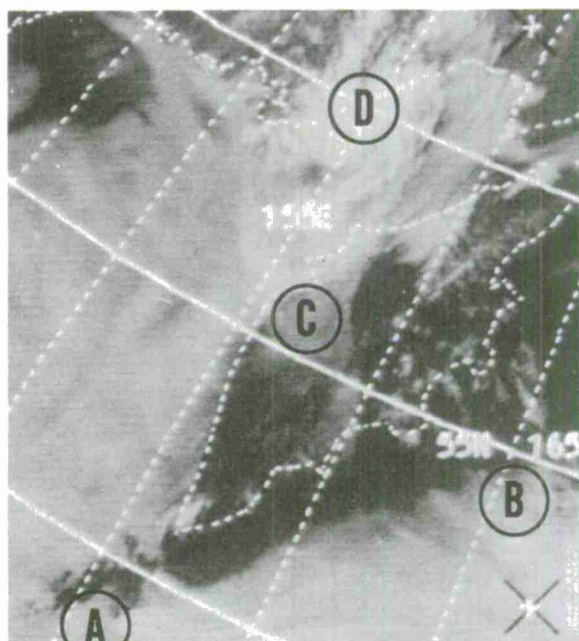


ITOS-1 2059-3 0259 GMT July 7, 1970

Figure 5-B-6. This stratus over the western Gulf of Mexico terminates abruptly along the foothills of eastern Mexico. The stratus deck has a flat texture except where some cirrus (A) casts shadows on the lower clouds.
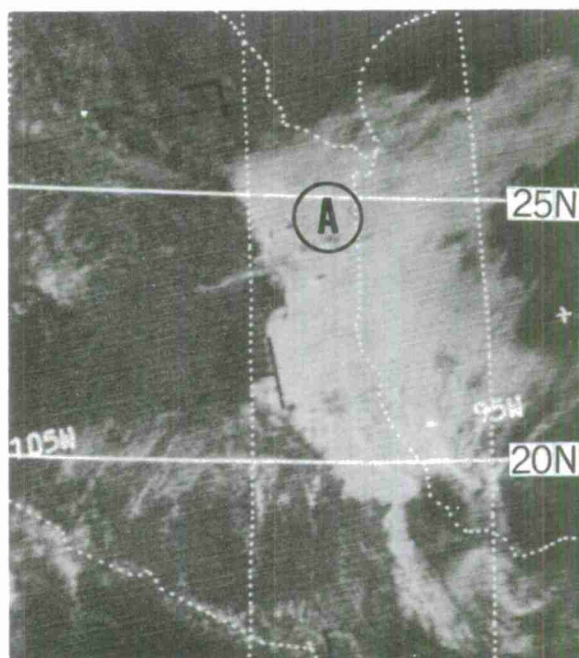


E-7 1307-4 2138 GMT November 28, 1968
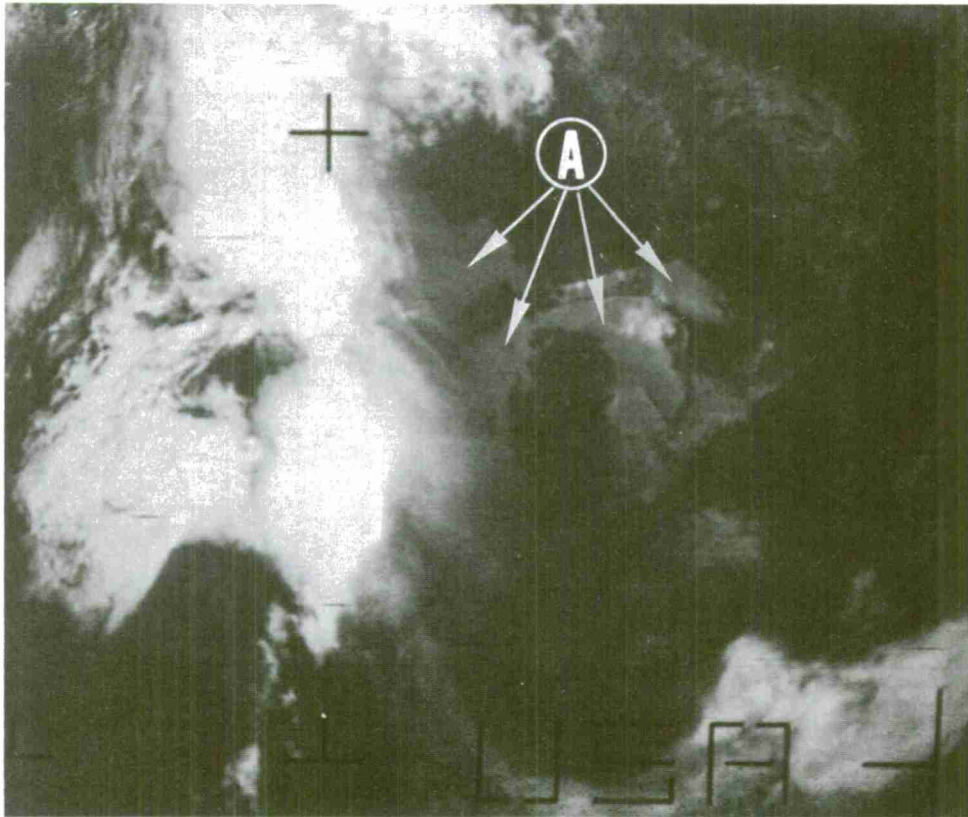
E-8   1178-8   1635 GMT   July 12, 1971

Figure 5-B-7. The light gray area (A) has a smooth texture, terminates abrupt-
ly along a coastline, and contrasts with the surrounding land. This strongly
suggests a fog bank over the water. Actually, the light gray area is a sun-
glint on parts of the Great Lakes. (See p. 2-27, figure 2-46, this report.)
The following techniques can be used as a guide for the detection and approxi-
mate location of the sun-glint. The sun-glint is to the right (east) of the
center fiducial mark for morning satellite pictures and to the left (west) of
the center fiducial for afternoon satellites. The sun-glint appears to move
northward on successive frames on a southbound polar-orbiting satellite
(ESSA-8). The inverse relationship is valid for northbound satellites (ESSA-9)
with the sun-glint appearing to move southward on successive frames. The sun-
glints will be at different latitudes from day to day.

Pictures from geostationary satellites have sun-glints that progress westward
with the sun and are at a constant latitude throughout the day. The latitude
of the sun-glint follows the sun as the seasons change.

Chapter 5

Section C

Turbulence


## Introduction

The presence of turbulence can often be assessed from distinctive cloud forms
which appear in satellite imagery. Lenticular cloud formations and wave
cloud patterns reveal areas of orographically induced turbulence, jet stream
cirrus locates regions of turbulence induced by strong horizontal shear in
the upper troposphere, and convective cloud forms indicate the strength and
relative depth of turbulent convection. Turbulence also occurs in certain
areas of fronts, vortices, and vorticity maxima. Cloud imagery can be used
to precisely locate these features and the general regions where turbulence
is probable. Sometimes it is possible to assign specific turbulence intensi-
ties based on the appearance of the satellite observed cloud forms (5, 61,
62, 63, 64). It is important to remember that it is impossible to identify
turbulent areas where there are no clouds or where the turbulent cloud forms
are obscured by higher clouds.

The illustrations in this section are limited geographically because they were
obtained from areas where a high density of aircraft reports was available.
They show typical turbulence distributions in the vicinity of the cloud forms
discussed. Turbulence reports plotted on the photographs are within six
hours of picture time. The symbol ⋀ indicates severe turbulence, ⋀ indi-
cates moderate turbulence, and ∧ represents light turbulence. Heights of
reported turbulence are shown in hundreds of feet.

## Mountain Waves

Mountain wave turbulence occurs downwind of mountains. The turbulent energy
is dissipated downstream. The most severe turbulence is close to the moun-
tains; lesser degrees of turbulence occur further downstream. Mountain wave
turbulence is generally confined to altitudes below 20,000 feet. The wave
clouds seen on satellite photographs are usually low or middle level clouds.
Concurrent higher level turbulence, i.e., above 30,000 feet, usually can be
attributed to a jet stream above the wave clouds. The intermediate levels
between 20,000 and 30,000 feet have a minimum of turbulence (64, 65, 66).
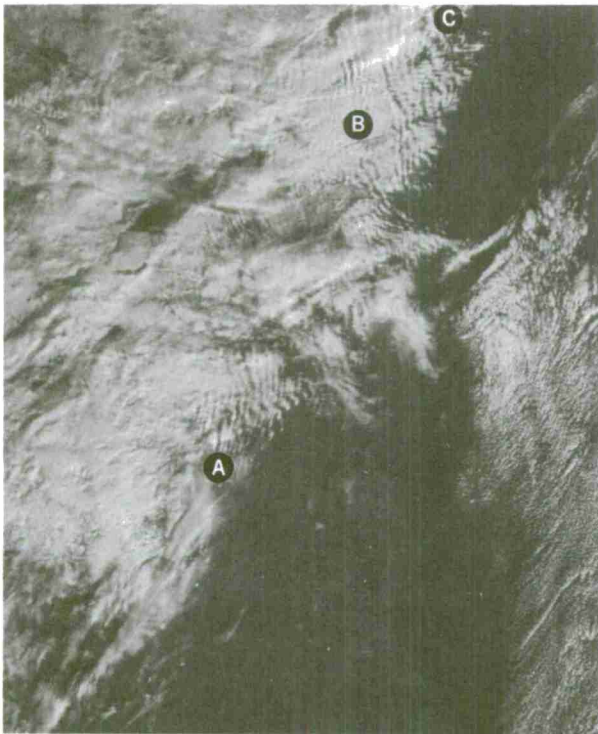


Figure 5-C-1a. NOAA-2 VHRR Visible        Figure 5-C-1b. NOAA-2 VHRR Daytime
537-2 November 27, 1972                   IR 537-2 November 27, 1972
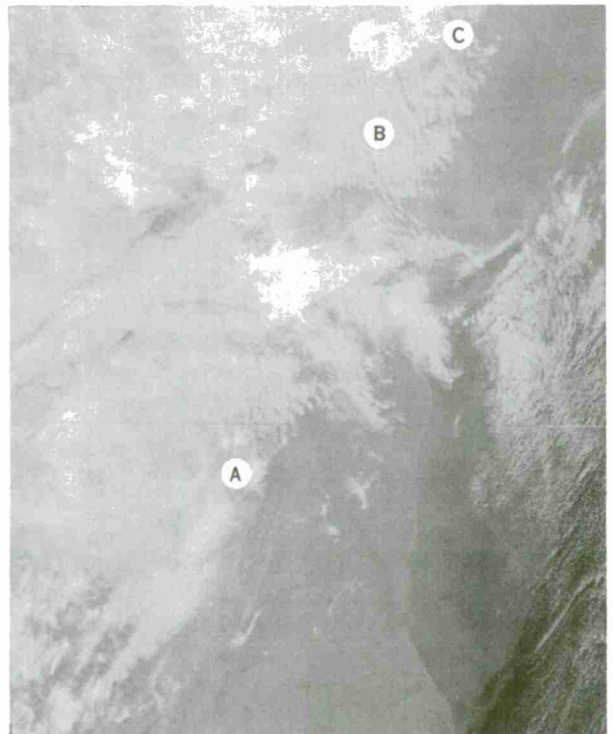
Figures 5-C-1a and b. This example of mountain wave clouds is a simultaneous
view of the clouds in the visible and infrared spectra. The mountain wave
clouds exist over and to the east of the Appalachian Mountain range from
Virginia, at A, and northward across the New England States to C. Resolution
of these two Very High Resolution Radiometer (VHRR) photographs is about one
nautical mile. At B, the interval between successive wave cloud elements is
small and the cloud elements merge forming a solid deck of clouds. However,
the wave crests are still distinguishable in this high resolution imagery.
On lower resolution imagery the wave clouds in this area would not be discern-
ible. When wave clouds are discernible, areas of high turbulence risk asso-
ciated with the wave action can be isolated, by using the empirical rule that
the turbulence is most severe close to the mountains and is less severe down-
wind. In this case, only light turbulence was reported above 25,000 feet.
The position of the polar jet stream is off the East Coast. The severity of
the mountain wave turbulence throughout the area was not reported.

## Jet Streams

Except where cumulonimbus clouds are present, most turbulence of moderate or greater intensity that occurs above 30,000 feet is associated with jet streams in which strong horizontal or vertical shear is present (61, 62, 63, 64). Cirrus is often present equatorward of the jet axis on the western side of and across the top of the upper air ridges, thus permitting identification of this portion of the jet stream in satellite imagery. Turbulence occurs on both sides of the sharp edge of the cirrus shield or its associated shadow line and is generally confined to within three degrees latitude of the jet axis.

There is a higher probability of turbulence of moderate or greater intensity with dense overcast jet stream cirrus than with thin, broken, or scattered cirrus. Scattered cirrus, when seen on satellite photographs, is generally associated with light turbulence or non-turbulent conditions. Moderate turbulence is generally encountered in the top two thirds of a heavy cirrus overcast associated with a polar jet stream. The greatest probability of moderate or greater turbulence is associated with the lower two thirds of the dense overcast cirrus layer of subtropical jet streams. Light turbulence is generally found in the lower third of polar jet stream cirrus and in the upper third of subtropical jet stream cirrus (61). A higher risk of severe or extreme turbulence exists when transverse bands or cloud trails are observed near the jet than when they are not present (5, 61).
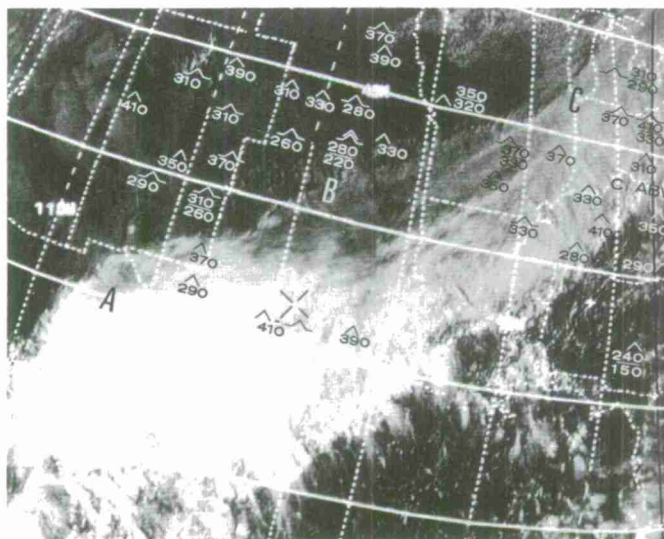


ITOS-1 3082-4 2130 GMT September 26, 1970

Figure 5-C-2. A large area of light to moderate and occasionally severe turbulence is associated with this jet stream over the central United States. This jet stream originates in the subtropics southwest of Baja California and reaches a maximum velocity of more than 100 knots over Oklahoma and to the northeast. The jet stream is located in the clear air just to the north of points A, B, and C at 200 mb. The cirrus at A and the cirrus spissatus at B originated in the subtropics and was advected northward where it merged in the main belt of hemispheric westerlies. In this case the turbulence was generally above 30,000 feet on both sides of the jet stream.
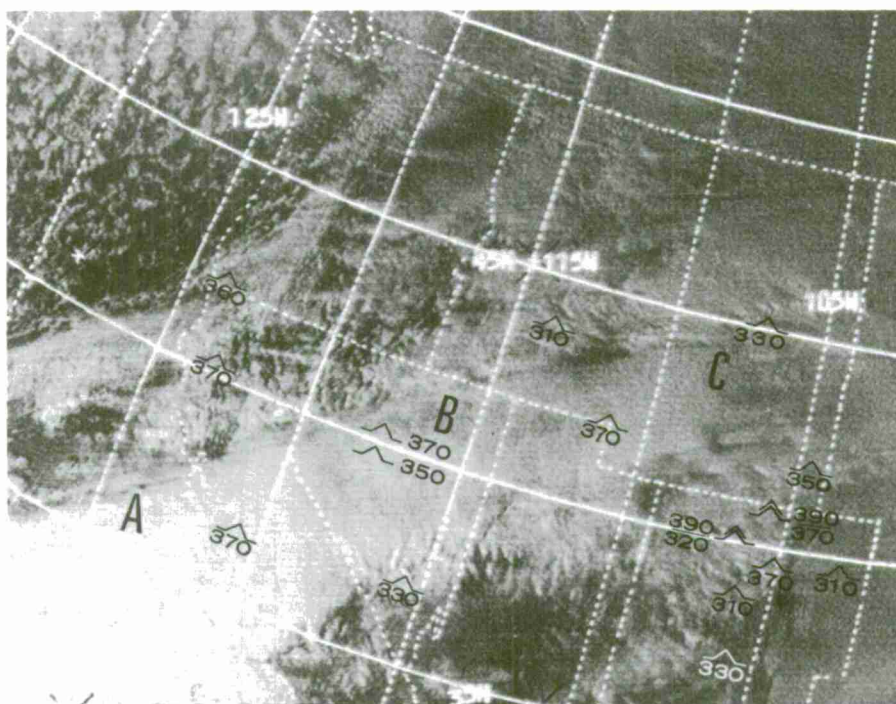
ITOS-1 3833-2 2215 GMT November 25, 1971

Figure 5-C-3. This outbreak of moderate to occasionally severe turbulence over the western United States, generally above 30,000 feet, is associated with an anticyclonically curved jet (A, B, C). A continuous shadow (B, C) appears on the lower clouds north of the jet stream cirrus. Numerous reports of light turbulence (not plotted) also were reported in the region of the jet stream. In this case, the westerlies first split over the central Pacific then merged again just west of California. Cirrus from the tropics was advected northeastward in the southern branch of the westerlies to the merge point, and then eastward over the United States. Wind speeds at 200 mb were generally in excess of 120 knots from California to North Dakota.


## Convection

Convective clouds seen on satellite photographs identify turbulent areas. Cumulus and towering cumulus clouds have a typical lumpy, uneven texture and indicate the presence of light to moderate turbulence. Cumulonimbus clouds appearing either as individual cells or in clusters indicate the presence of moderate or severe turbulence. The turbulence associated with cumulonimbus clouds is not restricted to the clouds themselves, but also can occur in the clear air immediately surrounding the clouds. Significant turbulence also can occur up to 5,000 feet above developing cumulonimbus clouds (61, 64). The specific intensity of turbulence encountered by an aircraft around convective cells will vary depending on the exact location of the aircraft relative to the cloud and on the stage of development of the cloud.

The open cellular cumulus pattern frequently observed to the rear of polar fronts indicates the presence of turbulence at the low and middle levels.

5-C-4

As the open cells develop vertically, and take on a larger and brighter appearance, the probability of encountering more intense turbulence increases.

Figure 5-C-4. Turbulence occurs in and around convective clouds. Here, the large area of thunderstorms over the Rocky Mountains had tops near 40,000 feet. Two reports of moderate turbulence at 41,000 feet indicate that significant turbulence extends to at least 1,000 feet above these thunderstorms.
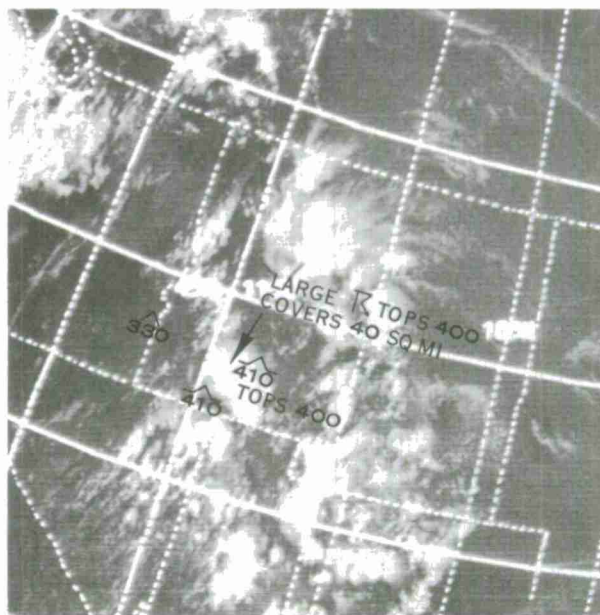


ITOS-1 2757-3 2200 GMT August 31, 1970

Figure 5-C-5. Moderate to severe turbulence occurred between 19,000 and 25,000 feet in association with the intense convective activity of Tropical Storm FELICE along the Gulf Coast. Other areas of high turbulence risk associated with convection probably occurred with the thunderstorms visible over the eastern Gulf of Mexico and Florida.
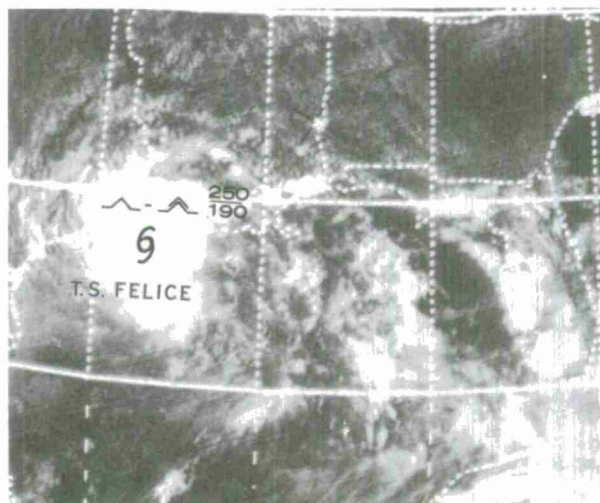


ITOS-1 2944-4 2100 GMT September 15, 1970

Figure 5-C-6. At the time of this picture, moderate to severe low level turbulence was reported in the vicinity of open cellular clouds. Clouds of this type form in a strong cyclonically curved wind flow to the rear of a cold front when sufficient moisture is available. This unstable air is a favored region for turbulence; the presence of open cellular clouds is useful for outlining the region of high turbulence risk.
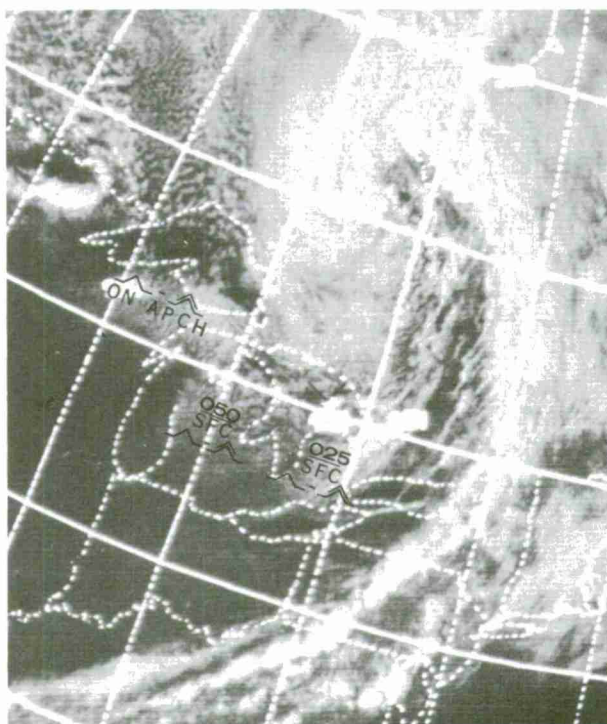


ITOS-1 2881-3 2000 GMT September 10, 1970

Other Turbulent Regions

Turbulence also is associated with fronts, developing frontal waves, and positive vorticity advection (PVA) maxima. These features have distinctive, recognizable cloud forms which make possible identification and isolation of areas where turbulence is most probable. Turbulence is most likely when the thermal gradients associated with these synoptic features are becoming stronger with time.

The entire frontal cloud band should be considered as an area of high turbulence probability, especially in areas where imbedded convective activity appears. A developing frontal wave and its associated jet stream contains areas of strong horizontal temperature gradient and strong vertical wind shear. Frequently there is a large area of significant turbulence extending through a thick atmospheric layer. In this synoptic situation, the turbulence below 20,000 feet usually is associated with the frontal clouds and the higher level turbulence is related to the jet stream (5, 63, 64).

PVA maxima, seen in satellite photographs as areas of enhanced cumulus or comma-shaped cloud patterns in the cold air behind the polar front, are associated with mid-tropospheric short-wave patterns and are areas of probable turbulence. The favored area for turbulence is the northeast quadrant of PVA maxima.
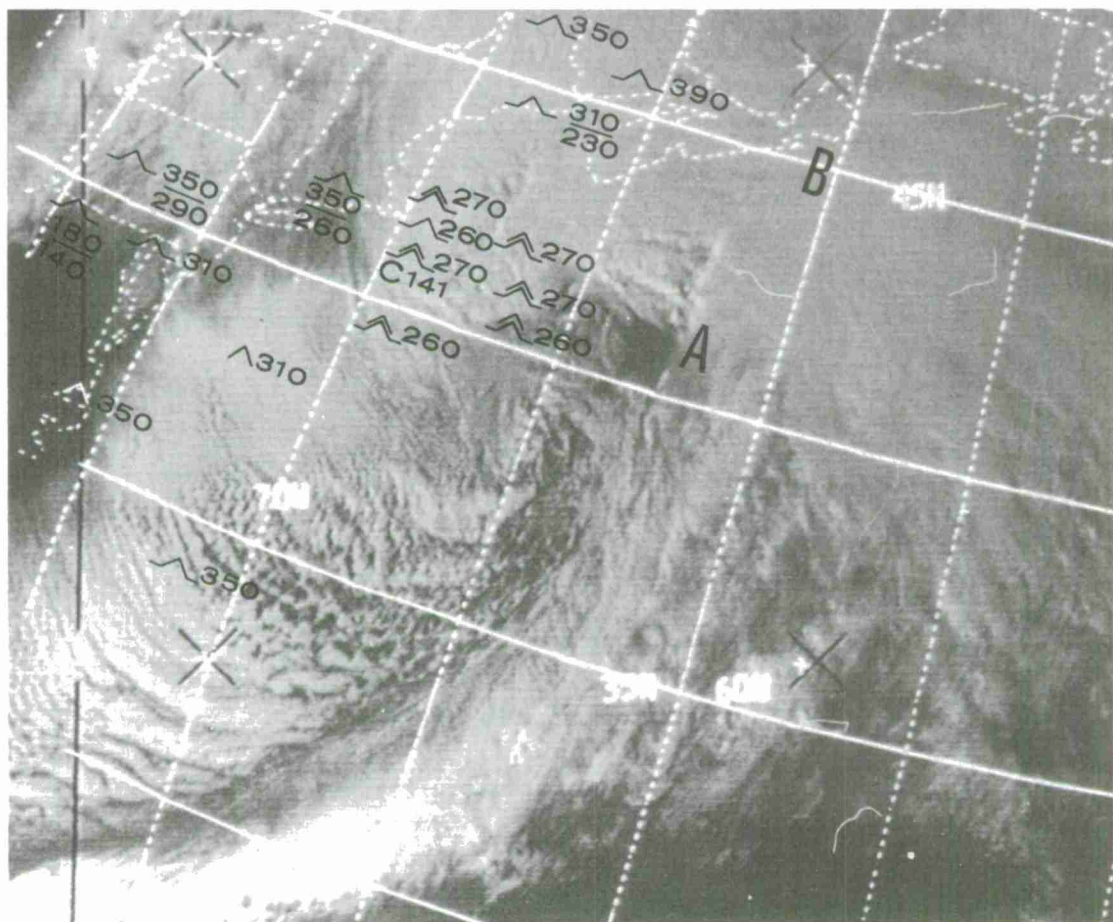
ITOS-1 4219-2 1900 GMT December 26, 1970

Figure 5-C-7. This figure and figure 5-C-8 illustrate the turbulence associ-
ated with two major East Coast storms. The December 26 storm (above) is
fully occluded (1800 GMT, central pressure 957 mb) and the December 31 storm
(figure 5-C-8) is still an open wave (1800 GMT, central pressure 998 mb).
Most of the severe turbulence with the above storm was reported to be between
26,000 and 27,000 feet, to the north and somewhat to the west of the surface
low center, and to the west, or poleward of the anticyclonically curved jet
stream cirrus (A to B). Light and moderate turbulence extended many hundreds
of miles through a deep layer of the atmosphere along the East Coast--a direct
result of the thermal and wind shear patterns associated with this major storm.
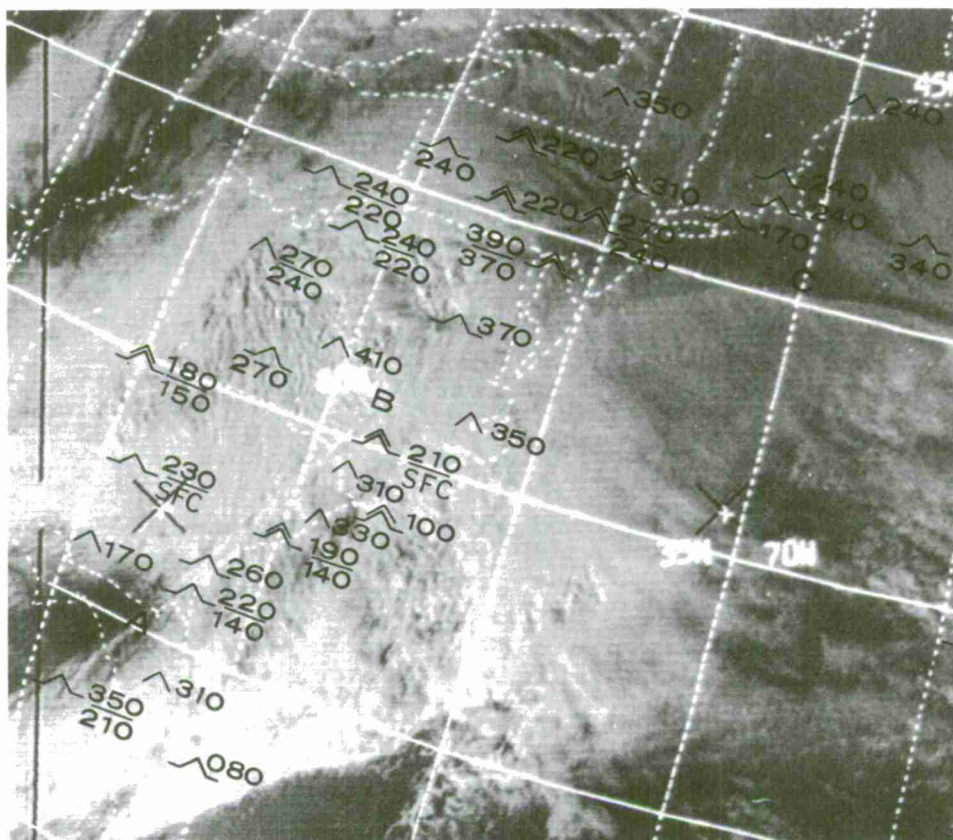
ITOS-1 4282-2 1900 GMT December 31, 1970

Figure 5-C-8. There were numerous reports of moderate and severe turbulence with this major storm in the high air traffic areas of the East Coast. As in the December 26 storm, most of the turbulence was reported poleward of the jet stream (A, B, C). Again the turbulence extended through a deep layer of the atmosphere from the surface to well above 30,000 feet.

This storm and the one in figure 5-C-7 illustrate how one can associate turbulent areas with particular cloud patterns. By using satellite pictures to locate major storms, one can infer wind shears and thermal patterns favorable for the production of significant turbulence and can identify turbulent areas not only in data-rich areas, but also in data-sparse areas.

Chapter 5


Section D


Mesoscale and Subsynoptic Scale Vortices


Introduction

Frequently, small-scale spirallike cloud patterns appear in satellite photo-
graphs. These patterns may exist at any cloud level. This section will dis-
cuss those occurring in the lower cloud layers, primarily because they are
observed most frequently. These small-scale spirallike cloud patterns range
in size from the mesoscale (10 to 100 n.mi.) eddies, which occur downwind
from island barriers, to the subsynoptic scale (100 to 300 n.mi.) spiral
patterns which occur in stratocumulus clouds adjacent to coastlines. Small
vortices or eddies also are observed within the large areas of fog that occur
under oceanic highs, as well as in cumulus fields of polar air masses.

As with the study of many mesoscale cloud patterns, the observation and in-
vestigation of subsynoptic scale vortices was facilitated by the advent of
satellite photographs. The detection of small-scale vortices by means of
conventional synoptic data is extremely difficult because vortices of this
size are too small to show up in the "wide mesh" standard weather-observation
network, and normally are too large to be recognized by ground observers (67).
As operational satellite imagery with a resolution of one mile or less becomes
available, it will be possible to detect local scale eddies (1 to 10 n.mi.).

Subsynoptic and mesoscale vortices should not be confused with those of a
larger scale since they are generally formed by different mechanisms and do
not represent a potential for development. Small-scale vortices can affect
the local cloud distribution when they occur in areas of local, short-range
forecast interest. These patterns also give insight into the wind field in
data-sparse regions.

## Mesoscale Vortices in Stratocumulus

Mesoscale eddies occur most often in the stratocumulus field on the eastern side of a subtropical high downwind from mountainous islands. These eddies are most often seen in the satellite photographs downwind from the Canary Islands, the Cape Verde Islands, Madeira Island, and Guadalupe Island. The conditions necessary for development of these eddies are a strong low-level inversion which caps the stratocumulus field, an island barrier that pierces the inversion, and a persistent low-level wind flow in the 10- to 25-knot range. If the wind speed exceeds 25 knots, the eddy pattern will tend to break down, and, if the wind speeds are less than 10 knots, the eddies usually will not form. Ideally, mesoscale vortices are shed from alternating sides of an island, one spiraling to the right, the other to the left. After forming, the eddies move downwind with the surrounding air flow. The eddies will persist until the flow pattern or the inversion changes, or until the region of influence of one eddy overlaps and counteracts the motion of a neighboring eddy of an opposite circulation (67).



BAJA
CALIFORNIA

Figure 5-D-1. A Gemini XII picture of mesoscale eddies that developed downwind of Guadalupe Island (point A). The eddies formed in the dense stratocumulus cloud deck that dominated the eastern side of the subtropical high. Note the detail of the eddies visible from this low altitude (153 mi.) photograph.

Gemini XII Orbit 30 Frame 108 November 13, 1966
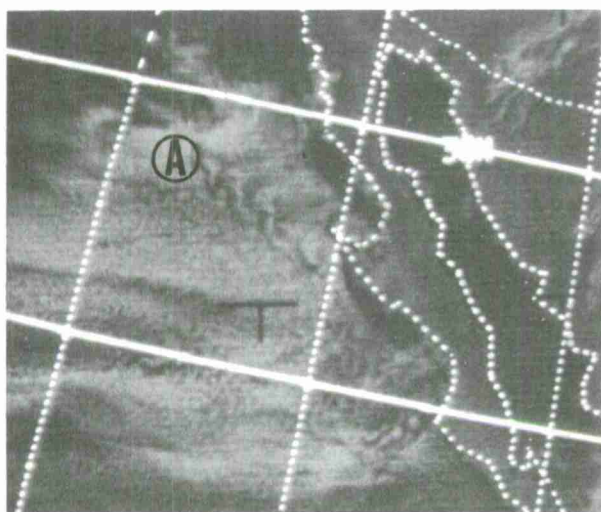
Figure 5-D-2. An eddy pattern extending 200 miles downwind from Guadalupe Island (A), viewed from an altitude of 900 miles. In this example the eddies are embedded in the strato-cumulus cloud deck associated with the subtropical high off the west coast of the United States. The eddies extend southeastward from the island, indicating a persistent north-west low level wind flow.

ESSA-9 2842-5 2149 GMT October 11, 1969
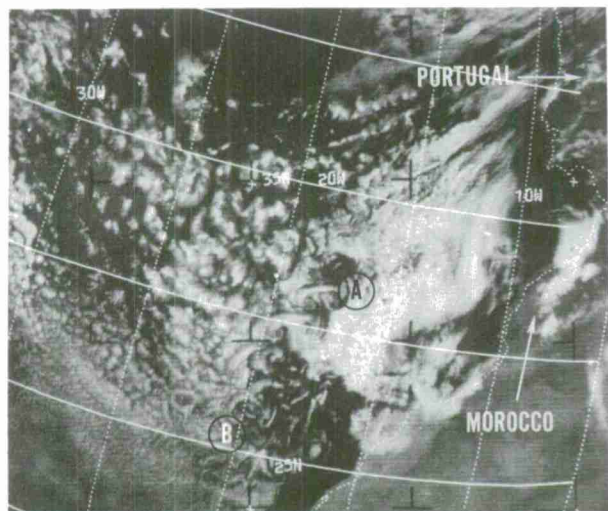


Figure 5-D-3. An eddy pattern extends downwind from Madeira Island (point A). The eddies extend approximately 400 miles to point B, indicating that the synoptic situation of the area has remained stable for at least 24 hours. These eddies formed in the stratocumulus cloud deck on the east-ern side of the subtropical high in the western North Atlantic.

ESSA-9 1627-5 1522 GMT July 6, 1969

Mesoscale Vortices in Cumulus Clouds

Mesoscale spirallike cloud patterns are frequently observed in the cumulus cloud field poleward of polar fronts east and southeast of the Kamchatka Peninsula, the Kuril Islands, Japan, and Greenland. These patterns can vary in size from mesoscale to synoptic scale and form in the cyclonic flow associated with a surface or low level vortex or trough. The primary cause of these patterns is horizontal shear in the low levels that results in cyclonic twisting of the cloud pattern. In addition, the patterns seem to occur when the atmosphere aloft is extremely cold and the winds are light. The vortices may or may not be located downwind of a land barrier.
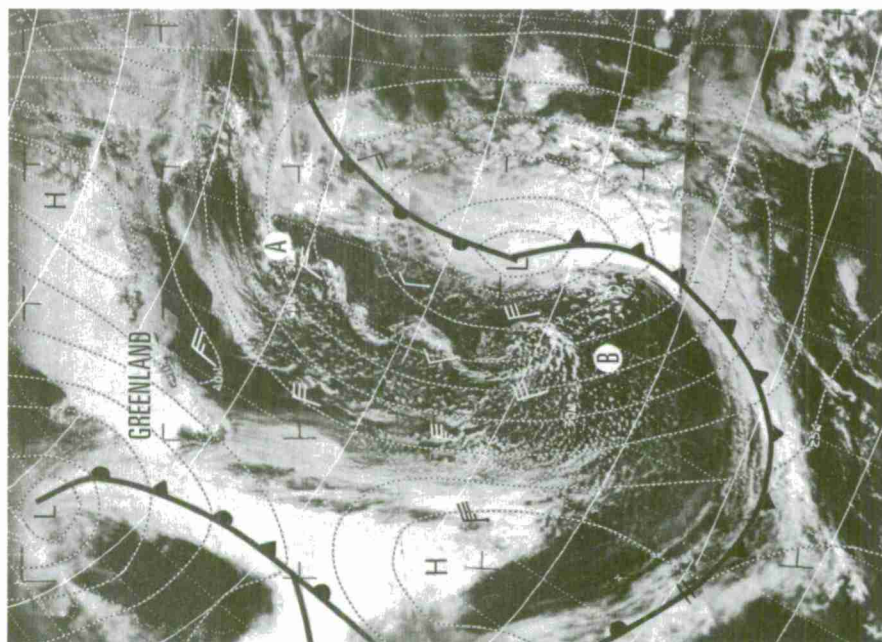
Figure 5-D-4a. ESSA-9 1352-3,4 June 14, 1969.
Surface Analysis 1200 GMT June 14, 1969.
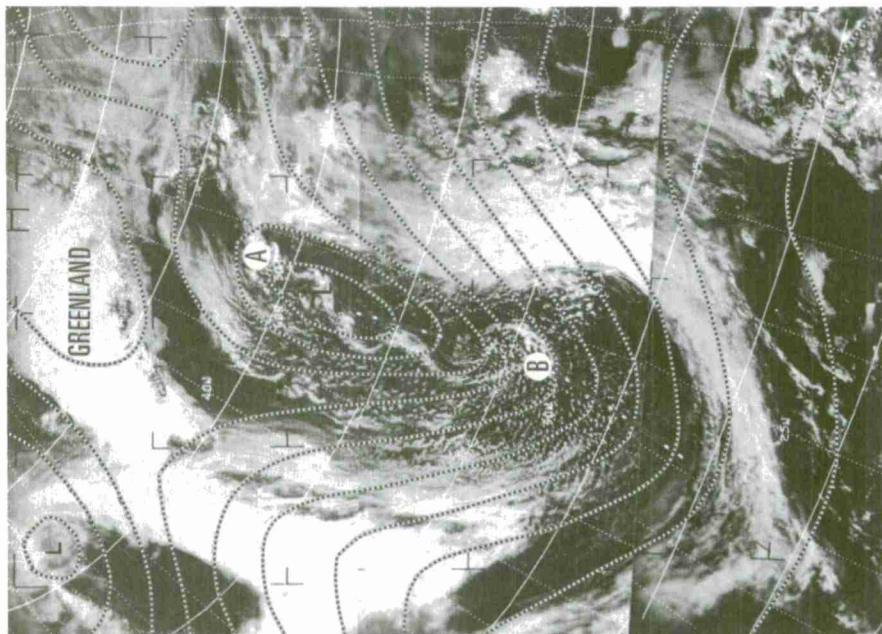
Figure 5-D-4b. ESSA-9 1352-3,4 1350 GMT
June 14, 1969. 500-mb Analysis 1200 GMT June
14, 1969.

Figures 5-D-4a and b show an example of a mesoscale spirallike cloud pattern southeast of Greenland (A
to B). The pattern in this situation was caused by the cyclonic shear in the low-level wind field and
is reflected in the cumulus cloud field. The pattern also lies along or just to the west of a high am-
plitude mid-tropospheric trough line. The surface winds shown in figure 5-D-4a are for 1200 GMT on
June 14, 1969.

## Mesoscale Vortices in Fog

Mesoscale vortices or eddies are observed frequently in the fog or stratus
areas associated with stationary or quasi-stationary oceanic highs. In gen-
eral, the winds are light at the surface and at the low levels in the region
where the eddies form. Even though the winds are light, there is sufficient
horizontal shear in the wind field to create the eddy pattern. Such hori-
zontal shear may or may not be due to a land barrier.
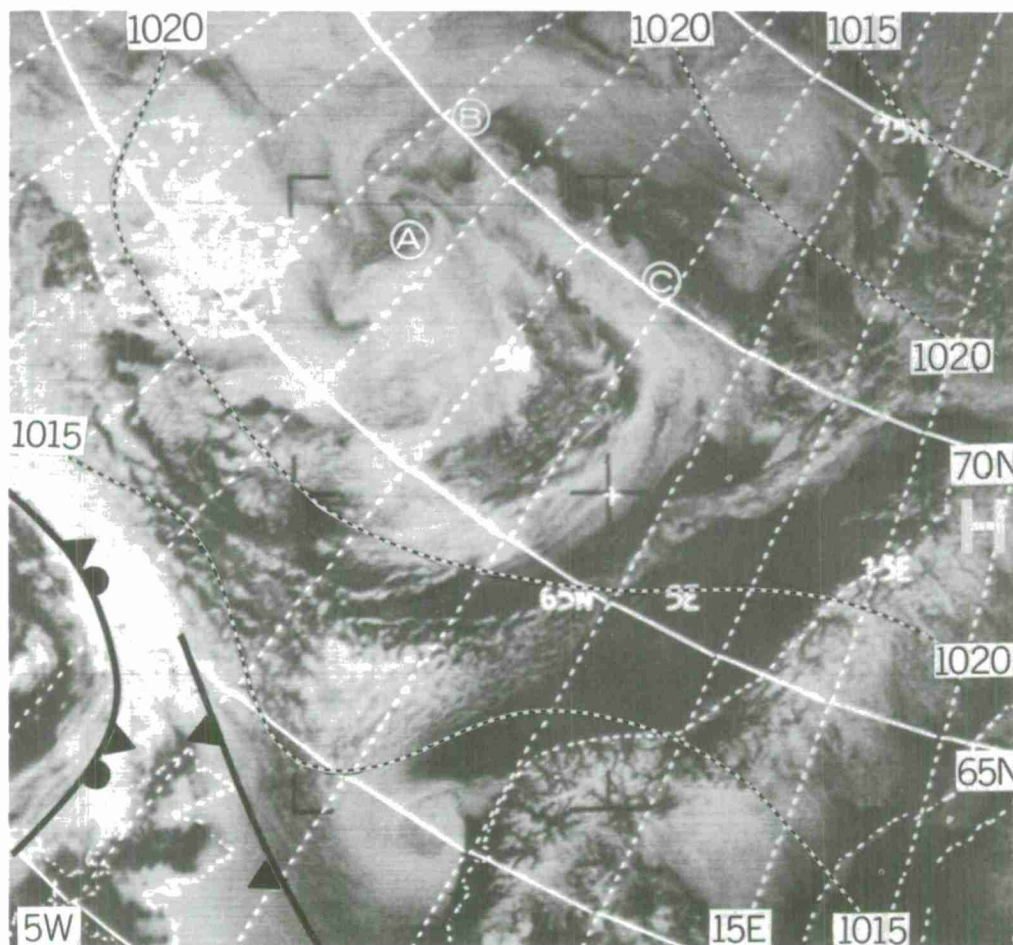


ESSA-9 5535-2  1226 GMT  May 15, 1970
Surface Analysis 0700 GMT May 15, 1970 Berlin Weather Chart

_igure 5-D-5. In this photograph, at A, B, and C, are examples of mesoscale
vortices or eddies that appear in fog and stratus areas associated with sta-
tionary or quasi-stationary oceanic highs. The area is dominated by a quasi-
stationary high pressure cell with the main center over Greenland. Fog and
stratus is the predominant cloud type in the region of the eddies. The
surface analysis shows the very flat pressure-gradient across the region on
May 15, 1970; thus, light surface winds can be inferred. The eddies exist
in this area of light winds. The eddies from B to C have formed along or just
equatorward of the shear zone associated with the surface ridge line.

## Subsynoptic Scale Vortices

Subsynoptic scale vortices form, as do other types of eddies, as a result of horizontal shear in the surface or low-level wind field. This shear can be induced on the wind field dynamically or orographically. Subsynoptic scale vortices or eddies usually are seen in the cumulus cloud field poleward of a polar front, or in stratocumulus clouds adjacent to coastlines.
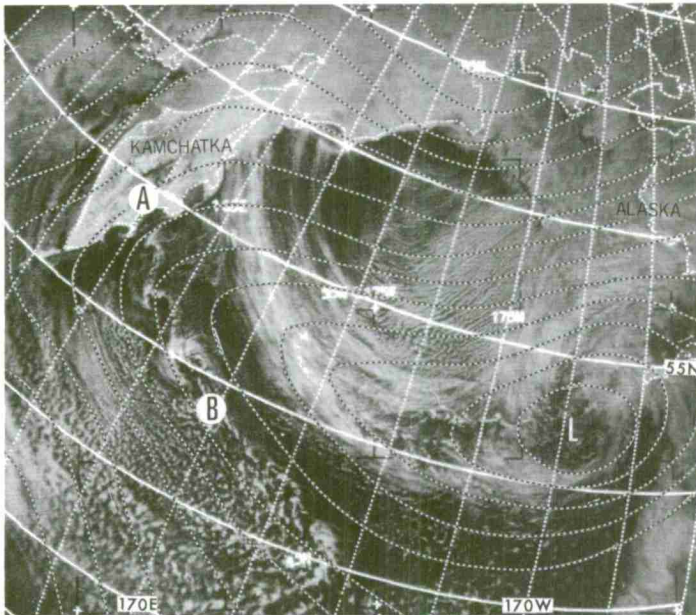


Figure 5-D-6a. ESSA-9 4705-2 0136 GMT March 10, 1970; Surface Analysis 0000 GMT March 10, 1970.

Figures 5-D-6a and b. A subsynoptic scale vortex train extends from A to B, southeastward from the Kamchatka Peninsula. The vortices were formed in the cumulus cloud field by cyclonic shear in the low-level wind field (figure 5-D-6a). In the region of the vortices, light surface winds were reported, while to the southwest the winds were 20 to 30 knots; the result was the cyclonic shear that created the vortex pattern. At 500-mb (figure 5-D-6b), a narrow, elongated cold low overlies the vortex train. This factor also may have contributed to the formation of the vortices.



Figure 5-D-6b. ESSA-9 4705-2 0136 GMT March 10, 1970; 500-mb Analysis 0000 GMT March 10, 1970.

The subsynoptic scale vortex or eddy pattern that forms in the Atlantic Ocean west of the Mediterranean Sea is an example of the type of eddy that occurs in stratus or stratocumulus clouds adjacent to coastlines. This subsynoptic scale eddy is observed less frequently than those which form in subtropical highs or cumulus cloud fields. The formation of this eddy pattern is a result of orographically induced cyclonic shear in the low levels. This region of cyclonic shear exists at the mouth of the Mediterranean Sea when the synoptic scale wind flow from the north and east first traverses the higher terrain of the Iberian Peninsula. When conditions are favorable for low-level cloud formation, the eddy pattern will appear on the satellite photographs. This pattern will remain stationary and will persist as long as conditions are favorable for its formation.



Figure 5-D-7a.  Gemini X Orbit 26 Frame 28 July 20, 1966



Figures 5-D-7a and b. This is an example of the subsynoptic scale eddy that forms at the mouth of the Mediterranean Sea (figure 5-D-7a). Cyclonic shear in the region of the eddy pattern was caused by both the northerly and the easterly wind flow (figure 5-D-7b). Note that the pattern consists of a single eddy and not a group of eddies as in previous examples. The streamline analysis is based on the surface winds for 0600 GMT on July 20, 1966.

Figure 5-D-7b.  Surface Streamline Analysis
0600 GMT July 20, 1966

Chapter 5

Section E

Severe Weather


## Introduction

Specific atmospheric conditions accompany the occurrence of severe weather,
particularly tornadoes (68). Usually, a severe weather watch is issued
several hours in advance of the severe weather event and identifies a large
area (usually 120 by 240 miles) in which severe weather is expected to occur.
Combined use of imagery from meteorological satellites and conventional data
yields a better assessment of the behavior of the atmosphere than is possible
with the use of conventional data alone; this leads to more reliable and
accurate warnings of severe weather. Satellite imagery gives the viewer an
immediate feeling for the dynamics of a severe weather situation. Synoptic
and mesoscale features, important in severe weather development, are readily
detectable in satellite imagery. Visible and infrared imagery from polar-
orbiting and geostationary satellites provide valuable information for: (1)
locating the active squall line (the area of maximum severe weather threat);
(2) locating the low-level jet (850-mb) and the axes of the polar and sub-
tropical jets; (3) determining vertical wind shear between the lower and upper
troposphere; (4) locating the area where the low-level and mid-level jets in-
tersect (the major axis of latent tornado activity) and (5) isolating small
(15 miles square) areas of immediate tornado threat; these areas are located
by the combined use of satellite imagery, the surface wind field, and radar
information.

## Squall Lines

In most cases convectively unstable squall lines form along the convergent low-level streamline which separates warm, moist, maritime air from warm, dry, continental air; this air mass boundary is the so-called "dry line". An excellent example of a dry line in the process of becoming an active squall line is shown in figure 5-E-6c.

> "...these so-called "dry lines" may remain quasi-stationary
> for days...without becoming active; but under certain conditions,
> they appear to act as mechanisms aiding the formation of large
> thunderstorms and organized squall lines...this is most likely
> when a supporting feature...exists at 500 mb" (69).

Most severe weather occurs in the area of deep, moist convection which is associated with this boundary.

The squall line appears in satellite imagery as a line of cumulonimbus clusters which have merged together to form a bright band. The threat of severe weather is greatest in the area where the squall line takes on a characteristic tapering shape in the imagery (figure 5-E-1). The narrowing of the line to the south should be expected since the preferred region of the squall line for new storm formation is its southernmost portion. Here the smaller, less mature storms are located; while the older, more mature storms are further north (70).

## Locating the 850-mb Wind Maximum

The axis of the low-level jet parallels an active squall line. Its exact location beneath the squall line cloud shield depends on the curvature of the low-level flow and the isotach field. However, if the axis is assumed to be near the back edge of the active squall line clouds and its direction parallel to the squall line, its location will be very close to the actual position.

## Middle and Upper-Level Jets

An important factor in forecasting severe weather is the presence of a mechanism that produces upper-level divergence. In most cases this is a jet stream. The locating of jet streams from satellite imagery has been discussed in Chapter 3 of this Technical Report.

The polar jet stream has long been recognized as an important factor in the development of severe weather. Miller (68) has pointed out that the major activity in a tornado outbreak will be located near the intersection of a low-level and upper-level jet. The axis of the polar jet stream can be either south (figure 5-E-2) or north (figure 5-E-3) of the region in which severe weather occurs.
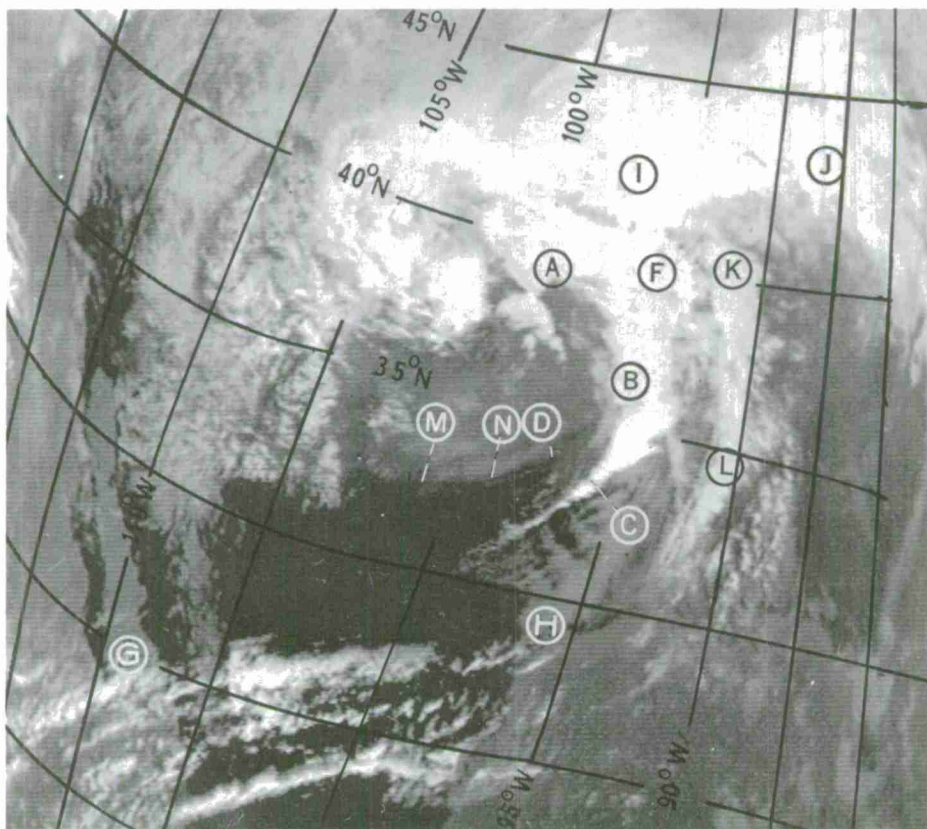
NOAA-1 Daytime Infrared   2125 GMT   February 18, 1971

Figure 5-E-1.  This figure is a classic example of an infrared picture re-
ceived during a severe weather outbreak.  The tapering cloud system, with its
back edge extending from A to B to C, is associated with an active squall
line and represents the area of maximum severe weather threat.  Four tornadoes
were reported near A between 1930 GMT and 2210 GMT, one near B at 2045 GMT,
and three near C between 2055 GMT and 2335 GMT.  The 850-mb jet axis is
parallel to the squall line; in this case it is within the convective cloud-
iness from C to F.  The axis of the polar jet stream at 500-mb extends along
the cloud edge M-N-D.  The subtropical jet is easily detected from its cloud
shield which extends from G to H; however, in this case, the polar jet stream
was the dominant triggering mechanism in the severe weather outbreak.  High
clouds associated with a warm front extend from I to J, and a band of cirrus
(remnants of the convection on February 17, 1971) from K to L.

In figure 5-E-2, the axis of the polar jet is easy to locate along the cloud edge B-C-D. The presence of the jet is also indicated by the anticyclonic curvature along the western edge of the upper-level cloudiness near A. Extension of the jet axis from D to A places the jet axis south of the squall line (Q'LINE). From the imagery, one may compare the vertical wind shear at the southern portion of the squall line to that at its northern end; the change in shear also indicates the jet is south of the squall line (shear is discussed on page 5-E-6). In figure 5-E-3, the axis of the polar jet is easy to locate along the cloud edge A-B-C; however, its location past C is not apparent from the satellite imagery. When a situation of this kind occurs, the current 500-mb analysis is used to help locate those portions of the jet which are not detectable in the satellite imagery; in the case of figure 5-E-3, the extension is from C to E.
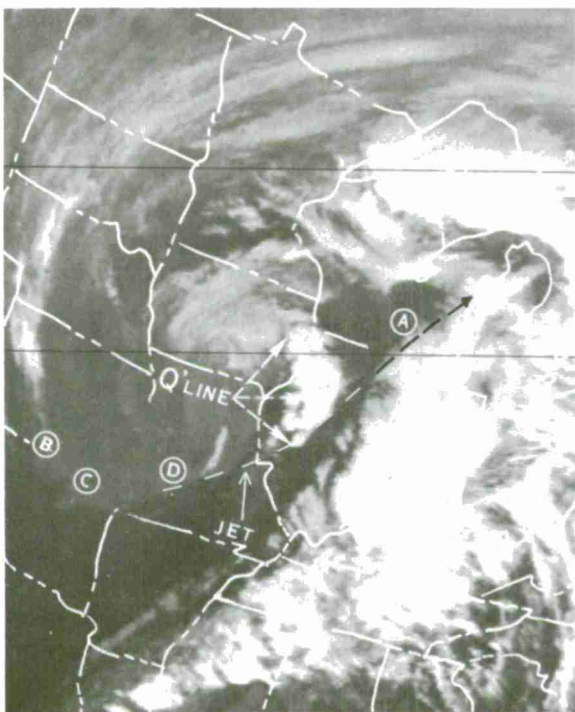


NOAA-1 Daytime Infrared   2026 GMT
February 19, 1971

Figure 5-E-2.  A squall line (Q'LINE)
extends from eastern Iowa through
western Illinois.  Tornadoes were
reported in the southern end of the
squall line between 1935 GMT and
2100 GMT.
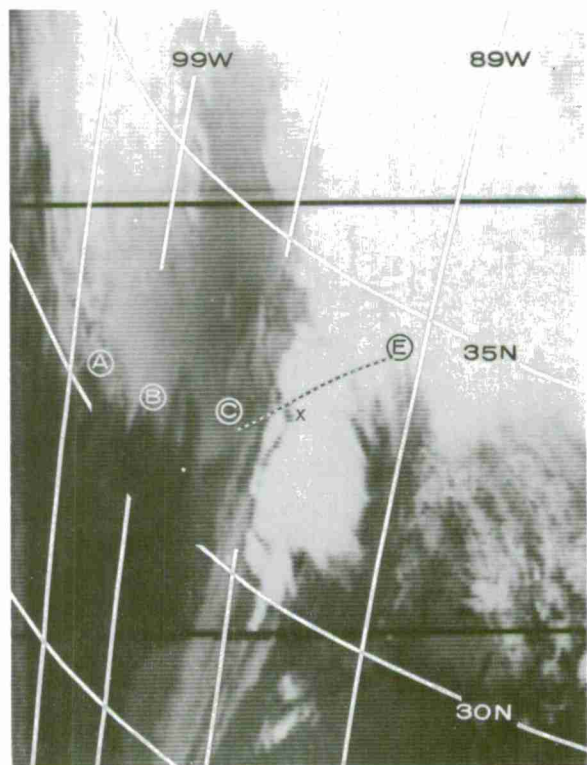
NOAA-1 Daytime Infrared   2016 GMT
February 21, 1971

Figure 5-E-3.  Mississippi tornadoes
began at 2100 GMT near X, beneath the
intersection of the low and mid-level
jets.

The subtropical jet stream has been found to play a key role in a large num-
ber of severe weather outbreaks (figure 5-E-4). Tornadoes occurring in the
presence of the subtropical jet stream are normally beneath its intersection
with the squall line and to the north of the jet axis. Prior to the availa-
bility of satellite observations, the role of the subtropical jet in severe
weather situations was not fully appreciated because of the paucity of data
along the path of the subtropical jet stream. In fact, the subtropical jet
may well have been mistaken for the southern branch of a split polar jet
during some severe weather outbreaks.
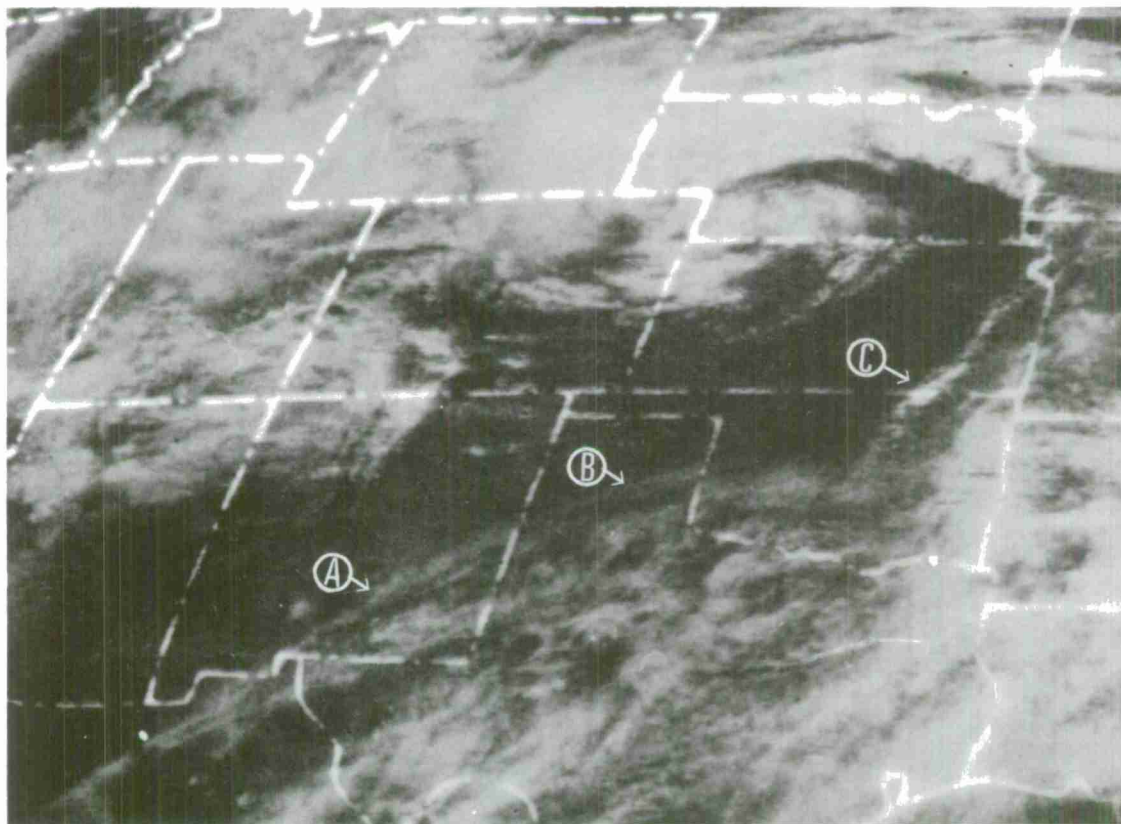


ATS-3  Frame 29  2016 GMT  May 5, 1971

Figure 5-E-4. The axis of the subtropical jet stream is made apparent by
the anticyclonically-curved cloud shield that extends from A to B. Extrapo-
lation of the jet from several consecutive ATS pictures (or extension from
just one picture) showed that the main axis of the subtropical jet would
intersect the north-south oriented squall line (C) that is forming in eastern
Kansas and northern Oklahoma. Several devastating tornadoes occurred beneath
this intersection. The May 5, 1971 outbreak is described in detail later in
this section of Chapter 5.

## Detection of Shear

Convective clouds building through a shearing current are stretched out horizontally so that the elongated axis of the anvil is parallel to the direction of the vertical shear. In most severe weather situations, when thunderstorms develop in a strong shear environment, their anvils will extend to the right of the squall line and will be parallel to the vertical wind shear between the lower and upper troposphere. Since the vertical wind shear vector between the lower and upper troposphere is parallel to the mid-tropospheric isotherms, it is possible to use satellite imagery to locate the mid-tropospheric thermal ridge, a place where the maximum instability often occurs. This is done by using the thermal patterns from the current mid-tropospheric analysis and the shear orientation from the subsequent satellite imagery to reposition the thermal ridge. In figure 5-E-3, the cirrus anvils are oriented from northwest to southeast (winds from approximately 300°) across the squall line. If we move the mid-level thermal ridge from the 1200 GMT upper air analysis to fit the 300° shear vector, we must place it near the western edge of the squall line; this is verified by upper air data at 0000 GMT, February 22, 1971.

From the location of the low-level jet and the 500-mb jet axis in the satellite imagery, it is possible to infer the amount of veering between the two. Veering of winds with height is an important parameter in forecasting severe weather (68). In figure 5-E-3, the axis of the low-level jet is located parallel to the western edge of the squall line while the 500-mb jet axis extends across the squall line from C to E. Using this information, a veering of 40 degrees may be inferred; the 0000 GMT analysis for February 22, 1971 showed that the winds turned from 190° at 850 mb to 235° at 500 mb.

## Squall Line Growth Characteristics as Observed by ATS-3

The ATS-3 meteorological satellite, with its ability to view the same area of the earth at frequent intervals during daylight, provides information valuable for use in issuing severe weather warnings. During days when severe weather is expected, the spacecraft is programmed to take pictures of the Northern Hemisphere at 11-minute intervals. Information from these frequent observations permits the issuance of warnings of severe weather in mesoscale detail.

Cumulus cloud formation along the dry line is often observable in satellite imagery up to two hours prior to the time it becomes a squall line sufficiently active to be detected by radar. This squall line predecessor cloud formation first appears as a long thin line in the satellite imagery. Next, small areas of convective cloudiness begin to form along the thin line, organize into clusters as they grow, and form the initial stages of an active squall line. These intense thunderstorm complexes can remain active for several hours and interact vigorously with their surrounding environment. They are readily identified by the subsidence zones surrounding them. The subsidence zones appear as narrow gray areas within the squall line cloud band. In the initial stages of squall line development, clear areas usually surround the entire complex. Later as the thunderstorm complex grows and interacts with its environment, its anvil clouds may overlap other clouds and merge with other complexes; however, each individual complex usually makes its presence known by developing some clear areas around its periphery. When tornadoes

occur, they are located in the low-level inflow region of a complex; hail, however, may occur anywhere within a complex.

## Isolation of Threat Areas

It is possible to isolate very small areas of immediate tornado threat from satellite imagery, radar, and surface wind field data; the method is graphically demonstrated in figures 5-E-5 (a-d). To locate immediate tornado threat areas, first identify the boundary of each individual convective cluster along the squall line. Second, draw a streamline analysis of the surface wind field to define the asymptote of convergence in the low-level streamline field (this will usually parallel the back edge of the active squall line) and mark the area of low-level inflow into the thunderstorm complex. Lastly, identify the area on the inflow side of the cluster where the cluster boundary and the asymptote of convergence intersect. The portion of the cluster immediately adjacent to this point of intersection represents the area favorable for tornadoes. The threat area can be further reduced in size by comparing the moist inflow region with the echo patterns from the radar scope or with radar echo lines as they appear on the facsimile radar chart. Identify the radar echo within the cluster which is associated with the moist inflow region. The area of this echo near its tapered end represents the smallest threat area that can be defined. As a rule, the threat area should not cover more than one-half of a radar echo or enter more than 15 miles into its boundary. Once identification of a threat area has been made, its movement should be forecast from cell movement on radar. If possible, successive ATS pictures should be used since the complexes undergo changes in time which can alter the threat area patterns; this occurred in the May 5, 1971 example which is discussed next.
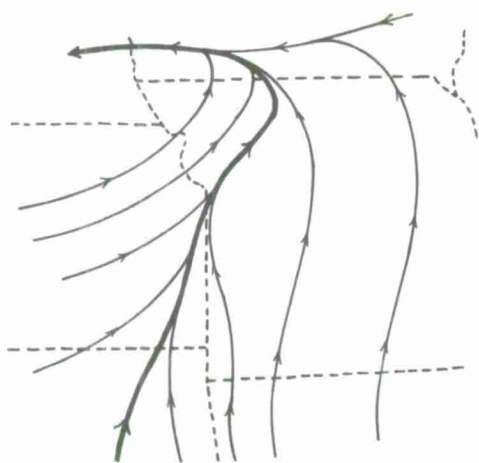


Surface Streamline Analysis 2300 GMT May 5, 1971

Figure 5-E-5a. Melding this analysis with the satellite picture to the right makes it possible to identify the low-level inflow region of each complex, marked with a dot in the picture.
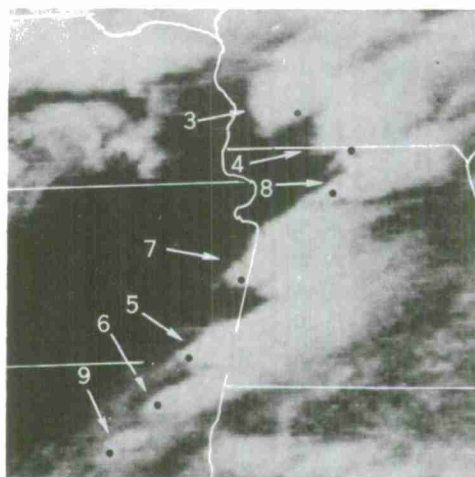


ATS-3 Frame 41 2256 GMT May 5, 1971

Figure 5-E-5b. There are seven active convective clusters within this squall line (numbered 3 to 9 for continuity with the next section). The portion of each complex favorable for tornadoes is marked with a dot.
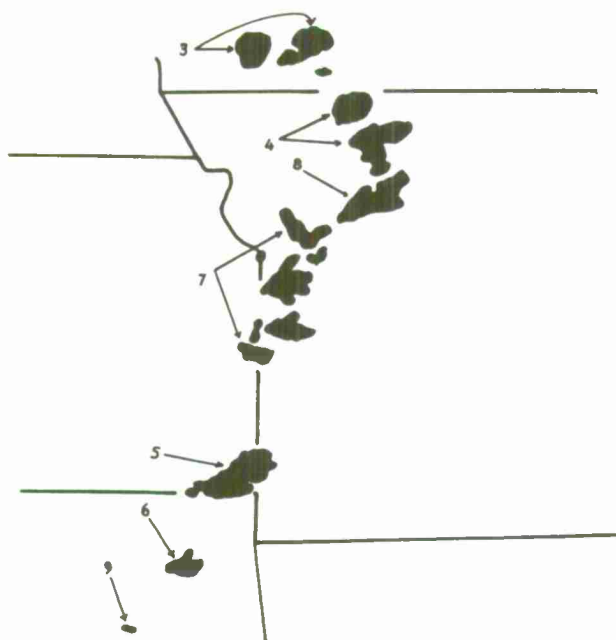
Radar Echoes   2256 GMT   May 5, 1971

Tornado Threat Areas   2256 GMT
May 5, 1971

Figure 5-E-5c.  Arrows point to the
radar echoes which make up the
thunderstorm clusters in figure
5-E-5b.  An area which is one-half
the echo size or 15 miles, which-
ever is less, should be isolated at
the low-level inflow region of each
echo cluster.

Figure 5-E-5d.  The tornado threat
areas (shown above as white portions
of the echoes) are isolated by in-
tegrating the information in the
three previous figures.  The expect-
ed movement of each threat area as
determined from radar and successive
ATS pictures is indicated by the wind
vectors.

## The Tornado Outbreak of May 5, 1971, An Illustrative Example

The synoptic situation on May 5, 1971 was ideal for a tornado outbreak over
the midwestern United States.  Considerable streamline convergence existed at
the lower levels along the "dry line" which separated warm, moist maritime air
and warm, dry continental air.  A well defined southwesterly subtropical jet
intersected the highly unstable area and triggered the severe weather.  Fig-
ures 5-E-6 (a-q) show the step-by-step development of this outbreak.  The
location where a tornado or tornadoes occurred is marked by an asterisk (*)
on each figure.
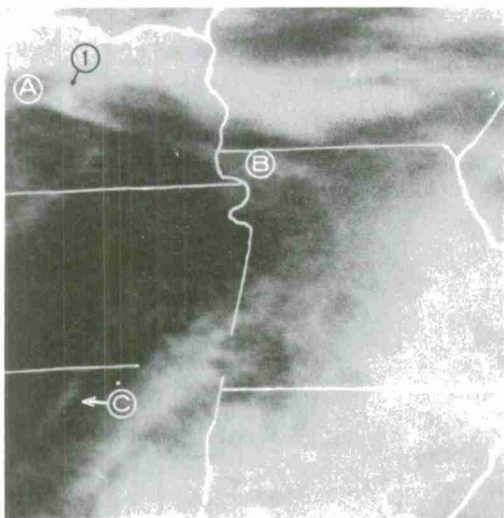
ATS-3 Frame 21   1833 GMT May 5, 1971

Figure 5-E-6a. Convective activity has just become apparent at point 1 along the line A-B. Cloudiness has just become visible at C along the dry line. It was nearly 2½ hours before the line B-C was detected by radar and identified as an active squall line.
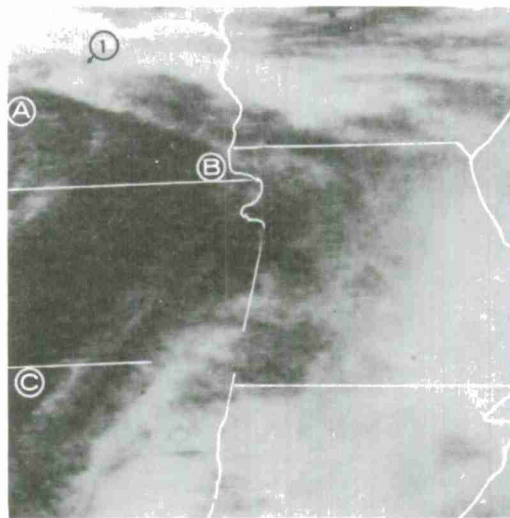


ATS-3 Frame 23   1858 GMT May 5, 1971

Figure 5-E-6b. Cloudiness along the dry line B-C is more evident. The thunderstorm complex at 1 bears watching; notice the clearing around it. The low-level inflow region of 1 should be identified as an area with a high potential for tornadoes.
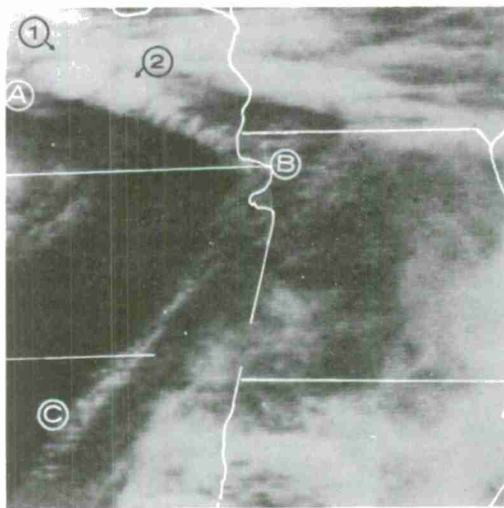


ATS-3 Frame 27   1951 GMT May 5, 1971

Figure 5-E-6c. A second thunderstorm complex has formed on A-B at 2. The danger of tornadoes at 1 still exists. Cloudiness along the dry line is now well defined. The area around C is where the major tornado activity should be expected; here the line is intersected by the subtropical jet (see figure 5-E-4).
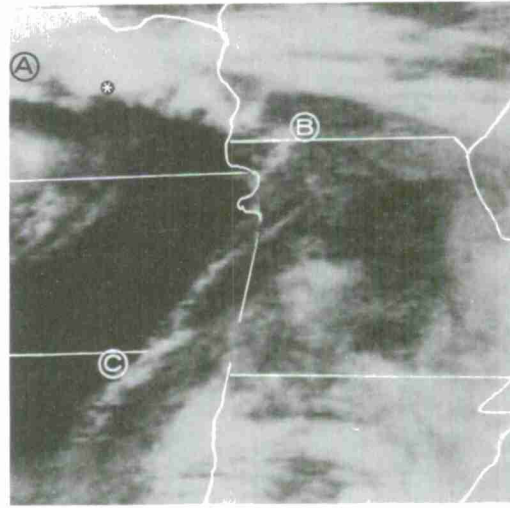


ATS-3 Frame 30   2027 GMT May 5, 1971

Figure 5-E-6d. Convective activity has increased along the dry line near C. The thunderstorm complexes at 1 and 2 have grown in size and are merging. Tornadoes were reported (as indicated by asterisk) between 2025 GMT and 2030 GMT.
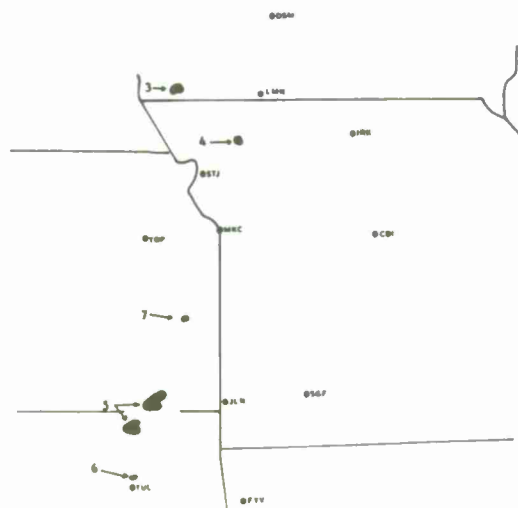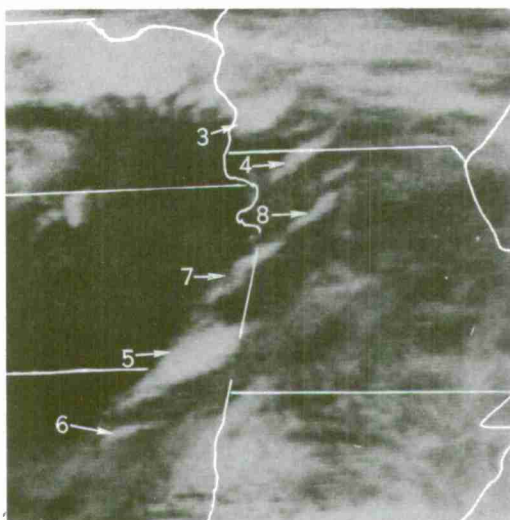
ATS-3 Frame 33   2109 GMT May 5, 1971   Radar Echoes   2109 GMT May 5, 1971

Figures 5-E-6e and f.  There are six distinct thunderstorm complexes visible in the ATS imagery along the dry line.  The storm complex at 3 can be traced back nearly an hour, the complex at 4 and the large complex at 5 can be traced back for nearly 50 minutes, the storm complex at 6 has been in existence for about 40 minutes, and the clusters at 7 and 8 have been going for 25 minutes.  The squall line has just begun to take shape in the radar presentation.
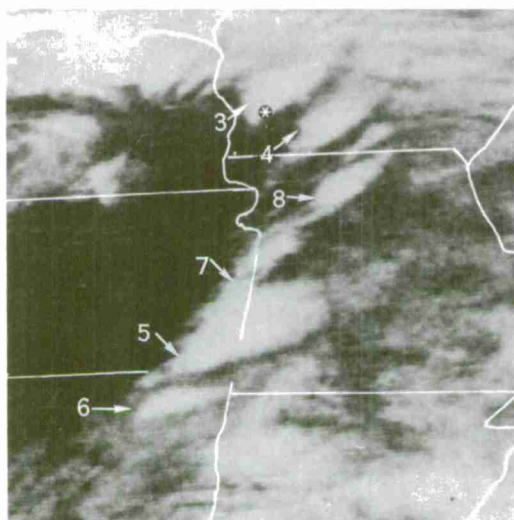


ATS-3 Frame 36   2147 GMT May 5, 1971   Radar Echoes   2147 GMT  May 5, 1971

Figures 5-E-6g and h.  The squall line shows up very clearly in both the satellite imagery and the radar.  The clear portions of the radar echoes represent the tornado threat areas which were located using the method previously described.  The only tornado activity reported near picture time was a funnel cloud (*) at 2150 GMT beneath cluster 3.
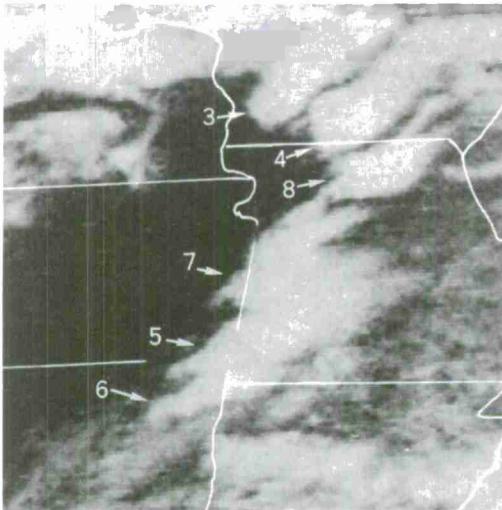
ATS-3 Frame 39  2229 GMT May 5, 1971     Radar Echoes  2229 GMT May 5, 1971

Figures 5-E-6i and j.  All of the storm complexes are easily located in the
satellite imagery and radar.  The white portions of the radar echoes represent
tornado threat areas.  Notice the bulge in complex 4 at its northwestern cor-
ner; this is associated with the northern echo in that cluster which is moving
to the west on a collision course with complex 3.  A junction actually occurred
as the northern echo in cluster 4 changed complexes and became the new threat
area in complex 3 (see radar in figure 5-E-6l).  The same type of split also
is occurring in complex 8, which will transfer the northern portion of its
echo to complex 4.
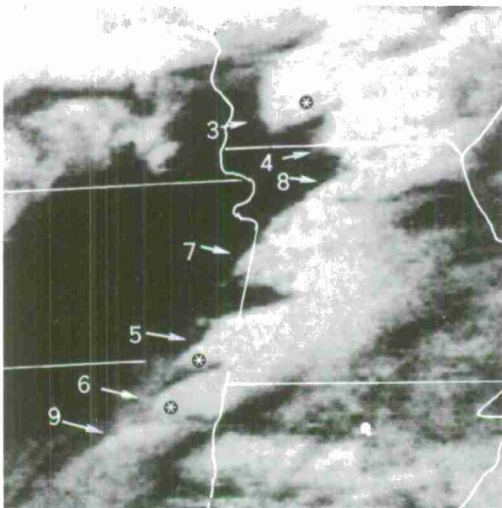


ATS-3 Frame 42  2307 GMT May 5, 1971     Radar Echoes  2307 GMT May 5, 1971

Figures 5-E-6k and l.  The echo transfers mentioned above are apparent in
both the satellite imagery and the radar.  The white portions of each echo
represent areas of tornado threat.  Tornadoes indicated by asterisks occurred
at 2308 GMT beneath cluster 6, at 2315 GMT beneath complex 3, and at 2315 GMT
beneath cluster 5.  A new threat area in the storm at 9 is evident in both
the radar and satellite imagery.

5-E-11
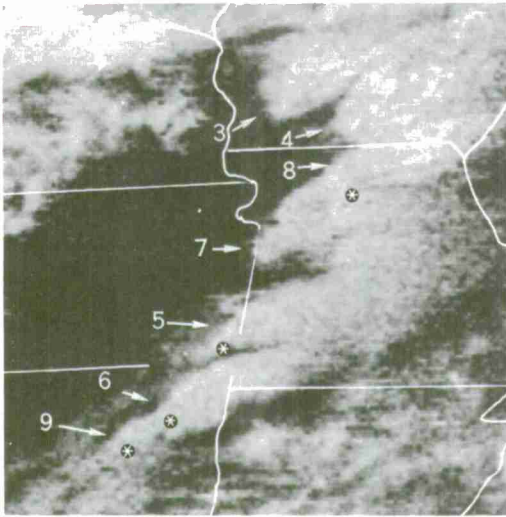
ATS-3 Frame 45   2347 GMT May 5, 1971      Radar Echoes   2347 GMT May 5, 1971

Figures 5-E-6m and n.  A significant amount of detail is lost in the ATS
picture because of poor solar illumination; however, most of the clusters are
still easily detected.  Tornadoes (*) were underway beneath clusters 5, 6, 8,
and 9 at the time of this picture.



Radar Echoes   0007 GMT May 6, 1971      Radar Echoes   0045 GMT May 6, 1971

Figures 5-E-6o and p.  Although no ATS imagery was available because of in-
sufficient illumination for picture taking, the known threat areas were
followed on radar.  A devastating tornado (indicated by * in cluster 5) oc-
curred in Joplin, Missouri at 0000 GMT, May 6, 1971.  A tornado was reported
beneath cluster 9 at 0044 GMT, and another beneath cluster 3 at 0045 GMT.
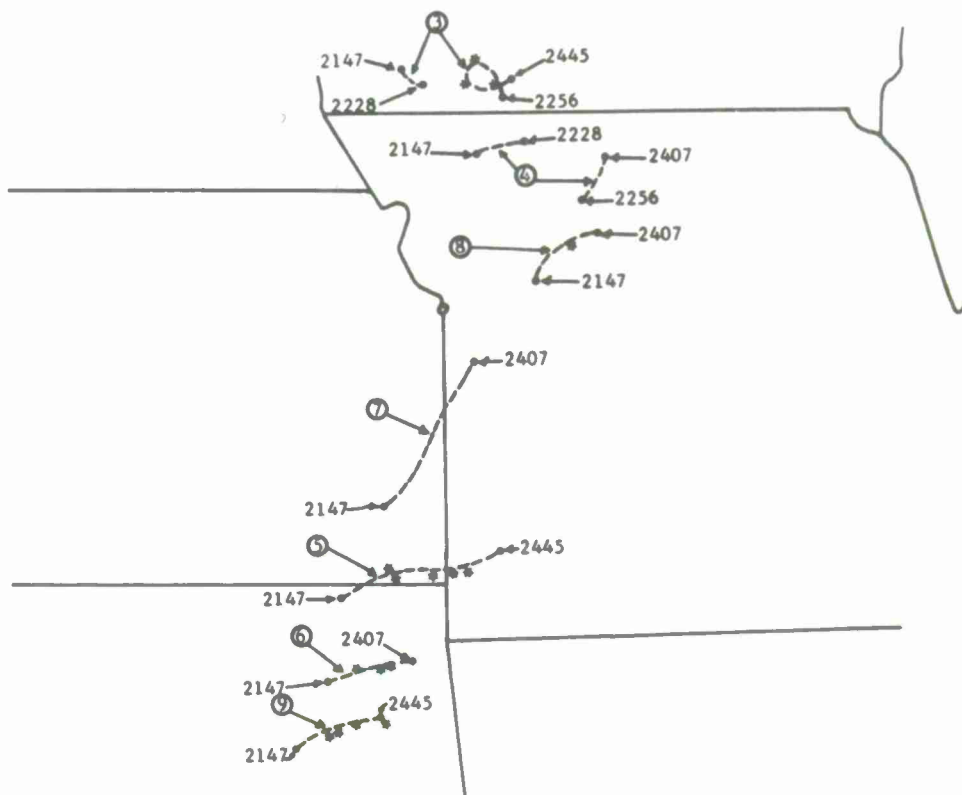
Threat Area Summary

Figure 5-E-6q. This figure shows the tracks of the center of each of the
tornado threat areas (dashed lines) and the relationship of each track to
the tornadoes which were reported. The GMT times that each threat area was
first identified, plus the time it was last recognized, are also indicated.
Each star (*) represents one tornado report; notice that no tornadoes occurred
outside of a threat area. The threat tracks of the tornado-producing storms
are all oriented at a far greater angle to the right of the low-level flow
than those of the non-tornado producers. This indicates that the tornado-
producing thunderstorms were all cyclonically rotating, right-deviating
severe storms, while the slight right-offset of the non-tornado producers is
due to the eastward progression of the squall line.

Chapter 5


Section F


Sea Breeze


## Introduction

The existence of a sea breeze has been acknowledged by meteorologists for
many years, but its region of influence was considerably underestimated until
observations were made from satellites. Numerous investigations of the sea
breeze show that many factors influence its development. At any particular
location such things as the temperature difference between the land and sea
surface, the strength and direction of the large-scale gradient-wind flow,
the stability of the air mass which overlies the land and adjacent water,
topography, friction, and the earth's rotation influence the sea breeze (71).
Each coastal station must develop its own sea breeze study because the net
effect of the parameters that influence the development of a sea breeze differs
from station to station.

The basic cause of the sea breeze is the differential heating of adjacent land
and water masses. Equal insolation over the land and adjacent water yields
a higher air temperature over the land. The warmer air over land rises and
is replaced by denser air. This denser air comes primarily from over the
water because of the density gradient established by the differential heating.
To compensate for the landward movement of the marine air, a portion of the
air at a level above the ground drifts seaward and subsides, thus, creating
a closed circulation cell (72). After its initial development, the sea
breeze cell is located near the shoreline in the morning and then expands
both landward and seaward as the day progresses. This expansion is not
symmetric about the shoreline. The greatest expansion normally occurs over
the water and may vary from approximately 10 to 20 miles out to 100 or more
miles depending on the strength of the sea breeze cell. The inland penetra-
tion may vary from a few miles on steep, mountainous coastlines to 100 or
more miles on flat, unobstructed coastlines. Vertically, the sea breeze may
vary from as little as 50 feet up to as much as 8,000 feet, depending on the
strength of the onshore flow (72). The maximum sea breeze flow is normally
located between 100 and 200 feet above the surface.
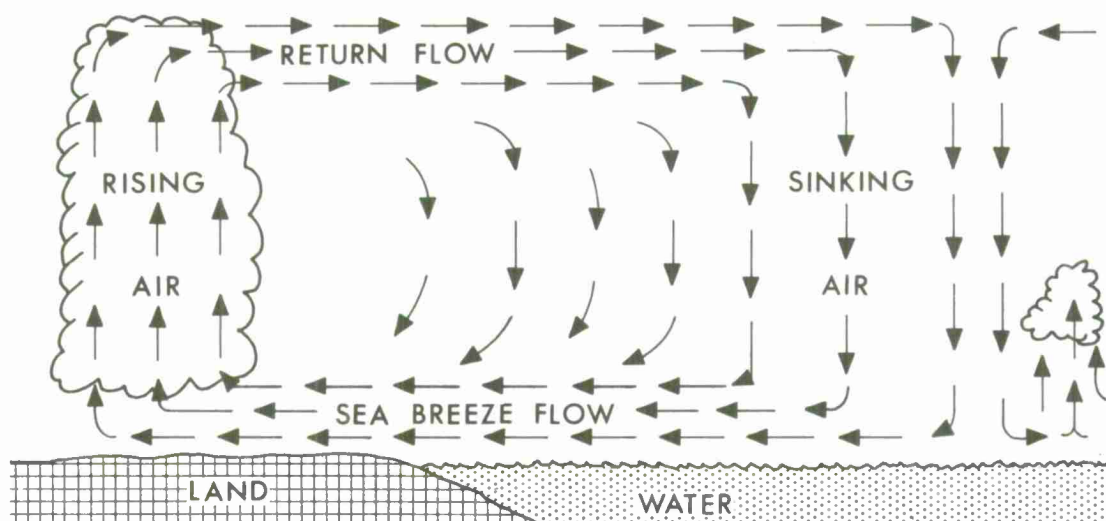
Figure 5-F-1. A schematic showing the classical sea breeze cell.

One of the most striking features of the sea breeze is the front-like zone at its leading edge over land. This zone, commonly referred to as the sea breeze front, moves inland as the sea breeze cell expands and then, as the cell deteriorates, moves seaward. The sea breeze front may result in showers as it moves inland, accompanied by a slight drop or leveling off of the temperature, a humidity change, and a wind direction change. As the sea breeze front moves seaward, its intensity will normally be decreasing, but may still result in showers, a humidity change, and a wind direction change.

In the case of a peninsula or an island, sea breeze circulations can develop along opposite shores. These multiple sea breeze zones lead to an area of increased convergence over the central region of the island or peninsula. The shape of a coastline also has an effect on the sea breeze. Various coastline curvatures result in convergence or divergence of the sea breeze flow.
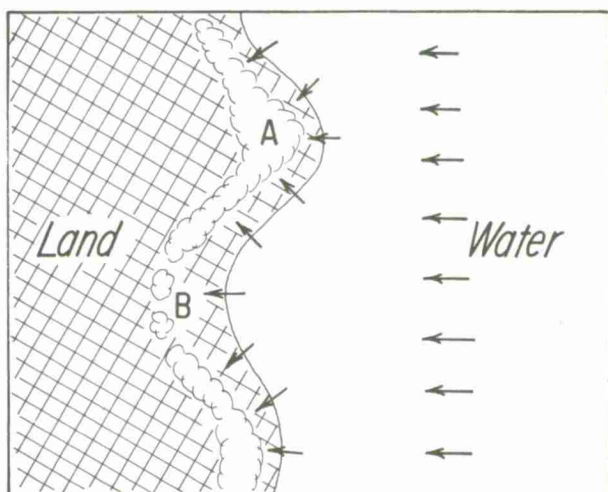


Assuming a uniform, steady sea breeze flow onto an uneven coastline, the frictional drag acting on the flow over land results in mass convergence at A and mass divergence at B. These effects are portrayed by strengthening at A and weakening at B in the cloud pattern associated with the sea breeze front.

Figure 5-F-2. Schematic showing the relationship between coastline curvature and sea breeze frontal cloudiness.

## Sea Breeze Cloud Patterns

The effect of the sea breeze appears on satellite photographs as a line of
clouds (sea breeze front) inland from the coast with a relatively cloud-free
region along and off the coastline. The sea breeze front may or may not be
continuous depending on terrain and other effects. The clear area ends
abruptly over water where either random cloudiness or another line of clouds
appears. The vertical development of this secondary line of clouds over the
water in most cases is less than the vertical development of the line of
clouds inland from the coast.
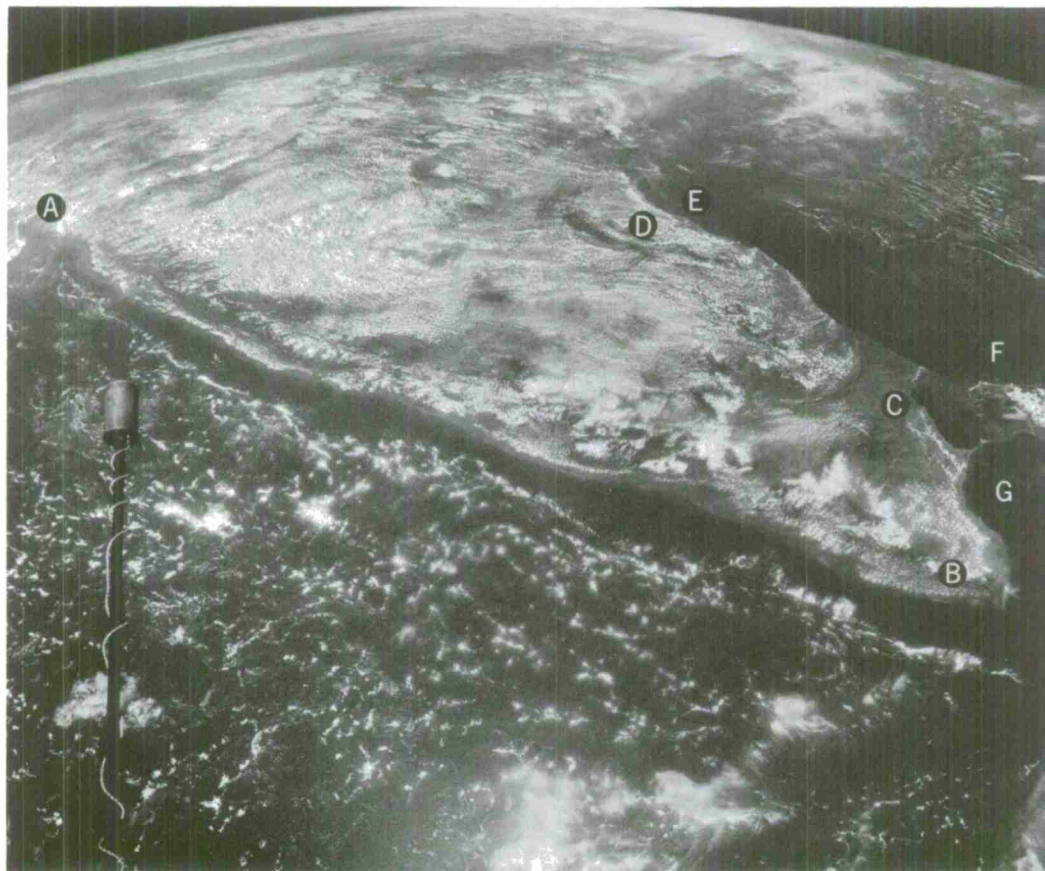


Gemini XI   Orbit 26   Frame 27   September 14, 1966.

Figure 5-F-3.  The cloud pattern resulting from a well-developed sea breeze
is apparent along the entire western coast of India (A to B).  The sea breeze
front is seen inland from the coast.  The cloud-free area associated with the
sea breeze circulation extends seaward about 30 miles.  Other sea breeze
fronts exist along the southern and eastern coast of India from B to C to D.
The extensive clear areas E, F, and G off the east coast are attributed to
the sea breeze circulation cell and also to the effects of persistent upwell-
ing (73).
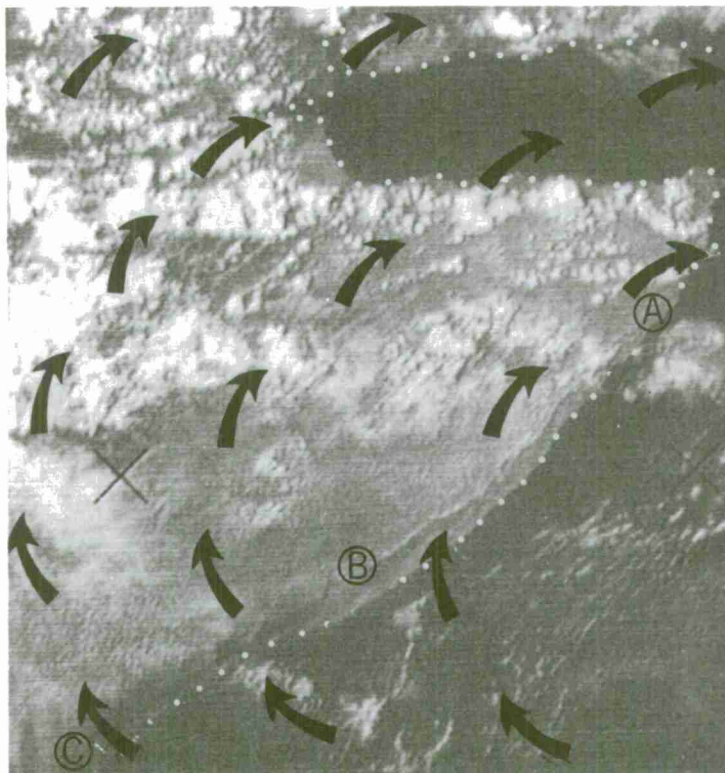
ITOS-1   3027-6   1029 GMT   September 22, 1970.

Figure 5-F-4.  This is an example of the cloud pattern resulting from a sea
breeze which has developed along the coast of the Somali Republic.  From A to
B, the sea breeze front appears as a line of clouds about 30 miles inland.
Offshore, the subsidence zone is clear.  From B to C, the sea breeze circula-
tion has produced onshore clearing, but no inland cloud line is present.  This
may be due to divergence in the low-level wind flow in this region.  Arrows
show the wind flow at the gradient level.

Observational studies of the sea breeze (74) show that when the gradient wind
flow is directed onshore, thus reinforcing the sea breeze, the sea breeze
front will penetrate further inland and will be more intense than with an
offshore gradient wind flow.  The clouds associated with a sea breeze front
in most cases will have a greater horizontal and vertical extent with an on-
shore flow than with an offshore flow.  The subsidence region associated with
the sea breeze circulation will be well defined in both cases.  Occasionally,
with an onshore gradient flow, the advection of clouds into the subsidence
region makes the seaward extent of the subsidence less apparent.
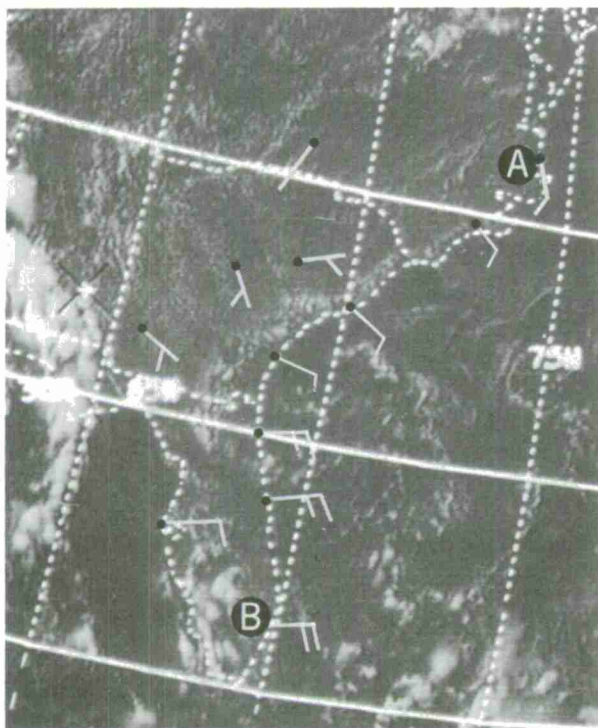
Figure 5-F-5. The cloud pattern resulting from a sea breeze is seen along the southeast coast of the United States from near Cape Hatteras (A) to just south of Miami (B). The sea breeze front has moved inland 50 or more miles over Georgia and Florida assisted by a strong easterly gradient-wind flow. The subsidence region off the coast is ill-defined in some areas, due to the advection of clouds into the area. Surface wind reports are shown on the picture.

ITOS-1  3044-4  1923 GMT  September 23, 1970
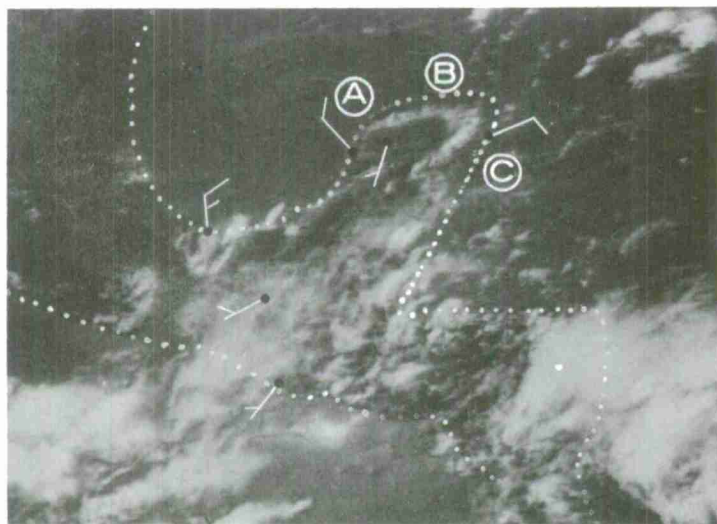


Figure 5-F-6. This is an example of the cloud pattern associated with the sea breeze along the north coast (A-B-C) of the Yucatan Peninsula. The inland penetration of the sea breeze front varies from approximately 10 miles on the northwest coast to 20 miles on the north and northeast coasts. The offshore subsidence regions are apparent at A and B, while at C, some clouds are being advected into the region by a northeast gradient-wind flow. The sea breeze front is enhanced by the onshore gradient-wind flow along the north and northeast coasts. Surface wind reports appear on the picture.

ATS-3 Frame 14  2004 GMT  June 15, 1970
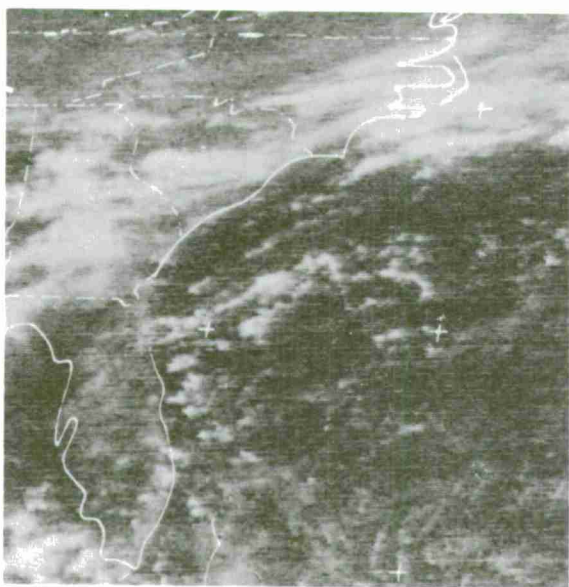
Figure 5-F-7a. ATS-3 Frame 2 1344
GMT August 28, 1970.



Figure 5-F-7b. ATS-3 Frame 5 1502
GMT August 28, 1970.



Figure 5-F-7c. ATS-3 Frame 7 1555
GMT August 28, 1970.
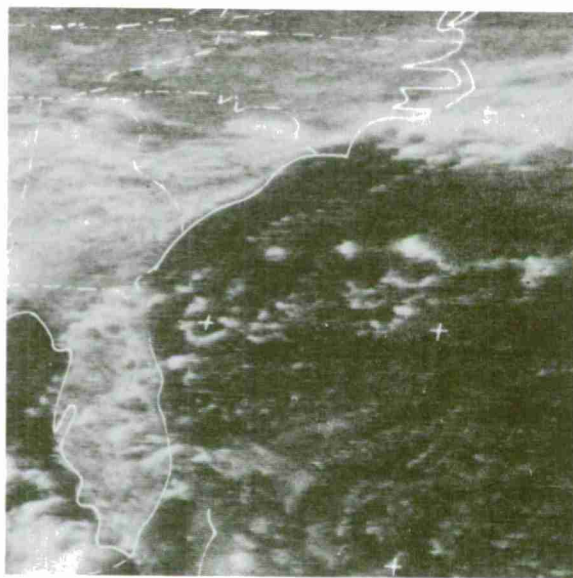


Figure 5-F-7d. ATS-3 Frame 10 1654
GMT August 28, 1970
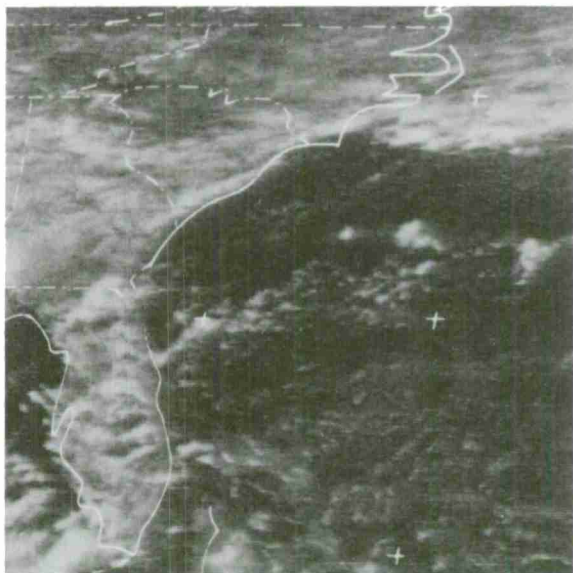
Figure 5-F-7e. ATS-3 Frame 12
1747 GMT August 28, 1970.

Figure 5-F-7f. ATS-3 Frame 15
1905 GMT August 28, 1970.

Figures 5-F-7(a-f). This series portrays the development of the sea breeze
along the southeast coast of the United States from North Carolina to south-
ern Florida. The time period of the series is approximately 5½ hours. In
photograph (a), the sea breeze is in its initial stage of development, with
just a slight dissipation of the low clouds along the coast from North Carolina
to northern Florida. In photograph (b), the sea breeze is stronger and more
fully reflected in the cloud pattern. The low clouds along and off the coast
from North Carolina to northern Florida dissipated as subsidence associated
with the sea breeze cell increased. In photograph (c), the subsidence region
expanded and became noticeable along the entire east coast of Florida. A
faint line of clouds along the seaward edge of the subsidence region can also
be seen from North Carolina to Florida. In photograph (d), the sea breeze
front is just along the South Carolina and Georgia coasts, while over Florida
it is developing further inland. The subsidence region continues off the
coast. In photograph (e), the subsidence region continues to expand seaward
and the clouds associated with the sea breeze front continue to develop. In
photograph (f), the sea breeze front has pushed further inland along the en-
tire coast and the clouds show significant vertical development. The subsi-
dence area offshore remains quite large and easily recognized.
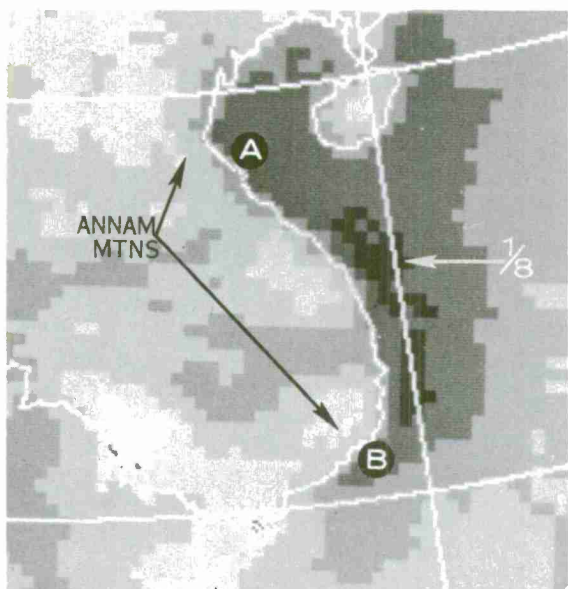
Figure 5-F-8a. Mean Eighths of
Relative Cloud Cover for June.
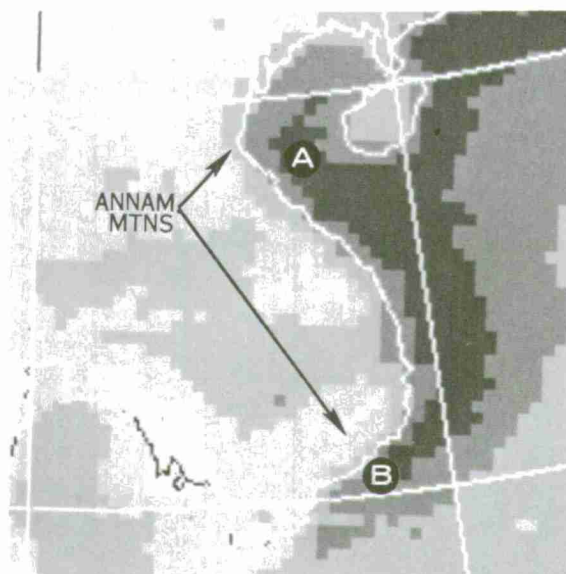


Figure 5-F-8b. Mean Eighths of
Relative Cloud Cover for July.

Figure 5-F-8(a-c). These photographs
are examples of satellite cloud clima-
tology based on four years of satel-
lite imagery near 1400 local time (75).
Mean cloud cover in these pictures is
depicted in nine gray shades. The
darkest shade represents clear skies
while the whitest shade represents
overcast clouds. Each intermediate,
brighter, gray shade corresponds to
an increase of one-eighth mean cloud
cover. The summer months shown are
the period of the Southwest Monsoon
over Southeast Asia.
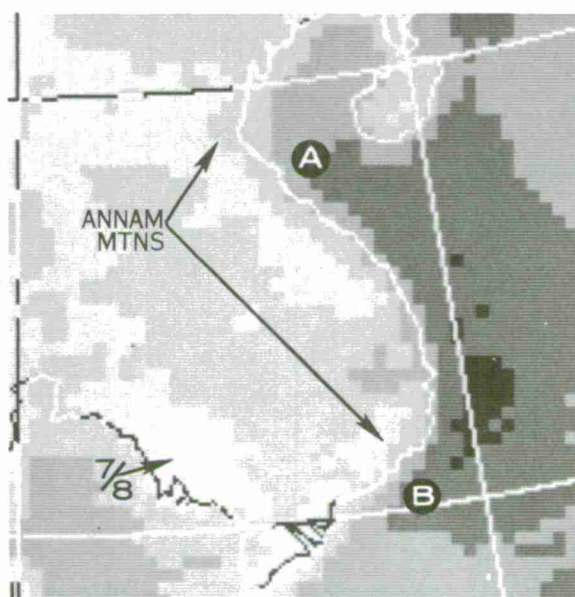


Figure 5-F-8c. Mean Eighths of
Relative Cloud Cover for August.

The Annam Mountain Range blocks the southwest gradient-wind flow which results
in a period of light winds in the low levels along the coast. During the
period, the sea breeze circulation is dominant along the east coast of Viet-
nam. The influence of the sea breeze circulation, accompanied by downslope
effects to the lee of the mountains, is reflected in the mean cloud cover
from point A to B by a low percentage of cloud cover due to the two effects.

Chapter 6

INFRARED

Section A

Basic Characteristics of Infrared Data

## Introduction

Infrared (IR) sensors measure long-wave radiation emitted by cloud, land and water surfaces. These measurements are converted to temperatures which generally represent the temperatures of the surfaces viewed. The IR data are obtained by a scanning radiometer (SR) which measures radiances in the 10.5 to 12.5 $\mu m$ portion of the electromagnetic spectrum[1]. These measurements are recorded and processed by computer to provide global coverage. They are also available by direct readout (DRIR). In the future, SR data from other portions of the electromagnetic spectrum will also be transmitted to direct readout stations.

IR measurements commonly are converted to imagery in which the clouds and earth appear as different shades of gray. The darkest areas represent the warmest surfaces, while the brightest represent the coldest surfaces. IR imagery also shows relative cloud height. Satellite television pictures measure reflected sunlight in the visible spectral range. Dark areas correspond to areas with low albedo while bright areas are produced by highly reflective surfaces.

## IR and Television Pictures Compared

A comparison in coinciding IR imagery and TV pictures shows many cloud and land features are similar in appearance while other features are quite different in appearance. For example, in IR imagery the gray shade of oceans varies with temperature, while in a television picture, oceans are uniformly dark except in areas of sunglint. Thick cloud formations, such as those associated with storms, are cold and highly reflective; such formations appear bright in both the IR and video.

[1] Section C describes the scanning radiometer and discusses the overall accuracy of cloud and surface temperatures obtained by ITOS/NOAA satellites.

Figure 6-A-1. This tabulation shows the relative shades of gray for various cloud and land features as they appear in television and in daytime IR pictures. The shades shown for the features are typical but can vary depending on display device settings. This comparison shows which features appear similar in either type of display and which ones appear different. Some of the features in figure 6-A-1 appear in figure 6-A-2, which shows coincident IR and TV views of the United States and adjacent areas. The circled numbers in the tabulation locate features in figure 6-A-2. The relative gray shades assigned each feature for each type of data can vary over a range, so this diagram should be considered for illustrative purposes only.

| LONG WAVE RADIATION - IR IMAGE \ ALBEDO - TV PICTURE | White | Lt.Gray | Gray | Dk.Gray | Black |
|---|---|---|---|---|---|
| Black | | | | Fair Wea. Cu ⑬  Deserts ⑤⑧ | Warm Ocean ⑯ |
| Dk.Gray | St. ⑭ | | | | Cold Ocean ①⑱ |
| Gray | St. & Sc ⑦⑩  Middle Cloud | | Thin Ci | | High Forested Terrain ② |
| Lt.Gray | | | | | |
| White | Ci & As ⑥  Cb ⑨①⑮  Front ⑰⑲  Artic Snow | | Dead Cb Anvil ⑫ | Dense Ci ④ | |

Figures 6-A-2a, b. The IR and TV data displayed here are coincident. Examination of these two views reveals both differences and similarities in the appearance of the two types of data. The clouds associated with a surface low between Lake Superior and James Bay are cold and have a high albedo, so they appear white in both pictures (17). A cold front extends southwestward from the low to the Texas panhandle. The IR display delineates areas of cold middle and high clouds (17 and 11) and causes the frontal band to appear discontinuous. It is not possible to differentiate between middle and high clouds and low clouds of this front in the TV picture; they are equally reflective so the band appears more continuous. A deep pool of cold air is behind the front. The cumulus along the northern Montana border, in the center of the cold pool, extend through the middle troposphere; their tops appear white in the IR. These cumulus are also highly reflective so they appear much the same in the TV picture. The stratocumulus west of California (7) does not appear the same on both displays. It is bright and has sharply defined edges in the TV but appears gray in the IR because of its relatively warm cloud top temperatures. In the video the stratocumulus contrasts sharply with the adjacent land and water because of large differences in albedo, while in the IR the boundary is ill-defined because of the small temperature contrast between the cloud tops and the water surface. The characteristics of other numbered areas in these pictures can be identified by referring to the gray-scale chart of figure 6-A-1.
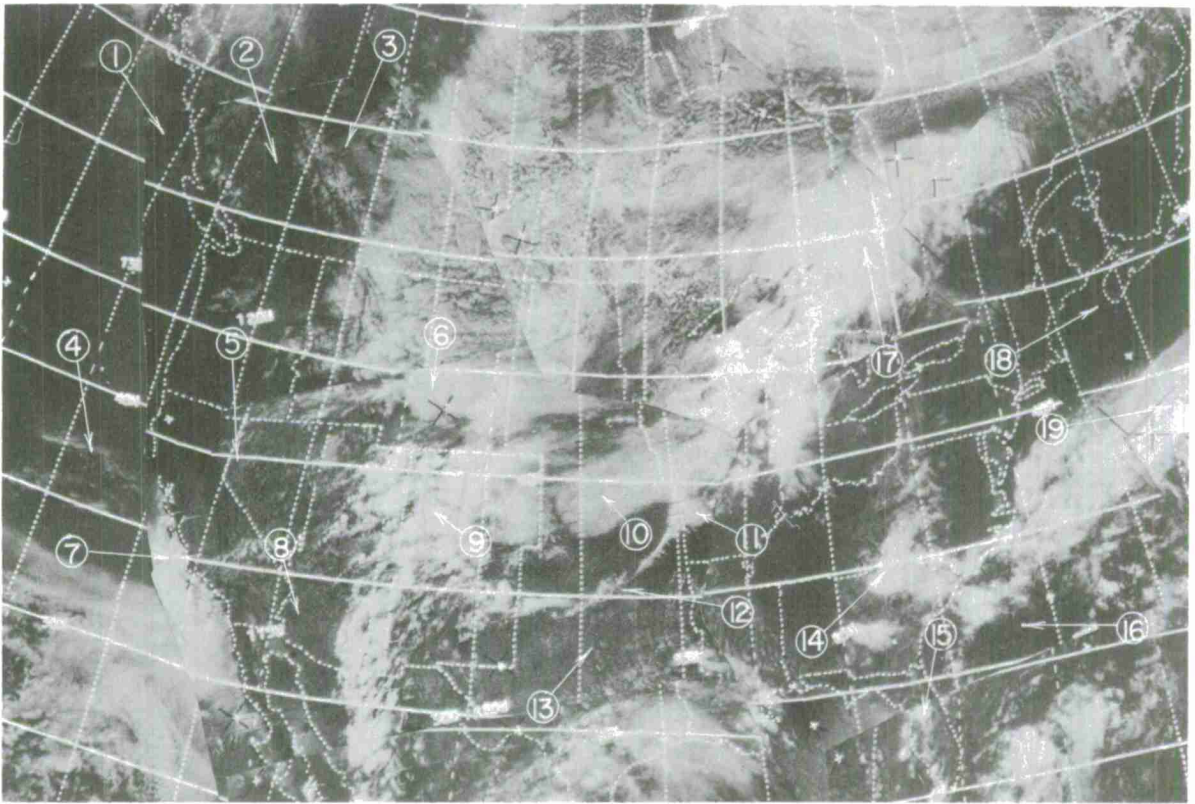
Figure 6-A-2a.  NOAA-1 Visible (TV)  September 12, 1970
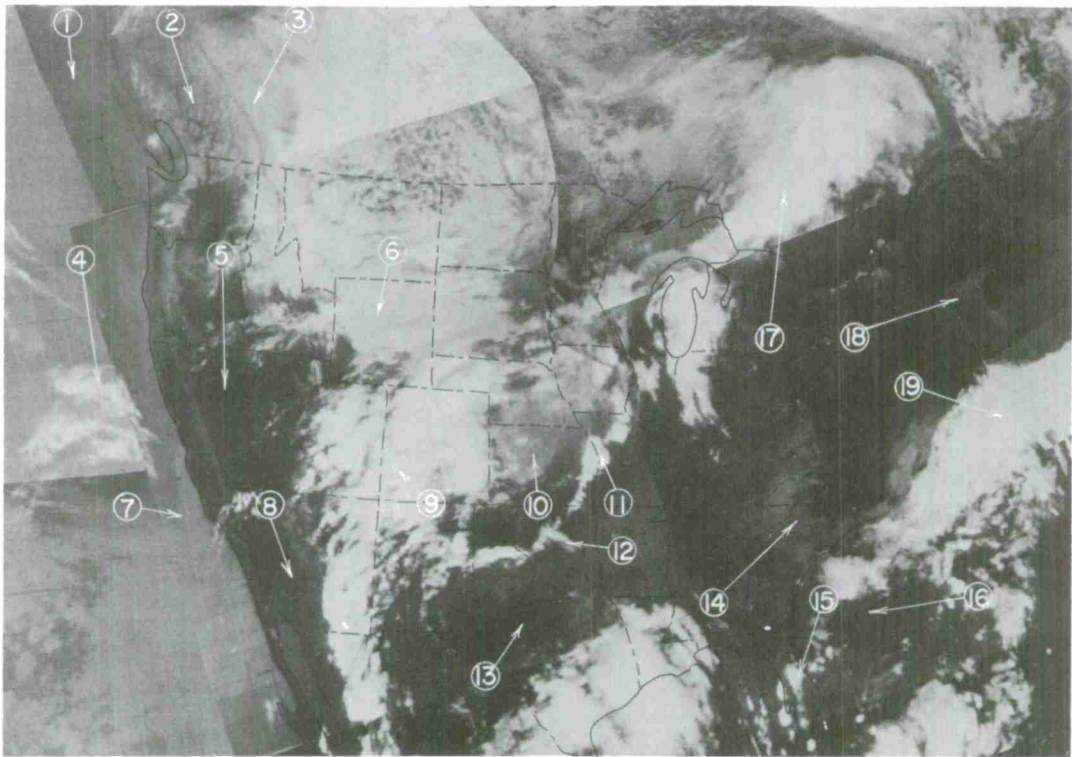


Figure 6-A-2b.  NOAA-1 Daytime Infrared (IR)  September 12, 1970

## Effects of Naturally-Occurring Temperature Variations on IR Pictures

The large diurnal temperature variation over land surfaces produces a marked difference in appearance between daytime and nighttime IR pictures. In the daytime, the warm land appears darkest in IR imagery and contrasts well with cool water bodies which appear gray and with cold middle and high clouds which appear white.

As the land cools at night, it appears a lighter shade of gray in the IR image. The closer the land temperature comes to that of water bodies, the less the contrast between land, water and clouds in the image; thus, their boundaries are less obvious. If land and water surfaces become the same temperature, the boundaries disappear.

Seasonal and latitudinal temperature variations are another cause of variation in the appearance of IR imagery. In the winter, especially at night, clouds over cold land are not easily detectable. In the tropics, there is always a large temperature contrast between the land surface and middle and high clouds, so these clouds are easily recognizable.

The effects of diurnal, latitudinal, and seasonal temperature variations can be compensated for, to a degree, when IR data are displayed. (See Enhanced Displays, Section C.) It is usually necessary to apply the compensation procedure described in Section C so clouds can be recognized in areas of small cloud-earth temperature difference.
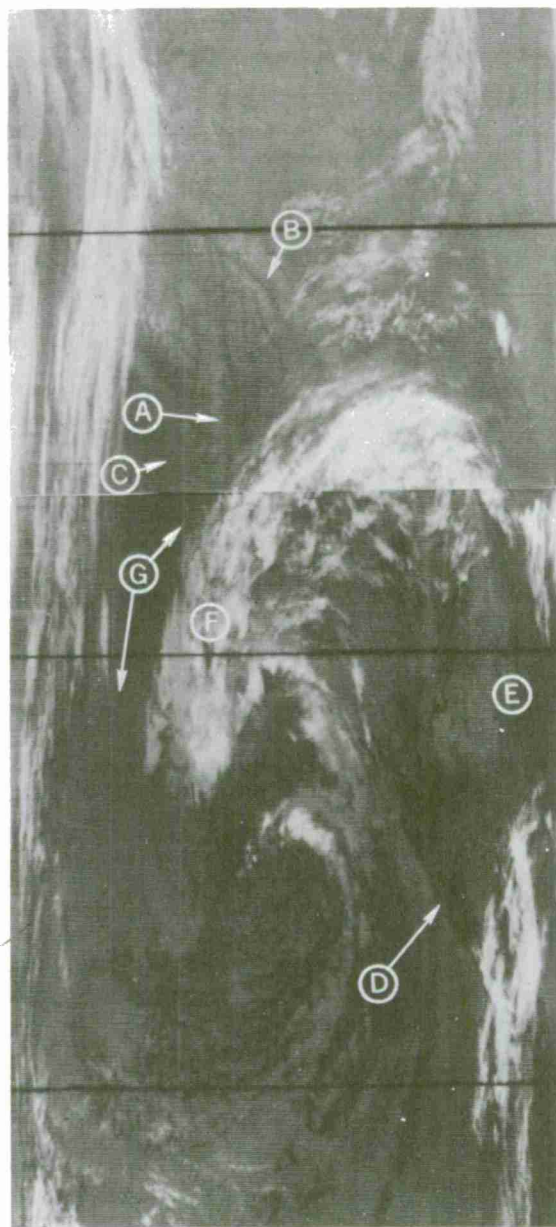


Figure 6-A-3a  NOAA-1  1791 Nighttime IR  1200 GMT  May 3, 1971.

Figure 6-A-3a and b. These two IR pictures taken 12 hours apart show the effect of the diurnal change of land temperatures during spring on an infrared scene. In the daytime (figure 6-A-3b) the Cascade Mountains (A), the Rockies (B), and the coastlines (C and D), are easier to identify than in the nighttime view 12 hours earlier (figure 6-A-3a). Also note in this picture pair that the cold ground of the
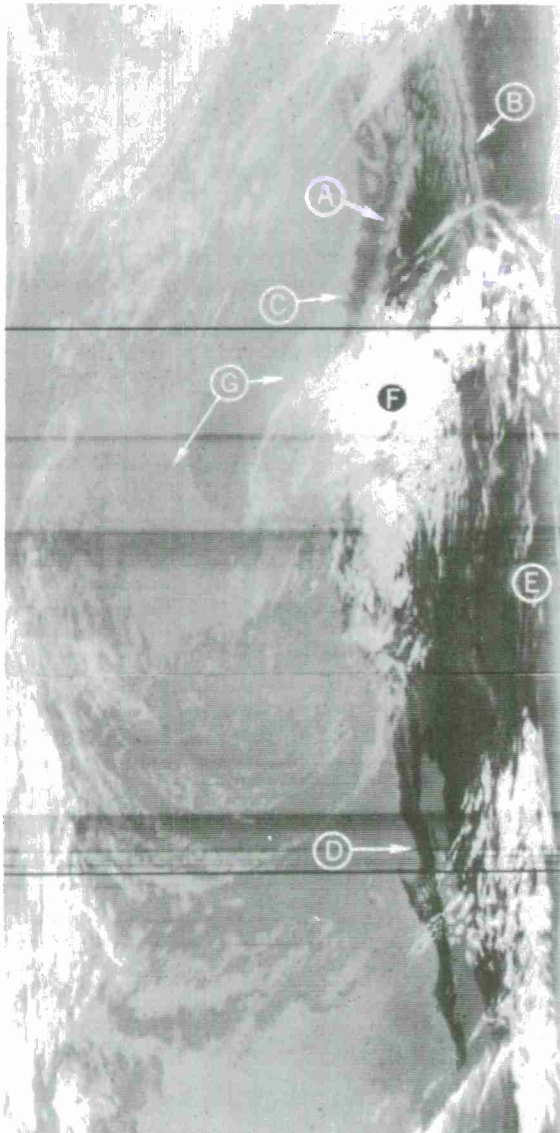
Figure 6-A-3b.  NOAA-1  1798 Daytime
IR  2300 GMT  May 3, 1970



Figure 6-A-3c.  NOAA-1  1798-3, 4, 5
Visible (TV)  2300 GMT  May 3, 1970

inter-mountain plateau (E) turns gray
at night and could be confused with
an area of low clouds.  The major
cloud system (F), associated with a
deep cold low, is moving eastward.
The vortex pattern of this system,
defined by the cold high clouds in
the IR, is equally detectable by day
and by night.

Figure 6-A-3c.  This TV picture coin-
cides with the daytime IR (figure
6-A-3b).  The large-scale cloud system
associated with the closed low is more
easily recognized in the IR than in
the TV imagery.  In this figure, the
highly reflective stratus and strato-
cumulus over the water (G) could be
confused with the high clouds associ-
ated with the vortex pattern.

## Identifying Synoptic Scale Cloud Systems in IR

In general, pattern recognition skills developed for interpreting synoptic
scale cloud formations in television pictures can be used for interpreting
IR imagery. The geometry of frontal bands, vortices, and jet-stream cloud
formations is the same in both types of display. The gray shade displays of
a given cloud formation, depending on the type and characteristics of the
clouds involved, can be very different in simultaneous IR and TV imagery.
The relative heights of clouds, except for some forms of cirrus and low
clouds, are clearly depicted in IR. Thus, IR and TV data used together are
superior for synoptic scale diagnosis than either form of data alone. For
a discussion on how to interpret IR views of major cloud systems, see Chap-
ters 3 and 4 of this manual. Additional examples of IR imagery will be con-
tained in future additions or revisions to this manual.

Chapter 6

INFRARED

Section B

Interpretation of Cloud Forms and Surface Features

## Cirrus and Middle Cloud

Middle and high clouds are more easily identified in IR imagery than in TV pictures. The gray shades representing these clouds generally range from white to medium gray. Usually there is a large contrast between the gray shade of an upper cloud and that of the much warmer earth or that of lower clouds beneath them. An exception occurs during winter in polar regions. Here the difference between the temperature of the earth's surface and that of middle and high clouds is small; thus it becomes difficult to differentiate between clouds and the earth's surface. To further complicate cloud analysis, the clouds above a polar snow surface can look darker in the presence of a strong temperature inversion.

It is often difficult to differentiate between cirrus and middle clouds in infrared imagery because of the transmission characteristics of the ice crystals that form the cirrus. Cirrus is semi-transparent to infrared radiation at $11\,\mu m$. Its transmissivity depends on its vertical thickness and the ice concentration within the cloud. Thin cirrus is much more transparent to IR radiation than thick cirrus. For example, a cirrus sheet of a given ice concentration and cloud particle size transmits 80 percent of the radiation from below if it is 0.5 km thick but only 20 percent if it is 5.0 km thick (47).

A satellite IR radiometer senses a combination of cold radiation from cirrus tops and warmer radiation transmitted upward through the cirrus and records a single integrated measurement. For this reason, some cirrus cloud top temperatures derived from SR data will be too warm and the cloud top heights calculated from these temperatures will be too low.

The gray shade of cirrus in an IR display is quite variable because it is dependent on the thickness of the cirrus, the temperature of the surface immediately below, and the temperature structure of the atmosphere. In an atmosphere with no strong inversions, thin cirrus with middle clouds beneath will appear much colder in an IR display than will the same cirrus by itself. Here the sensor detects radiation from both the cold middle cloud and the cirrus. The same thin cirrus occurring alone often approximates the gray shade of lower warmer middle clouds. In this case, the sensor has detected radiation from both the cirrus and the warm ground or ocean surface below. In an atmosphere where strong inversions are present, cirrus can appear a darker gray than land. This is most frequently observed at polar latitudes in the winter where warm air advection is occurring over very cold snow-

covered ground. The low or middle cloud beneath the cirrus in this situation
can be appreciably warmer than the land. This results in a scene where the
relative brightness of clouds and land is as follows: the cold cirrus over
the cold land appears brightest; the cold land alone is the next brightest;
cirrus over lower cloud is gray, and the warmer lower cloud is the grayest.

More cirrus is detectable in IR imagery than in TV pictures. Relatively
thin cirrus over land or water has a low albedo in the visible part of the
spectrum so there is very low contrast between areas covered with thin cirrus
and clear areas. At times, thin cirrus is almost impossible to detect in TV
pictures. The same cirrus in an IR image still appears bright enough to con-
trast well with the warmer and hence darker land and water surfaces. Thus
IR reveals the presence of relatively thin cirrus even though it cannot pro-
vide an accurate measure of its temperature. Many types of cirrus have
similar characteristics in both the infrared and visible data. Dense cirrus
shields and cirrus anvils associated with active cumulonimbus have high
albedos and also radiate at cold temperatures, and so appear quite bright in
both the visible and IR.
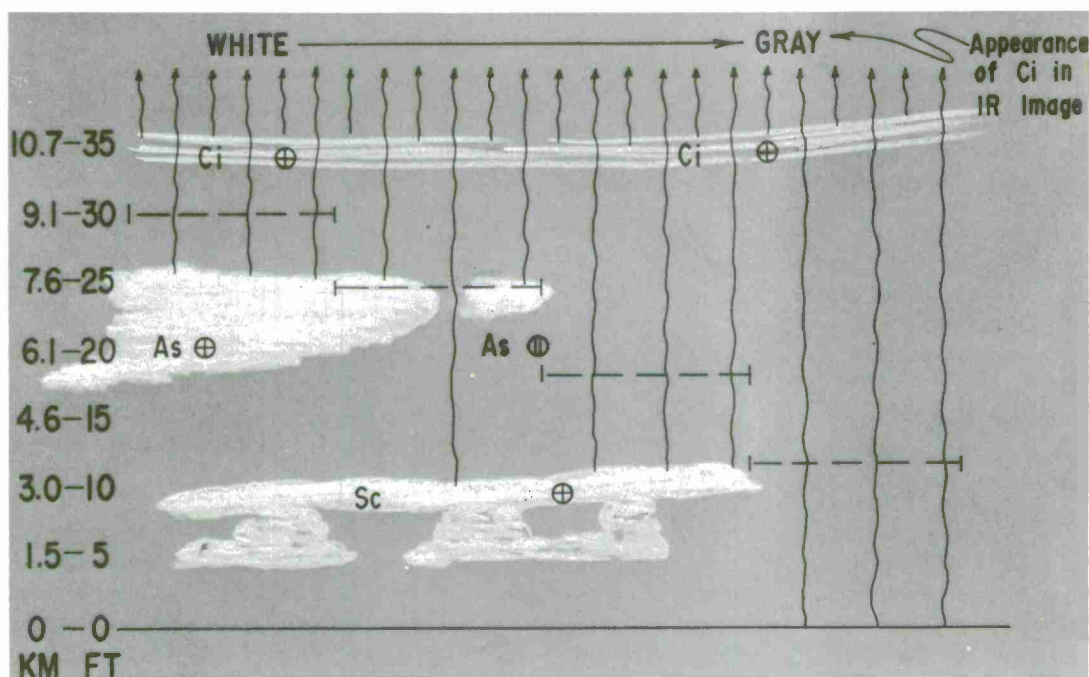


Figure 6-B-1. This diagram shows the effect of lower cloud on radiation
emitted by a uniform layer of thin cirrus. It is assumed that no large tem-
perature inversion is present. The vertical wavy lines represent schemat-
ically the source of the radiation reaching the satellite sensor. The hori-
zontal dashed lines represent the height of the cirrus tops computed on the
basis of the integrated temperature received by the SR. The horizontal lines
are of equal length and represent the smallest distance that the IR sensor
can resolve. As the clouds below the cirrus become less in amount and lower,
the cirrus appears progressively grayer and warmer in an IR display. The
heights and gray shades shown here are for illustration purposes only, but
are considered representative of changes that actually can occur. Cirrus can
appear to be as low as 10,000 feet if it is almost transparent, and occurs
where the surface below is sufficiently warm.

Middle cloud generally appears as an intermediate shade of gray in an IR display, somewhere between the gray shades representing the coldest and warmest clouds observed in a given area. It is difficult to differentiate between middle clouds and thin cirrus since both often have the same gray shade. If an area of middle cloud is broken with cloud elements at or below sensor resolution, it will appear to be warmer than it actually is[1] and so may be improperly identified as low cloud.

Satellite observations show that most middle clouds are associated with synoptic scale storms or with areas in which large numbers of thunderstorms are occurring. In both cases, much of the middle cloudiness occurs beneath higher cirrus or cirrostratus. Middle clouds are observed directly only
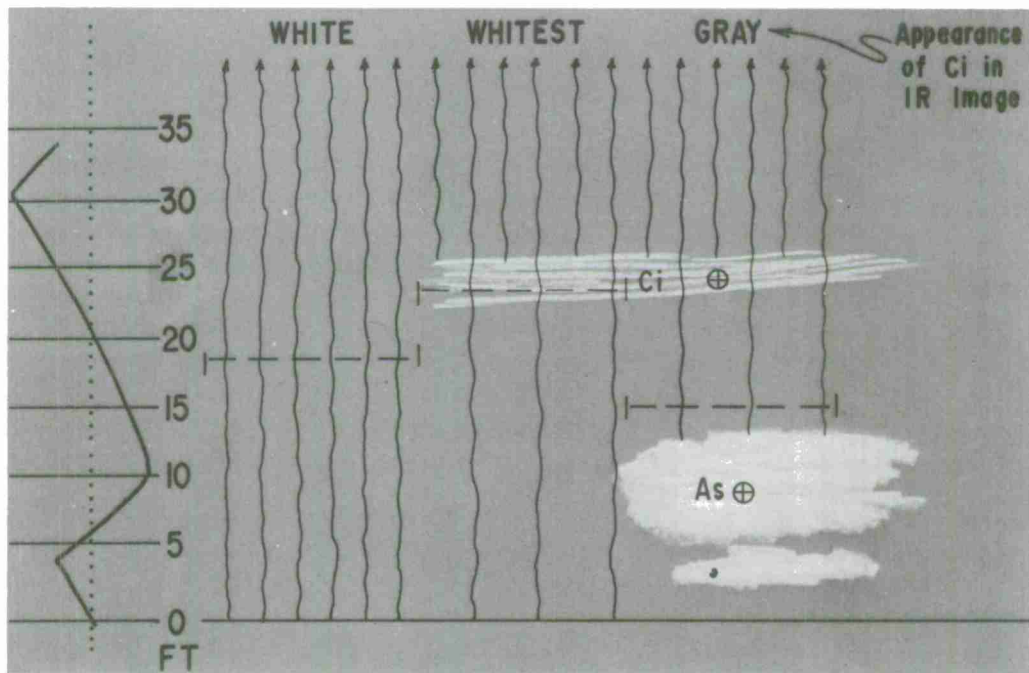


Figure 6-B-2. This diagram shows a uniform, thin cirrus layer over a cloud layer that is warmer than the earth's surface. The dashed horizontal cloud height lines and the schematic representation of radiation follow the same convention as in figure 6-B-1. The schematic sounding curve on the left indicates the strength of the inversion for this example. The ground temperature shown is the same as the temperature at 500-mb. In this example the cirrus over the cold ground appears whiter than the ground alone. The cirrus is now grayer when over low cloud, rather than whiter as shown in figure 6-B-1.

1/ See Section C, "Effect of Spatial Resolution on Indicated Cloud Top Temperature".

around the fringes of storms or in small isolated patches. When temperature
decreases with height, cirrus over storms appears brightest when middle or
low clouds are present beneath it. This characteristic of IR response can
be used as an indirect indication of the presence of lower cloud. Generally,
the brighter the cirrus, the more likely it is that middle cloud, rather than
low cloud, is present beneath it.

If a number of cloud layers are present and their relative heights can be
established from other data, it is usually possible to identify them in the
IR display by their relative shades of gray. Once the gray shade associated
with a middle cloud layer is identified, the IR image reveals the extent of
the layer much more precisely than do the other data.
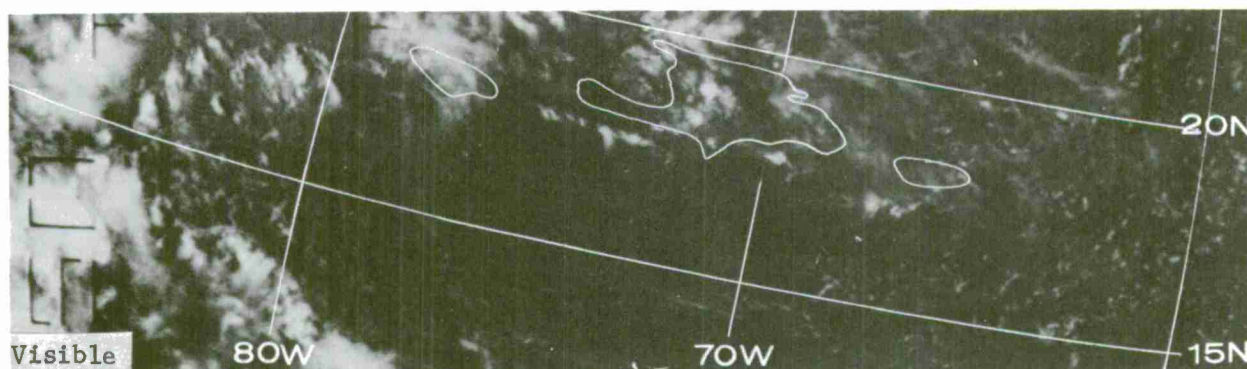


ITOS-1   2807 Visible (APT TV)   1945 GMT   September 4, 1970



ITOS-1   2807 Daytime IR   1945 GMT   September 4, 1970

Figure 6-B-3. This shows simultaneous daytime views of cirrus over the
Caribbean area. More clouds appear in the infrared than in the visible in
the area north of 17°N and between 65°W and 70°W. A careful examination of
the visible data shows some cirrus, but the exact extent of high clouds is
uncertain.
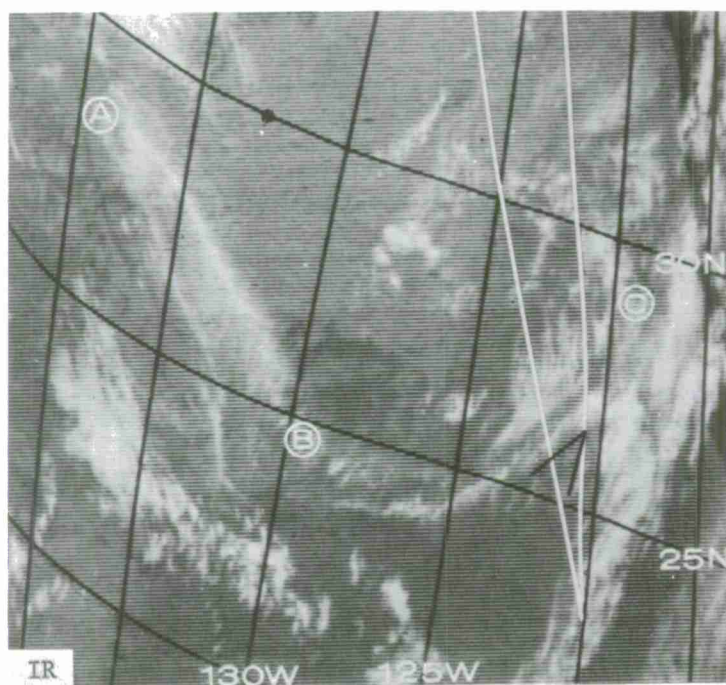
ITOS-1  270 Daytime DRIR  2308 GMT  May 4, 1970
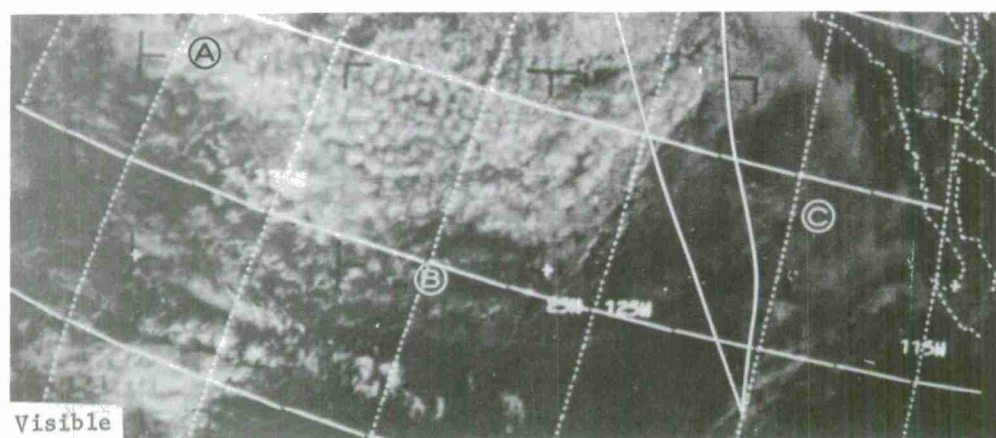


ESSA-9  5403-5 Visible (TV)  2235 GMT  May 4, 1970

Figure 6-B-4.  Cirrus overlying eastern Pacific stratocumulus is often diffi-
cult to identify positively in the visible data, but can be easily detected
in the IR.  These two views, 27 minutes apart, are a good example of this.
Cirrus is quite obvious in the IR image; here high clouds extend from A to B
to C and appear much whiter than the lower, warmer stratocumulus.  Most of
the cirrus is not detectable in the TV picture.  In the TV picture, the only
evidence of cirrus is between A and B.  Here the stratocumulus appears some-
what blurred by the nearly transparent cirrus but it is not noticeably bright-
er.  This blurring of the stratocumulus by cirrus is often overlooked and
only becomes apparent after examination of an IR image.  The white lines show
the track of an aircraft reconnaissance flight made at the altitude of the
cirrus tops.  The height of the cirrus was near 37,000 feet and cloud top
temperatures were around -55°C (from 48).

6-B-5
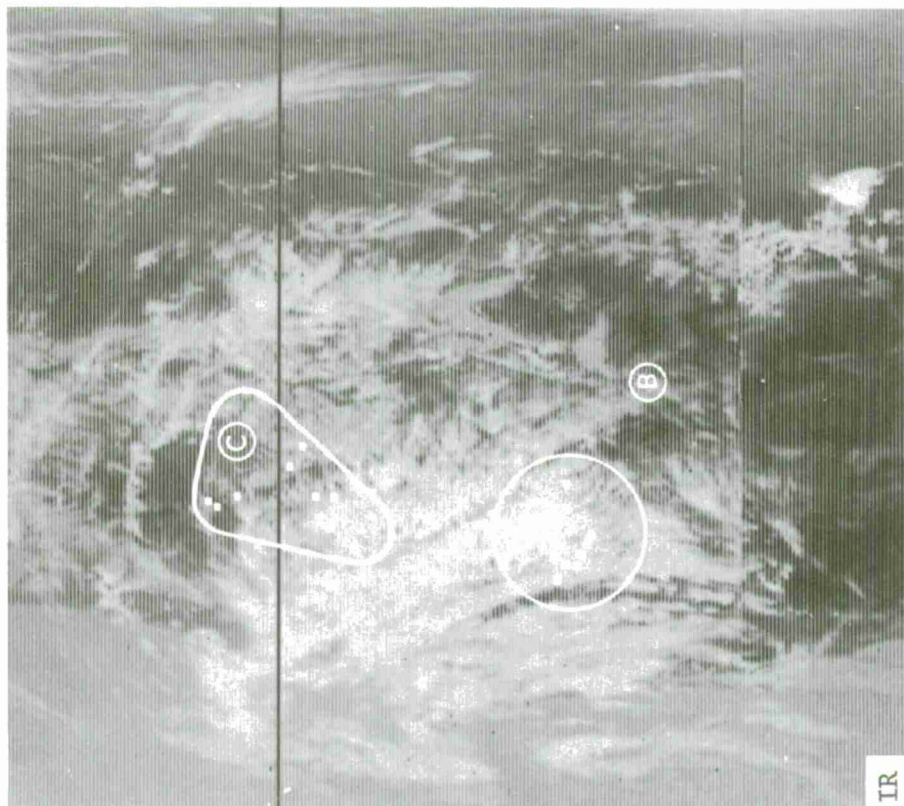
a. NOAA-1 1785 Daytime DRIR 2203 GMT May 2, 1971
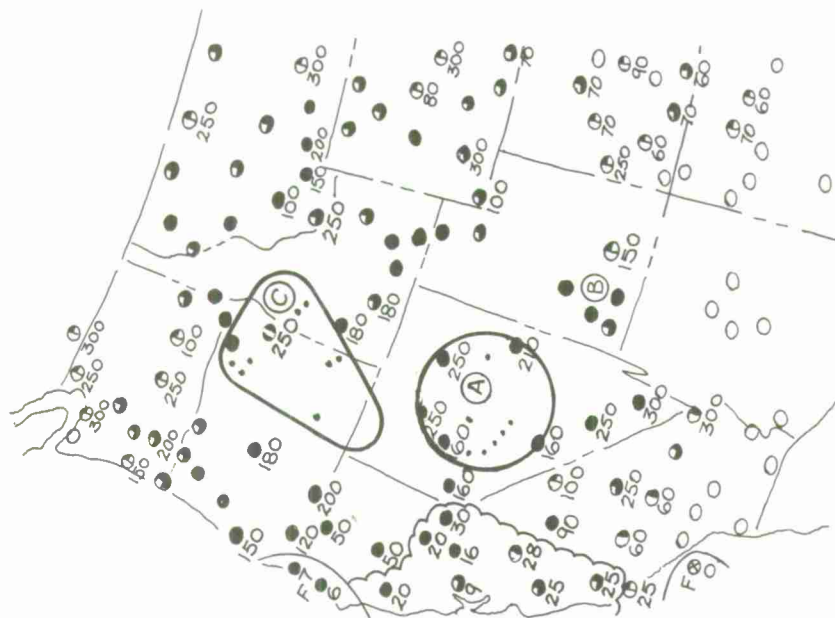
c. National Meteorological Center Weather Depiction Chart 2200 GMT May 2, 1971. Cloud bases in hundreds of feet.
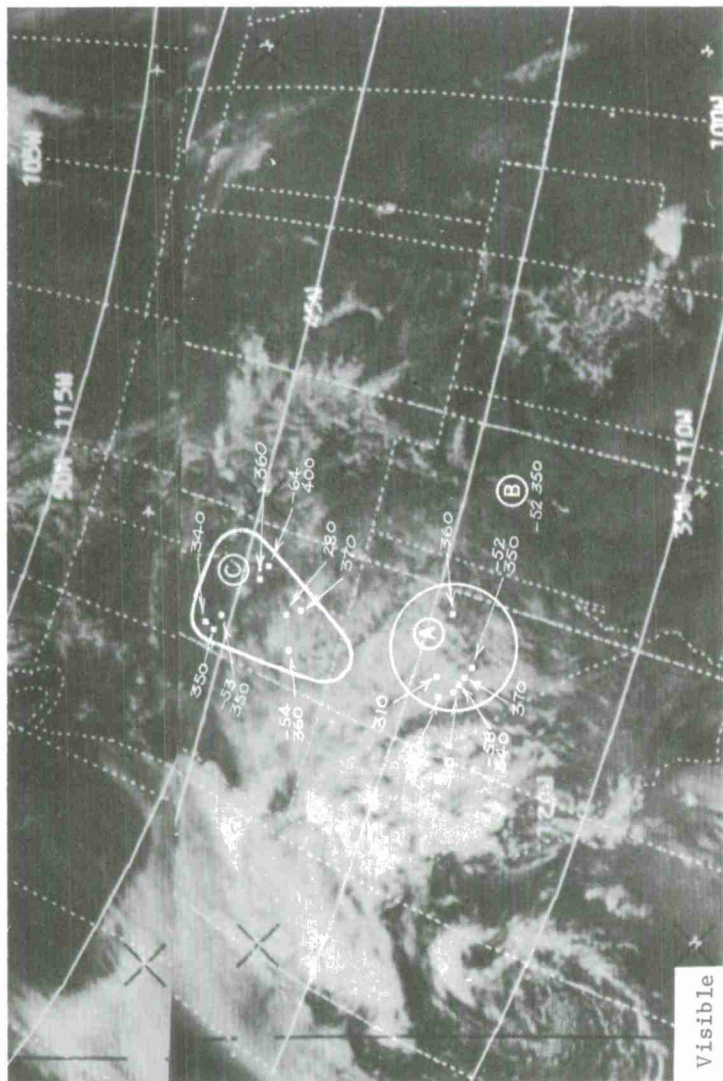
Visible

b. NOAA-1 1785-4, 5 Visible (TV) 2203 GMT May 2, 1971

Figure 6-B-5a, b, c. Variations in the brightness of cirrus clouds are well illustrated in these simultaneous daytime NOAA-1 IR and TV views (a, b). Special observations of cirrus cloud heights and temperatures were made at the time of this satellite pass. This information has been entered on the TV photograph, the corresponding points indicated on the IR data, and on the weather depiction chart (c). The height of the cirrus is indicated in hundreds of feet (three-digit group), and the cloud top temperature in °C. Notice that the brightness of the clouds ranges from near white around point A to dark gray around points B and C (6-B-5a), but aircraft reports indicate cirrus at about the same height at all three locations. This suggests that either the cirrus around point A is thicker than at points B and C or there are lower clouds beneath the cirrus at point A. The weather depiction chart shows a cloud base of 16,000 feet west of A which suggests that middle clouds are present in the area near where the infrared display is brightest. Only cirrus is reported at points B and C. The darker gray shade at B and C represents radiation from both the earth's surface and the high clouds.
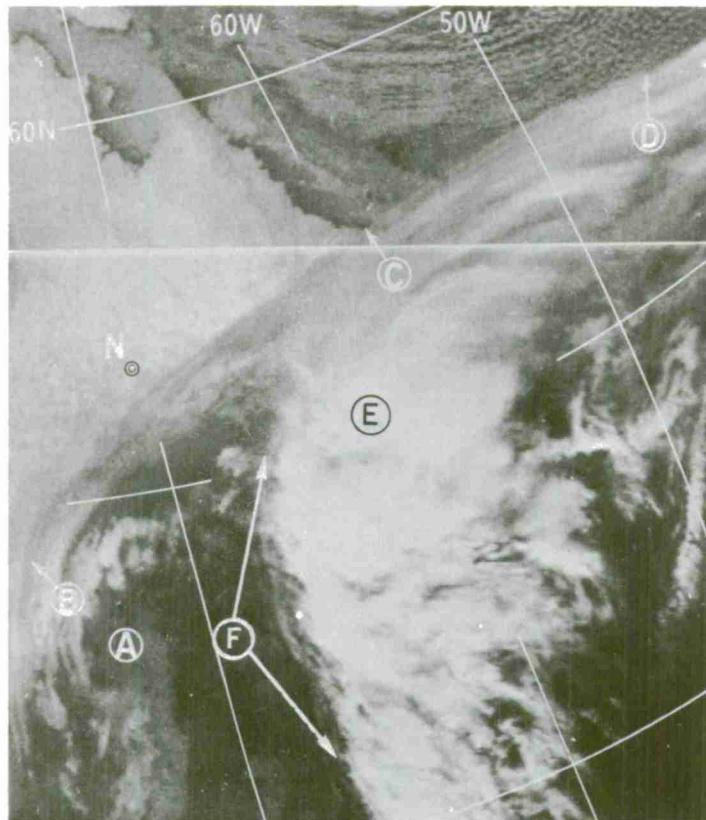
ITOS-1   4839 Nighttime IR   0840 GMT February 14, 1971

Figure 6-B-6.  This IR view of eastern Canada shows clouds associated with a
vortex centered at A.  A sharp cloud edge extends across the picture from B to
C to D.  From the coastline (C) westward, the cloud shield appears darker than
the bright clouds around E and the cloud-free snow to the north.  At first im-
pression, the dark gray clouds south of line B-C-D appear to be middle clouds
because their gray shade indicates that they are much warmer than the clouds
at E.  Radiosonde data showed that this gray cloud extended to 20,000 feet
where the temperature was -33°C.  The surface temperature at (N) north of the
cloud band was near -28°C.  Warm air advection was occurring between the sur-
face and 12,000 feet within the cloud band.  The warmest temperature was -10°C
at 8,500 feet, and -12°C at 12,000 feet.  Thus, the cirrus appears dark gray
because it is semi-transparent to the warmer radiation from below.  SR mea-
surements indicated that the temperature of the cirrus along and south of the
line B-C was -20°C, which would place the cloud tops at 14,000 feet, or 6,000
feet below the actual tops.  The temperature of the snow surface to the north
is the same as that at 500 millibars.  The edge of the jet stream cirrus is
indicated by F.  The coldest temperatures measured by the satellite were for
the cirrus south of the jet where the integrated temperature averaged near
-43°C (around E).  No reports were available to verify the actual cloud top
heights in this region.
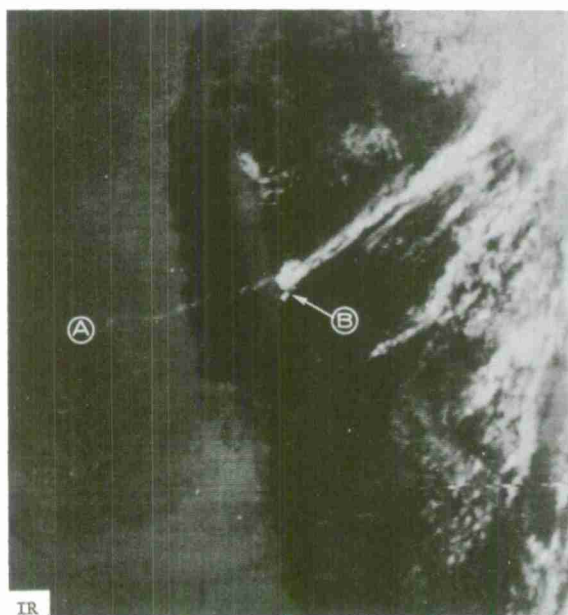
ITOS-1 2921 Daytime DRIR 2240 GMT
September 13, 1970
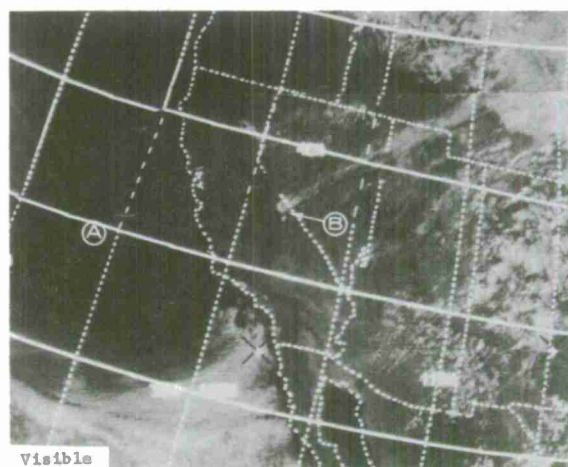
ITOS-1 2921-3, 4 Visible (TV) 2240
GMT September 13, 1970

Figure 6-B-7. Jet-associated cirrus in daytime IR and TV views of western
North America. A jet-associated band of high clouds extends northeast from
point A. This band is discontinuous and quite narrow for the first 400 miles
northeast of point A and is detectable only in the IR data. (The narrow por-
tion of the band was faintly visible in the original high quality video data,
but was noticed only after the infrared data were examined.) The band of
cirrus broadens abruptly at the Sierra Nevada range (B) because of mountain
effects. The broad portion of the band in the visible data is a dark shade
of gray and less conspicuous than the stratocumulus field in the lower left
corner of the TV picture. This same part of the band is much more obvious in
the IR imagery.

Figure 6-B-9a, b. These coincident views of the central United States show the advantage of IR in revealing multilayer cloud structure. The most obvious difference between the pictures is that a large dark area centered at A in the IR view is completely white in the TV view. In the TV picture the white area forms part of what appears to be a continuous and equally white cloud sheet that extends to the north of a line of thunderstorms in Oklahoma (B). A sounding at A showed that the tops of the clouds were 3,500 feet above the ground and were radiating at the relatively warm temperature of +13°C. Other soundings indicated that both cirrus and middle clouds were present between the thunderstorms (B) and the cloud edge (C, D). The cloud edge is clearly visible in the IR view but not in the TV picture, where it is barely perceptible. This cloud edge was not identified as such until the IR imagery was examined.

Two gray shades (E and F) appear in an area where soundings indicated the presence of middle and high clouds. The light gray shade at E suggests that cirrus is more likely here than at F where the clouds are darker but still sufficiently bright to be middle cloud.



ITOS-1  4790 Nighttime IR  0850 GMT  Feb. 10, 1971

Figure 6-B-8. This infrared image shows anti-cyclonically-curved, jet-associated cirrus off the east coast of North America. A polar jet stream lies just to the west of the cloud band A-B. The cold, high clouds contrast well with lower clouds at C and with the cold water at D. Transverse bands, which appear in the region of strong horizontal shear along the poleward edge of the high clouds, are observed in both the visible and infrared imagery.

Figure 6-B-9b. ITOS-1 2920 Daytime IR 2045 GMT
September 13, 1970
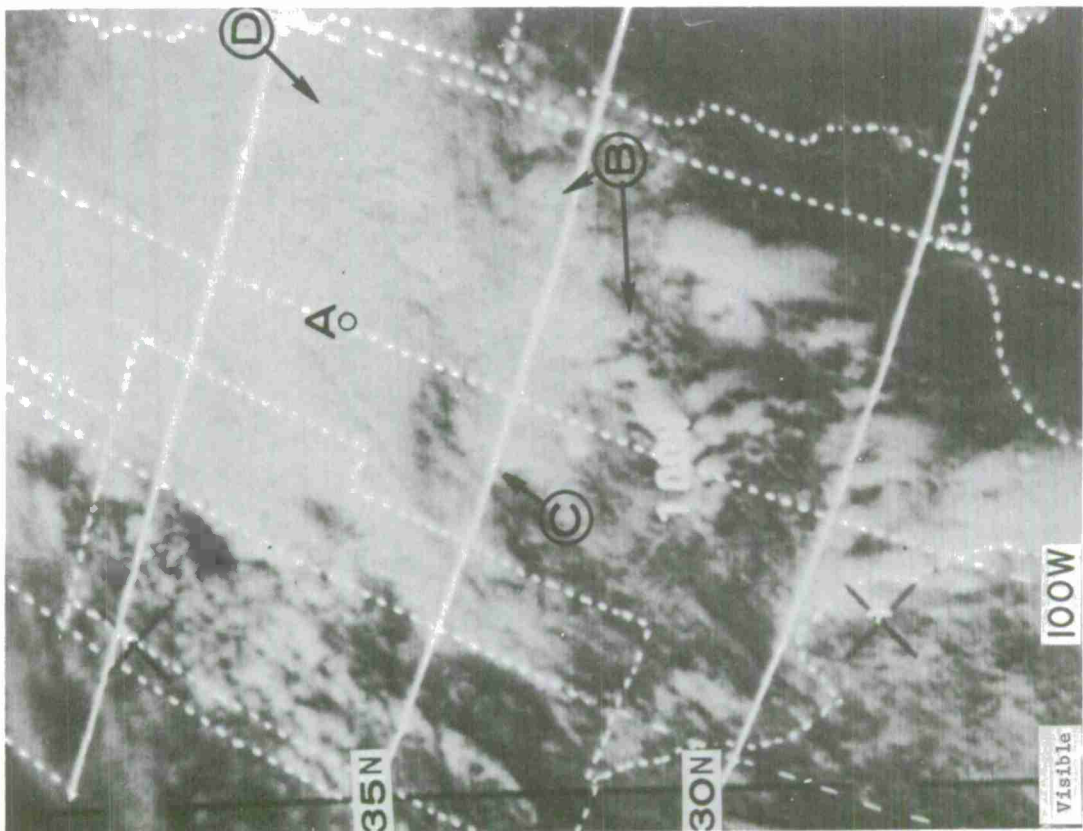
Figure 6-B-9a. ITOS-1 2919-4 Visible (TV) 2045
GMT September 13, 1970

Visible

Figure 6-B-10b. ITOS-1 4908-2, 3 Visible (TV)
2030 GMT February 19, 1971



Figure 6-B-10a. NOAA-1 882 Daytime IR 2000 GMT
February 19, 1971

There are several striking differences between the IR and the visible images of this storm. The areas of middle and high clouds are much more readily identified in the IR view. The combination of cirrus and middle clouds produced by the thunder-storms along the warm sector squall line (A, B) and at the cold front (at C), make these areas of strong convection stand out clearly in the IR.

Most of the middle cloud generated by this storm is covered by higher cirrus. Only small areas of middle cloud are viewed directly by the satellite. The narrow cloud band (D in 3a) which lies across eastern Arkansas appears as an intermediate shade of gray. Surface reports showed this to be only middle clouds. Otherwise, middle cloud occurs in conjunction with cirrus and cannot be positively identified. Outside the thunderstorm and rain areas, the clouds are brightest where cirrus and altostratus, cirrus and altocumulus, or all three in combination, were reported. On the extreme eastern and northern periphery of the cloud system, where no middle cloud was present, cirrus alone appears as a dark gray shade in the IR. This cirrus is not detectable in the visible but can be identified in the IR.

Within the precipitation area, (heavy broken line, 3c) there is a considerable variation in brightness in the IR which is not evident in the visible. The darker portions very likely represent areas where either no precipitation was occurring or the precipitation was from very low clouds and insignificant in amount. This could not be verified due to sparseness of surface reports.



Figure 6-B-10c. NOAA-1 882 Daytime DRIR 2000 GMT February 19, 1971

Figure 6-B-10a, b, c. Parts a and b of this figure show an intense winter storm in both the IR and the visible. Part c shows the surface fronts and a cloud and precipitation analysis superimposed over the IR image. The cloud types are based on surface reports and an analysis of the radiosonde data nearest in time to the pictures. The satellite image was used to define precisely the boundaries of the general cloud areas. The precipitation envelope (heavy broken line) encloses all stations where precipitation was occurring at the time of the picture and is based on reports from the synoptic network.

## Cumulus

Convective clouds are similar in appearance in both infrared imagery and in
television pictures. The shapes and patterns which serve to identify cumuli-
form clouds in the visible are usually present in an IR display. In a TV
picture, a large cloud mass with imbedded convection has a bumpy, uneven
appearance when shadows are present. The same cloud mass viewed in the IR
has a similar texture resulting from the contrast between the colder (whiter)
tops of the convective clouds with the somewhat warmer (grayer) tops of the
main deck of clouds. The strength or vertical extent of cumulus convection
appearing in television pictures can be determined by estimating the relative
brightnesses of the cumulus and by measuring or estimating the sizes of their
shadows at a given latitude. Cumulus clouds with the brightest appearance
and the largest shadows extend high into the atmosphere and indicate the
presence of areas of vigorous convective activity. The strength of the con-
vection and vertical extent of cumulus clouds in IR imagery is determined
from the brightness (radiant temperature) of the cloud. The smallest, lowest,
and therefore, warmest cumulus are gray while convective clouds having more
vertical development appear as brighter (colder) areas.
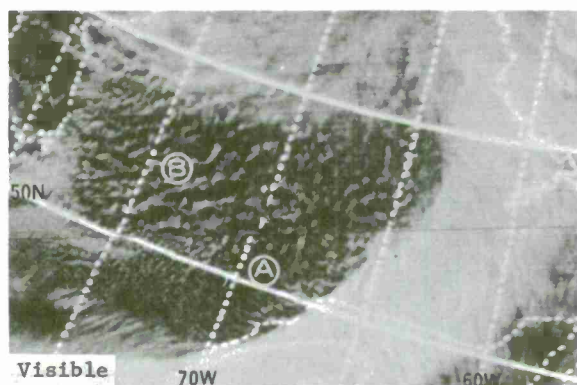


ITOS-1   2918-3 Visible (TV) 1900 GMT     ITOS-1   2918 Daytime DRIR   1900 GMT
September 13, 1970                         September 13, 1970
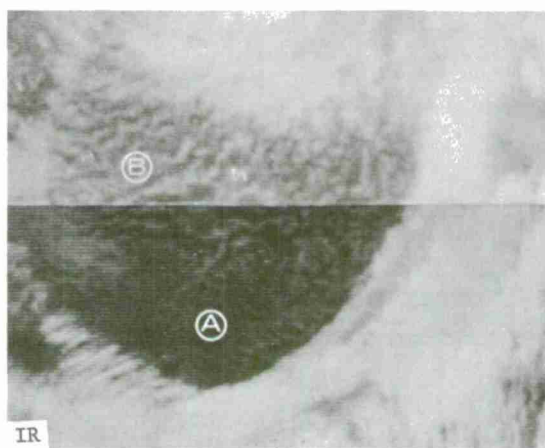
Figure 6-B-11. A cellular cloud pattern behind a cold front. The front is
located over the Maritime Provinces of Canada. The cellular pattern is com-
posed mainly of cumulus and cumulus congestus and has a similar appearance
in both the IR and visible imagery. The moderately gray aspect of the pattern
at A in the IR indicates the clouds here are lower than those at B where the
cloud elements are both larger and whiter.
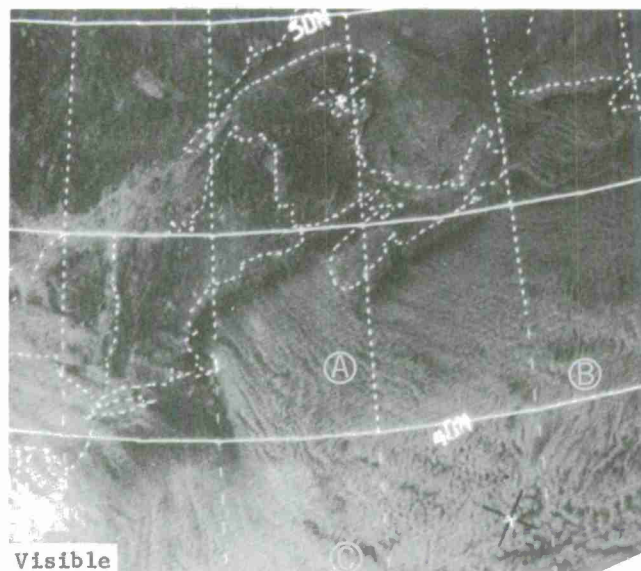
ITOS-1  4707-1 Visible (TV) 1900 GMT  Feb. 3, 1971

Figure 6-B-12.  This TV picture shows cumulus in lines (A), formed as cold continental air moves over the Atlantic Ocean east of Nova Scotia and New England.  Further east (B) the cumulus are organized in a cellular cloud pattern.
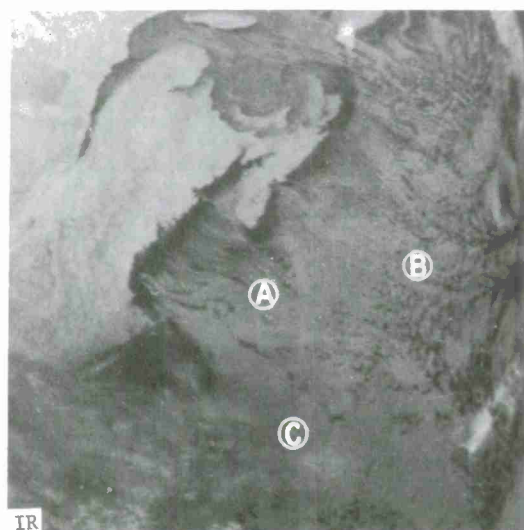


ITOS-1  4715 Nighttime IR  0900 GMT  Feb. 4, 1971

This DRIR display of the same area, taken 14 hours later, shows the same line structure near A and also the cellular cloud pattern further east (B).  Compare the irregular cumuliform appearance at A with the uniformly gray strato-cumulus clouds to the south (C).  The medium gray shade of the cumulus and stratocumulus in the IR indicates relatively low cloud tops.

6-B-15
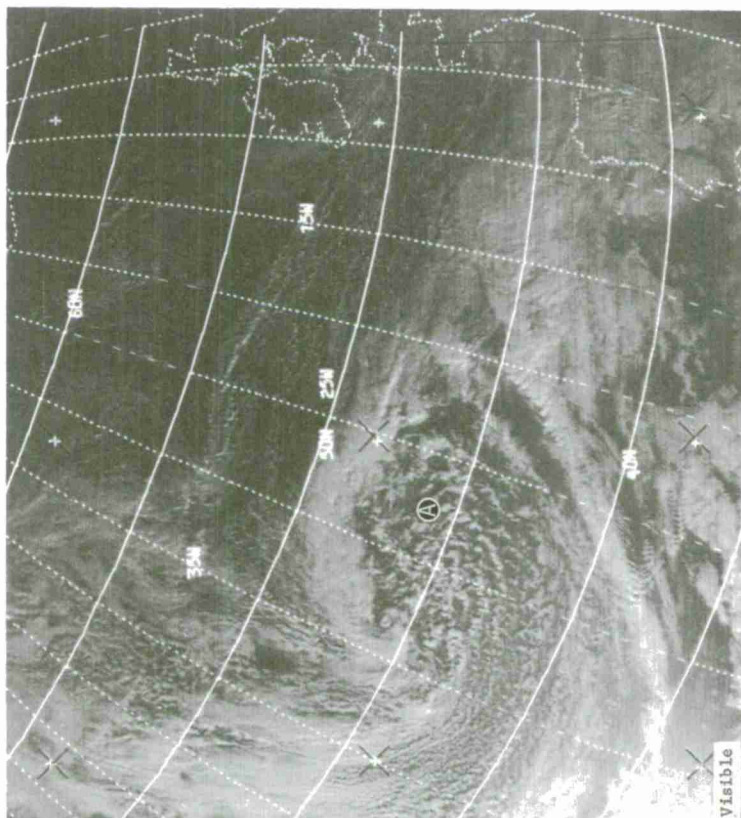
ITOS-1  4593-1 Visible (TV)  1615 GMT  Jan. 25, 1971

ITOS-1  4589 Nighttime IR  0710 GMT  Jan. 25, 1971

Figure 6-B-13.  This video picture shows a vortex and frontal band.  The cellular cloud pattern indicates cold air advection and cyclonic flow in the lower levels behind the front.  The larger cumuliform cloud elements (A) represent a region of maximum upward vertical motion in advance of a vorticity center.

The IR image of this vortex nine hours earlier shows the same general pattern.  The cumulus clouds (A) in advance of the vorticity center are brighter than the rest of the cumulus field because of their considerable vertical development.  This vertical development is more clearly determined on the IR image than on video pictures.
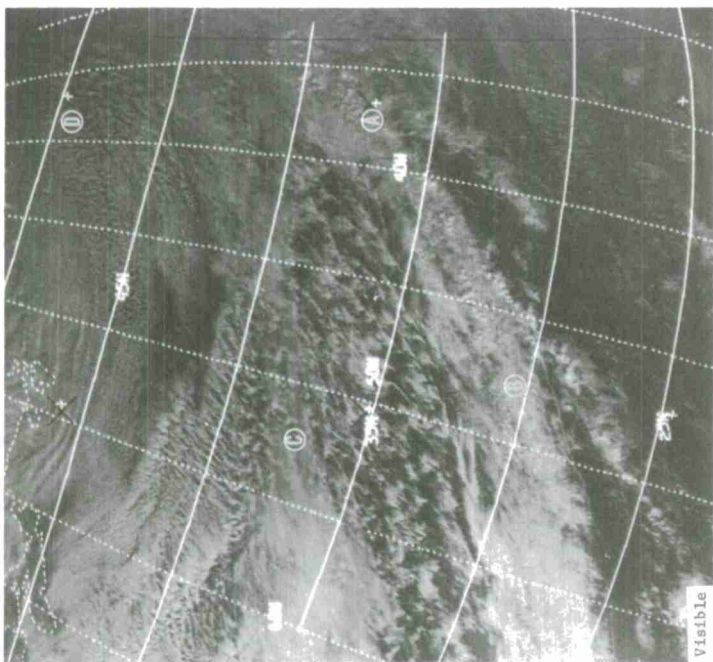
ITOS-1 4494-2 Visible (TV) 1815 GMT Jan. 17, 1971

Figure 6-B-14. Above is a television picture showing a cold front and a large area of cellular clouds over the north Atlantic Ocean. Highlights and shadows (A to B) in the southern portion of the cold front indicate convective activity imbedded in the frontal band. The field of cellular clouds around the vortex and behind the cold front have the normal pattern associated with cumulus clouds. In the vicinity of C, the cumulus are covered by thin cirrus; at D, cumulus have developed into towering cumulus and cumulonimbus.
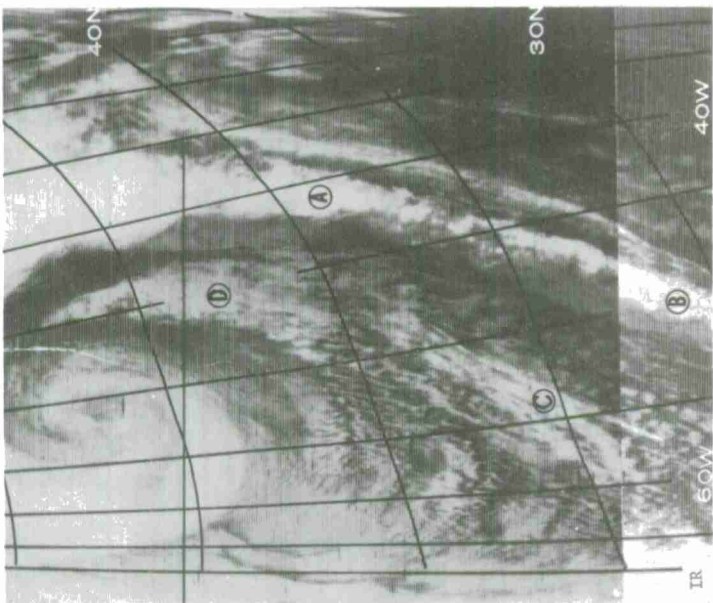


ITOS-1 4489 Nighttime IR 0715 GMT Jan. 17, 1971

This IR display, acquired eleven hours earlier, shows a vortex and the same frontal band. Bright areas (A to B) in the frontal band indicate thunderstorms. Areas of convection within the frontal band are more easily identifiable in the IR than in the visible. The cumulus in the cellular pattern behind the front are gray indicating tops lower than those of the white cumulonimbus along the front. The whiter area (C) indicates the presence of high clouds over the cellular cumulus clouds. Tops of the clouds at D, while somewhat higher than those of the cellular pattern, are not as high as those of the cumulonimbus embedded in the front.

6-B-17
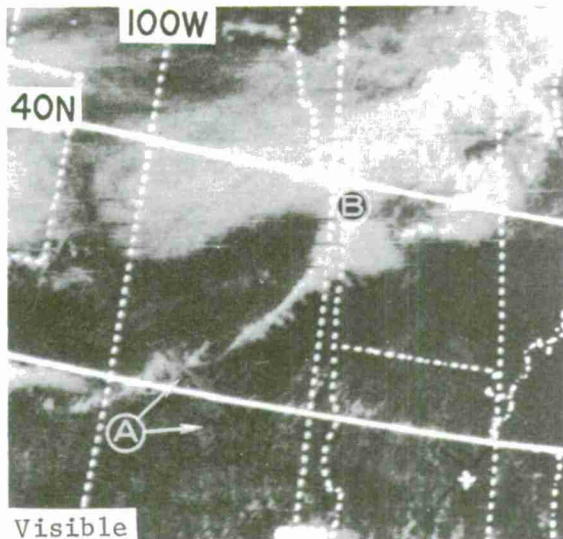
ITOS-1  2907-3 Visible (TV) 2130 GMT   ITOS-1  2907 Daytime IR  2130 GMT
September 12, 1970                      September 12, 1970
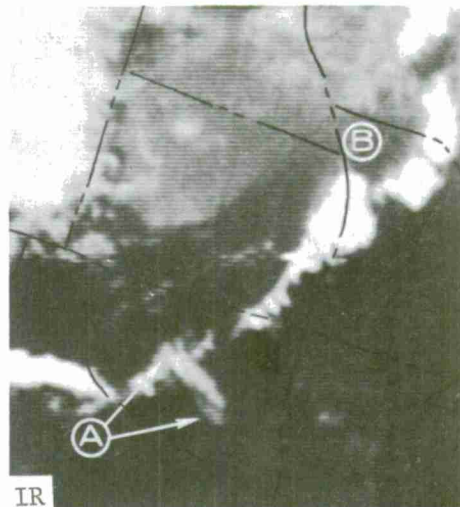
Figure 6-B-15.  The video display shows a line of cumulonimbus from Texas (A)
through eastern Kansas (B).  The cumulonimbus can be recognized by their
sharp western (windward) edges and fuzzy eastern (lee) edges, and their rela-
tive brightnesses.

In the IR display, as in the video display, the cumulonimbus have sharp edges
and fuzzy edges.  The cumulonimbus are the whitest (coldest) clouds in this
view.  The clouds over Oklahoma (A) are decaying anvils; this is suggested
by the gray response in the visual and nearly white shade in the IR.  The
cumulonimbus in western Missouri (B) are very bright in both the visual and
the IR; this indicates an area of active thunderstorms.
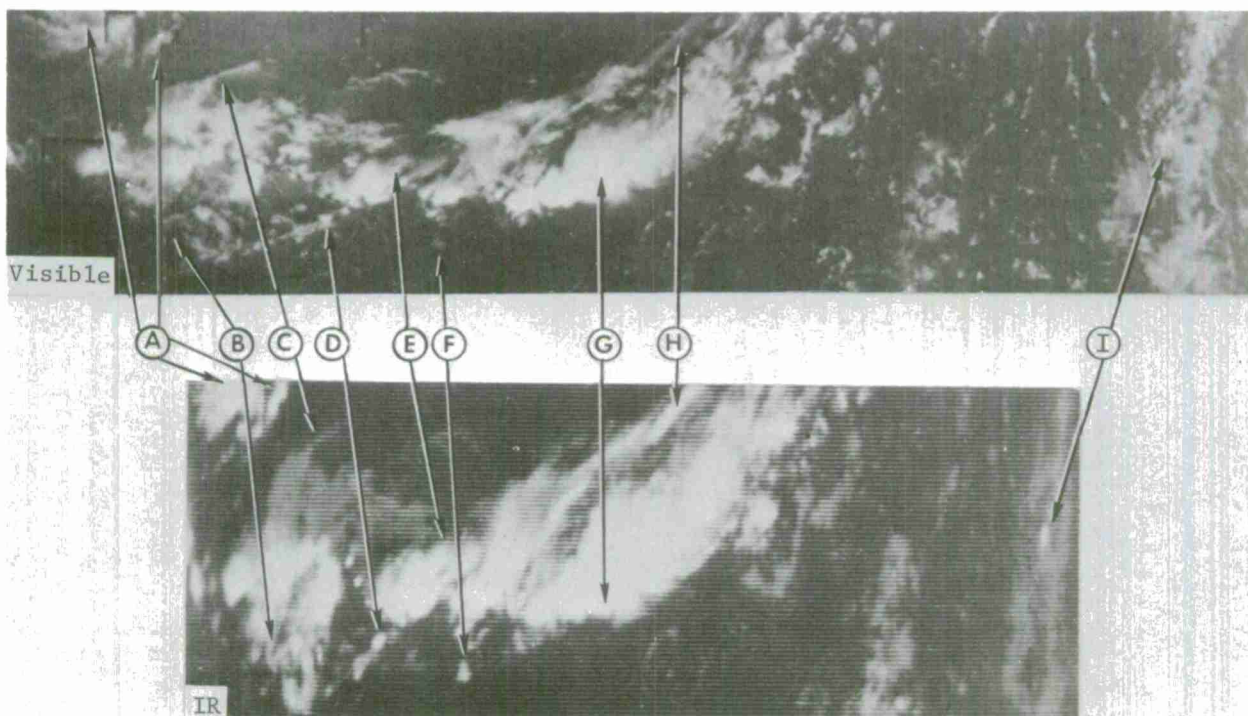
ITOS-1   2806 Visible (TV) - top, Daytime IR - bottom, 1830 GMT   Sept. 4, 1970

Figure 6-B-16.   A comparison of concurrent video and IR data of cumulonimbus activity along a front (49).   Of particular interest is that the cirrus originating from the cumulonimbus are more detectable in the IR than in the video.   This is evident at points A, B, and F, and between points E and H. In the visible the cirrus is gray or not seen, while on the IR it is white. This simultaneous comparison of visible and IR data also permits differentiation between active cbs and dead cb anvils.   For example, at G, the clouds are equally bright on both displays.   This indicates active cb clouds with cold tops.   At D and F, the clouds are nearly equal in brightness on the IR but in the visible, the element at F is darker than the one at D.   This indicates the element at D is an active cb while the one at F is a dead anvil. The cb at point I is detectable in the visible data but somewhat masked by the surrounding clouds.   It is much more easily detectable in the IR display.
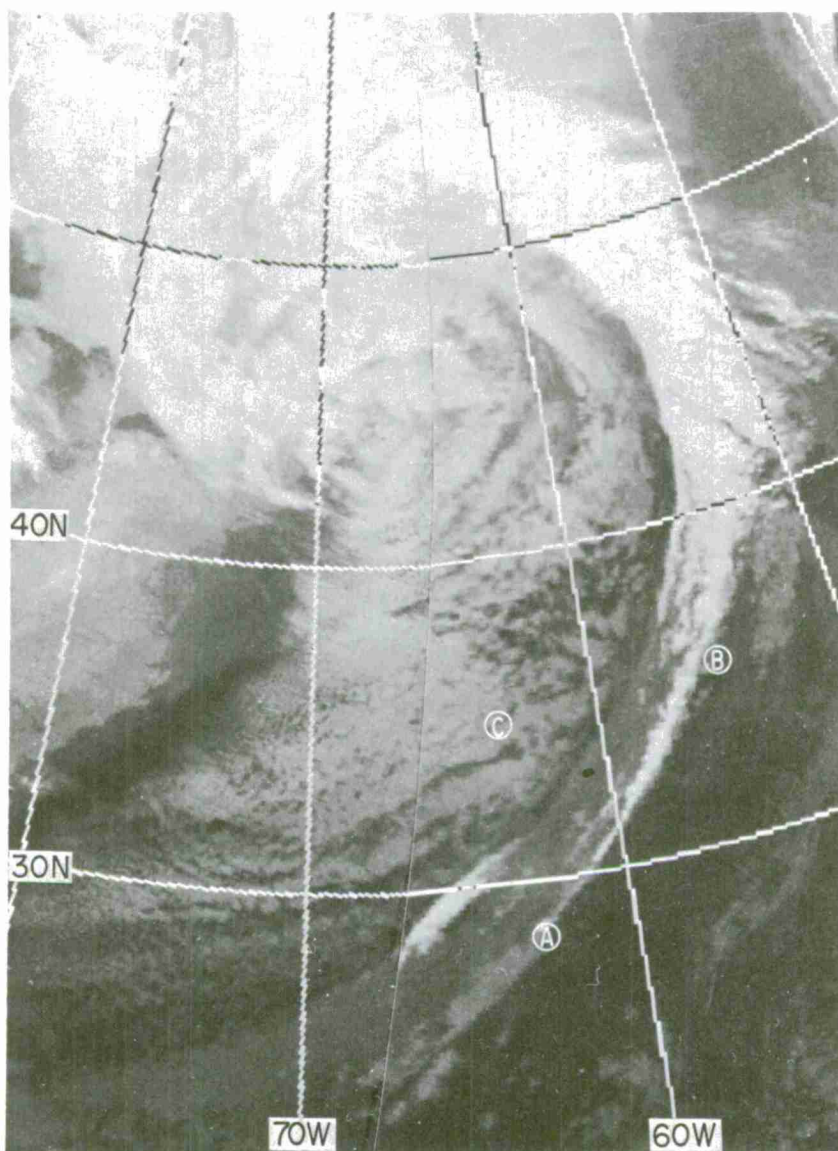
ITOS-1   5076-5077 Nighttime IR   0830 GMT   March 5, 1971

Figure 6-B-17.  This mapped direct-readout infrared display shows a large
area of convective cellular cumulus clouds east of North America and a narrow
line of cumulonimbus clouds, from A to B, along the leading edge of a broader
band of clouds associated with a cold front.  The brightness values of the
different cloud patterns indicate their relative heights.  The line of cumulo-
nimbus in the front southwest of B are the brightest and hence the highest;
the cellular convective clouds (C) to the rear of the front are much grayer
and lower, but still higher than the dark gray part of the frontal band to
the rear of the thunderstorms.

ITOS-1  2769 Visible (TV) - top, Daytime DRIR - bottom, 1900 GMT
September 1, 1970

Figure 6-B-18.  A comparison of concurrent video and IR data of fair weather
cumulus over Pennsylvania.  The fair weather cumulus in the video (A) appear
light gray, individual cloud elements are too small to be resolved.  In the
IR the fair weather cumulus (A) is barely detectable and appears as a faint,
slightly whiter (cooler) area than the surrounding terrain.  The relatively
warm tops of these clouds plus radiation from the warm ground combine to
produce this dark gray image.  In this IR image it is difficult to distinguish
between the cumulus field and the variations in gray shade produced by tem-
perature variations of the terrain.

## Fog and Stratus

A fog or stratus layer appears as a smooth, fairly uniform area, slightly
gray or milky in color in satellite cloud photographs.  In video pictures,
the edges of fog or stratus are often sharp and distinct; the clouds termi-
nate abruptly along mountains or coastlines or along a wind shear line in the
low levels.  The sharp edges of fog and stratus over land are not as easily
detected on nighttime IR displays because the temperature contrast between
the fog or stratus and its surroundings are less at night than during the day.
If a strong surface inversion is present at night the tops of the fog and
stratus radiate at warmer temperatures than does the surrounding terrain.
Thus the fog and stratus region appears darker than the surrounding cloud-
free region.  In IR imagery this phenomenon is referred to as "black fog" or
"black stratus".

At times, the temperature radiated by the top of the fog or stratus layer
will be nearly the same as that of the surrounding terrain.  This produces
an infrared display in which the top of the cloud layer and the adjacent
terrain are the same gray shade.  Such areas of thick fog and stratus will be
devoid of landmarks such as coastlines, rivers, and lakes.  One must be fa-
miliar with the topographical features which normally appear in a cloud-free
IR display to be able to determine the distribution of fog and stratus over
a region where terrain and fog are at equal temperatures.

If the fog and stratus appear lighter (cooler) than the surrounding area at
night, the fog and stratus must be thick and may contain some internal or
induced convection.  Drizzle may be falling at the surface in these regions.
Stratocumulus clouds, not in a cellular pattern, and areas of cold water,
completely or partly surrounded by warmer water have an appearance very
similar to fog and stratus.  Thin fog reported in surface observations may
not be detectable in IR displays.
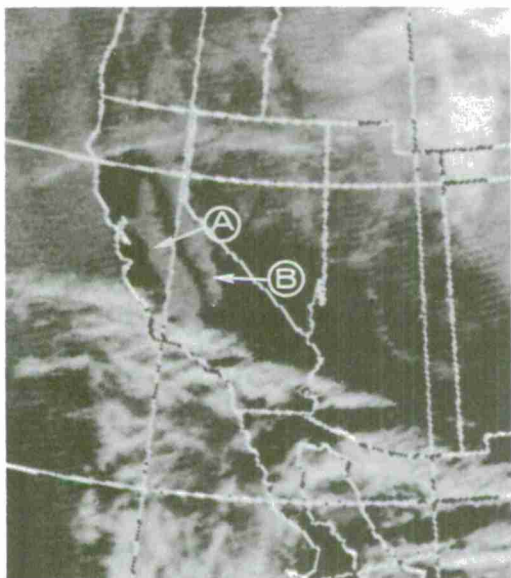


Figure 6-B-19.  This figure is an ex-
ample of a digitized daytime infrared
display showing fog and stratus in the
San Joaquin Valley of California (A).
The region is dominated by a stagnant
high pressure cell; under this condi-
tion, thick radiation fog and stratus
can form at night and persist through-
out the day.  The surrounding terrain,
with the exception of the snow-covered
mountain tops (B), appears black and
the fog and stratus appear a lighter
gray.  The fog and stratus are cooler
than the surrounding mountains which
are heated by solar insolation.

ITOS-1  4634 Daytime IR  2230 GMT
January 28, 1971
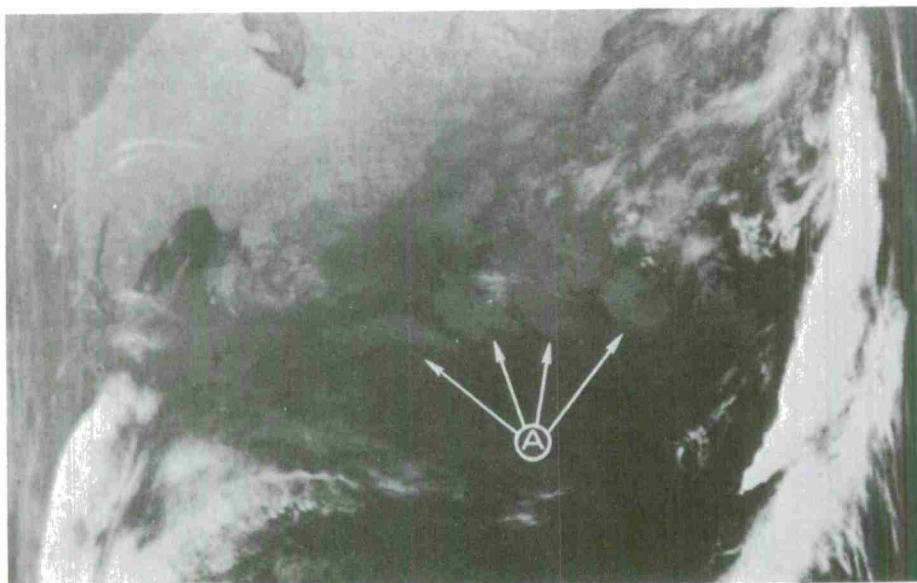
ITOS-1  4927 Nighttime IR  0830 GMT  February 21, 1971

Figure 6-B-20.  This nighttime IR display is an example of fog and stratus
(confirmed by surface observations) extending from northern Ohio to Massachu-
setts and Connecticut.  The fog and stratus (A) appear as a lighter gray
(cooler) in comparison to the surrounding area.  This indicates that the fog
and stratus in these regions are so thick that their tops are cooler than the
surface.  Some light precipitation was reported at the surface in these
regions.
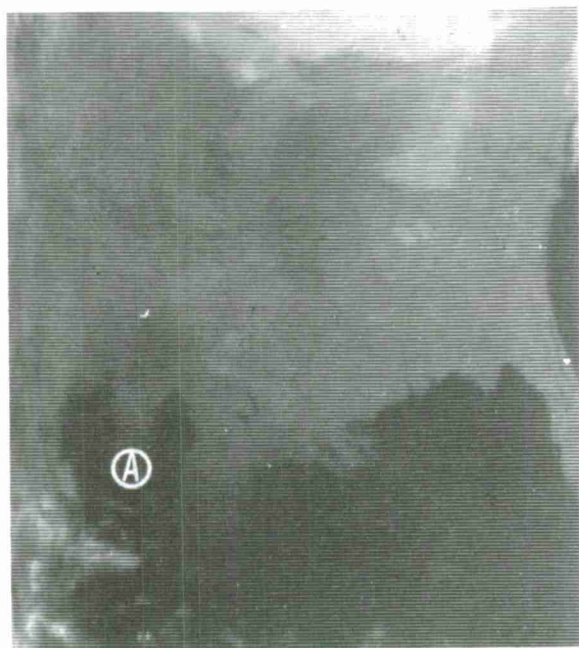


Figure 6-B-21.  This nighttime IR view
shows a good example of "black stratus".
The region of interest (A) is over
southeast Texas where warm moist air is
being advected northward from the Gulf
of Mexico.  The added moisture in-
creased the dew point sufficiently to
cause the formation of fog and stratus.
The surrounding cloud-free terrain is
a lighter gray (cooler) than the fog
and stratus region which is black
(warmer).  Black fog looks very similar
to a large inland lake or bay extending
inland from the ocean.  Therefore, one
must know or check terrain features
such as coastlines, rivers, and lakes
in the area of interest to make accurate
interpretations.

ITOS-1  4628 Nighttime IR  1000 GMT
January 28, 1971
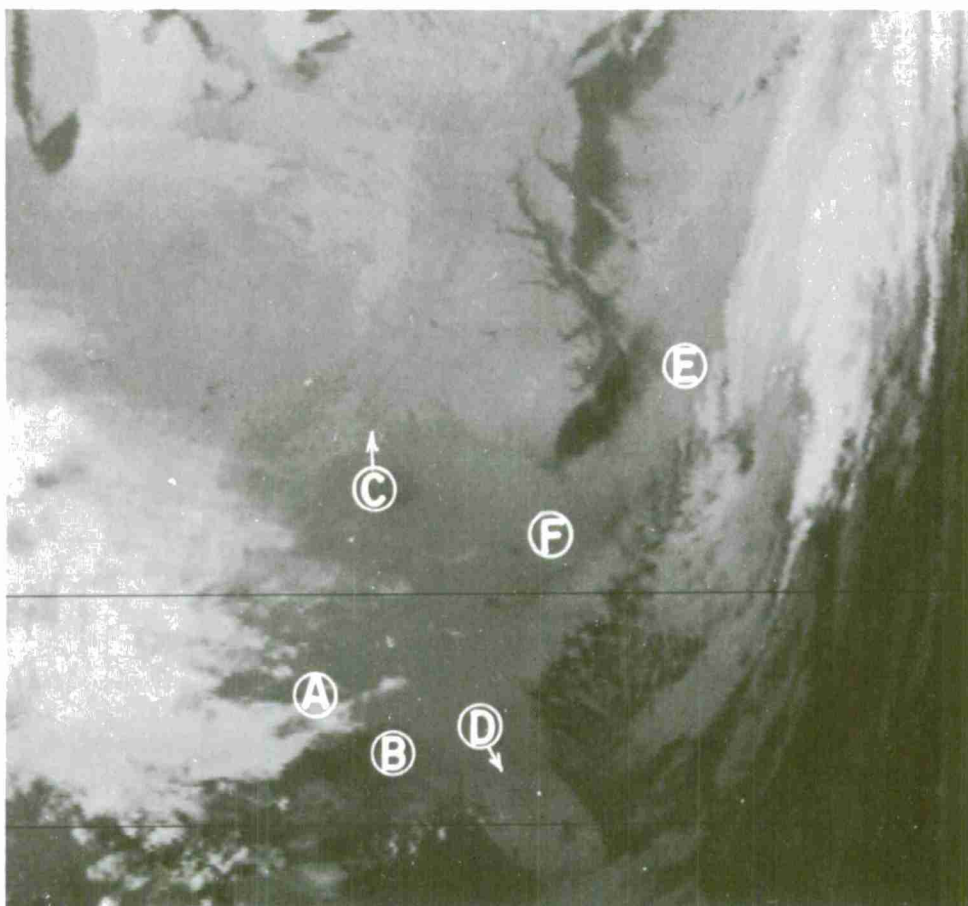
ITOS-1  4264  Nighttime IR  0830 GMT  December 30, 1970

Figure 6-B-22.  An extensive fog and stratus layer appears as a dark gray area
in the nighttime IR over the southeastern U. S. from North Carolina to central
Florida.  The temperature contrasts between the fog and stratus and its sur-
roundings are large at A and B and small at C and D.  At A, cold high clouds
sharply contrast with the warmer fog and stratus, while at B, the waters of
the Gulf of Mexico are warmer than the fog and stratus.  At C, a slight tem-
perature contrast is seen along the northern boundary of the layer where the
terrain is slightly cooler than the top of the fog and stratus.  The tempera-
ture contrast between the fog and stratus in central Florida (D) is minimal
so the gray shades of the land and clouds are similar.  The coastline of north-
ern Florida and Georgia and the rivers in northern Florida, Georgia, and South
Carolina are not detectable: this indicates the presence of a fog layer.  The
clouds from E to F appear similar in temperature to the inland fog and stratus,
but synoptic reports indicate that these clouds were stratocumulus rather than
fog or stratus.
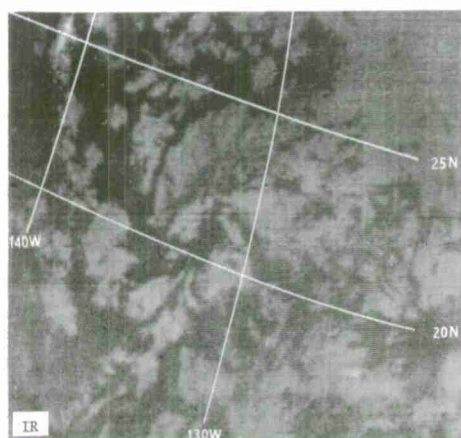
ITOS-1  2908 Daytime IR  0000 GMT        ITOS-1  2908-5 Visible (TV) 0000 GMT
September 13, 1970                        September 13, 1970
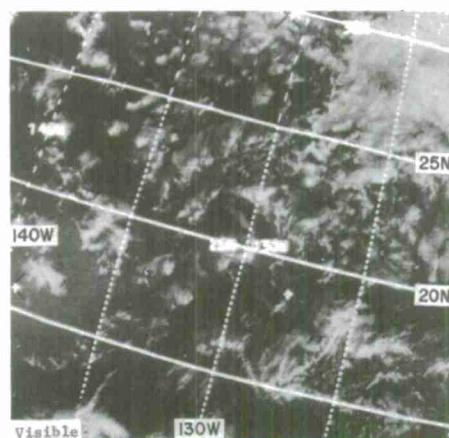
Figure 6-B-23.  These two pictures are concurrent IR and video views of stra-
tocumulus in a subtropical high over the eastern Pacific.  The same cellular
cloud pattern is evident on both views but the brightness values of the clouds
are quite different in the two displays.  The differences in brightness in the
TV picture are due to variations in the thickness of the cloud elements.
These differences in brightness are not visible in the IR because the tops of
the cloud elements are all at approximately the same height, are radiating
the same cloud top temperature, and apparently are not thin enough to trans-
mit warmer radiation from below.
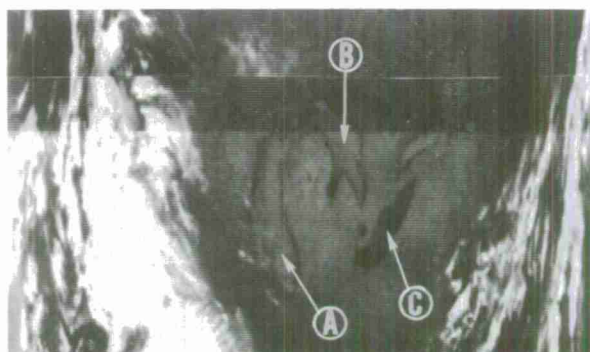




a.  ITOS-1 Nighttime IR 0846 GMT        b.  ITOS-1 Nighttime IR 0846 GMT June
    April 17, 1971                          10, 1971

Figures 6-B-24a, b.  These two nighttime IR displays show patterns similar to
fog and stratus.  In both examples, the areas of interest have clear skies and
the different gray shades represent the different temperatures of the surface
of the Atlantic Ocean and the Great Lakes.  In figure 6-B-24a, an early spring
case, the shelf water (A) is cool and appears dark gray, similar to fog or
stratus, in the IR.  An abrupt termination of the gray area is seen further
offshore along the western edge of the Gulf Stream.  The IR shows the warm
Gulf Stream water (B) as black.  The temperature contrast between the shelf
water and the Gulf Stream, indicated by U.S. Coast Guard Airborne Radiation
Thermometer measurements, is about 10°C.  In figure 6-B-24b, a late spring
view of the Great Lakes, the shallow waters along the shoreline and all of
shallow Lake Erie (C) have warmed and appear dark.  The colder waters of the
deeper portions of the lakes (A and B) have a lighter gray shade than the ad-
jacent warm waters and could be mistaken for fog or stratus.

## Earth's Surface

Coastlines, mountains, lakes, rivers, snow, ice, and ocean currents can all be detected in IR data displays. The larger the temperature difference and the steeper the gradient across the boundary of a surface feature, or between the feature and its surroundings, the more detectable the feature is. Temperature differences and gradients vary with latitude, season, and time of day. For instance, coastlines are seen most clearly in the summer daytime when land-sea temperature differences are at a maximum.

The gray shade contrast seen at a land-water boundary often appears to reverse at night. In daytime land may appear darker than an adjacent body of water; at night the water, although retaining approximately the same gray shade, appears darker than the land which has cooled by radiation and so appears lighter.

Some mountain ranges are easily detectable in IR imagery. Those with a large temperature difference between the top and lower adjacent land and those with steep slopes produce a strong temperature gradient visible in the IR image. The Sierra Nevada, which rises from near sea level, is more visible in IR imagery than the equally high and cold Rocky Mountains.

Snow-covered terrain usually appears whiter in the IR imagery than its surroundings. The brightness of a snow area depends, among other things, on whether there is vegetation within the area, on the type of vegetation, and on how much of the vegetation is snow-covered. Light snow on the tops of high mountain ranges is less detectable in IR than in TV visible data because the temperature difference between cold land and snow is small while the difference in albedo between snow and land is large.

To map areas of snow cover, it is necessary to distinguish snow from clouds. In the IR data, the clouds can be warmer than the snow-covered terrain, and appear as darker areas or they may be the same temperature or colder than the terrain and appear as bright as, or brighter than, the areas of snow cover. Except for terrain-induced cloudiness, clouds seldom persist in one location for more than a few hours. Therefore, snow fields can be identified by comparing data taken on successive days (See Chapter 5, Snow Cover and Snow Depth).

Sea-surface temperatures can be obtained from IR data where clouds are absent. Sharp temperature gradients along the edges of strong ocean currents such as the Gulf Stream can be seen clearly in IR imagery.

Figure 6-B-25. The most dramatic changes in IR imagery are produced by the diurnal variation of land surface temperatures, especially in the desert regions. Equally marked are seasonal changes in the polar regions*. These changes are illustrated in parts (a) through (d) of this figure which show

*See Section C, "Enhancement of IR Imagery to Compensate for Latitudinal Temperature Changes", for an example of how the mean surface temperature varies with season and how this can be compensated for on a display of mapped digital data.
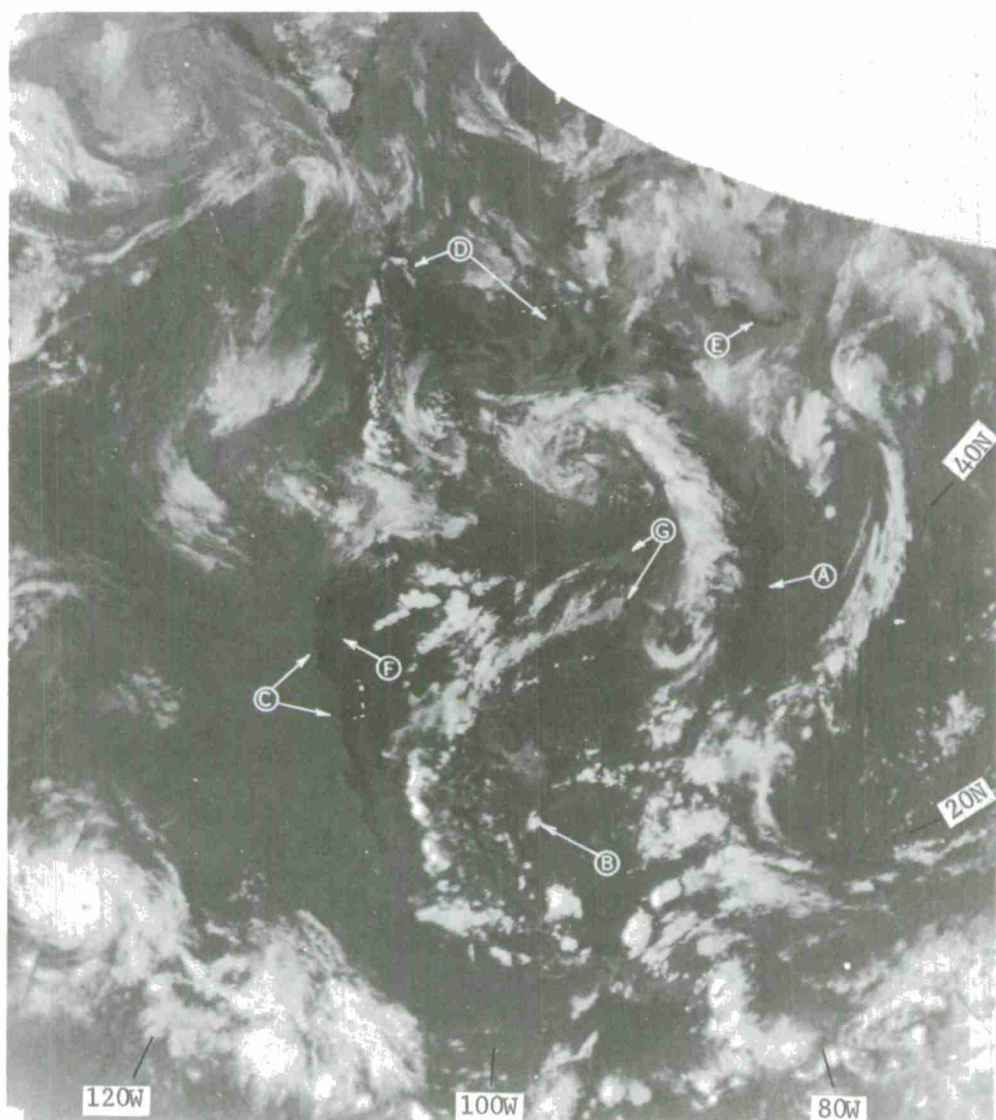
NOAA-1   Daytime IR   July 8, 1971

daytime and nighttime views of North America 12 hours apart for a day in July
and for a day in January. The pictures are IR data mapped digitally on a
polar stereographic projection. Grids have been omitted so coastlines can be
seen where present. Data for all four pictures are displayed within the same
temperature range but this range varies between equator and pole; at the
equator the temperature varies between +53°C (earth surface) and -86°C (high
cloud tops) and between +10°C and -42°C at the poles. Temperature compari-
sons can be made among all four pictures by comparing gray shades at the same
latitudes but not at different latitudes.


Figure 6-B-25a - Summer Daytime. More coastlines are visible in this picture
than in the three that follow. The east coast of the United States (A), the
Gulf Coast (B), the Mexican and California coasts (C), the northern coasts
of Alaska and Canada (D), and the Greenland coast (E), are all warmer than
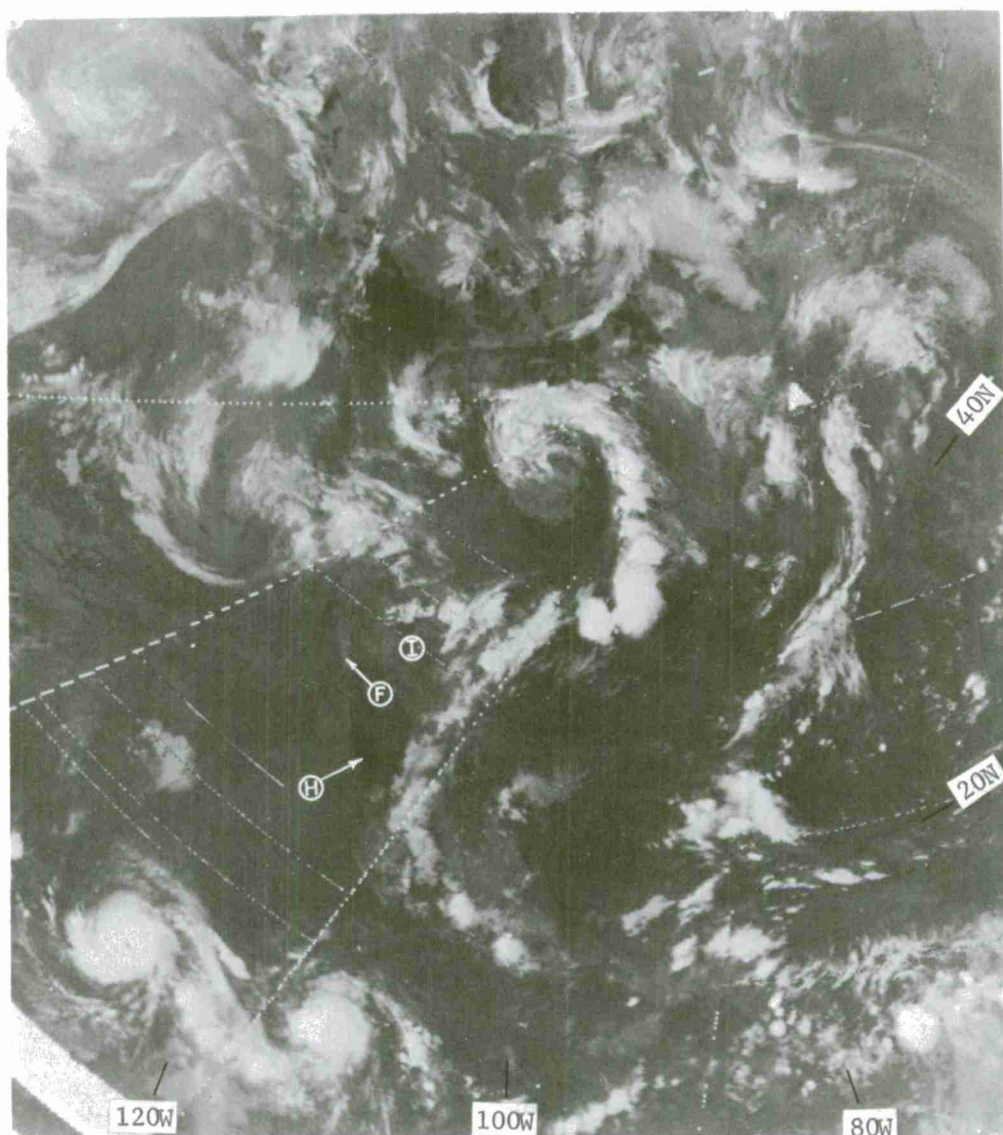
NOAA-1 Nighttime IR   July 8, 1971

the adjacent oceans and stand out clearly.  The high, cold Sierra Nevada (F)
is easily seen.  Lake Michigan and Lake Superior (G) are cooler than their
surroundings and can be identified where not obscured by clouds.


Figure 6-B-25b - Summer Nighttime.  In the summertime, the land forming the
coastlines of the United States cools to very nearly the same temperature as
the oceans; thus the coastlines are undetectable in the IR data.  Only the
warm waters of the Gulf of California (H) still provide enough contrast to
make the shoreline visible.  In the Arctic, land-water contrast changes little
during the 12 hours between the pictures, so the coastlines are equally visi-
ble in figures 6-B-25a and b.  At night, the Sierra Nevada (F) and the Rocky
Mountains (I) can be distinguished from warmer lower terrain.
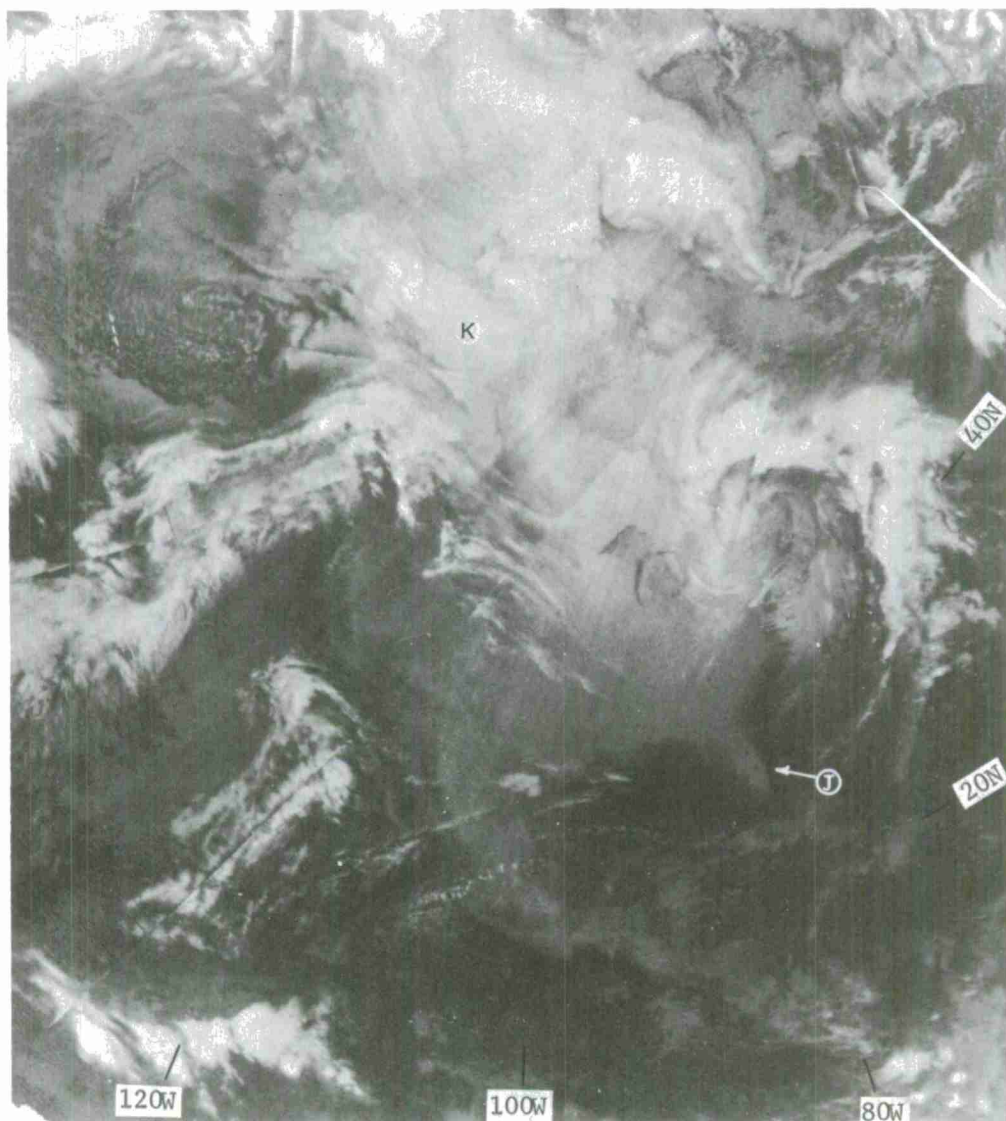
ITOS-1  Nighttime IR  January 27, 1971

Figure 6-B-25c - Winter Nighttime.  In a nighttime winter view, the coast-lines of the United States again become visible but now the cold land is grayer than the warm water.  The land-water contrast is greater along the east coast from Florida (J) northward.  The Arctic regions (K) appear quite bright with some snow surfaces radiating at temperatures as cold as middle and high clouds further south.  It is very difficult to differentiate between clouds and the earth's surface near the pole.  Compare this picture with the summer views of the same area.
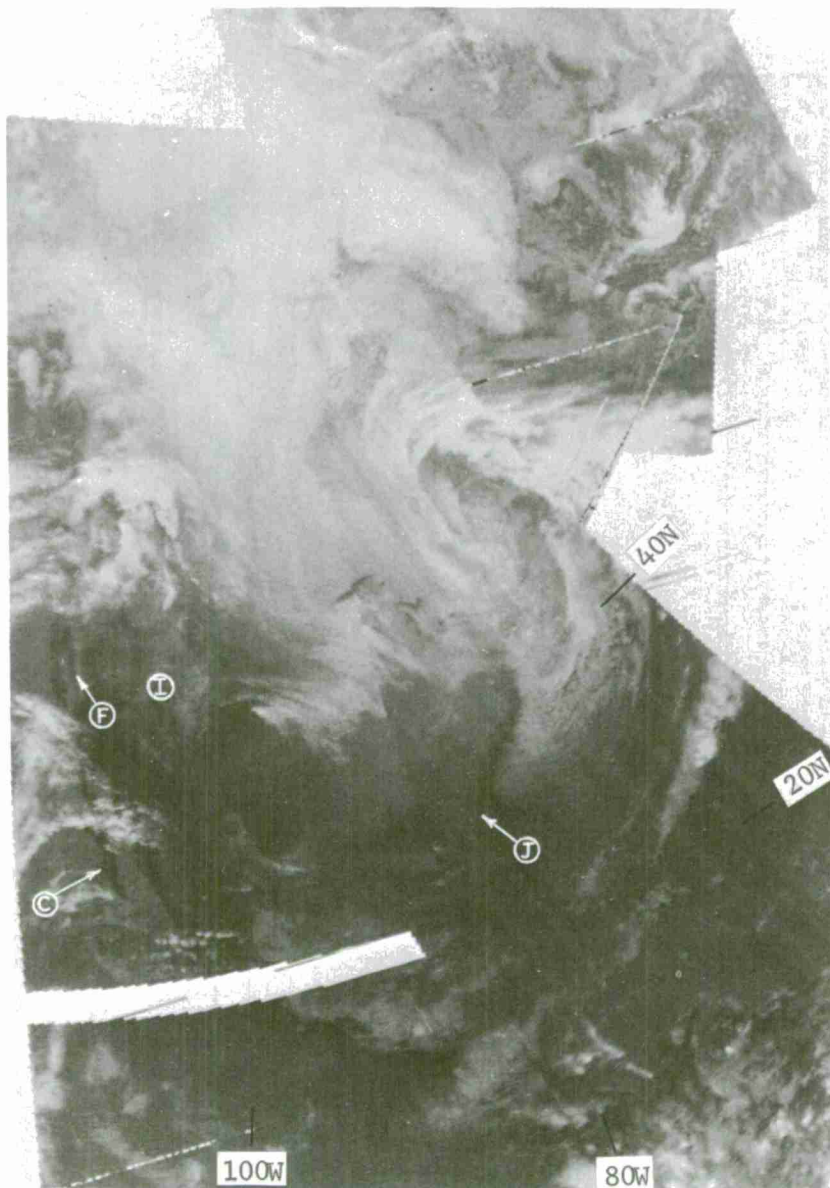
ITOS-1   Daytime IR   January 27, 1971

Figure 6-B-25d - Winter Daytime.   South of about 30°N, (note west coast of
Mexico, C) the land reverses shade with respect to the oceans as night be-
comes day.   To the north, as along the east coast of the United States (J),
the land remains colder than the offshore waters even in the daytime.   The
Rocky Mountains (I) and Sierra Nevada (F) appear colder than lower terrain.
The Arctic regions again appear the same for both times of day in the winter.
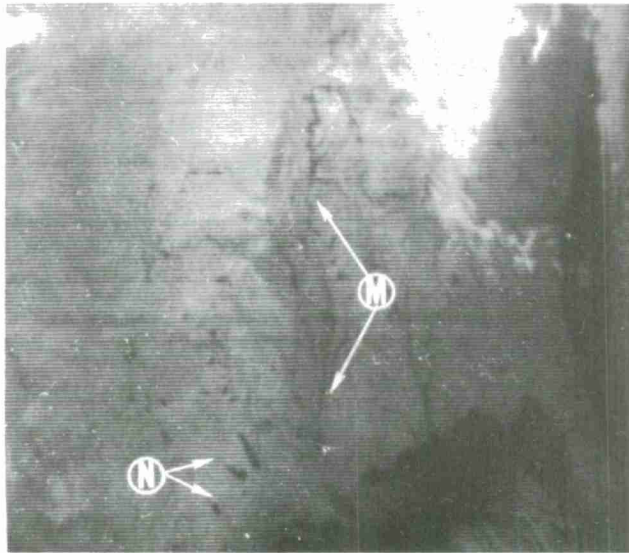
ITOS-1 5066 Nighttime IR  1020 GMT March 4, 1971

Figure 6-B-26.  Many water bodies can be identified in this nighttime IR image by their dark appearance.  The Mississippi River (M) and its tributaries produce a dark, thread-like pattern across the terrain.  A number of small lakes in eastern Texas can be seen at N.
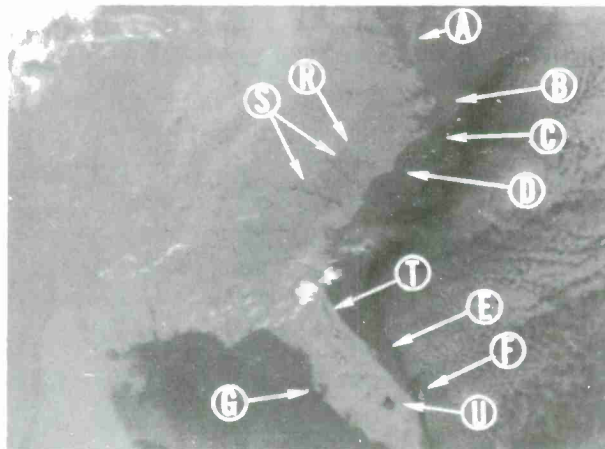


ITOS-1 5078 Nighttime IR  0920 GMT March 5, 1971

Figure 6-B-27.  This cloud-free nighttime view of the eastern United States shows the temperature difference between the warmer Gulf and Atlantic waters and the colder mainland.  The coastlines stand out clearly.  Some of the land forms seen are the Delmarva Peninsula (A), the inlets around Norfolk and Cape Hatteras (B), Cape Lookout (C), Cape Fear (D), Cape Kennedy (E), Cape Sable (F), and Tampa Bay (G).  Inland, a series of lakes and rivers (R, S) in South Carolina, the St. John's River (T) in Florida, and a large number of lakes stretching through central Florida to Lake Okeechobee (U) can be seen.  All these inland water bodies are warmer than the surrounding land so appear dark.
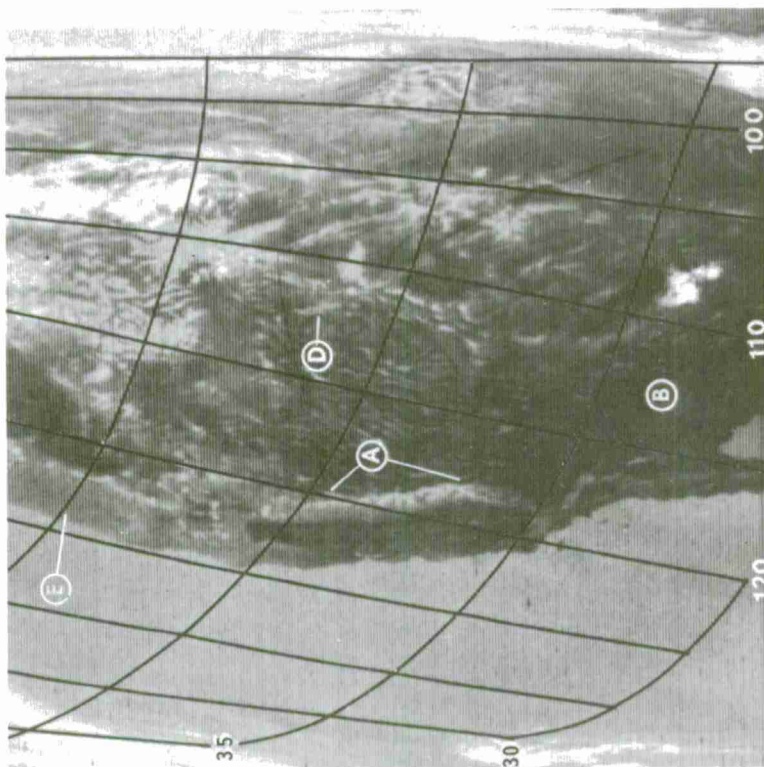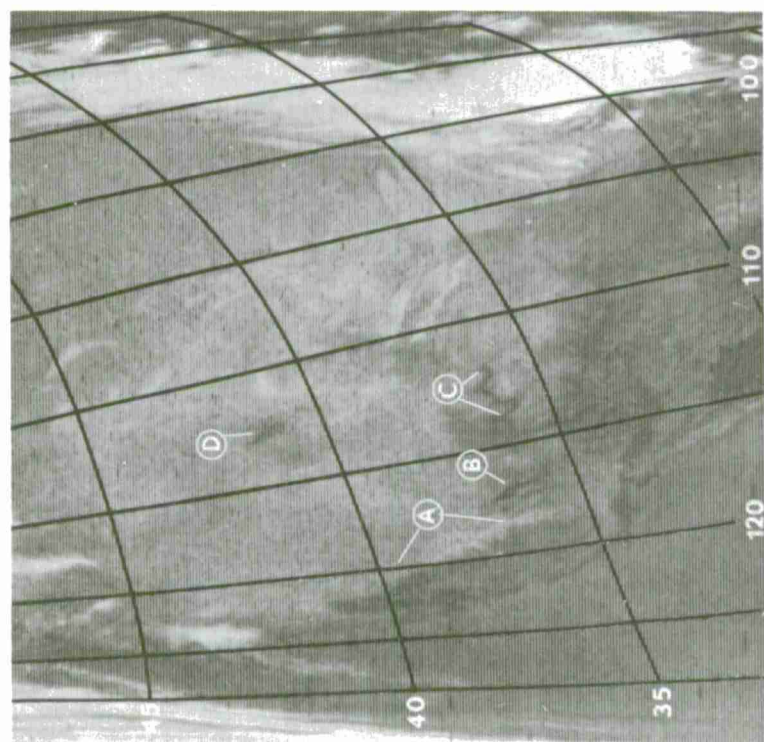
a. ITOS-1 1401 Nighttime DRIR 1030 GMT May 15, 1970  b. ITOS-1 1407 Daytime DRIR 2207 GMT May 15, 1970

Figures 6-B-28a, b. This figure shows both day and night IR views of the western United States. In the nighttime view, the slightly warmer coast of California can be distinguished from the adjacent Pacific waters between 34°N, 120°W and 40°N, 124°W. A more distinct temperature difference is seen between the colder Sierra Nevada (A), and the San Joaquin and Sacramento Valleys which lie west of this mountain range. Death Valley (B), the Grand Canyon (C) and the Great Salt Lake (D) appear as warm areas in this view. The daytime view of the same area clearly shows the coastline from Baja California to Washington. Note how the temperature of the terrain gradually changes with latitude; the warmest spot is near the Gulf of California (B) and the coolest is near Seattle (E). The snow-covered Sierra Nevada (A) and Rocky Mountain Ranges are easily distinguished from the lower, warmer terrain. The Great Salt Lake (D) is colder than the surrounding land masses.
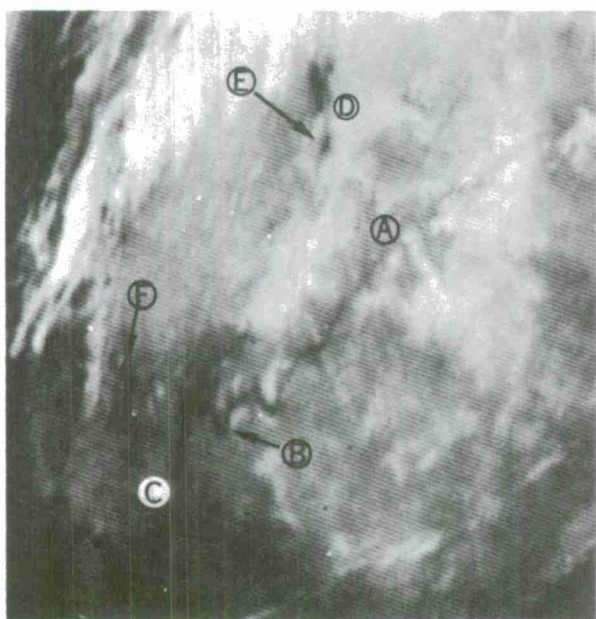
Figure 6-B-29. The most striking terrain feature in this nighttime IR view is the dark pattern of the Colorado River Valley (A-C) and the Grand Canyon (B). The temperature difference between the canyon rim and the valley floor is large during the night, sometimes as much as 14°C (50). This landmark appears in IR nighttime imagery equally well in summer and winter. The Great Salt Lake, Utah Lake, and Death Valley, all warm features, are seen at D, E, and F, respectively.

ITOS-1  5004 Nighttime DRIR   1120 GMT
February 27, 1971
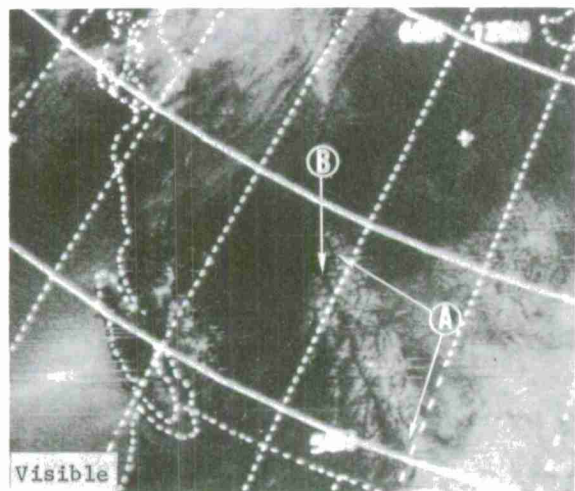


ITOS-1  2907-2 Visible (TV) 2152 GMT
September 12, 1970
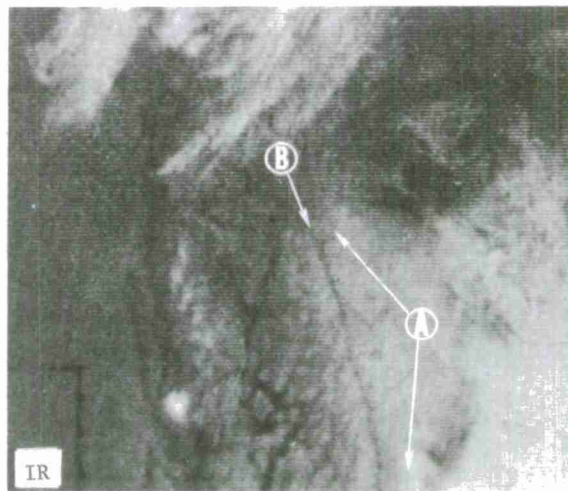


ITOS-1  2907 Daytime IR  2152 GMT
September 12, 1970

Figure 6-B-30. These are nearly simultaneous TV and infrared views of the snow cover on the Rocky Mountains in southwestern Canada (A). The TV view reveals the typical dendritic pattern of snow on mountainous terrain. The IR view shows a dendritic pattern which reflects temperature variations due to altitude. It is nearly impossible to identify the snow-covered terrain in the IR imagery in this example. The most obvious feature in the TV picture is the snow on the ridges; in the IR view it is the warm Columbia-Frazier River Valley which appears as a dark line running to the southeast of B.
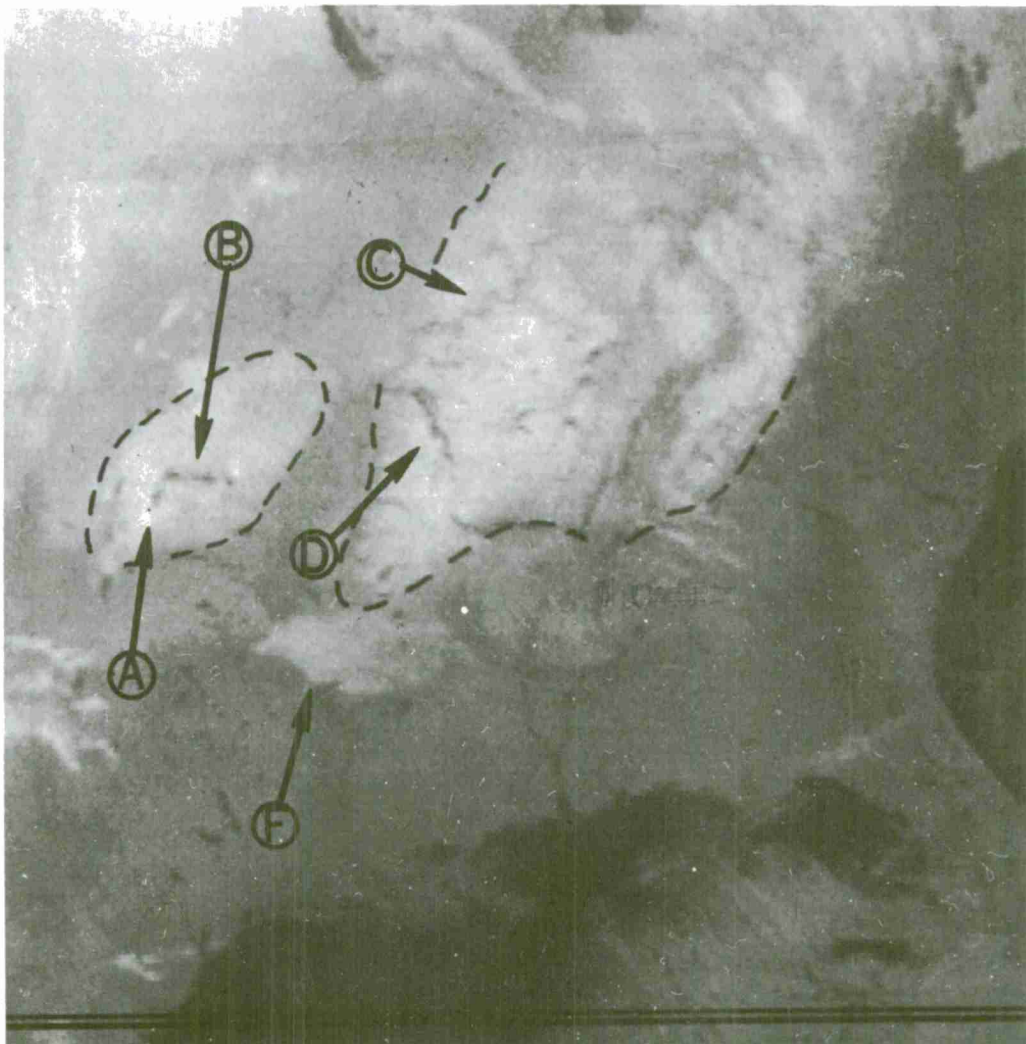
ITOS-1  4778 Nighttime IR 0900 GMT February 9, 1971

Figure 6-B-31.  Two areas of snow (outlined by dashed lines) are easily dis-
tinguished in this nighttime IR view.  The bright snow-covered Ozark Plateau
appears on the left.  One to four inches of snow were reported in this area,
but a heavier accumulation may be present at the higher elevations (A).  Ice-
free Table Rock Lake and Bull Shoals Reservoir are the dark areas at B.

The second area of snow stretches from Illinois southward to Tennessee and
eastward to the Blue Ridge Mountains.  The Ohio River (C), Kentucky Lake (D),
and numerous other lakes appear dark within the snow field.  The heaviest
snow accumulations are five to seven inches in the area northeastward from
Kentucky Lake.

The dashed lines show areas having an inch or more of snow.  Although the
gray area at F appears to be as cold as the one-inch snow field, this is not
snow but an area of clouds.  The presence of cloud is revealed by the absence
of visible terrain features such as the Mississippi River.
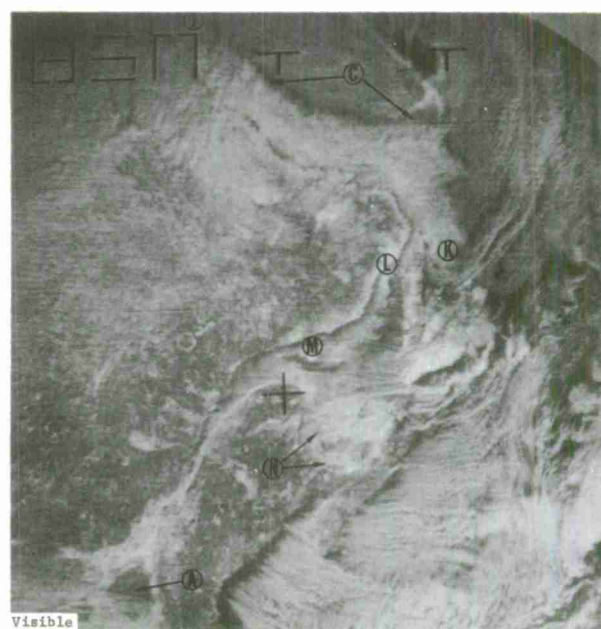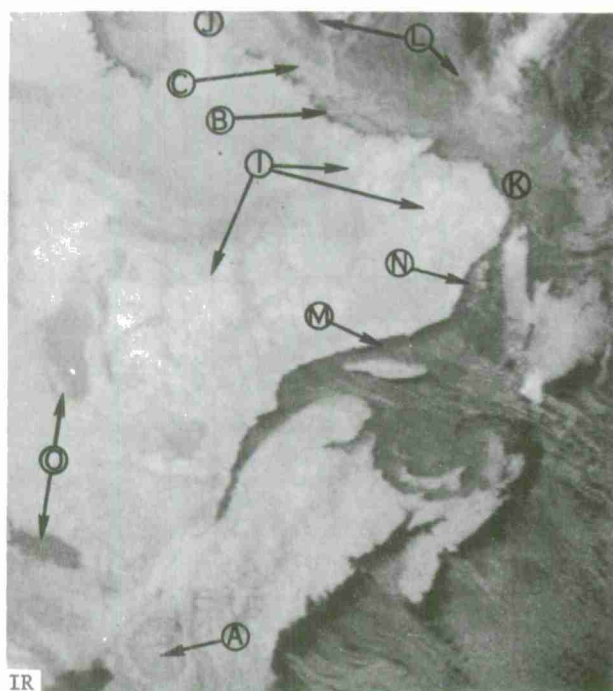
ITOS-1  4715 Nighttime IR  0900 GMT       ESSA-8  9791 Video  1435 GMT February
February 4, 1971                          3, 1971

Figure 6-B-32.  Shown here are views of snow-covered northeastern United
States and Canada.  The tree-covered Adirondack Mountains (A) appear dark in
both views compared to the snow-covered valleys which surround them.  The dark
appearance of the mountains is caused by the forests.  In the IR, the tree
tops radiate at a warmer temperature than the snow-covered ground; in the
visible, trees have a much lower albedo than snow.  In Canada, the higher
terrain of the Mealy, Hope and Otish Mountains (I) appear the brightest and
coldest.  The darkest areas (O) are fog and stratus.

The APT photograph shows the extent of the heavy pack ice along the coast of
Labrador (J-K).  Some ice can also be seen from the Strait of Belle Isle to
Anticosti Island (L-M).

In the IR view, the pack ice (J-K) appears to be at three distinct tempera-
tures.  The dark thin area (B) immediately offshore is an area of open water
or wind-driven and broken ice.  Further east (C), the ice appears whitest.
This is solid pack ice and is thought to be colder because of its heavy snow
cover and thickness.  Near the edge of the pack ice (L), the ice becomes
grayer.  Further south (near K), the pack ice appears warmer than the adjacent
land mass, and near the temperature of the cold air cumulus clouds to the
east.  A brighter area of pack ice can be seen near N.  The remaining ice-
covered areas from M-N appear warm, suggesting open water or wind-driven and
broken ice.
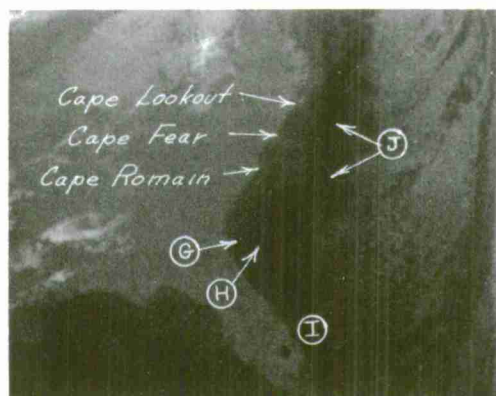
a. ITOS-1 4853 Nighttime IR 0900
   GMT February 15, 1971



b. Sea-Surface Temperature Analysis from
   Nighttime IR Data. ITOS-1, 4853,
   0900 GMT February 15, 1971.



c. ITOS-1 5078 Nighttime IR 0900
   GMT March 5, 1971
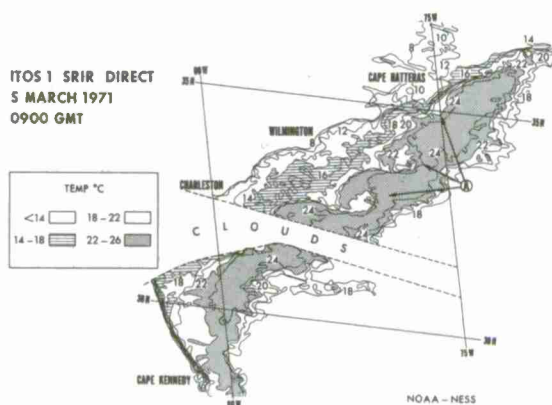


d. Sea-Surface Temperature Analysis from
   Nighttime IR Data. ITOS-1, 5078,
   0900 GMT March 5, 1971.

Figure 6-B-33a, b, c, d. The cold land area of the eastern United States, as
well as the slightly warmer offshore waters and the Gulf Stream are clearly
visible in these nighttime IR data.

Three offshore temperature fields can be seen in the IR gray shade display
(a). The coldest area at G marks the shelf water, the warmer water at H is
the intermediate slope water and the warmest area (I) is the Gulf Stream (51).

The two meanders in the Gulf Stream east of Cape Romain and Cape Lookout are
caused by cold water intrusions (J). The SR-measured sea-surface temperatures
for this area are shown in the detailed temperature analysis (b). The coldest
shelf waters were 8-14°C, the intermediate slope waters and meanders were 14-
22°C, and the Gulf Stream temperatures 26-28°C.

In the cloud-free IR view taken on March 5 (c), three cold eddies (A) can be
seen along the northern edge of the Gulf Stream (51).

These cold water eddies are easily identifiable in the SRIR sea-surface tem-
perature map (d). The detailed analysis shows that the warmer water has

completely surrounded the central eddy; the southernmost eddy is nearing the cut-off stage, and the northernmost eddy appears to be in the formation stage. These eddies occur in the region of strong shear between the relatively slow-moving slope water and the fast-moving Gulf Stream.
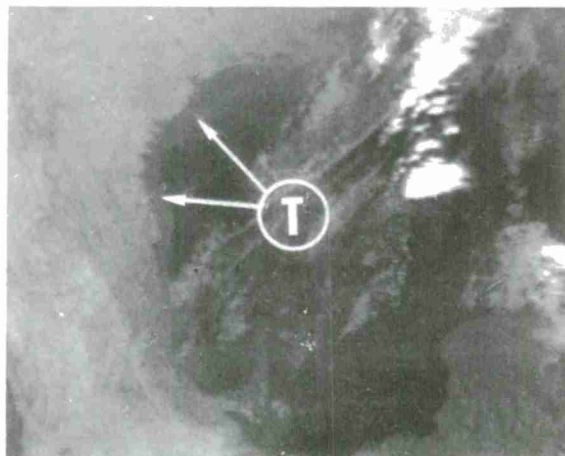


ITOS-1  4728  Nighttime IR 1000 GMT February 5, 1971

Figure 6-B-34.  During the winter, cold water from the continent flows into the Gulf of Mexico and reduces the temperature of the shallow waters.  This IR view shows the colder shelf waters along the Texas coast (T).
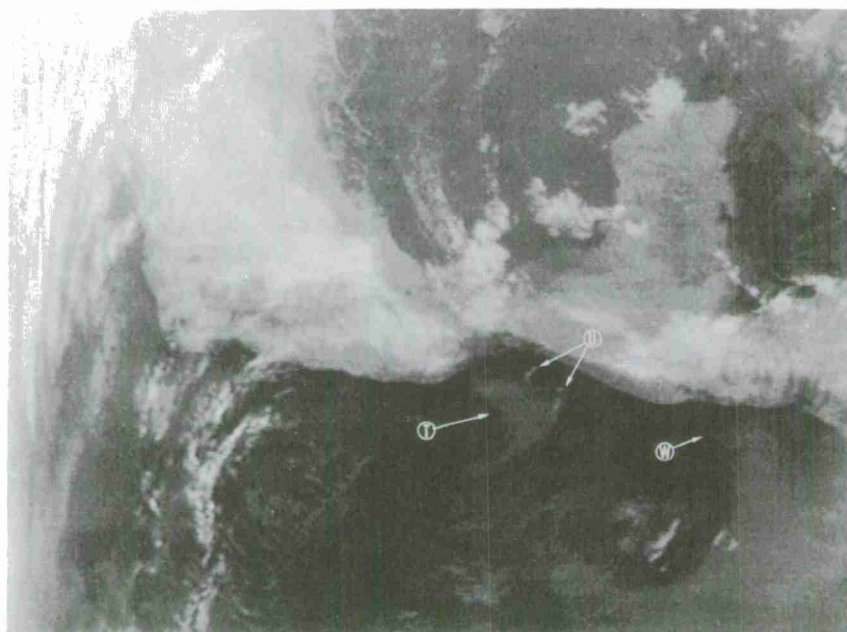


ITOS-1  4703 Nighttime IR 1000 GMT February 3, 1971

Figure 6-B-35.  This ITOS IR view shows an area of cold water (T) upwelling in the Gulf of Tehuantepec.  The SRIR data were used to find the sea-surface temperatures of these features.  The temperature of the cold gyre was 28°C and that of the surrounding warmer equatorial current waters was 30-32°C.  Some low cloudiness appears to be present along the northern edge (U) of this colder water.  Another tongue of cold water (W) can be seen along the San Salvador coast.

Chapter 6

INFRARED

Section C

APPENDIX

Infrared Radiation From the Earth and Atmosphere

The IR portion of the electromagnetic spectrum ($0.8 \mu m$ to $1,000 \mu m$) is
bounded at its lower end by visible radiation and at its upper end by micro-
wave radiation. The earth and atmosphere, whose mean temperature is 250°K,
radiates in the IR with maximum intensity at about $10 \mu m$. At this wave-
length, the earth's surface and thick clouds have an emissivity close to one
and are assumed to be black body radiators. Thus, IR radiances detected by
satellite are related directly to the temperatures of the emitting land,
water, and cloud surfaces. Radiation from these surfaces is transferred to
space through complex radiative transfer processes which involve absorption
and re-emission by several atmospheric gases. The strongest absorbers for IR
radiation are water vapor, carbon dioxide, and ozone. The absorptivity of
these gases varies with wavelength. Between 8 to $12 \mu m$, atmospheric absorp-
tion is at a minimum and IR radiation escapes directly to space. This spec-
tral region is called an "atmospheric window". Satellite IR sensors are de-
signed to detect radiation within this window so that the attenuating effect
of atmospheric absorption on the satellite IR measurements is minimized.

Figure 6-C-1. The upper portion of the
diagram shows normalized curves of
black-body radiation for a body of
6,000°K, corresponding to the radia-
tion emitted by the sun, and for a
body of 250°K corresponding roughly
to the radiation emitted by the earth
and atmosphere. The radiation of the
earth and the sun covers two separate
spectral ranges with little overlap.
The bottom part of the diagram shows
the absorption spectrum of the atmos-
phere. The atmosphere is much more
transparent to incoming solar radia-
tion than it is to outgoing infrared
terrestrial radiation. This produces
the well known greenhouse effect.
The shaded band is the IR region
(10.5- $12.5 \mu m$) sensed by NOAA scan-
ning radiometers. The line at $.63 \mu m$
is centered in the region where NOAA
SR visible measurements are made.
(Diagram from (52)).
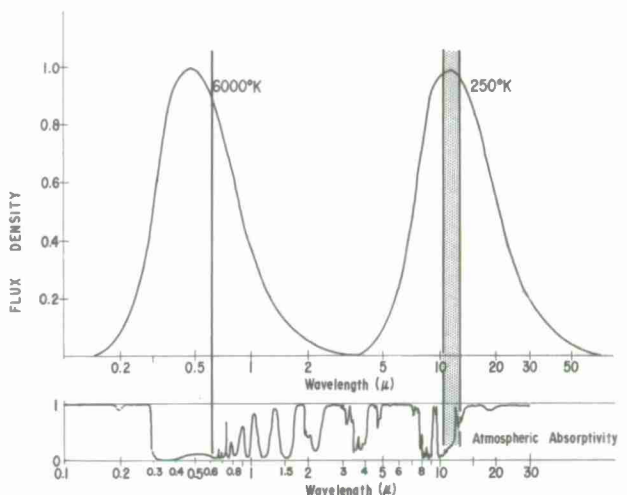
## Effects of Atmospheric Absorption (Limb-Darkening)

A small amount of atmospheric absorption does take place in the 11.5- to 12-$\mu m$ window, principally by $CO_2$ and water vapor. Along the radiation path length these gases re-radiate energy at a lower temperature. This causes a radiating surface in the atmosphere to appear colder in the satellite data than it actually is.

This is most pronounced near the horizons where the path length of the radiation becomes quite long, and in the tropics where water vapor concentrations are high. IR data that are centrally processed in digital form are corrected for limb-darkening (54). IR data readout directly in the field must be evaluated qualitatively for this error.
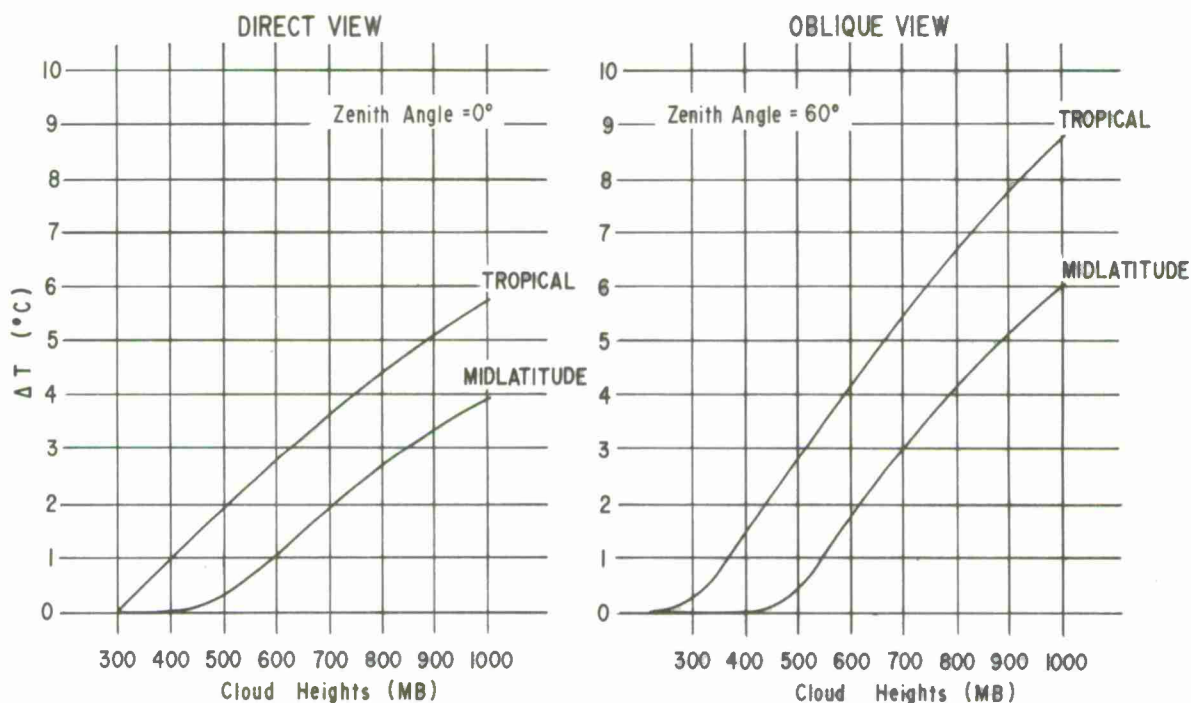


## LIMB DARKENING WHEN VIEWING CLOUDS

Figure 6-C-2. This figure shows the error introduced in cloud top temperature as radiation path length increases. Graphs are presented for both direct and oblique views. The curves represent typical air masses for the tropics and mid-latitudes. When the satellite sensor is pointing straight down, (direct view) there is no error if the clouds are at or above 300 millibars. For the same case, clouds at 1,000 millibars will appear to be 4°C colder than they actually are at mid-latitude and 6°C colder in the tropics. The errors become greater for oblique-viewing angles. These curves are based on a model and are calculated from data obtained from ITOS-1. They are applicable to the NOAA/ITOS series.

Figure 6-C-3. This figure shows the
error introduced in the earth's sur-
face temperature as the radiation
path length increases. The graphs
here show the range of maximum errors
to be expected between the case where
the satellite sensor is pointing
straight down (zenith angle = 0) and
the case where the sensor is viewing
the earth's horizon (zenith angle =
90°). The curves are for surface
temperatures of tropical, mid-latitude
and polar regions. The scale on the
bottom relates the corrections to the
distance from the satellite subpoint
of each datum point along a scan line
(see figure 6-C-4). For example, when
the satellite views the earth's sur-
face 900 nautical miles on either side
of the satellite subpoint track at
mid-latitude, the sensor measures a
temperature of 265°K rather than an
actual temperature of 270°K.
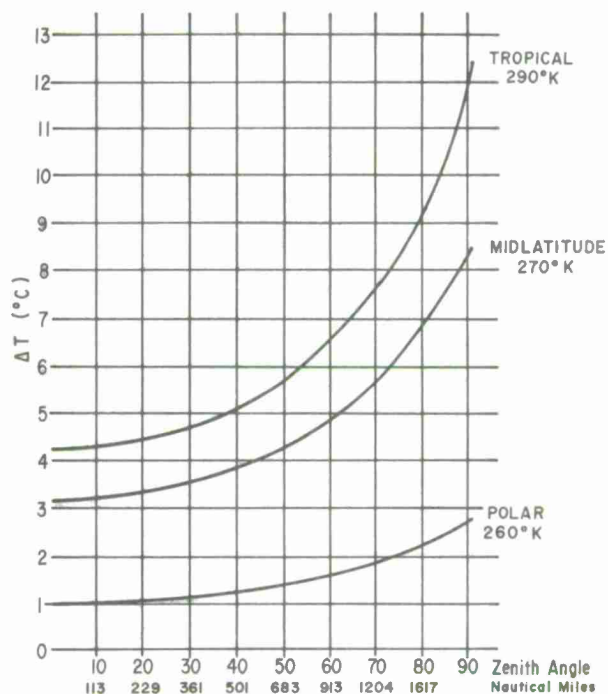


## The Scanning Radiometer (SR)

Unlike the TV cameras carried on earlier satellites, the scanning radiometer
(SR) (54) does not take a picture. Instead, it provides narrow swaths of data
from which an image can be constructed. As the satellite moves around the
earth, a rotating mirror provides an optical scan perpendicular to the direc-
tion of spacecraft motion. The data content for each scan depends on the
orbit and instrument characteristics of a given satellite. For ITOS, each
scan "sees" a 3,622 nautical-mile-long area of the earth. In the 1.25-second
interval between scans, the satellite advances five nautical miles along the
subpoint track. Each successive data scan is either recorded for later play-
back or transmitted directly to ground stations where consecutive swaths are
displayed side by side to form an image. Data in an IR display always extends
over an interval of time, whereas all the data in a single TV picture are for
the same time.
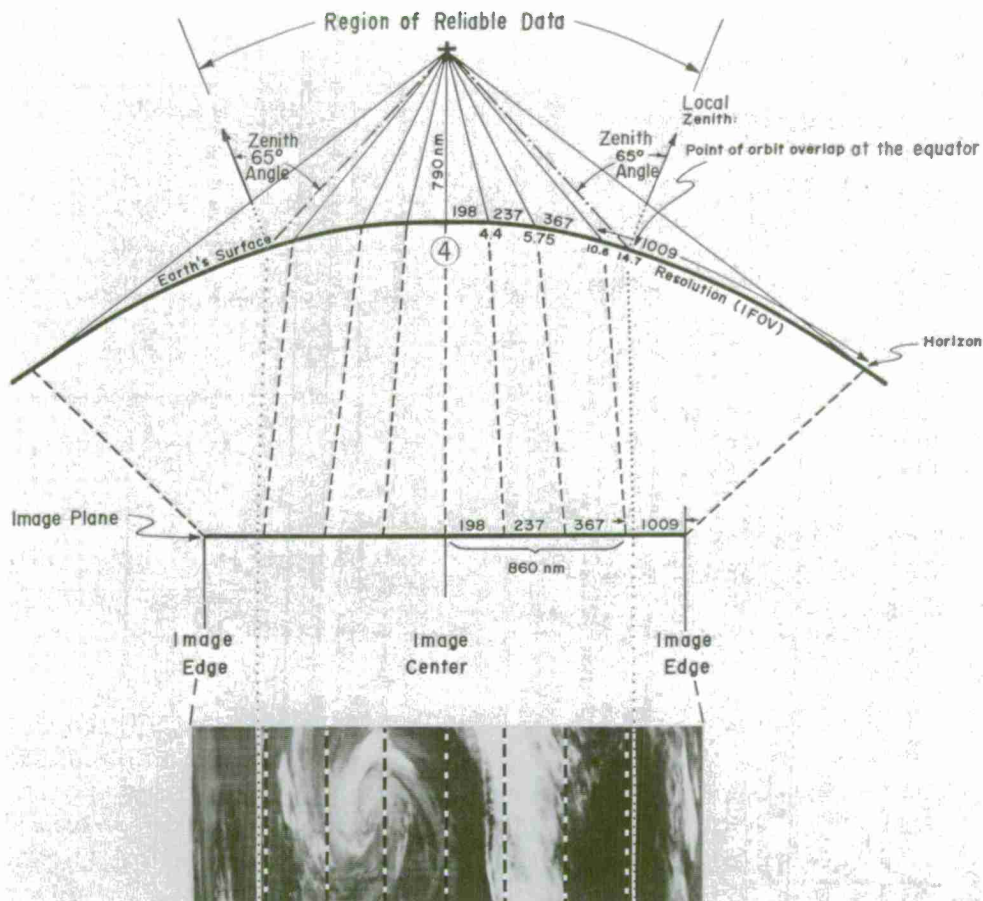
Figure 6-C-4. This diagram shows how an SR view of the earth's curved surface
is displayed on the flat plane of an IR imaging device. In this diagram, the
image plane is divided into eight equal segments. The number above each seg-
ment of the image plane is the length in nautical miles of the arc of the
earth's surface displayed in that segment. These numbers show the rate at
which foreshortening increases toward the edge of an IR display. The numbers
plotted below the curved line representing the earth's surface are the size
of the instrument field of view. It is four nautical miles wide at the satel-
lite subpoint and increases to 14.7 nautical miles where the zenith angle is
65°. Beyond this point resolution decreases markedly and location errors in-
crease because of foreshortening. The reliable data region is restricted to
the inner 860 nautical miles of the scan. At the Equator these regions are
contiguous from pass to pass; poleward they overlap.


## Spatial Resolution of the SR

The maximum resolution of the scanning radiometer sensor is four miles along
the subpoint track. As the sensor completes its sweep to the horizon, the
viewing angle becomes more oblique and the area viewed becomes much larger.
For data whose local zenith angle is 60°, the area viewed increases to a spot
of about eight nautical miles by twelve nautical miles (see figure 6-C-4).
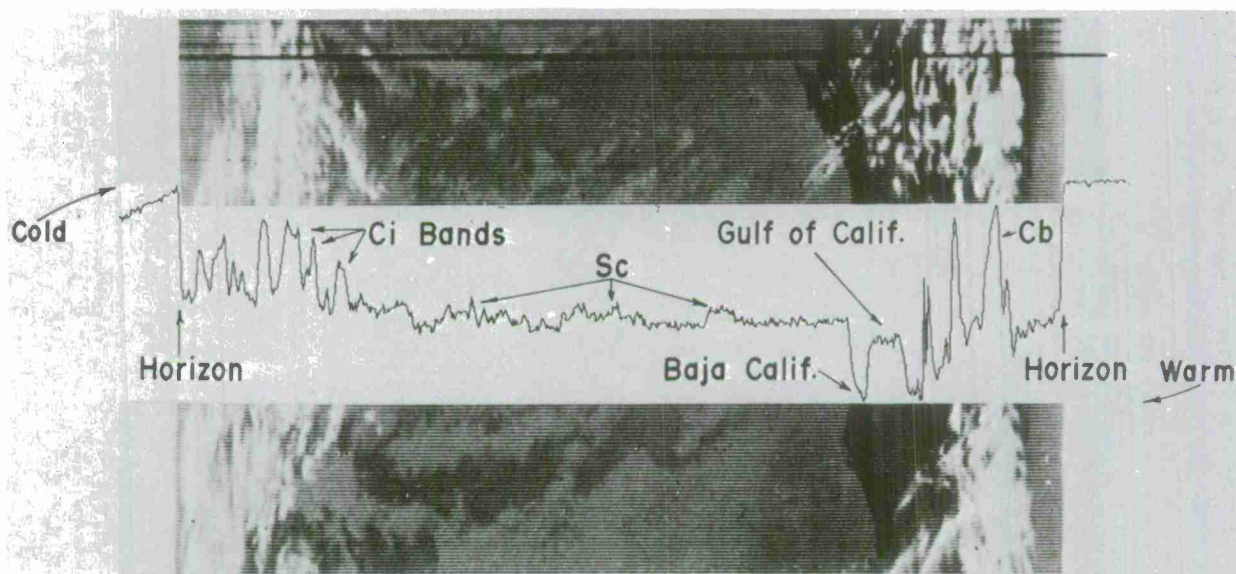
Figure 6-C-5. A plot of a single scan line from a DRIR transmission appears in the middle of the figure. Above and below, the preceding and following data are displayed in analog form as shades of gray. The warmest point along the scan line is the eastern coast of Baja California; the coldest clouds are the cumulonimbus over western Mexico and the cirrus near the western horizon.

## Effect of Spatial Resolution on Indicated Cloud-Top Temperature

Radiometers measure the total long-wave radiation entering the sensor. This radiation usually comes from many sources radiating at different temperatures. If these sources are below the resolution of the sensor, the instrument integrates the radiances into a single response. For this reason, SR cloud-top temperature measurements are most accurate when clouds fill the entire field of view of the sensor. The satellite-derived temperature of clouds that are continuous, and opaque to terrestrial radiation, closely approximate the actual cloud-top temperature. Clouds that have breaks or holes which are below the sensor's resolution appear warmer in the data than they actually are.

The relative accuracy of satellite-measured cloud-top temperatures depends on the size of the cloud elements (or holes) in the cloud layer, the total amount and opaqueness of the clouds, and their location relative to the viewing angle of the sensor.
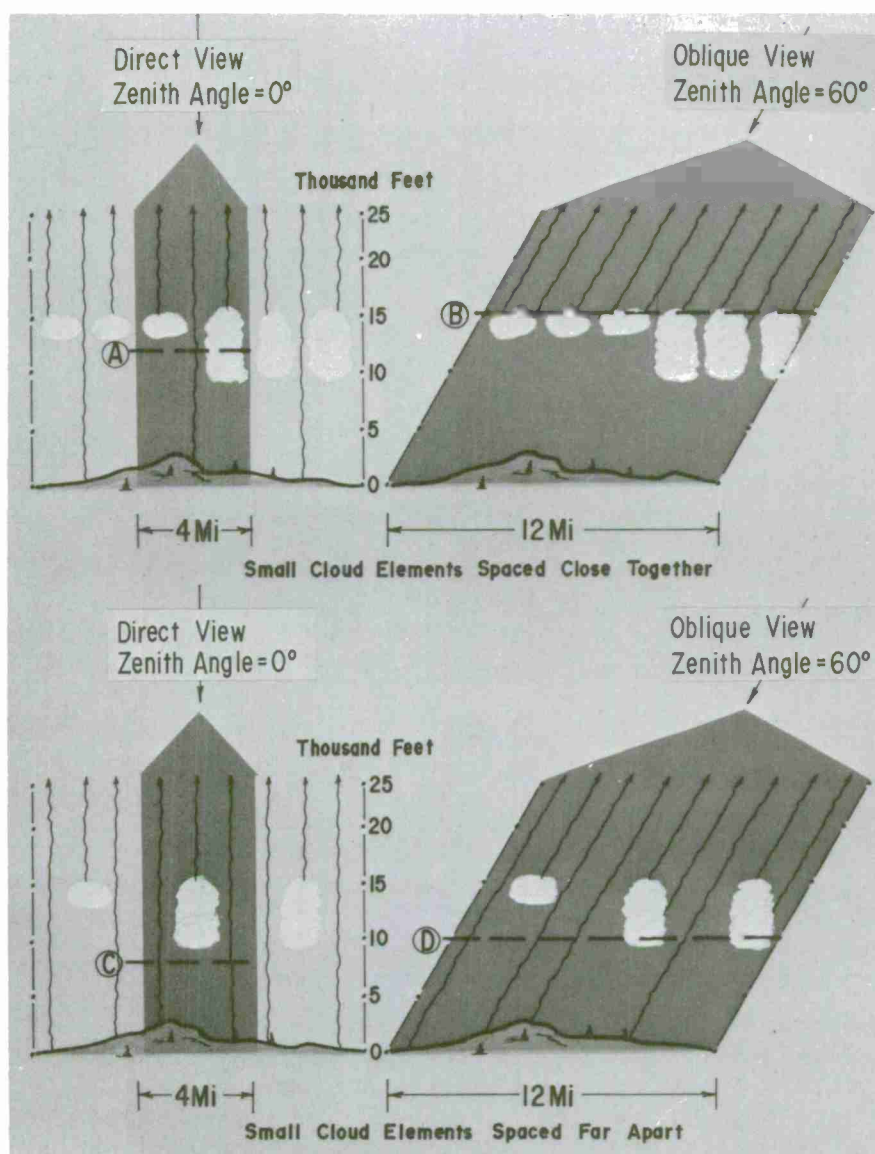
Figure 6-C-6. This schematic diagram shows how cloud element size and viewing angle make clouds appear warmer and lower than they actually are. The horizontal dashed lines, identified by letters, represent the cloud-top heights as they might be derived from the two cloud fields shown. The cloud fields on the left and right-hand side of the diagram are identical. Only the viewing angle and field of view changes. The cloud-top height measurements observed for a broken cloud layer with closely spaced, thick and thin, opaque cloud elements appear at the top of the figure. When these clouds are viewed directly (nadir angle = 0), the SR measures both cloud-top and ground radiation; thus, the height of the clouds appears to be at a lower level (A). The same clouds, viewed at an oblique angle (top, right), appear to be higher (B) due to the absence of ground radiation. At the bottom of the figure, the clouds are spaced farther apart. Here the ground contributes more energy and the clouds appear warmer and lower (C, D). The numerical values for height changes shown here are for purposes of illustration only.

## Temperature Resolution of the SR

The capability of the NOAA/ITOS scanning radiometer (SR) to measure radiances accurately varies with the temperature of the scene. Inaccuracy results from noise introduced by the sensing system itself, and from variations in instrument stability. In terms of temperature, the error ranges from $\pm 2°C$ at the warm end (300°K) to $\pm 8°$ at the cold end (185°K). Applying these figures to the U. S. Standard Atmosphere gives an indication of the effect of instrument error on the accuracy of derived cloud-top heights. At 3,000 feet it is $\pm 1,000$ feet; at 13,000 feet it is $\pm 2,000$ feet; at 23,000 feet it is $\pm 3,000$ feet, and at 33,000 feet it is $\pm 4,000$ feet. These figures should be considered approximate only. The temperature-resolving power of the instrument is quite high, being 1°C for cold temperatures and 1/2°C for warm temperatures.

## The Conversion of Measured Radiances to Temperature

Cloud and earth surfaces are considered black body radiators. This is a relatively good approximation for radiation at $11 \mu m$ . Before launch, an SR is calibrated by placing a variable temperature black body target in the field of view of the sensor. The response signature of the sensor to the 190°K to 340°K temperature range is recorded. This calibration curve is used to convert the radiance measurements received from the satellite to temperatures. The radiances measured by the satellite when in orbit are converted to equivalent black body temperatures; derived temperature accuracy depends on the assumption that the clouds and earth surfaces observed are emitting as black bodies.

## Computer-Processed IR Data

The energy detected by a scanning radiometer is transmitted to earth as an analog signal. This signal can be converted either directly to gray shade displays, such as the ones produced at APT DRIR (Direct Readout Infrared) stations, or it can be digitized and processed by computer to quantify the data before being displayed. The advantages of computer processing are:

(1) The data can be corrected for variations in spacecraft temperature and limb-darkening errors;

(2) Quantitative temperature values can be assigned on the basis of pre-launch instrument calibration;

(3) The data can be rectified to different map scales and displayed with grids. This removes the distortions present in direct readout displays and puts the display in a more convenient form for operation use.

(4) The gray shade range for selected temperature intervals can be expanded to facilitate interpretation.

Computer processing has the disadvantage of delaying the availability of the data. IR computer products currently are distributed over domestic facsimile networks and relayed by ATS satellites to APT receivers within telemetry range.

Figure 6-C-7. The same IR data appear
in this diagram in two different for-
mats. The lower portion of the figure
shows the IR imagery as it is dis-
played and gridded at an APT station.
The grids furnished APT stations are
distorted to fit the data display.
The central portion of the diagram
shows the same data, processed by com-
puter and mapped to a polar stereo-
graphic projection. The top of the
diagram represents the portion of the
earth's curved surface viewed by the
satellite. The mapping program does
not display the data near the horizon
where location errors, due to fore-
shortening, are large and limb-darken-
ing corrections reach a maximum. The
edge of the mapped data is indicated
by dashed lines in all three portions
of the diagram. The format of the
mapped IR data in this example is
that used for operational distribu-
tion over U. S. National Weather
Service facsimile networks.

## Mapped NOAA Data

IR data received from the NOAA/ITOS
satellites are processed by computer
at the National Environmental Satellite
Service in the following manner: The
raw data are in the form of an analog
voltage which varies as a function of
the energy impinging on the satellite
sensor. The raw data signal for each
scan of the SR is sampled 1,250 times
between horizons. Each sample along
the line is assigned a value over a
number range of 256 depending on the
voltage strength. These raw sample
counts are converted to temperature by
means of the calibration relationships
determined prior to the launch of the
SR. This calibration takes into ac-
count variations in spacecraft temper-
ature which take place as the satellite
moves from day to night along its or-
bit. The data are also corrected for
the effects of atmospheric absorption
(limb-darkening).
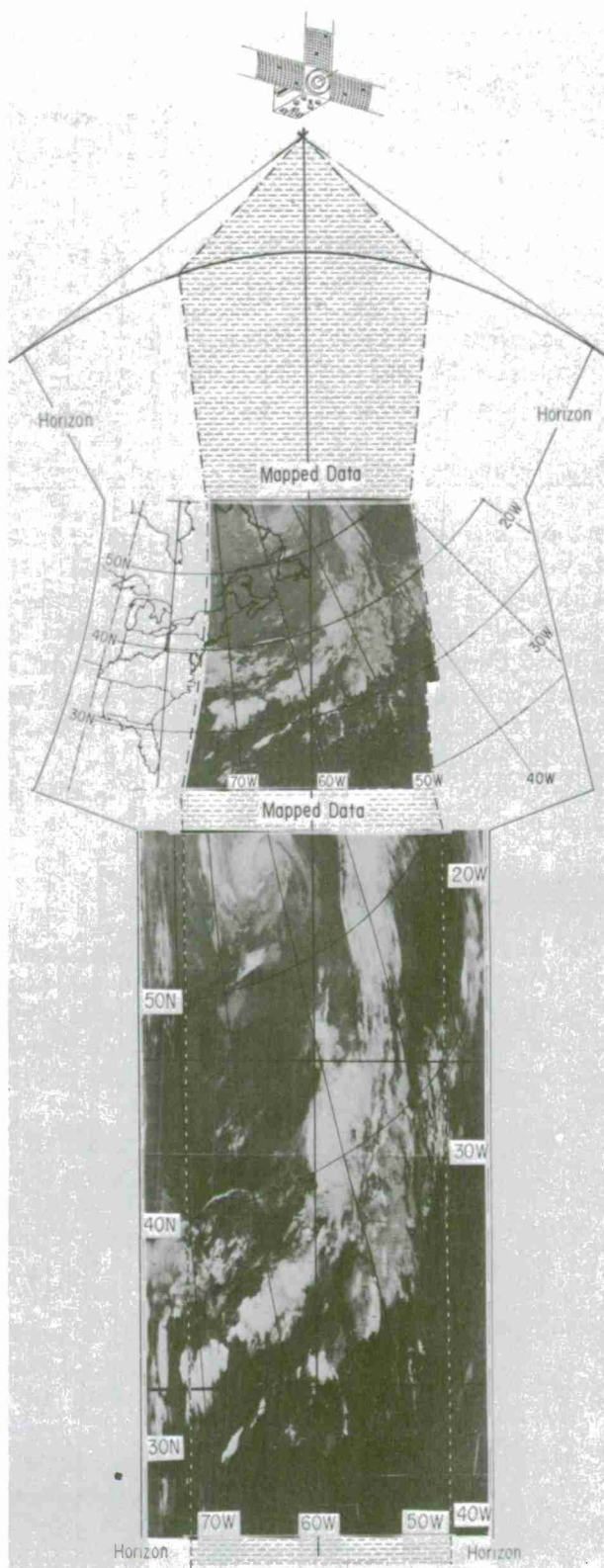
The earth's position for each of the 1,250 scan line samples is then located. Precise knowledge of spacecraft position and attitude are required to do this. This information is obtained from telemetry data received from the satellite at the same time as the SR data. A mapping program (55) next arranges the data so that it can be displayed either as a polar stereographic or Mercator
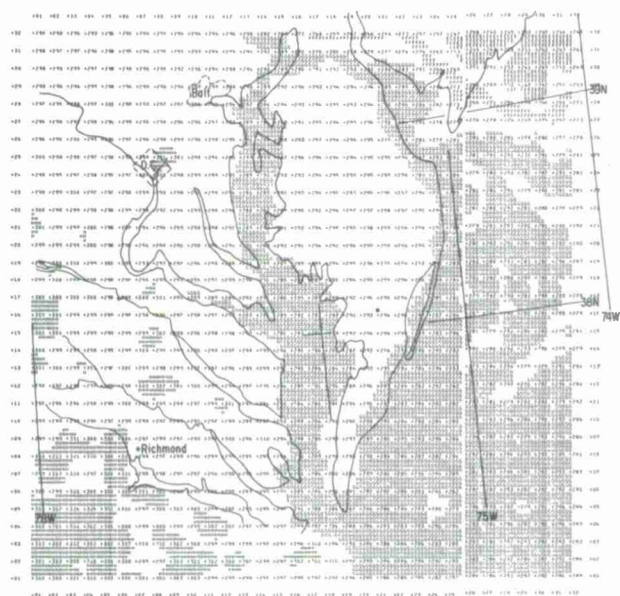


Figure 6-C-8. This is a numerical printout of polar stereographic mapped data which shows the Delmarva Peninsula, Chesapeake Bay and eastern Virginia. A temperature is plotted for each grid point within the array. The array shown here is the size of one square in the grid used by the National Meteorological Center for their hemispheric Numerical Weather Prediction model. The shading over water represents temperatures less than 290°K. The shading over land represents temperatures greater than 300°K. This type of numerical data display is necessary for detailed analysis of mapped data. The coast-line, as well as small bays and inlets, are easily detectable by means of temperature values. Even the urban areas of Washington and Baltimore can be identified in the display as they are two to three degrees warmer than the surrounding countryside. This display illustrates the inherent resolution of mapped IR data produced by the National Environmental Satellite Service.

Figure 6-C-9. This is a gray shade display of the same data shown in figure 6-C-8. Here, each temperature has been converted into a gray shade so an array of contiguous boxes rather than numbers appear. This is the same format, but much enlarged, in which digital data are transmitted over domestic facsimile circuits and by WEFAX. This illustration shows the maximum spatial resolution present in the mapped data transmitted by facsimile circuit to users. The reduced resolution of the product as received is due to the size of the image displayed, and to the quality of transmission lines and display equipment.

image with superimposed latitude-longitude grids. There is some loss in spatial resolution toward the poles in data mapped on a polar stereographic projection because it is not an equal area projection. For mapped IR data, resolution remains four nautical miles within 20 degrees of the Equator, but decreases to eight miles at the poles. Mapped data can be displayed in shades of gray which represent specific temperatures or ranges of temperature, or as numbers.

## Enhanced Displays

A gray-shade display of IR digital data represents temperatures over a given range by use of a finite number of gray shades. At the present time, display devices at NESS produce IR imagery with 64 gray shades, transmissions over facsimile are made in 16 gray shades. (Most facsimile recorders will only reproduce 8 to 12 of these 16.) Gray-shade assignments to specific temperature values can be made in several ways depending on the purpose of the display.

In a straight display, temperature increments are equal for each shade of gray displayed. This type of display gives a true picture of the relative levels of radiant energy detected by the sensor over the whole scene, but does not necessarily provide the best means for recognizing significant cloud and surface features in the data. To do this, the number of gray shades is increased within a small portion of the total temperature range. For example, the highest, coldest tops within a convective cloud cluster are best identified by assigning most of the gray shades to the temperature range of clouds above 500 millibars. This procedure is called enhancing the data.

Another variation of enhancing is to restrict the number of gray shades used in the display in order to increase the contrast between individual shades so that they can be easily recognized.

A third variation of enhancing is to display certain gray shades out of sequence (e.g., alternate light and dark shades are used instead of increasingly darker shades) in order to emphasize particular cloud features.

## Enhancement of IR Imagery to Compensate for Latitudinal Temperature Changes

The gray shade range of displayed IR data shifts toward whiter values poleward from the Equator. This is caused by the natural latitudinal temperature decrease of the earth's surface and atmosphere. The temperatures of low clouds are more affected by this variation than those of higher clouds. For this reason, middle and high clouds are less easy to identify at higher latitudes where the temperature difference between them and lower clouds or the surface is at a minimum. This is particularly true in the winter. In the tropics and subtropics there is a difference of more than 100°C between high clouds and the surface; over continental polar regions this range is often less than 20°C. The small range in temperature between earth and clouds at high latitudes results in very small brightness contrasts in the IR imagery, which makes it more difficult to distinguish clouds from the cold earth.

Latitude effect can be compensated for, to a degree, by varying the settings
on DRIR receivers as the data are received. It can also be done by computer
when the data are digitized. The mapped IR displays transmitted over fac-
simile are enhanced to compensate for latitude variation. The aim is to make
the images easier to interpret by maximizing the number of gray shades in the
IR display for imagery at each latitude. This is done by reassigning gray
shades so the image ranges from black to white at all latitudes no matter what
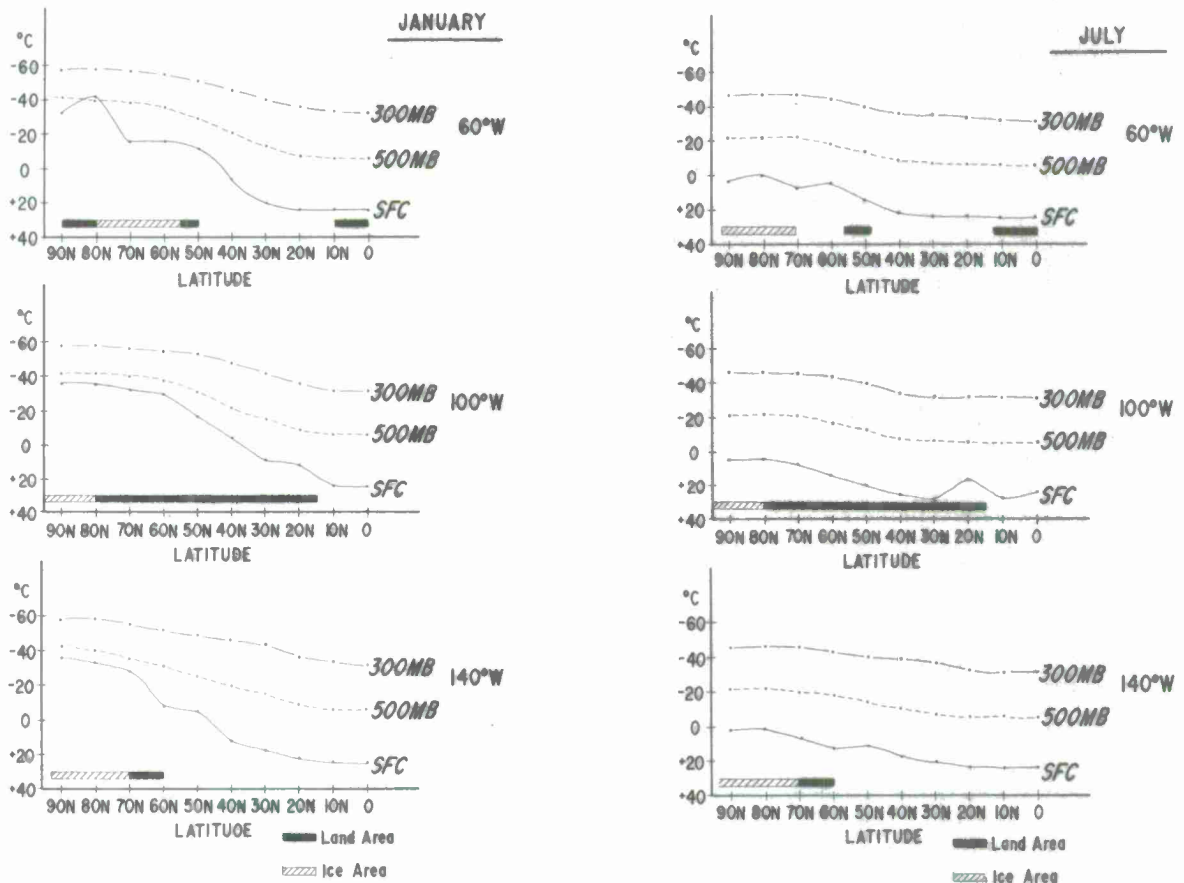


Figure 6-C-10. These six graphs show how temperature varies with latitude
and with season (56). Mean temperatures representative of summer and winter
are plotted for the surface, 500- and 300-mb levels. The graphs for 60°W are
representative for conditions over water immediately east of North America;
the graphs for 100° represent continental conditions over North America; and
the graphs for 140°W represent the maritime atmosphere west of North America.

The January curves show that low cloud temperatures are much more affected by
latitude change than high cloud temperatures. Note the very small tempera-
ture range between low and high clouds in the Arctic during winter. This is
responsible for the small brightness contrast between clouds and land in
wintertime Arctic IR imagery. Comparing the January and July temperature
curves, we see that IR imagery should display little seasonal change in the
tropics, and that the brightness of high clouds between Equator and pole vary
much less with season than does the brightness of low clouds. Compare the
data in this figure with the seasonal IR displays of figure 6-B-25.
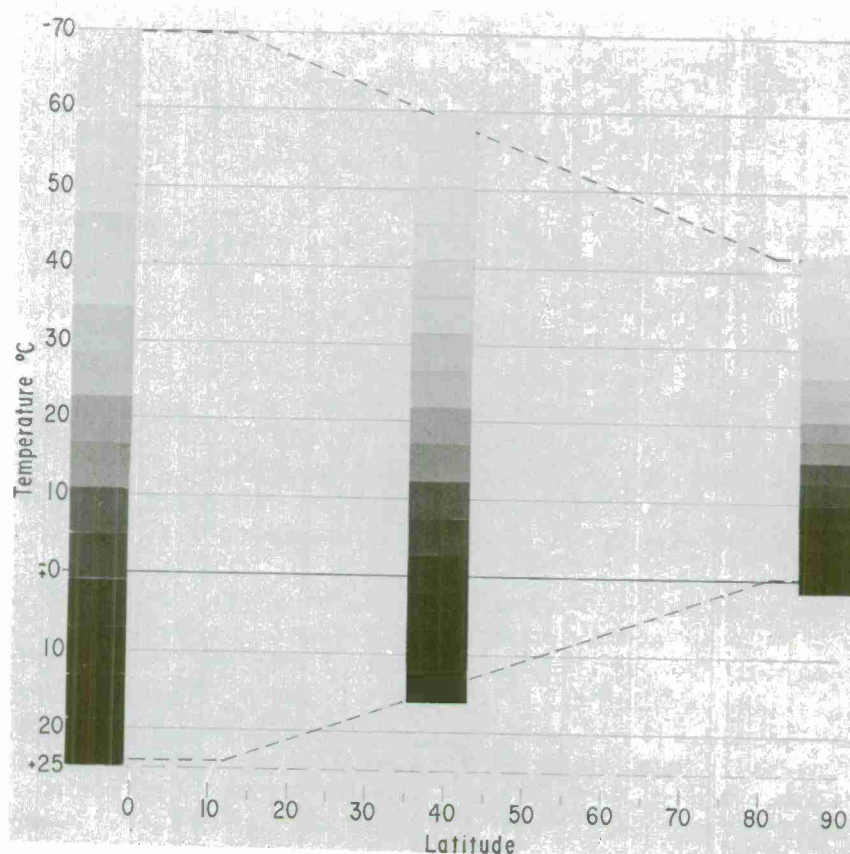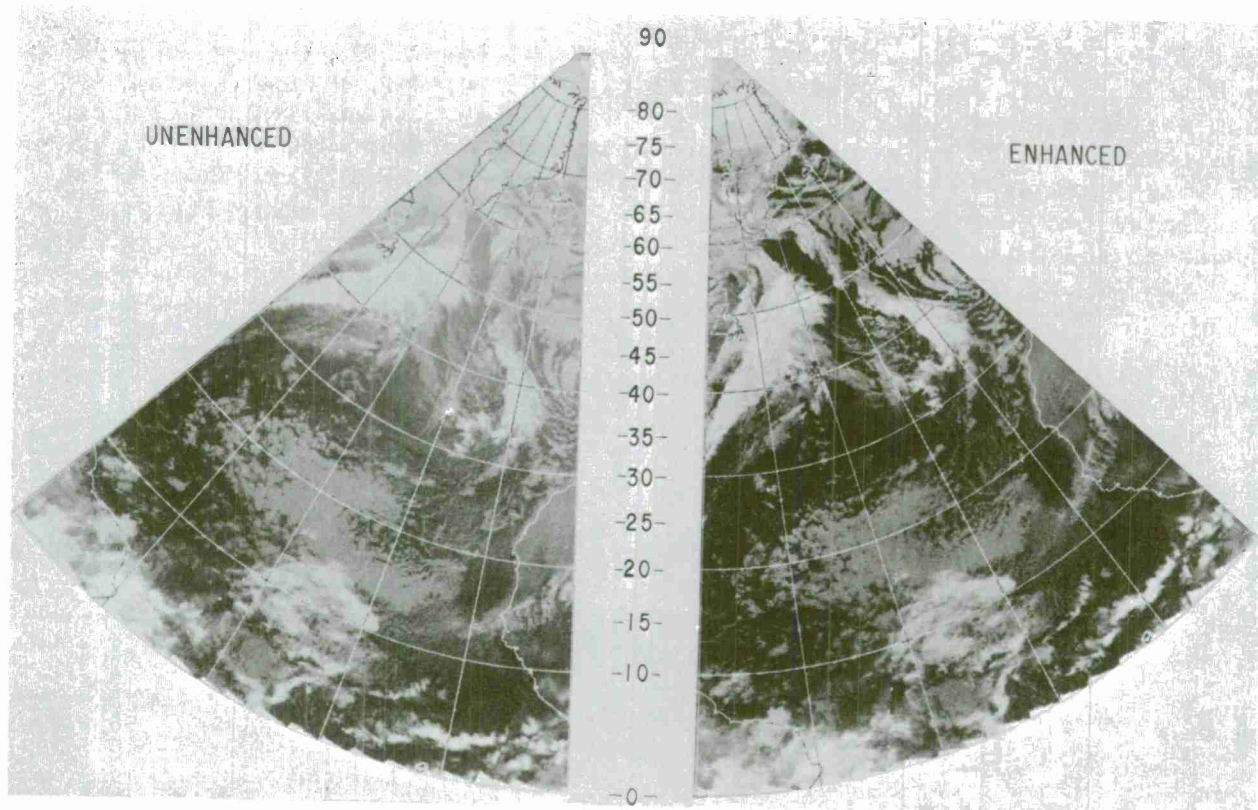
the strength of the signal from the IR detector. While this procedure produces a display more easily interpretable in terms of cloud distribution, the temperature values assigned to each of the gray shades change with latitude throughout the display.

## Enhancement of IR Imagery to Optimize the Display of Clouds in Certain Temperature Ranges

It is difficult to distinguish between cloud layers whose temperatures are very close in a normal IR display. This is because of the small contrast between the shades of gray representing the cloud top temperatures. The same problem exists with clouds close to the earth's surface. If we increase the number of gray shades assigned to a given temperature range we increase the contrast between the features which we wish to distinguish. There is a penalty with this type of enhancement in that there must be a corresponding decrease in gray shade contrast over other regions of temperature. This type of enhancement is used to better display low clouds, to better identify the structure of convective storms and to locate sea-surface temperature gradients.

It is possible to perform this enhancement with DRIR display devices that have been modified so that the output voltage can be appropriately varied. Computer-processed data distributed by facsimile circuit incorporate this type of enhancement.

Figure 6-C-11. This example illustrates the effects of the latitude enhancement method used by NESS. This type of enhancement is present in many of the operational IR displays produced by NESS and distributed by Weather Service facsimile and WEFAX. Latitude enhancement is accomplished by making the correspondence of gray shade to temperature different for each 5-degree latitude band between $10°N$ (S) and $80°N$ (S) latitude. (At the poles and Equator the bands are $10°$ wide.) The bottom diagram shows how the temperature range and the gray shade assignment vary with latitude when the data are latitudinally enhanced. In this example, white represents temperatures of $-70°C$ at the Equator, $-58°C$ at $40°N$ and $-43°C$ at the pole. Similarly at the warm end, black represents $+25°C$ at the Equator, $+15°C$ at $40°N$ and $\pm 0°C$ at the pole. Gray shade temperature correspondence is different for each of 16 latitude bands between the Equator and the pole. Only three of the 16 gray wedges are shown here.

Displays of data with and without latitude enhancement appear in the upper portion of the figure. In the unenhanced version temperature gray shade assignment is the same, $+25°$ to $-70°C$, from the Equator to the pole. The enhanced version displays the data over temperature ranges which vary with latitude as indicated in the bottom diagram. Up to about $30°$ north, both displays appear very similar. As the ocean surface becomes colder north of $30°$, the contrast between low clouds and the ocean becomes less in the unenhanced display. The oceans in the enhanced display remain black past $70°N$. This increases the contrast between clouds and ground and makes the clouds more detectable.
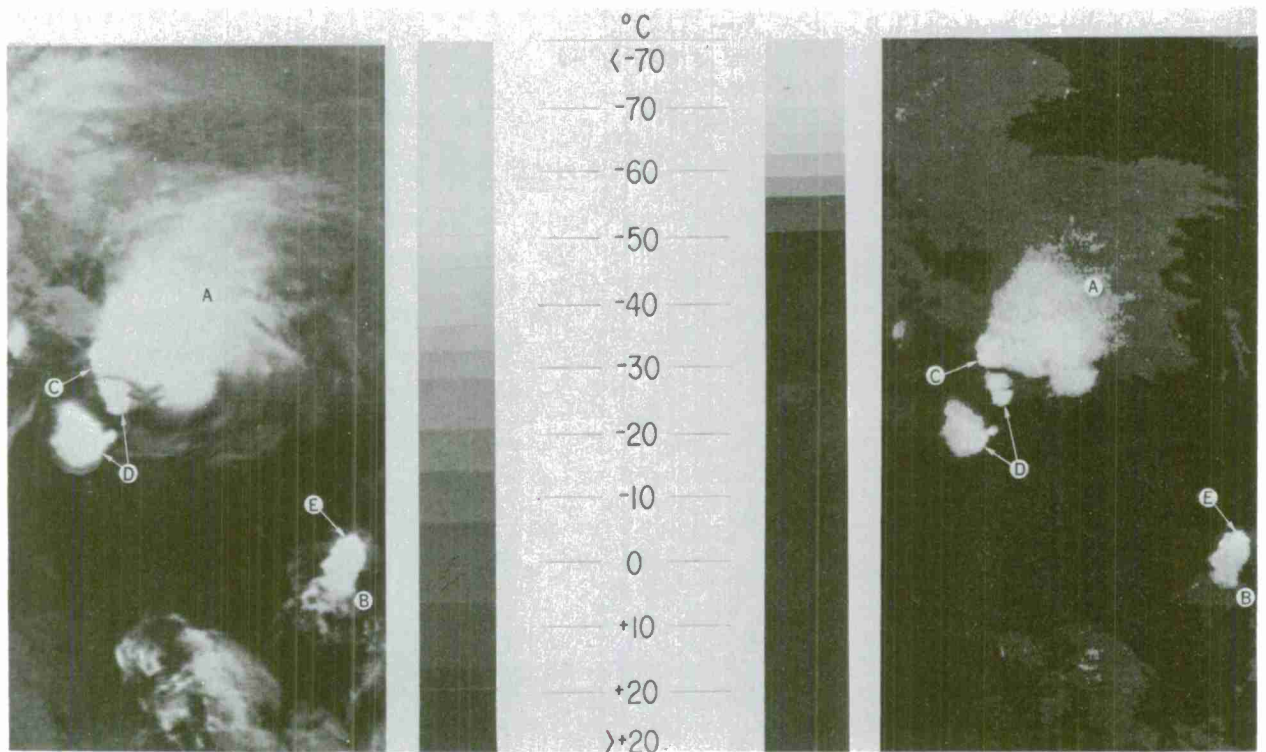
NOAA-1   1905 Nighttime IR   1230 GMT   May 5, 1971

Figure 6-C-12.   Another example of data enhancement is shown here.   The IR
data on the left are displayed in 16 gray shades; the same data are displayed
on the right using seven shades.   The gray wedges next to each display show
the temperature ranges assigned to the different hues in the respective dis-
plays.   The temperature intervals for each gray shade are not equal in either
display.   In the image on the left, all clouds with temperatures colder than
-50°C appear white.   In the display on the right, cloud tops with tempera-
tures between -50°C and -70°C are displayed in six gray shades, while all
those with temperatures warmer than -50°C appear black.   The IR image shows
two thunderstorm complexes over the central United States, one in North
Dakota (A), and one near Des Moines, Iowa (B).   The display on the left uses
a large number of gray shades spread over a wide temperature range to best
depict the entire cloud scene.   The display on the right uses a small number
of shades to display the coldest temperatures in order to best depict the
structure of the thunderstorms.   With this kind of enhancement, it is possi-
ble to identify the coldest areas within the thunderstorm anvils.   The cold
spots (C, D, and E) represent the tops of the convective cells.
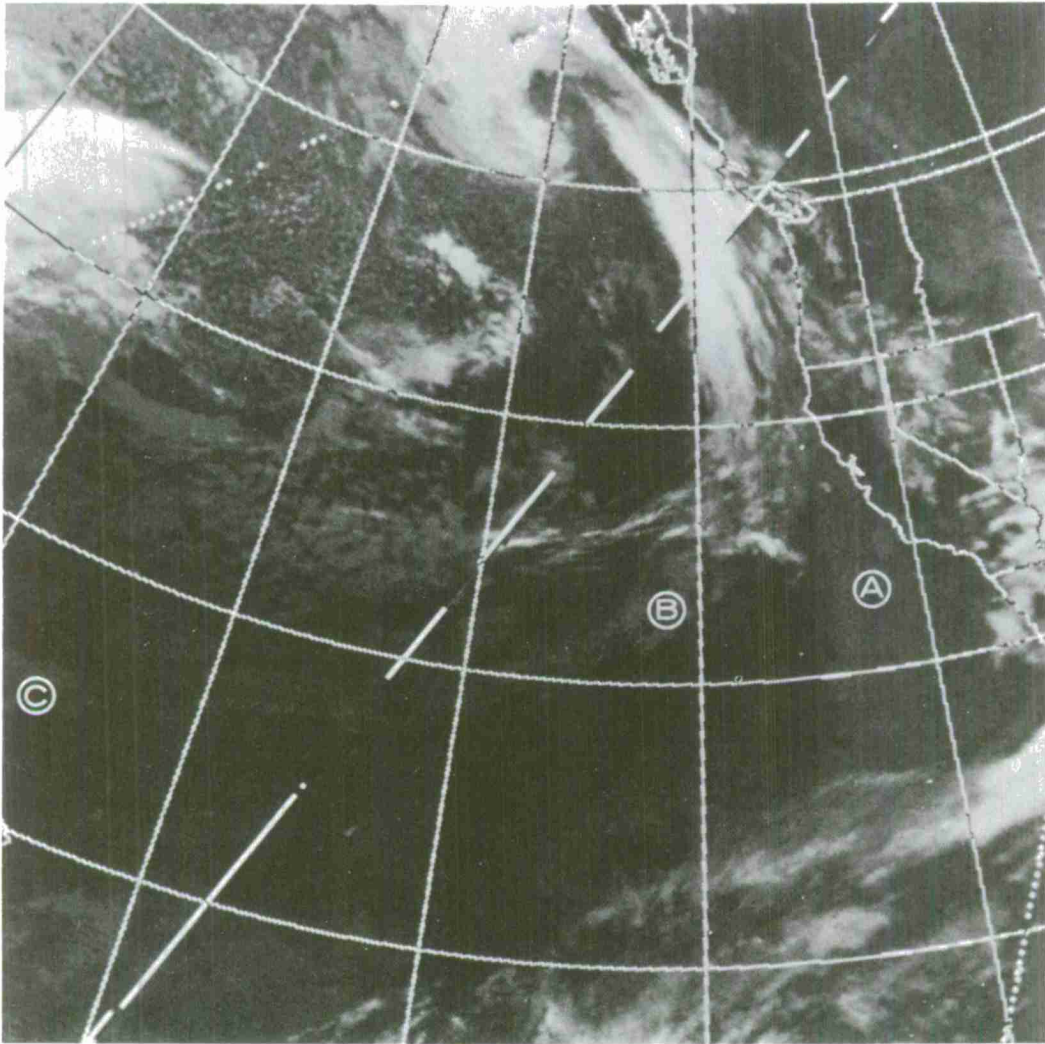
Figure 6-C-13.  Only one form of enhancement has been used in this IR dis-
play.  It incorporates the scheme of latitude enhancement shown in figure
6-C-11.  The temperature gray shade assignment is linear over the temperature
range of all the data in this display.  (See figure 6-C-15.)  Equal incre-
ments of temperature have equal increments of gray shade value (as measured
by a densitometer).  The high, cold clouds stand out well in this display but
low clouds, such as the stratocumulus off California (A), are dark and hard
to identify.
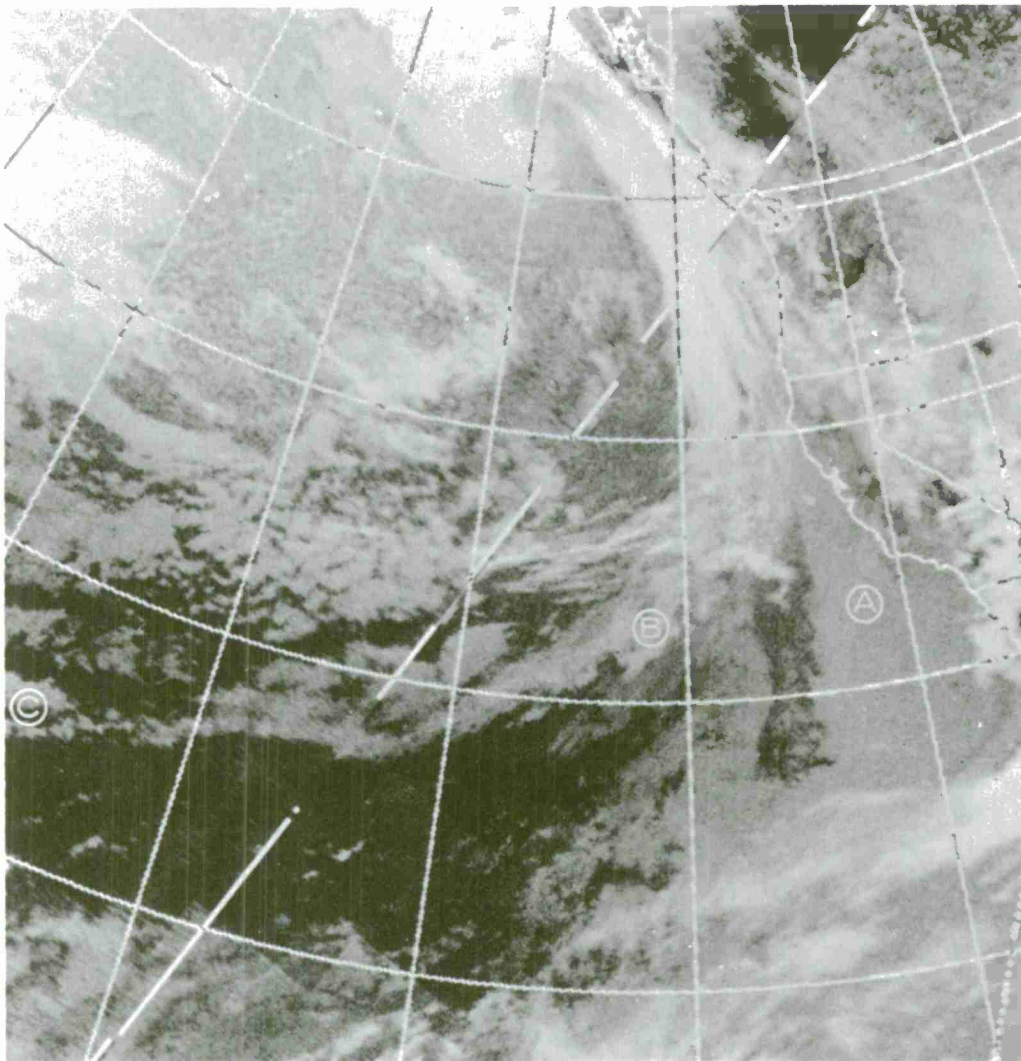
Figure 6-C-14. This is the same image as figure 6-C-13 but with two forms of
enhancement. It has the latitude enhancement of figure 6-C-13 plus a non-
linear temperature gray shade assignment to make the warm low clouds stand
out more clearly. In this image, gray shade values change more rapidly at
warm temperature values. This increases the contrast between low clouds and
the earth's surface. The breaks in the stratocumulus (A) and the weak por-
tion of the front (B to C) stand out clearly and are more easily identifiable
than in the display of figure 6-C-13.
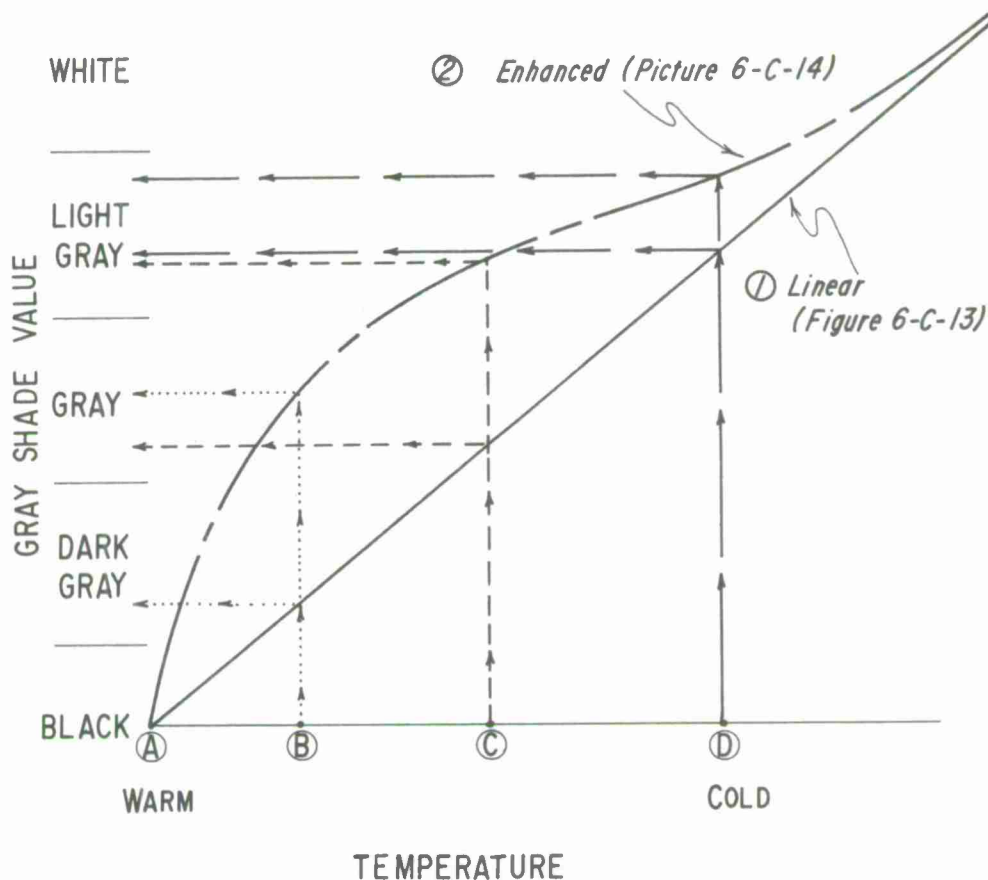
Figure 6-C-15. This graph shows the temperature gray shade assignments used in figures 6-C-13 and 6-C-14. For example, if point A on the abscissa represents the temperature of the earth's surface and point B represents the temperature of low clouds, then display curve 2 markedly increases the gray shade contrast between the low clouds and their background. Enhancement of one portion of the IR data is accomplished only at the expense of another portion of the data; e.g., the gray shade contrast between two cloud layers whose temperatures correspond to points C and D is less for curve 2 than for curve 1.

Figure 6-C-16. Above is an APT DRIR facsimile display of one of the four
passes used to make the mapped composite displays in figures 6-C-13
and 6-C-14. This display has latitude enhancement introduced by subjective
adjustment of the gain on the APT receiver as the data were received. The
contrast between low clouds and the earth's surface in this display falls
somewhere between that of figures 6-C-13 and 6-C-14.

REFERENCES

[1]   Anderson, R. K., E. W. Ferguson, and V. J. Oliver, 1966: "The Use of
      Satellite Pictures in Weather Analysis and Forecasting," World Meteor-
      ological Organization Technical Note No. 75, WMO - NO. 190.TP.96.

[2]   Widger, W. K. Jr., P. E. Sherr, and C. W. C. Rogers, 1965: "Practical
      Interpretation of Meteorological Satellite Data," Air Weather Service
      Technical Report 185, AFCRL Contract No. AF 19(628)-2471, Aracon
      Geophysics Company.

[3]   National Weather Satellite Center, 1965: APT Users Guide, US Department
      of Commerce, Environmental Sciences Services Administration.

[4]   Krueger, A. F., and S. Fritz, 1961: "Cellular Cloud Patterns Revealed by
      TIROS I," Tellus, Vol. 12, No. 1, pp. 1-7.

[5]   Viezee, W., et al, 1966: "Tiros-Viewed Jet Stream Cloud Patterns in Re-
      lation to Wind, Temperature, and Turbulence," Stanford Research Insti-
      tute, Final Report, Contract Cwb 11129.

[6]   Smith, A. H., 1968: "Statistical Test of Rules for Determining Points on
      Surface Ridgelines from Weather Satellite Photographs," Monthly
      Weather Review, Vol. 96, No. 5, May 1968, pp. 315-318.

[7]   Mendez-Vigo, C., 1967:  Unpublished notes for determining surface ridge-
      lines in the Southern Hemisphere.  ETAC Satellite Section.

[8]   Smith, A. H., 1968:  Unpublished notes regarding the correlation of sun
      glints and the location and orientation of surface ridgelines.  ETAC
      Satellite Section.

[9]   Boucher, R. J., et al, 1963: "Synoptic Interpretation of Cloud Vortex
      Patterns as Observed by Meteorological Satellites," Aracon Geophysics
      Company, Final Report, Contract No. Cwb-10630, pp. 176-180.

[10]  Hubert, L. F., 1963: "Middle Latitudes of the Northern Hemisphere -
      TIROS Data as an Analysis Aid," Rocket and Satellite Meteorology,
      pp. 312-316.

[11]  Merritt, E. S., 1963: "Fleet Applications, Meteorological Operational
      Satellites (Antarctic Area)," Final Report, Aracon Geophysics Company,
      Contract No. N189(188) 56507A.

[12]  Fritz, S., 1961: "Satellite Cloud Pictures of a Cyclone Over the Atlan-
      tic Ocean," Quarterly Journal of the Royal Meteorological Society,
      Vol. 87, No. 373, pp. 314-321.

[13]  Smith, A. H., 1968:  Unpublished notes for determining surface wind
      speed and direction from cellular cloud patterns to the rear of polar
      fronts.  ETAC Satellite Section.

[14]  Miller, R., and M. Young, 1968:  Unpublished notes correlating sun glints
      with surface wind speed.  ETAC Satellite Section.

[15]  Hubert, L. F., 1966: "Mesoscale Cellular Convection," Meteorological
      Satellite Laboratory Report No. 37, US Department of Commerce, En-
      vironmental Sciences Services Administration.

[16] Barnes, J. C., and C. J. Bowley, 1966: "Snow Cover Distribution as Mapped from Satellite Photography," Final Report, Contract No. Cwb-11269, Allied Research Associates (Aracon), Concord, Massachusetts.

[17] Barnes, J. C., and C. J. Bowley, 1968: "Operational Guide for Mapping Snow Cover from Satellite Photography," Report, Contract No. E-162-67(N), Allied Research Associates (Aracon), Concord, Massachusetts.

[18] Popham, R. S.: "Satellite Applications to Snow Hydrology," WMO (to be published).

[19] Nagle, R. E., and J. R. Clark, 1968: "A Quasi-Objective Method of Incorporating Meteorological Satellite Information in Numerical Weather Analyses," Meteorology International, Incorporated, Final Report, Contract No. E-93-67(N).

[20] Petterssen, S., 1956: Weather Analysis and Forecasting, Vol. 1, McGraw-Hill Book Company, New York, pp. 334-338.

[21] Williams, J. T. Jr., and F. C. Parmenter, 1967: "Cutoff Low Development in the Eastern Pacific as Observed in Satellite Data," Spaceflight Meteorology Group, Weather Bureau, Environmental Sciences Services Administration, unpublished manuscript.

[22] Briefings (V. J. Oliver, NESC).

[23] Personal conversations (V. J. Oliver, NESC).

[24] Parmenter, F. C., 1969: "Sunglint," Picture of the Month, Monthly Weather Review, Vol. 97, No. 2, pp. 155-156.

[25] USAF Environmental Technical Applications Center, September 1966: "Cellular Clouds," Report 5537A (unpublished).

[26] Simpson, R. H., et al, 1968: "Atlantic Disturbances, 1967," Monthly Weather Review, Vol. 96, No. 4, pp. 251-259.

[27] Simpson, J., et al, 1967: "A Study of a Non-Deepening Tropical Disturbance," Journal of Applied Meteorology, Vol. 6, No. 2, pp. 237-254.

[28] Merritt, E., 1964: "Easterly Waves and Perturbations, a Reappraisal," Journal of Applied Meteorology, Vol. 3, No. 4, pp. 367-382.

[29] Frank, N., 1968: "The 'Inverted V' Cloud Pattern - An Easterly Wave?" Monthly Weather Review, Vol. 97, No. 2, pp. 130-140.

[30] Frank, N., 1966: "The Weather Distribution with Upper Tropospheric Cold Lows in the Tropics," Southern Region Technical Memorandum No. 28, Weather Bureau, ESSA, National Hurricane Center, Miami, Florida.

[31] Frank, N., and H. M. Johnson, 1969: "Vortical Cloud Systems Over the Tropical Atlantic During the 1967 Hurricane Season," Monthly Weather Review, Vol. 97, No. 2, pp. 124-129.

[32] Fujita, T. T., et al, 1969: "Formation and Structure of Equatorial Anticyclones Caused by Large-Scale Cross-Equatorial Flows Determined by ATS-I Photographs," SMRP No. 78, University of Chicago.

[33] Gray, W. M., 1968: "Global View of the Origin of Tropical Disturbances and Storms," Monthly Weather Review, Vol. 96, No. 10, pp. 669-700.

[34]  Sadler, J., 1964: "Tropical Cyclones of the Eastern North Pacific as Re-
      vealed by TIROS Observations," Journal of Applied Meteorology, Vol. 3,
      No. 4, August 1964, pp. 347-366.

[35]  Sadler, J., 1967: "The Tropical Upper Tropospheric Trough as a Secondary
      Source of Typhoons and a Primary Source of Trade Wind Disturbances,"
      Hawaii Institute of Geophysics, Report HIG-67-12, University of Hawaii,
      44 p.

[36]  Mintz, Y., and G. Dean, 1951: "The Observed Mean Field of Motion of the
      Atmosphere," Part II, Report No. 7, Investigation of the General Cir-
      culation of the Atmosphere, University of California at Los Angeles,
      55 p.

[37]  Jager, G., W. Follansbee, and V. Oliver, 1965: "Operational Utilization
      of Upper Tropospheric Wind Estimates Based on Meteorological Satellite
      Photographs," ESSA Technical Memorandum NESCTM-8, October 1968, 23 p.

[38]  Kornfield, J., et al, 1967: "Photographic Cloud Climatology from ESSA-3
      and ESSA-5 Computer-Produced Mosaics," Bulletin American Meteorologi-
      cal Society, Vol. 48, No. 12, pp. 878-883.

[39]  Gaby, D. C., 1967: "Cumulus Cloud Lines vs Surface Wind in Equatorial
      Latitudes," Monthly Weather Review, Vol. 95, No. 4, pp. 203-208.

[40]  Hanson, K. J. and T. H. Vonder Haar, 1968: "Cloud Motion and Other
      Parameters from ATS-I Digital Data," Studies in Atmospheric Energetics
      Based on Aerospace Probings, Annual Report - 1967, Department of
      Meteorology, The University of Wisconsin, pp. 19-34.

[41]  Fujita, T. T. and D. L. Bradbury, 1968: "A Study of Mesoscale Cloud
      Motions Computed from ATS-I and Terrestrial Photographs," SMRP No. 71,
      University of Chicago.

[42]  Hubert, L. F. and L. F. Whitney, 1969: "Wind Estimates from Geostation-
      ary Satellites," Paper presented at New York Meeting of American
      Meteorological Society, January 22, 1969 (to be published).

[43]  Fett, Robert, 1966: "Upper Level Structure of the Formative Tropical
      Cyclone," Monthly Weather Review, Vol. 94, No. 1, pp. 9-18.

[44]  Fritz, S., L. Hubert, and A. Timchalk, 1966: "Some Inferences from
      Satellite Pictures of Tropical Disturbances," Monthly Weather Review,
      Vol. 94, No. 4, pp. 231-236.

[45]  Palmer, C., et al, 1955: "The Practical Aspect of Tropical Meteorology,
      Vol. I," Air Weather Service Manual 105-48, USAF, Washington, D. C.,
      202 pp.

[46]  Bittner, F. E., 1967: "Guide for Interpretation of Satellite Photography
      and Nephanalyses," Project FAMOS Research Report (4-67), Walter A.
      Bohan Company, Park Ridge, Illinois.

(47) Jacobowitz, H., 1970: "Emission, Scattering and Absorption in Cirrus Cloud Layers". PHD Thesis submitted in Department of Meteorology, Massachusetts Institute of Technology, Cambridge, Massachusetts.

(48) Keegan, Thomas J., 1972: "An Evaluation of Direct Readout Infrared", Monthly Weather Review, Vol. 100, No. 2.

(49) Anderson, R. K., 1970: Picture of the Month, "An Atlantic Cold Front, Satellite Infrared and Visual Data Compared", Monthly Weather Review, Vol. 98, No. 12, 2 pp.

(50) Fujita, T. T. and W. Bandeen, 1965: "Resolution of the Nimbus High Resolution Infrared Radiometer", Journal of Applied Meteorology, Vol. 4, No. 4, August 1965, pp. 493-503.

(51) Rao, P. Krishna, A. E. Strong, and R. Koffler, 1971: "Gulf Stream Meanders and Eddies as Seen in Satellite Infrared Imagery", Journal of Physical Oceanography, Vol. 1, July 1971, pp. 237-239.

(52) Fleagle, R. G. and J. A. Businger, 1963: "An Introduction to Atmospheric Physics", Academic Press, New York and London.

(53) Smith, W. L., P. K. Rao, R. Koffler and W. R. Curtis, 1970: "The Determination of Sea Surface Temperature From Satellite High Resolution Infrared Window Radiation Measurements", Monthly Weather Review, Vol. 98, No. 8, pp. 604-611.

(54) Albert, E. G., 1968: "The Improved TIROS Operational Satellite", ESSA Technical Memorandum NESC TM-7, (with Supplement 1), Environmental Science Services Administration, Washington, D. C., 25 pp.

(55) Bristor, C. L., W. M. Callicott and R. E. Bradford, 1966: "Operational Processing of Satellite Cloud Pictures by Computer", Monthly Weather Review, Vol. 94, No. 8, pp. 515-527.

(56) Crutcher, H. L. and J. M. Meserve, 1970: "Selected Level Heights, Temperatures and Dew Points for the Northern Hemisphere", NAVAIR 50-1C-52, Naval Weather Service Command, Washington, D. C.

(57)  Huschke, R. E., 1959: "Glossary of Meteorology", American Meteorological Society, p. 55.

(58)  Smith, A. H., 1971: "A Cyclonically Curved Jet Stream", Picture of the Month, Monthly Weather Review, Vol. 97, No. 2, pp. 136-137.

(59)  Fritz, S., 1965: "The Significance of Mountain Lee Waves as Seen from Satellite Pictures", Journal of Applied Meteorology, Vol. 4, pp. 31-37.

(60)  Byers, H. R., 1959: General Meteorology, McGraw Hill, pp. 481.

(61)  Kadlec, P. W., 1966: "Flight Observations of Atmospheric Turbulence", Federal Aviation Agency, Final Report, Contract No. FA 66 WA-1449, 52 pp.

(62)  Kadlec, P. W., 1965: "Flight Data Analysis of the Relationship Between Atmospheric Temperature Change and Clear Air Turbulence", Weather Bureau, Final Report, Contract No. Cwb-10888, 45 pp.

(63)  Sorenson, J. E., 1968: "Thermal Patterns and Clear Air Turbulence", United Airlines Meteorology Circular No. 62, 88 pp.

(64)  Wiegman, E. J., 1965: "The Distribution of Clear Air Turbulence Reports and Cloud Patterns as Seen in Satellite Photographs", Stanford Research Institute, Final Report, Contract Cwb-10791, 101 pp.

(65)  Foltz, H. P., 1967: "Prediction of Clear Air Turbulence", Colorado State University, Atmospheric Science Paper No. 106, 145 pp.

(66)  Woolridge, G. and P. F. Lester, 1969: "Detailed Observations of Mountain Lee Waves and a Comparison with Theory", Colorado State University, Atmospheric Science Paper No. 138, 87 pp.

(67)  Chopra, K. P. and L. F. Hubert, 1965: "Mesoscale Eddies in Wake of Islands", Journal of the Atmospheric Sciences, Vol. 22, No. 11, pp. 652-657.

(68)  Miller, R. C., 1967: "Notes on Analysis and Severe-Storm Forecasting Procedures of the Military Weather Warning Center", Air Weather Service Technical Report #200, 91 pp.

(69)  Frankhauser, J. C., 1971: "Thunderstorm-Environment Interactions Determined From Aircraft and Radar Observations", Monthly Weather Review, Vol. 99, No. 3, pp. 171-192.

(70)  Newton, C. W., 1962: "Dynamics of Severe Convective Storms", National Severe Storms Project Report Number 9, U. S. Weather Bureau, Washington, D. C., 44 pp.

(71)  Haurwitz, B., 1947: "Comments on the Sea Breeze Circulation", The Journal of Meteorology, Vol. 4, pp. 1-8.

(72)  Schroeder, M. J., M. A. Fosberg, O. P. Cramer and C. A. O'Dell, 1967:
      "Marine Air Invasion of the Pacific Coast: A Problem Analysis",
      Bulletin of the American Meteorological Society, Vol. 48, No. 11, pp.
      802-808.

(73)  Raghavan, K., 1969: "Satellite Evidence of Sea Air Interaction During
      Indian Monsoon", Monthly Weather Review, Vol. 97, No. 12, pp. 905-908.

(74)  Hsu, Shih-Ang, 1970: "Coastal Air Circulation System Observations and
      Empirical Model", Monthly Weather Review, Vol. 98, No. 7, pp. 487-509.

(75)  Miller, D. B., 1971: "Four Years of Satellite Relative Daytime Cloud
      Cover over Southeast Asia", Proceedings, Chinese American Air Forces
      Technical Meteorological Workshop, Headquarters 1st Weather Wing,
      Hickam AFB, Hawaii.

NESC 51  Application of Meteorological Satellite Data in Analysis and Forecasting. Ralph K. Anderson, Jerome P. Ashman, Fred Bittner, Golden R. Farr, Edward W. Ferguson, Vincent J. Oliver, and Arthur H. Smith, September 1969. Price $1.75 (AD-697-033) Supplement price $0.65 (AD-740-017)

NESC 52  Data Reduction Processes for Spinning Flat-Plate Satellite-Borne Radiometers. Torrence H. MacDonald, July 1970. Price $0.50 (COM-71-00132)

NESC 53  Archiving and Climatological Applications of Meteorological Satellite Data. John A. Leese, Arthur L. Booth, and Frederick A. Godshall, July 1970. Price $1.25 (COM-71-00076)

NESC 54  Estimating Cloud Amount and Height From Satellite Infrared Radiation Data. P. Krishna Rao, July 1970. Price $0.25 (PB-194-685)

NESC 56  Time-Longitude Sections of Tropical Cloudiness (December 1966-November 1967). J. M. Wallace, July 1970. Price $0.50 (COM-71-00131)

## NOAA Technical Reports

NESS 55  The Use of Satellite-Observed Cloud Patterns in Northern Hemisphere 500-mb Numerical Analysis. Roland E. Nagle and Christopher M. Hayden, April 1971. Price $0.55 (COM-73-50262)

NESS 57  Table of Scattering Function of Infrared Radiation for Water Clouds. Giichi Yamamoto, Masayuki Tanaka, and Shoji Asano, April 1971. Price $1.00 (COM-71-50312)

NESS 58  The Airborne ITPR Brassboard Experiment. W. L. Smith, D. T. Hilleary, E. C. Baldwin, W. Jacob, H. Jacobowitz, G. Nelson, S. Soules, and D. Q. Wark, March 1972. Price $1.25 (COM-72-10557)

NESS 59  Temperature Sounding From Satellites. S. Fritz, D. Q. Wark, H. E. Fleming, W. L. Smith, H. Jacobowitz, D. T. Hilleary, and J. C. Alishouse, July 1972. Price $0.55 (COM-72-50963)

NESS 60  Satellite Measurements of Aerosol Backscattered Radiation From the Nimbus F Earth Radiation Experiment. H. Jacobowitz, W. L. Smith, and A. J. Drummond, August 1972. Price $0.25 (COM-72-51031)

NESS 61  The Measurement of Atmospheric Transmittance From Sun and Sky With an Infrared Vertical Sounder. W. L. Smith and H. B. Howell, September 1972. Price $0.30 (COM-73-50020)

NESS 62  Proposed Calibration Target for the Visible Channel of a Satellite Radiometer. K. L. Coulson and H. Jacobowitz, October 1972. Price $0.35 (COM-73-10143)

NESS 63  Verification of Operational SIRS B Temperature Retrievals. Harold J. Brodrick and Christopher M. Hayden, December 1972. Price $0.55 (COM-73-50279)

NESS 64  Radiometric Techniques for Observing the Atmosphere From Aircraft. William L. Smith and Warren J. Jacob. January 1973. Price $0.35 (COM-73-50376)

NESS 65  Satellite Infrared Soundings From NOAA Spacecraft. L. M. McMillin, D. Q. Wark, J.M. Siomkajlo, P. G. Abel, A. Werbowetzki, L. A. Lauritson, J. A. Pritchard, D. S. Crosby, H. M. Woolf, R. C. Luebbe, M. P. Weinreb, H. E. Fleming, F. E. Bittner, and C. M. Hayden, September 1973. (COM-73-50936/6AS)

NESS 66  Effects of Aerosols on the Determination of the Temperature of the Earth's Surface From Radiance Measurements at 11.2 µm. H. Jacobowitz and K. L. Coulson, September 1973.

NESS 67  Vertical Resolution of Temperature Profiles for High Resolution Infrared Radiation Sounder (HIRS). Y. M. Chen, H. M. Woolf, and W. L. Smith, January 1974.

NESS 68  Dependence of Antenna Temperature on the Polarization of Emitted Radiation for a Scanning Microwave Radiometer. Norman C. Grody, January 1974.